European Commission

Plutonium Futures – The Science 2016

A Topical conference on plutonium and actinides, supporting safe and secure plutonium research as part of the global energy mix

18-22 August 2016, Baden-Baden, Germany
Abstract Booklet

Editor: Roberto Caciuffo

2016

EUR 28059 EN

Joint Research Centre

European Commission
EUR 28059 EN – European Commission, Joint Research Centre (JRC), Directorate for Nuclear Safety and Security (DNSS), Nuclear Safety Department, Advanced Nuclear Knowledge (Unit G.i.5)

Plutonium Futures – The Science 2016
A Topical conference on plutonium and actinides, supporting safe and secure plutonium research as part of the global energy mix
18 - 22 August 2016, Baden-Baden, Germany
Abstract Booklet
Editor: Roberto Caciuffo

Publications Office of the European Union, Luxembourg

Catalogue Number LC-NA-28059-EN-N (online)
EUR 28059 EN
ISBN 978-92-79-58851-8 (pdf)
ISSN 1831-9424 (online)
doi:10.2789/069707 (online)
PUBSY JRC 102724
© European Atomic Energy Community, 2016

Abstract
Plutonium Futures - The Science series of conferences provides an international forum for discussion of current research on physical and chemical properties of plutonium and other actinide elements in complex systems. In bringing the community together from diverse disciplines, the conference aims to enhance the dialogue among scientists and engineers on the fundamental properties of plutonium and their technological consequences.
Scientists, engineers, academics and students from universities, national laboratories, and the nuclear industry are encouraged to participate and make technical contributions..

Online abstracts are available via direct link: http://www.pufutures2016.eu/programme

Navigate through the tabs "Programme", "Titles", "Presenters", and "Topics" to get an overview of the programme and the sessions times, a list of the contribution titles and of the presenting authors in alphabetic order, or sorted by topic. Clicking hyperlinks on any of these lists will bring you to individual session pages.

Search for Author name using Bookmarks toolbar in .pdf.

Plutonium Futures - The Science 2016

A Topical conference on plutonium and actinides, supporting safe and secure plutonium research as part of the global energy mix.

18-22 September 2016

Kongresshaus Baden-Baden, Germany

European Commission | cea | AWE | NATIONAL NUCLEAR LABORATORY

Plutonium Futures - The Science

series of conferences provides an international forum for discussion of current research on physical and chemical properties of plutonium and other actinide elements in complex systems. In bringing the community together from diverse disciplines, the conference aims to enhance the dialogue among scientists and engineers on the fundamental properties of plutonium and their technological consequences.

Topical Areas

Condensed matter physics
Surface science and corrosion
Metallurgy and materials science
Compounds, complexes and coordination chemistry
Detection and analysis
Nuclear fuel cycle
Environmental behaviour and chemistry
Solution and gas-phase chemistry

European Commission | cea | AWE | NATIONAL NUCLEAR LABORATORY

Conference Chair

Hervé Bernard (CEA)
Roberto Caciuffo (EC-JRC)
David Geeson (AWE)

Local Organising Committee

Eric Colineau
Nicola Magnani
Dario Manara
Laura Martel
Philipp Poeml
Damien Prieur
Krisztina Varga

International Scientific Advisory Committee

Hervé Bernard (CEA, France)
Kerri Blobaum (Lawrence Livermore Nat. Lab., USA)
Roberto Caciuffo (EC, JRC, Germany)
David Clark (Los Alamos National Lab., USA)
Vladimir Dremov (RFNC - VNIIEF, Russia)
Rod Ewing (Stanford University, USA)
Thomas Fanghänel (EC, JRC, Belgium)
Jean Fuger (University of Liège, Belgium)
Horst Geckeis (KIT, Germany)
David Geeson (AWE, UK)
Claude Guet (Nanyang Tech. University, Singapore)
Yoshi Haga (Japan Atomic Energy Agency, Japan)
Ladia Havela (Charles University, Czech Republic)
Sig Hecker (Stanford University, USA)
Gordon Jarvinen (Los Alamos National Lab., USA)
Gerry Lander (ILL, France)
Scott McCall (Lawrence Livermore Nat. Lab., USA)
Boris Nadykto (RFNC - VNIIEF, Russia)
Alexander Petrovtsev (RFNC - VNIIEF, Russia)
P.R. Vasudeva Rao (IGCAR, India)
Lydia Timofeeva (RFNC - VNIIEF, Russia)
Tim Tinsley (Nuclear National laboratory, UK)
Gerrit van der Laan (Diamond Light Source, UK)
Philip Wilk (U.S. Department of Energy, USA)
Ping Zhang (IAPCM, China)

Ground floor

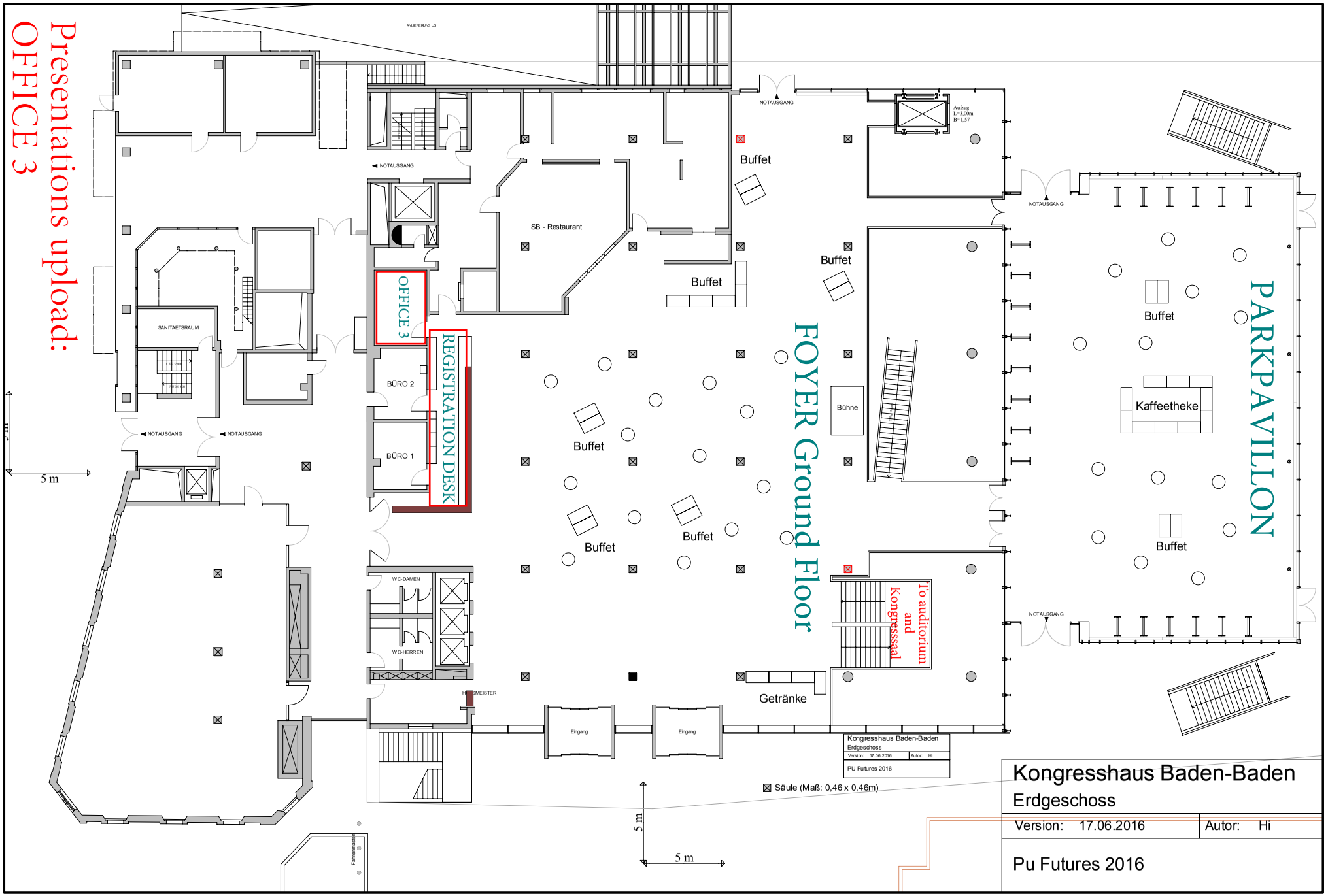

Auditorium - Basement Floor

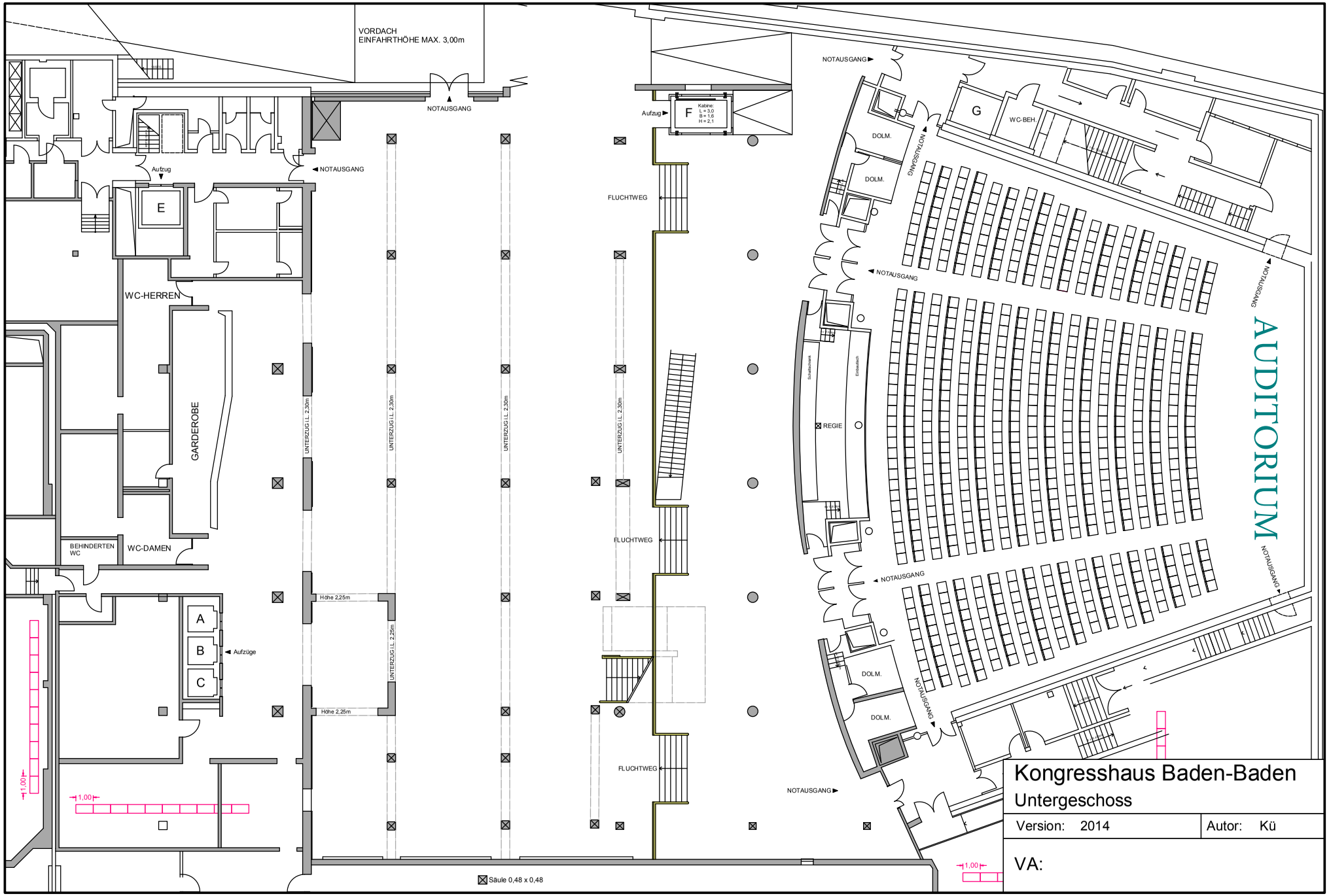

1st Floor

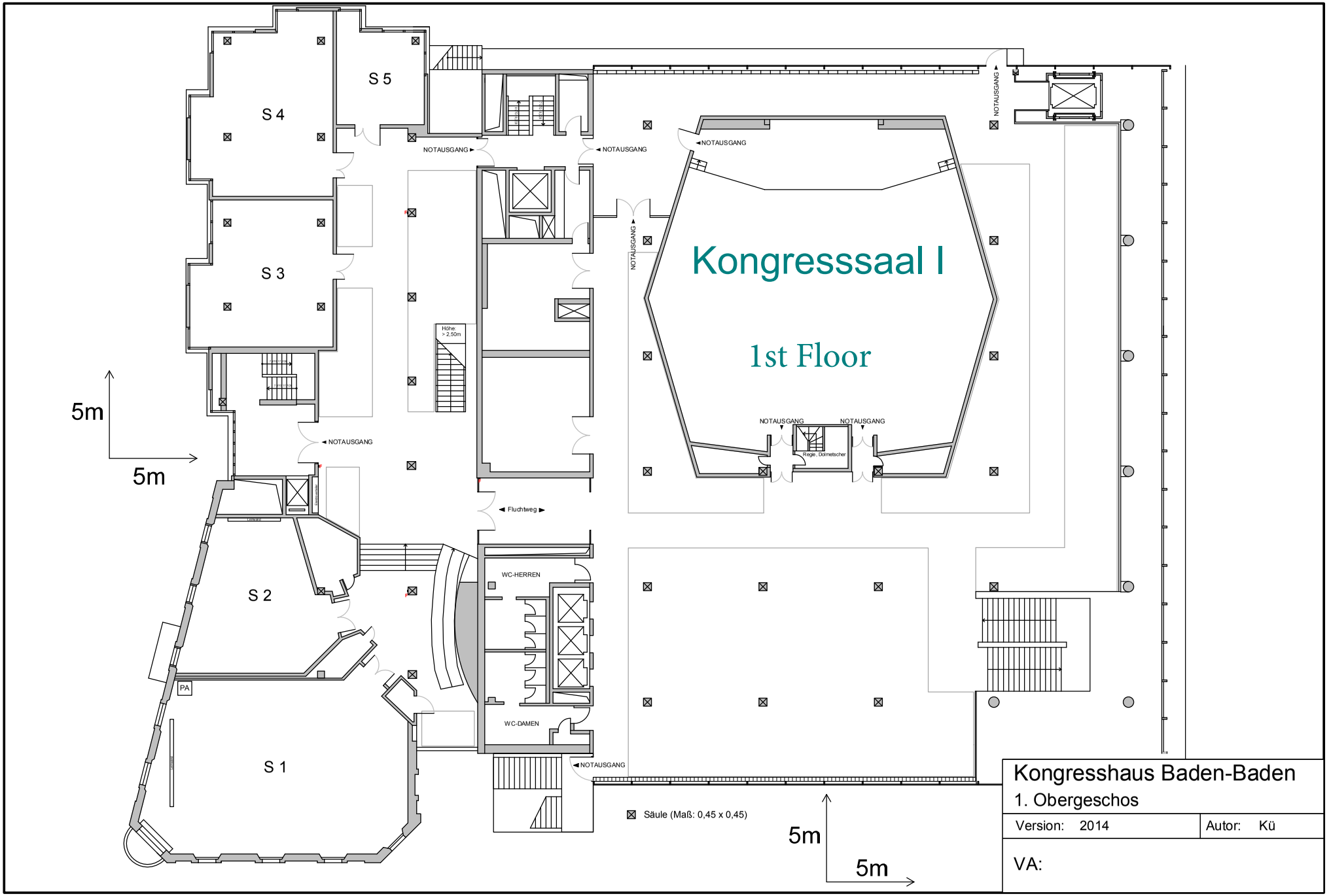
S 5
S 4
S 3
S 2
S 1
PA
Kongresssaal I
1st Floor
NOTAUSGANG
Höhe: > 2,50m
Fluchtweg
WC-HERREN
WC-DAMEN
Regie, Dolmetscher
5m
5m
5m
5m
Säule (Maß: 0,45 x 0,45)
Kongresshaus Baden-Baden
1. Obergeschos
Version: 2014
Autor: Kü
VA:

Opening hours

Cloakroom:
Monday: 8:00-18:00
Tuesday: closed
Wednesday: closed
Thursday: 8:00-17:00

Uploading presentations:
Office 3 (behind registration desk)
Monday: 8:00-14:00
Tuesday: 8:00-14:00
Wednesday: 8:00-14:00
Thursday: 8:00-14:00

To ensure keeping the schedule of the lectures, please upload your presentation on time, during the above opening hours.
Thank you.

Access to the venue:
http://www.kongresshaus.de/seiten/anfahrt/anfahrt-de.htm

Conference registration desk emergency number: +49-7221-304249 (from local network: 07221-304249).

Conference registration desk fax: +49-7221-304404 (from local network: 07221-304404)

Plutonium Futures - The Science 2016

Programme

European Commission | cea | AWE | NATIONAL NUCLEAR LABORATORY

	Sunday 18/9	Monday, 19/9		Tuesday,20/9		Wednesday, 21/9		Thursday, 22/9	
Time		**Chair A. Migliori**		**Chair H. Bernard**		**Chair T. Tinsley**		**Chair G. Lander**	
08:40-09:25		A-01 Alexander Lichtenstein		B-01 Thomas Albrecht-Schmitt		C-01 David Clark		D-01 Andrew Gaunt	
		Chair A. Migliori	Chair D. Clark	Chair H. Bernard	Chair J. Glascott	Chair T. Tinsley	Chair A. Gaunt	Chair G. Lander	Chair T. Albrecht-S
09:30-10:00		A-02 P. Söderlind	A-04 F. Quinto	B-02 D. Guillaumont	B-04 Y. Aregbe	C-02 M. Sarsfield	C-04 I. May	D-02 A. Shick	D-04 R. Maurice
10:00-10:30		A-03 G. Kotliar	A-05 J. Zsigrai	B-03 R. Wilson	B-05 S. Ennaceur	C-03 D. Kramer	C-05 W. Shi	D-03 K. Kvashnina	D-05 X. Gaona
10:30-11:00		**Coffee break**		**Coffee break**		**Coffee break**		**Coffee break**	
11:00-11:15		A-06 S. Hernandez	A-10 A. Romanchuk	B-06 E. Acher	B-10 B. Sun	C-06 A. Casella	C-10 G. Creff	D-06 B. Nadykto	D-10 P. Zhang
11:15-11:30		A-07 K.Gofryk	A-11 R. Harker	B-07 A. Arico	B-11 A. Pugmire	C-07 F. Freibert	C-11 A. Hixon	D-07 J. Jeffries	D-11 L. Jones
11:30-11.45		A-08 L. Havela	A-12 O. Benes	B-08 H. Cho	B-12 L. Venault	C-08 B. Ravat	C-12 N. Martin	D-08 P. Raison	D-12 E. Dalodiere
11.45-12:00		A-09 H. Liu	A-13 K. Dardenne	B-09 B. Dorado	B-13 M. Virot	C-09 B. Tegner	C-13 D. Meier	D-09 M. Silver	D-13 C. Zarzana
12:00-12:30		A-14 B. Maiorov	A-15 R. Vauchy	B-14 J.-C. Griveau	B-15 A. Geist	C-14 R. Wham	C-15 C. Dares	D-14 J. Joyce	D-15 R. Abergel
12:30-14:15		Poster Session (A-29 to A-66) & working lunch		Poster Session (A-29 to A-66) & working lunch		Poster Session (C-29 to C-67) & working lunch		Poster Session (C-29 to C-67) & working lunch	
		Chair T. Gouder		Chair K. Blobaum		Chair D. Warin		Chair C. Guet	
14:15-15:00		A-16 Joseph Glascott		B-16 Peter Steier		C-16 Danny Fox		D-16 Brian Powell	
		Chair T. Gouder	Chair P. Roussel	Chair K. Blobaum	Chair B. Powell	Chair D. Warin	Chair A. Shick	Chair C. Guet	Chair M. Sarsfield
15:05-15:35		A-17 M. Brierley	A-18 B. Chung	B-17 M. Joyce	B-18 E. Buck	C-17 J. Gibson	C-18 R. Eloirdi	D-17 C. Jégou	D-18 A. Kersting
15:35-15:50		A-19 D. Moore	A-21 K. Blobaum	B-19 M. Wilkerson	B-21 M. Altmaier	C-19 Y. Kitatsuji	C-21 D. Schwartz	D-19 E. Welcomme	D-21 S. Hellebrandt
15:50-16:05		A-20 G. Li	A-22 B. Ao	B-20 C. Willberger	B-22 R. Kierepko	C-20 X. Shi	C-22 A. Smith	D-20 Y. Ziouane	D-22 C. Tamain
16:05-16:30		**Coffee break**		**Coffee break**		**Coffee break**		**Closing Ceremony**	
16:30-17:00	Registration begins	A-23 T. Wiss	A-25 J. Mitchell	B-23 M. Naji	B-25 J. Li	C-23 R. Orr	C-25 S. Peuget		
17:00-17:30		A-24 M. Freyss	A-26 D. Olive	B-24 C. Walther	B-26 T. Vitova	C-24 R. Hania	C-26 K. Popa		
17:30-17.45	Welcome address by Maria Betti	A-27 A. Savchenko	A-28 A. Karavaev	B-27 L. Paolasini	B-28 P. Martin	C-27 K. Ivanov	C-28 T. Gouder		
17:45-18:30	Opening Talk by Roland Schenkel								
18:30-20:00	Welcome drink								
20:00-23:00						**Conference Dinner at Kurhaus Casino Restaurant**			

Kongresshaus Baden-Baden

Arrival

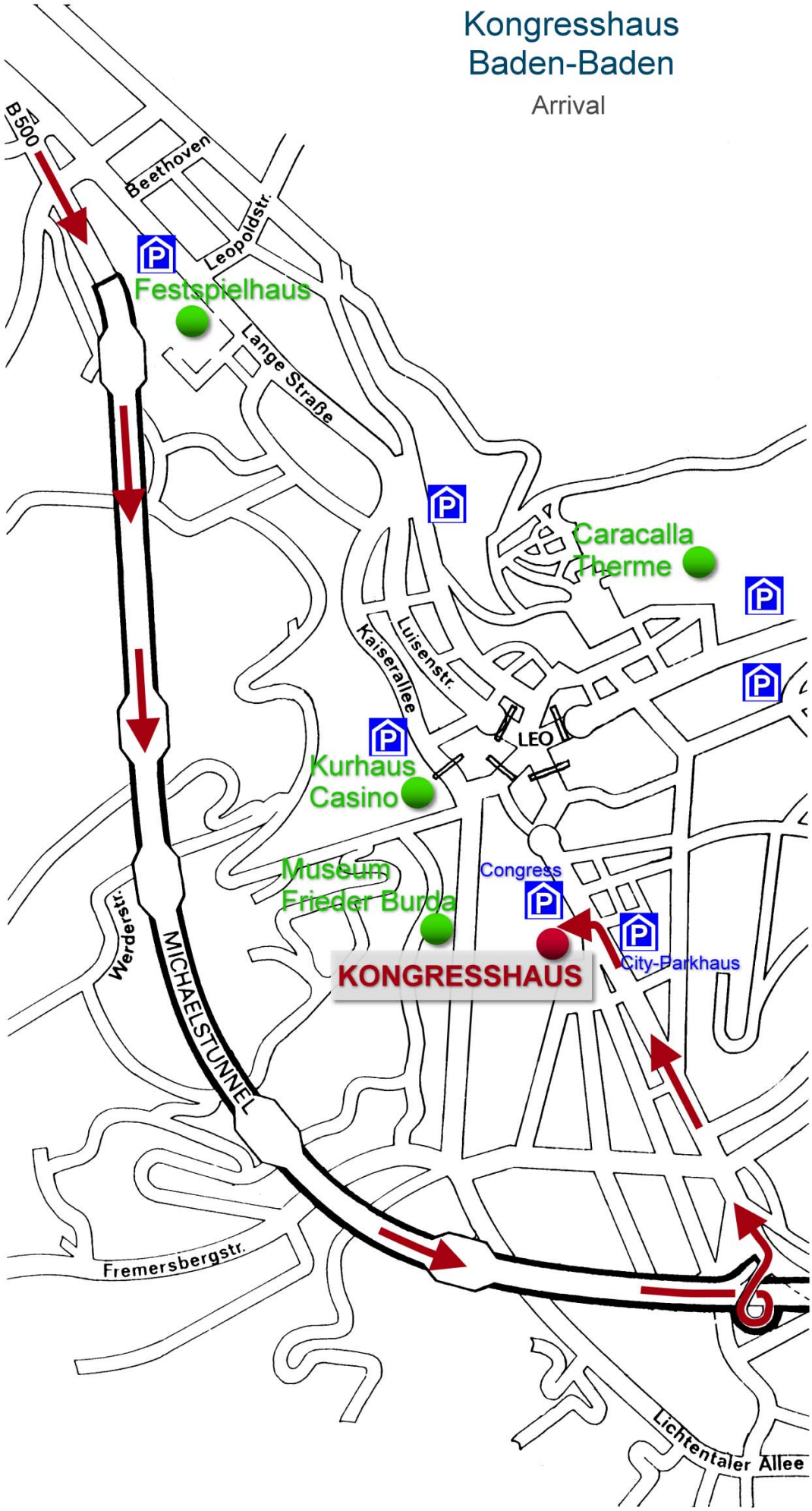

Programme number index

A-01 Racah materials: atomic multiplets and f-bands
*Alexander B. Shick, Jindrich Kolorenc, Mikhail I. Katsnelson, Alexander I. Lichtenstein**

A-02 Phase stability, elasticity, and phonons for plutonium from electronic-structure theory
*Per Soderlind**

A-03 Plutonium as a Mixed Valent Metal
*Gabriel Kotliar**

A-04 Multi-Actinides analysis with AMS: a novel method for ultra-trace determination and small sample sizes
Francesca Quinto, Markus Lagos, Markus Plaschke, Thorsten Schäfer, Peter Steier, Horst Geckeis*

A-05 Non-destructive analysis for Pu accountancy in reprocessing
Jozsef Zsigrai, Klaus Lutzenkirchen, Artur Muhleisen, Magdalena Toma, Peter Schwalbach, Sotiris Synetos*

A-06 Insights into point-defects of δ-Pu and δ-Pu-Ga alloys using density functional theory
Sarah Hernandez, Franz Freibert*

A-07 Thermoelectric power as a probe of density of states in $PuCoGa_5$
Krzysztof Gofryk, Jean-Christophe Griveau, Tomasz Durakiewicz*

A-08 Hydrogen as a tool to modify electronic structure: are there common features in U and Pu hydrides?
Ladislav Havela, Mykhaylo Paukov, Volodymyr Buturlim, Ilja Turek, Martin Divis, Daria Drozdenko, Zdenek Matej, Milan Dopita, Milan Cieslar, Frank Huber, Thomas Gouder*

A-09 Quantum molecular dynamics simulations of transport properties in liquid plutonium
Haifeng Liu, Shuaichuang Wang, Gongmu Zhang, Bo Sun, Haifeng Song, Mingfeng Tian*

A-10 Properties of PuO2 nanoparticles together with its analogues CeO2 and ThO2
Anna Romanchuk, Tatiana Plakhova, Stepan Kalmykov*

A-11 Development of point defect Raman signatures in PuO_2 through self-irradiation
Robert M Harker, Christopher Puxley*

A-12 Oxygen stoichiometry determination in Pu-fuel by vapour pressure measurement
Ondrej Benes, Rudy Konings, Jean-Yves Colle*

A-13 XAFS and μ-XRF investigations of highly radioactive nuclear waste samples: spent nuclear fuel and zircaloy cladding segments.
Kathy Dardenne, Ernesto Gonzalez-Robles, Michel Herm, Bernhard Kienzler, Gerd Christill, Nikolaus Müller, Volker Metz, Jörg Rothe*

A-14 Real Time Studies of ^{239}Pu Elastic Moduli using Resonant Ultrasound Spectroscopy
Boris Maiorov, Jonathan Betts, Maxime Leroux, Franz Freibert, Albert Migliori*

A-15 *In situ* high temperature X-ray diffraction studies of the phase equilibria in the UO_2-PuO_2-Pu_2O_3 system
Romain Vauchy, Renaud C. Belin, Alexis Joly, Christophe Valot*

A-16 Plutonium corrosion: some insights and some mysteries
*Joseph Glascott**

A-17 Recent progress in plutonium hydride research
Martin Brierley, John Knowles*

A-18 Metallurgical Properties of Aged Plutonium Alloys and the Need for Advanced Microstructural Characterization
Brandon Chung, Kenneth Lema, Robert Erler, Nick Teslich, Patrick Allen*

A-19 Auger Electron Spectroscopy of Plutonium Surfaces
David Moore, Alison Pugmire, Thomas Venhaus, Sarah Hernandez, David Pugmire*

A-20 The influence of hydrogen pressure and reaction temperature on the nucleation and growth kinetics of plutonium hydride
Gan Li, Huilong Yu, Haibo Li*

A-21 Small-scale production and characterization of high-purity plutonium metal
Kerri J.M. Blobaum, Mark A. Wall, Roger A. Henderson, Mike J. Singleton, Gary R. Eppich, Kiel S. Holliday, Jason R. Jeffries, Jeff A. Stanford, Elizabeth G. Dzenitis, Athanasios Arsenlis*

A-22 First-principles DFT+*U* Energetics of Impurity Atoms in PuO_2 and Pu_2O_3
*Bingyun Ao**

A-23 Radiation damage studies in plutonium oxides for energy production
Thierry Wiss, Rudy Konings, Vincenzo V. Rondinella, Oliver Dieste, Ondrej Benes, Jean-Yves Colle, Dragos Staicu, Philippe E. Raison*

A-24 First-principles modelling of point defects in fast reactor MOX fuels
Michel Freyss, Marjorie Bertolus, Ibrahim Cheik Njifon, Yaguang Li, Lei Shi*

A-25 Thermal Expansion of Delta Plutonium
Jeremy Mitchell, Franz Freibert, Scott Richmond, Daniel Schwartz, Michael Ramos*

A-26 EXAFS studies of self-irradiation damage in Pu
Daniel Olive, Deborah Wang, Corwin Booth, Eric D. Bauer, Alison Pugmire, Franz Freibert, Scott McCall, Mark A. Wall, Patrick Allen*

A-27 Fuel Cycle Concept with dispersion type Fuel in LWRs
Aleksei Savchenko, Leonid Karpyuk, Dmitry Shamin, Oleg Uferov*

A-28 MD study of self-irradiation effects on dislocation dynamics in δ-Pu
Alexey Karavaev, Vladimir Dremov, Gennady Ionov*

A-29 Secure and certify studies to work on production of spiked plutonium
*Ashraf Elsayed**

A-30 Plutonium Handbook, Second Edition
Patrice Stevens, David L. Clark, David Geeson, Robert Hanrahan, Jr, Natanya Civjan*

A-31 On dislocation mechanism of dynamic deformation of uranium
Victor Pushkov, Dmitry Tsisar*

A-32 Laser Spectroscopy and Detection of Actinides and Lanthanides in Solutions
*Igor Izosimov**

A-33 An in-situ X-ray diffraction study of plutonium oxidation
*Paul Roussel, Wayne Lake**

A-34 Temperature dependent hydriding and dehydriding energies of PuHx from *ab initio* calculations
Yu Yang, Ping Zhang*

A-35 Characterization of point defects in α-Pu
Vladimir Dremov, Gennady Ionov, Alexey Karavaev, Sergey Samarin, Filipp Sapozhnikov*

A-36 Theoretical studies on the extraction behaviors of Am(III) and Cm(III) with amide-type ligands
Cong-Zhi Wang, Jian-Hui Lan, Qun-Yan Wu, Zhi-Fang Chai, Wei-Qun Shi*

A-37 Properties of solids under compression and shock : Role of electronic and structural phase transitions
*Boris Nadykto**

A-38 2NN MEAM potential for Plutonium
Piheng Chen, Xinchun Lai*

A-39 Atom Probe Tomography of Niobium Redistribution in U-14 at.% Nb After High Temperature Age-Hardening
Clarissa Yablinsky, Amy Clarke, Yaqiao Wu, Robert Hackenberg*

A-40 Chitin-chitozan - a Sorbent Preventing Release of Radioactive Actinide Compounds under Emergency Submersion
Tatiana Kazakovskaya, Victor Scherbakov, Edvard Goryachev, Alexander Gorelov*

A-41 Cerium Behavior in Various Media as Compared with Plutonium
Tatiana Kazakovskaya, Yulia Belova*

A-43 Raman Spectroscopy Characterization of Uranium and Plutonium Hydride from the Hydrogen Corrosion
Xiaolin Wang, Guangfeng Zhang, Junbo Lv*

A-44 XPS study of radiation effect on UO2 single-crystal films
Yury Teterin, Alexey Popel, Konstantin Maslakov, Anton Teterin, Kirill Ivanov, Stepan Kalmykov, Ross Springell, Thomas Scott, Ian Farnan*

A-45 Pd-hybridization and paramagnon superconductivity mechanism $PuCoGa_5$
*Aleksandr Povzner**

A-46 Auger line-shape analysis and electron energy loss spectroscopy investigation of Pu surface chemistry
Art Nelson, Scott Donald, Wigbert Siekhaus, Patrick Allen, William McLean*

A-47 Research Shape Memory Effect in the U6.3wt%Nb Alloy by Dilatometry
Aleksandr Troshev, Chentzov Denis, Golunov Anatoliy, Shestakov Evgeniy, Baluev Alexey*

A-48 On the equation of state and elastoplastic and strength properties of beryllium
Maria Shirshova, Boris Nadykto, Ivan Pavlusha*

A-49 The Structure of Thick-walled Spherical Shell of U-1,5% Mo Alloy After Explosive Loading
Dmitry Belyaev, Eugen Kozlov, Yury Zouev, Igor Svyatov, Alexey Aleksandrov, Ekaterina Levi*

A-50 Dynamic Magnetic Response across the Pressure-Induced Structural Phase Transition in CeNi
Alexey Mirmelstein, Andrey Podlesnyak, Alexander Kolesnikov, Georg Ehlers, Douglas Abernathy, Vladimir Matvienko, Gregory Halder, Antonio dos Santos*

A-51 Development of AFM and STM Capabilities for Plutonium
Miles Beaux, Adam Zocco, Miguel Santiago Cordoba, Douglas Vodnik, Stephen Joyce, Michael Ramos, Scott Richmond, Thomas Venhaus, Jeremy Mitchell, Brian Scott, Eve Bauer, Igor Usov*

A-53 CALPHAD approach a complementary way to solve the plutonium mystery.
Benoît Oudot, Brice Ravat, Aurelien Perron, Christine Guéneau, Lionel Jolly, Patrice Turchi, François Delaunay*

A-54 Evolution of electronic structures of γ-Pu, δ-Pu, and ε-Pu
*Li Huang**

A-55 Pu Alloy Oxidation by Water Vapor.
*Lionel Jolly, Brice Ravat, Benoît Oudot, François Delaunay**

A-56 Oxidation of Pu-Ga alloyed surfaces and PuO_2 PAD films using Time-of-Flight SIMS
Sarah Hernandez, Thomas Venhaus, David Pugmire, David Moore, Brian Scott*

A-57 Some results of investigations of particle ejection from a free surface of metals under a shock wave effect
Michael Antipov, Alla Georgievskaya, Vladislav Igonin, Margarita Lebedeva, Konstantin Panov, Valeriy Sadunov, Alexander Utenkov, Igor Yurtov*

A-58 Experimental and calculation parameters of benchmark spherical critical assemblies with metal plutonium in α-phase core and in beryllium and depleted uranium reflectors
Alexey Kaygorodov, Sergey Vorontsov, Mikhail Kuvshinov, Valentin Khoruzhyi*

A-59 Carbonate Oxidation of Electrorefining Salts
Robert Watson, Clare Stawarz*

A-60 Hydrolysis of plutonium under reducing conditions controlled by electrolysis
Hye-Ryun Cho, Young-Sang Youn, E. C. Jung, W. Cha*

A-61 U(VI) adsorption onto alumina, silica, and kaolinite in U(VI)-OH / U(VI)-CO_3 / Ca-U(VI)-CO_3 aqueous systems
Yongheum Jo, Jun-Yeop Lee, Jong-Il Yun*

A-62 Structural properties of actinides from first principles: important role of Hund's exchange.
*Bernard Amadon**

A-63 Solubility, Hydrolysis and Carbonate Complexation of Plutonium and Neptunium under Repository-Relevant Conditions
Julian Schepperle, David Fellhauer, Xavier Gaona, Marcus Altmaier, Horst Geckeis*

A-64 Thermodynamic stability of the UO_2 surfaces: Interplay between over-stoichiometry and polarity compensation
François Bottin, Gérald Jomard, Grégory Geneste*

A-65 Analysis of surface chemistry on Pu-Ga alloyed surfaces by Time-of-Flight SIMS
Thomas Venhaus, Sarah Hernandez, Joseph Anderson, David Moore, David Pugmire*

A-66 ToF-SIMS Determination of the Partitioning between H and F in Aged Uranium Materials
Scott Donald, Wigbert Siekhaus, Art Nelson*

B-01 Does the Electrochemistry of Plutonium Signal the Unravelling of the Seaborg Concept of the Actinide Series?
*Thomas E. Albrecht-Schmitt**

B-02 Quantum chemistry and spectroscopic studies of actinide ions with oxygen- and nitrogen- donor ligands in solution
Dominique Guillaumont, Eleonor Acher, Thomas Dumas, Matthieu Audras, Laurence Berthon, Olivia Pecheur*

B-03 Thiocyanate complexes of the tri- and tetravalent actinides.
Richard Wilson, Tyler Carter*

B-04 Quality control tools for the analysis of plutonium in nuclear safeguards, security and safety
Yetunde Aregbe, Rozle Jakopic, Stephan Richter, Goedele Sibbens*

B-05 Impurity effects in plutonium alloys
Sue Ennaceur, Paul Roussel*

B-06 Structure of Plutonium(IV) with O-donor ligands from crystallography, extended X-ray absorption fine structure and theoretical calculations
Eleonor Acher, Thomas Dumas, Christelle Tamain, Dominique Guillaumont*

B-07 Semiconductivity in Plutonium and Americium Chromates and Molybdates: The Smoking Gun for Energy-Degeneracy-Driven Covalency
Alexandra Arico, Alejandro Garza, Justin Cross, Thomas E. Albrecht-Schmitt*

B-08 Evaluation of Covalency in PuF_4 by ^{19}F NMR Spectroscopy
Herman Cho, Cigdem Capan, Richard Dempsey, Sergey Sinkov, Bruce McNamara*

B-09 Insight Into Stabilization Mechanisms of the Delta Phase of Plutonium by Deltagen Elements
Boris Dorado, Jordan Bieder, Marc Torrent*

B-10 Density Functional Theory Study on Hydriding Resistance and Surface Initial Oxidation of Plutonium Nitride
Bo Sun, Haifeng Liu, Haifeng Song, Hui Zheng*

B-11 Understanding the Oxide Layer on Plutonium under Ambient Conditions
Alison Pugmire, David Pugmire, David Moore, Thomas Venhaus*

B-12 Alpha radiolysis of nitric acid solutions with plutonium
Laurent Venault, Guillaume Garaix, Amaury Costagliola, Philippe Moisy, Guillaume Blain, Johan Vandenborre, Massoud Fattahi-Vanani, Nicolas Vigier*

B-13 Reductive Dissolution of PuO_2 and CeO_2 in the Presence of Ti Particles and Ultrasound Irradiation
Matthieu Virot, Xavier Beaudoux, Tony Chave, Gilles Leturcq, Gauthier Jouan, Laurent Venault, Philippe Moisy, Sergey I. Nikitenko*

B-14 Shedding a new light on the superconductivity of $PuCoGa_5$: A heat capacity study on single crystals below 1 K.
Jean-Christophe Griveau, Eric Colineau, Rachel Eloirdi, Pedro Amador Celdran, Roberto Caciuffo*

B-15 Plutonium and Americium Solvent Extraction Processes: Recent Development in Europe
*Andreas Geist**

B-16 From the stars through the ocean abyss: the long travel of super-nova Pu-244 into VERA's particle detector
Peter Steier, Anton Wallner, Thomas Faestermann, Jenny Feige, Chana Feldstein, Klaus Knie, Gunther Korschinek, Walter Kutschera, Avishai Ofan, Michael Paul, Francesca Quinto, Georg Rugel*

B-17 Real-time, fast neutron assay of plutonium and related materials
*Malcolm J. Joyce**

B-18 Nanoparticle Plutonium Formation, Growth, and Morphology with in-situ Liquid Cell Electron Microscopy
*Edgar Buck**

B-19 Chemical Speciation of uranium oxide and plutonium oxide materials for forensic science
Marianne Wilkerson, Miles Beaux, Sarah Hernandez, Stephen Joyce, Andrew Nelson, Alison Pugmire, David Pugmire, Amy Ross, Brian Scott, Igor Usov, Gregory Wagner, Angelique Wall, Laura Wolfsberg*

B-20 Redox speciation of actinides using capillary electrophoresis coupled to ICP-MS
Christian Willberger, Samer Amayri, Verena Häußler, Raphael Scholze, Tobias Reich*

B-21 ThermAc - a collaborative project investigating aquatic chemistry and thermodynamics of actinides at elevated temperature conditions
Marcus Altmaier, Felix Brandt, Vinzenz Brendler, Ion Chiorescu, Elisenda Colas, Hilde Curtius, Francesco Endrizzi, Carola Franzen, Xavier Gaona, Mireia Grive, Seven Hagemann, Carsten Koke, Dmitrii A. Kulik, Sven Krüger, Jun-Yeop Lee, Martin Maiwald, Tres Thoenen, Petra J. Panak, Andrej Skerencak-Frech, Robin Steudtner*

B-22 Traces of Pu isotopes originated from burnt-up fuel in Fukushima exclusion zone
Renata Kierepko, Atsuyuki Sorimachi, Shinji Tokonami, Sarat Sahoo*

B-23 On the Raman Spectrum of Plutonium dioxide: vibrational and crystal electric field modes
Mohamed Naji, Nicola Magnani, Laura Bonales, Sara Mastromarino, Jean-Yves Colle, Joaquin Cobos, Dario Manara*

B-24 Resonant Laser-SNMS on actinides for spatially resolved ultra-trace analysis
Clemens Walther, Hauke Bosco, Michael Franzmann, Linda Hamann, Mohammad Tanha, KLaus Wendt*

B-25 On the Highest Oxidation State of Plutonium in Compounds
*Jun Li**

B-26 Structural properties of plutonium systems revealed by high resolution XANES and RIXS techniques
*Tonya Vitova**

B-27 Crystal dynamics of neptunium dioxide
Luigi Paolasini, Pablo Maldonado, Peter M. Oppeneer, Tom R. Forrest, Nicola Magnani, Alexei Bosak, Gerard H. Lander, Roberto Caciuffo*

B-28 Study of the 5f electronic states in uranium-plutonium mixed oxides using high resolution XANES
Philippe Martin, Michal Strach, Damien Prieur, René Bès, Renaud C. Belin, Dario Manara, Christophe Valot, Tonya Vitova, Tim Prussmann, Kathy Dardenne, Jörg Rothe*

C-01 Pu-238 and the Pu sustainment work at Los Alamos
*David L. Clark**

C-02 ^{241}Am Production for Use in Radioisotope Power Systems
Catherine Campbell, Cheryl Carrigan, Michael Carrott, Chris Maher, Bliss McLuckie, Chris Mason, Colin Gregson, Tamara Griffiths, Josh Holt, Mark Sarsfield, Robin Taylor, Tim Tinsley, Keith Stephenson*

C-03 Studies Related to the Fabrication of $^{238}PuO_2$ Ceramic Fuel Pellets and the Surrogate CeO_2
*Daniel Kramer**

C-04 Redox Stability and Separation Chemistry of Actinyl Cations Coordinated by Schiff Base Ligands
Christiain Bustillos, Roy Copping, Andrew Gaunt, Cory Hawkins, Iain May, Mikael Nilsson, Sean Reilly, Brian Scott*

C-05 Actinide Polyrotaxanes: From Hydrothermal Synthesis to Structural Regulation
*Wei-Qun Shi**

C-06 PuF_4 Lattice Effects Due to Aging
Amanda Casella, Calvin Delegard, Kaylyn McCoy, Bruce McNamara, William Karl Pitts, Sergey Sinkov*

C-07 The Kinetic Evolution of Self-Irradiation Damage in Face-Centered Cubic Pu-Ga Alloys
*Franz Freibert**

C-08 Oxidation study of Pu stabilized in δ-phase
Brice Ravat, Lionel Jolly, Benoît Oudot, François Delaunay*

C-09 Water Interactions with Actinide Oxide Surfaces
Bengt Tegner, Andrew Kerridge, Nikolas Kaltsoyannis*

C-10 How does Pu(IV) interact with hyperphosphorylated protein osteopontin ?
Gaëlle Creff, Hervé Michel, Jérôme Roques, Claude Vidaud, Christophe Den Auwer*

C-11 Self-assembly of plutonium sulfate dimers from a chloride matrix
Amy Hixon, Ginger Sigmon*

C-12 Coordination polymers of tetravalent neptunium with aromatic polycarboxylate ligands
Nicolas Martin, Juliane März, Natacha Henry, Christophe Volkringer, Atsushi Ikeda-Ohno, Christoph Hennig, Thierry Loiseau*

C-13 Plutonium Oxide Processing Platform for Nuclear Forensics Applications
David Meier, Joel Tingey, Gregg Lumetta*

C-14 Production of Plutonium-238 for Deep Space Missions
*Robert Wham**

C-15 Selective Separation of Electrochemically Generated Am(VI
Christopher Dares, Thomas J Meyer, Bruce Mincher*

C-16 Reprocessing and beyond --- the management of spent oxide and Magnox fuel in the UK held by the NDA
*Danny Fox**

C-17 Gas-Phase Reactions of Water with Actinide Dioxide Cations, PaO_2^+ to CfO_2^+: The "Enigmatic" Behavior of Plutonium
John K. Gibson, Monica Vasiliu, Phuong Diem Dau, Richard Wilson, Kirk Peterson, David Dixon*

C-18 Thermal expansion study of the heavy-fermion superconductor 242PuCoGa5
Rachel Eloirdi, Nicola Magnani, Carlotta Giacobbe, Pedro Amador Celdran, Jean-Christophe Griveau, Eric Colineau, Gerard H. Lander, Roberto Caciuffo*

C-19 Electrode reduction of actinyl ions followed by deposition in weak acid solution
Yoshihiro Kitatsuji, Kazuki Ouchi, Haruyoshi Otobe*

C-20 Numerical Simulation on Breeding and Burning Process of Plutonium in Fusion Fission Hybrid Reactor for Energy(FFHR-E)
Xueming Shi, Xianjue Peng*

C-21 Thermodynamic Properties of Pu as a Function of Ga Content
Daniel Schwartz, Jeremy Mitchell, Franz Freibert*

C-22 A Temperature Investigation of δ-phase ^{239}Pu-Ga Alloys
Alice I. Smith, Adrian S. Losko, Sven C. Vogel, Scott Richmond, Michael Ramos*

C-23 Experimental studies to support storage of PuO_2 in the UK
Colin Gregson, Robin Orr, Howard Sims, Robin Taylor, Kevin Webb, David Woodhead, Paul Cook, Jeff Hobbs, Helen Steele*

C-24 Irradiation testing of fuels for plutonium and minor actinide transmutation
*P. Ralph Hania**

C-25 How alpha decays of actinides will affect the nuclear glass structure: evidence of competitive effects between damage generation from recoil nuclei and recovery processes from alpha particles
Sylvain Peuget, Anamul Haq Mir, Thibault Charpentier, Laura Martel, Joseph Somers, Thierry Wiss, Jean-Marc Delaye, Marcel Toulemonde, Serge Bouffard, Christophe Jégou*

C-26 Recent progress in actinide phosphates chemistry
Karin Popa, Gilles Wallez, Damien Bregiroux, Philippe E. Raison, Laura Martel, Yulia Arinicheva, Stefan Neumeier, Joseph Somers, Rudy Konings*

C-27 Chemical bond nature in $Cs_2AnO_2Cl_4$
Yury Teterin, Anton Teterin, Kirill Ivanov, Mikhail Ryzhkov, Konstantin Maslakov, Stepan Kalmykov, Vladimir Petrov, Dmitry Suglobov*

C-28 Integrated surface science lab station for spent corrosion studies
Thomas Gouder, Rachel Eloirdi, Frank Huber, Roberto Caciuffo*

C-29 Effect of Doping Level on Dissolution Behavior of Rare-Earth Doped UO_2
Jeongmook Lee, Jandee Kim, Young-Sang Youn, Jong-Goo Kim, Sang-Eun Bae, Yeong-Keong Ha, Jong-Yun Kim*

C-30 A New Strategy for Stabilizing Uncommon Oxidation States Learned from an Extraordinarily Complex Mixed-Valent Uranium Phosphonate Framework
Chengliang Xiao, Lanhua Chen, Juan Diwu, Thomas E. Albrecht-Schmitt, Shuao Wang*

C-31 Uranium-hydride initiation iimes before and after outgassing in vacuum at 300 C to determine the influence of hydrogen content in uranium on hydride initiation time.
*Wigbert J. Siekhaus**

C-32 Lipophilic pyridine-2,6-bis(1H-1,2,3-triazol-4-yl) structure as selective chelating unit for direct actinides extraction from purex raffinate
Annalisa Ossola, Eros Mossini, Elena Macerata, Marco Giola, Mario Mariani, Arturo Arduini, Alessandro Casnati*

C-33 Incorporation of soluble radionuclides into High Oxidation State Actinide Solid Matrix
Yaxing Wang, Xuemiao Yin, Juan Diwu, Thomas E. Albrecht-schmitt, Shuao Wang*

C-34 Recent Investigations of Solid State Chemistry of Actinides at Soochow University
*Shuao Wang**

C-35 Vibrational properties of uranium and plutonium
Johann Bouchet, François Bottin, Boris Dorado*

C-36 A state-of-the-art report within NEA-TDB to assess modeling and experimental approaches in aqueous high ionic-strength solutions
Marcus Altmaier, Davide Costa, Andrew Felmy, Helge Moog, Roberto Pabalan, Marilena Ragoussi, Don T. Reed, Wolfgang Runde, Punam Thakur, Wolfgang Voigt*

C-37 The OECD/NEA update book on the chemical thermodynamics of U, Np, Pu, Am and Tc
Ingmar Grenthe, Xavier Gaona, Andrey Plyasunov, Linfeng Rao, Wolfgang Runde, Andrew Felmy, Bernd Grambow, Rudy Konings, Anna L. Smith, Emily Moore, Kastriot Spahiu, Davide Costa, Marilena Ragoussi*

C-38 Solubility, hydrolysis and chloride complexation of Np(V) in alkaline, dilute to concentrated NaCl, MgCl2 and CaCl2 solutions
David Fellhauer, Xavier Gaona, Kathy Dardenne, Marcus Altmaier*

C-40 Examination of actinide (Pu(IV,V,VI), Np(V), and U(VI)) sorption on rutile (TiO_2)
Andreas Schnurr, Brian Powell*

C-41 Evolution of the morphology of $(U_{0.45}Pu_{0.55})O_2$ powder during dissolution in nitric acid
Gilles Leturcq, Alexis Neuschwander, Yannis Ziouane, Bénédicte Arab-Chapelet*

C-42 Overview: National Research Laboratory in Nuclear Forensic from México
Héctor Hernández-Mendoza, Elizabeth Teresita Romero-Guzmán*

C-43 Diffusion Characteristics of Surrogate Nuclear Material Alloys
John Auxier II, Christopher Eley, Joshua Gurka, Duncan Brocklehurst, Howard Hall*

C-44 benchmark spherical critical assemblies with PLUTONIUM metal ^{239}Pu (98 %) in δ - phase core and compound reflectors
Alexey Kaygorodov, Sergey Vorontsov, Mikhail Kuvshinov, Valentin Khoruzhyi*

C-45 Characterization of Ce, U, and Pu Metal Produced by Calcium Reduction
Kaylyn McCoy, William Karl Pitts, Amanda Casella, Calvin Delegard*

C-46 The Multi-Isotope Process Monitor: Deployment at the H-Canyon Nuclear Separation Facility
David Meier, Lindsay Sexton, Jamie Coble*

C-47 Investigation of the Electronic Structure of Transuranic Elements Utilizing a Redox Active Ligand.
Shane S. Galley, Scott A. Pattenaude, Suzanne C. Bart, Thomas E. Albrecht-Schmitt*

C-48 Fast neutron multiplicity counting with zero accidentals
Rashed Sarwar, Malcolm J Joyce, Colin H Zimmerman*

C-49 Synthesis and Vapor Pressure Determination of Volatile Quadrivalent Neptunium Complexes
Aaron Johnson, Jacon Davies, Kevin Carney*

C-50 Simulant corium materials for investigations in the frame of severe accident studies
Alice Seibert, David Bottomley, Dario Manara, Sara Mastromarino, Luca Soldi, Emtethal Kassim, Damien Prieur, Phillippe E. Raison, Thierry Wiss, Didier Pellotiero, Joseph Somers, Vincenzo V. Rondinella*

C-51 New insight in the Am-O phase diagram by coupling experimental HT-XRD and Calphad thermodynamic modelling
Enrica Epifano, Romain Vauchy, Renaud C. Belin, Florent Lebreton, Alexis Joly, Christine Guéneau, Philippe Martin*

C-52 Structure and stability of EDTMP and DOTMP complex with Th(IV) for nuclear medicine
Tomoo Yamamura, Masaru Furuya, Suguru Ohta, Koshin Washiyama*

C-53 Assessment of PuO_2^{2+} solubility in high borate media
*Mark Silver**

C-54 Elastic Modulii of Various Innovative Fuel Materials
Tarik A. Saleh, Joshua White, Ursula Caraval Nunez, Laura A. Tucker, Ryan Leon*

C-55 Aging Effects Interacting with Microstructure
Saryu Fensin, Steve Valone*

C-56 Electrical transport in uranium compounds $URhX_5$ (X = Ga, In)
Yoshinori Haga, Yuji Matsumoto, Naoyuki Tateiwa, Etsuji Yamamoto, Jiri Pospisil, Zachary Fisk*

C-57 Experimentally Validated Casting Simulations of Unalloyed Plutonium
Meghan Gibbs, Deniece Korzekwa*

C-58 Magnetic susceptibility and fluctuations of the electron density in the δ-plutonium
Arkadij Volkov, Aleksandr Povzner*

C-59 Modeling and validation of the Pu 239 surface alpha spectrum using MCNPX coupled with CINDER'90LA-UR-16-23017
Laura A. Tucker, Scott Richmond, Tarik A. Saleh*

C-60 Effects of Aqueous Phase Complexants on Lanthanide and Actinide Oxalate Solubilities
Hannah Colledge, Cheryl Carrigan, Robin Taylor, Mark Sarsfield*

C-61 Characterization of *f*-element oxide stoichiometry and phases through Raman Spectroscopy
Jared Stritzinger, George Goff, Dave Wayne*

C-62 Physical Properties and Nuclear Magnetic Resonance of Antiferromagnetic $PuPt_3$
Eric D. Bauer, Andrew M. Mounce, Adam P. Dioguardi, Paul H. Tobash, Jeremy Mitchell, Thomas E. Albrecht-Schmitt, Joe D. Thompson*

C-64 Complexation Behavior and Solubility of the Ternary Systems Ca/Mg-UO_2-CO_3 under Weakly Alkaline Conditions
Jun-Yeop Lee, Marika Vespa, Ezgi Yalcintas, Xavier Gaona, Kathy Dardenne, Jörg Rothe, Thomas Rabung, Marcus Altmaier, Jong-Il Yun*

C-65 Physical nature of light actinides longevity in the dynamic failure phenomenon
Alexandr Uchaev, Nadezda Selchenkova, Valeriy Punin, Elena Kosheleva*

C-66 Effect of geometry and time-amplitude characteristics of external high-intensity action on metals longevity employed in the nuclear power engineering
Alexandr Uchaev, Valeriy Punin, Nadezda Selchenkova, Elena Kosheleva*

C-67 Measurement of the diffusivity and permeability of hydrogen in plutonium
*Scott Richmond**

D-01 Synthetic Transuranic Chemistry: Bridging the Knowledge Gap to Uranium
*Andrew Gaunt**

D-02 Role of atomic multiplets in intermediate valence PuB_6
Alexander B. Shick, Ladislav Havela, Alexander I. Lichtenstein, Mikhail I. Katsnelson*

D-03 Resonant Inelastic X-ray Scattering of Actinide Materials
*Kristina Kvashnina**

D-04 Synthesis, reactions, and structures of gas-phase actinide oxide nitrate complexes: Relative stabilities and An oxidation states in $AnO_3(NO_3)_2^-$ (An = U, Np, Pu)
Rémi Maurice, Eric Renault, Phuong Diem Dau, Yu Gong, Philip X. Rutkowski, John K. Gibson*

D-05 Redox chemistry of Pu, Np and U under alkaline to hyperalkaline pH conditions
*Xavier Gaona**

D-06 Towards explaining anomalous properties of unalloyed and alloyed Pu appearing after the long-term storage at the liquid He temperature
*Boris Nadykto**

D-07 Probing He bubbles in naturally aged and annealed δ-Pu alloys using small-angle x-ray scattering
Jason R. Jeffries, Tony van Buuren, Trevor Willey, Mark A. Wall, Dave Ruddle, Jan Ilavsky, Patrick Allen*

D-08 Oxidation states of Plutonium: Recent Studies in Inorganic Compounds
*Denis Bykov, Anna L. Smith, Karin Popa, Damien Prieur, Philippe Martin, Rudy Konings, Philippe E. Raison**

D-09 Synthesis, Structure, and Characterization of a Pair of Berkelium Iodates: Developments in assessing bonding character in actinides beyond Plutonium
*Mark Silver**

D-10 First-principles studies of plutonium oxides and their surface interactions with gaseous molecules
*Ping Zhang**

D-11 Radiolysis of H_2-O_2 mixtures at the interface with ceramic oxides
Luke Jones, Howard Sims, Robin Orr, Simon Pimblott*

D-12 Preparation and Characterization of Intrinsic Plutonium Colloids by Sonolysis of PuO_2 in Water
Elodie Dalodière, Matthieu Virot, Vincent Morosini, Tony Chave, Thomas Dumas, Christoph Hennig, Thierry Wiss, Oliver Dieste Blanco, Tolek Tyliszcak, David Shuh, Laurent Venault, Philippe Moisy, Sergey I. Nikitenko*

D-13 Spectroscopic and Mass Spectral Characterization of Uranium Fluoroanions Formed from an Ionic Liquid
Christoper Zarzana, Gary Groenewold, Michael Benson, Kristyn Johnson-Roscioli, Jonathan Martens, Jos Oomens, Rika Hagiwara, Tetsuya Tsuda*

D-14 Electronic Structure of PuTe and Related Materials from Photoemission
John Joyce, Kevin Graham, Tomasz Durakiewicz, Gerard H. Lander, Miles Beaux, Paul H. Tobash, Eric D. Bauer, Jeremy Mitchell, Scott Richmond*

D-15 Exploring actinide recognition, sensitization, and cellular uptake by bio-inspired platforms
*Rebecca Abergel**

D-16 Examination of aging processes occurring during plutonium sorption to solid phases
*Brian Powell**

D-17 characterization of actinides oxides by raman spectroscopy: from model systems to real spent fuel
Christophe Jégou, Sylvain Peuget, Sandrine Miro, Zeynep Talip, Lionel Desgranges, Ritesh Mohun, Guillaume Guimbretière, Aurelien Canizares, Patrick Simon*

D-18 Identification of Processes Controlling Pu Transport Behavior Under Field Conditions
*Annie Kersting**

D-19 Study of combustion synthesis of solid solutions $(U_{1-y}An/Ln_y)O_{2\pm x}$ under air atmosphere
Guillaume Peter-Soldani, Eléonore Welcomme, Xavier Deschanels, Francis Abraham, Stéphane Grandjean*

D-20 Synthesis and dissolution of mixed oxides $(U_{1-x}Pu_x)O_2$ with different morphologies
Yannis Ziouane, Gilles Leturcq, Bénédicte Arab-Chapelet, Sophie Lalleman*

D-21 Differential sorption behavior of U(VI) and Pu(VI) dependent on their redox chemistry
Stefan Hellebrandt, Karah E. Knope, Sang Soo Lee, Aaron J. Lussier, Joanne E. Stubbs, Peter J. Eng, Lynda Soderholm, Paul Fenter, Moritz Schmidt*

D-22 Synthesis and structural characterization of a new water soluble actinide(IV) hexanuclear cluster $[An_6(OH)_4O_4]^{12+}$ (with An(IV) = U(IV), Np(IV), Pu(IV)).
Christelle Tamain, Thomas Dumas, Dominique Guillaumont, Christoph Hennig, Philippe Guilbaud*

Subject index

Compounds, complexes and coordination chemistry

A-34 Temperature dependent hydriding and dehydriding energies of PuHx from *ab initio* calculations

A-60 Hydrolysis of plutonium under reducing conditions controlled by electrolysis

B-01 Does the Electrochemistry of Plutonium Signal the Unravelling of the Seaborg Concept of the Actinide Series?

B-03 Thiocyanate complexes of the tri- and tetravalent actinides.

B-06 Structure of Plutonium(IV) with O-donor ligands from crystallography, extended X-ray absorption fine structure and theoretical calculations

B-07 Semiconductivity in Plutonium and Americium Chromates and Molybdates: The Smoking Gun for Energy-Degeneracy-Driven Covalency

B-25 On the Highest Oxidation State of Plutonium in Compounds

C-04 Redox Stability and Separation Chemistry of Actinyl Cations Coordinated by Schiff Base Ligands

C-05 Actinide Polyrotaxanes: From Hydrothermal Synthesis to Structural Regulation

C-10 How does Pu(IV) interact with hyperphosphorylated protein osteopontin ?

C-11 Self-assembly of plutonium sulfate dimers from a chloride matrix

C-12 Coordination polymers of tetravalent neptunium with aromatic polycarboxylate ligands

C-26 Recent progress in actinide phosphates chemistry

C-27 Chemical bond nature in $Cs_2AnO_2Cl_4$

C-30 A New Strategy for Stabilizing Uncommon Oxidation States Learned from an Extraordinarily Complex Mixed-Valent Uranium Phosphonate Framework

C-33 Incorporation of soluble radionuclides into High Oxidation State Actinide Solid Matrix

C-34 Recent Investigations of Solid State Chemistry of Actinides at Soochow University

C-47 Investigation of the Electronic Structure of Transuranic Elements Utilizing a Redox Active Ligand.

C-52 Structure and stability of EDTMP and DOTMP complex with Th(IV) for nuclear medicine

C-64 Complexation Behavior and Solubility of the Ternary Systems Ca/Mg-UO_2-CO_3 under Weakly Alkaline Conditions

D-01 Synthetic Transuranic Chemistry: Bridging the Knowledge Gap to Uranium

D-04 Synthesis, reactions, and structures of gas-phase actinide oxide nitrate complexes: Relative stabilities and An oxidation states in $AnO_3(NO_3)_2^-$ (An = U, Np, Pu)

D-08 Oxidation states of Plutonium: Recent Studies in Inorganic Compounds

D-09 Synthesis, Structure, and Characterization of a Pair of Berkelium Iodates: Developments in assessing bonding character in actinides beyond Plutonium

D-15 Exploring actinide recognition, sensitization, and cellular uptake by bio-inspired platforms

D-22 Synthesis and structural characterization of a new water soluble actinide(IV) hexanuclear cluster $[An_6(OH)_4O_4]^{12+}$ (with An(IV) = U(IV), Np(IV), Pu(IV)).

Condensed matter physics

A-01 Racah materials: atomic multiplets and f-bands

A-02 Phase stability, elasticity, and phonons for plutonium from electronic-structure theory

A-03 Plutonium as a Mixed Valent Metal

A-06 Insights into point-defects of δ-Pu and δ-Pu-Ga alloys using density functional theory

A-07 Thermoelectric power as a probe of density of states in $PuCoGa_5$

A-08 Hydrogen as a tool to modify electronic structure: are there common features in U and Pu hydrides?

A-09 Quantum molecular dynamics simulations of transport properties in liquid plutonium

A-14 Real Time Studies of ^{239}Pu Elastic Moduli using Resonant Ultrasound Spectroscopy

A-24 First-principles modelling of point defects in fast reactor MOX fuels

A-37 Properties of solids under compression and shock : Role of electronic and structural phase transitions

A-45 Pd-hybridization and paramagnon superconductivity mechanism $PuCoGa_5$

A-48 On the equation of state and elastoplastic and strength properties of beryllium

A-50 Dynamic Magnetic Response across the Pressure-Induced Structural Phase Transition in CeNi

A-54 Evolution of electronic structures of γ-Pu, δ-Pu, and ε-Pu

A-57 Some results of investigations of particle ejection from a free surface of metals under a shock wave effect

A-62 Structural properties of actinides from first principles: important role of Hund's exchange.

B-08 Evaluation of Covalency in PuF_4 by ^{19}F NMR Spectroscopy

B-09 Insight Into Stabilization Mechanisms of the Delta Phase of Plutonium by Deltagen Elements

B-14 Shedding a new light on the superconductivity of $PuCoGa_5$: A heat capacity study on single crystals below 1 K.

B-23 On the Raman Spectrum of Plutonium dioxide: vibrational and crystal electric field modes

B-27 Crystal dynamics of neptunium dioxide

C-18 Thermal expansion study of the heavy-fermion superconductor 242PuCoGa5

C-25 How alpha decays of actinides will affect the nuclear glass structure: evidence of competitive effects between damage generation from recoil nuclei and recovery processes from alpha particles

C-35 Vibrational properties of uranium and plutonium

C-56 Electrical transport in uranium compounds $URhX_5$ (X = Ga, In)

C-58 Magnetic susceptibility and fluctuations of the electron density in the δ-plutonium

C-62 Physical Properties and Nuclear Magnetic Resonance of Antiferromagnetic $PuPt_3$

C-65 Physical nature of light actinides longevity in the dynamic failure phenomenon

C-66 Effect of geometry and time-amplitude characteristics of external high-intensity action on metals longevity employed in the nuclear power engineering

D-02 Role of atomic multiplets in intermediate valence PuB_6

D-03 Resonant Inelastic X-ray Scattering of Actinide Materials

D-06 Towards explaining anomalous properties of unalloyed and alloyed Pu appearing after the long-term storage at the liquid He temperature

D-14 Electronic Structure of PuTe and Related Materials from Photoemission

---

A-04 **Detection and analysis**

Multi-Actinides analysis with AMS: a novel method for ultra-trace determination and small sample sizes

A-05 Non-destructive analysis for Pu accountancy in reprocessing

A-32 Laser Spectroscopy and Detection of Actinides and Lanthanides in Solutions

A-47 Research Shape Memory Effect in the U6.3wt%Nb Alloy by Dilatometry

B-16 From the stars through the ocean abyss: the long travel of super-nova Pu-244 into VERA's particle detector

B-17 Real-time, fast neutron assay of plutonium and related materials

B-20 Redox speciation of actinides using capillary electrophoresis coupled to ICP-MS

B-24 Resonant Laser-SNMS on actinides for spatially resolved ultra-trace analysis

B-26 Structural properties of plutonium systems revealed by high resolution XANES and RIXS techniques

C-42 Overview: National Research Laboratory in Nuclear Forensic from México

C-48 Fast neutron multiplicity counting with zero accidentals

C-59 Modeling and validation of the Pu 239 surface alpha spectrum using MCNPX coupled with CINDER'90LA-UR-16-23017

Environmental behaviour and chemistry

A-10 Properties of PuO2 nanoparticles together with its analogues CeO2 and ThO2

A-40 Chitin-chitozan - a Sorbent Preventing Release of Radioactive Actinide Compounds under Emergency Submersion

A-61 U(VI) adsorption onto alumina, silica, and kaolinite in U(VI)-OH / U(VI)-CO_3 / Ca-U(VI)-CO_3 aqueous systems

A-63 Solubility, Hydrolysis and Carbonate Complexation of Plutonium and Neptunium under Repository-Relevant Conditions

B-18 Nanoparticle Plutonium Formation, Growth, and Morphology with in-situ Liquid Cell Electron Microscopy

B-21 ThermAc - a collaborative project investigating aquatic chemistry and thermodynamics of actinides at elevated temperature conditions

B-22 Traces of Pu isotopes originated from burnt-up fuel in Fukushima exclusion zone

C-36 A state-of-the-art report within NEA-TDB to assess modeling and experimental approaches in aqueous high ionic-strength solutions

C-40 Examination of actinide (Pu(IV,V,VI), Np(V), and U(VI)) sorption on rutile (TiO_2)

C-53 Assessment of PuO_2^{2+} solubility in high borate media

D-16 Examination of aging processes occurring during plutonium sorption to solid phases

D-18 Identification of Processes Controlling Pu Transport Behavior Under Field Conditions

D-21 Differential sorption behavior of U(VI) and Pu(VI) dependent on their redox chemistry

---

Metallurgy and materials science

A-18 Metallurgical Properties of Aged Plutonium Alloys and the Need for Advanced Microstructural Characterization

A-21 Small-scale production and characterization of high-purity plutonium metal

A-22 First-principles DFT+*U* Energetics of Impurity Atoms in PuO_2 and Pu_2O_3

A-25 Thermal Expansion of Delta Plutonium

A-26 EXAFS studies of self-irradiation damage in Pu

A-28 MD study of self-irradiation effects on dislocation dynamics in δ-Pu

A-30 Plutonium Handbook, Second Edition

A-31 On dislocation mechanism of dynamic deformation of uranium

A-35 Characterization of point defects in α-Pu

A-38 2NN MEAM potential for Plutonium

A-39 Atom Probe Tomography of Niobium Redistribution in U-14 at.% Nb After High Temperature Age-Hardening

A-49 The Structure of Thick-walled Spherical Shell of U-1,5% Mo Alloy After Explosive Loading

A-53 CALPHAD approach a complementary way to solve the plutonium mystery.

A-59 Carbonate Oxidation of Electrorefining Salts

B-05 Impurity effects in plutonium alloys

C-01 Pu-238 and the Pu sustainment work at Los Alamos

C-03 Studies Related to the Fabrication of $^{238}PuO_2$ Ceramic Fuel Pellets and the Surrogate CeO_2

C-06 PuF_4 Lattice Effects Due to Aging

C-07 The Kinetic Evolution of Self-Irradiation Damage in Face-Centered Cubic Pu-Ga Alloys

C-21 Thermodynamic Properties of Pu as a Function of Ga Content

C-22 A Temperature Investigation of δ-phase ^{239}Pu-Ga Alloys

C-43 Diffusion Characteristics of Surrogate Nuclear Material Alloys

C-51 New insight in the Am-O phase diagram by coupling experimental HT-XRD and Calphad thermodynamic modelling

C-55 Aging Effects Interacting with Microstructure

C-57 Experimentally Validated Casting Simulations of Unalloyed Plutonium

C-67 Measurement of the diffusivity and permeability of hydrogen in plutonium

D-07 Probing He bubbles in naturally aged and annealed δ-Pu alloys using small-angle x-ray scattering

---

Nuclear fuel cycle

A-12 Oxygen stoichiometry determination in Pu-fuel by vapour pressure measurement

A-13 XAFS and μ-XRF investigations of highly radioactive nuclear waste samples: spent nuclear fuel and zircaloy cladding segments.

A-15 *In situ* high temperature X-ray diffraction studies of the phase equilibria in the UO_2-PuO_2-Pu_2O_3 system

A-23 Radiation damage studies in plutonium oxides for energy production

A-27 Fuel Cycle Concept with dispersion type Fuel in LWRs

A-29 Secure and certify studies to work on production of spiked plutonium

A-36 Theoretical studies on the extraction behaviors of Am(III) and Cm(III) with amide-type ligands

A-44 XPS study of radiation effect on UO2 single-crystal films

A-58 Experimental and calculation parameters of benchmark spherical critical assemblies with metal plutonium in α-phase core and in beryllium and depleted uranium reflectors

B-04 Quality control tools for the analysis of plutonium in nuclear safeguards, security and safety

B-12 Alpha radiolysis of nitric acid solutions with plutonium

B-13 Reductive Dissolution of PuO_2 and CeO_2 in the Presence of Ti Particles and Ultrasound Irradiation

B-15 Plutonium and Americium Solvent Extraction Processes: Recent Development in Europe

B-28 Study of the 5f electronic states in uranium-plutonium mixed oxides using high resolution XANES

C-02 ^{241}Am Production for Use in Radioisotope Power Systems

C-13 Plutonium Oxide Processing Platform for Nuclear Forensics Applications

C-14 Production of Plutonium-238 for Deep Space Missions

C-15 Selective Separation of Electrochemically Generated Am(VI

C-16 Reprocessing and beyond --- the management of spent oxide and Magnox fuel in the UK held by the NDA

C-20 Numerical Simulation on Breeding and Burning Process of Plutonium in Fusion Fission Hybrid Reactor for Energy(FFHR-E)

C-24 Irradiation testing of fuels for plutonium and minor actinide transmutation

C-32 Lipophilic pyridine-2,6-bis(1H-1,2,3-triazol-4-yl) structure as selective chelating unit for direct actinides extraction from purex raffinate

C-41 Evolution of the morphology of $(U_{0.45}Pu_{0.55})O_2$ powder during dissolution in nitric acid

C-44 benchmark spherical critical assemblies with PLUTONIUM metal ^{239}Pu (98 %) in δ - phase core and compound reflectors

C-45 Characterization of Ce, U, and Pu Metal Produced by Calcium Reduction

C-46 The Multi-Isotope Process Monitor: Deployment at the H-Canyon Nuclear Separation Facility

C-50 Simulant corium materials for investigations in the frame of severe accident studies

C-54 Elastic Modulii of Various Innovative Fuel Materials

C-60 Effects of Aqueous Phase Complexants on Lanthanide and Actinide Oxalate Solubilities

D-17 characterization of actinides oxides by raman spectroscopy: from model systems to real spent fuel

D-19 Study of combustion synthesis of solid solutions $(U_{1-y}An/Ln_y)O_{2\pm x}$ under air atmosphere

D-20 Synthesis and dissolution of mixed oxides $(U_{1-x}Pu_x)O_2$ with different morphologies

---

Solution and gas-phase chemistry

B-02 Quantum chemistry and spectroscopic studies of actinide ions with oxygen- and nitrogen- donor ligands in solution

C-17 Gas-Phase Reactions of Water with Actinide Dioxide Cations, PaO_2^+ to CfO_2^+: The "Enigmatic" Behavior of Plutonium

C-19 Electrode reduction of actinyl ions followed by deposition in weak acid solution

C-37 The OECD/NEA update book on the chemical thermodynamics of U, Np, Pu, Am and Tc

C-38 Solubility, hydrolysis and chloride complexation of Np(V) in alkaline, dilute to concentrated NaCl, MgCl2 and CaCl2 solutions

C-49 Synthesis and Vapor Pressure Determination of Volatile Quadrivalent Neptunium Complexes

D-05 Redox chemistry of Pu, Np and U under alkaline to hyperalkaline pH conditions

D-11 Radiolysis of H_2-O_2 mixtures at the interface with ceramic oxides

D-12 Preparation and Characterization of Intrinsic Plutonium Colloids by Sonolysis of PuO_2 in Water

D-13 Spectroscopic and Mass Spectral Characterization of Uranium Fluoroanions Formed from an Ionic Liquid

Surface science and corrosion

A-11 Development of point defect Raman signatures in PuO_2 through self-irradiation

A-16 Plutonium corrosion: some insights and some mysteries

A-17 Recent progress in plutonium hydride research

A-19 Auger Electron Spectroscopy of Plutonium Surfaces

A-20 The influence of hydrogen pressure and reaction temperature on the nucleation and growth kinetics of plutonium hydride

A-33 An in-situ X-ray diffraction study of plutonium oxidation

A-41 Cerium Behavior in Various Media as Compared with Plutonium

A-43 Raman Spectroscopy Characterization of Uranium and Plutonium Hydride from the Hydrogen Corrosion

A-46 Auger line-shape analysis and electron energy loss spectroscopy investigation of Pu surface chemistry

A-51 Development of AFM and STM Capabilities for Plutonium

A-55 Pu Alloy Oxidation by Water Vapor.

A-56 Oxidation of Pu-Ga alloyed surfaces and PuO_2 PAD films using Time-of-Flight SIMS

A-64 Thermodynamic stability of the UO_2 surfaces: Interplay between over-stoichiometry and polarity compensation

A-65 Analysis of surface chemistry on Pu-Ga alloyed surfaces by Time-of-Flight SIMS

A-66 ToF-SIMS Determination of the Partitioning between H and F in Aged Uranium Materials

B-10 Density Functional Theory Study on Hydriding Resistance and Surface Initial Oxidation of Plutonium Nitride

B-11 Understanding the Oxide Layer on Plutonium under Ambient Conditions

B-19 Chemical Speciation of uranium oxide and plutonium oxide materials for forensic science

C-08 Oxidation study of Pu stabilized in δ-phase

C-09 Water Interactions with Actinide Oxide Surfaces

C-23 Experimental studies to support storage of PuO_2 in the UK

C-28 Integrated surface science lab station for spent corrosion studies

C-29 Effect of Doping Level on Dissolution Behavior of Rare-Earth Doped UO_2

C-31 Uranium-hydride initiation iimes before and after outgassing in vacuum at 300 C to determine the influence of hydrogen content in uranium on hydride initiation time.

C-61 Characterization of *f*-element oxide stoichiometry and phases through Raman Spectroscopy

D-10 First-principles studies of plutonium oxides and their surface interactions with gaseous molecules

Author Index

Abergel, Rebecca D-15
Abernathy, Douglas A-50
Abraham, Francis D-19
Acher, Eleonor B-02, B-06
Albrecht-Schmitt, Thomas B-01, B-07, C-30, C-33, C-47, C-62
Aleksandrov, Alexey A-49
Alexey, Baluev A-47
Allen, Patrick A-18, A-26, A-46, D-07
Altmaier, Marcus A-63, B-21, C-36, C-38, C-64
Amadon, Bernard A-62
Amador Celdran, Pedro B-14, C-18
Amayri, Samer B-20
Anatoliy, Golunov A-47
Anderson, Joseph A-65
Antipov, Michael A-57
Ao, Bingyun A-22
Arab-Chapelet, Bénédicte C-41, D-20
Arduini, Arturo C-32
Aregbe, Yetunde B-04
Arico, Alexandra B-07
Arinicheva, Yulia C-26
Arsenlis, Athanasios A-21
Audras, Matthieu B-02
Auxier II, John C-43
Bae, Sang-Eun C-29
Bart, Suzanne C C-47
Bauer, Eric D A-26, C-62, D-14
Bauer, Eve A-51
Beaudoux, Xavier B-13
Beaux, Miles A-51, B-19, D-14
Belin, Renaud C A-15, B-28, C-51
Belova, Yulia A-41
Belyaev, Dmitry A-49
Benes, Ondrej A-12, A-23
Benson, Michael D-13
Berthon, Laurence B-02
Bertolus, Marjorie A-24
Bès, René B-28
Betts, Jonathan A-14
Bieder, Jordan B-09
Blain, Guillaume B-12
Blobaum, Kerri JM A-21
Bonales, Laura B-23
Booth, Corwin A-26
Bosak, Alexei B-27
Bosco, Hauke B-24
Bottin, François A-64, C-35
Bottomley, David C-50
Bouchet, Johann C-35
Bouffard, Serge C-25
Brandt, Felix B-21
Bregiroux, Damien C-26
Brendler, Vinzenz B-21
Brierley, Martin A-17
Brocklehurst, Duncan C-43
Buck, Edgar B-18
Bustillos, Christiain C-04
Buturlim, Volodymyr A-08
Bykov, Denis D-08
Caciuffo, Roberto B-14, B-27, C-18, C-28
Campbell, Catherine C-02

Canizares, Aurelien	D-17
Capan, Cigdem	B-08
Caraval Nunez, Ursula	C-54
Carney, Kevin	C-49
Carrigan, Cheryl	C-02, C-60
Carrott, Michael	C-02
Carter, Tyler	B-03
Casella, Amanda	C-06, C-45
Casnati, Alessandro	C-32
Chai, Zhi-Fang	A-36
Charpentier, Thibault	C-25
Chave, Tony	B-13, D-12
Cha, W	A-60
Cheik Njifon, Ibrahim	A-24
Chen, Lanhua	C-30
Chen, Piheng	A-38
Chiorescu, Ion	B-21
Cho, Herman	B-08
Cho, Hye-Ryun	A-60
Christill, Gerd	A-13
Chung, Brandon	A-18
Cieslar, Milan	A-08
Civjan, Natanya	A-30
Clark, David L	A-30, C-01
Clarke, Amy	A-39
Coble, Jamie	C-46
Cobos, Joaquin	B-23
Colas, Elisenda	B-21
Colineau, Eric	B-14, C-18
Colledge, Hannah	C-60
Colle, Jean-Yves	A-12, A-23, B-23
Cook, Paul	C-23
Copping, Roy	C-04
Costa, Davide	C-36, C-37
Costagliola, Amaury	B-12
Creff, Gaëlle	C-10
Cross, Justin	B-07
Curtius, Hilde	B-21
Dalodière, Elodie	D-12
Dardenne, Kathy	A-13, B-28, C-38, C-64
Dares, Christopher	C-15
Dau, Phuong Diem	C-17, D-04
Davies, Jacon	C-49
Delaunay, François	A-53, A-55, C-08
Delaye, Jean-Marc	C-25
Delegard, Calvin	C-06, C-45
Dempsey, Richard	B-08
Den Auwer, Christophe	C-10
Denis, Chentzov	A-47
Deschanels, Xavier	D-19
Desgranges, Lionel	D-17
Dieste Blanco, Oliver	D-12
Dieste, Oliver	A-23
Dioguardi, Adam P	C-62
Divis, Martin	A-08
Diwu, Juan	C-30, C-33
Dixon, David	C-17
Donald, Scott	A-46, A-66
Dopita, Milan	A-08
Dorado, Boris	B-09, C-35
dos Santos, Antonio	A-50
Dremov, Vladimir	A-28, A-35
Drozdenko, Daria	A-08
Dumas, Thomas	B-02, B-06, D-12, D-22
Durakiewicz, Tomasz	A-07, D-14
Dzenitis, Elizabeth G	A-21

Ehlers, Georg	A-50
Eley, Christopher	C-43
Eloirdi, Rachel	B-14, C-18, C-28
Elsayed, Ashraf	A-29
Endrizzi, Francesco	B-21
Eng, Peter J	D-21
Ennaceur, Sue	B-05
Epifano, Enrica	C-51
Eppich, Gary R	A-21
Erler, Robert	A-18
Evgeniy, Shestakov	A-47
Faestermann, Thomas	B-16
Farnan, Ian	A-44
Fattahi-Vanani, Massoud	B-12
Feige, Jenny	B-16
Feldstein, Chana	B-16
Fellhauer, David	A-63, C-38
Felmy, Andrew	C-36, C-37
Fensin, Saryu	C-55
Fenter, Paul	D-21
Fisk, Zachary	C-56
Forrest, Tom R	B-27
Fox, Danny	C-16
Franzen, Carola	B-21
Franzmann, Michael	B-24
Freibert, Franz	A-06, A-14, A-25, A-26, C-07, C-21
Freyss, Michel	A-24
Furuya, Masaru	C-52
Galley, Shane S	C-47
Gaona, Xavier	A-63, B-21, C-37, C-38, C-64, D-05
Garaix, Guillaume	B-12
Garza, Alejandro	B-07
Gaunt, Andrew	C-04, D-01
Geckeis, Horst	A-04, A-63
Geeson, David	A-30
Geist, Andreas	B-15
Geneste, Grégory	A-64
Georgievskaya, Alla	A-57
Giacobbe, Carlotta	C-18
Gibbs, Meghan	C-57
Gibson, John K	C-17, D-04
Giola, Marco	C-32
Glascott, Joseph	A-16
Goff, George	C-61
Gofryk, Krzysztof	A-07
Gong, Yu	D-04
Gonzalez-Robles, Ernesto	A-13
Gorelov, Alexander	A-40
Goryachev, Edvard	A-40
Gouder, Thomas	A-08, C-28
Graham, Kevin	D-14
Grambow, Bernd	C-37
Grandjean, Stéphane	D-19
Gregson, Colin	C-02, C-23
Grenthe, Ingmar	C-37
Griffiths, Tamara	C-02
Griveau, Jean-Christophe	A-07, B-14, C-18
Grive, Mireia	B-21
Groenewold, Gary	D-13
Guéneau, Christine	A-53, C-51
Guilbaud, Philippe	D-22
Guillaumont, Dominique	B-02, B-06, D-22
Guimbretière, Guillaume	D-17
Gurka, Joshua	C-43

Hackenberg, Robert	A-39
Haga, Yoshinori	C-56
Hagemann, Seven	B-21
Hagiwara, Rika	D-13
Halder, Gregory	A-50
Hall, Howard	C-43
Hamann, Linda	B-24
Hania, P Ralph	C-24
Hanrahan, Jr, Robert	A-30
Harker, Robert M	A-11
Häußler, Verena	B-20
Havela, Ladislav	A-08, D-02
Hawkins, Cory	C-04
Ha, Yeong-Keong	C-29
Hellebrandt, Stefan	D-21
Henderson, Roger A	A-21
Hennig, Christoph	C-12, D-12, D-22
Henry, Natacha	C-12
Herm, Michel	A-13
Hernández-Mendoza, Héctor	C-42
Hernandez, Sarah	A-06, A-19, A-56, A-65, B-19
Hixon, Amy	C-11
Hobbs, Jeff	C-23
Holliday, Kiel S	A-21
Holt, Josh	C-02
Huang, Li	A-54
Huber, Frank	A-08, C-28
Igonin, Vladislav	A-57
Ikeda-Ohno, Atsushi	C-12
Ilavsky, Jan	D-07
Ionov, Gennady	A-28, A-35
Ivanov, Kirill	A-44, C-27
Izosimov, Igor	A-32
Jakopic, Rozle	B-04
Jeffries, Jason R	A-21, D-07
Jégou, Christophe	C-25, D-17
Johnson, Aaron	C-49
Johnson-Roscioli, Kristyn	D-13
Jolly, Lionel	A-53, A-55, C-08
Joly, Alexis	A-15, C-51
Jomard, Gérald	A-64
Jones, Luke	D-11
Jouan, Gauthier	B-13
Joyce, John	D-14
Joyce, Malcolm J	B-17, C-48
Joyce, Stephen	A-51, B-19
Jo, Yongheum	A-61
Jung, E C	A-60
Kalmykov, Stepan	A-10, A-44, C-27
Kaltsoyannis, Nikolas	C-09
Karavaev, Alexey	A-28, A-35
Karpyuk, Leonid	A-27
Kassim, Emtethal	C-50
Katsnelson, Mikhail I	A-01, D-02
Kaygorodov, Alexey	A-58, C-44
Kazakovskaya, Tatiana	A-40, A-41
Kerridge, Andrew	C-09
Kersting, Annie	D-18
Khoruzhyi, Valentin	A-58, C-44
Kienzler, Bernhard	A-13
Kierepko, Renata	B-22
Kim, Jandee	C-29
Kim, Jong-Goo	C-29
Kim, Jong-Yun	C-29
Kitatsuji, Yoshihiro	C-19

Knie, Klaus	B-16
Knope, Karah E	D-21
Knowles, John	A-17
Koke, Carsten	B-21
Kolesnikov, Alexander	A-50
Kolorenc, Jindrich	A-01
Konings, Rudy	A-12, A-23, C-26, C-37, D-08
Korschinek, Gunther	B-16
Korzekwa, Deniece	C-57
Kosheleva, Elena	C-65, C-66
Kotliar, Gabriel	A-03
Kozlov, Eugen	A-49
Kramer, Daniel	C-03
Krüger, Sven	B-21
Kulik, Dmitrii A	B-21
Kutschera, Walter	B-16
Kuvshinov, Mikhail	A-58, C-44
Kvashnina, Kristina	D-03
Lagos, Markus	A-04
Lai, Xinchun	A-38
Lake, Wayne	A-33
Lalleman, Sophie	D-20
Lander, Gerard H	B-27, C-18, D-14
Lan, Jian-Hui	A-36
Lebedeva, Margarita	A-57
Lebreton, Florent	C-51
Lee, Jeongmook	C-29
Lee, Jun-Yeop	A-61, B-21, C-64
Lee, Sang Soo	D-21
Lema, Kenneth	A-18
Leon, Ryan	C-54
Leroux, Maxime	A-14
Leturcq, Gilles	B-13, C-41, D-20
Levi, Ekaterina	A-49
Lichtenstein, Alexander I	A-01, D-02
Li, Gan	A-20
Li, Haibo	A-20
Li, Jun	B-25
Liu, Haifeng	A-09, B-10
Li, Yaguang	A-24
Loiseau, Thierry	C-12
Losko, Adrian S	C-22
Lumetta, Gregg	C-13
Lussier, Aaron J	D-21
Lutzenkirchen, Klaus	A-05
Lv, Junbo	A-43
Macerata, Elena	C-32
Magnani, Nicola	B-23, B-27 C-18
Maher, Chris	C-02
Maiorov, Boris	A-14
Maiwald, Martin	B-21
Maldonado, Pablo	B-27
Manara, Dario	B-23, B-28, C-50
Mariani, Mario	C-32
Martel, Laura	C-25, C-26
Martens, Jonathan	D-13
Martin, Nicolas	C-12
Martin, Philippe	B-28, C-51, D-08
März, Juliane	C-12
Maslakov, Konstantin	A-44, C-27
Mason, Chris	C-02
Mastromarino, Sara	B-23, C-50
Matej, Zdenek	A-08
Matsumoto, Yuji	C-56

Matvienko, Vladimir	A-50
Maurice, Rémi	D-04
May, Iain	C-04
McCall, Scott	A-26
McCoy, Kaylyn	C-06, C-45
McLean, William	A-46
McLuckie, Bliss	C-02
McNamara, Bruce	B-08, C-06
Meier, David	C-13, C-46
Metz, Volker	A-13
Meyer, Thomas J	C-15
Michel, Hervé	C-10
Migliori, Albert	A-14
Mincher, Bruce	C-15
Mir, Anamul Haq	C-25
Mirmelstein, Alexey	A-50
Miro, Sandrine	D-17
Mitchell, Jeremy	A-25, A-51, C-21, C-62, D-14
Mohun, Ritesh	D-17
Moisy, Philippe	B-12, B-13, D-12
Moog, Helge	C-36
Moore, David	A-19, A-56, A-65, B-11
Moore, Emily	C-37
Morosini, Vincent	D-12
Mossini, Eros	C-32
Mounce, Andrew M	C-62
Muhleisen, Artur	A-05
Müller, Nikolaus	A-13
Nadykto, Boris	A-37, A-48, D-06
Naji, Mohamed	B-23
Nelson, Andrew	B-19
Nelson, Art	A-46, A-66
Neumeier, Stefan	C-26
Neuschwander, Alexis	C-41
Nikitenko, Sergey I	B-13, D-12
Nilsson, Mikael	C-04
Ofan, Avishai	B-16
Ohta, Suguru	C-52
Olive, Daniel	A-26
Oomens, Jos	D-13
Oppeneer, Peter M	B-27
Orr, Robin	C-23, D-11
Ossola, Annalisa	C-32
Otobe, Haruyoshi	C-19
Ouchi, Kazuki	C-19
Oudot, Benoît	A-53, A-55, C-08
Pabalan, Roberto	C-36
Panak, Petra J	B-21
Panov, Konstantin	A-57
Paolasini, Luigi	B-27
Pattenaude, Scott A	C-47
Paukov, Mykhaylo	A-08
Paul, Michael	B-16
Pavlusha, Ivan	A-48
Pecheur, Olivia	B-02
Pellotiero, Didier	C-50
Peng, Xianjue	C-20
Perron, Aurelien	A-53
Peter-Soldani, Guillaume	D-19
Peterson, Kirk	C-17
Petrov, Vladimir	C-27
Peuget, Sylvain	C-25, D-17
Pimblott, Simon	D-11
Pitts, William Karl	C-06, C-45
Plakhova, Tatiana	A-10

Plaschke, Markus	A-04
Plyasunov, Andrey	C-37
Podlesnyak, Andrey	A-50
Popa, Karin	C-26, D-08
Popel, Alexey	A-44
Pospisil, Jiri	C-56
Povzner, Aleksandr	A-45, C-58
Powell, Brian	C-40, D-16
Prieur, Damien	B-28, C-50, D-08
Prussmann, Tim	B-28
Pugmire, Alison	A-19, A-26, B-11, B-19
Pugmire, David	A-19, A-56, A-65, B-11, B-19
Punin, Valeriy	C-65, C-66
Pushkov, Victor	A-31
Puxley, Christopher	A-11
Quinto, Francesca	A-04, B-16
Rabung, Thomas	C-64
Ragoussi, Marilena	C-36, C-37
Raison, Philippe E	A-23, C-26, D-08
Raison, Phillippe E	C-50
Ramos, Michael	A-25, A-51, C-22
Rao, Linfeng	C-37
Ravat, Brice	A-53, A-55, C-08
Reed, Don T	C-36
Reich, Tobias	B-20
Reilly, Sean	C-04
Renault, Eric	D-04
Richmond, Scott	A-25, A-51, C-22, C-59, C-67, D-14
Richter, Stephan	B-04
Romanchuk, Anna	A-10
Romero-Guzmán, Elizabeth Teresita	C-42
Rondinella, Vincenzo V	A-23, C-50
Roques, Jérôme	C-10
Ross, Amy	B-19
Rothe, Jörg	A-13, B-28, C-64
Roussel, Paul	A-33, B-05
Ruddle, Dave	D-07
Rugel, Georg	B-16
Runde, Wolfgang	C-36, C-37
Rutkowski, Philip X	D-04
Ryzhkov, Mikhail	C-27
Sadunov, Valeriy	A-57
Sahoo, Sarat	B-22
Saleh, Tarik A	C-54, C-59
Samarin, Sergey	A-35
Santiago Cordoba, Miguel	A-51
Sapozhnikov, Filipp	A-35
Sarsfield, Mark	C-02, C-60
Sarwar, Rashed	C-48
Savchenko, Aleksei	A-27
Schäfer, Thorsten	A-04
Schepperle, Julian	A-63
Scherbakov, Victor	A-40
Schmidt, Moritz	D-21
Schnurr, Andreas	C-40
Scholze, Raphael	B-20
Schwalbach, Peter	A-05
Schwartz, Daniel	A-25, C-21
Scott, Brian	A-51, A-56, B-19, C-04
Scott, Thomas	A-44

Seibert, Alice	C-50
Selchenkova, Nadezda	C-65, C-66
Sexton, Lindsay	C-46
Shamin, Dmitry	A-27
Shick, Alexander B	A-01, D-02
Shi, Lei	A-24
Shirshova, Maria	A-48
Shi, Wei-Qun	A-36, C-05
Shi, Xueming	C-20
Shuh, David	D-12
Sibbens, Goedele	B-04
Siekhaus, Wigbert	A-46, A-66
Siekhaus, Wigbert J	C-31
Sigmon, Ginger	C-11
Silver, Mark	C-53, D-09
Simon, Patrick	D-17
Sims, Howard	C-23, D-11
Singleton, Mike J	A-21
Sinkov, Sergey	B-08, C-06
Skerencak-Frech, Andrej	B-21
Smith, Alice I	C-22
Smith, Anna L	C-37, D-08
Soderholm, Lynda	D-21
Soderlind, Per	A-02
Soldi, Luca	C-50
Somers, Joseph	C-25, C-26, C-50
Song, Haifeng	A-09, B-10
Sorimachi, Atsuyuki	B-22
Spahiu, Kastriot	C-37
Springell, Ross	A-44
Staicu, Dragos	A-23
Stanford, Jeff A	A-21
Stawarz, Clare	A-59
Steele, Helen	C-23
Steier, Peter	A-04, B-16
Stephenson, Keith	C-02
Steudtner, Robin	B-21
Stevens, Patrice	A-30
Strach, Michal	B-28
Stritzinger, Jared	C-61
Stubbs, Joanne E	D-21
Suglobov, Dmitry	C-27
Sun, Bo	A-09, B-10
Svyatov, Igor	A-49
Synetos, Sotiris	A-05
Talip, Zeynep	D-17
Tamain, Christelle	B-06, D-22
Tanha, Mohammad	B-24
Tateiwa, Naoyuki	C-56
Taylor, Robin	C-02, C-23, C-60
Tegner, Bengt	C-09
Teslich, Nick	A-18
Teterin, Anton	A-44, C-27
Teterin, Yury	A-44, C-27
Thakur, Punam	C-36
Thoenen, Tres	B-21
Thompson, Joe D	C-62
Tian, Mingfeng	A-09
Tingey, Joel	C-13
Tinsley, Tim	C-02
Tobash, Paul H	C-62, D-14
Tokonami, Shinji	B-22
Toma, Magdalena	A-05
Torrent, Marc	B-09
Toulemonde, Marcel	C-25
Troshev, Aleksandr	A-47
Tsisar, Dmitry	A-31
Tsuda, Tetsuya	D-13

Tucker, Laura A	C-54, C-59
Turchi, Patrice	A-53
Turek, Ilja	A-08
Tyliszcak, Tolek	D-12
Uchaev, Alexandr	C-65, C-66
Uferov, Oleg	A-27
Usov, Igor	A-51, B-19
Utenkov, Alexander	A-57
Valone, Steve	C-55
Valot, Christophe	A-15, B-28
van Buuren, Tony	D-07
Vandenborre, Johan	B-12
Vasiliu, Monica	C-17
Vauchy, Romain	A-15, C-51
Venault, Laurent	B-12, B-13, D-12
Venhaus, Thomas	A-19, A-51, A-56, A-65, B-11
Vespa, Marika	C-64
Vidaud, Claude	C-10
Vigier, Nicolas	B-12
Virot, Matthieu	B-13, D-12
Vitova, Tonya	B-26, B-28
Vodnik, Douglas	A-51
Vogel, Sven C	C-22
Voigt, Wolfgang	C-36
Volkov, Arkadij	C-58
Volkringer, Christophe	C-12
Vorontsov, Sergey	A-58, C-44
Wagner, Gregory	B-19
Wall, Angelique	B-19
Wallez, Gilles	C-26
Wall, Mark A	A-21, A-26, D-07
Wallner, Anton	B-16
Walther, Clemens	B-24
Wang, Cong-Zhi	A-36
Wang, Deborah	A-26
Wang, Shuaichuang	A-09
Wang, Shuao	C-30, C-33, C-34
Wang, Xiaolin	A-43
Wang, Yaxing	C-33
Washiyama, Koshin	C-52
Watson, Robert	A-59
Wayne, Dave	C-61
Webb, Kevin	C-23
Welcomme, Eléonore	D-19
Wendt, KLaus	B-24
Wham, Robert	C-14
White, Joshua	C-54
Wilkerson, Marianne	B-19
Willberger, Christian	B-20
Willey, Trevor	D-07
Wilson, Richard	B-03, C-17
Wiss, Thierry	A-23, C-25, C-50, D-12
Wolfsberg, Laura	B-19
Woodhead, David	C-23
Wu, Qun-Yan	A-36
Wu, Yaqiao	A-39
Xiao, Chengliang	C-30
Yablinsky, Clarissa	A-39
Yalcintas, Ezgi	C-64
Yamamoto, Etsuji	C-56
Yamamura, Tomoo	C-52
Yang, Yu	A-34
Yin, Xuemiao	C-33
Youn, Young-Sang	A-60, C-29
Yu, Huilong	A-20

Yun, Jong-Il	A-61, C-64
Yurtov, Igor	A-57
Zarzana, Christoper	D-13
Zhang, Gongmu	A-09
Zhang, Guangfeng	A-43
Zhang, Ping	A-34, D-10
Zheng, Hui	B-10
Zimmerman, Colin	C-48
H Ziouane, Yannis	C-41, D-20
Zocco, Adam	A-51
Zouev, Yury	A-49
Zsigrai, Jozsef	A-05

Presenting Authors

Abergel, Rebecca
Lawrence Berkeley National Laboratory, USA
Exploring actinide recognition, sensitization, and cellular uptake by bio-inspired platforms
Thursday 22/9: INV Thu4 - 12:00-12:30

Acher, Eleonor
CEA MARCOULE, France
Structure of Plutonium(IV) with O-donor ligands from crystallography, extended X-ray absorption fine structure and theoretical calculations
Tuesday 20/9: OR Tu1 - 11:00-11:15

Albrecht-Schmitt, Thomas E.
Florida State University, USA
Does the Electrochemistry of Plutonium Signal the Unravelling of the Seaborg Concept of the Actinide Series?
Tuesday 20/9: PL Tu1 - 08:40-09:25

Altmaier, Marcus
Karlsruhe Institute of Technology, Institute for Nuclear Waste Disposal (KIT-INE), Germany
A state-of-the-art report within NEA-TDB to assess modeling and experimental approaches in aqueous high ionic-strength solutions
Wednesday 21/9: Poster session II 12:30-14:15 (continues on Thur. 22/9)

ThermAc - a collaborative project investigating aquatic chemistry and thermodynamics of actinides at elevated temperature conditions
Tuesday 20/9: OR Tu4 - 15:35-15:50

Amadon, Bernard
CEA, France
Structural properties of actinides from first principles: important role of Hund's exchange.
Monday 19/9: Poster session I - 12:30-14:15 (continues on Tuesday 20/9)

Ao, Bingyun
China Academy of Engineering Physics, P.O. Pox 919-71, China
First-principles DFT+*U* Energetics of Impurity Atoms in PuO_2 and Pu_2O_3
Monday 19/9: OR Mo4 - 15:50-16:05

Aregbe, Yetunde
EC-JRC-IRMM, Belgium
Quality control tools for the analysis of plutonium in nuclear safeguards, security and safety
Tuesday 20/9: INV Tu2 - 09:30-10:00

Arico, Alexandra
Florida State University, USA
Semiconductivity in Plutonium and Americium Chromates and Molybdates: The Smoking Gun for Energy-Degeneracy-Driven Covalency
Tuesday 20/9: OR Tu1 - 11:15-11:30

Auxier II, John
Radiochemistry Center of Excellence, USA
Diffusion Characteristics of Surrogate Nuclear Material Alloys
Wednesday 21/9: Poster session II 12:30-14:15 (continues on Thur. 22/9)

Bauer, Eric D.
Los Alamos National Laboratory, USA
Physical Properties and Nuclear Magnetic Resonance of Antiferromagnetic $PuPt_3$
Wednesday 21/9: Poster session II 12:30-14:15 (continues on Thur. 22/9)

Beaux, Miles
Los Alamos National Laboratory, USA
Development of AFM and STM Capabilities for Plutonium
Monday 19/9: Poster session I 12:30-14:15 (continues on Tuesday 20/9)
12:30-14:15

Belyaev, Dmitry
Russian Federal Nuclear Center – Zababakhin All-Russia Research Institute of Technical Physics, (RFNC-VNIITF), Russia
The Structure of Thick-walled Spherical Shell of U-1,5% Mo Alloy After Explosive Loading
Monday 19/9: Poster session I - 12:30-14:15 (continues on Tuesday 20/9)

Benes, Ondrej
European Commission - Joint Research Centre, Germany
Oxygen stoichiometry determination in Pu-fuel by vapour pressure measurement
Monday 19/9: OR Mo2 - 11:30-11:45

Blobaum, Kerri J.M.
Lawrence Livermore National Laboratory, USA
Small-scale production and characterization of high-purity plutonium metal
Monday 19/9: OR Mo4 - 15:35-15:50

Bottin, François
CEA, France
Thermodynamic stability of the UO_2 surfaces: Interplay between over-stoichiometry and polarity compensation
Monday 19/9: Poster session I - 12:30-14:15 (continues on Tuesday 20/9)

Bouchet, Johann
Commissariat a l'Energie Atomique, France
Vibrational properties of uranium and plutonium
Wednesday 21/9: Poster session II 12:30-14:15 (continues on Thur. 22/9)

Brierley, Martin
AWE, UK
Recent progress in plutonium hydride research
Monday 19/9: INV Mo5 - 15:05-15:35

Buck, Edgar
Pacific Northwest National Laboratory, USA
Nanoparticle Plutonium Formation, Growth, and Morphology with in-situ Liquid Cell Electron Microscopy
Tuesday 20/9: INV Tu6 - 15:05-15:35

Casella, Amanda
Pacific Northwest National Laboratory, USA
PuF_4 Lattice Effects Due to Aging
Wednesday 21/9: OR Wed1 - 11:00-11:15

Chen, Piheng
China Academy of Engineering Physics, China
2NN MEAM potential for Plutonium
Monday 19/9: Poster session I - 12:30-14:15 (continues on Tuesday 20/9)

Cho, Herman
Pacific Northwest National Laboratory, USA
Evaluation of Covalency in PuF_4 by ^{19}F NMR Spectroscopy
Tuesday 20/9: OR Tu1 - 11:30-11:45

Cho, Hye-Ryun
Korea Atomic Energy Research Institute, Republic of Korea
Hydrolysis of plutonium under reducing conditions controlled by electrolysis
Monday 19/9: Poster session I - 12:30-14:15 (continues on Tuesday 20/9)

Chung, Brandon
Lawrence Livermore National Laboratory, USA
Metallurgical Properties of Aged Plutonium Alloys and the Need for Advanced Microstructural Characterization
Monday 19/9: INV Mo6 - 15:05-15:35

Clark, David L.
Los Alamos National Laboratory, USA
Pu-238 and the Pu sustainment work at Los Alamos
Wednesday 21/9: PL Wed1 - 08:40-09:25

Colledge, Hannah
National Nuclear Laboratory, UK
Effects of Aqueous Phase Complexants on Lanthanide and Actinide Oxalate Solubilities
Wednesday 21/9: Poster session II 12:30-14:15 (continues on Thur. 22/9)

Creff, Gaëlle
ICN-Université de Nice Sophia Antipolis, France
How does Pu(IV) interact with hyperphosphorylated protein osteopontin ?
Wednesday 21/9: OR Wed2 - 11:00-11:15

Dalodière, Elodie
Institut de chimie separative de Marcoule, France
Preparation and Characterization of Intrinsic Plutonium Colloids by Sonolysis of PuO_2 in Water
Thursday 22/9: OR Thu2 - 11:30-11:45

Dardenne, Kathy
Institute for Nuclear Waste Disposal (KIT-INE), Karlsruhe Institute of Technology (KIT), Germany
XAFS and µ-XRF investigations of highly radioactive nuclear waste samples: spent nuclear fuel and zircaloy cladding segments.
Monday 19/9: OR Mo2 - 11:45-12:00

Dares, Christopher
The University of North Carolina at Chapel Hill, USA
Selective Separation of Electrochemically Generated Am(VI
Wednesday 21/9: INV Wed4 -12:00-12:30

Delaunay, François
CEA - VALDUC, France
Pu Alloy Oxidation by Water Vapor.
Monday 19/9: Poster session I - 12:30-14:15 (continues on Tuesday 20/9)

Donald, Scott
Lawrence Livermore National Laboratory, USA
ToF-SIMS Determination of the Partitioning between H and F in Aged Uranium Materials
Monday 19/9: Poster session I - 12:30-14:15 (continues on Tuesday 20/9)

Dorado, Boris
CEA, France
Insight Into Stabilization Mechanisms of the Delta Phase of Plutonium by Deltagen Elements
Tuesday 20/9: OR Tu1 - 11:45-12:00

Dremov, Vladimir
Russian Federal Nuclear Centre - Institute of Technical Physics, Russia
Characterization of point defects in α-Pu
Monday 19/9: Poster session I - 12:30-14:15 (continues on Tuesday 20/9)

Eloirdi, Rachel
European Commission, Joint Research Centre (JRC), Institute for Transuranium Elements (ITU), Germany
Thermal expansion study of the heavy-fermion superconductor 242PuCoGa5
Wednesday 21/9: INV Wed6 -15:05-15:35

Elsayed, Ashraf
Brno University, Czech Republic
Secure and certify studies to work on production of spiked plutonium
Monday 19/9: Poster session I 12:30-14:15 (continues on Tuesday 20/9)

Ennaceur, Sue
AWE, UK
Impurity effects in plutonium alloys
Tuesday 20/9: INV Tu2 - 10:00-10:30

Epifano, Enrica
DEN/DTEC/SECA/LCC CEA, France
New insight in the Am-O phase diagram by coupling experimental HT-XRD and Calphad thermodynamic modelling
Wednesday 21/9: Poster session II 12:30-14:15 (continues on Thur. 22/9)

Fellhauer, David
Karlsruhe Institute of Technology, Institute for Nuclear Waste Disposal, Germany
Solubility, hydrolysis and chloride complexation of Np(V) in alkaline, dilute to concentrated NaCl, MgCl2 and CaCl2 solutions
Wednesday 21/9: Poster session II - 12:30-14:15 (continues on Thur. 22/9)

Fensin, Saryu
Los Alamos National Lab, USA
Aging Effects Interacting with Microstructure
Wednesday 21/9: Poster session II - 12:30-14:15 (continues on Thur. 22/9)

Fox, Danny
Nuclear Decommissioning Authority, UK
Reprocessing and beyond --- the management of spent oxide and Magnox fuel in the UK held by the NDA
Wednesday 21/9: PL Wed2 - 14:15-15:00

Freibert, Franz
Los Alamos National Laboratory, USA
The Kinetic Evolution of Self-Irradiation Damage in Face-Centered Cubic Pu-Ga Alloys
Wednesday 21/9: OR Wed1 - 11:15-11:30

Freyss, Michel
CEA, DEN, Cadarache, France
First-principles modelling of point defects in fast reactor MOX fuels
Monday 19/9: INV Mo7 - 17:00-17:30

Galley, Shane S.
Florida State University, USA
Investigation of the Electronic Structure of Transuranic Elements Utilizing a Redox Active Ligand.
Wednesday 21/9: Poster session II - 12:30-14:15 (continues on Thur. 22/9)

Gaona, Xavier
Karlsruhe Institute of Technology, Institute for Nuclear Waste Disposal, Germany
1) Redox chemistry of Pu, Np and U under alkaline to hyperalkaline pH conditions
Thursday 22/9: INV Thu2 - 10:00-10:30
2) The OECD/NEA update book on the chemical thermodynamics of U, Np, Pu, Am and Tc
Wednesday 21/9: Poster session II - 12:30-14:15 (continues on Thur. 22/9)

Gaunt, Andrew
Los Alamos National Laboratory, USA
Synthetic Transuranic Chemistry: Bridging the Knowledge Gap to Uranium
Thursday 22/9: PL Thu1 - 08:40-09:25

Geist, Andreas
Karlsruhe Institute of Technology (KIT), Germany
Plutonium and Americium Solvent Extraction Processes: Recent Development in Europe
Tuesday 20/9: INV Tu4 - 12:00-12:30

Georgievskaya, Alla
RFNC-VNIIEF, Russia
Some results of investigations of particle ejection from a free surface of metals under a shock wave effect
Monday 19/9: Poster session I - 12:30-14:15 (continues on Tuesday 20/9)

Gibbs, Meghan
Los Alamos National Laboratory, USA
Experimentally Validated Casting Simulations of Unalloyed Plutonium
Wednesday 21/9: Poster session II - 12:30-14:15 (continues on Thur. 22/9)

Gibson, John K.
Lawrence Berkeley National Laboratory, USA
Gas-Phase Reactions of Water with Actinide Dioxide Cations, PaO_2^+ to CfO_2^+: The "Enigmatic" Behavior of Plutonium
Wednesday 21/9: INV Wed5 -15:05-15:35

Glascott, Joseph
Bristol University, UK
Plutonium corrosion: some insights and some mysteries
Monday 19/9: PL Mo2 - 14:15-15:00

Gofryk, Krzysztof
Idaho National Laboratory, USA
Thermoelectric power as a probe of density of states in $PuCoGa_5$
Monday 19/9: OR Mo1 - 11:15-11:30

Gouder, Thomas
European Commission, Joint Research Centre, Institute for Transuranium Elements, Germany
Integrated surface science lab station for spent corrosion studies
Wednesday 21/9: OR Wed6 - 17:30-17:45

Griveau, Jean-Christophe
ITU, Germany
Shedding a new light on the superconductivity of $PuCoGa_5$: A heat capacity study on single crystals below 1 K.
Tuesday 20/9: INV Tu3 - 12:00-12:30

Guillaumont, Dominique
CEA, France
Quantum chemistry and spectroscopic studies of actinide ions with oxygen- and nitrogen- donor ligands in solution
Tuesday 20/9: INV Tu1 - 09:30-10:00

Haga, Yoshinori
Japan Atomic Energy Agency, Japan
Electrical transport in uranium compounds $URhX_5$ (X = Ga, In)
Wednesday 21/9: Poster session II - 12:30-14:15 (continues on Thur. 22/9)

Hania, P. Ralph
NRG, The Netherlands
Irradiation testing of fuels for plutonium and minor actinide transmutation
Wednesday 21/9: INV Wed7 -17:00-17:30

Harker, Robert M
AWE Aldermaston, UK
Development of point defect Raman signatures in PuO_2 through self-irradiation
Monday 19/9: OR Mo2 - 11:15-11:30

Havela, Ladislav
Charles University, Czech Republic
Hydrogen as a tool to modify electronic structure: are there common features in U and Pu hydrides?
Monday 19/9: OR Mo1 - 11:30-11:45

Hellebrandt, Stefan
Helmholtz-Zentrum Dresden-Rossendorf, Germany
Differential sorption behavior of U(VI) and Pu(VI) dependent on their redox chemistry
Thursday 22/9: OR Thu4 - 15:35-15:50

Hernández-Mendoza, Héctor
Instituto Nacional de Investigaciones Nucleares, Mexico
Overview: National Research Laboratory in Nuclear Forensic from México
Wednesday 21/9: Poster session II - 12:30-14:15 (continues on Thur. 22/9)

Hernandez, Sarah
Los Alamos National Laboratory, USA
1) Insights into point-defects of δ-Pu and δ-Pu-Ga alloys using DFT
Monday 19/9: OR Mo1 - 11:00-11:15
2) Oxidation of Pu-Ga alloyed surfaces and PuO_2 PAD films using TOF SIMS
Monday 19/9: Poster session I 12:30-14:15 (continues on Tuesday 20/9)

Hixon, Amy
University of Notre Dame, USA
Self-assembly of plutonium sulfate dimers from a chloride matrix
Wednesday 21/9: OR Wed2 - 11:15-11:30

Huang, Li
Institute of Materials, China Academy of Engineering Physics, China
Evolution of electronic structures of γ-Pu, δ-Pu, and ε-Pu
Monday 19/9: Poster session I 12:30-14:15 (continues on Tuesday 20/9)

Ivanov, Kirill
NRC "Kurchatov Institute", Russia
Chemical bond nature in $Cs_2AnO_2Cl_4$
Wednesday 21/9: OR Wed5 - 17:30-17:45

Izosimov, Igor
Joint Institute for Nuclear Research, Russia
Laser Spectroscopy and Detection of Actinides and Lanthanides in Solutions
Monday 19/9: Poster session I - 12:30-14:15 (continues on Tuesday 20/9)

Jeffries, Jason R.
LLNL, USA
Probing He bubbles in naturally aged and annealed δ-Pu alloys using small-angle x-ray scattering
Thursday 22/9: OR Thu1 - 11:15-11:30

Jégou, Christophe
CEA DEN DTCD, France
Characterization of actinides oxides by Raman spectroscopy: from model systems to real spent fuel
Thursday 22/9: INV Thu5 - 15:05-15:35

Johnson, Aaron
Idaho National Laboratory, USA
Synthesis and Vapor Pressure Determination of Volatile Quadrivalent Neptunium Complexes
Wednesday 21/9: Poster session II - 12:30-14:15 (continues on Thur. 22/9)

Jones, Luke
University of Manchester, UK
Radiolysis of H_2-O_2 mixtures at the interface with ceramic oxides
Thursday 22/9: OR Thu2 - 11:15-11:30

Joyce, John
Los Alamos National Laboratory, USA
Electronic Structure of PuTe and Related Materials from Photoemission
Thursday 22/9: INV Thu3 - 12:00-12:30

Joyce, Malcolm J.
Lancaster University, UK
Real-time, fast neutron assay of plutonium and related materials
Tuesday 20/9: INV Tu5 - 15:05-15:35

Jo, Yongheum
Department of Nuclear and Quantum Engineering, KAIST, Republic of Korea
U(VI) adsorption onto alumina, silica, and kaolinite in U(VI)-OH / U(VI)-CO_3 / Ca-U(VI)-CO_3 aqueous systems
Monday 19/9: Poster session I - 12:30-14:15 (continues on Tuesday 20/9)

Karavaev, Alexey
Russian Federal Nuclear Center - Zababakhin Institute of Technical Physics (RFNC-VNIITF), Russia
MD study of self-irradiation effects on dislocation dynamics in δ-Pu
Monday 19/9: OR Mo6 - 17:30-17:45

Kaygorodov, Alexey
RFNC-VNIIEF, Russia

1) Benchmark spherical critical assemblies with plutonium metal ^{239}Pu (98 %) in δ - phase core and compound reflectors
Wednesday 21/9: Poster session II - 12:30-14:15 (continues on Thur. 22/9)

2) Experimental and calculation parameters of benchmark spherical critical assemblies with metal plutonium in α-phase core and in beryllium and depleted uranium reflectors
Monday 19/9: Poster session I - 12:30-14:15 (continues on Tuesday 20/9)

Kazakovskaya, Tatiana
RFNC-VNIIEF, Russia
1) Cerium Behavior in Various Media as Compared with Plutonium
2) Chitin-chitozan - a Sorbent Preventing Release of Radioactive Actinide Compounds under Emergency Submersion

Monday 19/9: Poster session I - 12:30-14:15 (continues on Tuesday 20/9)

Kersting, Annie
LLNL, USA
Identification of Processes Controlling Pu Transport Behavior Under Field Conditions
Thursday 22/9: INV Thu6 - 15:05-15:35

Kierepko, Renata
Fukushima Research Headquarter, National Institute for Quantum and Radiological Science and Technology, Japan
Traces of Pu isotopes originated from burnt-up fuel in Fukushima exclusion zone
Tuesday 20/9: OR Tu4 - 15:50-16:05

Kitatsuji, Yoshihiro
Japan Atomic Energy Agency, Japan
Electrode reduction of actinyl ions followed by deposition in weak acid solution
Wednesday 21/9: OR Wed3 - 15:35-15:50

Kotliar, Gabriel
Department of Physics and Astronomy, Rutgers University, USA
Plutonium as a Mixed Valent Metal
Monday 19/9: INV Mo1 - 10:00-10:30

Kramer, Daniel
University of Dayton, USA
Studies Related to the Fabrication of $^{238}PuO_2$ Ceramic Fuel Pellets and the Surrogate CeO_2
Wednesday 21/9: INV Wed1 -10:00-10:30

Kvashnina, Kristina
ESRF,Grenoble, France
Resonant Inelastic X-ray Scattering of Actinide Materials
Thursday 22/9: INV Thu1 - 10:00-10:30

Lake, Wayne
AWE, UK
An in-situ X-ray diffraction study of plutonium oxidation
Monday 19/9: Poster session I 12:30-14:15 (continues on Tuesday 20/9)

Lee, Jeongmook
Korea Atomic Energy Research Institute, Republic of Korea
Effect of Doping Level on Dissolution Behavior of Rare-Earth Doped UO_2
Wednesday 21/9: Poster session II - 12:30-14:15 (continues on Thur. 22/9)

Lee, Jun-Yeop
KIT-INE, Germany
Complexation Behavior and Solubility of the Ternary Systems Ca/Mg-UO_2-CO_3 under Weakly Alkaline Conditions
Wednesday 21/9: Poster session II - 12:30-14:15 (continues on Thur. 22/9)

Leturcq, Gilles
CEA, France
Evolution of the morphology of $(U_{0.45}Pu_{0.55})O_2$ powder during dissolution in nitric acid
Wednesday 21/9: Poster session II - 12:30-14:15 (continues on Thur. 22/9)

Lichtenstein, Alexander I.
Institute for Theoretical Physics, University of Hamburg, Germany
Racah materials: atomic multiplets and f-bands
Monday 19/9: PL Mo1 - 08:40-09:25

Li, Gan
China academy of engineering physics,
The influence of hydrogen pressure and reaction temperature on the nucleation and growth kinetics of plutonium hydride
Monday 19/9: OR Mo3 - 15:50-16:05

Li, Jun
Theoretical Chemistry Center, Department of Chemistry, Tsinghua University, China
On the Highest Oxidation State of Plutonium in Compounds
Tuesday 20/9: INV Tu8 - 16:30-17:30

Liu, Haifeng
Institute of Applied Physics and Computational Mathematics, China
Quantum molecular dynamics simulations of transport properties in liquid plutonium
Monday 19/9: OR Mo1 - 11:45-12:00

Maiorov, Boris
Los Alamos National Laboratory, USA
Real Time Studies of ^{239}Pu Elastic Moduli using Resonant Ultrasound Spectroscopy
Monday 19/9: INV Mo3 - 12:00-12:30

Martin, Nicolas
Université de Lille, France
Coordination polymers of tetravalent neptunium with aromatic polycarboxylate ligands
Wednesday 21/9: OR Wed2 - 11:30-11:45

Martin, Philippe
CEA, DEN, DTEC, Centre d'études nucléaires de Marcoule, France
Study of the 5f electronic states in uranium-plutonium mixed oxides using high resolution XANES
Tuesday 20/9: OR Tu6 - 17:30-17:45

Maurice, Rémi
SUBATECH, UMR CNRS 6457, IN2P3/EMN Nantes/Université de Nantes, France
Synthesis, reactions, and structures of gas-phase actinide oxide nitrate complexes: Relative stabilities and An oxidation states in $AnO_3(NO_3)_2^-$ (An = U, Np, Pu)
Thursday 22/9: INV Thu2 - 09:30-10:00

May, Iain
Science, Technology and Engineering, Los Alamos National Laboratory, USA
Redox Stability and Separation Chemistry of Actinyl Cations Coordinated by Schiff Base Ligands
Wednesday 21/9: INV Wed2 -09:30-10:00

McCoy, Kaylyn
Pacific Northwest National Laboratory, USA
Characterization of Ce, U, and Pu Metal Produced by Calcium Reduction
Wednesday 21/9: Poster session II - 12:30-14:15 (continues on Thur. 22/9)

Meier, David
Pacific Northwest National Laboratory, USA
1) Plutonium Oxide Processing Platform for Nuclear Forensics Applications
Wednesday 21/9: OR Wed2 - 11:45-12:00
2) The Multi-Isotope Process Monitor: Deployment at the H-Canyon Nuclear Separation Facility
Wednesday 21/9: Poster session II - 12:30-14:15 (continues on Thur. 22/9)

Mirmelstein, Alexey
RFNC-VNIITF, Russia
Dynamic Magnetic Response across the Pressure-Induced Structural Phase Transition in CeNi
Monday 19/9: Poster session I - 12:30-14:15 (continues on Tuesday 20/9)

Mitchell, Jeremy
Los Alamos National Laboratory, USA
Thermal Expansion of Delta Plutonium
Monday 19/9: INV Mo8 -16:30-17:00

Moore, David
Los Alamos National Laboratory, USA
Auger Electron Spectroscopy of Plutonium Surfaces
Monday 19/9: OR Mo3 - 15:35-15:50

Nadykto, Boris
Russian Federal Nuclear Center VNIIEF, Russia
1) Properties of solids under compression and shock : Role of electronic and structural phase transitions
Monday 19/9: Poster session I - 12:30-14:15 (continues on Tuesday 20/9)
2) Towards explaining anomalous properties of unalloyed and alloyed Pu appearing after the long-term storage at the liquid He temperature
Thursday 22/9: OR Thu1 - 11:00-11:15

Naji, Mohamed
European Commission, Joint Research Centre, Institute for Transuranium Elements (ITU), Germany
On the Raman Spectrum of Plutonium dioxide: vibrational and crystal electric field modes
Tuesday 20/9: INV Tu7 - 16:30-17:00

Nelson, Art
LLNL, USA
Auger line-shape analysis and electron energy loss spectroscopy investigation of Pu surface chemistry
Monday 19/9: Poster session I - 12:30-14:15 (continues on Tuesday 20/9)

Olive, Daniel
Los Alamos National Laboratory, USA
EXAFS studies of self-irradiation damage in Pu
Monday 19/9: INV Mo8 - 17:00-17:30

Orr, Robin
National Nuclear Laboratory, UK
Experimental studies to support storage of PuO_2 in the UK
Wednesday 21/9: INV Wed7 16:30-17:00

Ossola, Annalisa
Politecnico di Milano, Italy
Lipophilic pyridine-2,6-bis(1H-1,2,3-triazol-4-yl) structure as selective chelating unit for direct actinides extraction from purex raffinate
Wednesday 21/9: Poster session II - 12:30-14:15 (continues on Thur. 22/9)

Oudot, Benoît
CEA-VALDUC, France
CALPHAD approach a complementary way to solve the plutonium mystery.
Monday 19/9: Poster session I - 12:30-14:15 (continues on Tuesday 20/9)

Paolasini, Luigi
ESRF, Grenoble, France
Crystal dynamics of neptunium dioxide
Tuesday 20/9: OR Tu5 - 17:30-17:45

Peuget, Sylvain
CEA, DEN, DTCD, SECM, Laboratoire d'Étude des Matériaux et Procédés Actif, France
How alpha decays of actinides will affect the nuclear glass structure: evidence of competitive effects between damage generation from recoil nuclei and recovery processes from alpha particles
Wednesday 21/9: INV Wed8 -16:30-17:00

Popa, Karin
European Commission, JRC, Germany
Recent progress in actinide phosphates chemistry
Wednesday 21/9: INV Wed8 -17:00-17:30

Povzner, Aleksandr
Ural Federal University, Russia
Pd-hybridization and paramagnon superconductivity mechanism $PuCoGa_5$
Monday 19/9: Poster session I - 12:30-14:15 (continues on Tuesday 20/9)

Powell, Brian
Clemson University, USA
Examination of aging processes occurring during plutonium sorption to solid phases
Thursday 22/9: PL Thu2 - 14:15-15:00

Pugmire, Alison
Los Alamos National Laboratory, USA
Understanding the Oxide Layer on Plutonium under Ambient Conditions
Tuesday 20/9: OR Tu2 - 11:15-11:30

Pushkov, Victor
Russian Federal Nuclear Center-VNIIEF, Russia
On dislocation mechanism of dynamic deformation of uranium
Monday 19/9: Poster session I - 12:30-14:15 (continues on Tuesday 20/9)

Quinto, Francesca
Karlsruhe Institute of Technology (KIT), Institute for Nuclear Waste Disposal (INE), Germany
Multi-Actinides analysis with AMS: a novel method for ultra-trace determination and small sample sizes
Monday 19/9: INV Mo2 - 09:30-10:00

Raison, Philippe E.
European Commission- JRC-ITU, Germany
Oxidation states of Plutonium: Recent Studies in Inorganic Compounds
Thursday 22/9: OR Thu1 - 11:30-11:45

Ravat, Brice
CEA - VALDUC, France
Oxidation study of Pu stabilized in δ-phase
Wednesday 21/9: OR Wed1 - 11:30-11:45

Richmond, Scott
Los Alamos National Laboratory, USA
Measurement of the diffusivity and permeability of hydrogen in plutonium
Wednesday 21/9: Poster session II - 12:30-14:15 (continues on Thur. 22/9)

Romanchuk, Anna
Lomonosov Moscow State University, Russia
Properties of PuO2 nanoparticles together with its analogues CeO2 and ThO2
Monday 19/9: OR Mo2 - 11:00-11:15

Saleh, Tarik A.
Los Alamos National Laboratory, USA
Elastic Modulii of Various Innovative Fuel Materials
Wednesday 21/9: Poster session II - 12:30-14:15 (continues on Thur. 22/9)

Sarsfield, Mark
National Nuclear Laboratory, UK
^{241}Am Production for Use in Radioisotope Power Systems
Wednesday 21/9: INV Wed1 -09:30-10:00

Sarwar, Rashed
Engineering Department, Lancaster University, UK
Fast neutron multiplicity counting with zero accidentals
Wednesday 21/9: Poster session II - 12:30-14:15 (continues on Thur. 22/9)

Savchenko, Aleksei
A.A. Bochvar Institute (VNIINM), Russia
Fuel Cycle Concept with dispersion type Fuel in LWRs
Monday 19/9: OR Mo5 - 17:30-17:45

Schepperle, Julian
Institute for Nuclear Waste Disposal, Karlsruhe Institute of Technology, Germany
Solubility, Hydrolysis and Carbonate Complexation of Plutonium and Neptunium under Repository-Relevant Conditions
Monday 19/9: Poster session I - 12:30-14:15 (continues on Tuesday 20/9)

Schnurr, Andreas
Environmental Engineering and Earth Sciences, Clemson University, USA
Examination of actinide (Pu(IV,V,VI), Np(V), and U(VI)) sorption on rutile (TiO_2)
Wednesday 21/9: Poster session II - 12:30-14:15 (continues on Thur. 22/9)

Schwartz, Daniel
Los Alamos National Laboratory, USA
Thermodynamic Properties of Pu as a Function of Ga Content
Wednesday 21/9: OR Wed4 - 15:35-15:50

Seibert, Alice
Europäische Kommission, Joint Research Centre, Institut für Transurane, Germany
Simulant corium materials for investigations in the frame of severe accident studies
Wednesday 21/9: Poster session II - 12:30-14:15 (continues on Thur. 22/9)

Selchenkova, Nadezda
Russian Federal Nuclear Center – VNIIEF, Russia
Physical nature of light actinides longevity in the dynamic failure phenomenon
Wednesday 21/9: Poster session II - 12:30-14:15 (continues on Thur. 22/9)

Shick, Alexander B.
Institute of Physics ASCR, Czech Republic
Role of atomic multiplets in intermediate valence PuB_6
Thursday 22/9: INV Thu1 - 09:30-10:00

Shirshova, Maria
RFNC-VNIIEF, Russia
On the equation of state and elastoplastic and strength properties of beryllium
Monday 19/9: Poster session I - 12:30-14:15 (continues on Tuesday 20/9)

Shi, Wei-Qun
Laboratory of Nuclear Energy Chemistry, Institute of High Energy Physics, Chinese Academy of Sciences, China
Actinide Polyrotaxanes: From Hydrothermal Synthesis to Structural Regulation
Wednesday 21/9: INV Wed2 10:00-10:30

Shi, Xueming
Institute of Applied Physics and Computational Mathematics, China
Numerical Simulation on Breeding and Burning Process of Plutonium in Fusion Fission Hybrid Reactor for Energy(FFHR-E)
Wednesday 21/9: OR Wed3 - 15:50-16:05

Siekhaus, Wigbert J.
Lawrence Livermore National Laboraoty, USA
Uranium-hydride initiation iimes before and after outgassing in vacuum at 300 C to determine the influence of hydrogen content in uranium on hydride initiation time.
Wednesday 21/9: Poster session II - 12:30-14:15 (continues on Thur. 22/9)

Silver, Mark
Florida State University, USA
1) Assessment of PuO_2^{2+} solubility in high borate media
Wednesday 21/9: Poster session II - 12:30-14:15 (continues on Thur. 22/9)

2) Synthesis, Structure, and Characterization of a Pair of Berkelium Iodates: Developments in assessing bonding character in actinides beyond Plutonium
Thursday 22/9: OR Thu1 - 11:45-12:00

Smith, Alice I.
Los Alamos National Laboratory, USA
A Temperature Investigation of δ-phase ^{239}Pu-Ga Alloys
Wednesday 21/9: OR Wed4 - 15:50-16:05

Soderlind, Per
Lawrence Livermore National Laboratory, USA
Phase stability, elasticity, and phonons for plutonium from electronic-structure theory
Monday 19/9: INV Mo1 -09:30-10:00

Steier, Peter
University of Vienna, Austria
From the stars through the ocean abyss: the long travel of super-nova Pu-244 into VERA's particle detector
Tuesday 20/9: PL Tu2 - 14:15-15:00

Stevens, Patrice
Los Alamos National Laboratory, USA
Plutonium Handbook, Second Edition
Monday 19/9: Poster session I - 12:30-14:15 (continues on Tuesday 20/9)

Stritzinger, Jared
Los Alamos National Laboratory, USA
Characterization of *f*-element oxide stoichiometry and phases through Raman Spectroscopy
Wednesday 21/9: Poster session II - 12:30-14:15 (continues on Thur. 22/9)

Sun, Bo
Institute of Applied Physics and Computational Mathematics, China
Density Functional Theory Study on Hydriding Resistance and Surface Initial Oxidation of Plutonium Nitride
Tuesday 20/9: OR Tu2 - 11:00-11:15

Tamain, Christelle
CEA, Nuclear Energy Division, Marcoule, RadioChemistry & Processes Department, France
Synthesis and structural characterization of a new water soluble actinide(IV) hexanuclear cluster $[An_6(OH)_4O_4]^{12+}$ (with An(IV) = U(IV), Np(IV), Pu(IV)).
Thursday 22/9: OR Thu4 - 15:50-16:05

Tegner, Bengt
The University of Manchester, UK
Water Interactions with Actinide Oxide Surfaces
Wednesday 21/9: OR Wed1 - 11:45-12:00

Teterin, Yury
Chemistry Department, Lomonosov Moscow State University, Russia
XPS study of radiation effect on UO2 single-crystal films
Monday 19/9: Poster session I - 12:30-14:15 (continues on Tuesday 20/9)

Troshev, Aleksandr
Russian Federal Nuclear Center – VNIITF, Russia
Research Shape Memory Effect in the U6.3wt%Nb Alloy by Dilatometry
Monday 19/9: Poster session I - 12:30-14:15 (continues on Tuesday 20/9)

Tucker, Laura A.
Los Alamos National Laboratory, USA
Modeling and validation of the Pu 239 surface alpha spectrum using MCNPX coupled with CINDER'90LA-UR-16-23017
Wednesday 21/9: Poster session II - 12:30-14:15 (continues on Thur. 22/9)

Uchaev, Alexandr
Russian Federal Nuclear Center – VNIIEF, Russia
Effect of geometry and time-amplitude characteristics of external high-intensity action on metals longevity employed in the nuclear power engineering
Wednesday 21/9: Poster session II - 12:30-14:15 (continues on Thur. 22/9)

Vauchy, Romain
CEA, DEN, DTEC, Marcoule, France
In situ high temperature X-ray diffraction studies of the phase equilibria in the UO_2-PuO_2-Pu_2O_3 system
Monday 19/9: INV Mo4 - 12:00-12:30

Venault, Laurent
CEA Marcoule, France
Alpha radiolysis of nitric acid solutions with plutonium
Tuesday 20/9: OR Tu2 - 11:30-11:45

Venhaus, Thomas
Los Alamos National Laboratory, USA
Analysis of surface chemistry on Pu-Ga alloyed surfaces by Time-of-Flight SIMS
Monday 19/9: Poster session I - 12:30-14:15 (continues on Tuesday 20/9)

Virot, Matthieu
Institut de Chimie Separative de Marcoule (ICSM), France
Reductive Dissolution of PuO_2 and CeO_2 in the Presence of Ti Particles and Ultrasound Irradiation
Tuesday 20/9: OR Tu2 - 11:45-12:00

Vitova, Tonya
Karlsruhe Institute of Technology (KIT), Insitute for Nuclear Waste Disposal (INE), Germany
Structural properties of plutonium systems revealed by high resolution XANES and RIXS techniques
Tuesday 20/9: INV Tu8 - 17:00-17:30

Volkov, Arkadij
Ural Federal University, Russia
Magnetic susceptibility and fluctuations of the electron density in the δ-plutonium
Wednesday 21/9: Poster session II - 12:30-14:15 (continues on Thur. 22/9)

Walther, Clemens
Leibniz Universität Hannover, Institute for Radioecology and Radiation Protection, Germany
Resonant Laser-SNMS on actinides for spatially resolved ultra-trace analysis
Tuesday 20/9: INV Tu7 - 17:00-17:30

Wang, Cong-Zhi
Institute of High Energy Physics, Chinese Academy of Sciences, China
Theoretical studies on the extraction behaviors of Am(III) and Cm(III) with amide-type ligands
Monday 19/9: Poster session I - 12:30-14:15 (continues on Tuesday 20/9)

Wang, Shuao
Soochow University, China
Recent Investigations of Solid State Chemistry of Actinides at Soochow University
Wednesday 21/9: Poster session II - 12:30-14:15 (continues on Thur. 22/9)

Wang, Xiaolin
China Academy of Engineering Physics, P.O. Pox 919-71, China
Raman Spectroscopy Characterization of Uranium and Plutonium Hydride from the Hydrogen Corrosion
Monday 19/9: Poster session I - 12:30-14:15 (continues on Tuesday 20/9)

Wang, Yaxing
Soochow University, China
Incorporation of soluble radionuclides into High Oxidation State Actinide Solid Matrix
Wednesday 21/9: Poster session II - 12:30-14:15 (continues on Thur. 22/9)

Watson, Robert
AWE plc, UK
Carbonate Oxidation of Electrorefining Salts
Monday 19/9: Poster session I - 12:30-14:15 (continues on Tuesday 20/9)

Welcomme, Eléonore
CEA, DEN, DRCP/SERA/LCAR, France
Study of combustion synthesis of solid solutions $(U_{1-y}An/Ln_y)O_{2\pm x}$ under air atmosphere
Thursday 22/9: OR Thu3 - 15:35-15:50

Wham, Robert
Oak Ridge National Laboratory, USA
Production of Plutonium-238 for Deep Space Missions
Wednesday 21/9: INV Wed3 -12:00-12:30

Wilkerson, Marianne
Los Alamos National Laboratory, USA
Chemical Speciation of uranium oxide and plutonium oxide materials for forensic science
Tuesday 20/9: OR Tu3 - 15:35-15:50

Willberger, Christian
Johannes Gutenberg University Mainz, Germany
Redox speciation of actinides using capillary electrophoresis coupled to ICP-MS
Tuesday 20/9: OR Tu3 -15:50-16:05

Wilson, Richard
Argonne National Laboratory, USA
Thiocyanate complexes of the tri- and tetravalent actinides.
Tuesday 20/9: INV Tu1 - 10:00-10:30

Wiss, Thierry
European Commission, Joint research Centre, Institute for Transuranium Elements, Germany
Radiation damage studies in plutonium oxides for energy production
Monday 19/9: INV Mo7 - 16:30-17:00

Xiao, Chengliang
Soochow University, China
A New Strategy for Stabilizing Uncommon Oxidation States Learned from an Extraordinarily Complex Mixed-Valent Uranium Phosphonate Framework
Wednesday 21/9: Poster session II - 12:30-14:15 (continues on Thur. 22/9)

Yablinsky, Clarissa
Los Alamos National Laboratory, USA
Atom Probe Tomography of Niobium Redistribution in U-14 at.% Nb After High Temperature Age-Hardening
Monday 19/9: Poster session I - 12:30-14:15 (continues on Tuesday 20/9)

Yamamura, Tomoo
Institute for Materials Research, Tohoku University, Japan
Structure and stability of EDTMP and DOTMP complex with Th(IV) for nuclear medicine
Wednesday 21/9: Poster session II - 12:30-14:15 (continues on Thur. 22/9)

Yang, Yu
Institute of Applied Physics and Computational Mathematics, China
Temperature dependent hydriding and dehydriding energies of PuHx from *ab initio* calculations
Monday 19/9: Poster session I - 12:30-14:15 (continues on Tuesday 20/9)

Zarzana, Christoper
Idaho National Laboratory, USA
Spectroscopic and Mass Spectral Characterization of Uranium Fluoroanions Formed from an Ionic Liquid
Thursday 22/9: OR Thu2 - 11:45-12:00

Zhang, Ping
Institute of Applied Physics and Computational Mathematics, China
First-principles studies of plutonium oxides and their surface interactions with gaseous molecules
Thursday 22/9: OR Thu2 - 11:00-11:15

Ziouane, Yannis
CEA, France
Synthesis and dissolution of mixed oxides $(U_{1-x}Pu_x)O_2$ with different morphologies
Thursday 22/9: OR Thu3 - 15:50-16:05

Zsigrai, Jozsef
EC Joint Research Centre, Germany
Non-destructive analysis for Pu accountancy in reprocessing
Monday 19/9: INV Mo2 - 10:00-10:30

Conference Programme

Sunday 18/9

Registration begins
17:00-20:00 **Foyer (Ground Floor)**

Welcome address by Maria Betti
17:30-17:45 **Foyer (Ground Floor)**

Opening talk by Roland Schenkel
17:45-18:30 **Foyer (Ground Floor)**

Welcome drink
18:30-20:00 **Parkpavillon**

Monday 19/9

Registration

08:00-18:00 **Reception desk (ground floor)**

PL Mo1

08:40-09:25 **Auditorium** **Chair: Albert Migliori**

A-01
08:40-09:25

Racah materials: atomic multiplets and f-bands
Alexander B. Shick[1], Jindrich Kolorenc[1], Mikhail I. Katsnelson[2], Alexander I. Lichtenstein[3]
[1]Institute of Physics, ASCR, Na Slovance 2, CZ-18221 Prague, Czech Republic, [2]Radboud University Nijmegen, Heyendaalseweg 135, 6525 AJ Nijmegen, The Netherlands, [3]Institute for Theoretical Physics, University of Hamburg, 20355 Hamburg, Germany

INV Mo1

09:30-10:30 **Auditorium** **Chair: Albert Migliori**

A-02
09:30-10:00

Phase stability, elasticity, and phonons for plutonium from electronic-structure theory
Per Soderlind
Lawrence Livermore National Laboratory, Livermore, CA, USA

A-03
10:00-10:30

Plutonium as a Mixed Valent Metal
Gabriel Kotliar
Department of Physics and Astronomy, Rutgers University, Piscataway, NJ, USA

INV Mo2

09:30-10:30 **Kongreßsaal I** **Chair: David Clark**

A-04
09:30-10:00

Multi-Actinides analysis with AMS: a novel method for ultra-trace determination and small sample sizes
Francesca Quinto[1], Markus Lagos[1], Markus Plaschke[1], Thorsten Schäfer[1], Peter Steier[2], Horst Geckeis[1]
[1]Karlsruhe Institute of Technology (KIT), Institute for Nuclear Waste Disposal (INE), Eggenstein Leopoldshafen, Germany, [2]University of Vienna, VERA Laboratory, Faculty of Physics-Isotope Research and Nuclear Physics, Vienna, Austria

A-05
10:00-10:30

Non-destructive analysis for Pu accountancy in reprocessing
Jozsef Zsigrai[1], Klaus Lutzenkirchen[1], Artur Muhleisen[1], Magdalena Toma[1], Peter Schwalbach[2], Sotiris Synetos[2]
[1]EC Joint Research Centre, Karlsruhe, Germany, [2]EC Directorate General for Energy, Luxembourg, Luxembourg

Coffee break

10:30-11:00 **Parkpavillon**

OR Mo1

11:00-12:00 **Auditorium** **Chair: Albert Migliori**

A-06
11:00-11:15
Insights into point-defects of δ-Pu and δ-Pu-Ga alloys using density functional theory
Sarah Hernandez, Franz Freibert
Los Alamos National Laboratory, Los Alamos, NM, USA

A-07
11:15-11:30
Thermoelectric power as a probe of density of states in $PuCoGa_5$
Krzysztof Gofryk[1], Jean-Christophe Griveau[2], Tomasz Durakiewicz[3]
[1]Idaho National Laboratory, Idaho Falls, Idaho, USA, [2]Institute for Transuranium Elements, Karlsruhe, Baden-Wurttemberg, Germany, [3]Los Alamos National Laboratory, Los Alamos, New Mexico, USA

A-08
11:30-11:45
Hydrogen as a tool to modify electronic structure: are there common features in U and Pu hydrides?
Ladislav Havela[1], Mykhaylo Paukov[1], Volodymyr Buturlim[1], Ilja Turek[1], Martin Divis[1], Daria Drozdenko[1], Zdenek Matej[1], Milan Dopita[1], Milan Cieslar[1], Frank Huber[2], Thomas Gouder[2]
[1]Charles University, Prague, Czech Republic, [2]European Commission, JRC, Institute for Transuranium Elements, Karlsruhe, Germany

A-09
11:45-12:00
Quantum molecular dynamics simulations of transport properties in liquid plutonium
Haifeng Liu, Shuaichuang Wang, Gongmu Zhang, Bo Sun, Haifeng Song, Mingfeng Tian
Institute of Applied Physics and Computational Mathematics, Beijing, China

OR Mo2

11:00-12:00 **Kongreßsaal I** **Chair: David Clark**

A-10
11:00-11:15
Properties of PuO2 nanoparticles together with its analogues CeO2 and ThO2
Anna Romanchuk, Tatiana Plakhova, Stepan Kalmykov
Lomonosov Moscow State University, Moscow, Russia

A-11
11:15-11:30
Development of point defect Raman signatures in PuO_2 through self-irradiation
Robert M Harker, Christopher Puxley
AWE Aldermaston, Reading, UK

A-12
11:30-11:45
Oxygen stoichiometry determination in Pu-fuel by vapour pressure measurement
Ondrej Benes, Rudy Konings, Jean-Yves Colle
European Commission - Joint Research Centre, Karlsruhe, Germany

A-13
11:45-12:00

XAFS and μ-XRF investigations of highly radioactive nuclear waste samples: spent nuclear fuel and zircaloy cladding segments.
Kathy Dardenne[1], Ernesto Gonzalez-Robles[1], Michel Herm[1], Bernhard Kienzler[1], Gerd Christill[2], Nikolaus Müller[1], Volker Metz[1], Jörg Rothe[1]
[1]Institute for Nuclear Waste Disposal (KIT-INE), Karlsruhe Institute of Technology (KIT), Karlsruhe, Germany, [2]Sicherheit und Umwelt (KIT-SUM), Karlsruhe Institute of Technology (KIT), Karlsruhe, Germany

INV Mo3

12:00-12:30 **Auditorium** **Chair: Albert Migliori**

A-14
12:00-12:30

Real Time Studies of ^{239}Pu Elastic Moduli using Resonant Ultrasound Spectroscopy
Boris Maiorov, Jonathan Betts, Maxime Leroux, Franz Freibert, Albert Migliori
Los Alamos National Laboratory, Los Alamos, New Mexico, USA

INV Mo4

12:00-12:30 **Kongreßsaal I** **Chair: David Clark**

A-15
12:00-12:30

In situ high temperature X-ray diffraction studies of the phase equilibria in the UO_2-PuO_2-Pu_2O_3 system
Romain Vauchy[1], Renaud C. Belin[2], Alexis Joly[1], Christophe Valot[1]
[1]CEA, DEN, DTEC, Marcoule, 30207 Bagnols-sur-Cèze, France, [2]CEA, DEN, DEC, Cadarache, 13108 Saint-Paul-lez-Durance, France

Poster session I & working lunch

12:30-14:15 **Foyer ground floor and Parkpavillon**

(continues on Tuesday 20/9)

A-29
12:30-14:15

Secure and certify studies to work on production of spiked plutonium
Ashraf Elsayed
Brno University, Brno, Czech Republic

A-30
12:30-14:15

Plutonium Handbook, Second Edition
Patrice Stevens[1], David L. Clark[1], David Geeson[2], Robert Hanrahan, Jr[3], Natanya Civjan[1]
[1]Los Alamos National Laboratory, Los Alamos, New Mexico, USA, [2]Atomic Weapons Establishment, Aldermaston, Reading, UK, [3]National Nuclear Security Administration, Washington, DC, USA

A-31
12:30-14:15

On dislocation mechanism of dynamic deformation of uranium
Victor Pushkov, Dmitry Tsisar
Russian Federal Nuclear Center-VNIIEF, Sarov, Nizhni Novgorod reg., Russia

A-32
12:30-14:15

Laser Spectroscopy and Detection of Actinides and Lanthanides in Solutions
Igor Izosimov
Joint Institute for Nuclear Research, Dubna, Moscow region, Russia

A-33
12:30-14:15

An in-situ X-ray diffraction study of plutonium oxidation
Paul Roussel, Wayne Lake
AWE, Aldermaston, Reading, Berkshire., UK

A-34
12:30-14:15

Temperature dependent hydriding and dehydriding energies of PuHx from *ab initio* calculations
Yu Yang, Ping Zhang
Institute of Applied Physics and Computational Mathematics, Beijing, China

A-35
12:30-14:15

Characterization of point defects in α-Pu
Vladimir Dremov, Gennady Ionov, Alexey Karavaev, Sergey Samarin, Filipp Sapozhnikov
Russian Federal Nuclear Centre - Institute of Technical Physics, Snezhinsk, Chelyabinsk region, Russia

A-36
12:30-14:15

Theoretical studies on the extraction behaviors of Am(III) and Cm(III) with amide-type ligands
Cong-Zhi Wang, Jian-Hui Lan, Qun-Yan Wu, Zhi-Fang Chai, Wei-Qun Shi
Institute of High Energy Physics, Chinese Academy of Sciences, Beijing, China

A-37
12:30-14:15

Properties of solids under compression and shock : Role of electronic and structural phase transitions
Boris Nadykto
Russian Federal Nuclear Center VNIIEF, Sarov, Russia

A-38
12:30-14:15

2NN MEAM potential for Plutonium
Piheng Chen, Xinchun Lai
China Academy of Engineering Physics, Mianyang, Sichuan, China

A-39
12:30-14:15

Atom Probe Tomography of Niobium Redistribution in U-14 at.% Nb After High Temperature Age-Hardening
Clarissa Yablinsky[1], Amy Clarke[1,2], Yaqiao Wu[3,4], Robert Hackenberg[1]
[1]Los Alamos National Laboratory, Los Alamos, NM, USA, [2]Colorado School of Mines, Golden, CO, USA, [3]Center for Advanced Energy Studies, Idaho Falls, ID, USA, [4]Boise State University, Boise, ID, USA

A-40
12:30-14:15

Chitin-chitozan - a Sorbent Preventing Release of Radioactive Actinide Compounds under Emergency Submersion
Tatiana Kazakovskaya, Victor Scherbakov, Edvard Goryachev, Alexander Gorelov
RFNC-VNIIEF, Sarov, Nizhny Novgorod Region, Russia

A-41
12:30-14:15

Cerium Behavior in Various Media as Compared with Plutonium
Tatiana Kazakovskaya, Yulia Belova
RFNC-VNIIEF, Sarov, Nizhny Novgorod Region, Russia

A-43
12:30-14:15

Raman Spectroscopy Characterization of Uranium and Plutonium Hydride from the Hydrogen Corrosion
Xiaolin Wang, Guangfeng Zhang, Junbo Lv
China Academy of Engineering Physics, P.O. Pox 919-71, Mianyang, 621900, China

A-44
12:30-14:15

XPS study of radiation effect on UO2 single-crystal films
Yury Teterin[1,3], Alexey Popel[2], Konstantin Maslakov[1], Anton Teterin[3], Kirill Ivanov[3], Stepan Kalmykov[1], Ross Springell[4], Thomas Scott[4], Ian Farnan[2]
[1]Chemistry Department, Lomonosov Moscow State University, Moscow, Russia, [2]Department of Earth Sciences, University of Cambridge, Cambridge, UK,
[3]NRC "Kurchatov Institute", Moscow, Russia, [4]Interface Analysis Centre, School of Physics, University of Bristol, Bristol, UK

A-45
12:30-14:15

Pd-hybridization and paramagnon superconductivity mechanism $PuCoGa_5$
Aleksandr Povzner
Ural Federal University, Ekaterinburg, Russia

A-46
12:30-14:15

Auger line-shape analysis and electron energy loss spectroscopy investigation of Pu surface chemistry
Art Nelson, Scott Donald, Wigbert Siekhaus, Patrick Allen, William McLean
LLNL, Livermore, CA, USA

A-47
12:30-14:15

Research Shape Memory Effect in the U6.3wt%Nb Alloy by Dilatometry
Aleksandr Troshev, Chentzov Denis, Golunov Anatoliy, Shestakov Evgeniy, Baluev Alexey
Russian Federal Nuclear Center – VNIITF, Snezhinsk, Russia

A-48
12:30-14:15

On the equation of state and elastoplastic and strength properties of beryllium
Maria Shirshova, Boris Nadykto, Ivan Pavlusha
RFNC-VNIIEF, Sarov, Nizhny Novgorod Region, Russia

A-49
12:30-14:15

The Structure of Thick-walled Spherical Shell of U-1,5% Mo Alloy After Explosive Loading
Dmitry Belyaev, Eugen Kozlov, Yury Zouev, Igor Svyatov, Alexey Aleksandrov, Ekaterina Levi
Russian Federal Nuclear Center – Zababakhin All-Russia Research Institute of Technical Physics, (RFNC-VNIITF), Snezhinsk, Chelyabinsk region, Russia

A-50
12:30-14:15

Dynamic Magnetic Response across the Pressure-Induced Structural Phase Transition in CeNi
Alexey Mirmelstein[1], Andrey Podlesnyak[2], Alexander Kolesnikov[2], Georg Ehlers[2], Douglas Abernathy[2], Vladimir Matvienko[1], Gregory Halder[3], Antonio dos Santos[2]
[1]RFNC-VNIITF, Snezhinsk, Chelyabinsk region, Russia, [2]Oak Ridge National Laboratory, Oak Ridge, TN, USA, [3]Argonne National Laboratory, Argonne, IL, USA

A-51
12:30-14:15

Development of AFM and STM Capabilities for Plutonium
Miles Beaux, Adam Zocco, Miguel Santiago Cordoba, Douglas Vodnik, Stephen Joyce, Michael Ramos, Scott Richmond, Thomas Venhaus, Jeremy Mitchell, Brian Scott, Eve Bauer, Igor Usov
Los Alamos National Laboratory, Los Alamos, NM, USA

A-53
12:30-14:15

CALPHAD approach a complementary way to solve the plutonium mystery.
Benoît Oudot[1], Brice Ravat[1], Aurelien Perron[2], Christine Guéneau[3], Lionel Jolly[1], Patrice Turchi[2], François Delaunay[1]
[1]CEA-VALDUC, Is-sur-Tille, France, [2]LLNL, Livermore, CA, USA, [3]CEA-SACLAY, Gif-sur-Yvette, France

A-54
12:30-14:15

Evolution of electronic structures of γ-Pu, δ-Pu, and ε-Pu
Li Huang
Institute of Materials, China Academy of Engineering Physics, Sichuan Jiangyou, China

A-55
12:30-14:15

Pu Alloy Oxidation by Water Vapor.
Lionel Jolly, Brice Ravat, Benoît Oudot, François Delaunay
CEA - VALDUC, Is-sur-Tille, France

A-56
12:30-14:15

Oxidation of Pu-Ga alloyed surfaces and PuO_2 PAD films using Time-of-Flight SIMS
Sarah Hernandez, Thomas Venhaus, David Pugmire, David Moore, Brian Scott
Los Alamos National Laboratory, Los Alamos, NM, USA

A-57
12:30-14:15

Some results of investigations of particle ejection from a free surface of metals under a shock wave effect
Michael Antipov, Alla Georgievskaya, Vladislav Igonin, Margarita Lebedeva, Konstantin Panov, Valeriy Sadunov, Alexander Utenkov, Igor Yurtov
RFNC-VNIIEF, Sarov, Russia

A-58
12:30-14:15

Experimental and calculation parameters of benchmark spherical critical assemblies with metal plutonium in α-phase core and in beryllium and depleted uranium reflectors
Alexey Kaygorodov, Sergey Vorontsov, Mikhail Kuvshinov, Valentin Khoruzhyi
RFNC-VNIIEF, Sarov, Nizhny Novgorod Region, Russia

A-59
12:30-14:15

Carbonate Oxidation of Electrorefining Salts
Robert Watson, Clare Stawarz
AWE plc, Aldermaston, Reading, UK

A-60
12:30-14:15

Hydrolysis of plutonium under reducing conditions controlled by electrolysis
Hye-Ryun Cho, Young-Sang Youn, E. C. Jung, W. Cha
Korea Atomic Energy Research Institute, Daejeon, Republic of Korea

A-61
12:30-14:15

U(VI) adsorption onto alumina, silica, and kaolinite in U(VI)-OH / U(VI)-CO_3 / Ca-U(VI)-CO_3 aqueous systems
Yongheum Jo[1], Jun-Yeop Lee[2], Jong-Il Yun[1]
[1]Department of Nuclear and Quantum Engineering, KAIST, 291 Daehak-ro, Yuseong-gu, Daejeon 34141, Republic of Korea, [2]Institute for Nuclear Waste Disposal, Karlsruhe Institute of Technology, Karlsruhe, Baden-Württemberg, Germany

A-62
12:30-14:15

Structural properties of actinides from first principles: important role of Hund's exchange.
Bernard Amadon
CEA, Bruyeres le Chatel, France

A-63
12:30-14:15

Solubility, Hydrolysis and Carbonate Complexation of Plutonium and Neptunium under Repository-Relevant Conditions
Julian Schepperle, David Fellhauer, Xavier Gaona, Marcus Altmaier, Horst Geckeis
Institute for Nuclear Waste Disposal, Karlsruhe Institute of Technology, Karlsruhe, Germany

A-64
12:30-14:15

Thermodynamic stability of the UO_2 surfaces: Interplay between over-stoichiometry and polarity compensation
François Bottin[1], Gérald Jomard[2], Grégory Geneste[1]
[1]CEA, Arpajon, France, [2]CEA, Saint-Paul-lez-Durance, France

A-65
12:30-14:15

Analysis of surface chemistry on Pu-Ga alloyed surfaces by Time-of-Flight SIMS
Thomas Venhaus, Sarah Hernandez, Joseph Anderson, David Moore, David Pugmire
Los Alamos National Laboratory, Los Alamos, NM, USA

A-66
12:30-14:15

ToF-SIMS Determination of the Partitioning between H and F in Aged Uranium Materials
Scott Donald, Wigbert Siekhaus, Art Nelson
Lawrence Livermore National Laboratory, Livermore, CA, USA

PL Mo2

14:15-15:00 **Auditorium** **Chair: Thomas Gouder**

A-16
14:15-15:00

Plutonium corrosion: some insights and some mysteries
Joseph Glascott
Bristol University, Bristol, UK

INV Mo5

15:05-15:35 **Auditorium** **Chair: Thomas Gouder**

A-17
15:05-15:35

Recent progress in plutonium hydride research
Martin Brierley, John Knowles
AWE, Aldermaston, Berkshire, UK

INV Mo6

15:05-15:35 **Kongreßsaal I** **Chair: Paul Roussel**

A-18
15:05-15:35

Metallurgical Properties of Aged Plutonium Alloys and the Need for Advanced Microstructural Characterization
Brandon Chung, Kenneth Lema, Robert Erler, Nick Teslich, Patrick Allen
Lawrence Livermore National Laboratory, Livermore, CA, USA

OR Mo3

15:35-16:05 **Auditorium** **Chair: Thomas Gouder**

A-19
15:35-15:50

Auger Electron Spectroscopy of Plutonium Surfaces
David Moore, Alison Pugmire, Thomas Venhaus, Sarah Hernandez, David Pugmire
Los Alamos National Laboratory, Los Alamos, NM, USA

A-20
15:50-16:05

The influence of hydrogen pressure and reaction temperature on the nucleation and growth kinetics of plutonium hydride
Gan Li, Huilong Yu, Haibo Li
china academy of engineering physics, mianyang, sichuan, China

OR Mo4

15:35-16:05 **Kongreßsaal I** **Chair: Paul Roussel**

A-21
15:35-15:50

Small-scale production and characterization of high-purity plutonium metal
Kerri J.M. Blobaum, Mark A. Wall, Roger A. Henderson, Mike J. Singleton, Gary R. Eppich, Kiel S. Holliday, Jason R. Jeffries, Jeff A. Stanford, Elizabeth G. Dzenitis, Athanasios Arsenlis
Lawrence Livermore National Laboratory, Livermore, CA, USA

A-22
15:50-16:05

First-principles DFT+*U* Energetics of Impurity Atoms in PuO_2 and Pu_2O_3
Bingyun Ao
China Academy of Engineering Physics, P.O. Pox 919-71, Mianyang 621900, China

Coffee break

16:05-16:30 **Parkpavillon**

INV Mo7

16:30-17:30 **Auditorium** **Chair: Thomas Gouder**

A-23
16:30-17:00

Radiation damage studies in plutonium oxides for energy production
Thierry Wiss, Rudy Konings, Vincenzo V. Rondinella, Oliver Dieste, Ondrej Benes, Jean-Yves Colle, Dragos Staicu, Philippe E. Raison
European Commission, Joint research Centre, Institute for Transuranium Elements, Karlsruhe, Germany

A-24
17:00-17:30

First-principles modelling of point defects in fast reactor MOX fuels
Michel Freyss, Marjorie Bertolus, Ibrahim Cheik Njifon, Yaguang Li, Lei Shi
CEA, DEN, Cadarache, Saint-Paul lez Durance, France

INV Mo8

16:30-17:30 **Kongreßsaal I** **Chair: Paul Roussel**

A-25
16:30-17:00

Thermal Expansion of Delta Plutonium
Jeremy Mitchell, Franz Freibert, Scott Richmond, Daniel Schwartz, Michael Ramos
Los Alamos National Laboratory, Los Alamos, NM, USA

A-26
17:00-17:30

EXAFS studies of self-irradiation damage in Pu
Daniel Olive[1,2], Deborah Wang[2,3], Corwin Booth[2], Eric D. Bauer[1], Alison Pugmire[1], Franz Freibert[1], Scott McCall[4], Mark A. Wall[4], Patrick Allen[4]
[1]Los Alamos National Laboratory, Los Alamos, NM, USA, [2]Lawrence Berkeley National Laboratory, Berkeley, CA, USA, [3]University of California Berkeley, Berkeley, CA, USA, [4]Lawrence Livermore National Laboratory, Livermore, CA, USA

OR Mo5

17:30-17:45 **Auditorium** **Chair: Thomas Gouder**

A-27
17:30-17:45

Fuel Cycle Concept with dispersion type Fuel in LWRs
Aleksei Savchenko, Leonid Karpyuk, Dmitry Shamin, Oleg Uferov
A.A. Bochvar Institute (VNIINM), Moscow, Russia

OR Mo6

17:30-17:45 **Kongreßsaal I** **Chair: Paul Roussel**

A-28
17:30-17:45

MD study of self-irradiation effects on dislocation dynamics in δ-Pu
Alexey Karavaev, Vladimir Dremov, Gennady Ionov
Russian Federal Nuclear Center - Zababakhin Institute of Technical Physics (RFNC-VNIITF), Snezhinsk, Chelyabinsk region, Russia

Tuesday 20/9

Registration

08:00-17:00 **Registration desk (Ground Floor)**

PL Tu1

08:40-09:25 **Auditorium** **Chair: Hervé Bernard**

B-01
08:40-09:25 Does the Electrochemistry of Plutonium Signal the Unravelling of the Seaborg Concept of the Actinide Series?
Thomas E. Albrecht-Schmitt
Florida State University, Tallahassee, Florida, USA

INV Tu1

09:30-10:30 **Auditorium** **Chair: Hervé Bernard**

B-02
09:30-10:00 Quantum chemistry and spectroscopic studies of actinide ions with oxygen- and nitrogen- donor ligands in solution
Dominique Guillaumont, Eleonor Acher, Thomas Dumas, Matthieu Audras, Laurence Berthon, Olivia Pecheur
CEA, Bagnols sur Cèze, France

B-03
10:00-10:30 Thiocyanate complexes of the tri- and tetravalent actinides.
Richard Wilson, Tyler Carter
Argonne National Laboratory, Argonne, Illinois, USA

INV Tu2

09:30-10:30 **Kongreßsaal I** **Chair: Joe Glascott**

B-04
09:30-10:00 Quality control tools for the analysis of plutonium in nuclear safeguards, security and safety
Yetunde Aregbe, Rozle Jakopic, Stephan Richter, Goedele Sibbens
EC-JRC-IRMM, Geel, Belgium

B-05
10:00-10:30 Impurity effects in plutonium alloys
Sue Ennaceur, Paul Roussel
AWE, Aldermaston, Reading, Berkshire., UK

Coffee break

10:30-11:00 **Parkpavillon**

OR Tu1

11:00-12:00 **Auditorium** **Chair: Hervé Bernard**

B-06
11:00-11:15 Structure of Plutonium(IV) with O-donor ligands from crystallography, extended X-ray absorption fine structure and theoretical calculations
Eleonor Acher, Thomas Dumas, Christelle Tamain, Dominique Guillaumont
CEA MARCOULE, Bagnols sur Cèze, France

B-07
11:15-11:30 Semiconductivity in Plutonium and Americium Chromates and Molybdates: The Smoking Gun for Energy-Degeneracy-Driven Covalency
Alexandra Arico[1], Alejandro Garza[2], Justin Cross[3], Thomas E. Albrecht-Schmitt[1]
[1]Florida State University, Tallahassee, FL, USA, [2]Rice University, Houston, TX, USA, [3]Los Alamos National Laboratory, Los Alamos, NM, USA

B-08 11:30-11:45
Evaluation of Covalency in PuF_4 by ^{19}F NMR Spectroscopy
Herman Cho[1], Cigdem Capan[2], Richard Dempsey[2], Sergey Sinkov[1], Bruce McNamara[1]
[1]Pacific Northwest National Laboratory, Richland, Washington, USA, [2]Washington State University, Richland, Washington, USA

B-09 11:45-12:00
Insight Into Stabilization Mechanisms of the Delta Phase of Plutonium by Deltagen Elements
Boris Dorado, Jordan Bieder, Marc Torrent
CEA, Arpajon, France

OR Tu2

11:00-12:00 **Kongreßsaal I** **Chair: Joe Glascott**

B-10 11:00-11:15
Density Functional Theory Study on Hydriding Resistance and Surface Initial Oxidati on of Plutonium Nitride
Bo Sun, Haifeng Liu, Haifeng Song, Hui Zheng
Institute of Applied Physics and Computational Mathematics, Beijing, China

B-11 11:15-11:30
Understanding the Oxide Layer on Plutonium under Ambient Conditions
Alison Pugmire, David Pugmire, David Moore, Thomas Venhaus
Los Alamos National Laboratory, Los Alamos, NM, USA

B-12 11:30-11:45
Alpha radiolysis of nitric acid solutions with plutonium
Laurent Venault[1], Guillaume Garaix[1], Amaury Costagliola[2], Philippe Moisy[1], Guillaume Blain[2], Johan Vandenborre[2], Massoud Fattahi-Vanani[2], Nicolas Vigier[3]
[1]CEA Marcoule, Bagnols sur Ceze, France, [2]Subatech EMN, Nantes, France, [3]AREVA NC, Paris La Défense, France

B-13 11:45-12:00
Reductive Dissolution of PuO_2 and CeO_2 in the Presence of Ti Particles and Ultrasound Irradiation
Matthieu Virot[1], Xavier Beaudoux[1,2], Tony Chave[1], Gilles Leturcq[2], Gauthier Jouan[3], Laurent Venault[2], Philippe Moisy[2], Sergey I. Nikitenko[0]
[1]Institut de Chimie Separative de Marcoule (ICSM), Bagnols sur Ceze, France, [2]CEA Marcoule - CEA/DEN/MAR/DRCP, Bagnols sur Ceze, France, [3]CEA Marcoule - CEA/DEN/MAR/DTEC/SECA/LCC, Bagnols sur Ceze, France

INV Tu3

12:00-12:30 **Auditorium** **Chair: Hervé Bernard**

B-14 12:00-12:30
Shedding a new light on the superconductivity of $PuCoGa_5$: A heat capacity study on single crystals below 1 K.
Jean-Christophe Griveau, Eric Colineau, Rachel Eloirdi, Pedro Amador Celdran, Roberto Caciuffo
ITU, Karlsruhe, Germany

INV Tu4

12:00-12:30 **Kongreßsaal I** **Chair: Joe Glascott**

B-15 12:00-12:30
Plutonium and Americium Solvent Extraction Processes: Recent Development in Europe
Andreas Geist
Karlsruhe Institute of Technology (KIT), Karlsruhe, Germany

Poster session I & working lunch

12:30-14:15 **Foyer ground floor and Parkpavillon**

PL Tu2

14:15-15:00 **Auditorium** **Chair: Kerri Blobaum**

B-16
14:15-15:00
From the stars through the ocean abyss: the long travel of super-nova Pu-244 into VERA's particle detector
Peter Steier[1], Anton Wallner[1,2], Thomas Faestermann[3], Jenny Feige[1,8], Chana Feldstein[4], Klaus Knie[3,5], Gunther Korschinek[3], Walter Kutschera[1], Avishai Ofan[4], Michael Paul[4], Francesca Quinto[1,6], Georg Rugel[3,7]
[1]University of Vienna, Vienna, Austria, [2]Australian National University, Canberra, Australia, [3]Technische Universität München, Garching, Germany, [4]Hebrew University, Jerusalem, Israel, [5]GSI Helmholtz-Zentrum fu ¨r Schwerionenforschung, Darmstadt, Germany, [6]Institute for Nuclear Waste Disposal, Eggenstein-Leopoldshafen, Germany, [7]Helmholtz-Zentrum Dresden-Rossendorf, Rossendorf, Germany, [8]Technische Universität Berlin, Berlin, Germany

INV Tu5

15:05-15:35 **Auditorium** **Chair: Kerri Blobaum**

B-17
15:05-15:35
Real-time, fast neutron assay of plutonium and related materials
Malcolm J. Joyce
Lancaster University, Lancaster, UK

INV Tu6

15:05-15:35 **Kongreßsaal I** **Chair: Brian Powell**

B-18
15:05-15:35
Nanoparticle Plutonium Formation, Growth, and Morphology with in-situ Liquid Cell Electron Microscopy
Edgar Buck
Pacific Northwest National Laboratory, Richland, WA, USA

OR Tu3

15:35-16:05 **Auditorium** **Chair: Kerri Blobaum**

B-19
15:35-15:50
Chemical Speciation of uranium oxide and plutonium oxide materials for forensic science
Marianne Wilkerson, Miles Beaux, Sarah Hernandez, Stephen Joyce, Andrew Nelson, Alison Pugmire, David Pugmire, Amy Ross, Brian Scott, Igor Usov, Gregory Wagner, Angelique Wall, Laura Wolfsberg
Los Alamos National Laboratory, Los Alamos, NM, USA

B-20
15:50-16:05
Redox speciation of actinides using capillary electrophoresis coupled to ICP-MS
Christian Willberger, Samer Amayri, Verena Häußler, Raphael Scholze, Tobias Reich
Johannes Gutenberg University Mainz, Mainz, Germany

OR Tu4

15:35-16:05 **Kongreßsaal I** **Chair: Brian Powell**

B-21 15:35-15:50
ThermAc - a collaborative project investigating aquatic chemistry and thermodynamics of actinides at elevated temperature conditions
Marcus Altmaier[1], Felix Brandt[5], Vinzenz Brendler[2], Ion Chiorescu[6], Elisenda Colas[7], Hilde Curtius[5], Francesco Endrizzi[1], Carola Franzen[2], Xavier Gaona[1], Mireia Grive[7], Seven Hagemann[4], Carsten Koke[3], Dmitrii A. Kulik[8], Sven Krüger[6], Jun-Yeop Lee[1], Martin Maiwald[3], Tres Thoenen[8], Petra J. Panak[3], Andrej Skerencak-Frech[3], Robin Steudtner[2]
[1]Karlsruhe Institute of Technology, Institute for Nuclear Waste Disposal (KIT-INE), Karlsruhe, Germany, [2]Helmholtz-Zentrum Dresden-Rossendorf, Institute of Resource Ecology, Dresden, Germany, [3]University of Heidelberg, Institute for Physical Chemistry, Heidelberg, Germany, [4]Gesellschaft für Reaktor und Anlagensicherheit (GRS), Braunschweig, Germany, [5]Jülich Research Center, Institute of Energy and Climate Research (IEK-6), Jülich, Germany, [6]Technische Universität München, Theoretical Chemistry, München, Germany, [7]Amphos21 Consulting, Barcelona, Spain, [8]Paul Scherrer Institute, Laboratory for Waste Management (PSI-LES), Villigen, Switzerland

B-22 15:50-16:05
Traces of Pu isotopes originated from burnt-up fuel in Fukushima exclusion zone
Renata Kierepko[1,2], Atsuyuki Sorimachi[3,4], Shinji Tokonami[4], Sarat Sahoo[1]
[1]Fukushima Research Headquarter, National Institute for Quantum and Radiological Science and Technology, Chiba, Japan, [2]Institute of Nuclear Physics, Polish Academy of Sciences, Krakow, Poland, [3]Department of Radiation Physics and Chemistry, Fukushima Medical University, Fukushima, Japan, [4]Institute of Radiation Emergency Medicine, Hirosaki University, Hirosaki, Japan

Coffee break

16:05-16:30 **Parkpavillon**

INV Tu7

16:30-17:30 **Auditorium** **Chair: Kerri Blobaum**

B-23 16:30-17:00
On the Raman Spectrum of Plutonium dioxide: vibrational and crystal electric field modes
Mohamed Naji[1], Nicola Magnani[1], Laura Bonales[2], Sara Mastromarino[1,3], Jean-Yves Colle[1], Joaquin Cobos[2], Dario Manara[1]
[1]European Commission, Joint Research Centre, Institute for Transuranium Elements (ITU), Karlsruhe, Germany, [2]Centro de Investigaciones Energéticas, Medioambientales y Tecnológicas (CIEMAT), Madrid, Spain, [3]Università degli di Roma La Sapienza, Rome, Italy

B-24 17:00-17:30
Resonant Laser-SNMS on actinides for spatially resolved ultra-trace analysis
Clemens Walther[1], Hauke Bosco[1], Michael Franzmann[1,2], Linda Hamann[1], Mohammad Tanha[1], KLaus Wendt[2]
[1]Leibniz Universität Hannover, Institute for Radoioecology and Radiation Protection, Hannover, Germany, [2]Johannes Gutenberg-Universität Mainz, Institute of Physics, Mainz, Germany

INV Tu8

16:30-17:30 **Kongreßsaal I** **Chair: Brian Powell**

B-25 16:30-17:00
On the Highest Oxidation State of Plutonium in Compounds
Jun Li
Theoretical Chemistry Center, Department of Chemistry, Tsinghua University, Beijing, China

B-26
17:00-17:30

Structural properties of plutonium systems revealed by high resolution XANES and RIXS techniques

Tonya Vitova
Karlsruhe Institute of Technology (KIT), Insitute for Nuclear Waste Disposal (INE), Karlsruhe, Germany

OR Tu5

17:30-17:45 **Auditorium** **Chair: Kerri Blobaum**

B-27
12:30-14:15

Crystal dynamics of neptunium dioxide

Luigi Paolasini[1], Pablo Maldonado[2], Peter M. Oppeneer[2], Tom R. Forrest[3], Nicola Magnani[4], Alexei Bosak[1], Gerard H. Lander[4], Roberto Caciuffo[4]
[1]ESRF – The European Synchrotron, 71 avenue des Martyrs CS 40220, 38043 Grenoble cedex 9, France, [2]Department of Physics and Astronomy, Uppsala University, Box 516, S-75120 Uppsala, Sweden, [3]Diamond Light Source,, Harwell Science and Innovation Campus, Didcot Oxfordshire OX11 0DE, UK, [4]European Commission, JRC-ITU, Postfach 2340, D-76125 Karlsruhe, Germany

OR Tu6

17:30-17:45 **Kongreßsaal I** **Chair: Brian Powell**

B-28
17:30-17:45

Study of the 5f electronic states in uranium-plutonium mixed oxides using high resolution XANES

Philippe Martin[1], Michal Strach[1], Damien Prieur[2], René Bès[3], Renaud C. Belin[4], Dario Manara[2], Christophe Valot[1], Tonya Vitova[5], Tim Prussmann[5], Kathy Dardenne[5], Jörg Rothe[5]
[1]CEA, DEN, DTEC, Centre d'études nucléaires de Marcoule, Bagnols-sur-Cèze F-30207, France, [2]European Commission, Joint Research Centre, Institute for Transuranium Elements, , P.O.Box 2340, D-76125 Karlsruhe, Germany, [3]Antimatter and Nuclear engineering, Department of applied Physics, Aalto University, Finland, [4]CEA, DEN, DEC, Centre d'études nucléaires de Cadarache, Saint Paul lez Durance, F-13115, France, [5]Karlsruhe Institute of Technology (KIT), Institute for Nuclear Waste Disposal, P.O. Box 3640, D-76021 Karlsruhe, Germany

Wednesday 21/9

Registration

08:00-17:00 **Registration desk (groundfloor)**

PL Wed1

08:40-09:25 **Auditorium** **Chair: Tim Tinsley**

C-01
08:40-09:25

Pu-238 and the Pu sustainment work at Los Alamos
David L. Clark
Los Alamos National Laboratory, Los Alamos, NM, USA

INV Wed1

09:30-10:30 **Auditorium** **Chair: Tim Tinsley**

C-02
09:30-10:00

^{241}Am Production for Use in Radioisotope Power Systems
Catherine Campbell[1], Cheryl Carrigan[1], Michael Carrott[1], Chris Maher[1], Bliss McLuckie[1], Chris Mason[1], Colin Gregson[1], Tamara Griffiths[1], Josh Holt[1], Mark Sarsfield[1], Robin Taylor[1], Tim Tinsley[1], Keith Stephenson[2]
[1]National Nuclear Laboratory, Sellafield, UK, [2]European Space Agency, Noordwijk, The Netherlands

C-03
10:00-10:30

Studies Related to the Fabrication of $^{238}PuO_2$ Ceramic Fuel Pellets and the Surrogate CeO_2
Daniel Kramer
University of Dayton, Dayton, Ohio, USA

INV Wed2

09:30-10:30 **Kongreßsaal I** **Chair: Andrew Gaunt**

C-04
09:30-10:00

Redox Stability and Separation Chemistry of Actinyl Cations Coordinated by Schiff Base Ligands
Christiain Bustillos[1,2], Roy Copping[2,3], Andrew Gaunt[2], Cory Hawkins[1,4], Iain May[2], Mikael Nilsson[1], Sean Reilly[2], Brian Scott[2]
[1]Department of Chemical Engineering and Materials Science, University of California, Irvine, CA, USA, [2]Science, Technology and Engineering, Los Alamos National Laboratory, Los Alamos, NM, USA, [3]Medical Radioisotope Program – Isotope Development Group, Oak Ridge National Laboratory, Oak Ridge, TN, USA, [4]Chemistry Department, Tennessee Tech University, Cookeville, TN, USA

C-05
10:00-10:30

Actinide Polyrotaxanes: From Hydrothermal Synthesis to Structural Regulation
Wei-Qun Shi
Laboratory of Nuclear Energy Chemistry, Institute of High Energy Physics, Chinese Academy of Sciences, Beijing, China

Coffee break

10:30-11:00 **Parkpavillon**

OR Wed1

11:00-12:00 **Auditorium** **Chair: Tim Tinsley**

C-06
11:00-11:15
PuF_4 Lattice Effects Due to Aging
Amanda Casella, Calvin Delegard, Kaylyn McCoy, Bruce McNamara, William Karl Pitts, Sergey Sinkov
Pacific Northwest National Laboratory, Richland, WA, USA

C-07
11:15-11:30
The Kinetic Evolution of Self-Irradiation Damage in Face-Centered Cubic Pu-Ga Alloys
Franz Freibert
Los Alamos National Laboratory, Los Alamos, NM, USA

C-08
11:30-11:45
Oxidation study of Pu stabilized in δ-phase
Brice Ravat, Lionel Jolly, Benoît Oudot, François Delaunay
CEA - VALDUC, Is-sur-Tille, France

C-09
11:45-12:00
Water Interactions with Actinide Oxide Surfaces
Bengt Tegner[1], Andrew Kerridge[2], Nikolas Kaltsoyannis[1]
[1]The University of Manchester, Manchester, UK, [2]Lancaster University, Lancaster, UK

OR Wed2

11:00-12:00 **Kongreßsaal I** **Chair: Andrew Gaunt**

C-10
11:00-11:15
How does Pu(IV) interact with hyperphosphorylated protein osteopontin ?
Gaëlle Creff[1], Hervé Michel[1], Jérôme Roques[3], Claude Vidaud[2], Christophe Den Auwer[1]
[1]ICN-Université de Nice Sophia Antipolis, Nice, France, [2]CEA Marcoule, Bagnol-sur-Cèze, France, [3]IPN-Université Paris Orsay, Orsay, France

C-11
11:15-11:30
Self-assembly of plutonium sulfate dimers from a chloride matrix
Amy Hixon, Ginger Sigmon
University of Notre Dame, Notre Dame, IN, USA

C-12
11:30-11:45
Coordination polymers of tetravalent neptunium with aromatic polycarboxylate ligands
Nicolas Martin[1], Juliane März[2], Natacha Henry[1], Christophe Volkringer[1,3], Atsushi Ikeda-Ohno[2], Christoph Hennig[2], Thierry Loiseau[1]
[1]Université de Lille, Lille, France, [2]Helmhotz Zentrum Dresden Rossendorf, Dresden, Germany, [3]Institut Universitaire de France, Paris, France

C-13
11:45-12:00
Plutonium Oxide Processing Platform for Nuclear Forensics Applications
David Meier, Joel Tingey, Gregg Lumetta
Pacific Northwest National Laboratory, Richland, WA, USA

INV Wed3

12:00-12:30 **Auditorium** **Chair: Tim Tinsley**

C-14
12:00-12:30
Production of Plutonium-238 for Deep Space Missions
Robert Wham
Oak Ridge National Laboratory, Oak Ridge, TN, USA

INV Wed4

12:00-12:30 **Kongreßsaal I** **Chair: Andrew Gaunt**

C-15
12:00-12:30

Selective Separation of Electrochemically Generated Am(VI
Christopher Dares[1,2], Thomas J Meyer[1], Bruce Mincher[3]
[1]The University of North Carolina at Chapel Hill, Chapel Hill, NC, USA, [2]Florida International University, Miami, FL, USA, [3]Idaho National Laboratory, Idaho Falls, ID, USA

Poster session II & working lunch

12:30-14:15 **Foyer ground floor and**

(continues on Thursday 22/9) **Parkpavillon**

C-29
12:30-14:15

Effect of Doping Level on Dissolution Behavior of Rare-Earth Doped UO_2
Jeongmook Lee[1], Jandee Kim[1], Young-Sang Youn[1], Jong-Goo Kim[1], Sang-Eun Bae[1,2], Yeong-Keong Ha[1], Jong-Yun Kim[1,2]
[1]Korea Atomic Energy Research Institute, Daejeon, Republic of Korea, [2]University of Science and Technology, Daejeon, Republic of Korea

C-30
12:30-14:15

A New Strategy for Stabilizing Uncommon Oxidation States Learned from an Extraordinarily Complex Mixed-Valent Uranium Phosphonate Framework
Chengliang Xiao[1], Lanhua Chen[1], Juan Diwu[1], Thomas E. Albrecht-Schmitt[2], Shuao Wang[1]
[1]Soochow University, Suzhou, Jiangsu, China, [2]Florida State University, Tallahassee, Florida, USA

C-32
12:30-14:15

Lipophilic pyridine-2,6-bis(1H-1,2,3-triazol-4-yl) structure as selective chelating unit for direct actinides extraction from purex raffinate
Annalisa Ossola[1], Eros Mossini[1], Elena Macerata[1], Marco Giola[1], Mario Mariani[1], Arturo Arduini[2], Alessandro Casnati[2]
[1]Politecnico di Milano, Milano, Italy, [2]University of Parma, Parma, Italy

C-33
12:30-14:15

Incorporation of soluble radionuclides into High Oxidation State Actinide Solid Matrix
Yaxing Wang[1], Xuemiao Yin[1], Juan Diwu[1], Thomas E. Albrecht-schmitt[2], Shuao Wang[1]
[1]Soochow University, suzhou, China, [2]Florida State University, talahassee, USA

C-34
12:30-14:15

Recent Investigations of Solid State Chemistry of Actinides at Soochow University
Shuao Wang
Soochow University, Suzhou, China

C-35
12:30-14:15

Vibrational properties of uranium and plutonium
Johann Bouchet, François Bottin, Boris Dorado
Commissariat a l'Energie Atomique, Bruyeres le Chatel, France

C-36
12:30-14:15

A state-of-the-art report within NEA-TDB to assess modeling and experimental approaches in aqueous high ionic-strength solutions

Marcus Altmaier[1], Davide Costa[2], Andrew Felmy[3], Helge Moog[4], Roberto Pabalan[5], Marilena Ragoussi[2], Don T. Reed[6], Wolfgang Runde[7], Punam Thakur[8], Wolfgang Voigt[9]
[1]Karlsruhe Institute of Technology, Institute for Nuclear Waste Disposal (KIT-INE), Karlsruhe, Germany, [2]OECD Nuclear Energy Agency, Boulogne-Billancourt, France, [3]Washington State University, Pullman WA, USA, [4]Gesellschaft für Anlagen- und Reaktorsicherheit, Braunschweig, Germany, [5]U.S. Nuclear Waste Technical Review Board, Arlington VA, USA, [6]Los Alamos National Laboratory, Carlsbad NM, USA, [7]Los Alamos National Laboratory, Los Alamos NM, USA, [8]Carlsbad Environmental Monitoring & Research Center, Carlsbad NM, USA, [9]Technical University of Freiberg, Freiberg, Germany

C-37
12:30-14:15

The OECD/NEA update book on the chemical thermodynamics of U, Np, Pu, Am and Tc

Ingmar Grenthe[1], Xavier Gaona[2], Andrey Plyasunov[3], Linfeng Rao[4], Wolfgang Runde[5], Andrew Felmy[6], Bernd Grambow[7], Rudy Konings[8], Anna L. Smith[9], Emily Moore[8], Kastriot Spahiu[10], Davide Costa[11], Marilena Ragoussi[11]
[1]Royal Institute of Technology, Stockholm, Sweden, [2]Karlsruhe Institute of Technology, Institute for Nuclear Waste Disposal, Karlsruhe, Germany, [3]Institute of Experimental Mineralogy, Russian Academy of Sciences, Moscow, Russia, [4]Lawrence Berkeley National Laboratory, Berkeley, USA, [5]Los Alamos National Laboratory, Los Alamos, USA, [6]Washington State University, Pullman, USA, [7]SUBATECH, Nantes, France, [8]European Commission, JRC, Institute for Transuranium Elements, Karlsruhe, Germany, [9]Delft University of Technology, Delft, The Netherlands, [10]SKB, Stockholm, Sweden, [11]OECD Nuclear Energy Agency (NEA), Paris, France

C-38
12:30-14:15

Solubility, hydrolysis and chloride complexation of Np(V) in alkaline, dilute to concentrated NaCl, MgCl2 and CaCl2 solutions

David Fellhauer, Xavier Gaona, Kathy Dardenne, Marcus Altmaier
Karlsruhe Institute of Technology, Institute for Nuclear Waste Disposal, Karlsruhe, Germany

C-40
12:30-14:15

Examination of actinide (Pu(IV,V,VI), Np(V), and U(VI)) sorption on rutile (TiO_2)

Andreas Schnurr, Brian Powell
Environmental Engineering and Earth Sciences, Clemson University, Clemson, SC, USA

C-41
12:30-14:15

Evolution of the morphology of $(U_{0.45}Pu_{0.55})O_2$ powder during dissolution in nitric acid

Gilles Leturcq, Alexis Neuschwander, Yannis Ziouane, Bénédicte Arab-Chapelet
CEA, Marcoule, France

C-42
12:30-14:15

Overview: National Research Laboratory in Nuclear Forensic from México

Héctor Hernández-Mendoza, Elizabeth Teresita Romero-Guzmán
Instituto Nacional de Investigaciones Nucleares, Estado de México, Mexico

C-43
12:30-14:15

Diffusion Characteristics of Surrogate Nuclear Material Alloys

John Auxier II[1,2], Christopher Eley[1,2], Joshua Gurka[1,2], Duncan Brocklehurst[1,2], Howard Hall[1,2]
[1]Radiochemistry Center of Excellence, Knoxville, TN, USA, [2]Institute for Nuclear Security, University of Tennessee, Knoxville, TN, USA

C-44
12:30-14:15

benchmark spherical critical assemblies with PLUTONIUM metal ^{239}Pu (98 %) in δ - phase core and compound reflectors

Alexey Kaygorodov, Sergey Vorontsov, Mikhail Kuvshinov, Valentin Khoruzhyi
RFNC-VNIIEF, Sarov, Nizhny Novgorod Region, Russia

C-45
12:30-14:15

Characterization of Ce, U, and Pu Metal Produced by Calcium Reduction

Kaylyn McCoy[1,2], William Karl Pitts[1], Amanda Casella[1], Calvin Delegard[1]
[1]Pacific Northwest National Laboratory, Richland, WA, USA, [2]University of Utah, Salt Lake City, UT, USA

C-46
12:30-14:15

The Multi-Isotope Process Monitor: Deployment at the H-Canyon Nuclear Separation Facility

David Meier[1], Lindsay Sexton[2], Jamie Coble[3]
[1]Pacific Northwest National Laboratory, Richland, WA, USA, [2]Savannah River National Laboratory, Aiken, SC, USA, [3]University of Tennessee-Knoxville, Knoxville, TN, USA

C-47
12:30-14:15

Investigation of the Electronic Structure of Transuranic Elements Utilizing a Redox Active Ligand.

Shane S. Galley[1], Scott A. Pattenaude[2], Suzanne C. Bart[2], Thomas E. Albrecht-Schmitt[1]
[1]Florida State University, Tallahassee, Fl, USA, [2]Purdue University, West Lafayette, IN, USA

C-48
12:30-14:15

Fast neutron multiplicity counting with zero accidentals

Rashed Sarwar[1], Malcolm J Joyce[1], Colin H Zimmerman[2]
[1]Engineering Department, Lancaster University, Lancaster, Lancashire, UK, [2]Central Laboratory, National Nuclear Laboratory, Sellafield, Cumbria, UK

C-49
12:30-14:15

Synthesis and Vapor Pressure Determination of Volatile Quadrivalent Neptunium Complexes

Aaron Johnson, Jacon Davies, Kevin Carney
Idaho National Laboratory, Idaho Falls, Idaho, USA

C-50
12:30-14:15

Simulant corium materials for investigations in the frame of severe accident studies

Alice Seibert[1], David Bottomley[1], Dario Manara[1], Sara Mastromarino[2], Luca Soldi[3], Emtethal Kassim[1], Damien Prieur[1], Phillippe E. Raison[1], Thierry Wiss[1], Didier Pellotiero[1], Joseph Somers[1], Vincenzo V. Rondinella[1]
[1]Europäische Kommission, Joint Research Centre, Institut für Transurane, Karlsruhe, Germany, [2]Delft University of Technology Faculty of Applied Sciences, Nuclear Energy and Radiation Applications, Delft, The Netherlands, [3]Politecnico di Milano, Energy Department, Milan, Italy

C-51
12:30-14:15

New insight in the Am-O phase diagram by coupling experimental HT-XRD and Calphad thermodynamic modelling

Enrica Epifano[1], Romain Vauchy[1], Renaud C. Belin[3], Florent Lebreton[1], Alexis Joly[1], Christine Guéneau[2], Philippe Martin[1]
[1]DEN/DTEC/SECA/LCC CEA, Cadarache Saint-Paul-Lez-Durance, France, [2]DEN/DPC/SCCME/LM2T CEA, Saclay Gif-sur-Yvette, France, [3]DEN/DEC/SESC/LLCC, Cadarache Saint-Paul-Lez-Durance, France

C-52
12:30-14:15

Structure and stability of EDTMP and DOTMP complex with Th(IV) for nuclear medicine

Tomoo Yamamura[1], Masaru Furuya[1], Suguru Ohta[1], Koshin Washiyama[2]
[1]Institute for Materials Research, Tohoku University, Sendai, Miyagi, Japan, [2]School of Health Sciences, Faculty of Medicine, Kanazawa University, Kanazawa, Ishikawa, Japan

C-53
12:30-14:15

Assessment of PuO_2^{2+} solubility in high borate media

Mark Silver
Florida State University, Tallahassee, Florida, USA

C-54
12:30-14:15

Elastic Modulii of Various Innovative Fuel Materials

Tarik A. Saleh, Joshua White, Ursula Caraval Nunez, Laura A. Tucker, Ryan Leon
Los Alamos National Laboratory, Los Alamos, NM, USA

C-55
12:30-14:15

Aging Effects Interacting with Microstructure

Saryu Fensin, Steve Valone
Los Alamos National Lab, Los Alamos, NM, USA

C-56
12:30-14:15

Electrical transport in uranium compounds $URhX_5$ (X = Ga, In)

Yoshinori Haga[1], Yuji Matsumoto[2], Naoyuki Tateiwa[1], Etsuji Yamamoto[1], Jiri Pospisil[1], Zachary Fisk[3]
[1]Japan Atomic Energy Agency, Tokai, Japan, [2]Nagoya Institute of Technology, Nagoya, Japan, [3]University of California, Irvine, Irvine, USA

C-57
12:30-14:15

Experimentally Validated Casting Simulations of Unalloyed Plutonium

Meghan Gibbs, Deniece Korzekwa
Los Alamos National Laboratory, Los Alamos, NM, USA

C-58
12:30-14:15

Magnetic susceptibility and fluctuations of the electron density in the δ-plutonium

Arkadij Volkov, Aleksandr Povzner
Ural Federal University, Ekaterinburg, Russia

C-59
12:30-14:15

Modeling and validation of the Pu 239 surface alpha spectrum using MCNPX coupled with CINDER'90LA-UR-16-23017

Laura A. Tucker, Scott Richmond, Tarik A. Saleh
Los Alamos National Laboratory, Los Alamos, NM, USA

C-60
12:30-14:15

Effects of Aqueous Phase Complexants on Lanthanide and Actinide Oxalate Solubilities

Hannah Colledge, Cheryl Carrigan, Robin Taylor, Mark Sarsfield
National Nuclear Laboratory, Cumbria, UK

C-61
12:30-14:15

Characterization of *f*-element oxide stoichiometry and phases through Raman Spectroscopy

Jared Stritzinger, George Goff, Dave Wayne
Los Alamos National Laboratory, Los Alamos, NM, USA

C-62
12:30-14:15

Physical Properties and Nuclear Magnetic Resonance of Antiferromagnetic $PuPt_3$
Eric D. Bauer[1], Andrew M. Mounce[1], Adam P. Dioguardi[1], Paul H. Tobash[1], Jeremy Mitchell[1], Thomas E. Albrecht-Schmitt[2], Joe D. Thompson[1]
[1]Los Alamos National Laboratory, Los Alamos, NM, USA, [2]Florida State University, Tallahassee, FL, USA

C-64
12:30-14:15

Complexation Behavior and Solubility of the Ternary Systems Ca/Mg-UO_2-CO_3 under Weakly Alkaline Conditions
Jun-Yeop Lee[1], Marika Vespa[1], Ezgi Yalcintas[1], Xavier Gaona[1], Kathy Dardenne[1], Jörg Rothe[1], Thomas Rabung[1], Marcus Altmaier[1], Jong-Il Yun[2]
[1]KIT-INE, Karlsruhe, BW, Germany, [2]KAIST, Daejeon, Daejeon, Republic of Korea

C-65
12:30-14:15

Physical nature of light actinides longevity in the dynamic failure phenomenon
Alexandr Uchaev, Nadezda Selchenkova, Valeriy Punin, Elena Kosheleva
Russian Federal Nuclear Center – VNIIEF, Sarov, Russia

C-66
12:30-14:15

Effect of geometry and time-amplitude characteristics of external high-intensity action on metals longevity employed in the nuclear power engineering
Alexandr Uchaev, Valeriy Punin, Nadezda Selchenkova, Elena Kosheleva
Russian Federal Nuclear Center – VNIIEF, Sarov, Russia

C-67
12:30-14:15

Measurement of the diffusivity and permeability of hydrogen in plutonium
Scott Richmond
Los Alamos National Laboratory, Los Alamos, NM, USA

C-31
12:30-14:15

Uranium-hydride initiation iimes before and after outgassing in vacuum at 300 C to determine the influence of hydrogen content in uranium on hydride initiation time.
Wigbert J. Siekhaus
Lawrence Livermore National Laboraoty, Livermore, USA

PL Wed2

14:15-15:00 **Auditorium** **Chair: Dominique Warin**

C-16
14:15-15:00

Reprocessing and beyond --- the management of spent oxide and Magnox fuel in the UK held by the NDA
Danny Fox
Nuclear Decommissioning Authority, Moor Row, Cumbria, UK

INV Wed5

15:05-15:35 **Auditorium** **Chair: Dominique Warin**

C-17
15:05-15:35

Gas-Phase Reactions of Water with Actinide Dioxide Cations, PaO_2^+ to CfO_2^+: The "Enigmatic" Behavior of Plutonium
John K. Gibson[1], Monica Vasiliu[2], Phuong Diem Dau[1], Richard Wilson[3], Kirk Peterson[4], David Dixon[2]
[1]Lawrence Berkeley National Laboratory, Berkeley, California, USA, [2]University of Alabama, Tuscaloosa, Alabama, USA, [3]Argonne National Laboratory, Argonne, Illinois, USA, [4]Washington State University, Pullman, Washington, USA

INV Wed6

15:05-15:35 **Kongreßsaal I** **Chair: Alexander Shick**

C-18
15:05-15:35

Thermal expansion study of the heavy-fermion superconductor 242PuCoGa5

Rachel Eloirdi[1], Nicola Magnani[1], Carlotta Giacobbe[2], Pedro Amador Celdran[1], Jean-Christophe Griveau[1], Eric Colineau[1], Gerard H. Lander[1], Roberto Caciuffo[1]
[1]European Commission, Joint Research Centre (JRC), Institute for Transuranium Elements (ITU), Karlsruhe, Germany, [2]European Synchrotron Radiation Facility, Grenoble, France

OR Wed3

15:35-16:05 **Auditorium**

C-19
15:35-15:50

Electrode reduction of actinyl ions followed by deposition in weak acid solution

Yoshihiro Kitatsuji, Kazuki Ouchi, Haruyoshi Otobe
Japan Atomic Energy Agency, Tokai, Ibaraki 319-1195, Japan

C-20
15:50-16:05

Numerical Simulation on Breeding and Burning Process of Plutonium in Fusion Fission Hybrid Reactor for Energy(FFHR-E)

Xueming Shi, Xianjue Peng
Institute of Applied Physics and Computational Mathematics, Beijing, China

OR Wed4

15:35-16:05 **Kongreßsaal I** **Chair: Alexander Shick**

C-21
15:35-15:50

Thermodynamic Properties of Pu as a Function of Ga Content

Daniel Schwartz, Jeremy Mitchell, Franz Freibert
Los Alamos National Laboratory, Los Alamos, New Mexico, USA

C-22
15:50-16:05

A Temperature Investigation of δ-phase ^{239}Pu-Ga Alloys

Alice I. Smith[1], Adrian S. Losko[1,2], Sven C. Vogel[1], Scott Richmond[1], Michael Ramos[1]
[1]Los Alamos National Laboratory, Los Alamos, NM, USA, [2]University of California Berkeley, Berkeley, CA, USA

Coffee break

16:05-16:30 **Parkpavillon**

INV Wed7

16:30-17:30 **Auditorium** **Chair: Dominique Warin**

C-23
16:30-17:00

Experimental studies to support storage of PuO_2 in the UK

Colin Gregson[1], Robin Orr[1], Howard Sims[2], Robin Taylor[1], Kevin Webb[1], David Woodhead[1], Paul Cook[3], Jeff Hobbs[3], Helen Steele[3]
[1]National Nuclear Laboratory, Sellafield, Cumbria, UK, [2]National Nuclear Laboratory, Culham Science Park, Abingdon, Oxfordshire, UK, [3]Sellafield Ltd, Sellafield, Cumbria, UK

C-24
17:00-17:30

Irradiation testing of fuels for plutonium and minor actinide transmutation
P. Ralph Hania
NRG, Petten, The Netherlands

INV Wed8

16:30-17:30 **Kongreßsaal I** **Chair: Alexander Shick**

C-25
16:30-17:00

How alpha decays of actinides will affect the nuclear glass structure: evidence of competitive effects between damage generation from recoil nuclei and recovery processes from alpha particles
Sylvain Peuget[1], Anamul Haq Mir[1], Thibault Charpentier[2], Laura Martel[3], Joseph Somers[3], Thierry Wiss[3], Jean-Marc Delaye[1], Marcel Toulemonde[4], Serge Bouffard[4], Christophe Jégou[1]
[1]CEA, DEN, DTCD, SECM, Laboratoire d'Étude des Matériaux et Procédés Actif, Bagnols sur Cèze, France, [2]NIMBE, CEA, CNRS, Université Paris-Saclay, CEA Saclay, Gif sur Yvette, France, [3]European Commission, Joint Research Centre (JRC), Institute for Transuranium Elements (ITU), Karlsruhe, Germany, [4]CIMAP-GANIL (CEA-CNRS-ENSICAEN-Univ. Caen), Caen, France

C-26
17:00-17:30

Recent progress in actinide phosphates chemistry
Karin Popa[1], Gilles Wallez[2], Damien Bregiroux[2], Philippe E. Raison[1], Laura Martel[1], Yulia Arinicheva[3], Stefan Neumeier[3], Joseph Somers[1], Rudy Konings[1]
[1]European Commission, Joint Research Centre, Institute for Transuranium Elements, Karlsruhe, Germany, [2]Sorbonne Universités, UPMC Univ Paris, Paris, France, [3]Forschungszentrum Jülich, IEK-6, Juelich, Germany

OR Wed5

17:30-17:45 **Auditorium** **Chair: Dominique Warin**

C-27
17:30-17:45

Chemical bond nature in $Cs_2AnO_2Cl_4$
Yury Teterin[1,3], Anton Teterin[1], Kirill Ivanov[1], Mikhail Ryzhkov[2], Konstantin Maslakov[3], Stepan Kalmykov[3], Vladimir Petrov[3], Dmitry Suglobov[3]
[1]NRC "Kurchatov Institute", Moscow, Russia, [2]Ural Department of RAS, Institute of Solid State Chemistry, Ekaterinburg, Russia, [3]Radiochemistry Division, Chemistry Department, Lomonosov Moscow State University, Moscow, Russia, [4]V.G. Khlopin Radium Institute, St.-Petersburg, Russia

OR Wed6

17:30-17:45 **Kongreßsaal I** **Chair: Alexander Shick**

C-28
17:30-17:45

Integrated surface science lab station for spent corrosion studies
Thomas Gouder, Rachel Eloirdi, Frank Huber, Roberto Caciuffo
European Commission, Joint Research Centre, Institute for Transuranium Elements, Karlsruhe, Germany

Thursday 22/9

PL Thu1

08:40-09:25 Auditorium **Chair: Gerard Lander**

D-01 08:40-09:25
Synthetic Transuranic Chemistry: Bridging the Knowledge Gap to Uranium
Andrew Gaunt
Los Alamos National Laboratory, Los Alamos, New Mexico, USA

INV Thu1

09:30-10:30 Auditorium **Chair: Gerard Lander**

D-02 09:30-10:00
Role of atomic multiplets in intermediate valence PuB_6
Alexander B. Shick[1], Ladislav Havela[2], Alexander I. Lichtenstein[3], Mikhail I. Katsnelson[4]
[1]Institute of Physics ASCR, Prague, Czech Republic, [2]Charles University, Prague, Czech Republic, [3]University of Hamburg, Hamburg, Germany, [4]Radboud University, Nijmegen, The Netherlands

D-03 10:00-10:30
Resonant Inelastic X-ray Scattering of Actinide Materials
Kristina Kvashnina[1,2]
[1]The European Synchrotron, Grenoble, France, [2]Helmholtz-Zentrum Dresden-Rossendorf, Dresden, Germany

INV Thu2

09:30-10:30 Kongreßsaal I **Chair: T. Albrecht-Schmitt**

D-04 09:30-10:00
Synthesis, reactions, and structures of gas-phase actinide oxide nitrate complexes: Relative stabilities and An oxidation states in $AnO_3(NO_3)_2^-$ (An = U, Np, Pu)
Rémi Maurice[1], Eric Renault[2], Phuong Diem Dau[3], Yu Gong[3], Philip X. Rutkowski[3], John K. Gibson[3]
[1]SUBATECH, UMR CNRS 6457, IN2P3/EMN Nantes/Université de Nantes, Nantes, France, [2]CEISAM, UMR CNRS 6230, Université de Nantes, Nantes, France, [3]Chemical Sciences Division, Lawrence Berkeley National Laboratory, Berkeley, California, USA

D-05 10:00-10:30
Redox chemistry of Pu, Np and U under alkaline to hyperalkaline pH conditions
Xavier Gaona
Karlsruhe Institute of Technology, Institute for Nuclear Waste Disposal, Karlsruhe, Germany

Coffee break

10:30-11:00 Parkpavillon

OR Thu1

11:00-12:00 Auditorium **Chair: Gerard Lander**

D-06 11:00-11:15
Towards explaining anomalous properties of unalloyed and alloyed Pu appearing after the long-term storage at the liquid He temperature
Boris Nadykto
Russian Federal Nuclear Center VNIIEF, Sarov, Russia

D-07 11:15-11:30
Probing He bubbles in naturally aged and annealed δ-Pu alloys using small-angle x-ray scattering
Jason R. Jeffries[1], Tony van Buuren[1], Trevor Willey[1], Mark A. Wall[1], Dave Ruddle[1], Jan Ilavsky[2], Patrick Allen[1]
[1]Lawrence Livermore National Laboratory, Livermore, CA, USA, [2]Argonne National

Laboratory, Argonne, IL, USA

D-08 11:30-11:45 Oxidation states of Plutonium: Recent Studies in Inorganic Compounds
Denis Bykov[2], Anna L. Smith[2], Karin Popa[1], Damien Prieur[1], Philippe Martin[3], Rudy Konings[1], Philippe E. Raison[1]
[1]European Commission- JRC-ITU, Karlsruhe, Germany, [2]Delft University of Technology, Delft, The Netherlands, [3]Commissariat à l'Energie Atomique. CEA-DEC, Saint Paul Lez Durance, France

D-09 11:45-12:00 Synthesis, Structure, and Characterization of a Pair of Berkelium Iodates: Developments in assessing bonding character in actinides beyond Plutonium
Mark Silver
Florida State University, Tallahassee, Florida, USA

OR Thu2

11:00-12:00 Kongreßsaal I **Chair: T. Albrecht-Schmitt**

D-10 11:00-11:15 First-principles studies of plutonium oxides and their surface interactions with gaseous molecules
Ping Zhang
Institute of Applied Physics and Computational Mathematics, Beijing, China

D-11 11:15-11:30 Radiolysis of H_2-O_2 mixtures at the interface with ceramic oxides
Luke Jones[1], Howard Sims[2], Robin Orr[3], Simon Pimblott[1]
[1]University of Manchester, Moor Row, Cumbria, UK, [2]National Nuclear Laboratory, Abingdon, Oxfordshire, UK, [3]National Nuclear Laboratory, Seascale, Cumbria, UK

D-12 11:30-11:45 Preparation and Characterization of Intrinsic Plutonium Colloids by Sonolysis of PuO_2 in Water
Elodie Dalodière[1], Matthieu Virot[1], Vincent Morosini[1], Tony Chave[1], Thomas Dumas[2], Christoph Hennig[3], Thierry Wiss[4], Oliver Dieste Blanco[4], Tolek Tyliszcak[5], David Shuh[5], Laurent Venault[2], Philippe Moisy[2], Sergey I. Nikitenko[1]
[1]Institut de chimie separative de Marcoule, bagnols sur ceze, France, [2]CEA, nuclear energy division, bagnols sur ceze, France, [3]Helmholtz zentrum dresden-rossendorf, Dresden, Germany, [4]European commission JRC ITU, Karlsruhe, Germany, [5]Advanced light source LBNL, Berkeley, USA

D-13 11:45-12:00 Spectroscopic and Mass Spectral Characterization of Uranium Fluoroanions Formed from an Ionic Liquid
Christoper Zarzana[1], Gary Groenewold[1], Michael Benson[1], Kristyn Johnson-Roscioli[1], Jonathan Martens[2], Jos Oomens[2], Rika Hagiwara[3], Tetsuya Tsuda[4]
[1]Idaho National Laboratory, Idaho Falls, Idaho, USA, [2]Radboud University, Institute for Molecules and Materials, FELIX Laboratory, Nijmegen, The Netherlands, [3]Kyoto University, Kyoto, Japan, [4]Osaka University, Suita, Suita, Japan

INV Thu3

12:00-12:30 Auditorium **Chair: Gerard Lander**

D-14 12:00-12:30 Electronic Structure of PuTe and Related Materials from Photoemission
John Joyce[1], Kevin Graham[1], Tomasz Durakiewicz[1], Gerard H. Lander[2], Miles Beaux[1], Paul H. Tobash[1], Eric D. Bauer[1], Jeremy Mitchell[1], Scott Richmond[1]
[1]Los Alamos National Laboratory, Los Alamos, NM, USA, [2]European Commission, Joint Research Centre, Institute for Transuranium Elements, Karlsruhe, Germany

INV Thu4

12:00-12:30 Kongreßsaal I **Chair: T. Albrecht-Schmitt**

D-15 12:00-12:30 Exploring actinide recognition, sensitization, and cellular uptake by bio-inspired platforms
Rebecca Abergel
Lawrence Berkeley National Laboratory, Berkeley, CA, USA

Poster session II & working lunch

12:30-14:15 Foyer ground floor and Parkpavillon

PL Thu2

14:15-15:00 Auditorium **Chair: Claude Guet**

D-16 14:15-15:00 Examination of aging processes occurring during plutonium sorption to solid phases
Brian Powell
Clemson University, Anderson, SC, USA

INV Thu5

15:05-15:35 Auditorium **Chair: Claude Guet**

D-17 15:05-15:35 characterization of actinides oxides by raman spectroscopy: from model systems to real spent fuel
Christophe Jégou[1], Sylvain Peuget[1], Sandrine Miro[1], Zeynep Talip[1], Lionel Desgranges[2], Ritesh Mohun[2], Guillaume Guimbretière[3], Aurelien Canizares[3], Patrick Simon[3]
[1]CEA DEN DTCD, 30207 Bagnols sur Ceze Cedex, France, [2]CEA DEN DEC, 13108 Saint Paul Lez Durance Cedex, France, [3]CNRS UPR3079 CEMHTI, 45071 Orleans Cedex, France

INV Thu6

15:05-15:35 Kongreßsaal I **Chair: Mark Sarsfield**

D-18 15:05-15:35 Identification of Processes Controlling Pu Transport Behavior Under Field Conditions
Annie Kersting
LLNL, Livermore, CA, USA

OR Thu3

15:35-16:05 Auditorium **Chair: Claude Guet**

D-19 15:35-15:50 Study of combustion synthesis of solid solutions $(U_{1-y}An/Ln_y)O_{2\pm x}$ under air atmosphere
Guillaume Peter-Soldani[1], Eléonore Welcomme[1], Xavier Deschanels[2], Francis Abraham[3], Stéphane Grandjean[4]
[1]CEA, DEN, DRCP/SERA/LCAR, F-20207 Bagnols-sur-Cèze Cedex, France, [2]CEA, DEN, DRCP/ICSM/LNER, F-20207 Bagnols-sur-Cèze Cedex, France, [3]Université Lille Nord de France- UCCS/UMR CNRS 8181 ENSCL-USTL, F-59652 Villeneuve d'Ascq Cedex, France, [4]CEA, DEN, DRCP, F-20207 Bagnols-sur-Cèze Cedex, France

D-20 15:50-16:05 Synthesis and dissolution of mixed oxides $(U_{1-x}Pu_x)O_2$ with different morphologies
Yannis Ziouane, Gilles Leturcq, Bénédicte Arab-Chapelet, Sophie Lalleman
CEA, Marcoule, France

OR Thu4

15:35-16:05 Kongreßsaal I **Chair: Mark Sarsfield**

D-21 15:35-15:50 Differential sorption behavior of U(VI) and Pu(VI) dependent on their redox chemistry
Stefan Hellebrandt[1], Karah E. Knope[2,5], Sang Soo Lee[2], Aaron J. Lussier[3], Joanne E. Stubbs[4], Peter J. Eng[4], Lynda Soderholm[2], Paul Fenter[2], Moritz Schmidt[1]
[1]Helmholtz-Zentrum Dresden-Rossendorf, Dresden, Saxony, Germany, [2]Argonne National Laboratory, Lemont, IL, USA, [3]University of Notre Dame, Notre Dame, IN, USA, [4]University of Chicago, Chicago, IL, USA, [5]Georgetown University, Washington, DC, USA

D-22 15:50- Synthesis and structural characterization of a new water soluble actinide(IV) hexanuclear cluster $[An_6(OH)_4O_4]^{12+}$ (with An(IV) = U(IV), Np(IV), Pu(IV)).

16:05 *Christelle Tamain[1], Thomas Dumas[1], Dominique Guillaumont[1], Christoph Hennig[2], Philippe Guilbaud[1]*
[1]CEA, Nuclear Energy Division, Marcoule, RadioChemistry & Processes Department, F-30207 Bagnols sur Cèze, France, [2]Helmholtz-Zentrum Dresden-Rossendorf, Institute of Resource Ecology, Bautzner Landstr. 400, D-01314 Dresden, Germany

Closing Ceremony

16:05-16:30 Auditorium (basement floor)

Abstracts

A-01

Racah materials: atomic multiplets and f-bands

Alexander B. Shick[1], Jindrich Kolorenc[1], Mikhail I. Katsnelson[2], Alexander I. Lichtenstein[3]

[1]Institute of Physics, ASCR, Na Slovance 2, CZ-18221 Prague, Czech Republic, [2]Radboud University Nijmegen, Heyendaalseweg 135, 6525 AJ Nijmegen, The Netherlands, [3]Institute for Theoretical Physics, University of Hamburg, 20355 Hamburg, Germany

The theoretical description of many actinide systems with strongly interacting f-electrons is still far from being perfect. The local density approximation scheme often fails for correlated materials containing f-elements with complicated spectral function. Dynamical mean field theory in combination with the first-principle scheme which takes into account full non-spherical local interaction vertex for f-shell can resolve the long-standing mystery of the nonmagnetic state of delta-Pu. Combination of atomic-like multiplets and pronounced hybridization to conducting bands are essential to describe complicated electronic structure of many actinide systems. Comparison with experimental photoemission spectra support the crucial role of complex spin-orbital multiplets from f-configurations in such Racah materials.

A-02

Phase stability, elasticity, and phonons for plutonium from electronic-structure theory

Per Soderlind

Lawrence Livermore National Laboratory, Livermore, CA, USA

We apply electronic-structure theory to compute phase stability, elasticity, and phonons for plutonium. The model accurately predicts this very broad range of properties for plutonium because the character of the 5f electrons is very well captured by itinerant (band-like) states that are perturbed by spin and orbital interactions. The computed total energy is obviously quite accurate because otherwise phase stability, elastic constants, and lattice dynamics could not be computed realistically.

This work was performed under the auspices of the U.S. DOE by LLNL under Contract DE-AC52-07NA27344.

A-03

Plutonium as a Mixed Valent Metal

Gabriel Kotliar

Department of Physics and Astronomy, Rutgers University, Piscataway, NJ, USA

The combination of modern implementations of electronic structure methods in conjunction with Dynamical Mean Field Theory (DMFT) in combination with massively parallel computers, are giving new system specific insights into the properties of strongly correlated electron sytems.

The predictions of this "theoretical spectroscopies" can be directly compared with experimental results, and give insights into previously untractable problems.

In this talk I will briefly outline the state of the art of this methodology focusing on the determination of the inelastic neutron scattering spectra of the delta phase of Pu. We will stress how the theory and the experiments fits with the Dynamical Mean Field Theory physical picture of plutonium as a mixed valent metal, and with previous theoretical calculations on this material.

A-04

Multi-Actinides analysis with AMS: a novel method for ultra-trace determination and small sample sizes

Francesca Quinto[1], Markus Lagos[1], Markus Plaschke[1], Thorsten Schäfer[1], Peter Steier[2], Horst Geckeis[1]

[1]Karlsruhe Institute of Technology (KIT), Institute for Nuclear Waste Disposal (INE), Eggenstein Leopoldshafen, Germany, [2]University of Vienna, VERA Laboratory, Faculty of Physics-Isotope Research and Nuclear Physics, Vienna, Austria

Introduction

The knowledge of the environmental behaviour of uranium, neptunium, plutonium and americium is of great relevance for the safe geological disposal of nuclear waste. In particular, ^{236}U ($t_{1/2}$ = 2.342 x 10^7 y), ^{237}Np ($t_{1/2}$ = 2.144 x 10^6 y), ^{239}Pu ($t_{1/2}$ = 24110 y), ^{240}Pu ($t_{1/2}$ = 6563 y), ^{242}Pu ($t_{1/2}$ = 3.733 x 10^5 y), ^{241}Am ($t_{1/2}$ = 432.2 y) and ^{243}Am ($t_{1/2}$ = 7370 y) are among the main contributors to the long term radiotoxicity of irradiated nuclear fuel. Such long-lived nuclides are not only inherent to the nuclear fuel cycle but are as well widespread in the environment at ultra-trace concentrations, commonly below ppq levels, as consequence of the fallout from atmospheric nuclear testing (AD 1945 – 1980). Trace concentrations of actinides are also employed in the setup of *in situ* tracers experiments, like the Colloid Formation and Migration (CFM) Project at the Grimsel Test Site (http://www.grimsel.com/gts-phase-vi/cfm-section).

The analytical capability of investigating actinides in natural samples below ppq levels can, therefore, be exploited in the study of their environmental behaviour, both in the frame of *in situ* tracers tests and diffusion experiments and in the determination of ultra-trace contamination of the environment from global fallout and nuclear reprocessing.

Accelerator mass spectrometry (AMS) enables an extremely high suppression of interferences from molecular isobars and tailing from neighbouring abundant masses. In this way, the actinide nuclides can be unambiguously determined with detection limits at a value of 10^4 atoms in a sample [1] and with abundance sensitivities for ^{236}U, ^{237}Np and ^{239}Pu relative to ^{238}U at levels ≤ 10^{-15} [2]. Exploiting such an advantageous abundance sensitivity, we have developed a novel analytical method consisting in the simultaneous determination of several actinide nuclides without previous chemical separation from each other and with the use of non-isotopic tracers for the ultra-trace determination of ^{237}Np and ^{243}Am [3].

The investigation of ^{237}Np and ^{243}Am at ultra-trace levels is, in fact, particularly challenging due to the non-availability of pure enough isotopic yield tracers for their mass spectrometric determination. In the actual method the use of non-isotopic tracers is combined with a simplified chemical procedure, namely one concentration step using $Fe(OH)_3$ as actinides scavenger, that once converted to oxides, is directly used as sample material for AMS measurements. In this way different actinide nuclides can be measured sequentially from the same AMS sample. Such simplified chemical treatment is favoured by the reduced amount of matrix elements that is a consequence of the small sample size required for the analysis. We will present the recent findings from the application of the multi-actinide analysis with AMS to the *in situ* tracers experiments at the Grimsel Test Site and, with the aid of this example, discuss the advantages and drawbacks of the actual method.

Multi-actinide analysis with AMS applied to the CFM Project – in situ tracers tests

At the Grimsel Test Site, two *in situ* tracers tests (run 12-02 and run 13-05) devoted to investigate the colloid mediated transport and retention of actinides in near natural flow conditions were performed in 2012 and 2013, . In these experiments ^{233}U, ^{237}Np, ^{242}Pu and

^{243}Am, among other radionuclides dissolved in a solution of Grimsel groundwater, were injected into dipoles of a water conducting granodiorite shearzone fracture in the presence of bentonite colloids. Groundwater samples were continuously collected at the exit of the dipole and the concentration of the injected actinides in the eluted samples was investigated with SF-ICPMS. In this way a dense group of data describing the peak of the breakthrough curves were obtained limited to ca. one month from the injection of the actinide tracers. In the tailing of the curves the actinides were present in the samples at levels lower than the detection limits of the employed SF-ICPMS, equal to 10 ppb (ca. 2x 10^7 atoms of an actinide nuclide).

The limited sample size, which for the actual study was of 250 ml, taken together the ultra-trace concentration of the actinides required the use of an appropriately sensitive analytical technique. In order to investigate the behaviour of the actinides in the tailing of the breakthrough curves below the detection limits of SF-ICPMS, the multi-actinide analysis with AMS was employed. Furthermore, a chosen group of groundwater samples belonging to the peak of the breakthrough curve of run 13-05 and previously analysed with SF-ICPMS were investigated with AMS.

The groundwater samples were sized according to the expected concentration of the actinides from 0.1 ml to 250 ml. ^{233}U, ^{237}Np and ^{242}Pu were determined by using ^{239}Pu as yield tracer, while ^{243}Am by using ^{248}Cm. In order to normalize the measured concentrations relative to the corresponding yield tracer, the chemical and the ionization yields of the five actinides in the Cs negative ions sputtering source of AMS were obtained according to the procedure described in [3]. The method was validated with the determination of ^{236}U, ^{237}Np, ^{239}Pu and ^{242}Pu using ^{233}U as yield tracer in the Reference Material IAEA-443, radionuclides in Irish Seawater.

The determination of the ^{233}U, ^{237}Np, ^{242}Pu and ^{243}Am in the groundwater samples was possible with AMS over six orders of magnitude, in particular from 10 ppt down to 0.1 ppq. The lowest concentrations corresponded to the last sampling time at ca. six and eight months after the injection of the actinide tracers in run 12-02 and run 13-05, respectively.

With the sensitivity of AMS, actinides nuclides can be determined at levels down to 10^5 atoms in a sample with a relative statistical uncertainty of ca. 32%. Similarly, the detection of 10^7 atoms is associated to an error of ca. 0.02%. The use of non-isotopic tracers has led to a higher uncertainty in the determination of ^{233}U, ^{237}Np and ^{243}Am than of ^{242}Pu. In fact, the relative uncertainties of the measured values of ^{242}Pu, solely due to counting errors, were equal to ca. 1 to 5%. The uncertainty propagation associated to the ionization yield of Np relative to Pu and Am relative to Cm resulted in errors of ca. 10 - 16 % and 12 - 24% on the measured concentrations of ^{237}Np and ^{243}Am, respectively. The variability of the ionization yield of U relative to Pu has been higher, so that for the concentrations of ^{233}U an uncertainty of up to 35% was obtained.

However, even considering such high relative uncertainty, the multi-actinide analysis with AMS enabled the quantitative determination of ^{233}U, ^{237}Np and ^{243}Am far below the detection limits of SF-ICPMS, making possible field studies of multiple actinide tracers at unrivaled low concentration levels. Such an analytical capability is of particular importance when investigating samples that are unique and available to the study only in a limited size. These findings prove that the behaviour of actinide tracers can be studied with the developed analytical method in samples collected up to eight months after the start of the experiments, providing extremely valuable information on their long-term retention and migration under geochemical conditions expected in crystalline formations at near natural conditions.

References

1. Steier P, Dellinger F, Forstner O, Golser R, Knie K, Kutschera W, et al. Nuclear Instruments and Methods in Physics Research B: 2010;268(7–8):1045-9.

2. Winkler SR, Steier P, Buchriegler J, Lachner J, Pitters J, Priller A, et al. Nuclear Instruments and Methods in Physics Research B: 2015;361:458-64.

3. Quinto F, Golser R, Lagos M, Plaschke M, Schafer T, Steier P, et al. Anal Chem. 2015;87(11):5766-73.

A-05
Non-destructive analysis for Pu accountancy in reprocessing

Jozsef Zsigrai[1], Klaus Lutzenkirchen[1], Artur Muhleisen[1], Magdalena Toma[1], Peter Schwalbach[2], Sotiris Synetos[2]

[1]EC Joint Research Centre, Karlsruhe, Germany, [2]EC Directorate General for Energy, Luxembourg, Luxembourg

Introduction

This work is an overview of non-destructive methods enabling nuclear safeguards inspectors to timely verify the Pu balance in nuclear fuel reprocessing. These methods are equally applied to samples from reprocessing plants and from mixed-oxide (MOX) fuel plants either on-site or in dedicated analytical laboratories. Here we focus on hybrid K-edge densitometry, neutron coincidence counting, calorimetry, and gamma spectrometry.

In order to timely detect or exclude possible Pu diversion scenarios, two on-site laboratories were set up by the European Commission (EC) at the reprocessing plants in Europe [1]. These laboratories are operated by the Joint Research Centre (JRC) on behalf of the EC's Directorate General for Energy (Euratom safeguards). A similar laboratory is run by the International Atomic Energy Agency (IAEA) at a reprocessing plant in Japan. In large Pu handling facilities the flow of items is often followed by automated measurement systems [2]. By a combination of on-site measurements on Pu in items and results from samples analyzed in analytical laboratories, the safeguards authorities can keep track of Pu from chemical separation to MOX fuel fabrication and can ensure that it is not diverted from peaceful uses.

Methods

Hybrid K-edge/K-XRF densitometry

Hybrid K-edge/K-XRF densitometry (HKED) uses X-rays to determine the Pu and U concentration in liquid samples [3, 4]. The Pu in reprocessing plants is available in dissolved form and HKED does not alter the solutions in any way. Therefore HKED provides a non-destructive measurement of the Pu concentration in reprocessing solutions. The term "hybrid" indicates that HKED is a combination of two techniques. The first of them is X-ray transmission spectrometry at the element-specific K-shell absorption edge energies, or shortly K-edge densitometry. The other technique is spectrometry of fluoresced characteristic K-shell X-rays, or shortly K-XRF. For both techniques the measured signal relates to the number of atoms in the observed volume, so one needs the isotopic composition to convert to mass units.

For K-edge densitometry a highly collimated continuous-energy X-ray beam from a 160 kV X-ray tube is sent through the liquid sample. The transmitted spectrum is recorded by a high-resolution high-purity Germanium (HPGe) detector. The abrupt change of the photon mass attenuation coefficient at the binding energy of K-shell electrons produces a sharp edge in the recorded spectrum (Fig. 1a). The height of this edge depends on the concentration of the analyzed element in the solution. The sample spectrum is normalized to the spectrum of a blank sample, and the concentration of the analyte is calculated from the transmission ratio at the corresponding absorption edge. Relative accuracies down to 0.2 % can be achieved by HKED for Pu concentrations around 300 g/L.

For K-XRF the same X-ray beam is used to irradiate the sample and produce X-ray florescence in the elements present in the sample. The fluoresced spectrum is recorded in another HPGe detector (Fig. 1b) The intensity of the K-shell XRF peaks in the spectrum depends on the element concentration. It requires careful sample-type specific calibration to relate the intensity

of the peaks to the concentration. However, if there is much more U than Pu in the solution, the ratio of the Pu and U X-ray peak intensities is used to get the Pu to U mass ratio. In this relative mode the technique is less sensitive to matrix effects and it enables more accurate measurements of the minor element. Using the Pu/U mass ratio measured by K-XRF combined with the U concentration measured by K-edge, the Pu concentration can be obtained with accuracies below 0.5%.

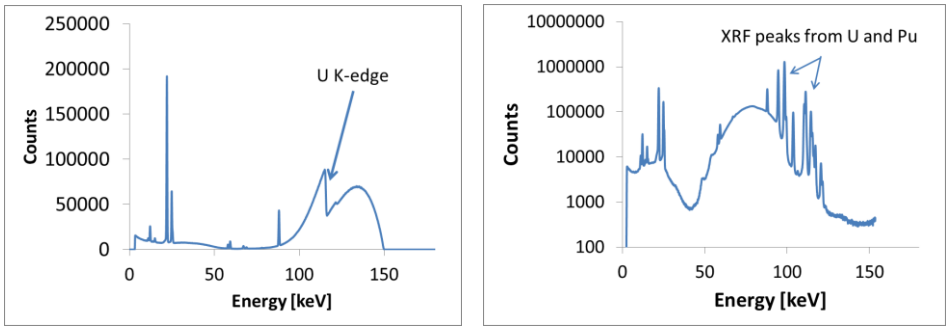

a) b)

Fig. 1. a) Spectrum of photons transmitted through a solution containing about 136 g/L of U and 14 g/L of Pu. The U K-edge is clearly seen, the Pu K-edge is much smaller and hardly visible for this sample. b) X-ray fluorescence spectrum of the same solution showing K-shell XRF peaks from both elements.

Neutron coincidence counting

Neutron coincidence counting (NCC) is used for Pu accountancy when distinct Pu items are available in solid form and on-site dissolution is not feasible. This is the case, e.g. in MOX fuel production facilities. NCC uses the fact that fissile material, including Pu, emits multiple neutrons in each fission. Neutrons are registered in discrete short time intervals called "events". The Pu mass is determined from the number of events in which multiple neutrons are registered within the short time interval. These events are called "coincidences". As each Pu isotope has different neutron emission rate per unit mass, the number of coincidences is calibrated in terms of "^{240}Pu-effective mass". This is the mass of a hypothetical isotopically pure ^{240}Pu sample which would produce the same number of coincidences as the real sample. To get the Pu mass, the ^{240}Pu effective mass is divided by the specific neutron emission rate of the sample.

For registering the neutrons the sample is placed inside a detector that usually contains several proportional counters filled with ^{3}He gas [4, 5]. The signals from the detector are processed by specialized electronics. Counting the coincidences is either done on-the-fly in the electronics ("shift register") or the time stamps of the events are recorded and later analyzed on a computer ("list mode counting") [6]. Due to the large penetrability of neutrons NCC enables timely verification of the Pu content of large bulk items in the field. The EURATOM Safeguards Directorate has many neutron coincidence counters installed in large facilities to follow the flow of Pu-containing items through the facilities [7-8]. However, for detailed material balance evaluations samples from MOX fuel production plants are sent by safeguards inspectors to analytical laboratories for exhaustive analysis.

Calorimetry

Calorimetry for Pu accountancy measures the heat release rate from the decay of Pu isotopes and of the always present ^{241}Am. The measured rate is independent of sample geometry, matrix composition, and of the distribution of Pu in the sample [4, 5]. Therefore, no calibration is needed to convert the measured heat rate to Pu mass. To get the Pu mass, the measured heat

rate is simply divided by the effective specific decay heat of the sample, which is calculated using the known isotopic composition. In solid Pu samples usually no concurrent reactions releasing or consuming heat take place. However, in Pu solutions a large part of decay energy is consumed by radiolysis of the solvent, so calorimetry is not applicable to Pu solutions. So-called small sample calorimeters are used for measuring gram quantities of Pu in MOX pellets and powders, with accuracies close to chemical assay [9]. Calorimeters for kilogram sized samples are used by operators of some nuclear facilities for Pu accountancy [10]. Calorimetry is not yet widely used in international safeguards, but with technological advances it may become a viable option for non-destructive Pu measurements in the field.

Gamma spectrometry

The main application of gamma spectrometry in Pu accountancy is measuring the Pu isotopic composition. All the above-described techniques require the knowledge of the isotopic composition to report results in terms of Pu mass or Pu concentration. In addition, the isotopic composition is valuable information for categorizing the type of Pu (e.g. weapons-grade or reactor-grade). For determining the isotopic composition of Pu by gamma spectrometry high-resolution gamma spectrometers based on high-purity Germanium detectors are routinely applied in accountancy measurements [4, 5]. The applicability of so-called “medium-resolution gamma spectrometers” for Pu isotopic measurements is being evaluated [11]. Computer codes exist that automatically fit the peaks in the Pu spectra and calculate the isotopic composition.

Determining Pu isotopic composition by gamma spectrometry does not require external calibration and it is independent of sample geometry and sample form. To get the isotope ratios, one only needs the peak areas and the ratio of detection efficiencies at different gamma energies. All this information is available from the sample spectrum. Unfortunately, the gamma peaks of ^{242}Pu are not visible in the very complex Pu spectra, so the ^{242}Pu fraction is estimated from empirical correlations. Although the accuracy of gamma spectrometric measurement of the isotopic composition is not as good as that of destructive techniques, gamma spectrometry is an indispensable tool in non-destructive verifications of Pu accountancy.

Conclusion

Non-destructive methods for Pu accountancy help keep track of the Pu balance in reprocessing. The uncertainty of the HKED technique is low enough for material balance evaluations at reprocessing facilities, making the HKED technique the "workhorse" of the on-site laboratories. Other non-destructive techniques, such as neutron coincidence counting, calorimetry and gamma spectrometry, are used for timely on-site verifications and usually they are combined with destructive analyses for detailed material balance evaluations.

References

1. P. Schwalbach, F. Lipcsei, M. Boella, P. Chare, K. Casteleyn, L. Duinslaeger, K. Luetzenkirchen, P. van Belle, E. Zuleger, Y. Aregbe, The EURATOM safeguards on-site laboratories at the reprocessing plants of La Hague and Sellafield – ten years of operation; Proceedings IAEA Symposyum 2010, IAEA-CN-184/241, Vienna (2010), https://www.iaea.org/safeguards/symposium/2010/Documents/PapersRepository/241.pdf Accessed 31th May 2015.

2. P Schwalbach, A Smejkal, D Ancius, M Boella, W Koehne, P Chare, Data Acquisition Systems in Large Nuclear Facilities – challenges, experiences, solutions; Proceedings IAEA Symposyum 2010, IAEA-CN-184/240, Vienna (2010), https://www.iaea.org/safeguards/symposium/2010/Documents/PapersRepository/240.pdf Accessed 31th May 2015.

3. H. Ottmar, H. Eberle, The Hybrid K-Edge / K-XRF Densitometer: Principles - Design – Performance; Report KfK 4590, Kernforschungszentrum Karlsruhe (1991), http://digbib.ubka.uni-karlsruhe.de/volltexte/270030394 Accessed 31th May 2015.

4. K. Casteleyn, H. Ottmar, M. Wallenius, T. Wiss, Selected methods for the Analysis of Plutonium; JRC Report TN2009/39 (2009)

5. Passive Non-Destructive Assay of Nuclear Materials, edited by D. Reilly, N. Ensslin, and H. Smith, Jr., NUREG/CR5550, (1991), http://www.lanl.gov/orgs/n/n1/FMTTD/neut_mc/pdfs/LA_UR_90_0732.pdf Accessed 31th May 2015.

6. D. Henzlova , H. O. Menlove, M. T. Swinhoe, J. B. Marlow, I. P. Martinez, C. D. Rael, Neutron Data Collection and Analysis Techniques Comparison for Safeguards; Proceedings IAEA Symposyum 2010 IAEA-CN-184/129, Vienna (2010), https://www.iaea.org/safeguards/symposium/2010/Documents/PapersRepository/178F.pdf Accessed 31th May 2015.

7. H. Tagziria,_, P. Peerani, P. De Baere, P. Schwalbach, Neutron coincidence counter for the verification of PuO2 cans; Nuclear Instruments and Methods in Physics Research A 580 (2007) 377–379

8. P. Schwalbach, V. Leiner, M. Boella, P. de Baere, F Lipcsei: Current instrumentation for physical verification in nuclear material safeguards as used by DG TREN; Proceedings 29th ESARDA Symposium, Aix en Provence (2007), https://esarda.jrc.ec.europa.eu/index.php?option=com_jifile&filename=NzcyZWE2Mzg2N2I1MjdiMThiZGZlNGZjYzhhMTFiM2Y= Accessed 31th May 2015.

9. Ottmar, H., Abousahl, S., Morgenstern, A., & Vincent, M.C. Plutonium Assay by Calorimetry - An Experimental Case Study for Reactor-Grade Plutonium Materials; Proceedings 25th ESARDA Symposium, Stockholm (2003), https://esarda.jrc.ec.europa.eu/index.php?option=com_jifile&filename=MWJkOWQ2OTY4NjFhOGU0YTA5ZDk3Yjg1NTE0YzNiMzI= Accessed 31th May 2015.

10. J. D. Nutter, F.A. O`Hara, W. W. Rodenburg, The use of calorimetry in nuclear materials management; United States UNT Digital Library. http://digital.library.unt.edu/ark:/67531/metadc666732/ Accessed May 9, 2016. (1996)

11. J. Zsigrai, A. Mühleisen. M. Ramos Pascual, Collection of medium-resolution gamma spectra of certified Pu reference materials; JRC Technical report JRC98337, http://publications.jrc.ec.europa.eu/repository/handle/JRC98337 Accessed May 9, 2016. (2015)

A-06

Insights into point-defects of δ-Pu and δ-Pu-Ga alloys using density functional theory

Sarah Hernandez, Franz Freibert

Los Alamos National Laboratory, Los Alamos, NM, USA

Introduction

Aging of δ-plutonium (Pu) is becoming a forefront challenging problem in Pu science, as we try to understand the effects of radiological decay on the phase stability of face-centered-cubic (fcc) δ-Pu. Recent studies have shown that δ-Pu that is 20-40 years of age does not void swell [1], unlike austenitic steel. This only deepens the problems and concerns, since currently we do not know why δ-Pu does not void swell, or if aging of δ-Pu in the future will cause void swelling.

Since aging of δ-Pu may affect the mechanical and electronical properties, it is vital to understand the most influential drivers of aging, which includes helium ingrowth, radiation-induced lattice defect accumulation, and phase instability of the fcc structure. These drivers are dependent on temperature, gallium (Ga) concentration, radioactive α-decay dose, and α-decay rate. Due to multiple processes that occur while δ-Pu ages, computational efforts, such as density functional theory (DFT), may provide fundamental insight and guidance into the most prominent defects that will impact the stability of the lattice and the electronic properties.

Computational details

Using DFT we have explored a variety of point defects in an unalloyed and Ga-alloyed δ-Pu 3x3x3 supercells (108 atoms), which consisted of vacancies, octahedral and <100> dumbbell interstitials, and Frenkel pairs. Formation energy, E_f, of these defects will be reported. DFT calculations were performed using the PBE formulation to GGA to approximate the exchange-correlation functional of the system as implemented in *VASP*. A spin-polarized anti-ferromagnetic configuration was applied to the Pu atoms within the cell.

Due to cell size, all calculations were done at the Γ-point, and in addition, underwent a three step process to determine the ground state: 1) volume optimization; 2) uniaxial strain of the lattice; and 3) relaxation of the ions at a fixed volume. As previously shown by Söderlind et al. [2,3], a tetragonal distortion of the lattice (without defects) was calculated for unalloyed δ-Pu, while the addition of Ga in a substitutional lattice site in the alloyed δ-Pu structure minimized the tetragonal distortion.

Results

In a pure Pu lattice, energies thus far indicate that a mono-vacancy (E_f = 0.75 eV) and a Pu octahedral interstitial (E_f = 0.56 eV) are energetically more favorable than a uranium (U) interstitial (E_f = 1.35 eV) or Ga interstitial (E_f = 1.47 eV). In addition, a Pu Frenkel pair will annihilate when the Pu interstitial and vacancy are at nearest neighboring distance, whereas when the distance is increased the energy significantly increases to E_f = 1.95 eV. Interestingly, a U Frenkel pair annihilates when the pair is at nearest neighboring distance from each other with calculated E_f of 14.73 eV, thus indicating that this system is energetically unlikely. The energy is similar to the formation energy of a U substitutional lattice site, E_f = 14.01 eV. When a U interstitial and Pu interstitial exist at nearest neighboring distance from a vacancy (Figure 1a), the U interstitial relaxes back into the lattice site, while the Pu interstitial remains an interstitial atom (Figure 1b). The E_f is 1.00 eV, which implies that the Pu interstitial may aid in stabilizing a U substitutional atom in the lattice.

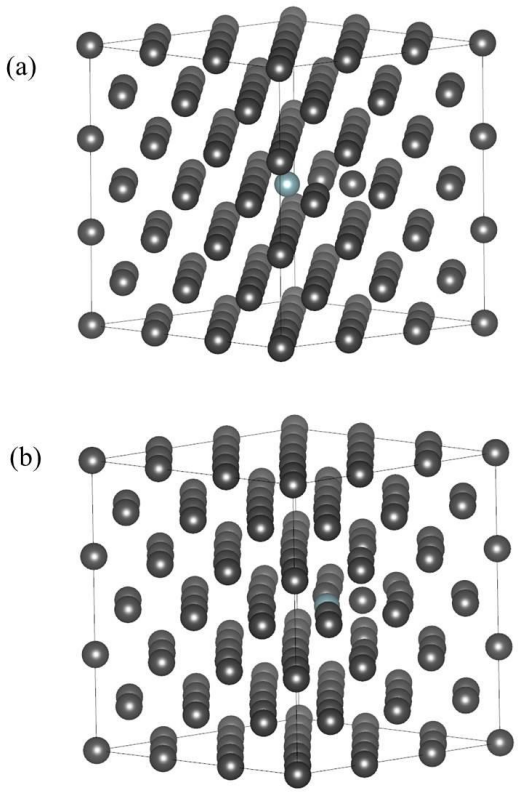

Figure 1: Pu interstitial, U interstitial, and vacancy structure before relaxation (a) and after relaxation (b). The gray atoms are Pu atoms and the light blue atom is a U atom.

The alloying impurity, Ga, is calculated to have an effect on the stabilization of defects. For instance, a Pu mono-vacancy and octahedral Pu interstitial is energetically more favorable when there is either no Ga or far away from the Ga alloyed impurity within the cell. Furthermore, when an octahedral Pu interstitial is a neighboring atom to a Ga atom, the Pu interstitial forms a Pu-Pu dumbbell with a neighboring Pu lattice atom. This does not occur when the interstitial atom is placed far from the Ga or in a pure Pu lattice.

In addition to discussing the energetic differences between the various defects investigated, we will also discuss the effect of these defects on the local geometric structure of the lattice, including an induced α-Pu phase-like bonding. We will also discuss if these local geometric distortions have an effect on the local electronic properties via partial density of states.

References

1. W. G. Wolfer, *Radiation Effects in Plutonium*, Los Alamos Science Vol. 1 26, 274-289 (2000).

2. P. Söderlind, A. Landa, B. Saidgh, *Density-functional investigation of magnetism in δ-Pu*, PRB 66, 205109 (2002).

3. P. Söderlind, A. Landa, *Theoretical confirmation of Ga-stabilized anti-ferromagnetism in plutonium metal*, J. Nucl. Mater. 448, 310-314 (2008).

Acknowledgement
This work is supported by Los Alamos National Laboratory LDRD program.

A-07

Thermoelectric power as a probe of density of states in $PuCoGa_5$

Krzysztof Gofryk[1], Jean-Christophe Griveau[2], Tomasz Durakiewicz[3]

[1]Idaho National Laboratory, Idaho Falls, Idaho, USA, [2]Institute for Transuranium Elements, Karlsruhe, Baden-Wurttemberg, Germany, [3]Los Alamos National Laboratory, Los Alamos, New Mexico, USA

In order to advance fundamental understanding of actinide materials and their thermophysical properties, so important in nuclear energy production, all aspects of the so-called 5*f*-electron challenge have to be addressed. However, in spite of large theoretical and experimental efforts their electronic structure is still not well understood. The band structure of solids is usually addressed by various photoelectron spectroscopy methods. In nuclear materials, however, this is very demanding due to the presence of radioactivity and radio-toxicity of actinide elements, especially plutonium. Here we present thermoelectric properties of plutonium-based unconventional superconductor $PuCoGa_5$. It has been characterized as a strongly correlated compound with a superconducting transition temperature T_c = 18.5 K. Despite many years of investigations, there is still not much known on the mechanism of Cooper pair formation in this material, neither the role of 5*f*-electrons. The photoemission measurements and electronic calculations obtained for $PuCoGa_5$ point to strongly renormalized electronic structure with sharp peak just below the Fermi level. Here we show that Seebeck coefficient of $PuCoGa_5$ is strongly enhanced and its magnitude and temperature dependence is characteristic of intermediate valence systems, indicating the presence of the 5*f*-band in close vicinity of the Fermi level. The thermoelectric data can be well described by the phenomenological picture of strongly renormalized quasiparticle bands just below the Fermi level. The results obtained point to itinerant nature of the 5*f*-electrons in $PuCoGa_5$ and its importance for unconventional superconductivity. We will compare the results obtained for $PuCoGa_5$ with other transuranium-based superconductor $NpPd_5Al_2$, which shows more localized nature of 5*f*-electrons. The electronic structure parameters obtained for $PuCoGa_5$ from the thermoelectric measurements agree well with the photoemission results and we show that this approach can be extended on other valence fluctuating correlated systems. The correlation between photoemission and thermoelectric power opens new possibilities in research approach to the electronic structure of correlated nuclear materials and fuels. This approach benefits from the interaction between fundamental and applied physics by aligning the two results obtained by two different methods, which previously have been found difficult to balance.

A-08

Hydrogen as a tool to modify electronic structure: are there common features in U and Pu hydrides?

Ladislav Havela[1], Mykhaylo Paukov[1], Volodymyr Buturlim[1], Ilja Turek[1], Martin Divis[1], Daria Drozdenko[1], Zdenek Matej[1], Milan Dopita[1], Milan Cieslar[1], Frank Huber[2], Thomas Gouder[2]

[1]Charles University, Prague, Czech Republic, [2]European Commission, JRC, Institute for Transuranium Elements, Karlsruhe, Germany

Besides its importance in materials processing, hydrides and their comparison with parent metals serve as an important probe into electronic structure. If a penetration of H atoms can reduce the energy of crystal structure of a metal or intermetallic compound, metal hydrides, which often preserve the metallicity, are formed, and the primary impact on actinides is the effect of expansion of the lattice, simulating a negative pressure. In this context, magnetic ordering found in different types of UH_3 and both Pu binary hydrides, UH_2 and UH_3, can be perceived as due to the enhanced separation of actinide atoms, leading to narrowing of the 5*f* band and enhancing the density of states at the Fermi level.

More detailed analysis reveals facts, which cannot be understood in such a simple conceptual framework. For U, it is mainly the fact that ferromagnetism with relatively very high Curie temperature (T_C = 165 K) appears at β-UH_3, which has the shortest U-U distances (330 pm) inferior to the Hill limit, i.e. in situation, where weak paramagnetism and superconductivity are more expected than magnetic order. We also confirmed the fact that the metastable form, α-UH_3, with much higher U-U spacing (360 pm), has practically identical magnetic properties [1]. This brings a conjecture that the interaction between U and H is actually more prominent in the U hydrides than the U-U spacing, believed to be the principle tuning parameter in light actinides. The fact, that the Pu-Pu spacing can be actually less important than changes of the 5*f* occupancy modulating the Pu magnetism, was actually articulated [2].

In the present work we developed a route of synthesis of UH_3 alloyed with various transition metals. It is based on using *bcc* U alloys (γ-U) as precursor, which has to be exposed to high pressures of H_2 gas. Depending on the type of alloying element, we obtained either conventional β-UH_3 type, or stable α-UH_3 type, or nanocrystalline β-UH_3 type, with a grain size 1-2 nm. The last case, which is observed for Mo alloying, can incorporate also many other different alloying elements (double alloying). Especially the last type of hydride can be obtained in the form of large monolithic pieces, which allows to investigate transport and thermodynamic properties. The results reveal that the hydrides, which have in all cases the H concentration close to 3 per 1 U atom, have quite uniform magnetic properties, which have only a weak dependence on structure and composition details. The T_C values are actually enhanced in most of cases even if the alloying includes elements, which are not typical sources of strong magnetic properties, as Mo, Zr, or Ti. The most striking increase has been found for Mo. The hydrides $(UH_3)_{1-x}Mo_x$ exhibit T_C exceeding 200 K for x = 0.13-0.15. For higher concentrations of Mo or other alloying elements, T_C tends to decrease again, and broadened ferromagnetic transition indicates an influence of inhomogeneities.

Besides the weak variations of magnetic properties, also the Sommerfeld coefficient of electronic specific heat is very little dependent on actual composition. The values around 30 mJ/mol K^2 do not reveal anything unusual as to electron-electron correlations. An interesting information is provided by electrical resistivity studies. Although UH_3 (studied in the form of UD_3 [3]) has a metallic character of its temperature dependence with resistivity decreasing strongly below T_C and reaching small residual resitivity, its absolute value, 600 $\mu\Omega$cm in the paramagnetic state, is an order of magnitude higher than expected for a metal. The resistivity of the nanocrystalline hydrides is even higher, reaching 1000 $\mu\Omega$cm. A very weak temperature dependence has to be attributed to the atomic disorder, inherited from the alloy precursors. It even leads to a weakly negative slope, caused by the weak localization. Below T_C it is

accompanied by a magnetization randomness in orientation over individual nanograins; application of magnetic field leads to strong negative magnetoresistance, reflecting the hysteresis loops observed ion magnetization measurements.

An attempt to understand the experimental findings can be based on assumption that the 5*f* states remain band-like and present at the Fermi level in UH_3-based materials, but the concentration of electrons with low effective masses (6*d*,7*s*) is low. The reason can be seen in results of the FPLO calculations [1], which indicate a significant depopulation of the 6*d* and 7*s* states. The H-1*s* states, which are populated more, are deep below the Fermi level. On the other hand, the 5*f* occupancy in the hydride even increases when compared with pure U *bcc* lattice with identical lattice parameters. Weakening of the 5*f* hybridization with the 6*d* and 7*s* states can eventually contribute towards the 5*f* moments formation, and the moments survive in a hypothetical experiment a compression to volumes smaller than for U metal (the volume increment between U and UH_3 is 75%). The UH_3-type materials represent thus a new class of materials in which a partial ionicity, including the 6*d* and 7*s* states, leaves around the Fermi level predominantly the 5*f* states only.

Similar effect of electron transfer was indicated in the past by calculations of Pu hydrides (see e.g ref. [4].), in which the Curie temperature increases with the H concentration and eventually also reaches relatively very high value (101 K) [5]. Interesting insight is provided by valence-band photoelectron spectroscopy, which exhibits only the $5f^4$ final-state multiplet (approx. 2 eV below the Fermi level), which implies that the $5f^5$ ground state has no admixture of $5f^6$, occurring e.g. in Pu metal [6]. Such situation, resembling strongly PuSb, is the only situation in Pu systems which give magnetic ordering. It is not, however, related to the 5*f* band as in UH_3, but dwells in essentially atomic character of the 5*f* states in PuH_3.

Acknowledgments

This work was supported by the Czech Science Foundation under the Grant 15-01100S.

References

[1] I. Tkach, M. Paukov, D. Drozdenko, M. Cieslar, B. Vondráčková, Z. Matěj, D. Kriegner, A.V. Andreev, N.-T.H. Kim-Ngan, I. Turek, M. Diviš, and L. Havela, :Phys. Rev. B 91 (2015) 115116.

[2] L. Havela, A. Shick, T. Gouder,.J.Appl.Phys. 105 (2009) 07E130

[3] J. W. Ward, L. E. Cox, J. L. Smith, G. R. Stewart and J. H. Wood, J. Phys. 40 (1979) C4-15.

[4] Jing-Jing Zheng, Bao-Tian Wang, Igor di Marco, Wei-Dong Li, J. Hydrogen Energy 39 (2014) 13255.

[5] A.T. Aldred, G. Cinader, D.J. Lam, L.W. Weber, Phys. Rev. B 19 (1979) 300.

[6] T. Gouder, A. Seibert, J. Rebizant, F. Huber, L. Havela, Mater. Res. Soc. Symp. Proc. 986 (2007) 17.

A-09

Quantum molecular dynamics simulations of transport properties in liquid plutonium

Haifeng Liu, Shuaichuang Wang, Gongmu Zhang, Bo Sun, Haifeng Song, Mingfeng Tian

Institute of Applied Physics and Computational Mathematics, Beijing, China

Introduction

Plutonium, a member of the actinides, has many applications. From physical and chemical perspectives, plutonium is one of the most complex and fascinating elements in the periodic table [1-3]. In order to elucidate the material properties of the solid allotropes, there are extensive experimental, theoretical, and computational works [4-7]. While the liquid phase has remained relatively unexplored except around the melt temperature due to its highly reactive, corrosive, and radioactive nature. Measurements of the shear viscosity and optical properties exist in Refs. [8-9]. Cherne [10] studied the fluid-phase transport properties, diffusivity and viscosity, by equilibrium and non-equilibrium techniques for Pu, whose interatomic interactions are described by the modified embedded-atom method. The transport coefficients are evaluated at zero pressure, for temperatures between 950 K and 1300 K. They find that the calculated viscosities are 3–4 times higher than the experiment. Kress [11] et. al. have employed quantum molecular dynamics (QMD) and orbital-free molecular dynamics (OFMD) simulation techniques to determine the transport properties, both diffusion and viscosity of Pu over a broad range of temperatures and compressions. The QMD viscosities of liquid plutonium are about 40% lower than the experiment. The shear viscosities computed from the autocorrelation function (Green-Kubo relation) of the off-diagonal component of the stress tensor [12]. In order to reduce the large computational requirements of QMD, the fitting routines of allow for shorter simulation are used in Ref. [11]. The method of extrapolating the off-diagonal stress tensor autocorrelation function in the $t \rightarrow +\infty$ limit leads to an unknown error for the viscosity and the desired statistical accuracy of viscosity depends on the entire simulation system and needs very long trajectories[13]. The main purpose of this paper is to revisit the viscosity and self-diffusion coefficient of Pu in liquid. We tested the numerical convergence of the viscosity and self-diffusion coefficient and obtained different results of liquid Pu from Ref. [11].

Methodology

The calculations are based on density functional theory, as implemented in the Vienna ab initio Simulation Package (VASP) [14-16]. The computational super cells were obtained as 3×3×6 original cells corresponding to 54 atoms, which guaranteed that a single k point is sufficient to sample the Brillouin zone. We conducted our AIMD simulations in the NVT ensemble. The ionic temperature was adjusted by Nose-Hoover thermostat, and the electron temperature was equal to the ionic temperature to achieve local thermo-dynamical equilibrium. The calculations were done at one fixed density of 17.4 g/cc, with the temperature spanning from 900 K to 12766 K. We set the time step of 2.5 fs with a negligible energy drift during tens of thousands of time steps. The first 3000 time steps were used for equilibrium, and subsequently atomic positions, velocities, stresses and other physical data were analyzed. The simulations run for from 30,000 to 100,000 time steps.

The self-diffusion coefficient is computed from the trajectory by the mean-square displacement or from the velocity autocorrelation function (VCF) and the viscosity is computed from the autocorrelation function of the off-diagonal components of the stress tensor (STACF) by the Green-Kubo formula.

Results and discussions

The shear viscosity and self-diffusion coefficients for liquid plutonium at the density ρ_L = 17.4

g/cm^3 and several temperatures are shown in Fig.1 and Fig.2, respectively. The fit of experimentally measured [8] viscosity of liquid plutonium, the results from QMD [11] simulations (N = 54) and the previous MEAM calculations [10] are plotted in Figs for comparison. Fig.1 shows that the QMD results are about 40% lower than the experiment, while the MEAM results are 3–4 times higher than the experiment, and our result agrees with the experiment well in the range of experiment. The difference of this work and QMD [11] decreases with increasing temperature. Fig.2 shows that the results of Ref. [11] QMD diffusion constants are about 7 times larger than the MEAM values at low temperature 900K, while the result of this work agrees with MEAM well at this point. The difference between this wok and Kress's is reduced with the increasing of temperature. Further studies show that there is obvious structure of VACFs and STACFs. The structures are indicative of correlated liquid. According to our knowledge, the single exponential which is not included the necessary physics is not adequate for fitting of the numerical data at lower temperature [17, 18]. In Ref. [11], the author fit the time dependence of the autocorrelation functions to a single exponential function, then to find viscosities in the t→∞ limit. This fitting procedure reduces the simulation duration and serves to damp long-time fluctuations. Unfortunately, this method fails to use for the correlated liquid. So we think this is the most important reason for difference in two results of QMD.

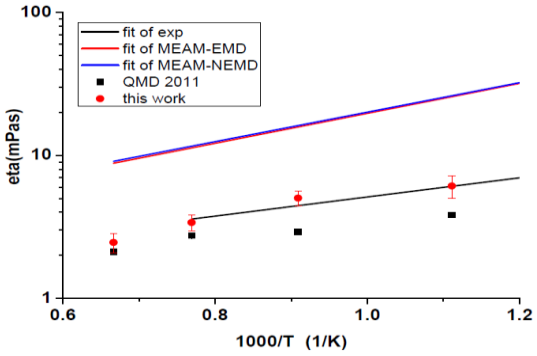

Fig.1 (Color online) Shear viscosity of liquid plutonium as a function of inverse temperature: experimental results [8, 10], the present QMD calculations (with statistical error bars), MEAM calculations [10], QMD calculation [11].

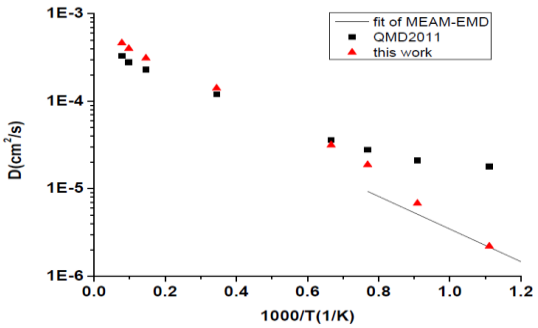

Fig. 2 (Color online) Diffusion coefficients of plutonium as a function of temperature for densities of 17.4 g/cm3: this work, QMD calculation [11], experimental results fits to the experiment data [8, 10].

Summary

We have studied the transport properties of liquid Pu with QMD simulations. We focused on calculation viscosity and diffusion properties from ACFs. Our results are agreement with experiment in the range of measurement. There is obvious difference between our result and Ref. [11] at lower temperature and two results show good agreement at relatively higher temperature. The structures of STACFs and VACFs at lower temperatures are observed and this exhibits correlated liquid-like behavior of liquid Pu. The method of extrapolating the autocorrelation function in the t→∞ limit leads a larger error for viscosity and diffusion coefficient of correlated liquid. We obtain the accuracy viscosity and diffusion coefficient of liquid Pu from the long simulation trajectories.

References

[1] D. L. Clark, *et al.*, Chapter 7 in The Chemistry of the Actinide and Trans actinide Elements, 4th Edition (Volumes 1–6), Springer (2011).

[2] S. S. Hecker and M. Stan, J. Nucl. Mater.383, 112(2008).

[3] V. P. Bobkov *et al.*, Thermo physical Properties of Materials for Nuclear Engineering: A Tutorial and Collection of Data (IAEA, Vienna, 2008), Sec. 2.2, pp. 14–21.

[4] S. P. Rudin, Phys. Rev. B 76, 195424 (2007).

[5] S.S.Hecker, Metall. Mater. Transations 35A, 2207 (2004).

[6] J.M.Wills, O.Erikssom, Actinide Ground-State Properties, Los Alamos Science 26, 128 (2000).

[7] M.Pénicaud, J. Phys. Condens. Matter 14, 3575 (2002).

[8] L. J. Wittenberg, D. Ofte, and W. G. Rohr, Nucl. Appl. 3, 550(1967).

[9] R. I. Sheldon, *et al.*, J. Nucl. Mater.312, 207 (2003).

[10] F. J. Cherne, M. I. Baskes, and B. L. Holian, Phys. Rev. B 67,092104 (2003).

[11] J. D. Kress, *et al.*, Phys. Rev. E 83, 026404 (2011).

[12] M. P. Allen *et al.*, Computer Simulation of Liquids (Oxford University Press, New York, 1987).

[13] J.-F. Danel, L. Kazandjian, and G. Z´erah, Phys. Rev. E 85, 066701 (2012).

[14] J. P. Perdew, K. Burke, and M. Ernzerhof, Phys. Rev. Lett. 77, 3865 (1996)

[15] G. Kresse and J. Furthmuuller, Phys. Rev. B 54, 11169 (1996)

[16] P. E. Blochl, Phys. Rev. B 50, 17953 (1994)

[17] J. Clerouin, J. Phys. Condens. Matter 14, 9089 (2002).

[18] E. R. Meyer, *et al.*, Phys. Rev. E 90, 043101 (2014)

A-10

Properties of PuO_2 nanoparticles together with its analogues CeO_2 and ThO_2

Anna Romanchuk, Tatiana Plakhova, Stepan Kalmykov

Lomonosov Moscow State University, Moscow, Russia

Plutonium is the chemical element of the major concern at the nuclear legacy sites. It was previously shown that plutonium can migrate in the subsurface environment with colloidal fraction. Colloidal migration of plutonium can be defined by the formation of pseudocolloids, when plutonium is sorbed onto various colloidal particles, or formation of intrinsic colloids. Additionally, it was shown that depending on the experimental conditions plutonium forms surface precipitates on various mineral colloids.

In this paper we aimed to study the behavior of $PuO_{2+x}\cdot nH_2O$ nanoparticles with average sizes of 1.5-5 nm. As an analogs to $PuO_{2+x}\cdot nH_2O$ nanosized ThO_2 and CeO_2 were synthesized. The attempt to compare the properties of PuO_2 nanoparticles with CeO_2 and ThO_2 nanoparticles is done. Typical images of studied nanoparticles present in Figure 1.

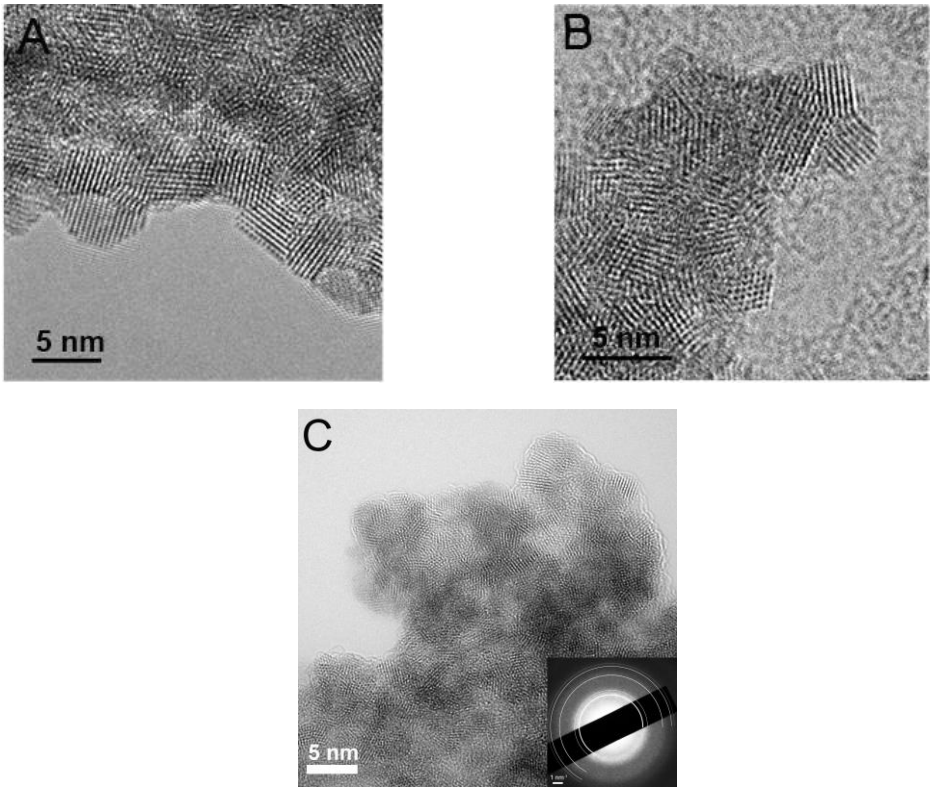

Figure 1. The HRTEM images of (A) ThO_2, (B) – CeO_2 and PuO_2 nanoparticles. ThO_2 nanoparticles were obtained by mixing 1 M $Th(NO_3)_4$ with 3M $NH_3\cdot H_2O$, CeO_2 – 0.001 M $Ce(NO_3)_3$ with 3M $NH_3\cdot H_2O$ and PuO_2 - $2\cdot10^{-4}$ M $Pu(NO_3)_4$ with NaOH (pH 11).

Thorium and cerium oxide nanoparticles were prepared by rapid chemical precipitation. These particles are thoroughly characterized by different techniques: XRD, HRTEM, SAED, DLS and ζ-potential measurements.

Effects of nature and concentration of precursor and pH of reaction on the morphology of nanoparticles were studied. It was found that concentration of thorium precursor did not influence the particles size distribution. At the same time ThO_2 nanoparticles that were obtained at various pH values were different in size. In case of CeO_2 the valence state of the precursors in highly important. If precursor is Ce(III) salt variation in its concentration effects the particles size. While in case of Ce(IV) precursor concentration did not change particles size as in case of ThO_2. It was also clearly found that the lattice parameter of ThO_2 and CeO_2 particles is increasing with decreasing of particles size. For ThO_2 this data was unknown previously.

PuO_2 nanoparticles were formed as a result of different reactions: redox reactions (equilibration of Pu(V) solution at pH around 8), chemisorption on inorganic mineral substrates, e.g. iron oxides and Pu(IV) hydrolysis reaction. These particles were characterized by HRTEM, SAED, Pu-L_3-XAFS, DLS and ζ-potential measurements. Leaching tests (at pH 1.3) were done for all types of $PuO_{2+x}\cdot nH_2O$ nanoparticles.

Solubility behavior of all three oxides was compared. For cerium dioxide experimental data on solubility was absent previously. In this work solubility of CeO_2 nanoparticles in broad pH range was determined by measuring cerium concentration in aqueous phase using inductively coupled plasma mass spectrometry (ICPMS) or by determining ^{141}Ce radioactive Ce isotope concentration with by γ-spectroscopy technique. For that reason CeO_2 with radioactive tracer was synthesized. Solid phase was examined too before and after interaction with aqueous solution. Experimental data on CeO_2 solubility were fitted using reductive dissolution model since Ce(III) species is dominated at pH < 5 similar to PuO_2 upon reducing condition.

This work was supported by Russian Foundation for Basic Research (projects No. 16-31-06000 mol_a_dk).

A-11

Development of point defect Raman signatures in PuO_2 through self-irradiation

Robert M Harker, Christopher Puxley

AWE Aldermaston, Reading, UK

It is known that degradation of the perfect fluorite PuO_2 lattice through cumulative □-event damage can be followed by Raman spectroscopy [1] but this has not been studied systematically before. In essence the solitary, symmetry-allowed T_{2g} band shifts, reduces in intensity and broadens. In addition, a number of formally symmetry-disallowed defect-related bands (1LO and a peak at 650 cm^{-1}) grow in intensity (see Fig. 1). Some have argued that this 650 cm^{-1} peak is related hyperstoichiometric defects in UO_{2+x} [2,3] but this will not be the case for PuO_2; additionally other reports have argued that both bands are related to the spectroscopic signature of extended defects.[4]

We have utilised Raman spectroscopy to follow a number of PuO_2 oxide powder samples over time with no annealing and after annealing in air (2hrs) at 1000, 800, 600, or 400°C. The oxides were of different ages at the start of the experiment, different source material and from preparation methods as shown in Table 1. We followed the samples with a range of lasers; the 633nm data is reported here. Spectra were collected at ambient temperatures with the laser at 1mW power. There were clear differences between the spectral response of the different samples, in part attributed to differences in particle size, but in each case we studied how each sample changed with respect to heating and age and compared those changes between samples.

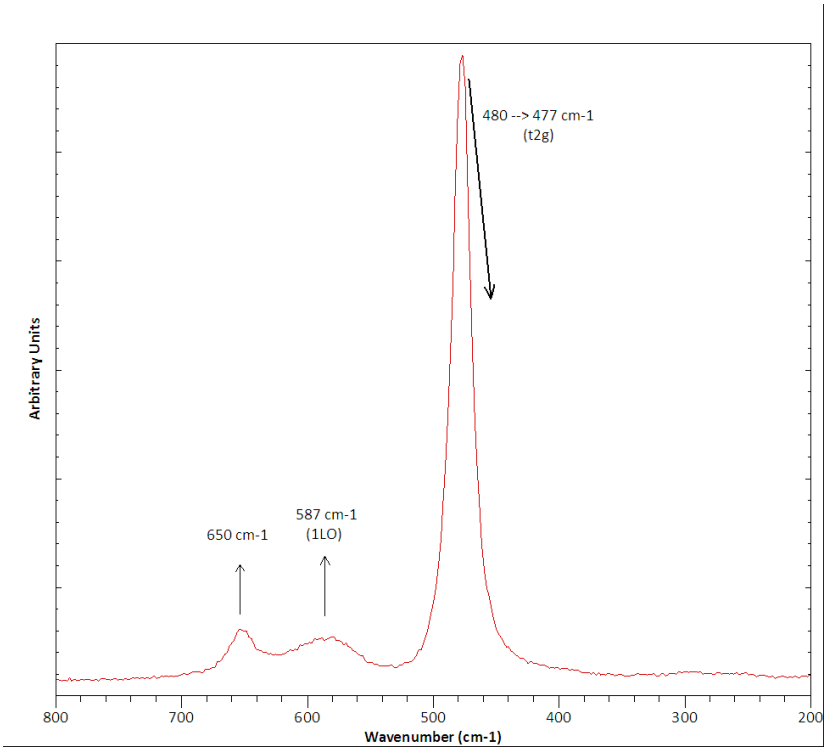

Fig.1 Example Raman spectra indicating changes in peaks with increasing age/defect concentration

With ageing of annealed samples, we observed both a reduction in T_{2g} peak intensity and peak area concurrent with a shift to lower wavenumber. The extent of change was related to the

sample set and anneal temperature with the highest anneal samples exhibiting the greatest change; for the 1000°C anneal samples the shift was 480.1 → 477.4 cm-1 over a period of 640 days. The reduction in T_{2g} area was found to fit best to a logarithmic relationship in each case.

Table 1. Oxide samples used in this study

Sample	**Source metal**	**Method of oxide preparation**	**Time since PuO_2 formation**
3625	δ-phase Pu	Coupon→PuH_x→Pu metal powder→+O_2@500°C	7.1 years
3626	α-phase Pu	Coupon→ +air@500°C	3.8 years
3627	δ-phase Pu	Coupon→PuH_x→Pu metal powder→+O_2@500°C	5.5 years
2500	δ-phase Pu	Coupon→ +air@500°C	5.1 years

We confidently identify the 1LO band at 587.0 ± 2.6 cm^{-1} and the additional defect band at 649.8 ± 2.2 cm^{-1}, and both are observed to increase with time. Our observation of 1LO at 587 cm^{-1} is higher than usually observed (for example 580 cm^{-1} in [1]). Our data at this time are not sufficient to allow conclusions to be drawn as to the exact form of the in-growth relationship; a linear form is assumed in the first case. The rate of increase of the 587 and 650 cm^{-1} bands would appear to be greater for the α-Pu sourced PuO_2 although we cannot rule out particle size effects at this time.

The air anneal procedure was shown to largely remove the 587 (1LO) and 650 cm^{-1} peak intensity between 600 and 800°C suggesting that their origin is related to Frenkel pairs. Given that anion and cation Frenkel pair annihilation is suggested for MOX at 150-500°C and 350-800°C respectively [5], it is more likely that these peaks are related, at least in part, to the cation Frenkel pairs. Interestingly, these defect related peaks appear to increase in intensity on annealing from room temperature to 500°C (Fig. 2). It is unclear whether this behaviour of increasing intensity to 500°C is related to defect migration to the surface or perhaps a simplification of the various defect environments due to removal of anion Frenkel pairs. This observation is in contrast to Guimbretiere et al. [4] who observed the complete removal of similar peaks over 375-525°C in MOX; there are obviously significant differences between defects in the two systems.

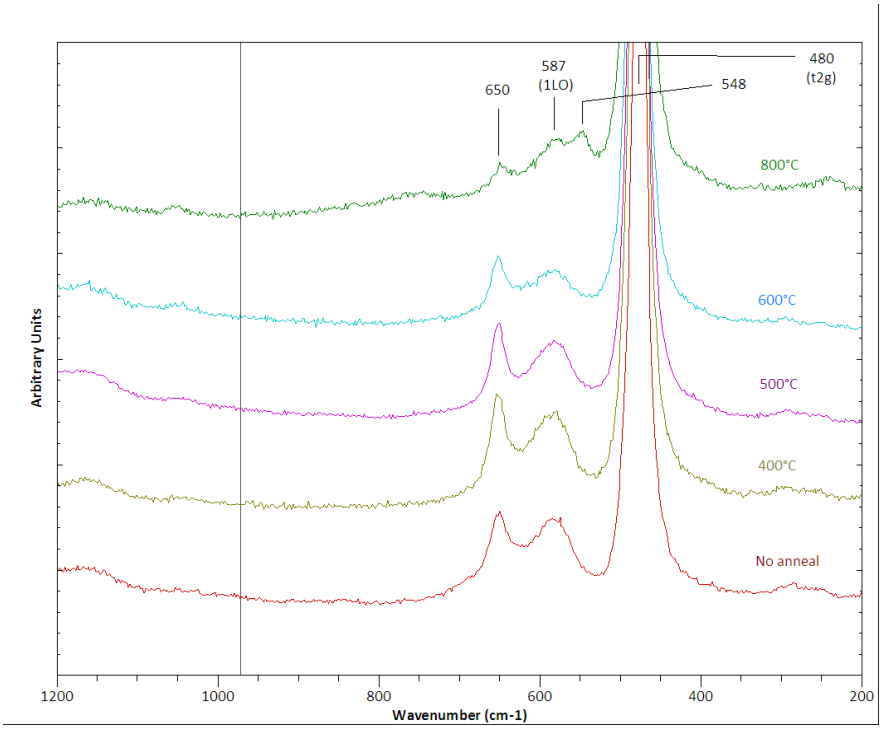

Fig.2 Raman spectra of sample 3627 within 2 days of heat treatments

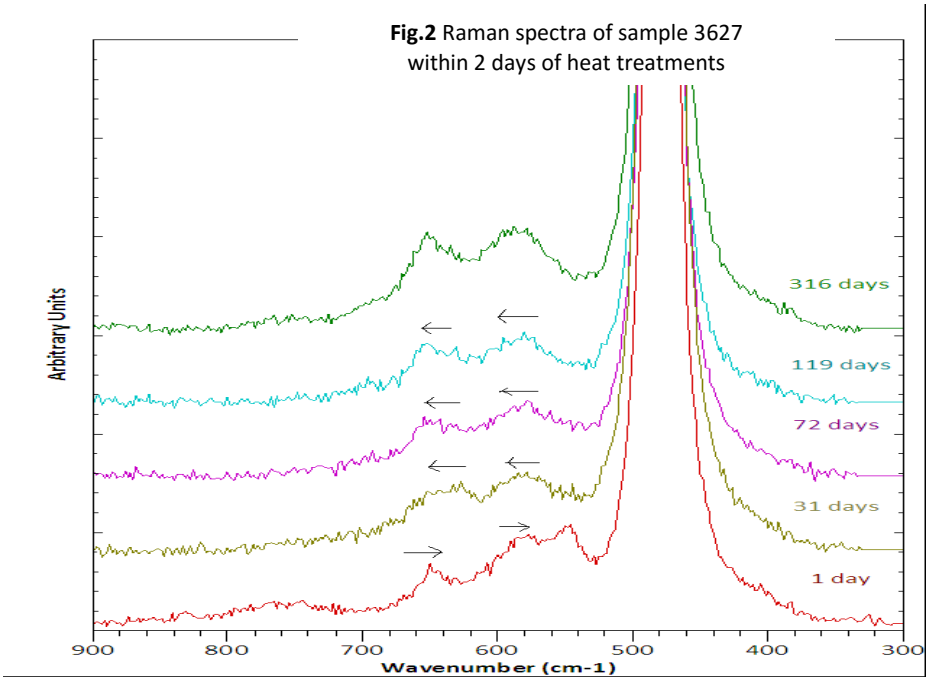

Fig.3 Raman spectra of sample 3625 heat treated to 800°C and followed over 316 days since heat treatment

Some of the sample-anneal combinations showed a more complicated spectral signature for a short period post-anneal that gradually developed into the more familiar aged PuO_2 spectra. This effect, identified in two samples, was particularly prominent in the 800°C anneal samples where an additional peak was identified at 548 cm^{-1} for some days post anneal (we are working to replicate this observation). It should be noted that according to the literature [4,5] for MOX, Frenkel pairs are supposedly annihilated by 800°C whereas other defects (dislocation loops, isolated He atoms, bubbles and voids) will remain. Thus, a tentative conclusion would be that this behaviour is related to a temporary interaction between still present defects, where some (possibly He[6]) have moved as a result of the 800°C anneal.

References:

[1] M.J. Sarsfield, R.J. Taylor, C. Puxley, H.M. Steele J. Nucl. Mater. 427, 333-342 (2012)

[2] C. Jegou, R. Caraballo, S. Peuget, D. Roudil, L. Desgranges, M. Magnin J. Nucl. Mater. 405, 235-243 (2010)

[3] C. Jegou, M. Gennisson, S. Peuget, L. Desgranges, G. Guimbretiere, M. Magnin, Z. Talip, P. Simon J. Nucl. Mater. 458, 343-349 (2015)

[4] G. Guimbretiere, L. Desgranges, C. Jegou, A. Canizares, P. Simon, R. Caraballo, N. Raimboux, M-F. Barthe, M-R. Ammar, O.A. Maslova, F. Duval, R. Omnee IEEE Trans. Nucl. Sci. 61 (4) 2045-2051 (2014)

[5] M. Kato, A. Komeno, H. Uno, H. Sugata, N. Nakae, K. Konashi, M. Kashimura J. Nucl. Mater. 393 134-140 (2009); D. Staicu, T. Wiss, V.V. Rondinella, J.P. Hiernaut, R.J.M. Konings, C. Ronchi J. Nucl. Mater. 397 8-18 (2010)

[6] T. Wiss, O. Dieste-Blanco, A. Tacu, A. Janssen, Z. Talip, J-Y. Colle, P. Martin, R. Konings J. Mater. Res. 30 (9) 1544-1554 (2015).

© British Crown Owned Copyright 2016/AWE

A-12

Oxygen stoichiometry determination in Pu-fuel by vapour pressure measurement

Ondrej Benes, Rudy Konings, Jean-Yves Colle

European Commission - Joint Research Centre, Karlsruhe, Germany

Two main types of fuel exist in commercial nuclear power plants. The first one is based on UO_2 pellets, while the second one utilizes produced plutonium which is mixed with uranium into the so-called MOX (mixed-oxide) fuel. One of the safety issues in light water reactors is the oxidizing potential of the fuel towards the cladding which is determined by the oxygen potential of the fuel, i.e. by its oxygen stoichiometry. While UO_2 fuel is likely stabilized at stoichiometric composition, thus at O/M ratio 2.0, the MOX fuel will tent to reduce due to the presence of plutonium which is stabilized in valence states 4 and 3. To be able to predict the behaviour of the MOX fuel with respect to temperature and plutonium concentration a thermodynamic model has been developed, but the correctness of such model always requires input of reliable experimental data. Among them are the partial pressure data which not only provide the information about the volatility of the fuel, but also provide activity data, which are a measure of the fuel stability.

At JRC the vapour pressures of oxide fuel samples are measured using a Knudsen effusion mass spectrometry and typical conditions of the measurement are temperatures well above 2000 K and vacuum. At such conditions actinide oxide samples tends to reduce into lower oxidation state and for the right data interpretation it is important to know the right fuel composition and oxygen stoichiometry which may significantly differ from the initial state. One way of measuring the oxygen stoichiometry is via oxygen pressure detection, but unfortunately oxygen cannot be directly measured due to its very high background signal. Therefore, novel approach has been proposed which takes into account the vapour equilibrium between various actinide oxide gaseous species which gives basis for the assessment of the fuel oxygen potential during the high temperature measurement.

In this paper we will show a systematic study of three intermediate MOX compositions (x(Pu) = 0.25, 0.5 and 0.75) which are correlated with independent measurements of oxygen potentials and we propose a method for estimation of the oxygen stoichiometry during the high temperature event.

A-13

XAFS and µ-XRF investigations of highly radioactive nuclear waste samples: spent nuclear fuel and zircaloy cladding segments.

Kathy Dardenne[1], Ernesto Gonzalez-Robles[1], Michel Herm[1], Bernhard Kienzler[1], Gerd Christill[2], Nikolaus Müller[1], Volker Metz[1], Jörg Rothe[1]

[1]Institute for Nuclear Waste Disposal (KIT-INE), Karlsruhe Institute of Technology (KIT), Karlsruhe, Germany, [2]Sicherheit und Umwelt (KIT-SUM), Karlsruhe Institute of Technology (KIT), Karlsruhe, Germany

Speciation information on radionuclides such as actinides and radioactive fission products incorporated into matrices of highly active nuclear waste (HAW) – in particular spent nuclear fuel (SNF) and HAW glass - is mandatory in safety assessment studies, as the chemical and physical state of these elements lastly determines their environmental mobility. The fate of SNF and HAW glass in a future deep bedrock repository (e.g., groundwater induced corrosive degradation and dissolution of the waste forms) and the associated release of actinides, fission and activation products depends mainly on the oxidation state and bonding characteristics of the radionuclides in the individual matrices. Hence, X-ray Absorption Fine Structure Spectroscopy (XAFS) and related techniques are ideally suited as speciation methods for the *in situ* investigation of such materials, as they are capable to provide chemical speciation information (i.e., oxidation states and coordination geometries) by means of X-ray Absorption Near Edge Structure (XANES) analysis and short-range structural details on local coordination environments (bond lengths, neighboring atom types and coordination numbers) by means of Extended X-ray Absorption Fine Structure (EXAFS) analysis. X-ray Fluorescence Spectroscopy (XRF) delivers information on the elemental composition of the sample. Those techniques applied with a µ-focus incident beam provide additional spatial resolution of the distribution of elements and chemical species. XAFS / XRF studies of simulated or radionuclide doped HAW surrogates (first of all matrices for nuclear waste conditioning like glasses or ceramics) are numerously reported in the material sciences literature (cf., e.g., the recent overview provided in [1] and references therein). Yet, reports on the investigation of irradiated nuclear fuel and its zircaloy cladding [2] by XAFS are sparse, reflecting the general difficulties to investigate even moderately radioactive samples at most synchrotron radiation laboratories. Research at KIT in Karlsruhe benefits from the unique situation, where a shielded box-line with a variety of instrumentation for radioactive sample manipulation and analysis operated at INE controlled area laboratories is situated in close proximity to X-ray absorption spectroscopy experimental stations dedicated to radionuclide research - the INE-Beamline and the new ACT station at the ANKA synchrotron radiation source [3], KIT Campus North.

Considering the long-term safety assessment of a deep geological repository, understanding structural and chemical characteristics of the irradiated uranium oxide matrix is mandatory, as they will control the fuel stability and possible release of redox sensitive long-lived fission / activation products. Mo isotopes in the fuel matrix occur in metallic Ɛ-particles. These solid solutions are considered as catalysts for the reduction of radiolytically oxidized uranium and actinide species as well as for reduction of radiolytic oxidants. Pu, Am and other minor actinides which are generated in the uranium oxide matrix following neutron capture are considered as safety relevant radionuclides in less probable scenarios, such as permeation of oxidizing water or colloid mediated radionuclide migration. Due to their long half-lives and relatively high mobility, a number of fission products (e.g. I-129, Cs-135, Zr-93) are relevant for the HAW long-term dose rate. Besides short-lived radionuclides (e.g. Ti-44), certain radionuclides (like Cs-137, Ba-137m) remain important heat sources for hundreds to thousands of years.

The present study demonstrates the feasibility of direct speciation investigations for the plethora of fission product and actinide elements contained in SNF fragments sampled from a test fuel rod irradiated at the Gösgen pressurized water reactor (Switzerland) achieving an average burn-up of 50.4 GWd/(t HM) and at the inner surface of a Zry-4 plenum ring segment derived

from the same rod. A millimeter-sized SNF fragment and two Zry-4 ring segments with contact dose rates of 3.45 mSv/h and 30 µSv/h, respectively, were removed from the shielded box-line in a contamination free vial and encapsulated in specially designed sample containers sealed by polyimide film. For recording XAFS and XRF spectra of the SNF fragments, the standard fluorescence yield detection setup at the INE-Beamline was used, where the monochromatic radiation is focused by a toroidal mirror into a beam spot of approx. 500 × 300 µm^2 at the sample position. The fluorescence signal emitted by the sample is recorded by a Canberra LEGe solid state detector system. Digital X-ray pulse processing is applied to derive energy dispersive emission spectra and filtered element emission lines for XAFS scans in fluorescence yield detection mode.

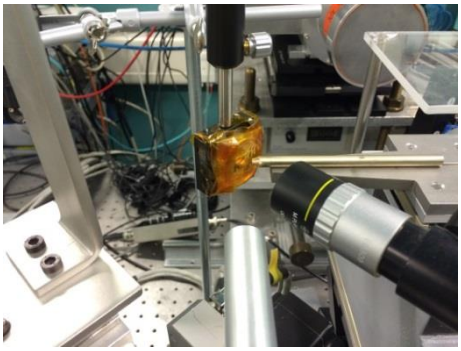

Fig. 1 µ-focus setup with an encapsulated Zry-4 ring segment.

The Zry-4 ring segments (the first one was mounted to investigate a material cross section and the second one to expose the inner surface to the beam) were additionally investigated by means of a µ-focus setup available at the beamline, where a 25µm spot is achieved by applying a polycapillary half lens (IfG Berlin) with an approx. 5mm focal length. The µ-XRF signal is recorded using a Silicon Drift Detector (Vortex-60EX, Hitachi High-Technologies Science), cf. the setup depicted in figure 1.

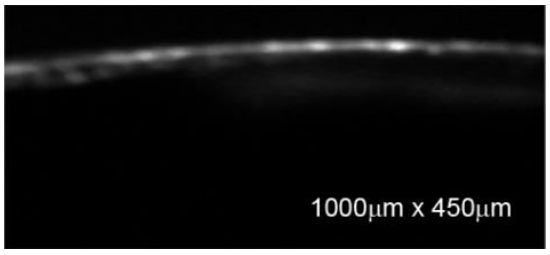

Fig. 2 U L Fluorescence map recorded for the Zry-4 ring segment cross section.

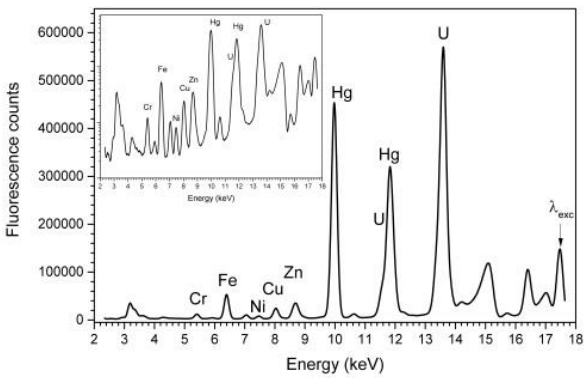

Fig. 3 Fluorescence lines recorded for the Zry-4 ring segment by excitation at 17500 eV. The insert shows the fluorescence intensity in log scale.

The presentation will focus on initial results obtained for the elements Am, Mo, Pu, Tc and U present in a SNF fragment and Ti, Ba, U detected for the zircaloy ring segments. Here the focus

was placed on the analysis of an uranium rich deposition layer on the inner ring surface by a combination of µ-XRF elemental mapping and µ-XANES, cf. the U L fluorescence map in figure 2 and the full MCA spectrum shown in figure 3. While semi-quantitative determination of the element compositions (i.e., applying an internal standard) was shown to be feasible for the HAW glass matrix (cf. our previous study in [1]), strong self-absorption effects hamper efficient detection of low-Z element fluorescence lines in case of the SNF matrix, mainly consisting of UO_2.

References

[1] K. Dardenne, E. González-Robles, J. Rothe, N. Müller, G. Christill, D. Lemmer, R. Praetorius, B. Kienzler, V. Metz, G. Roth, H. Geckeis, XAS and XRF investigation of an actual HAWC glass fragment obtained from the Karlsruhe vitrification plant (VEK), J. Nuc. Mat. 460 (2015) 209–215

[2] Kyu-Tae Kim, UO2/Zry-4 chemical interaction layers for intact and leak PWR fuel rods, J. Nuc. Mat. 404 (2010) 128–137

[3] J. Rothe, S. Butorin, K. Dardenne, M. A. Denecke, B. Kienzler, M. Löble, V. Metz, A. Seibert, M. Steppert, T. Vitova, C. Walther, H. Geckeis, The INE-Beamline for actinide science at ANKA, Rev. Sci. Instrum. 83 (2012) 043105

A-14

Real Time Studies of ^{239}Pu Elastic Moduli using Resonant Ultrasound Spectroscopy

Boris Maiorov, Jonathan Betts, Maxime Leroux, Franz Freibert, Albert Migliori

Los Alamos National Laboratory, Los Alamos, New Mexico, USA

Elastic moduli are fundamental thermodynamic susceptibilities that connect directly to thermodynamics, electronic structure and mechanic properties. It is important to determine the origin of changes in elastic properties in ^{239}Pu and it Ga alloys as a function of time. The most-likely sources of these changes include a) ingrowth of radioactive decay products like He and U, b) the introduction of radiation damage, c) δ-phase instabilities towards α-Pu or to Pu_3Ga. The measurement of mechanical resonance frequencies can be made with extreme precision and used to compute the elastic moduli without corrections giving important insight in this problem. Using Resonant Ultrasound Spectroscopy, time-dependent measurements were made of the mechanical resonance frequencies of fine-grained polycrystalline δ-phase ^{239}Pu, from room temperature up to 480K. At room temperature, both shear (G) and bulk (B) moduli increase in time with the rate of G at least a factor of 3 faster than that of B. As the temperature is increased, the rates of change increase exponentially with both G and B becoming stiffer with time. For T>420K an abrupt change in the time dependence is observed indicative of different G and B time dependence, however no changes in rate are observed when the temperature (400K) corresponding to the α-β lines is crossed. These measurement suggest that the changes in time observed in Ga-stabilized ^{239}Pu are consistent with the thermally activated creation of defects, that can be (partially) annealed for T>420K and in principle to rule out the decomposition of δ-Pu(Ga) towards α-Pu or Pu_3Ga in laboratory time frame.

A-15

In situ high temperature X-ray diffraction studies of the UO_2-PuO_2-Pu_2O_3 system

Romain Vauchy[1], Renaud C. Belin[2], Alexis Joly[1], Christophe Valot[1]

[1]CEA, DEN, DTEC, Marcoule, 30207 Bagnols-sur-Cèze, France, [2]CEA, DEN, DEC, Cadarache, 13108 Saint-Paul-lez-Durance, France

Uranium-plutonium mixed oxides with plutonium content less than 10 wt% are currently used as nuclear fuels in Pressurized Water Reactors. Within this compositional range, $U_{1-y}Pu_yO_{2-x}$ compounds have been extensively studied and their physico-chemical properties versus temperature are well known [1-3].

However, uranium-plutonium mixed oxides $U_{1-y}Pu_yO_{2-x}$ with high amounts of plutonium (*i.e.* $y > 0.20$) are envisaged as fuel for future Sodium-cooled Fast Reactors (SFRs) [4]. Although the exact nature of SFRs' nuclear fuels is still under consideration, general trends are already defined. The fuel will be oxygen-hypostoichiometric uranium-plutonium mixed oxides (O/(U+Pu) = Oxygen/Metal ratio < 2.0) with a plutonium content ranging between $0.20 < y < 0.30$. Furthermore, depending upon the fabrication route and raw materials used for nuclear fuel processing, *i.e.* upon cation distribution homogeneity, local high and low Pu content zones might be present within the mixed oxides that may have an influence on the behavior of the fuel under irradiation. In the UO_2-PuO_2-Pu_2O_3 sub-system, corresponding to the domain of interest for nuclear fuel for future SFRs, $U_{1-y}Pu_yO_{2-x}$ mixed oxides with high plutonium content ($y > 0.20$) are multiphasic at room temperature [5-20]. In this system, a miscibility gap exists and is composed of two fluorite face-centered cubic *fcc* phases for the lower Pu contents ($0.20 < y < 0.45$) and of an *fcc* phase in equilibrium with an α-Pu_2O_3-type body centred cubic *bcc* phase in the higher plutonium content range [7-11]. The two phases constituting the hypostoichiometric mixed oxides exhibit different oxygen content and are so called “high-oxygen” and “low-oxygen” phases, respectively [15-20]. Since these two phases have different physico-chemical properties, their co-existence may have detrimental effects on the fuel during its manufacturing, storage and irradiation. Thus, studying the phase equilibria in the UO_2-PuO_2-Pu_2O_3 system as a function of temperature in a wide composition range is required in order to obtain a nuclear fuel for Sodium-cooled Fast Reactors that matches the manufacturing specifications.

To do so, $U_{1-y}Pu_yO_{2-x}$ mixed oxides with homogeneous cation distribution (as evidenced by EPMA) with y ranging from 0.15 to 0.62 were prepared by our team using powder metallurgy processes [15,21].

The phase equilibria in the UO_2-PuO_2-Pu_2O_3 system were studied using a Bragg-Brentano θ-θ X-ray diffractometer equipped with a fast-counting PSD detector with an opening angle of 3° 2θ (see Figure 2). The entire apparatus is located in its own custom-built nitrogen-filled glove-box dedicated to handling of nuclear materials at the LEFCA facility (CEA Cadarache, France). The diffractometer is also equipped with a hot stage which can heat samples up to 2273 K [22]. Taking advantage of the angular window of the PSD, measurements in fixed-angle mode are also possible in a restricted angular range <3° 2θ. This procedure provides very fast measurements (15 s) and can be used to collect data while rapidly varying the temperature [15,16].

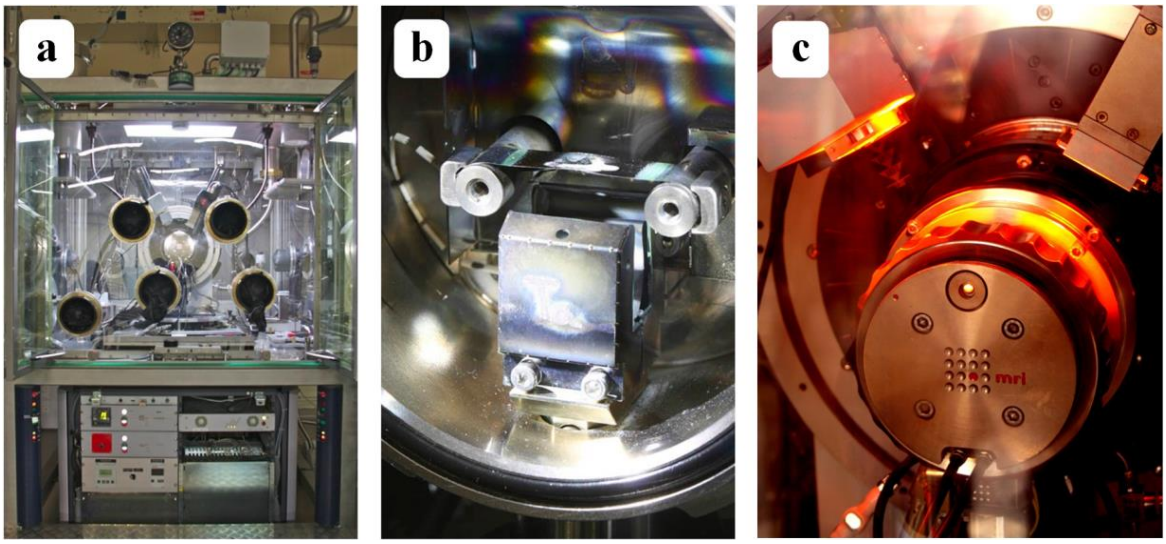

Figure 2. (a) Implementation of the BRUKER D8-Advance diffractometer in its glovebox, (b) MRI hot stage with direct and radiant heating elements and (c) the hot stage radiatingduring a heat treatment.

Reducing annealing was performed *in situ* in the High Temperature X-Ray Diffraction (HT-XRD) device at ~1800 K under He + 5% H_2 + ~20 vpm H_2O. Because the HT-XRD does not allow measurements to be performed in a closed system, at equilibrium, the oxygen chemical potential of the sample is equal to that of the gas mixture used. Thus, the samples were cooled down to room-temperature with various rates (ranging from 0.005 to 2 $K.s^{-1}$) in order to modify *in situ* the O/M ratio of the mixed oxides. Depending upon the plutonium content, the promptly cooled samples evidenced a phase separation (see the $U_{0.55}Pu_{0.45}O_{2-x}$ example given in Figure 3) whereas samples cooled slowly did not due to their complete oxidation in contact with the atmosphere during cooling (Figure 4). Besides the composition of the annealing gas mixture, the cooling rate plays a major role on the control of the O/M ratio and then on the crystallographic properties of the $U_{1-y}Pu_yO_{2-x}$ uranium-plutonium mixed oxides.

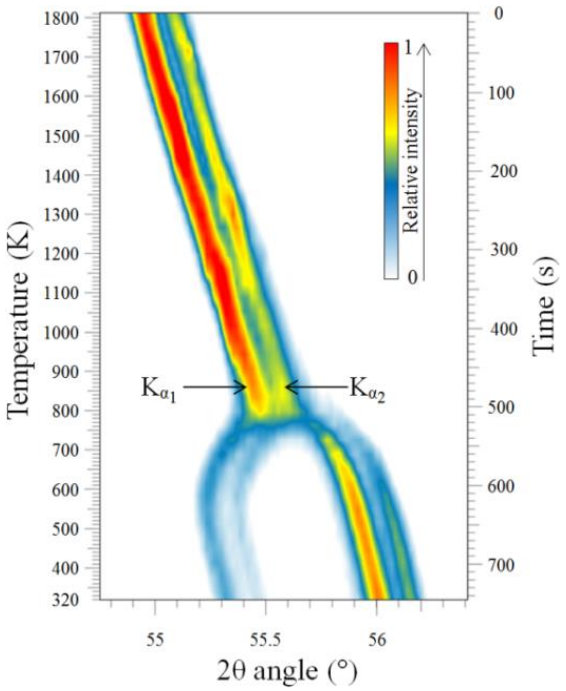

Figure 3. Isodentity map of the (311) peak intensity of the *fcc* structure of $U_{0.55}Pu_{0.45}O_{2-x}$ during cooling at 2 $K.s^{-1}$ under He + 5% H_2 + ~20 vpm H_2O.

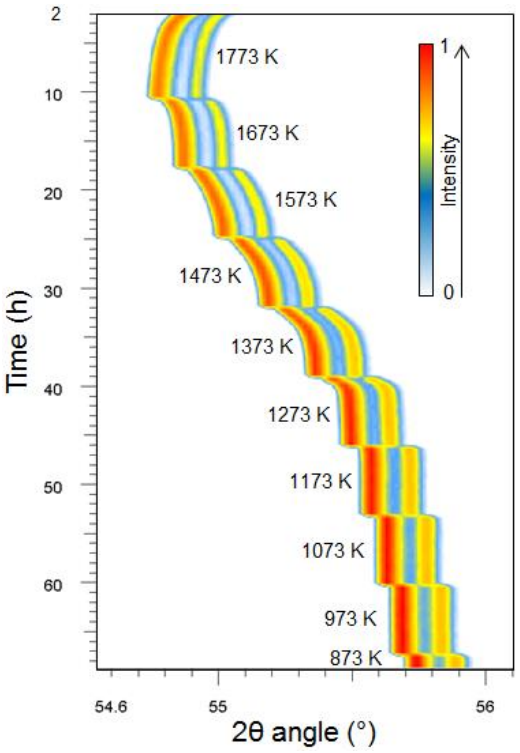

Figure 4. Isodentity map of the (311) peak intensity of the *fcc* structure of $U_{0.55}Pu_{0.45}O_{2-x}$ during cooling at 0.005 $K.s^{-1}$ under He + 5% H_2 + ~20 vpm H_2O.

The experiments were also performed to evaluate the kinetics of the phase separation phenomenon. Once phase separated and cooled to room-temperature, two (y = 0.28 and 0.45) of the obtained biphasic samples were re-heated at the same rate and a phase recombination was evidenced. Furthermore, regardless of the cooling/heating rate used (from ~0.05 $K.s^{-1}$ up to 2 $K.s^{-1}$), the temperatures of phase separation/recombination are identical for a given plutonium content and equal to 570 ± 20 K and 770 ± 20 K for y = 0.28 and 0.45, respectively. In addition, for given plutonium content, the lattice parameters of two *fcc* phases formed during the phase separation phenomenon do not depend upon the cooling rate used.

At elevated temperatures, the experimental phase equilibria data, *i.e.* temperature of phase separation, lattice parameters and phase fractions, will be presented at the Plutonium Futures – The Science 2016 conference and compared to literature data and to calculated results using a thermodynamic model of the U-Pu-O system based on the CALPHAD method [23].

References

[1] J.J. Carbajo, G.L. Yoder, S.G. Popov, V.K. Ivanov, *J. Nucl. Mater*. 299 (2001) 181.

[2] C. Guéneau, A. Chartier, L. Van Brutzel, *Compr. Nucl. Mater*, Elsevier, Oxford, 2012, 21-59.

[3] R.J.M. Konings, T. Wiss, C. Guéneau, in: L.R. Morss, N.M. Edelstein, J. Fuger (Eds.), Chem. Actin. Trans. Elem., Springer, Netherlands, 2011, 3665-3811.

[4] A Technology Roadmap for the Generation IV Nuclear Energy Systems, US Department of Energy Nuclear Energy Research Advisory Committee and the Generation IV International Forum, December 2002.

[5] L.E. Russell, N.H. Brett, J.D.L. Harrison, J. Williams, *J. Nucl. Mater.* 5 (1962), 216-227.

[6] N.H. Brett, L.E. Russell, *Trans. Brit. Ceram. Soc.* 62 (1962) 97-118.

[7] T.L. Markin, R.S. Street, *Inorg. Nucl. Chem.* 29 (1967) 2265-2280.

[8] T.L. Markin, E.J. McIver, Plutonium 1965, Chapman and Hall, London, 1967, 845-857.

[9] C. Sari, U. Benedict, H. Blank, *Thermo. Nucl. Mater.* (1968) 587-611.

[10] C. Sari, U. Benedict, H. Blank, *J. Nucl. Mater.* 35 (1970) 267-277.

[11] G. Dean, J.C. Boivineau, P. Chereau, J.-P. Marcon, Plutonium and Other Actinides, Plutonium 1970, 1970, 753-761.

[12] A. Komeno, M. Kato, H. Uno, K. Morimoto, M. Kashimura, Phase separation behaviour of (U0.7Pu0.3)O2-x (1.92<x<2.00) based fuels containing actinides and/or lanthanides, actinides 2009, IOP Conf. Ser. Mater. Sci. Eng. 9 (2010) 012016.

[13] T. Truphémus, R.C. Belin, J.-C. Richaud, J. Rogez, *Proc. Chem.* 7 (2012) 521-527.

[14] T. Truphémus, R.C. Belin, J.-C. Richaud, M. Reynaud, M.-A. Martinez, I. Félines, A. Arredondo, A. Miard, T. Dubois, F. Adenot, J. Rogez, *J. Nucl. Mater.* 432 (2013) 378-387.

[15] R. Vauchy, R.C. Belin, A.-C. Robisson, F. Hodaj, *J. Eur. Ceram. Soc.* 30 (10) (2014) 2543-2551.

[16] R. Vauchy, R.C. Belin, A.-C. Robisson, F. Hodaj, *M.R.S. Proc. Mater. Res. Soc.* 2014 (2013) 1645.

[17] R. Vauchy, A.-C. Robisson, P.M. Martin, R.C. Belin, L. Aufore, A.C. Scheinost, F. Hodaj, *J. Nucl. Mater.* 456 (2015) 115-119.

[18] R. Vauchy, A.-C. Robisson, R.C. Belin, P.M. Martin, A.C. Scheinost, F. Hodaj, *J. Nucl. Mater.* 465 (2015) 349-357.

[19] R.C. Belin, M. Strach, T. Truphémus, C. Guéneau, J.-C. Richaud, J. Rogez, *J. Nucl. Mater.* 465 (2015) 407-417.

[20] R. Vauchy, R.C. Belin, A.-C. Robisson, F. Hodaj, *J. Nucl. Mater.* 469 (2016) 125-132.

[21] R. Vauchy, A.-C. Robisson, F. Audubert, F. Hodaj, *Ceram. Int.* 40 (2014) 10991-10999.

[22] R. Vauchy, R.C. Belin, J.-C. Richaud, P.J. Valenza, F. Adenot, C. Valot, *App. Mater. Today* 3 (2016) 87-95

[23] C. Guéneau, N .Dupin, B. Sundman, C. Martial, J.-C. Dumas, S. Gossé, S. Chatain, F. De Bruycker, D. Manara, R.J.M. Konings, *J. Nucl. Mater.* 419 (2011) 145-167.

A-16

Plutonium Corrosion : Some Insights and Some Mysteries

Joseph Glascott

Bristol University, Bristol, UK

A comprehensive knowledge of all aspects of the corrosion of plutonium metal is important to fully understand any possible impact on all stages of the manufacture, life, storage and disposition of some nuclear weapons components. Unwanted plutonium corrosion at any stage could possibly have extreme consequences for cost, functionality, component life, and perhaps also safety.

Although metal corrosion generally can be limited by controlling the atmosphere the metal might see, the radiolytic properties of plutonium metal can sometimes cause severely detrimental gaseous species to be generated from nominally inert materials such as plastics or rubbers. The corrosion caused by gases generated in such circumstances might be of very limited extent but the surface films so generated can be catalytic and could have catastrophic consequences if the metal were later to be exposed to a different atmosphere, such as air or oxygen. In this respect, the characteristics of all corrosion films which could possibly be generated on plutonium metal surfaces by corrosion in oxygen, nitrogen, hydrogen , water and all combinations of these gases is of interest. Fully characterizing the mechanisms by which plutonium reacts with these gases is important, as is also quantifying reaction rates which can vary over a range of 10 orders of magnitude or more at room temperature.

The properties of the corrosion products themselves are of interest also not just because they may catalyse further reaction but because they might impact on other stages of the entire cycle of plutonium component manufacture to disposition. In this regard, the interaction of plutonium dioxide with water is of particular interest. Although conversion of metal to oxide is a more secure route for the long-term storage of excess plutonium from nuclear weapons stockpile reductions, the hygroscopic nature of the oxide, together with the possibility for adsorbed water to be radiolysed, could present safety hazards. Addressing such issues, relies on a full understanding of the relevant chemistry. However, many aspects of the chemistry of plutonium are still a matter of debate, including even fundamental matters such as the equilibrium Pu-O phase diagram, the activation energy for some important reactions metal-gas reactions and even the existence of certain plutonium corrosion species. Lastly, the native oxide film on the metal can influence not only its reaction with other gases such as hydrogen but also other characteristics such as its pyrophoricity.

In this review of plutonium corrosion, the general behaviour for some reactions is described as are a number of eccentricities particular to plutonium. Comment is also offered relating to some unanswered questions. The review illustrates how the rich chemistry of plutonium impacts on all aspects of its corrosion behaviour.

A-17

Recent progress in plutonium hydride research

Martin Brierley, John Knowles

AWE, Aldermaston, Berkshire, UK

The behaviour of the reaction between plutonium and hydrogen has been typically studied using gravimetric [1], volumetric [2] or visual methods [3] to elicit kinetic data. Initial hydride growth behaviour tends to follow a spot-wise growth as further hydride forms around existing hydride precipitates and each hydride reaction site grows radially at the surface. Additional reaction sites continue to nucleate on the surface while the initial sites grow. Given sufficient time, hydride reaction sites on the surface will impinge each other and form a continuous layer of hydride at the surface, after which the reaction continues at the bulk hydriding rate until either the plutonium or the gas is exhausted.

Recent work on δ-stabilised plutonium has demonstrated that anisotropy exists in the cross section of a typical hydride reaction site, with average lateral radius to penetration depth aspect ratio of 2.2:1 [4]. Anisotropic growth implies that there is a process that promotes lateral growth over penetrative growth. The anisotropy arises from local failure of the protective dioxide layer surrounding the hydride reaction sites as the volume expansion when transforming from Pu + H_2 → PuH_{2+x} imparts a stress into the surrounding plutonium metal. The ductile δ-Pu deforms plastically and the associated change in surface shape causes cracking in the surface oxide layers above it. The freshly formed cracks allow facile access for hydrogen to reach non-reacted metal at the metal/oxide interface surrounding the existing hydride reaction sites. This allows a small advantage to growth at the surface, favouring lateral growth and leading to anisotropy.

The work to be presented shows recent results obtained from plutonium samples of different microstructure, specifically a sample of mixed α/δ microstructure. Analysis of the reaction products was made *in situ* following reaction using scanning electron microscopy which prevented subsequent oxidation of the sample prior to analysis. Subsequent investigations of the reaction product microstructure obtained were also performed in cross section.

The sample was successively exposed to hydrogen for increasing durations of 60, 7200 and 70320 seconds. No evidence of reaction was evident following the 60 s and 7200 s exposures, unlike that observed in experiments carried out on gadolinium [5] and uranium [6]. Following the 70320 s exposure, 96 % of the available hydrogen was consumed and several large, anisotropic reaction sites had formed. The mixed α/δ phase sample exhibited traits similar to the δ-stabilised plutonium samples investigated previously [**Error! Bookmark not defined.**], with deformation of the δ-phases from the volume expansion of the hydride driving anisotropic growth. Cross sectional analysis of hydride reaction sites showed that plutonium metal surrounding the hydride reaction site at the surface had deformed by slip processes (Figure 5) and this deformed material affected the growth of hydride into the metal, strongly supporting our previously proposed mechanism for anisotropic growth [**Error! Bookmark not defined.**]. The α-phase domains resisted deformation and instead transferred the stresses from the hydride reaction front deeper into the surrounding metal. Fracture of the α-phase domains and plastic deformation of the δ-phase domains was observed at an increased distance from the reaction front. Post experimental cross sections through reaction sites suggest that regions associated with alpha domains had not undergone complete reaction with hydrogen.

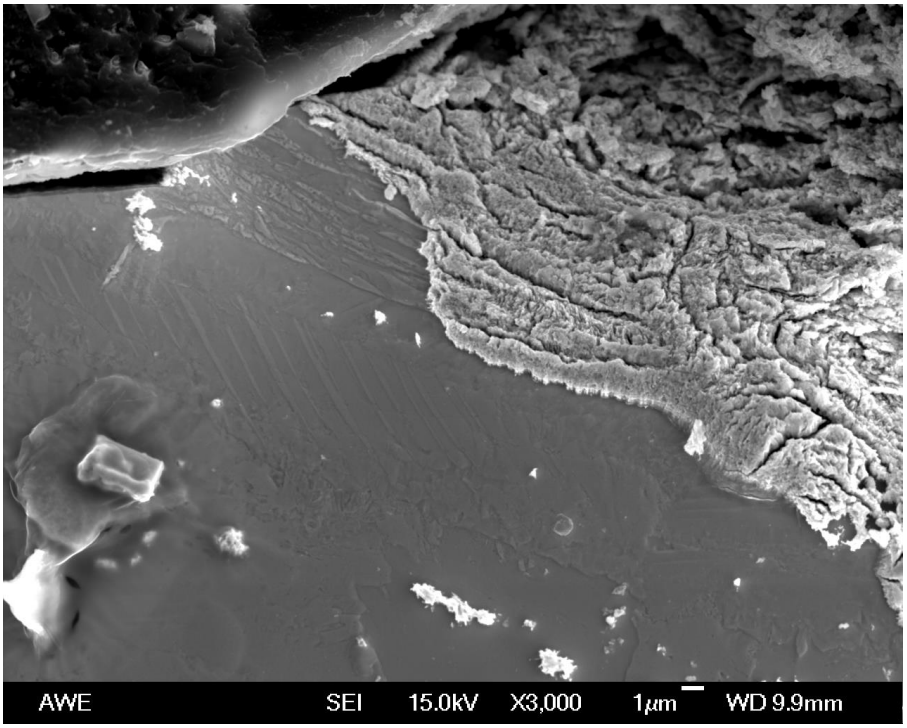

Figure 5 – cross section showing slip lines surrounding a hydride reaction site

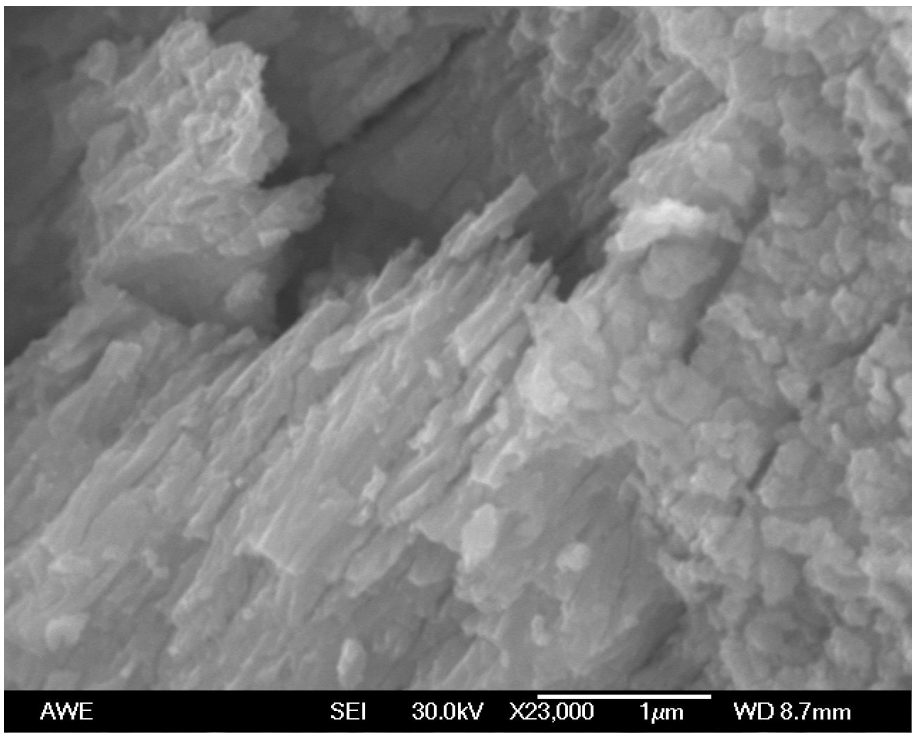

Figure 6 – High magnification image of Plutonium hydride produced from the mixed phase alloy

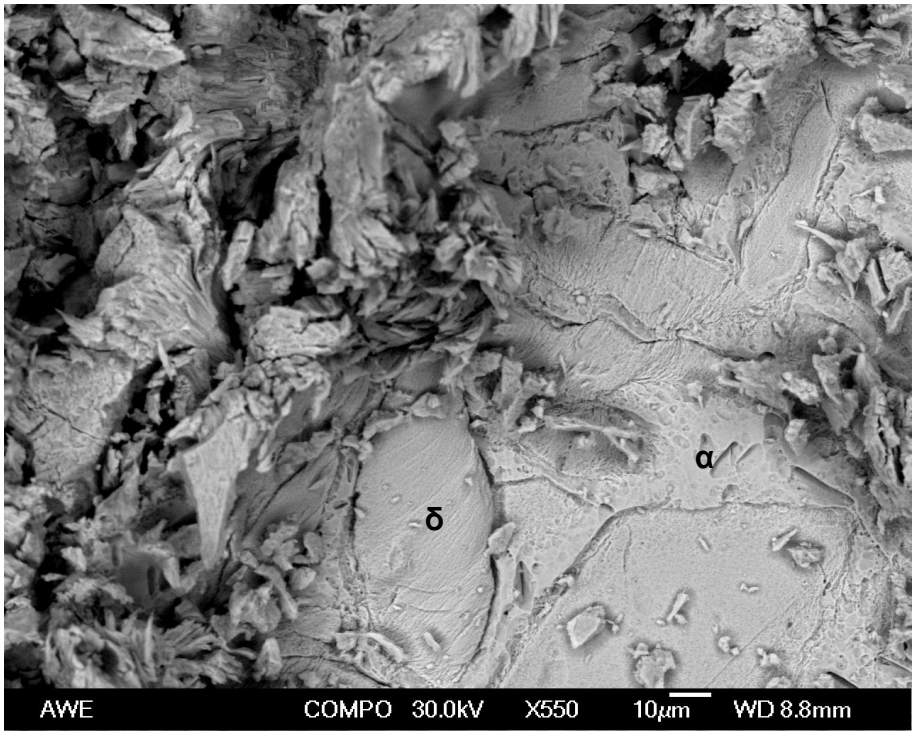

Figure 7 – deformation by plane slip was observed in δ-Pu domains

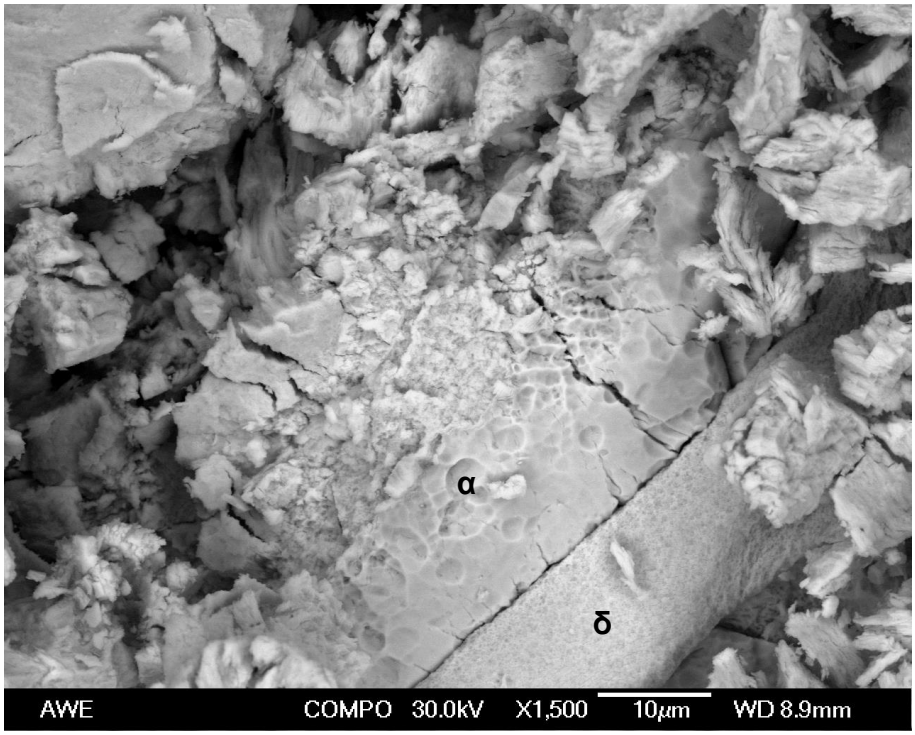

Figure 8 – fracturing and transformation of α-Pu to a powder with no deformation

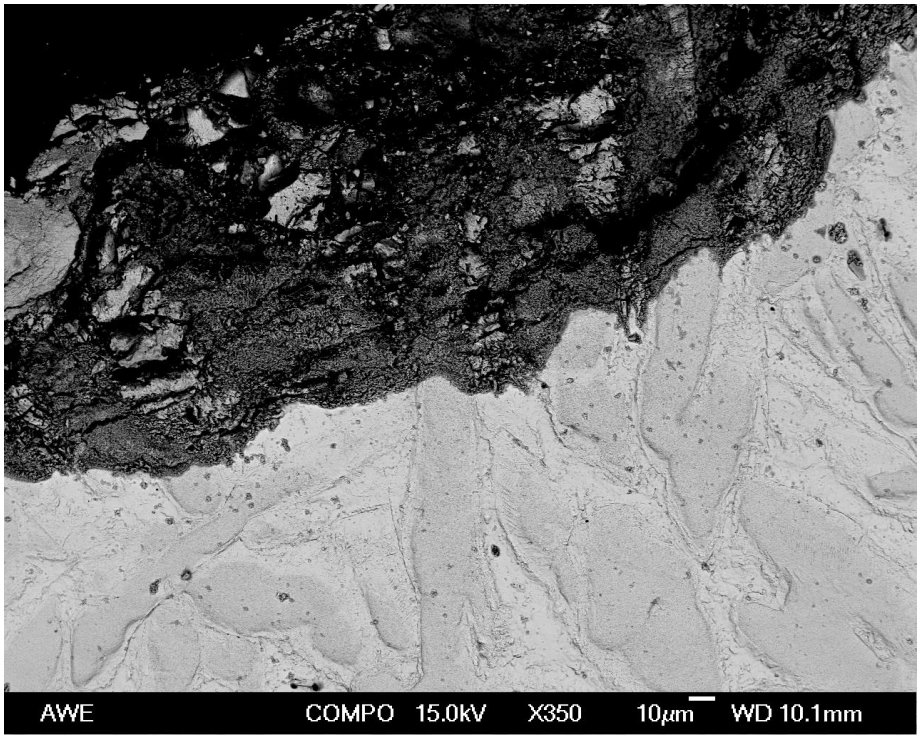

Figure 9 – regions of hydride associated with α-Pu had a brighter contrast using backscattered electrons, suggesting that the density was higher than the surrounding hydride

References

1. J.L. Stakebake, Summary Abstract: Kinetics for the hydriding of a plutonium-l w/o gallium alloy

powder, J. Vac. Sci. Technol. 17 (1980) 114.

2. R.N.R. Mulford, G.E. Sturdy, The Plutonium-Hydrogen System. I. Plutonium Dihydride and

Dideuteride, J. Am. Chem. Soc. 77 (1955) 3449–3452.

3. G.W. McGillivray, J.P. Knowles, I.M. Findlay, M.J. Dawes, Journal of Nuclear Materials 412 (2011) 35–40

4. M. Brierley, J.P. Knowles, A. Sherry, M. Preuss, Journal of Nuclear Materials 469 (2016) 145e152

5. G.M. Benamar, D. Schweke, G. Kimmel, M.H. Mintz, Journal of Alloys and Compounds 520 (2012) 98– 104.

6. R.M. Harker, A.H. Chohollo, MRS Online Proceedings Library Archive, 1444 (2012) 189

A-18

Metallurgical Properties of Aged Plutonium Alloys and the Need for Advanced Microstructural Characterization

Brandon Chung, Kenneth Lema, Robert Erler, Nick Teslich, Patrick Allen

Lawrence Livermore National Laboratory, Livermore, CA, USA

The plutonium alpha-decay leads to the formation and accumulation of numerous defects and transmutations, which affect metallurgical properties [1]. Plutonium and its alloys, when stored, accumulate radiation defects caused by self-irradiation damage which alter the underlying material microstructure, which leads to self-irradiation induced changes in physical and mechanical properties. The primary aging effects are believed to be lattice damage, helium bubble in-growth, and potential void swelling. The corresponding consequences to Pu metal include potential reduction in density, dimensional swelling, hardening, and embrittlement [1-3]. During the past decade, significant progress has been made in understanding the mechanisms of aging and its induced effects in metallurgical properties [3-10]. There remain, however, a number of outstanding questions regarding the role of microstructural contributions (e.g. impurities and defects) on the fundamental aging process of plutonium.

Figure 1 shows results of immersion density measurements on both standard (reference alloy) and ^{238}Pu-enriched alloys. The ages of reference samples for the immersion density range from 0.2 to 21 years. Following the initial stage showing rapid decrease in the measured density, the rate of density reduction becomes reduced. The rate of decrease in the immersion density due to helium in-growth is ~0.002% per year which corresponds well with the measured volumetric swelling rate from dilatometry [3]. Measurements past 90 equivalent years of age show minimal change in immersion densities. This behavior indicates potential higher order complexity in disorder in damaged plutonium than the simple accumulation of Frenkel pair and radiogenic helium bubbles [1-10].

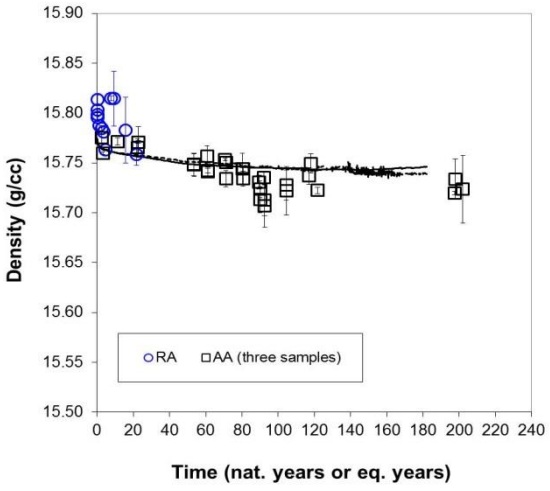

Figure 1. Immersion density measurement of enriched and reference alloys. Included in the plot are the dilatometry data converted to density for comparison with the initial density set to 15.78 g/cm^3. [8]

Figure 2 shows the engineering stress-strain curves of enriched alloys (AA) and reference alloys (RA) at different ages. The yield and ultimate tensile strength at different ages from Figure 2 are plotted in Figure 3. As can be seen from the data, both mechanical properties are about the same between the reference and enriched alloys at the early stage of aging. Data is also consistent with the values expected for alloys with ~2 atomic % gallium [11]. While there is a difference in the total elongation between two alloys, both alloys show increase in strength

and reduction in ductility from the aging process. At extended aging, the measurements continue to show gradual increase in strength, without signs of saturation. The ductility appears to reach around 10%. Based on the present results, the aging process still increases static strength of Pu alloys without any detrimental failure in mechanical properties. It is clear that the continued increase in the static strength is mostly linked to the continued in-growth of U and helium in the enriched alloys. Studies of the integrated effect from in-grown actinide daughters and helium bubbles to microstructural changes are needed to explain the changes in the static strength.

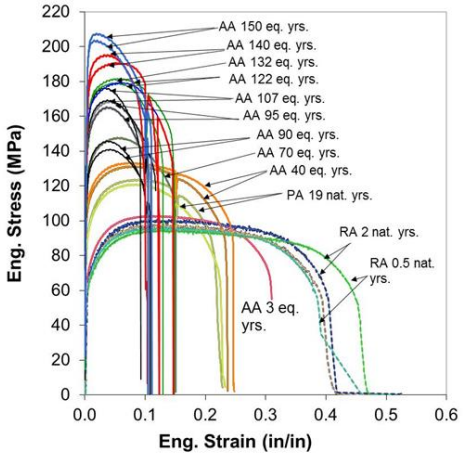

Figure 2. Tensile tests at room temperature show increase in strength and decrease in ductility as plutonium alloys are aged. RA is reference alloy and AA is enriched alloy. [8]

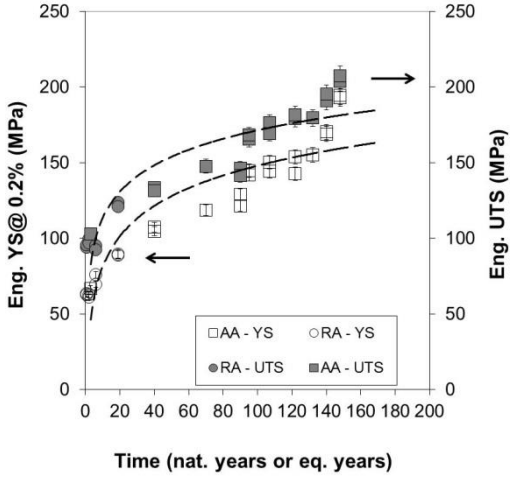

Figure 3. Engineering yield strength (YS) and ultimate tensile strength (UTS) for plutonium alloys from aging. Circles are reference alloys and squares are enriched alloys. [8]

While our continuing measurements in age-induced metallurgical changes in key plutonium alloys show very gradual changes in physical properties, we still know very little about the microstructure of plutonium alloys, and its influence in physical properties. With various options of manufacturing processes and complex self-irradiation damage, we need to improve our understanding of the process-property relation to determine if additional aging studies are needed. Figure 4 shows the three-dimensional (3D) representation of inner microstructures that reveals salient microstructural features that cannot be observed from conventional metallographic techniques. It demonstrates the benefit of FIB-SEM in improving microstructural characterization of microscopic inclusions, particularly with respect to improving process-structure-property relation in plutonium alloys.

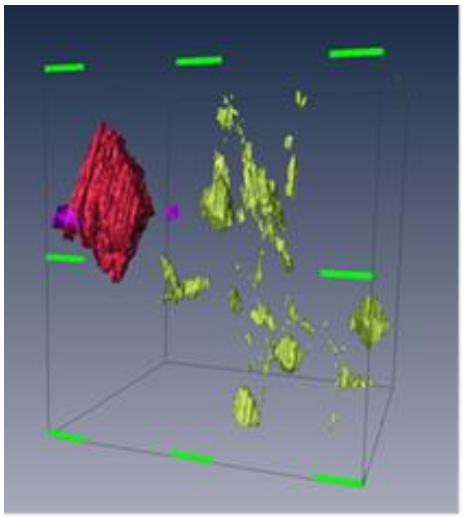

Figure 4. 3D inner microstructure of a plutonium metal. The 3D reconstruction of impurities and pores contained within the plutonium volume-of-interest: carbide (red), pore (purple), Pu_6Fe (yellow), and Pu (transparent). [12]

Our continuing measurements show aging in plutonium alloys leads to increasing static strength, gradual swelling in volume, and decrease in density without signs of void swelling. We obtained a self-irradiation equivalent time of nearly 200 years. At this extended aging, we find the rate of decrease in density has slowed significantly, stabilizing around 15.73 g/cm^3, without signs of void swelling. The volume expansion measured at 35°C also shows apparent saturation at less than 0.25%. Quasi-static tensile measurement still show gradual increase in the strength of plutonium alloys with age. Results from our quasi-static physical property tests suggest a different contribution of defects depending on the time scale. This work reveals that a better understanding of the integrated contribution from several self-irradiation induced defects to Pu alloys is needed. Detailed microstructural and chemical investigation could clearly help to explain the changes occurring in plutonium materials with age. Results of our initial 3D microscopy show the benefit of improved microstructural characterization that can improve our understanding of the role impurities and defects have on the properties of plutonium alloys.

This work performed under the auspices of the U.S. Department of Energy by Lawrence Livermore National Laboratory under Contract DE-AC52-07NA27344.

References

[1] W.G. Wolfer, Los Alamos Sci., 26 (2000) 26**,** 274

[2] S. S. Hecker, Los Alamos Sci., 26 (2000) 26, 290

[3] B.W. Chung, S.R. Thompson, K.E. Lema, D.S. Hiromoto, and B.B. Ebbinghaus, J. Nucl. Mater., 385 (2009) 91

[4] N. Baclet, B. Oudot, R. Grynszpan, L. Jolly, B. Ravat, P. Faure, L. Berlu and G. Jomard, Journal of Alloys and Compounds 444 (2007) 305

[5] B. W. Chung, C. K. Saw, S. R. Thompson, T. M. Quick, C. H. Woods, D. J. Hopkins and B. B. Ebbinghaus, Journal of Alloys and Compounds 444 (2007) 329

[6] B. W. Chung, S. R. Thompson and D. S. Hiromoto, Actinides 2008 - Basic Science, Applications and Technology 1104 (2008) 191

[7] B. W. Chung, S. R. Thompson, C. H. Woods, D. J. Hopkins, W. H. Gourdin and B. B. Ebbinghaus, J. Nucl. Mater. 355 (2006) 142

[8] B. W. Chung, K. E. Lema, and P. G. Allen, J. Nucl. Mater. 471 (2016) 239

[9] A.J. Schwartz, J. Alloys Compd., 444-445 (2007) 4

[10] W.G. Wolfer, B. Oudot, and N. Baclet, J. Nucl. Mater., 359 (2006) 185

[11] O. J. Wick, ed., Plutonium Handbook: A Guide to the Technology (American Nuclear Society, La Grange Park, IL, 1980)

[12] B. W. Chung, R. G. Erler and N. E. Teslich, J. Nucl. Mater. *accepted*

A-19

Auger Electron Spectroscopy of Plutonium Surfaces

David Moore, Alison Pugmire, Thomas Venhaus, Sarah Hernandez, David Pugmire

Los Alamos National Laboratory, Los Alamos, NM, USA

In recent years, many studies have focused on the properties of the thin film oxide layers that form on the plutonium metal surface under exposure to oxygen. Developing an accurate model of the structures, oxidation states, and concentration gradients present during oxidation are essential to understanding how oxide surfaces on plutonium interact with their environment. A prerequisite to the development of accurate models is having reliable data and comparison spectra for the base material and the chemical states of interest.

Surface-sensitive techniques, typically under ultra-high vacuum (UHV) conditions, are often used for the study of the surface chemistry of plutonium and its oxides. For these studies, x-ray photoelectron spectroscopy (XPS) has typically been the technique of choice as it is ideally suited for the study of oxidation states by analyzing XP peak shape and position changes [1-3]. This allows for the identification of relative changes in the Pu 4f manifold in going from Pu metal, to the Pu sesquioxide (Pu_2O_3), to the Pu dioxide (PuO_2). But there are advantages of other surface science techniques, specifically Auger electron spectroscopy (AES), over XPS for certain types of studies. Prime among them is that AES has a much higher spatial resolution than XPS allowing for analysis of specific areas and features on a surface down to a few tens of nanometers. The high spatial resolution is particularly relevant for investigating inclusions or impurity phases within the metal matrix such as Pu carbides (PuC_y) or iron intermetallics (Pu_6Fe). And although AES typically suffers from less sensitivity and specificity to chemical state differences in its peak shape and position, modern Auger systems have alleviated much of this shortcoming.

For plutonium, Auger peaks for the metal and dioxide have been used for investigation [4-5] whereas the Auger peaks for the sesquioxide, oxy-carbide (PuO_xC_y) and impurity phases have not received the same study. In order to more fully utilize AES for the study of the oxidation of plutonium surfaces, the relative changes in the Auger peaks in going from Pu metal to all of its oxides as well as other relevant phases must be quantified. Peak positions from both normal and derivative spectra, estimates of relative sensitivity factors, and quantification from peak-to-peak heights must be determined. For this work, relative changes in both the integrated and derivative Auger peak shapes and positions have been identified and will be presented.

Figure 1 shows both integrated and differentiated Auger spectra for Pu metal, PuO_2, and Pu_2O_3. For this data set, a Ga-stabilized delta Pu sample was sequentially sputtered to obtain a clean surface and O_2 dosing was performed in UHV to grow the oxides. It is important to note that both the peak position and shape of the Auger manifold are sensitive to sample conditions so care must be taken to fully characterize and understand the bulk Pu metal and any impacts from the surface preparation of the sample as they can dramatically influence the data. In particular, since some surface preparation techniques can induce the alpha phase at the surface, the delta-Pu surface was verified by electron backscatter diffraction (EBSD). The different chemical states are easily identified from both a 1 - 3 eV shift in peak position as well as changes to the overall shape of the AE manifold.

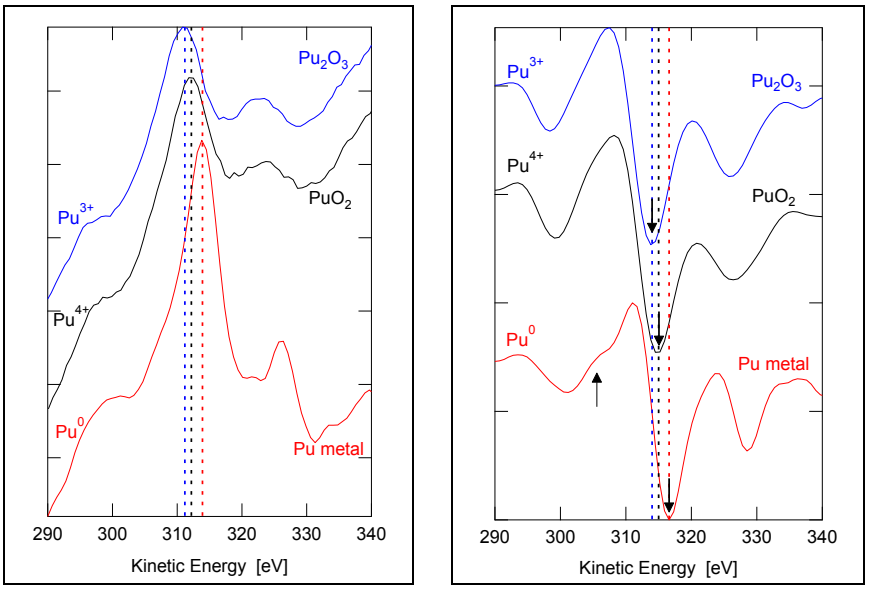

Figure 1: Integrated (left) and differential (right) Auger spectra for Pu metal and Pu oxide surfaces showing shifts in peak positions as well as differences in the structure of the AE manifold.

We have used high resolution AES to identify the Auger peak structure of Pu metal, oxides, and impurity phases including Pu, PuO_2, Pu_2O_3, PuO_xC_y, PuC_y, and Pu_6Fe. We have studied the OPP and OVV Auger transitions in the 80 – 110 eV range as well as the NOV transitions at approximately 315 eV. A variety of samples and sample preparation techniques have been utilized to obtain a comprehensive and coherent data set. Pu metal, PuC_y, and Pu_6Fe samples have been sputtered to a clean surface to identify the relevant phase. Oxide surfaces have been investigated via growth of a native oxide and oxygen (O_2) dosing on Pu metal surfaces. For the dosing studies, oxygen doses of less than a Langmuir up to over 1000 Langmuirs have been investigated.

We will present data and discussion of AES studies on the elemental and chemical state species present within the surface and near-surface region of plutonium samples. We will discuss studies of the metal, impurity phases, and oxides. Studies of the oxides include both oxidation and auto-reduction of plutonium with exposure to oxygen in UHV system as well as growth of a native oxide from atmospheric exposure. The surface and near-surface conditions of plutonium samples and their relationship to the plutonium thin-film system will be discussed. We will take advantage of the higher spatial resolution of AES to further study plutonium oxide properties such as layer structure, oxidation kinetics, and auto reduction on polycrystalline plutonium samples. We will additionally correlate the Auger data with other surface sensitive techniques such as XPS, spectroscopic ellipsometry (SE), and time-of-flight secondary mass spectrometry (ToF-SIMS).

References

[1] H.G. Flores, P. Roussel, D.P. Moore, D.L. Pugmire; Surf. Sci., **605**(3), 314 (2011).

[2] A.J. Nelson, P. Roussel; J. Vac. Sci. Technol. A **31**(3), 031406 (2013).

[3] M.T. Butterfield, T. Durakiewicz, E. Guziewicz, J.J. Joyce, A.J. Arko, K.S. Graham, D.P. Moore, L.A. Morales; Surf. Sci. **571**(1-3), 74 (2004).

[4] D.T. Larson; J. Vac. Sci. Technol. **17**(1), 55 (1979)

[5] D.T. Larson and R.O. Adams; Surf. Sci. **47**(2), 413 (1975).

A-20

The influence of hydrogen pressure and reaction temperature on the nucleation and growth kinetics of plutonium hydride

Gan Li, Huilong Yu, Haibo Li

China academy of engineering physics, Mianyang, Sichuan, China

Introduction

Due to the highly pyrophoric and catalytic nature of plutonium hydride, there are considerable technical and safety issues arising from hydride formation. For the safe and long term storage of plutonium, a comprehensive knowledge of plutonium hydriding kinetics is desirable. The hydriding kinetics can be separated into two independent stages, namely a nucleation and growth stage followed by a bulk reaction. The latter stage has been studied in detail and the associated kinetics and rates have been well defined, while the early stage has received relatively little attention. In the present study, the influence of hydrogen pressure, reaction temperature and the state of surface oxide on the hydride nucleation and growth velocities were determined.

Experimental method

The experiment was performed using a stainless steel reaction cell with an integrated viewing window. The δ-Pu sample was wet abraded to remove the gross oxide layer then located within the reaction cell. Once system base pressure was achieved, the sample was heated to 423 K to remove the adsorbed impurities, and then oxidized at 323 K for 1 hour under oxygen of 50 mbar to form a surface layer of PuO_2. For preparation of the sample with a surface layer of Pu_2O_3, the pre-oxidized sample was heated at 423 K for two hours under vacuum.

Following the pre-treatment, the reaction cell was evacuated and maintained at the reaction temperatures of 303-333 K, high purity hydrogen was introduced to react with the sample at the pressures of 0.1-1.0 bar. The digital microscope recorded images of the visible reacting surface every second during the course of the reaction. Once the sufficient hydride sites had appeared on the sample surface, the reaction was terminated by evacuation of hydrogen. The captured images were analyzed using image analysis software.

Results

By measuring the number of hydride sites formed in the visible area as function of time for the PuO_2-coated sample, the nucleation profiles at given experimentally applied *P-T* conditions were obtained. The nucleation at initial stage is relative slow, and then proceeded rapidly at an approximately constant rate. As may be expected, increasing the hydrogen pressure or reaction temperature significantly increase nucleation rate. Empirically, the variation of the nucleation rate with temperature and pressure was determined, which are broadly consistent with a protective oxide layer acting as a diffusion barrier.

The lateral growth velocity U_s was determined by measuring the diameter of a certain growing nucleus as a function of time and averaging this growth rate over the different nuclei. From the deduced values of U_s under a variety of experimental conditions, both the pressure and temperature dependence of U_s were evaluated. U_s was found to be linearly proportional to the square root of the hydrogen pressure, which indicated that the dominate step of the growth process is the hydrogen dissociation on the surface hydride. The apparent activation energy was estimated to be 24 kJ/mol by an Arrhenius plot of the slopes of U_s vs temperature, which is closed to the values of uranium (23 kJ/mol) and cerium (26 kJ/mol).

In addition, the influence of Pu_2O_3 surface on the early hydriding kinetics of plutonium was examined. Under equivalent hydrogen pressure of 0.4 bar and reaction temperature of 303 K, the nucleation rate and lateral growth velocity of the Pu_2O_3-coated sample were found to be about 15 times and 3 times higher than those of the PuO_2-coated sample, respectively. This significant difference may result from the large oxygen vacancy density in Pu_2O_3, which facilitate migration and accommodation of hydrogen on the one side, and decrease the growth-associated strain energy on the other hand.

A-21

Small-scale production and characterization of high-purity plutonium metal

Kerri J.M. Blobaum, Mark A. Wall, Roger A. Henderson, Mike J. Singleton, Gary R. Eppich, Kiel S. Holliday, Jason R. Jeffries, Jeff A. Stanford, Elizabeth G. Dzenitis, Athanasios Arsenlis

Lawrence Livermore National Laboratory, Livermore, CA, USA

Small-scale scientific experiments require high-purity, low activity plutonium metal that is formed into components with nanoscale surface finishes and micron-scale surface features. We have developed a process for winning micro-ingots (~300 mg) of alpha-phase Pu metal from plutonium oxide. This process involves chemical removal of Am-241, followed by a fluorination process. The metal is formed via a metallothermic reaction in an induction furnace (Figure 1).

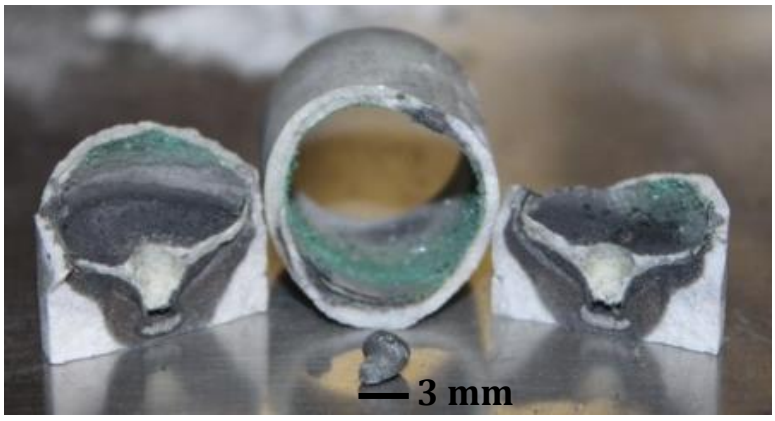

Figure 1: Pu micro-ingot produced via a metallothermic reaction (approximately 300 mg).

Optical metallography of the first Pu micro-ingots indicated a two-phase mixture (Figure 2), but the density, as measured with an immersion technique, was 19.3 ± 0.4 g/cm^3, indicating that the material had to be nearly all in the α-Pu phase (theoretical density = 19.84 g/cm^3; typical density of electrorefined, as cast material = 19.65 g/cm^3).

Extensive characterization of this material, including optical microscopy, Auger spectroscopy, mass spectrometry, x-ray diffraction, scanning electron microscopy, transmission electron microscopy, and electron microprobe, revealed that a few atomic percent of nickel contamination resulted in a euctectoid microstructure. The two phases seen in Figure 2 are α-Pu and a eutectoid mixture of $PuNi_x$ and α-Pu. This is particularly evident in the microprobe elemental maps shown in Figure 3. These images show regions of high Pu concentration (bright pink), where the material consists of α-Pu grains. The areas of lower Pu concentration (yellow areas) are mirrored in the nickel map as regions of enhanced Ni concentration. These areas are the eutectoid regions. The nickel contamination entered the process during the fluorination step, which involves high-temperature HF gas in nickel tubes.

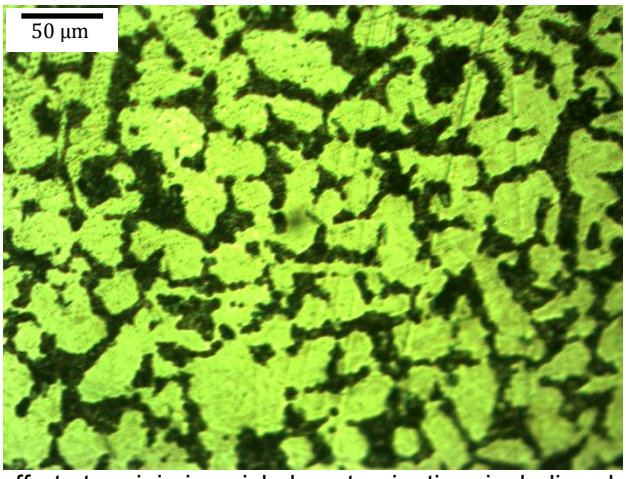

We will describe our efforts to minimize nickel contamination, including design and fabrication of a molten Pu centrifuge and use of platinum fluorination tubes. Recent batches of this Pu metal show significantly decreased impurity concentrations.

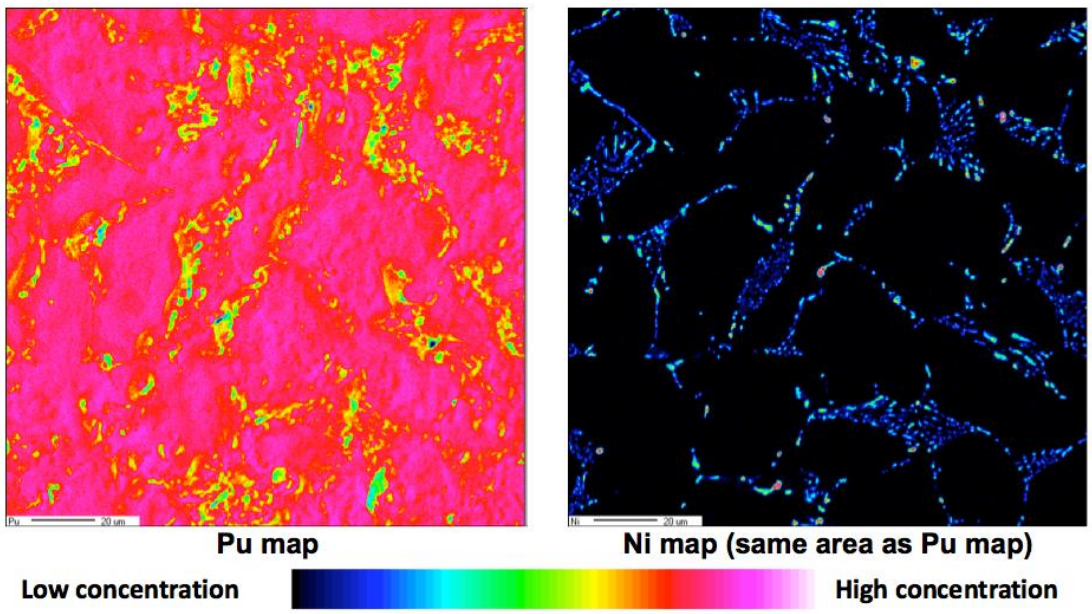

Figure 2: Optical micrograph of material produced in the Pu micro-ingot shown in Figure 1. A two-phase microstructure is indicated.

Figure 3: Electron microprobe maps showing the location of the α-Pu/PuNi$_x$ eutectoid. The bright pink regions in the Pu map indicate α-Pu grains; the yellow areas, which correspond with the blue areas of enhanced Ni concentration in the Ni map, are the eutectoid regions.

This work was performed under the auspices of the U.S. Department of Energy by Lawrence Livermore National Laboratory under Contract DE-AC52-07NA27344.

A-22

First-principles DFT+*U* Energetics of Impurity Atoms in PuO_2 and Pu_2O_3

Bingyun Ao

China Academy of Engineering Physics, P.O. Pox 919-71, Mianyang 621900, China

Plutonium (Pu) has been considered the most complicated and mysterious element in the Periodic Table because it exhibits many unusual physical and chemical properties rooted from its extremely complex 5f electronic states. Modern days problems regarding Pu involve in understanding its complex properties and predicting its aging. Among them, the solid-state properties and reaction behaviors of Pu oxides are the major concerns. However, taking solid-state properties for examples, available results focus on the two typical stoichiometric oxides, i.e., PuO_2 and Pu_2O_3. Very limited results have been reported on the behaviors of impurity atoms in PuO_2 and Pu_2O_3. From the point of view of applications, impurity atoms may play important roles in the solid-state properties and reaction behaviors of Pu oxides.

The energetics of some typical impurity atoms (H, He, B, C, N, O, F, Ne, Cl, Ar, Kr, Xe and Ga) in PuO_2, and two most-concerned impurity atoms (Ga and H) in Pu_2O_3, are calculated using a projector augmented-wave method under the framework of DFT+*U*. Three main incorporation sites for impurity atoms, i.e., octahedral interstitial, O vacancy, and Pu vacancy sites in both oxides, are considered. The results indicate that the energetics of impurity atoms depend significantly on the incorporation sites and on atomic properties such as atomic radius and electron affinity. Almost all impurity atoms considered here are energetically unfavorable at the three incorporation sites, with the exception of the F atom at the octahedral interstitial and O vacancy sites in PuO_2. The trends of incorporation energies of rare gas atoms generally reflect a size effect. Charge-transfer analysis reveals that the valence electrons can be polarized more easily with increasing atomic number of rare gas elements. Additionally, the energetics of Ga in the two oxides show that the distribution of Ga in the Pu oxide layers is strongly dependent on the distribution and the concentration of Pu vacancy. On the whole, Ga concentration might decrease with the transitions of Pu → Pu_2O_3 → PuO_2.

References

[1] B.Y. Ao, H.Y. Lu, R.Z. Qiu, X.Q. Ye, P. Shi, P.H. Chen, X. L. Wang, First-principles energetics of some nonmetallic impurity atoms in plutonium dioxide, *J. Phys. Chem. C*, 2015, 119: 14879.

[2] B.Y. Ao, R.Z. Qiu, H.Y. Lu, X.Q. Ye, P. Shi, P.H. Chen, X. L. Wang, New insights into the formation of hyperstoichiometric plutonium oxides, *J. Phys. Chem. C*, 2015, 119: 101.

[3] B.Y. Ao, H.Y. Lu, First-principles energetics of rare gases incorporation into uranium dioxide, *Nucl. Instr. Meth. Phys. Res. B*, 2016, 373: 102.

[4] S.C. Li, Y. Guo, T. Gao, B.Y. Ao, The structural, electronic, and optical properties of NpO_2 and PuO_2: a hybrid density functional theory study, *Eur. Phys. J. B*, 2015, 88: 230.

[5] R. Yang, B. Tang, T. Gao, B.Y. Ao, Structural, magnetic, electronic and optical properties of PuC and $PuC_{0.75}$: A hybrid density functional study, *J. Nucl. Mater*. 2016, 473: 54.

[6] B.Y. Ao, R.Z. Qiu, H.Y. Lu, P.H. Chen, First-principles DFT+*U* calculations on the energetics of gallium in the plutonium oxide layers, *Submitted*.

A-23

Radiation damage studies in plutonium oxides for energy production

Thierry Wiss, Rudy Konings, Vincenzo V. Rondinella, Oliver Dieste, Ondrej Benes, Jean-Yves Colle, Dragos Staicu, Philippe E. Raison

European Commission, Joint research Centre, Institute for Transuranium Elements, Karlsruhe, Germany

Plutonium is produced (almost) exclusively in nuclear reactors as a consequence of neutron capture by ^{238}U but also by decay from the other transplutonium actinides also produced by consecutive neutron captures. Plutonium is one of the main contributors to radiotoxic inventory of spent fuel and to the long-term decay heat generation. When separated from the spent fuel, plutonium can be used for energy production by fission of the ^{239}Pu and ^{241}Pu isotopes in nuclear reactors in mixed oxides fuels (MOX). Furthermore, the alpha-decay of ^{238}Pu can be used in radioisotopic thermal generators (RTG's) for space probes, but special production of substantial amounts of ^{238}Pu can only be realised by irradiation of ^{237}Np by neutrons.

Depending on their application, materials containing plutonium are subjected to radiation damage either by fission and/or by alpha-decay. This study reports on radiation damage studies in irradiated MOX fuels, in $^{238}PuO_2$ compounds used in RTGs, but also in ^{238}Pu-doped UO_2 used as analogue of aged spent fuel for the specific study of alpha-damage effects and radiogenic helium production.

Transmission electron Microscopy (TEM), Thermal Desorption Spectrometry (TDS), heat capacity measurements and X-ray diffraction (XRD), among others, have been used to characterize the damage accumulation and the helium behaviour. Conclusions will be presented on the stability of relevant materials used in different conditions of radiation, temperature and time.

A-24

First-principles modelling of point defects in fast reactor MOX fuel

Michel Freyss, Marjorie Bertolus, Ibrahim Cheik Njifon, Yaguang Li, Lei Shi

CEA, DEN, Cadarache, Saint-Paul lez Durance, France

First-principles calculations have proved to be an invaluable tool to get insight into radiation damage at the atomic scale of nuclear fuel materials. Most applications have been devoted to the standard UO_2 fuel, with great success in predicting, for instance, the mechanisms of oxygen migration [1], the location of fission products [2], and in supporting the interpretation of X-ray absorption and positron annihilation spectroscopy experiments [3,4]. First-principles calculations have, however, been scarcely used up to now to model the mixed oxide fuel (U, Pu)O_2, which will be the reference fuel for future fast reactors in France. Basic material data on (U, Pu)O_2 are, in particular, still needed for an efficient implementation of simulation of the material behavior at the mesoscopic scale, which in turn will lead to the refinement of performance codes applied to Gen IV MOX fuels.

In our study, we use the first-principles DFT+*U* method to study structural, electronic and thermodynamic properties of (U, Pu)O_2 and the stability and transport properties of point defects. The objective is to determine the effect of the chemical composition and of the deviation from stoichiometry on the properties of this mixed oxide.

In addition to the difficulty to describe the strong correlations and localization of the actinide *5f* electrons using DFT, we face one more challenge: taking into account the chemical disorder on the cation sublattice of (U, Pu)O_2 with a limited number of atoms in the simulation box. To tackle this problem, we use Special Quasirandom Structures (SQS) [5] which yield the most disordered cation mixing in a moderately sized (U, Pu)O_2 supercell containing 96 atoms, *i.e.* 32 cations, for various Pu contents [6].

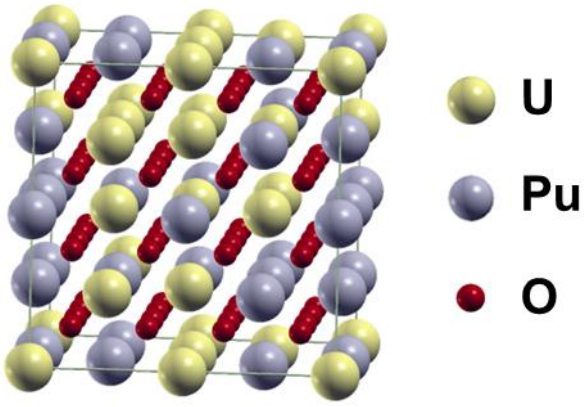

Figure 1: 96-atom supercell of (U, Pu)O_2 with 50% Pu.

We first determine bulk properties of (U, Pu)O_2 as a function of the Pu content: structural and elastic properties, mixing energies, etc. We then calculate the formation energies of various types of point defects in (U, Pu)O_2 (vacancies, interstitials, Schottky defects). The aim is to identify which type of point defects will accommodate deviations from stoichiometry, and to determine the structural and electronic modifications induced by the presence of such defects. In a disordered mixed oxide, such as (U, Pu)O_2, the defects can have various chemical environments, depending on the number of U or Pu neighbours. The effect of the defect chemical environment on their formation energy is also investigated. The results are confronted to experimental data from the literature, in particular those obtained by X-ray absorption

spectroscopy and X-ray diffraction [7,8], and to the results obtained in pure UO_2 by first-principles calculations [9,10].

Finally, atomic transport properties of defect are studied. Using the Nudged Elastic Band method (NEB), the migration energies are calculated for oxygen, plutonium and uranium defects considering various migration mechanisms. The effect of the charge state of the defects on the value of the migration energy is also considered. The determination of these migration activation energies will contribute to assess the diffusivity of point defects, which is a key parameter in the modelling of nuclear fuel behavior.

References

[1] B. Dorado *et al*., Phys. Rev. B **83**, 035126 (2011)

[2] P.M. Martin *et al*., J. Nucl. Mat. **466**, 379 (2015)

[3] R. Bes *et al.*, Appl. Phys. Lett. **106**, 114102 (2015)

[4] J. Wiktor *et al.*, Phys. Rev. B **90**, 184101 (2014)

[5] A. Zunger *et al.*, Phys. Rev. Lett. **65**, 353 (1990)

[6] J. von Pezold *et al.*, Phys. Rev. B **81**, 094203 (2010)

[7] J F. Vigier *et al.,* Inorg. Chem. **54**, 5358 (2015)

[8] R. Vauchy *et al.*, Ceramics International **40**, 10991 (2014)

[9] E. Vathonne *et al*., J. Phys.: Cond. Mat. **26** (2014)

[10] E. Vathonne, PhD Aix-Marseille University (2014)

A-25

Thermal Expansion of Delta Plutonium

Jeremy Mitchell, Franz Freibert, Scott Richmond, Daniel Schwartz, Michael Ramos

Los Alamos National Laboratory, Los Alamos, NM, USA

One of the many unusual properties of plutonium is the negative thermal expansion of its face-centered cubic δ phase. In pure plutonium, δ is stable from ~315-450 °C and the mean thermal expansion coefficient (α_m) over this temperature range is -9 x 10^{-6}. With the exception of tetragonal δ´-Pu (α_m = -66 x 10^{-6}), which has the most limited thermal stability field, all other phases have positive coefficients of thermal expansion that range from 35 x 10^{-6} to 43 x 10^{-6} [1]. Addition of as little as 1 atomic % Ga or other solutes will stabilize δ-Pu below room temperature. This stabilization has a dramatic effect on thermal expansion as a function of Ga content, with α_m ranging from 1 x 10^{-6} for Pu-2 atomic % Ga to 16 x 10^{-6} for Pu-12 atomic % Ga [2]. Thermal expansion of both thermally- and solute-stabilized δ-Pu can be quite variable depending on factors such as purity, prior thermal history, and microstructure. We have been studying other influences on the thermal expansion behavior of δ-Pu, and in this presentation we will discuss recent work on aging and hydrogen content effects coupled with bulk alloy composition.

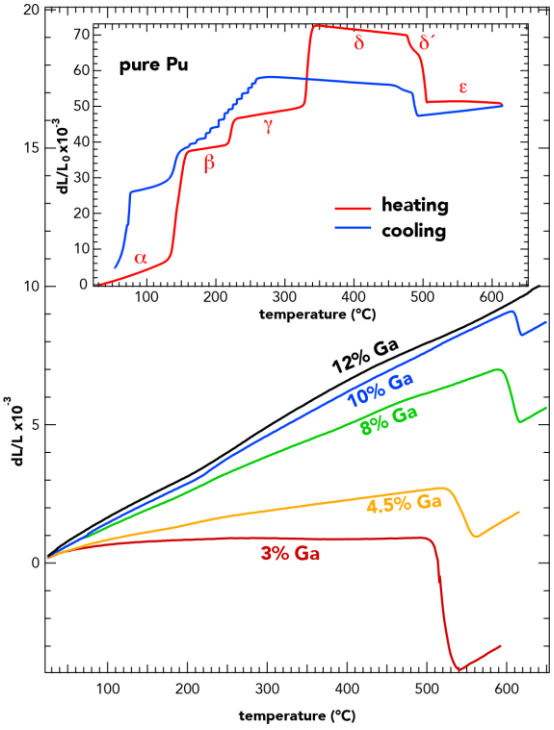

Figure 1. Dilatometric curves of pure Pu (top) and Pu-Ga alloys [2] (bottom).

References

[1] F.W. Schonfeld and R.E. Tate, The Thermal Expansion Behavior of Unalloyed Plutonium, LA-13034, September 1996.

[2] A. Goldberg and R.L. Rose, Plutonium 1970 and Other Actinides, p. 1056-1068, 1970.

A-26

EXAFS studies of self-irradiation damage in Pu

Daniel Olive[1,2], Deborah Wang[2,3], Corwin Booth[2], Eric D. Bauer[1], Alison Pugmire[1], Franz Freibert[1], Scott McCall[4], Mark A. Wall[4], Patrick Allen[4]

[1]Los Alamos National Laboratory, Los Alamos, NM, USA, [2]Lawrence Berkeley National Laboratory, Berkeley, CA, USA, [3]University of California Berkeley, Berkeley, CA, USA, [4]Lawrence Livermore National Laboratory, Livermore, CA, USA

Introduction

Plutonium metallurgy is inherently complicated, due in part to the complex role the 5f orbitals have in bonding, as well as the constant structural and chemical changes as a result of radioactive decay. The former leading to the presence of six allotropes of pure plutonium at ambient pressure, and the latter in a constant evolution of physical properties such as resistivity, length, and compressibility.

We have performed local structure measurements on Ga-stabilized δ-Pu using isochronal annealing and Extended X-ray Absorption Fine Structure (EXAFS), after a period of cryogenic storage, in order to separate damage production and annealing. The results are analyzed at various points on the annealing curve, using several techniques, to determine the damage fraction and environment from the perspective of both the Pu and the Ga sites. This enables a comparison to previous self-irradiation experiments on stabilized δ-Pu using resistivity [1], susceptibility [2], and dilatometry [3], as well as to molecular dynamics simulations of radiation damage in δ-Pu [4] and density functional theory calculations of defect sites in δ-Pu [5].

Methods

A sample of δ-Pu stabilized with 4.3 at.% Ga was placed in a closed cycle liquid He refrigerated cryostat (Montana Instruments) and stored for 72 days at the Stanford Synchrotron Radiation Lightsource (SSRL). During storage, the sample was exposed to 6.48×10^{-5} α-decays per atom, corresponding to approximately 0.02 displacements per atom (dpa). At the end of the storage period, the cryostat was moved to SSRL beamline 11-2 for isochronal annealing and EXAFS measurements. After an initial measurement at 15 K to collect data on the most damaged state, the sample was annealed to successively higher temperatures (35, 45, 55, 65, 75, 95, 105, 115, 125, 135, 156, 200, and 300 K) for 5 minutes each, before being cooled back down to 15 K for EXAFS measurements. EXAFS was collected at the Pu L_3-edge and the Ga K-edge in fluorescence geometry, using a 100-element Ge detector, and the data were corrected for self-absorption effects.

This experiment represents an improvement on a previous study on this sample [6] by taking data at 15 K instead of at the annealing temperature, and by recording additional points along the annealing curve at temperatures subject to the largest variations in damage fraction. In addition to the amplitude ratio method used in the previous study to determine damage fractions, full EXAFS fitting of the first near neighbor shell, and a method for estimated the undamaged region size were employed to characterize the sample. Additional details concerning the experimental methods and fitting methodologies are reported elsewhere [7].

Results

With the assumption that any loss of amplitude in the Fourier transformed EXAFS spectra is a result of becoming so disordered from their normal lattice positions by radiation damage that they no longer contribute to the EXAFS signal, we see approximately 60% of the Pu atoms, and 40% of the Ga atoms are considered heavily disordered. Using this method of damage estimation, a fractional change in damage, as a function of temperature can be calculated to generate comparisons to resistivity and susceptibility measurements. In doing so, we note that the annealing curve generated using EXAFS is a closer match to susceptibility measurements [2], with a recovery stage between 100 and 150 K for both the Pu and Ga edges. However,

using EXAFS fitting of the first near neighbor region, we account for signal lost due to highly disordered atoms, as well as a reduction in amplitude due to moderate static disorder that manifests as an increased EXAFS Debye-Waller factor.

Looking at the damaged fraction using this technique reveals a divergence in behavior between the Pu and Ga atoms. Ga appears less damaged overall, and the damage exhibits a recovery stage at a lower temperature, around 50 K, closer to resistivity results [1]. The start of this recovery is observed to coincide with an increase in moderate disorder (Debye-Waller factor). Additionally, below an annealing temperature of 135 K both data sets are best fit with a bond length contraction, but the effect is larger for Ga. A technique to estimate undamaged region size using the entire EXAFS range [8] was applied to these data. This revealed a steadily increasing region size of undamaged regions for both Pu and Ga, but the data are consistent with Ga having a greater fraction of atoms in the crystalline state before the annealing process starts. At the same temperature a jump in disorder is observed, the crystalline fraction drops to approximately the same value as Pu. They both increase together, reaching fully crystalline state by 135 K. These results, as well as additional EXAFS data collected on other samples, will be presented and discussed.

Acknowledgements

We gratefully acknowledge the support of the U.S. Department of Energy (DOE) through the Los Alamos National Laboratory (LANL) LDRD Program and the Glenn T. Seaborg Institute for Transactinium Science. LANL is operated by Los Alamos National Security, LLC, for the National Nuclear Security Administration of the U.S. DOE under Contract DE-AC52-06NA25396. Use of the Stanford Synchrotron Radiation Lightsource, SLAC National Accelerator Laboratory, is supported by the U.S. DOE, Office of Science, Office of Basic Energy Sciences under Contract No. DE-AC02-76SF00515. Work at Lawrence Berkeley National Laboratory was partially supported by the Director, Office of Science (OS), Office of Basic Energy Sciences (OBES), Chemical Sciences, Geosciences, and Biosciences Division of the U.S. DOE under Contract No. DE-AC02-05CH11231. Work at Lawrence Livermore National Laboratory was prepared under DOE Contract DE-AC52-07NA27344.

References

[1] M. J. Fluss, B. D. Wirth, M. Wall, T. E. Felter, M. J. Caturla, A. Kubota, and T. D. de la Rubia, “Temperature-dependent defect properties from ion-irradiation in Pu (Ga),” Journal of alloys and compounds, vol. 368, no. 1, pp. 62–74, 2004.

[2] S. K. McCall, M. J. Fluss, B. W. Chung, M. W. McElfresh, D. D. Jackson, and G. F. Chapline, “Emergent magnetic moments produced by self-damage in plutonium,” Proceedings of the National Academy of Sciences, vol. 103, no. 46, pp. 17179–17183, 2006.

[3] J. Jacquemin and R. Lallement, “Contraction des phases β et δ du plutonium sous l’effet de l’autoirradiation a 4.2 K,” Physics Letters A, vol. 33, no. 6, pp. 384–385, 1970.

[4] A. Kubota, W. G. Wolfer, S. M. Valone, and M. I. Baskes, “Collision cascades in pure δ-plutonium,” Journal of Computer-Aided Materials Design, vol. 14, no. 3, pp. 367–378, 2007.

[5] S. C. Hernandez, D. S. Schwartz, C. D. Taylor, and A. K. Ray, “Ab initio study of gallium stabilized δ-plutonium alloys and hydrogen–vacancy complexes,” Journal of Physics: Condensed Matter, vol. 26, no. 23, p. 235502, 2014.

[6] C. H. Booth, Y. Jiang, S. A. Medling, D. L. Wang, A. L. Costello, D. S. Schwartz, J. N. Mitchell, P. H. Tobash, E. D. Bauer, S. K. McCall, M. A. Wall, and P. G. Allen, “Self-irradiation damage to the local structure of plutonium and plutonium intermetallics,” Journal of Applied Physics, vol. 113, p. 093502, 2013.

[7] D. T. Olive, D. L. Wang, C. H. Booth, E. D. Bauer, A. L. Pugmire, F. J. Freibert, S. K. McCall, M. A. Wall, and P. G. Allen, “Isochronal annealing effects on local structure, crystalline fraction, and undamaged region size of radiation damage in Ga-stabilized δ-Pu,” arXiv preprint arXiv:1602.03913, 2016.

[8] D. T. Olive, H. Ganegoda, T. Allen, Y. Yang, C. Dickerson, and J. Terry, “Using a spherical crystallite model with vacancies to relate local atomic structure to irradiation defects in ZrC and ZrN,” Journal of Nuclear Materials, 2016, DOI:10.1016/j.jnucmat.2016.04.004, (in press).

A-27

Fuel Cycle Concept with dispersion type Fuel in LWRs

Aleksei Savchenko, Leonid Karpyuk, Dmitry Shamin, Oleg Uferov

A.A. Bochvar Institute (VNIINM), Moscow, Russia

Generation II Light Water Reactors (LWRs) are the dominant world commercial nuclear power plant. Currently, 90% of the installed reactors worldwide operate on a once-through nuclear fuel cycle, utilizing uranium dioxide fuel. To optimize the fuel cycle MOX fuel has been considered for thermal reactors, although some limitations exist, that make MOX fuel be used only in one fuel cycle. The most relevant are: the degradation of Pu isotopic vector, the insufficient uranium density, high operating fuel temperature and the low serviceability under transients.

We suggest replacing the container design fuel rod, for which possibilities are practically exhausted, by dispersion type fuel elements. Structurally, advanced METMET dispersion type fuel consists of uniformly distributed higher density fuel granules of U-Mo, U-Nb-Zr or U_3Si alloys that are metallurgically bonded between themselves and to fuel cladding with specially developed Zr-based matrix alloys. A fuel meat retains controllable porosity in the range of 16-38% to accommodate fuel swelling [1-2].

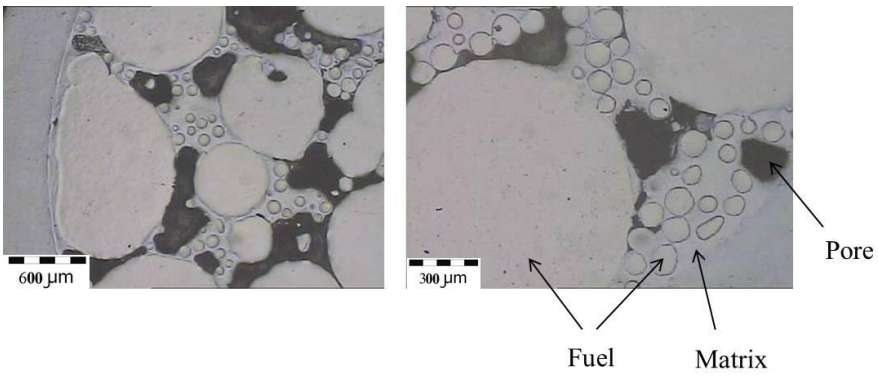

Fig. 1. Microstructure of modified composite fuel with higher uranium content. Conditions: 72% volume fraction of fuel under the cladding, technological parameters: t = 900°C and τ =60 s, fuel column length: 800 mm.

The primary advantages of advanced METMET fuel for application in thermal reactors are high uranium content (25-50% higher in comparison with the standard UO_2 pelletized fuel rod), low temperature of fuel (<500 ºC, cold fuel), the extension of burn-up (100 MW*d/kgU) and serviceability under transient conditions.

Due to high uranium content and hence intermediate neutron spectrum the main economically significant characteristics for PWR's can be improved:

1. Larger quantities of generated plutonium (~2.5-3 times higher).

2. Increasing of fissionable plutonium isotopes up to 75-78% in spent fuel (harder neutron spectrum).

3. Increasing the breeding ratio up to 0.7-0.8 (by reducing the hydrogen-to-heavy metal ratio).

4. The prolongation of the campaign will be more than 30% in effective days (up to 500 additional effective days).

5. Increasing the time between refuelling, in other words, increasing the Unit Capacity Factor (UCF). In this case instead of a year or a year and a half fuel cycle at two year cycle becomes feasible.

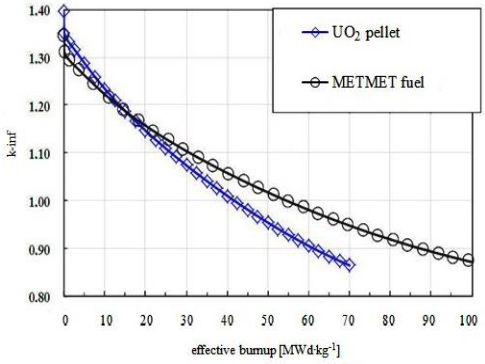

Fig. 2. K-inf versus effective burn-up for UO_2 and advanced METMET fuel

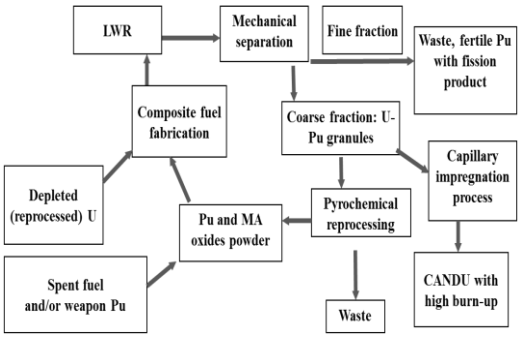

Fig. 3. LWR fuel cycle with composite fuel and multiply recycling of Pu

On the basis of METMET fuel, composite U(Th)-PuO_2 fuel (an analogue of MOX) can be fabricated where depleted uranium alloy and dioxide plutonium powder have initially separate arrangement [1-2]. The fuel element development approach consists of individual operations used to fabricate a fuel element with uranium as the main component and to fill it with plutonium dioxide powder, which minimizes dust producing operations on the fuel element fabrication. According to new fuel element design, a framework fuel element having a porous uranium alloy meat (U-Mo or U-Zr alloys) is filled with standard PuO_2 powder of less than 70 micron fraction prepared by pyrochemical or other methods. In this way a high uranium content fuel meat metallurgically bonded to cladding forms a heat conducting framework, pores of which contain PuO_2 powder. Instead/or in combination with Pu dioxide powder, other MA oxides can be used based on Am and Np. This approach can be also implemented with the use of Th granules in place of depleted uranium alloy granules. In this case the conversion ratio is increased.

Due to this as compared to MOX fuel the new one features higher thermal conductivity, higher uranium content, hence, high conversion ratio, does not interact with fuel cladding and fabrication technology is more environmentally clean. Composite fuel is intended for use in thermal and fast reactors as it features higher characteristics in comparison to MOX or metallic (U-Pu-Zr) fuel.

Mechanism of composite fuel operation: first PuO_2 burns up in metmet fuel form while Pu generates in the metmet fuel that first serves as a breeding blanket and then begins to burn up. Consequently, the components of the composite fuel have different Pu isotope compositions at the cycle end. The plutonium dioxide powder will basically accumulate non-fissionable isotopes while the METMET fuel – fissionable species.

In composite fuel U alloy and PuO_2 powder have initially separate arrangement in a fuel composition, so we can separate fissile Pu from fertile one. Mechanically evoked from cladding granules of generated U-Pu alloy can be used repeatedly in PWR and CANDU reactors using capillary impregnation method as they have high content of generated Pu. Hence in comparison to MOX we can multiply use of generated Pu in spent fuel and instead of partial recycling implement full recycling which drastically reduces the fuel waste.

Thus, using novel concept based on high density dispersion and composite fuel the closed U-Pu cycle in thermal reactors can be implemented – as the fuel available to these reactors may be increased by ~48% (18% in case of MOX). The remained Pu fissile isotopes can be used from the accumulated thermal reactor spent fuels.

References

[1] A. Savchenko, et al., Journal of Progress in Nuclear Energy **119-125**, 72 (2014).

[2] A. Savchenko, et al., Journal of Progress in Nuclear Energy **138-144**, 57 (2012).

A-28

MD study of self-irradiation effects on dislocation dynamics in δ-Pu

Alexey Karavaev, Vladimir Dremov, Gennady Ionov

Russian Federal Nuclear Center - Zababakhin Institute of Technical Physics (RFNC-VNIITF), Snezhinsk, Chelyabinsk region, Russia

Previously we performed intensive Molecular Dynamics (MD) study with the Modified Embedded Atom Model (MEAM) [1] into the phenomena caused by self-irradiation of δ-Pu-Ga alloys and their effects on mechanical and thermodynamic properties [2-9]. We demonstrated the primary radiation defects (PRDs) from the displacement cascades [2,3] to accumulate in the lattice during long-term storage [4] and to affect elastic properties, dynamic strength [5], phase transition boundaries [6] *etc*. In [7] we also investigated the behavior of He atoms in the lattice and compared it with that observed experimentally [10]. In [9] it is shown that at the ambient conditions vacancies feel mutual attraction, and it is thermodynamically "profitable" to form voids. Moreover, the formation of voids on edge dislocations is more thermodynamically preferable than in the bulk of the lattice, *i.e.* the edge dislocations are the effective drains of vacancies. The most thermodynamically stable form of vacancy clusters on edge dislocations is a nearly spherical void of size ~110 vacancies. The voids pin the dislocations and impede their sliding under shear stress. The pining is a plausible explanation of the observed increase of static yield stress in accelerated aged Pu-Ga alloys [11-13]. In the present work we focus on MD simulations to quantify the effect of the pining on edge dislocation dynamics and Peierls stress.

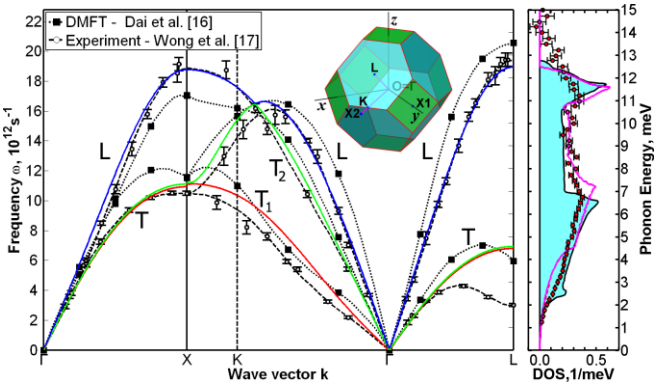

Figure 1. Phonon dispersion relations in δ-Pu 2 at. % Ga alloy. The experimental data at the ambient conditions [17] are shown by circles. The solid lines are calculated phonon dispersions in the MEAM MD. The dotted curves with black squares are dispersions for pure δ-Pu from DMFT [16]. Right panel: black line – DOS from experiment [17], red circles – experiment for δ-Pu 5 at. % Al alloy at 300 K [18], magenta line – DOS in the MEAM MD.

To model dislocation dynamics we have to be sure that the MEAM accurately reproduces the elastic properties of the material in particular elastic constants with huge Zener anisotropy (Z=7.03). The previous parameterization [5] of the MEAM qualitatively reproduces the elastic properties but gives low Zener anisotropy (Z≈3), high Debye temperature, and overestimates stacking fault energy (SFE) (60 mJ/m^2) compared to experiment (30 mJ/m^2) [14]. We decided to optimize the MEAM with the following targets: lattice parameters for pure Pu at T=600 K and for Pu 6 at. % Ga at T=300 K, phonon dispersion relations at the ambient conditions (based on DMFT [16] and experiment [17,18]), and the SFE value (see Table 1). In Fig.1 one can see that the MEAM is able to reproduce almost all the features of the phonon spectra except for the substantial softening of the TA[111] branch toward the L point. The quantitative reproduction of the experimental elastic constants and SFE results in the accurate description of the dislocation core structure (See Fig. 2) with width 5-6 Burgers.

Next we model dislocation dynamics under shear stress using stress relaxation [19] down to nearly zero dislocation velocity and thus estimate Peierls stress. We perform simulations in the absence of defects in the crystal structure and for samples with distributed vacancies and with small vacancy clusters in the form of voids seating on the dislocations. We demonstrate that the voids cause the pinning of the dislocations and impede their sliding (see Fig. 3). The quantitative estimates of the critical shear stress increase due to the dislocation pinning by the voids are made.

Table 1. Properties of δ-Pu-Ga alloys calculated with the MEAM (this work) and DMFT [16] in comparison with experimental values. C_{11}, C_{12}, C_{44}, $C'=(C_{11}-C_{12})/2$ are in GPa. $Z=C_{44}/C'$ is Zener anisotropy. Θ_D is Debye temperature in K is calculated from the elastic constants. E_{SF} is stacking fault energy in mJ/m^2. d is edge dislocations width in Burgers vectors. [a] – ref. [15]; [b] – ref. [14].

	C_{11}	C_{12}	C_{44}	C'	Z	Θ_D, K	E_{SF}	d
Experiment	36.28[a]	26.73[a]	33.59[a]	4.78	7.03	104.6	30[b]	~5[b]
MEAM	38.39	28.37	30.58	5.01	6.10	103.9	29.5	5-6
DMFT [16]	34.56	26.81	33.03	3.88	8.52	99.3	-	-

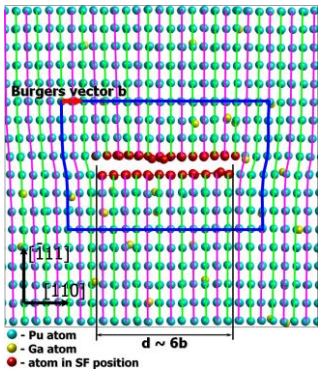

Figure 2. Structure of the edge dislocation in δ-Pu 3 at. % Ga alloy according to the MEAM MD. Burgers vector: **b**=1/2 [110]. The structure was determined by the ATA [20].

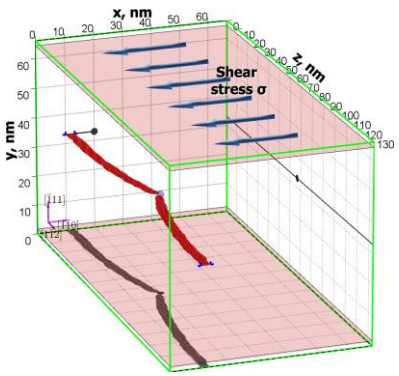

Figure 3. Thermodynamically equilibrium void of 110 vacancies (blue sphere) seating on edge dislocation (red) and pinning it. The host fcc lattice is not shown.

References

1. M.I. Baskes, Phys. Rev. B, 46, 2727 (1992).
2. V.V. Dremov *et al.*, J. Alloys Comp., 444-445, 197 (2007).
3. S.I. Samarin and V.V. Dremov, J. Nucl. Mater., 385, 83 (2009).
4. V.V. Dremov *et al.*, J. Nucl. Mater., 385, 79 (2009).
5. V.V. Dremov *et al.*, J. Nucl. Mater., 414, 471 (2011).
6. V.V. Dremov *et al.*, J. Nucl. Mater., 440, 478 (2013).
7. A.V. Karavaev et al., Acta Mater., 79, 248 (2014).
8. A.V.Karavaev and V.V. Dremov, J. Nucl. Mater., 457, 94 (2015).
9. A.V. Karavaev, V.V. Dremov, and G.V. Ionov, J. Nucl. Mater., 468, 46 (2016).
10. A.J. Schwartz *et al.*, Philos Mag., 85, 479 (2005).
11. B.W. Chung *et al.*, J. Nucl. Mater., 355, 142 (2006).
12. B.W. Chung *et al.*, J. Nucl. Mater., 385, 91 (2009).
13. B.W. Chung, K.E. Lema, and P.G. Allen, J. Nucl. Mater., 471, 239 (2016).
14. R.L. Moment, Met. Trans., 3, 1639 (1972).
15. H.M. Ledbetter and R.L. Moment, Acta Metall., 24, 891 (1976).
16. X. Dai *et al.*, Science, 300, 953 (2003).

17. J. Wong *et al.*, Science, 301, 1078 (2003).
18. R.J. McQueeney *et al.*, Phys. Rev. Lett., 92, 146401 (2004).
19. A.V. Karavaev, V.V. Dremov, and G.V. Ionov, EPJ Web of Conf., 94, 04007 (2015).
20. F.A. Sapozhnikov, G.V. Ionov, and V.V. Dremov, Rus. J. Phys. Chem. B, 2, 238 (2008).

A-29

Secure and certify studies to work on production of spiked plutonium

Ashraf Elsayed

Brno University, Brno, Czech Republic

In the nuclear weapons sites, work on materials include non-nuclear testing of components of weapons that are sitting in the sites that include fundamental physics and engineering experiments on plutonium and investigating technologies for remanufacture of plutonium parts in nuclear weapons and work on production of spiked plutonium which incorporates more of the isotope plutonium 238 than would normally be found in weapon-grade plutonium, 7.5 % rather than the typical 0.036 %. As plutonium 238 is more radioactive, the spiking process accelerates the formation of defects that occur within the metal during alpha decay of plutonium, the new alloy ages more quickly, on the equivalent of 16 years for every year of actual aging, which makes it perfect for experiments on plutonium decay, If typical weapon-grade plutonium, plutonium 239 is spiked with some plutonium 238, which decay more quickly, the self-irradiation process dramatically picks up speed. If 5% of plutonium 239 is replaced with plutonium 238, the sample will age 11 times faster than normal plutonium 239. Aging is faster by a factor of 16 over normal aging processes if 7.5% of the sample is plutonium 238. A useful measure of acceleration aging is defined as the number of years required to reach a radiation dose that results in 10 displacements per atom. Weapon-grade plutonium normally takes 100 years to reach this dose but will need just 6.25 years if it is spiked with 5% plutonium 238. In this paper, I discuss and present advanced studies to certify a weapons test that shake, drop, heat and cool sample of fissile materials take place inside the test building.

A-30

Plutonium Handbook, Second Edition

Patrice Stevens[1], David L. Clark[1], David Geeson[2], Robert Hanrahan, Jr[3], Natanya Civjan[1]

[1]Los Alamos National Laboratory, Los Alamos, New Mexico, USA, [2]Atomic Weapons Establishment, Aldermaston, Reading, UK, [3]National Nuclear Security Administration, Washington, DC, USA

Plutonium Handbook is considered the definitive reference text for plutonium science. First issued in 1967, it was given a minor update and reprinting in 1980 with O.J. Wick as the editor. Significant progress in plutonium science in the last 40 years provided a need to update this reference work. Expertise in plutonium science exists throughout the world. Los Alamos National Laboratory is leading the effort to update the Plutonium Handbook with publication by the American Nuclear Society in 2017. Contributions from 178 authors, representing 12 countries, are providing updates and additional chapters are being incorporated. Plutonium Handbook 2nd edition will be a comprehensive, modern reference text in the critically important field of plutonium science for the 21st century.

Plutonium Handbook consists of three unique volumes.

VOLUME 1: History of plutonium, the science of the physics, metallurgy, chemistry, fabrication and modern-day utilization of plutonium and its alloys, separation of plutonium from irradiated fuels and targets, plutonium inventories, conversion chemistry of plutonium, plutonium metal and alloys, mechanical properties, corrosion and oxidation, and physical, theoretical, and experimental structure of plutonium metal and alloys.

VOLUME 2: Aqueous solution, analytical, and coordination chemistry, plutonium hydrogen system, plutonium carbides, nitrides, and halides, thermodynamic trends, environmental chemistry, plutonium microbial interactions in the environment, and optical properties and electronic structure of plutonium molecules and compounds.

VOLUME 3: Plutonium in nuclear fuels, waste forms, use of plutonium in superheavy element research, heat sources, nuclear safeguards, biology, biochemistry, and decorporation, radiation and nuclear criticality safety, plutonium facility infrastructure, safety systems, and design, and laboratory techniques.

A-31

On dislocation mechanism of dynamic deformation of uranium

Victor Pushkov, Dmitry Tsisar

Russian Federal Nuclear Center-VNIIEF, Sarov, Nizhni Novgorod reg., Russia

Study of dynamic mechanical properties of uranium and its alloys is of significant attention both in Russia and abroad, for example, in [1-6]. Such characteristics as diagrams of compression, extension, spall and shear strengths, shock adiabats and other characteristics were determined in wide range of the temperature-velocity conditions of loading [1-6]. Also the authors of these works considered microstructural changes in tested samples up to changes of dislocation structures. For example, large number of twins was revealed in [5], where shear deformation of alloy of uranium with 6% of niobium was studied at strain rate of ~2000 s^{-1}. At the same time, kinetics of plastic deformation of uranium and its alloys has been poorly studied. In this work, basing on results of the tests with study of dynamic diagrams of compression of uranium–molybdenum alloy (~1% Mo) [1], we made an attempt to determine dislocation velocity, length of free run of dislocations, and increase of dislocation density during plastic deformation of alloy at strain rates of 600-1400 s^{-1}.

It is known that sliding and twinning are the basic mechanisms of plastic deformation [7]. The dislocation mechanism of twinning is rather complicated. Therefore this work is associated with kinetics of deformation mechanism by sliding. In [8], the formula was obtained for calculation of dislocation velocity depending on tangential stress applied to the sliding plane. Force f per unit of dislocation length is $f = \sigma_s \cdot b$, where σ_s is the tangential stress, b is the Burgers vector. Three forces are effecting on rectilinear dislocation line during dynamic equilibrium. One force tends to move it forward. This force is the moving force $f = \sigma_s \cdot b$, which is caused by the effecting stress. The other two forces prevent against its motion. These forces are the inertia force $f_i = m \cdot a$, where m is the dislocation mass; and the force of viscous deceleration $f_v = B \cdot v$, where B is the attenuation constant, v is the dislocation velocity. Thus $f = f_i + f_v$ or $\sigma_s \cdot b = m \cdot dv/dt + B \cdot v$. After separation of variables and integration, we obtain the following: $v(t) = \left(\frac{\sigma_s b}{B} \right) \left[1 - e^{-(B/m)t} \right]$. In the other words, dislocation velocity equals to zero at t=0. As velocity grows, value of the viscous force approaches value of the moving force, acceleration is reduced, and velocity approaches value of the stationary velocity $v_{ss} = \sigma_s \cdot b/B$.

Since stress of flow is changed during plastic deformation, velocity of dislocations is changed as well. So, for determination of tangential stresses, which cause sliding, the authors used stresses of flow from diagrams σ-ε presented in [1]. For turning from stress of flow to tangential stress, we used the Shmid criterion from [7]: $\sigma_s = \sigma \cdot k$, where k is the Shmid factor. For polycrystal, we choose average value $k_{av.}$ Assuming absence of texture, we take $k_{av.}$=0.25. Value B is assumed as ~ 10^{-4} Pa·sec [8], and the Burgers vector is b=2.8538·10^{-10} m [9]. Figure 1 presents the dependence of dislocation velocity on alloy deformation at various strain rates.

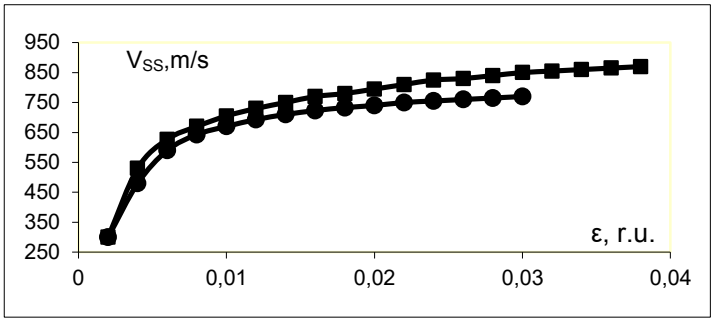

Fig. 1. Dislocation velocity versus degree of deformation of uranium-Mo alloy for 20^0C and various έ: -●-έ=740 s^{-1}; -■- έ =1200 s^{-1}.

If dislocation moved for all grain length ℓ_1 with formation of a step having value b at its edge, then the plastic deformation is $\varepsilon = b/\ell_1$ during run of one dislocation, and $\varepsilon_n = n \cdot b/\ell_1$ during run of n dislocations. However, not all of them are able to run through all crystal totally, i.e. dislocation stopped by a barrier will travel the distance $\ell_{fr} < \ell_1$, where ℓ_{fr} is length of free run of dislocation. In this case, value ε_n will be by ℓ_{fr}/ℓ_1 less, i.e. $\varepsilon_n = b\,\ell_{fr} \cdot n/\ell_1^2 = b\,\ell_{fr} \cdot N_n$, where $N_n = \acute{n}/\ell_1^2$ is density of movable dislocations, their number is $\acute{n} < n$. Further it is possible to determine increase of density of dislocations as plastic deformation grows by the formula $\Delta N = \varepsilon / b \cdot \ell_{fr}$.

With account for the theoretical background for calculation of ℓ_{fr} [7,8] and available experimental data, the dependence $\ell_{fr} = f(\varepsilon)$ was formulated. It is presented in fig.2. It is possible to see that ℓ_{fr} is sharply reduced in the beginning of plastic deformation. It facilitates formation of "forest" of dislocations when, after traveling ℓ_{fr}, dislocations are stopped, and successive dislocations are reacting with primary dislocations. Then after ~1.5% of deformation, ℓ_{fr} is smoothly reduced. Usually it occurs, if there is no a flowability site at the σ-ε diagram (alloy diagrams from [1] are such diagrams) after transition of yield strength, when cellular structure starts being formed. Figure 3 presents the dependence of dislocation density growth ΔN on strain ε obtained with account for ℓ_{fr} reduction as ε grows.

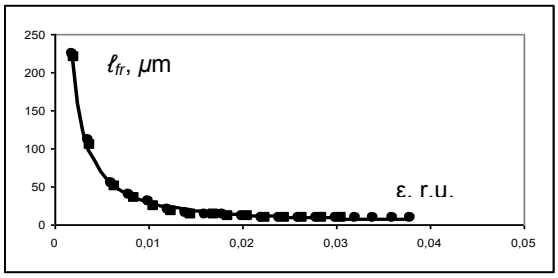

Fig. 2. Length of free run of dislocations versus degree of deformation of uranium-Mo alloy: -●-έ=740 s^{-1}; -■- έ =1200 s^{-1}.

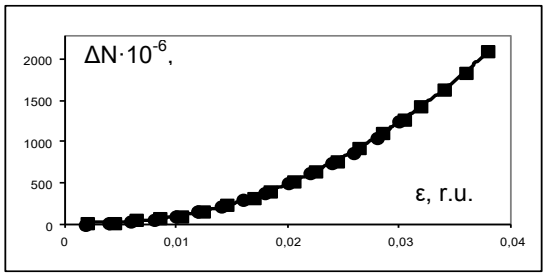

Fig. 3. Dislocation density growth vs degree of deformation of U-Mo alloy with account for reduction of ℓ_{fr}: -●-έ=740 s^{-1}; -■- έ =1200 s^{-1}.

References

1. V.A.Pushkov, A.P.Bol'shakov, G.A.Kvaskov, S.A.Novikov, V.A.Sinitsyn. Mechanical properties of uranium at quasi-static and shock-wave loading. Preprint, #54-97, Sarov, RFNC-VNIIEF, 1997, 44p.

2. E.A.Kozlov. On the problem of presence of two-wave configurations in range of 50.5-57.0 GPa in unalloyed depleted uranium and alloys of it with molybdenum. Proceedings of abstracts of papers for the V International Workshop "Fundamental properties of plutonium", 2005, Snezhinsk, Russia, p.138-141.

3. J.Buchar, S.Rolc et.al. Behaviour of uranium alloys at high loading rates. Proceed. of "DYMAT-1991", Strasbourg, France, pp.C3/191-C3/202.

4. G.T.Gray III, R.S.Hixson, C.M.Cady, S.R.Chen, M.Lopez. Influence of temperature, strain rate, and shock prestraining on the structure/property behavior of uranium and uranium 6%Nb. Abstracts of "V Int.Workshop "Fundamental Plutonium Properties", 2005, Snezhinsk, Russia, pp.118-120.

5. E.Cherreta, G.T.Gray III, P.J.Maudlin et.al. The characterization of shear deformation and shock damage in U6Nb. Abstracts of "6th US-Russian Workshop on Fundamentals of Pu Science", 2006, Lawrence Livermore National Laboratory, Livermore, CA, USA, p.66.

6. T. Le Bihan, S.Heathman, M.Idiri. Structural behavior of α-uranium with pressure to 100GPa. Phys. Rev.B, 2003, v.67, p.134102.

7. P.I.Polukhkin, S.S.Gorelik. Physical bases of plastic deformation. M., Metallurgiya, 1982.

8. J.J.Gilman. Dynamics of dislocations and behavior of materials at impact effect. Coll. book. “Mechanics”, M., Mir, v.2, #120, 1970, p. 96-124.

9. Yu.N.Sokursky, Ya.M.Sterlin, V.A.Fedorchenko. Uranium and its alloys. M., Atomizdat, 1971.

A-32

Laser Spectroscopy and Detection of Actinides and Lanthanides in Solutions

Igor Izosimov

Joint Institute for Nuclear Research, Dubna, Moscow region, Russia

The use of laser radiation with tunable wavelength allows selective excitation of actinide/lanthanide species with subsequent registration of luminescence/chemiluminescence for their detection. This work is devoted to applications of the time-resolved laser-induced luminescence spectroscopy and time-resolved laser-induced chemiluminescence spectroscopy for detection of lanthanides and actinides. Results of the experiments on Eu, Sm, U, and Pu detection are presented.

The use of luminescence methods for detection of lanthanides/actinides in solutions allows the sensitivity to reach the limit of detection (*LOD*) up to 10^{-13}mol/l (M). The background can be efficiently suppressed for lanthanides and actinides using time resolution [1-3]. Such value of limit of detection allows us to detect uranium in various samples of complicated chemical composition without separation of concomitant elements, since their quenching effect on luminescence can be diminished by dilution of the solutions to be analyzed. For Eu, Sm, and U analysis we used luminescence method with pulse (1ns) nitrogen laser excitation of the solution and time resolution for the signal registration (or Time Resolved Laser Induced Fluorescence - *TRLIF*). We performed both spectral and time resolution of the analytical signal. Time resolution is based on measurement of radiation after delay time t_d with respect to laser pulse with registration of the luminescence within a given time interval (strobe time, t_s). The optimum choice of t_d and t_s values allows excluding or significant decreasing interference of elements to be determined at level of background when these elements coexist in the solution. One of the most convenient way is the use of sodium polysilicate solution having a low self-background and providing limit of uranyl detection in our experiments up to 0.005 ng/ml. However, this method is suitable only for analysis of inorganic samples. Biological samples containing a large amount of organic substances should be preliminary mineralized. Typical concentration of uranium in blood plasma is about 0.05ng/ml – 0.5ng/ml, in urine is about 0.2ng/ml – 5ng/ml. Solution (2.2ml) was placed into a quartz cuvette and the background luminescence was measured. Then, an aliquot of the solution to be analyzed (in common case, 0.05ml – 0.2ml) was added and the total intensity of background and the sample was determined. The decay time of uranium luminescence in polysilicate was approximately 500 μs. After mineralization of the sample and preparation of a solution for analysis the decay time of uranium luminescence was about 300 μs. The limit of detection decreases by a factor of 1.5-2 in passing of blood plasma added into solution from 0.05ml to 0.15ml – 0.25 ml. Thus, the permissible volume of blood plasma does not exceed 0.15ml – 0.25 ml. Compare concentrations of the uranyl in blood plasma and in urine one can estimate the time when the uranyl was got into organism. Without mineralization the limit of uranyl detection in blood plasma was 0.1 ng/ml and after mineralization was up to 8pg/ml – 10pg/ml.The limit of uranyl detection in urine in our *TRLIF* experiments was up to 5 pg/ml. We applied *TRLIF* for samarium and europium detection in urine. We found that a high sensitivity of europium and samarium detection in aqueous solutions can be reached in the case of complex formation of these elements with fluorinated β-diketones and trioctylphosphine oxide (*TOPO*) in the presence of nonionic surfactants. In this work, we used pyvaloyltrifluoroacetone (*PTFA*), *TOPO*, and *Triton X-100*. The use of *PTFA* provides a low limit of detection of europium and samarium. The strongest luminescence radiation in the spectra of europium and samarium was observed at 614nm and 643 nm, respectively. The wavelength of radiation maximum for both elements does not vary in passing from neat solution to a solution with addition of urea samples. The life-times of europium and samarium luminescence are 800μs and 60μs, respectively, in both neat solution and solutions with addition of urine samples. By this is meant that in this case there is no dynamic quenching of luminescence and the variation of luminescence intensity is apparently caused by absorption of exciting laser radiation in the solution in addition of urine sample. When 0.2 ml of urine is

added into 2.2ml solution the intensity of luminescence decreases by a factor more than 2; hence, the volume of the sample required for analysis should be increased. The limit of detection was estimated from the 3σ background criterion, where σ is the standard deviation of the background measurements. In pure solution the limit of detection of europium was 0.005ng/ml and samarium, 0.07ng/ml. After addition of 0.2 ml of urine the limit of detection of europium was 0.015 ng/ml and samarium, 0.2 ng/ml.

Pu, Np, and some U compounds do not produce direct luminescence in solutions, but when excited by laser radiation, they can induce chemiluminescence of some chemiluminogen (luminol in our experiments) [1-3]. It is because of its high sensitivity (*LOD* from 10^{-6}M to 10^{-13} M) that chemiluminescence is widely used in many [4] fields. A key problem of chemiluminescence application to detection of lanthanides and actinides in solutions is an increase in the selectivity of detection. Appropriate selectivity can be reached when chemiluminescence is initiated by transitions within *4f/5f* electron shell of lanthanide/actinide ions, which correspond to visible spectral range. Since the energy of one quantum excitation in visible range is insufficient for initiation of luminol chemiluminescence it was proposed [1-3] to excite lanthanide/actinide ion by multi-quantum absorption of visible light.

The use of laser radiation with tunable wavelength allows selective excitation of actinide or lanthanide with subsequent registration of chemiluminescence of chemiluminogen initiated by excited actinide/lanthanide complexes. The schemes [1-3] two step-two color and two step-one color were used for chemiluminescence excitation. The intensity of chemiluminescence as a function of wavelength generated by the tunable laser (spectrum of chemiluminescence excitation) was measured. Data on luminol chemiluminescence in solutions containing Sm(III), U(IV), and Pu(IV) are analyzed. It is shown that appropriate selectivity of lanthanide/actinide detection can be reached when chemiluminescence is initiated by transitions within *4f*- or *5f*-electron shell of lanthanide/actinide ions corresponding to visible spectral range. In this case chemiluminescence of chemiluminogen (luminol) arises when the ion of *f* element is excited by multi-quantum absorption of visible light. The multi-photon scheme of chemiluminescence excitation makes chemiluminescence not only a highly sensitive but also a highly selective tool for the detection of lanthanides/actinides in solutions.

References

[1] I.N. Izosimov, Phys. Part. Nucl. **38**, 177 (2007). DOI: 10.1134/s1063779607020025

[2] I.N. Izosimov, N.G. Firsin, N.G. Gorshkov, et al., Hyperfine Interact. **227**, 271 (2014).

DOI: 10.1007/s10751-013-0990-7

[3] I.N. Izosimov, Journal of Radioanalytical and Nucl. Chem. **304**, 207 (2015).

DOI: 10.1007/s10967-014-3601-4

[4] C. Dodeigne, L. Thunus, R. Lejeune, Talanta, **51**, 415 (2000).

A-33

An in-situ X-ray diffraction study of plutonium oxidation

Paul Roussel, Wayne Lake

AWE, Aldermaston, Reading, Berkshire., UK

X-ray diffraction was used to follow the oxidation of α phase plutonium in oxygen at a pressure of 500 mbar. The composition of the growing oxide scale consisted of the trivalent cubic sesquioxide α-Pu_2O_3 and tetravalent fluorite dioxide PuO_2. The hexagonal β-sesquioxide phase was not detected. The quantity and lattice parameters of the oxide phases were determined from Rietveld analysis of the diffraction patterns. The lattice parameters of both oxides were found to decrease with increasing oxide quantity. Decreasing lattice parameters occur from increasing oxygen anion concentration in each oxide phase. The rate of oxidation for the total oxide composition at various temperatures below 100 °C was found to be linear, indicative of possible moisture enhanced oxidation. A detailed analysis of the contributions of the individual oxide compositions will be presented. Post oxidation optical microscopy of the coherent oxide scale showed areas of thicker scale typical of island growth. When the oxidation reaction was allowed to proceed to form olive green spalled oxide, X-ray diffraction analysis of the powder showed it to consist as a mixture of both cubic oxide phases.

A-34

Temperature dependent hydriding and dehydriding energies of PuH_x from *ab initio* calculations

Yu Yang, Ping Zhang

Institute of Applied Physics and Computational Mathematics, Beijing, China

Based on ab initio calculations within the density-functional theory DFT+*U* theoretical formalism, we systematically study the electronic properties of different PuHx compounds. We successfully obtain the antiferromagnetic ground state for PuH_2 and the ferromagnetic ground state for PuH_3. In combination with chemical potential calculations, we obtain the hydriding and dehydriding energies for PuH_x compounds at different temperatures, which accord well with available experimental results. The equilibrium hydrogen pressure along the hydriding and dehydriding processes is presented and carefully analyzed.

The hydriding or dehydriding process is modeled by adding or releasing a hydrogen atom in the PuHx compound. In this way, the hydriding energy corresponds to the formation energy of an interstitial hydrogen (E_{Hi}), while the dehydriding energy corresponds to the formation energy of a hydrogen vacancy (E_{Hv}). Accordingly, these two quantities are given by

$$E_{Hi} = E_{int} - E_{PuHx} - \mu_H(T, p) + qE_f, \qquad (1)$$

$$E_{Hv} = E_{vac} - E_{PuHx} + \mu_H(T, p) + qE_f, \qquad (2)$$

where E_{PuHx} and $E_{int}(E_{vac})$ are the total energies of PuH_x and of that with a hydrogen interstitial (hydrogen vacancy), respectively, $\mu_H(T, p)$ is the temperature- and pressure-dependent chemical potential of hydrogen, q and E_f are the charge state of hydrogen interstitial (hydrogen vacancy) and the Fermi energy. Charged state will not be discussed in the present work, thus the last term in the above equations vanishes.

Assuming that the environmental hydrogen atmosphere forms an ideal-gas-like reservoir, then the chemical potential $\mu_H(T, p)$ can be expressed as

$$\mu_H(T, p) = \mu_H(T, p_0) + (1/2)k_B T \ln(p/p_0), \qquad (3)$$

where k_B is the Boltzmann constant, p_0=1 atm, and

$$\mu_H(T, p_0) = \mu_H(0\ K, p_0) + (1/2)\ G(T, p_0, H_2). \qquad (4)$$

Following [1] and [2], we choose the zero reference state of $\mu_H(T, p)$ to be the total energy of hydrogen in an isolated molecule, i.e., $\mu_H(0\ K, p) \equiv 0$. With respect to this reference state, $\mu_H(T, p_0)$ is then given by

$$\mu_H(T, p_0) = (1/2)[H(T, p_0, H_2) - H(0\ K, p_0, H_2)] - (1/2)T\,[S(T, p_0, H_2) - S(0\ K, p_0, H_2)], \qquad (5)$$

where we have used the relation $G = H - TS$ between the Gibbs free energy and the enthalpy H. This allows us to obtain the aspired temperature dependence simply from the differences in the enthalpy and entropy of an H_2 molecule with respect to the T=0 K limit. For standard pressure, p_0=1 atm, these values are tabulated in thermochemical tables. Inserting them into Eq. (5) leads finally to $\mu_H(T, p_0)$. Letting a zero formation energy for hydrogen interstitial (vacancy), we also calculate and present the equilibrium criteria between different PuH_x compounds along the hydriding (dehydriding) process.

References

[1] K. Reuter and M. Scheffler, Phys. Rev. B **65**, 035406 (2002)

[2] Yufeng Zhao *et al.*, Phys. Rev. Lett. **94**, 155504 (2005)

A-35

Characterization of point defects in α-Pu

Vladimir Dremov, Gennady Ionov, Alexey Karavaev, Sergey Samarin, Filipp Sapozhnikov

Russian Federal Nuclear Centre - Institute of Technical Physics, Snezhinsk, Chelyabinsk region, Russia

Various phenomena linked with self-irradiation of δ-Pu-Ga alloys and their effects on mechanical and thermodynamic properties were investigated in [1-7] in the framework of the Molecular Dynamics (MD) approach with the Modified Embedded Atom Model (MEAM) [8] for interatomic interactions. But the MEAM failed to reproduce the stable monoclinic structure of α-Pu at finite temperatures. To enhance the flexibility of the MEAM it was generalized and the new model named GEAM [9] makes it possible to launch the whole research program for α-Pu similar to that carried out for δ-Pu-Ga alloys.

The first step is the determination of the displacement energy for hybrid Monte Carlo + MD [2] modeling of radiation damage cascades. The displacement energy averaged by escape angle for the probe particle energy 70 eV and 3 keV are 21 eV and 23 eV respectively (see Figure 1).

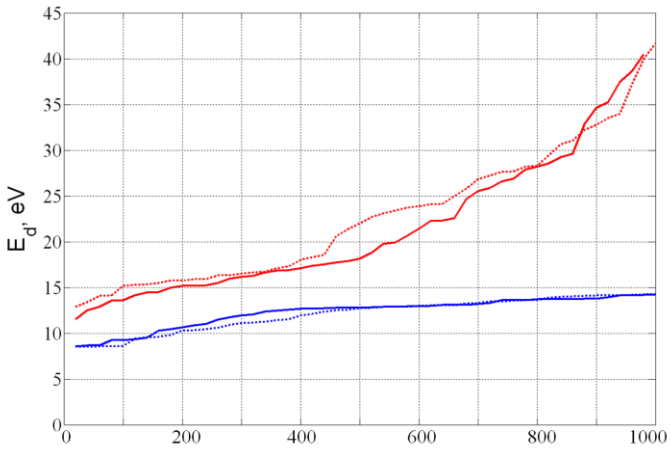

Fig. 1 Displacement energies E_d (sorted) for 1000 probe particles launched in different directions. Red curves – α-Pu, blue – δ-Pu. Dotted lines – probe particle energy 3 keV, solid lines – 70 eV.

As it was shown in MC+MD modeling the size of damaged region in monoclinic lattice was approximately the same but the number of Frenkel pairs produced is approximately half as many as in the case of the fcc material due to the higher value of the displacement energy. Subsequent MD modeling of the fast stage of annealing (4-5 ns) of damaged region in monoclinic material nevertheless resulted in approximately the same number of residual point defects (vacancies & interstitials). On the one hand, it may be explained by the lower average density of Frenkel pairs in monoclinic material which decreases the probability of vacancy-interstitial annihilation. On the other hand, at the same size of amorphous region formed around the cascade where the originally produced Frenkel pairs were dissolved, one may expect the same number of survived defects after annealing at the same temperature.

The direct MD simulations were carried out to determine parameters of Arrhenius law for the mobility of interstitials only. Figure 2 shows interstitial migration through the monoclinic lattice at T=300K. What draws attention is the two-dimensional character of diffusion in the plane (*ac*) unlike diffusion in the fcc lattice where it is essentially three-dimensional. Activation energies W and rate prefactors $1/\tau$ for other types of defects save the rate prefactor for single vacancy were determined using techniques described in [3,10]. The rate prefactor for single vacancy was

evaluated from the atomic vibrational spectrum. Results of calculations are presented in Table 1.

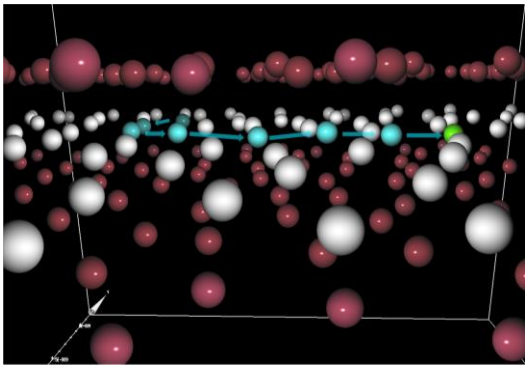

Fig. 2 Illustration of self-interstitial atom migration in monoclinic lattice of α-Pu. Cian – the chain of interstitial atom jumps within the atomic plane (*ac*) designated by white atoms, green – the position of interstitial at the end of simulation. Upper and lower neighbor planes are designated by dark red.

Table 1. Arrhenius parameters for defect mobility in α-Pu

Defect type	Activation energy W (eV)	$1/\tau_0$, s^{-1}
Interstitial	0.064	$9.85 \cdot 10^{11}$
Vacancy	1.34	$2.8 \cdot 10^{12}$
Divacancy	1.25	$3.9 \cdot 10^{12}$
Divacancy dissociation	1.47	$2.0 \cdot 10^{13}$
Trivacancy	0.72	$3.9 \cdot 10^{11}$
Trivacancy dissociation	1.35	$3.2 \cdot 10^{12}$

References

1. V.V. Dremov, F.A. Sapozhnikov, S.I. Samarin, D.G. Modestov, N.E. Chizhkova, J. of Alloys and Compounds, 444-445, (2007) 197-201.
2. S.I. Samarin, V.V. Dremov, J. Nucl. Mater., 385 (2009) 83-87.
3. V.V. Dremov, A.V. Karavaev, S.I. Samarin, F.A. Sapozhnikov, D.L. Preston, M.A. Zocher, Journal of Nuclear Materials, 385 (2009) 79–82.
4. V.V. Dremov, A.V. Karavaev, F.A. Sapozhnikov, M.A. Vorobyova, D.L. Preston, M.A. Zocher, J. Nucl. Mater. , 414 (2011) 471–478.
5. V.V. Dremov, F.A. Sapozhnikov, G.V. Ionov, A.V. Karavaev, M.A. Vorobyova, B.W. Chung, J. Nucl. Mater. , 440 (2013) 478–482.
6. A.V. Karavaev, V.V. Dremov, G.V. Ionov, B.W. Chung, Acta Materialia, 79 (2014), 248-257.
7. A.V. Karavaev, V.V. Dremov, G.V. Ionov, J. Nucl. Mater., 468 (2016), 46-55.
8. M.I. Baskes, Phys. Rev. B, 46 (1992), 2727-2742.

9. G.V. Ionov, F.A. Sapozhnikov, V.V. Dremov, M.A. Zocher, D.L. Preston, J. Nucl. Mater., 435 (2013),10-16.

10. B.P. Uberuaga, S.M. Valone, M.I. Baskes, J. of Alloys and Compounds, 444-445 (2007), 314-319.

A-36

Theoretical studies on the extraction behaviors of Am(III) and Cm(III) with amide-type ligands

Cong-Zhi Wang, Jian-Hui Lan, Qun-Yan Wu, Zhi-Fang Chai, Wei-Qun Shi

Institute of High Energy Physics, Chinese Academy of Sciences, Beijing, China

Nowadays, safe disposal of the spent nuclear fuel especially high level liquid waste (HLLW) generated during the PUREX (Plutonium Uranium Extraction) process is essential for the sustainable development of nuclear energy. Liquid-liquid extraction is an efficient method for the recovery and separation of actinides from HLLW. Due to the similar chemistries, the separation of Am^{3+} and Cm^{3+} is extremely challenging. Recently, the triamide extractant N, N, N', N', N'', N''-hexaalkyl-nitrilotriacetamide (NTAamide) was found to possess efficient extracting ability for Am(III)/Cm(III) separation in nitric acid solution. In this work, we have systematically investigated the extraction behaviors of Am^{3+} and Cm^{3+} with two amide-type ligands DMDOHEMA(N,N'- dimethyl-N,N'-dioctyl-2-(2-hexyloxyethyl)malonamide) and NTAamide(C4) in nitric acid solutions by using density functional theory (DFT). It has been found that in the 1:1 (ligand:metal) and 2:1 stoichiometric complexes, the NTAamide molecules are coordinated as tetradentate and tridentate chelating ligands, respectively, while all the DMDOHEMA ligands act as bidentate chelating ligands. The metal-ligand bonding is mainly ionic for all of these complexes. Nevertheless, molecular orbital analysis show that for all of these extraction complexes the 5f and 6d orbitals mainly contribute to the metal-ligand bonds. According to thermodynamic analysis, the 2:1 type complexes are predicted to be the most stable species in the extraction process, and the DMDOHEMA and NTAamide ligands exhibit higher selectivity for Am^{3+} over Cm^{3+}. Besides, NTAamide show relatively higher extractability for Am^{3+} and Cm^{3+}. This work might prove useful in exploring the origin of selectivity in extracting Am(III) and Cm(III) with amide-type ligands.

References

[1] Sasaki, Y.; Tsubata, Y.; Kitatsuji, Y.; Sugo, Y.; Shirasu, N.; Morita, Y., *Solvent Extr. Ion Exch.*, ***32***, 179-188 (2014)

[2] Ekberg, C.; Skarnemark, G., *Contract PARTNEW FIKT-CT2000-00087 (*2001).

A-37

Properties of solids under compression and shock : Role of electronic and structural phase transitions

Boris Nadykto

Russian Federal Nuclear Center VNIIEF, Sarov, Russia

In the present paper, pressure-induced crystalline structure and electronic phase transitions in solids are investigated. In the literature, there exist large number of experimental data sets on phase transformations of solids under high pressure and shock. Drastic changes in such solid properties as equilibrium density and bulk modulus occuring while the crystalline structure remains unchanged, are indicative of electronic phase transitions, changes in the energetic state of electrons of outer shell of atoms in solids.

Here we carry out a theoretical analysis of electronic phase transitions in solids and show that crystallyne structure phase transitions may or, more often, may not be accompanied by electronic phase transitions and that electronic phase transitions, which can occur while the crystalline structure remains unchanged, are the primary cause of sudden changes in solid properties. We demonstrate that in a number of cases, the pressure dependency of solid density for solids undergoing a series of crystalline structure phase transitions can be described by the same equation of state with the same parameters, which are independent of the lattice structure. This means that in this case the electronic state of the crystalline structures formed during a series of the structure phase transitions is identical and, hence, no electronic phase transition occurs.

For example, static compression of Na [1], [2] show that initial parameters of equation-of-state ρ_0 = 1.00 g cm^{-3}, B_0=7.8 GPa at T=0 change to ρ_0 = 1.145 g cm^{-3}, B_0=15.7 GPa at P=7.5 GPa, while the bcc structure of Na remains unchanged. New parameters ρ_0 = 1.145 g/cm^3, B_0=15.7 GPa, which characterize the new electronic state E1, adequately describe compression of Na in the pressure range of 7.5 GPa -160 GPa despite bcc-to-fcc transition in Na found in experiments [1] at 65 GPa followed by transitions to the c16, oP8, tI19 phases. The series of structural phase transitions bcc-fcc-c16-oP8- tI19 had no impact on the slope of the $P(\rho)$ curve at P>7.5 GPa. This means that the electronic state of all the bcc, fcc, c16, oP8 and tI19 structural phases is identical and that no electronic phase transition occurs in the pressure range of 7.5 GPa-160 GPa.

In [3], the tetragonal structure of Pa was observed to convert to the low-symmetry orthorhombic structure of α-uranium at P=77 GPa. However, the crystalline structure phase transition at P=77 GPa did not lead to any noticeable impact on the slope of the $P(\rho)$ curve despite drastic change in the crystalline structure. This means that the crystalline structure phase transition at P=77 GPa was not accompanied by the electronic phase transition. A sharp change in the slope of the $P(\rho)$ curve occurs at P=94 GPa, while low-symmetry orthorhombic structure of α-uranium remains unchanged. This is a clear indication of the electronic phase transition accompanied by the change in the state of electrons of outer shell in Pa atoms from initial E0 to E1. A thorough theoretical analysis of the behavior of a number of solids, including Li, Na, K, Rb, Zn, Si, Am and MgF_2 has also been carried out in the present paper.

The present work leads us to the following conclusions:

(1) Solids under compression exhibit very complex phase behavior and unusual properties, which are related directly to changes in the energy of outer electrons in the compressed elementary atomic/molecular cells due to changing electronic states and distributions of electrons in the atomic/molecular electronic shells indicating electronic phase transitions. The great variety of electronic phases of solids is a reflection of the great variety of exited electronic states observed in atomic spectroscopy;

(2) Complex phase behavior is found to be typical for not only complex solids but also elementary ones such as alkali metals including Li, K, Na and Rb. These metals under compression exhibit complex phase behavior due to changes in both the crystalline and electronic structures;

(3) In many cases, when phase transitions related to changes in the crystalline structure occur, $P(\rho)$ corresponding to different crystalline phases can be adequately described using the same set of parameters of equation of state. This means that the structural phase transitions may not be accompanied by the electronic phase transitions while the electronic phase transitions may or may not be accompanied by structural transformations;

(4) In many cases, high-pressure phases observed in static compression experiments in the diamond anvil cell were found to be also formed in shock-wave experiments behind the shock front.

The computed ρ_{0n} and B_{0n} derived from the experimental data can be utilized directly in the great variety of applications involving static and dynamic compression.

References

1. Hanfland M. et al. Phys. Rev. B. 2002. V. 65, N 18. 184109

2. Guillaume C.L. Nature Physics Letters. 2011. DOI: 10.1038/NPHYS1864

3. Haire R.G. et al. Phys. Rev., 2003, B67, 134101

A-38

2NN MEAM potential for Plutonium

Piheng Chen, Xinchun Lai

China Academy of Engineering Physics, Mianyang, Sichuan, China

Introduction

The α-decay of plutonium, resulting in an appreciable ingrowth of He and U in the microstructure, plays an important role in the aging of plutonium during storage. As of this point in time, several simulation works have been down using the molecular dynamics method with the MEAM potential [1]. The MEAM was formulated to consider only nearest neighbor interaction by using a strong screening function [2]. However, during the cascade simulation, the second nearest neighbor d istance is only a few percent larger than the first neighbor distance in the cascade zone. In such situation, the interaction between second nearest neighbor should be taken into account. In this work, an interatomic potential for plutonium has been derived based on the second-nearest-neighbor modified embedded-atom method scheme.

Description of the actual work

The potential parameters were constructed by fitting to the experimental information on the elastic constant, structural energy differences among alpha, beta, gamma, delta and epsilon structures, elastic constants, lattice constants and cohesive energy of delta Pu. Various physical properties including elastic constants, structural properties, and point-defect properties were calculated and compared with experiments in order to evaluate the reliability of the present empirical atomic-potential. We demonstrate that the present potential reasonably reproduce the unusual properties of plutonium.

Results

In this section, the fundamental physical properties of α, β, γ, δ and ε calculated using the 2NN MEAM potential shown in table 1 are presented, and compared with experimental results or first-principles calculations in order to evaluate the reliability of this 2NN MEAM potential. All the calculations were carried out using the LAMMPS code[3]. Details of calculations are shown below.

In table 2 we present the results of the calculations of some properties of bulk Pu in various crystal structures. This potential gives comparable lattice parameters and bulk modulus with experimental results.

In table 3 we present the calculated values for a number of point defects in the fcc structure. The cohesion energy for di-vacancies and tir-vacancies was found to be positive, which means that di-vacancies and tri-vacancies are energetically unfavorable than isolated vacancies. As for the larger vacancy-clusters (n>8), the cohesion energy transfer to negative, which means there is a critical size for vacancy-clusters to be stable in aged δ-Pu.

According to the saddle point and the vacancy formation energies, vacancy migration energy was found to be 0.72 eV which is agree with estimated value of ~0.55 eV by Fluss et al[4.] The sum of the formation and migration of mono-vacancy energies is 1.18 eV, which is in the range of experimental values of ~1.3$\pm$0.3 eV obtained from trace diffusion studies [5].

There are many possible interstitial configurations. The most stable configuration was found to be <1 0 0> dumbbell with a formation energy of 0.31 eV. The interstitials migration energy was evaluated by performing MSD calculations with a simulation cell containing one interstitial and with temperature ranging from 300 K to 700 K. The calculation results reveal a high mobility for the plutonium self -interstitial atoms. The interstitial migration energy was found to be 0.046 eV, and is reasonable consistent with the KMC evaluated values of ~0.1 eV [6].

Table 1: 2NN MEAM potential parameters for Plutonium

E_c	r_e	α	δ	A	β^0	β^1	β^2	β^3	t^1	t^2	t^3	C_{min}	C_{max}
3.80	4.648	3.285	0.433	1.043	1.960	2.685	5.900	8.580	1.196	4.104	-1.017	1.002	2.8

Table 2: Physical properties of bulk Pu in various crystal

	r_δ	$r_{\alpha(x)}$	$r_{\alpha(y)}$	$r_{\alpha(z)}$	$r_{\alpha(xz)}$	$r_{\gamma(x)}$	$r_{\gamma(y)}$	$r_{\gamma(z)}$	r_ε	$C11_\delta$	$C12_\delta$	$C44_\delta$
Expt.	4.63	11.21	4.93	6.18	-1.29	3.15	5.76	10.16	3.67	36.3	26.4	33.6
Cal.	4.64	11.26	5.03	6.31	-0.96	3.18	5.73	10.74	3.71	38.1	24.4	35.5

Table 3: Vacancies formation energies calculated within the 2NN MEAM

Configuration	1V	2V	3V	4V	5V	6V	7V	8V	9V	10V
E_f(eV) 4000 atoms	0.44	1.02	1.57	1.97	2.53	2.93	3.45	3.78	4.14	4.52
E_c(eV) 4000 atoms	–	0.14	0.11	-0.05	0.12	-0.04	0.07	-0.11	-0.07	-0.06

References

1. Baskes, M.I.: Atomistic model of plutonium. Phys. Rev. B 62, 15532 (2000)

2. M. I. Baskes, Phys. Rev. B 46, 2727 ~1992.

3. S. Plimpton, J. Comput. Phys. 117, 1 (1995).

4. M.J. Fluss, B.D. Wirth, M. Wall, T.E. Felter, M.J. Caturla, A. Kubota, T.D. de la Rubia, J. Alloys Compd. 368 (2004) 62

5. W.Z. Wade, D.W. Short, J.C. Walden, J.W. Magana, Metall. Trans. A, Phys. Metall. Mater. Sci. 9A (7) (1978) 965;

6. M.J. Fluss, B.D. Wirth, M. Wall, T.E. Felter, M.J. Caturla, A. Kubota, T.D. de la Rubia, J. Alloys Compd. 368 (2004) 62.

A-39

Atom Probe Tomography of Niobium Redistribution in U-14 at.% Nb After High Temperature Age-Hardening

Clarissa Yablinsky[1], Amy Clarke[1,2], Yaqiao Wu[3,4], Robert Hackenberg[1]

[1]Los Alamos National Laboratory, Los Alamos, NM, USA, [2]Colorado School of Mines, Golden, CO, USA, [3]Center for Advanced Energy Studies, Idaho Falls, ID, USA, [4]Boise State University, Boise, ID, USA

Uranium-niobium (U-Nb) alloys are of interest for defense applications and could potentially be used as metallic nuclear reactor fuels. U alloys near 14 at.% Nb have improved corrosion resistance and ductility relative to alloys with higher or lower Nb levels [1-3]. However, long term aging, aging temperature, and other thermal excursions may have an impact on corrosion resistance and mechanical properties. Aging results in complex microstructural evolution that occurs by time and temperature-dependent decomposition mechanisms, for which some chemistry and precipitation morphologies are known [4-7]. The precipitation reactions exhibit C-curve kinetics, and in this study, the non-lamellar (NL) mechanism is studied. It is our hypothesis that the NL is kinetically competitive with the discontinuous precipitation mechanism, competing for chemical driving force and storing or releasing energy at the interfaces that influences subsequent decomposition steps [8].

Preliminary scanning electron microscopy (SEM) suggested a non-lamellar, inter-connected precipitate microstructure in the NL precipitation regions in aged samples [9]. The chemical composition of the precipitates was better revealed by three-dimensional (3D) atom probe tomography (APT) characterization. This was done with the CAMECA® Local Electrode Atom Probe (LEAP) 4000X HR™ at the Microscopy and Characterization Suite (MaCS) in the Center for Advanced Energy Studies (CAES). Atom probe tips were made from the NL precipitation regions of samples aged at 500°C for 10, 100, and 10000 minutes, and investigated using APT. The data was analyzed using the IVAS® 3.2.8 software.

Figures 1 a-c show the tip reconstructions for each aging time studied. In the sample aged for 10 minutes, the precipitates are lenticular in shape and grow with aging to yield a microstructure of impinged Nb-lean α-U precipitates (purple) after 10,000 minutes. Figure 1d shows a proximity histogram, a statistical calculation of the concentration across the entire precipitate-matrix interfacial area, for each aging time. In this concentration graph, zero is the interface, precipitate concentrations are negative distance values, and matrix concentrations are positive distance values. At all aging times, the Nb has partitioned into the matrix, leaving Nb-depleted precipitates (3-4 at.% Nb), similar to expectation. As aging time increases, the Nb concentration increases from approximately 30 to 60 at.% in the matrix. In comparison, a bulk measurement of Nb yields ~12-13 at.% in all cases, consistent with bulk chemical and microprobe analysis. The proximity histograms show a downward gradient of Nb concentration as one moves away from the precipitate and into the matrix, as is expected for diffusional growth. Frequency vs. concentration profiles were also produced (not shown) in order to calculate ΔC, x_{Nb}(matrix)-x_{Nb}(precipitate), which is an indication of the energy released by progressive Nb partitioning. ΔC maps onto the phase diagram, Figure 1e, and describes the key transition concentrations in the NL regime.

This study advanced the understanding of niobium partitioning within aged samples of U-14 at.% Nb. Further analysis of these data will help to inform aging kinetics models that can be applied to a variety of thermal cycles in various manufacturing processes.

A-40

Chitin-chitozan - a Sorbent Preventing Release of Radioactive Actinide Compounds under Emergency Submersion

Tatiana Kazakovskaya, Victor Scherbakov, Edvard Goryachev, Alexander Gorelov

RFNC-VNIIEF, Sarov, Nizhny Novgorod Region, Russia

Introduction

It is widely known that under emergency submersion the seal failure could occur, so contaminating radioactivity could transfer to environment. One of the most promising methods to keep the environment safety is the use of powder sorbing agents. So the investigation of existing and search of new sorbents to prevent dangerous situations is a very actual task.

One of such natural sorbents is the natural sorbent -biopolymer on the basis of chitin-chitosan. The aim of this work is to investigate the sorption of various loose materials based on chitin-chitosan, to study the structure, to determine the physical stability in conditions imitating deep-water flooding.

Object and methods

Three kinds of materials based on chitin-chitosan were used: powdery material CHISIT-03 of three fractions, CHISIT-02 copper plated, and CHITOSAN acetilized. Besides two parties of gel chitin-chitosan were studied.

During research the specific weight, microhardness, swelling index in various solutions were measured, element composition of powders and gels was defined, such methods as dispersive analysis and electronic microscopy were used. The storage of CHISIT in the conditions of deep-water flooding was imitated using laboratory-scale plant . The tests were conducted in artificial sea water at temperature minus 1oC and pressure equal to 170 atm. The same plant was used to study sorption of the radioactive isotopes onto CHISIT under pressure. The concentration of radioactive isotopes in sea water was determined using mass - spectrometer method with isotope dilution.

Results

At room temperature the radioactive isotope content in sea water in the presence of chitin gel significantly decreases in the pH range 5.6 – 8.6.

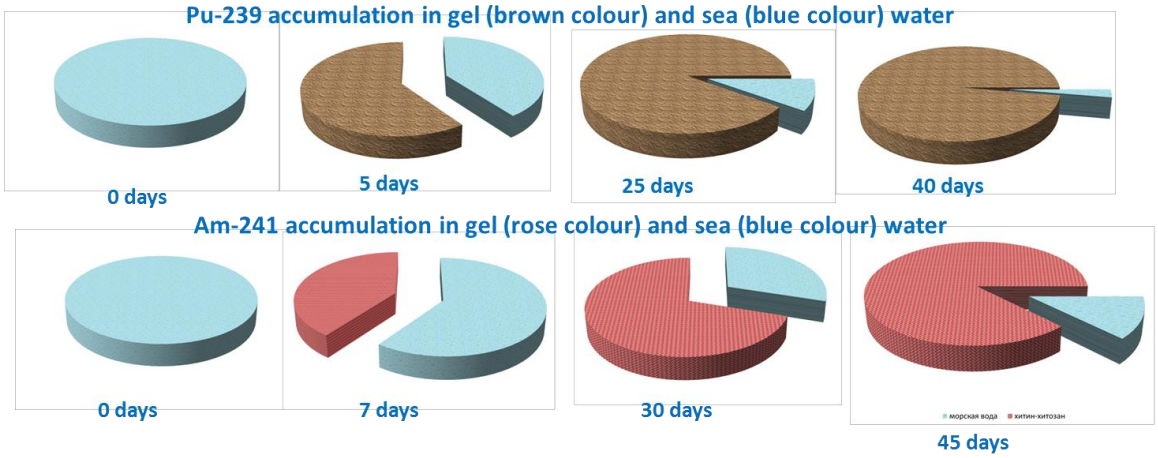

"Seeming" coefficients of distribution of a radioactive isotope between sea water and chitin gel were calculated.

It was demonstrated that chitin is a selective sorbent of various radioactive isotopes: it effectively absorbs Pu-239 and Am-241 isotopes, but is inefficient sorbent of uranium ions .

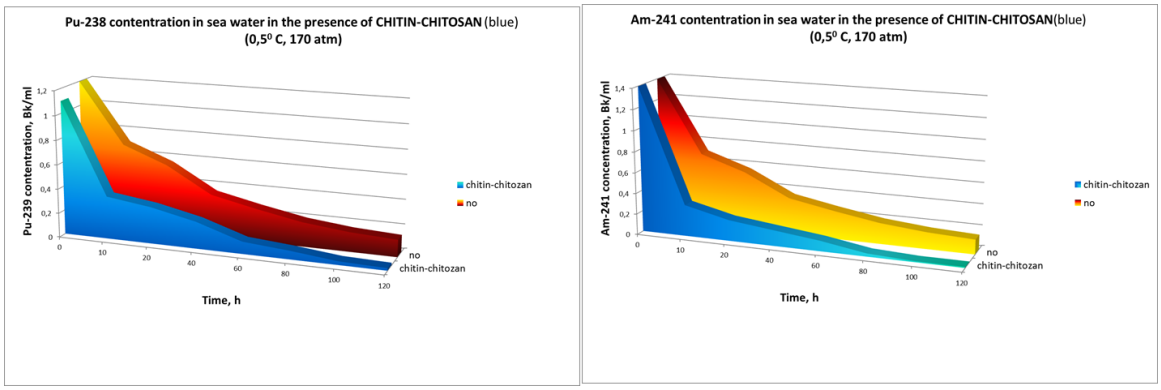

It can be explained supposing that reduction of the solution temperature leads to transformation of some radioactive metals into form of carbonates , and this fact significantly decreases the efficiency of sorption properties of chitin.

Besides, localizing properties of chitin were investigated. Study was carried out using 4 types of samples. It was shown that the 10 mm thick layer reliably holds radioactive materials within not less than 120 hours.

Conclusion

1. It was shown that plutonium-239 and americium-241 are effectively sorbed from sea water by all samples of chitin / chitosan in the conditions imitating emergency deep-water flooding.

2. The essential influence of preparation technology of composites on material microstructure was noted

3. During the exposure under pressure equal to 170 atm the non-predicted swelling was observed.

4. It is advisable to use chitin-chitosan for concentration and radiochemical purification of uranium and transuranium elements, and to increase the reliability of isolation of radioactive waste repositories.

References

1. V. V. Gromov. Dissolution of plutonium intermetallide in sea water. Radiochemistry, v..38/3, 1996.

2. V.V.Gromov, etc. Technogenic radioactivity of the World Ocean. M, Energoatomizdat.

A-41

Cerium Behavior in Various Media as Compared with Plutonium

Tatiana Kazakovskaya, Yulia Belova

RFNC-VNIIEF, Sarov, Nizhny Novgorod Region, Russia

Introduction

It is widely known that cerium and plutonium are very unusual metals with special properties, so they attract more and more investigators all over world. The most characteristic chemical features of these actinide metals are: a) the high chemical activity of their metallic states and b) the stable 3+ oxidation state in solids and solutions [1]. Numerous investigations of phase stability, phase transformations, electronic structure, and dynamic properties were done earlier. A great number of works is devoted to chemistry of Ce (a lanthanide) and Pu (an actinide). It seems very interesting to the authors to compare chemical behavior of cerium and plutonium in various media and to consider the probability to use some kinds of protective coatings to reduce corrosion and interaction with surroundings.

Peculiarities of Pu and Ce chemistry.

The element plutonium occupies a unique place in the history of chemistry. From physical, chemical, and technological perspectives, plutonium is one of the most complex and fascinating elements in the periodic table. The metal exhibits six solid allotropes at ambient pressure and its phases are notoriously unstable with temperature, pressure, chemical additions, and time [2]. With little provocation, the metal can change its density by as much as 25%. It can be as brittle as glass or as malleable as aluminum; it expands when it solidifies, and its freshly machined surface will tarnish in minutes. It is highly reactive in air, has five chemical oxidation states (six if the metal is included), and can form numerous compounds and complexes in the environment and during chemical processing [3]. Cerium is a rare-earth metal with unique properties, in some cases Ce is successfully used as a plutonium imitator [2].

Behavior in air media

To understand the essence of plutonium oxidation and corrosion processes is very important for safe and efficient use and storage of this chemically active metal. The overall rate of oxidation is less for alloyed plutonium than it is for unalloyed plutonium. Haschke (1999) has also speculated that gallium is not incorporated in the PuO_2 lattice and resides in octahedral sites of the fluorite structure. Pu–Ga alloys were found to oxidize at a lower rate than unalloyed plutonium at all temperatures in moist air. The oxidation rates were found to be greater in moist argon. However, the protection afforded by alloying was less for the case of moist argon than for moist air. Blank (1977) also summarized oxidation results for Pu–Al alloys.

At elevated temperatures, plutonium exhibits an autothermic reaction, igniting spontaneously in air when the temperature reaches 500 ^{o}C. Although the dioxide is the main corrosion product when plutonium metal is exposed to oxygen or air, there is always a layer of the cubic sesquioxide present at the metal-oxide interface. However, at room temperature, its thickness is small compared to that of the dioxide. The thickness of these various oxides depends upon a variety of factors including temperature and oxygen concentration. At temperatures exceeding 150 ^{o}C and in oxygen-poor environments, the cubic sesquioxide becomes the predominant phase, appearing as a surface product under oxygen-free environments.

Ce (even compact metal) starts oxidizing at room temperature. When temperature rises up to 300^{o} C the process in air is so fast that all metal mass could ignite, generating a considerable amount of heat enough for melting cerium dioxide (CeO_2) formed during the oxidation process. When Ce reacts with O_2 at the first stage Ce_2O_3 is formed, then Ce_2O_3 during further oxidation transforms into CeO_2. The finish corrosion products are hydrated carbonates.

Protective coatings

Sometimes in order to keep cerium samples safe (to prevent damage of samples) one needs to coat the sample with a protective film. The authors investigate the stability of Ce samples covered with varnish (2 types) and electroplated by copper. The technology of coating processes was worked out during the investigations. The corrosion tests in air media under room temperature and relative humidity equal to 75 % were done. The experiments demonstrate that the protective coatings raise the stability of cerium samples 4-12 times.

As for Pu at the present all attempts to coat plutonium metal with varnish or galvanic coating were not a success.

Behavior in water solutions

It is very important to appreciate the interaction of the investigated metals with water solutions including fresh and sea water. Because of its electropositive nature Pu atom in water solutions easily loses from 3 to 7 outer electrons [1]. The chemical behavior of plutonium depends on its oxidation state. If this parameter equals to 4, Pu is strongly hydrolyzed forming hydrogels or solid colloids. These colloids are aging, consequently their solubility decreases.

Cerium is also easily hydrolyzed in water solutions, forming cerium hydroxide. The prevailing oxidation state of cerium in water solutions is 4 (the same as Pu has).

Polarization in water electrolytes

In the literature it is difficult to find information about polarization of Pu and Ce in water solutions. So it was very interesting to compare the electrochemical behavior of these metals in various water solutions. The authors tried to get polarization curves of Pu and Ce in fresh water and in an imitator of sea water (3.5% NaCl solution). Polarization of Pu in water electrolytes were studied earlier by specialists of VNIINM, Russia. The authors repeated this investigation and provided the identical experiments with Ce. The experiments demonstrated that polarization curves for Pu and Ce in water solutions were similar. This fact corresponds to high electrochemical activity of these elements. Both for Pu and Ce there is no passivation area. The experimental results demonstrate that the electrochemical activity of Ce in sea water imitator is significantly lower than of Pu, while in fresh water the activity of both metals are practically the same.

Conclusions

The experiments confirmed that Ce is a metal with extremely high chemical and electrochemical activity.

The possibility of Ce protection with varnish or galvanic coatings is investigated. The protective coatings reduce the oxidation rate 4-12 times..

The electrochemical investigation demonstrate the necessity of further experiments to define the mechanism of Pu and Ce with water media.

References

1. V.F. Peretrukhin, C.H. Delegard, et.al. Identification of plutonium highest oxidation states in alkaline solutions by polarographic method. Proceedings of XII International Workshop “ Pu Fundamentals”, Sarov, Russia, 2013.

2. The Chemistry of the Actinide and Transactinide Elements, 4th edition, Shprienger;vol.2 David L. Clark, Siegfried S. Hecker et.al, Plutonium, p.813

3. Dunlap, B. D. and Kalvius, G. M. (1985) in Handbook on the Physics and Chemistry of Actinides, vol. 2.

A-43

Raman Spectroscopy Characterization of Uranium and Plutonium Hydride from the Hydrogen Corrosion

Xiaolin Wang, Guangfeng Zhang, Junbo Lv

China Academy of Engineering Physics, P.O. Pox 919-71, Mianyang, 621900, China

Hydriding corrosion is a significant issue for the safe, long-term storage of uranium and plutonium metal. To prevent and control the hydriding corrosion, an accurate method to identify the hydride is in great demand. Here, the uranium and plutonium hydride from the metal U/Pu-hydrogen corrosion was characterized by Raman spectroscopy.

Raman shift of uranium hydride and deuteride should match the following equation:

$$\omega_H / \omega_D \approx \sqrt{m_D / m_H} = \sqrt{2} \qquad (1)$$

Where ω_H, Raman shift of U-H bond vibration (cm^{-1}), ω_D, Raman shift of U-D bond vibration (cm^{-1}), m_H, atomic weight of hydrogen, m_D, atomic weight of deuterium. The typical Raman peaks of UH_3 and UD_3 can be characterized by the mass difference of hydrogen isotope for one another. Raman shifts of hydride and deuteride spots on uranium metal are identified to be at 738 and 950 cm^{-1} for UH_3 and 524 and 679 cm^{-1} for UD_3, respectively. It is found that the ratio between the Raman shifts of UH_3 and UD_3 pits is consistent with the expected harmonic value (1.40-1.41).

Based on the similar strategy, the hydriding spots on plutonium metal was characterized by Raman spectroscopy in situ. Raman shifts of plutonium hydride and deuteride spots are identified to be at 1061cm^{-1} and 757 cm^{-1} respectively, which also matches the above equation (1.40). According the research of Saw et al., the composition of hydriding in our study is approximate to PuH_2. Thus, the 1061cm^{-1} peak should be attributed to PuH_x (x close to 2.0) with FCC structure. According to our DFT calculation results (GGA+U+SP method), the vibration frequency at Gamma point for PuH_2 was 31.167 THz (1046.093 cm^{-1}), which further confirmed that Raman peak at 1061 cm^{-1} is the diagnostic Raman peak of PuH_x (x approach to 2.0).

References

[1] D. Avisar, T. Livneh. Raman scattering by phonons and crystal-field excitations in cerium hydrides. J. Alloy. Compd. 2010, 494: 11.

[2] G.F. Zhang, X.L. Wang, J.B. Lv. Raman spectroscopy characterization of uranium hydride and deuteride, J. Nucl. Mater. 2015, 458: 376.

[3] C.K. Saw, J.M. Haschke, P.G. Allen, W. Mclean II, L.N. Dinh, Hydrogen corrosion of plutonium: Evidence for fast grain-boundary reaction and slower intragrain reaction, J. Nucl. Mater. 2012, 429:128.

A-44

XPS study of radiation effect on UO_2 single-crystal films

Yury Teterin[1,3], Alexey Popel[2], Konstantin Maslakov[1], Anton Teterin[3], Kirill Ivanov[3], Stepan Kalmykov[1], Ross Springell[4], Thomas Scott[4], Ian Farnan[2]

[1]Chemistry Department, Lomonosov Moscow State University, Moscow, Russia, [2]Department of Earth Sciences, University of Cambridge, Cambridge, UK, [3]NRC "Kurchatov Institute", Moscow, Russia, [4]Interface Analysis Centre, School of Physics, University of Bristol, Bristol, UK

XPS determination of the oxygen coefficient k_O=2+x and ionic (U^{4+}, U^{5+} and U^{6+}) composition of oxides UO_{2+x} formed on the surfaces of differently oriented (*hkl*) planes of thin UO_2 films on LSAT ($Al_{10}La_3O_{51}Sr_{14}Ta_7$) and YSZ (yttria-stabilized zirconia) substrates was performed. The U 4f and O 1s core-electron peak intensities as well as the U 5f relative intensity before and after the $^{129}Xe^{23+}$ and $^{238}U^{31+}$ irradiations were employed. It was found that the presence of uranium dioxide film in air results in formation of oxide UO_{2+x} on the surface with mean oxygen coefficients k_O in the range 2.07-2.11 on LSAT and 2.17-2.23 on YSZ substrates. These oxygen coefficients depend on the substrate and weakly on the crystallographic orientation.

On the basis of the spectral parameters it was established that uranium dioxide films on the LSAT substrates have the smallest k_O values, and from the XRD and EBSD results it follows that these samples have a regular monocrystalline structure. The XRD and EBSD results indicate that samples on the YSZ substrates have monocrystalline structure, however, they have the highest k_O values. The observed difference in the k_O values, probably, caused by the different nature of the substrates: the YSZ substrates provide 6.4% compressive strain, whereas (001) LSAT substrates result only in 0.03% tensile strain in the UO_2 films.

$^{129}Xe^{23+}$ irradiation (92 MeV, 4.8×10^{15} ions/cm^2) of uranium dioxide films on the LSAT substrates was shown to destroy both long range ordering and uranium close environment, which results in increase of uranium oxidation state and regrouping of oxygen ions in uranium close environment. $^{238}U^{31+}$ (110 MeV, 5×10^{10}, 5×10^{11}, 5×10^{12} ions/cm^2) irradiations of uranium dioxide films on the YSZ substrates were shown to form the lattice damage only with partial destruction of the long range ordering.

A-45

pd-hybridization and paramagnon superconductivity mechanism in $PuCoGa_5$

A. A. Povzner, A. G. Volkov

Ural Federal University, Ekaterinburg, Russia

$PuCoGa_5$ is a superconductor with the relatively high superconducting transition temperature T_{SC}=18.5 K, which is significantly higher than the corresponding values for the other compounds of the group Pu-115. The experiments [1] indicate d-symmetry of the superconducting order parameter. This fact and the experimentally observed strong temperature dependence of the magnetic susceptibility near T_{SC} point to the important role of the spin-density fluctuations (SDF) in the formation of the magnetic properties and superconductivity $PuCoGa_5$.

The tetragonal crystal structure of $PuCoGa_5$ (symmetry group P4/mmm) formed by alternating layers of $PuGa_3$ and $CoGa_2$ [2], in which there is the hybridization of pd(f)- electronic states. Calculations of partial densities of electronic states for $PuCoGa_5$ show almost completely filled $f^{5/2}$-band [3], as well as a large value of the density d-electron states at the Fermi level [3]. The latter is due to the strong hybridization of the d-electron Co and p-electrons Ga.

To describe the electronic states in the layers $CoGa_2$, we use the Hamiltonian of the periodical Anderson model which been supplemented by the terms describing the electron jumps to a spin flip between the p- and d-states of neighbouring sites [4]

$$H = H_p^0 + H_d^0 + H_{pd} + H_U , \qquad (1)$$

Here: H_p^0 and H_d^o are the Hamiltonians of noninteracting p- and d-electrons, H_U is Hubbard Hamiltonian, $H_{pd} = \sum_{k,\sigma,\sigma'} V_k \left(p_{k,\sigma}^{+} d_{k,\sigma'} + h.c. \right)$ is the Hamiltonian describing the transitions between p- and d- states of neighbouring sites, $p_{k,\sigma}^{+}$, and $d_{k,\sigma}$ are operators of annihilation p- and d-electron.

The presence in (1) H_U-term does many-body problem. To solve it can use describe the effects of electron correlations in terms of internal stochastic exchange and charge fields [5]. It was shown that stochastic field split the spectrum of (pd)-electron states, as a result pd-hybridization and hybridization of spin states occur.

For analysis the occurrence of singlet pairs due to the exchange paramagnons, we used the potential of hybridization in the form

$$V_{\mathbf{k}} = \left((V_1 + V_2)/2\right)\left(\cos k_x + \cos k_y\right) + \left((V_1 - V_2)/2\right)\left(\cos k_x - \cos k_y\right), \qquad (2)$$

which explicitly takes into account the fact quasi-planar of crystal structure. In this case, we have introduced the anomalous Green function of the spin-symmetric and spin-antisymmetric states. For this function, the equation was found taking into account the most probable configuration of stochastic fields. In the immediate vicinity of T_{SC}, we found the equation for the order parameter, which repeats the d-symmetry of hybridization parameter

$$\Delta(\mathbf{k}) = \Delta \cdot V(\mathbf{k}) \Big/ \left(\sum_{\mathbf{k}} V(\mathbf{k})^2 \right)^{1/2} \qquad (3)$$

where

$$\Delta\left(T + (2U/3)\kappa \left\langle m^2 \right\rangle\right) = 0 , \qquad (4)$$

$\left\langle m^2 \right\rangle^{1/2}$ is the amplitude of SDF.

A non-zero solution of (4) occurs when the negative values of mode-mode coupling coefficient κ(<0), that corresponds to the thermodynamic instability of the ferromagnetic state [5], and takes place at the position of the chemical potential in the vicinity of the minimum function of the electron density of states or its concavity. It should be noted that the condition

κ<0 corresponds ...ɔtibility with increasing temperature.

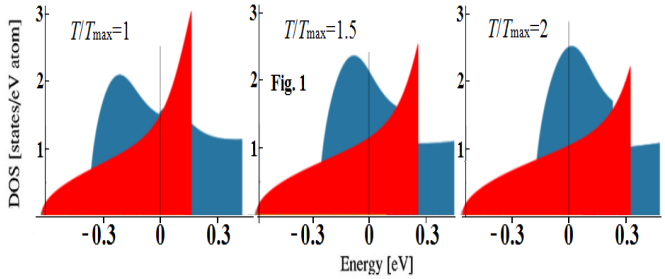

Analysis of the magnetic properties of the normal phase $PuCoGa_5$ was performed using the model in which the effects (fp)-hybridization neglected. The f-electrons are described under the LDA+U+SO-approximation [3] and spin-fluctuation approach [6]. The values of the partial density of states f-electrons are taken from [3]. In turn, the p- and d-electrons $CoGa_2$ layer is described using the Hamiltonian (1).

From the analysis of the magnetic state equation and (4) it follows that f-subsystem can only be magnetic instability (unlike for example $PuRhGa_5$ [6]). The spin hybridization does not lead to significant changes in the density of states of f-electrons. At the same time, DOS of (pd)-electrons has a strong change due to spin hybridization (see fig.1).

The calculation results of the magnetic susceptibility of $PuCoGa_5$ shown in Fig. 2. The inset shows the total magnetic susceptibility taking into account the orbital contribution (curve 3), and the experimental data [2].The spin magnetic susceptibility of f-electrons satisfies the Curie-Weiss law (curve 1), and the spin susceptibility of pd-electrons (curve 2) has a maximum prior to the formation of singlet pairs. The temperature at which, according to (4), appears a nonzero order parameter modulus (Cooper pairing mechanism for paramagnon) is shown in the inset to Fig. 2.

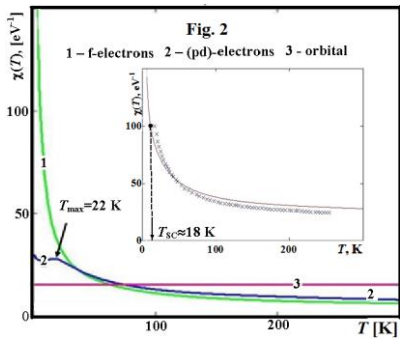

Thus, the electronic fluctuations into layers $CoGa_2$ lead to paramagnon singlet pairing of electrons. The pd-hybridization in layers $CoGa_2$ provides d-symmetry of the order parameter. Similar features of the crystal structure and magnetic properties have a place in the high-Tc cuprates [5, 7].

References

1. Curro N. J. et al., Nature 2005, **434**, p. 622
2. Sarrao J. L. et al., Nature, 2002, **420**, p. 297
3. Lukoyanov A. V. et al., JETP Letters, 2012, **96,** p. 452
4. Laughlin R. B. et al., Phys. Rev. B 2014, **89**, 035134
5. Povzner A. A. et al., JSCNM, 2015, **28**, p. 297
6. Povzner A. A. et al., JSCNM, 2014, **27**, p. 2347
7. Nakano T. et al., JLTP 1996, **105**, p. 395

A-46

Auger line-shape analysis and electron energy loss spectroscopy investigation of Pu surface chemistry

Art Nelson, Scott Donald, Wigbert Siekhaus, Patrick Allen, William McLean

LLNL, Livermore, CA, USA

Introduction

Oxidation/reduction reactions on plutonium metal continue to garner interest for establishing safe handling and storage procedures. X-ray photoelectron spectroscopy (XPS) core-level chemical shifts have established that the stable oxides of Pu are plutonium sesquioxide (Pu_2O_3, O/Pu = 1.5, Pu^{3+}) and plutonium dioxide (PuO_2, O/Pu = 2.0, Pu^{4+}) that typically form a layered structure on the surface of Pu metal. [1-6] However, XPS spatial resolution for characterizing the local chemical environment is limited to ~10 μm. Alternatively, Auger electron spectroscopy (AES) can be used to identify elemental composition and spatial distribution of contaminants on plutonium surfaces with nanometer scale spatial resolution. Yet using AES for chemical speciation has been limited. Also, employing electron energy loss spectroscopy (EELS) in combination with AES, one can gain additional information on the optical response of nanostructured surfaces and grain boundary interfaces.

Fundamental studies show that oxidation can be affected by surface electronic structure associated with crystal structure (e.g. monoclinic versus face-centered cubic), grain size, and the presence of defects (vacancies), contaminants or impurities. [7] Since plutonium oxidation/reduction studies have been predominantly performed on large grain gallium-stabilized δ-Pu with dry O_2 or O_2/H_2O mixtures, further investigations are required to quantify the effects of nanostructure.

This investigation utilizes AES line-shape analysis of the Pu PVV and $O_{45}VV$ peaks combined with EELS to provide definitive information on surface speciation. Figure 1 shows a schematic representation of these Auger transitions.

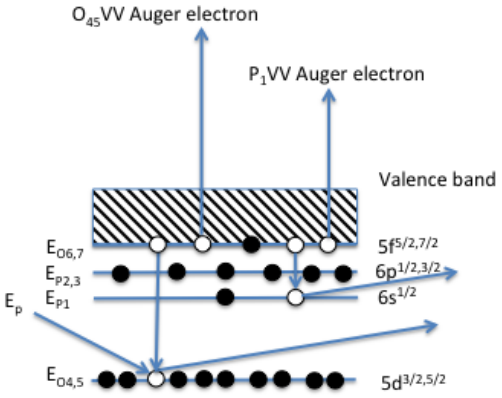

Fig 1. Schematic of PVV and OVV Auger transitions.

Description of the actual work

The samples studied were gallium stabilized □-Pu alloy (≈ 0.6 $^{w}/_{o}$), each having typical grain sizes of 30-50 μm. The δ-Pu alloy was electro-polished to remove any α phase from mechanical polishing before mounting. Gas dosing was performed at ~100 mtorr after Ar-ion sputter etching to remove the native oxide and any carbon contamination. AES and EELS experiments

were carried out using a PHI 710 scanning Auger nanoprobe equipped with a field-emission electron gun and co-axial cylindrical mirror analyzer having an energy resolution of ΔE/E = 0.5%. Secondary electron microscopy (SEM) and AES were performed with an incident electron beam at 20 kV and 10 nA (probe size ~10 nm) with a tilt angle of 30°. EELS was performed in reflection mode with an incident electron beam of 1 kV and 10 nA. Quantitative compositional analysis was obtained from the Auger peak intensities for each element present. Sputter etching was performed using 4 keV Ar+ ions (2 uA) with a raster size of 1 × 1 mm^2 having an estimated sputter rate of 3 nm/min.

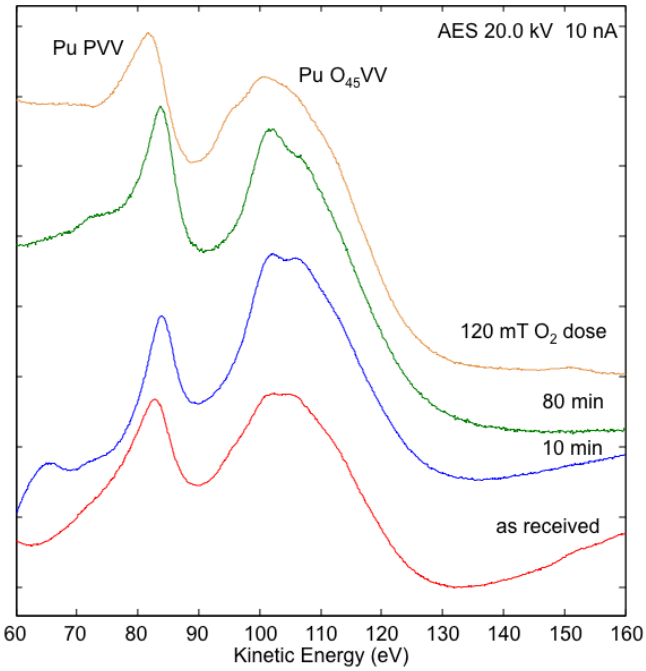

Fig. 2. N(E) versus kinetic energy plot of the Pu P_1VV and $O_{45}VV$ line-shapes for δ-Pu showing the evolution as a function of sputter time and O_2 dose.

Results

The evolution of the N(E) Pu P_1VV and $O_{45}VV$ line shapes for δ-Pu versus sputter etching and O_2 exposure at ambient temperature are presented in Figure 2. The as received $P_1VV/O_{45}VV$ line-shapes represent an oxidized surface, probably Pu_2O_3 since the surface oxide has been reduced in the UHV environment. [6] Note changes in Pu $P_1VV/O_{45}VV$ peak height ratio, changes in P_1VV kinetic energy and $O_{45}VV$ line-shape from the initial sputter cleaned Pu metal (Pu^0) after O_2 dosing. These changes are attributable to the initial presence of the Pu^{3+} valence state followed by a change to the Pu^0 after sputter etching, then to the Pu^{4+} valence state after O_2 dosing. These Auger line shapes can be correlated with features in the EELS spectra shown in Figure 3. The EELS spectra are displayed as N(E) versus energy loss below the 1 keV primary beam and $d^2N(E)/dE^2$ to accentuate the small loss features.

The loss features represent surface “oscillations” or surface plasmons, which are collective oscillations of conduction electrons. For the sputter etched δ-Pu surface, the loss features occur at 12.0 eV and 23.8 eV. Following O_2 dosing, the features shift by ~5 eV to 17.3 eV and 28.9 eV, which represents a change in the dielectric function and the consequent evolution of the optical constants due to 5f transitions to ligand p states. [8-10] Extracting the dielectric function from the N(E) EELS spectra to reveal the index of refraction *n* and the extinction coefficient *k* for Pu metal and Pu-oxide requires determining the single-scattering loss distribution which is beyond the scope of this study.

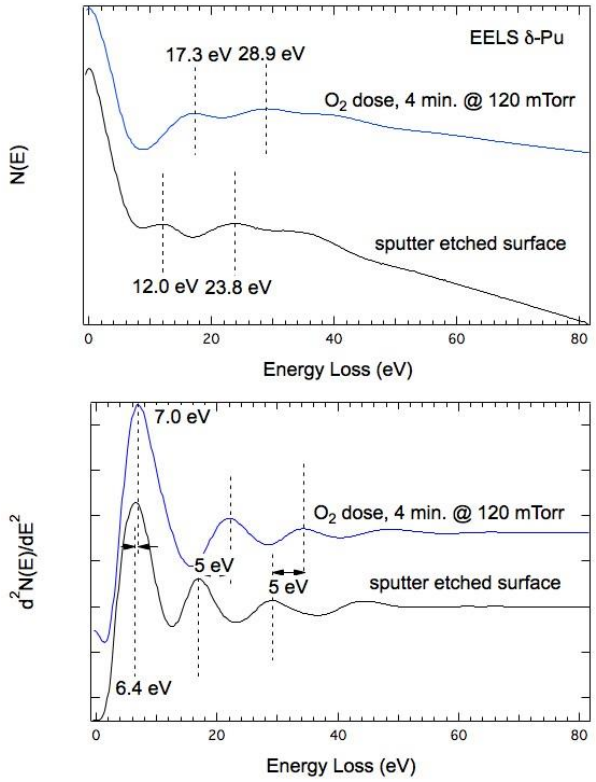

Fig. 3. EELS spectra for sputter etched δ-Pu and after O_2 dose.

In summary, the $P_1VV/O_{45}VV$ Auger lines shapes can be used to identify Pu species with nanoscale resolution. Correlating the Pu species with the corresponding energy loss features, one can extract the optical constants for the individual oxides.

This work performed under the auspices of the U.S. Department of Energy by Lawrence Livermore National Laboratory under Contract DE-AC52-07NA27344.

References

1. J. M. HASCHKE, T. H. ALLEN and L. A. MORALES, “Surface and Corrosion Chemistry of Plutonium,” *Los Alamos Sci.* **26,** 252 (2000).

2. M. T. BUTTERFIELD, T. DURAKIEWICZ, E. GUZIEWICZ, J. J. JOYCE, A. J. ARKO, K. S. GRAHAM, D. P. MOORE and L. A. MORALES, “Photoemission of Surface Oxides and Hydrides of Delta Plutonium,” *Surf. Sci.* **571**, 74 (2004).

3. P. MORRALL, S. TULL, J. GLASCOTT and P. ROUSSEL, “Plutonium Oxide Transformation Kinetics and Diffusion Coefficient Measurement,” *J. Alloy Compounds* **444-445**, 352 (2007).

4. H. G. GARCIA FLORES and D. L. PUGMIRE, “The growth and evolution of thin oxide films on δ-plutonium surfaces,” *IOP Conf. Series: Mater. Sci. Eng.* **9**, 012038 (2010).

5. A.J. NELSON, K.S. HOLLIDAY, J.A. STANFORD, W.K. GRANT, R.G. ERLER, P. ALLEN, W. McLEAN and P. ROUSSEL, “Adsorption of Atmospheric Gases on Pu Surfaces,” *Actinides and Nuclear Materials 2012*, San Francisco, California, April 2012, Materials Research Society (2012).

6. A. J. NELSON and P. ROUSSEL, “Low Temperature Oxidation of Plutonium,” *J. Vac. Sci. Technol.* A **31(3)**, 031406 (2013).

7. C. M. EGGLESTON, J.J. EHRHARDT, W. STUMM, “Surface structural controls on pyrite oxidation kinetics: An XPS-UPS, STM, and modeling study,” *Am. Mineralogist* **81**, 1036 (1996).

8. W. S. M. WERNER, K. GLANTSCHNIG and C. AMBROSCH-DRAXL, “Optical Constants and Inelastic Electron-Scattering Data for 17 Elemental Metals,” *Phys. Chem. Ref. Data,* **38**, 1013 (2009).

9. H. SHI, M. CHU, P. ZHANG, “Optical properties of UO_2 and PuO_2,” *J. Nucl. Materials,* **400**, 151 (2010).

10. Y. YANG, Y. LU, P. ZHANG, “Optical properties of PuO_2 and □-Pu_2O_3 by GGA + *U* + QA studies,” *J. Nucl. Materials,* **452**, 414 (2014).

A-47

Research Shape Memory Effect in the U6.3wt%Nb Alloy by Dilatometry

Aleksandr Troshev, Chentzov Denis, Golunov Anatoliy, Shestakov Evgeniy, Baluev Alexey

Russian Federal Nuclear Center – VNIITF, Snezhinsk, Russia

The present paper used the investigation approach that is similar to the one described in [1,2], i.e. dilatometry of the the alloy samples deformed at room temperature in the α′′-phase. The difference was in the deformation direction of the samples (compression instead of tension) and in their heating rates in the dilatometer (~0.5÷2°C/min instead of ~20°C/sec). The LFM-50 universal testing machine was used to deform samples by compression (~$10^{-3}s^{-1}$deformation rate) and a horizontal DIL-402C series dilatometer manufactured by NETZSCH was used to record the relative elongation and temperature of samples.

Similar investigations were made with the samples that experienced different levels of deformation from ~2 to ~16%.

The following results were obtained:

- The alloy shape is recovered under heating, whereas the shape of the samples is recovered up to the level corresponding to their state not only before deformation (in α''-phase) but also before quenching from the $\gamma°$-phase (when the alloy is prepared);
- The best recovery is observed when the alloy is heated up to ~250°C; if the temperature is higher, the alloy is decomposed into equilibrium phases (with this heating rate) and thus, the shape is not further recovered;
- Plastic deformation of the alloy up to ~2.6% can be recovered almost completely under heating;
- The alloy deformation greater than ~2.6% leads to the reduced deformation recovery under heating and this is associated with the change of the alloy deformation mechanism [3];
- Experimental data analysis supplemented with the X-ray diffraction study results demonstrate that the shape of the alloy samples is recovered not only due to reversible motion of the deformation carriers but also due to the thermoelastic $\alpha'' \leftrightarrow \gamma°$ phase transformation.

References

1. R.A. Vandermeer, J.C. Ogle, and W.B. Snyder. Shape Memory Effect In A Uranium+14 at.% Niobium Alloy. Scripta Metallurgica. Vol.12, 1978.
2. R.A. Vandermeer, J.C. Ogle, and W.G. Nortcutt. A Phenomenological Study of the Shape Memory Effect in Polycrystalline Uranium-Niobium Alloys. Metallurgical Transactions A. Vol.12A, May 1981.
3. R.D. Field, D.J. Thoma, P.S. Dunn, D.W. Brown and C.M. Cady. Martensitic Structures and Deformation Twinning in the U-Nb Shape-Memory Alloys. Philosophical Magazine A, 2001, Vol. 81, No. 7, p. 1691-1724

A-48

On the equation of state and elastoplastic and strength properties of beryllium

Maria Shirshova, Boris Nadykto, Ivan Pavlusha

RFNC-VNIIEF, Sarov, Nizhny Novgorod Region, Russia

Beryllium is an important engineering material. Beryllium has two solid phases at zero pressure. The hcp structure, which is stable at low temperatures, transforms into the bcc structure near the melting point. This transformation is not manifested on the Hugoniot. Simulations of beryllium response to shock loading require knowledge of the equation of state and elastoplastic properties of beryllium.

Hugoniot parameters for beryllium have been measured experimentally [1-2]. The normal (room) isotherm has been established by the diamond anvil method in [3]. The equation of state of beryllium providing a good description of available experimental data is given in [4]. SESAME also offers an equation of state for beryllium, SESAME 2024 [5].

Experiments with free surface velocity measurements provide important information on elastoplastic properties of materials. For S200F beryllium, free surface velocity profiles measured by laser interferometry in a series of planar experiments are presented in [6].

We know that the material behavior under static and quasistatic loading (at strain rates of 10^{-3} – 10^{3} s^{-1}) is described by a governing equation with an empirically added term representing stress as a function of strain rate and temperature [7-8].

In this case, stress in the material depends on the specific conditions of manufacturing, treatment and testing. This is attributed to the fact that, as distinct from compression or tension of a uniform material with micro-heterogeneities, external loading leads not only to a uniform variation in the interatomic distance, but also to a variation in micro-heterogeneities. Strength characteristics may vary with such deformation as a result of microscopic damage and deformation processes. Such variations depend both on the nature and duration of external loading and lead to a wide range of mechanical properties of materials. This is how elastoplastic properties of materials are related to the stress value and strain rate.

The comparison made in [9] shows that different models (for example, [7] and [8]) produce substantially different results for shock experiments at high strain rates and fail to provide a satisfactory description of the experiments [6].

In this paper, the experiments were simulated using the LEGAK-3D hydrodynamic code [10]. The simulations were done in the 1D approximation on a 25-micron Lagrange mesh. Elastoplastic properties were incorporated using a Wilkins-type model [11]. In the simulations for beryllium we used constant Poisson's ratio of 0.2, a constant yield point of 0.6 GPa, and a brittle failure model with σspall = 1.1 GPa.

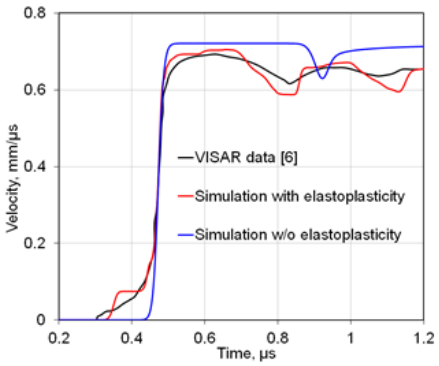

Fig. 1. Free surface velocity of Be as a function of time.

Fig. 1 shows the free surface velocity of beryllium as a function of time for a symmetric impact at a flyer plate velocity of 0.721 km/s and provides a comparison of our simulated values with the experimental results [6].

The target is 3.98 mm thick Be; the flyer is 2 mm thick. The flyer velocity is 0.721 km/s.

Fig. 2 shows a comparison of the experimental data [6] with simulated results produced by the PTW and MTS models (according to [9]) for the same flyer velocities.

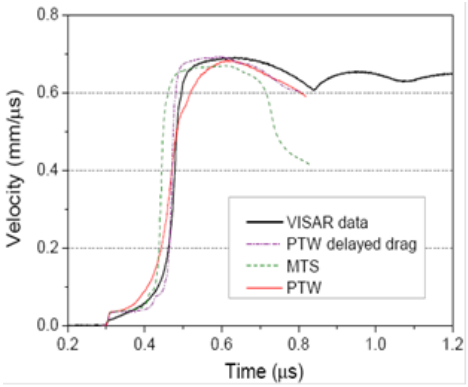

Fig. 2. Experimental data [6] and simulated results produced by the PTW and MTS models [9]

The comparison of Fig. 1 and Fig. 2 shows that the sufficiently accurate equation of state of beryllium and the simplified model of elastoplastic properties and damage provide a better description of shock experiments [6] than the sophisticated models [7], [8] used in [9].

Fig. 3 shows the free surface velocity of beryllium as a function of time for a symmetric impact at a flyer plate velocity of 1.246 km/s and provides a comparison of our simulated values with the experimental results [6].

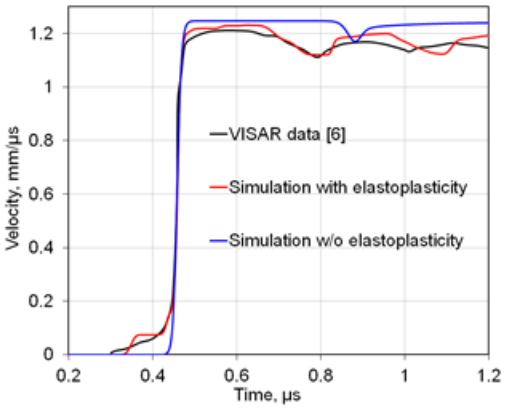

Fig. 3. Free surface velocity of Be as a function of time. The target is 3.98 mm thick Be; the flyer is 2 mm thick. The flyer velocity is 1.246 km/s.

The spall was not simulated in [9], so the simulated curves are limited in [9] by the time the spall appears in the experiment [6].

In Fig. 4, our simulated data are compared with the experimental results [6] for a 3.98 mm beryllium target, a 1 mm tantalum flyer and 1.418 km/s flyer velocity.

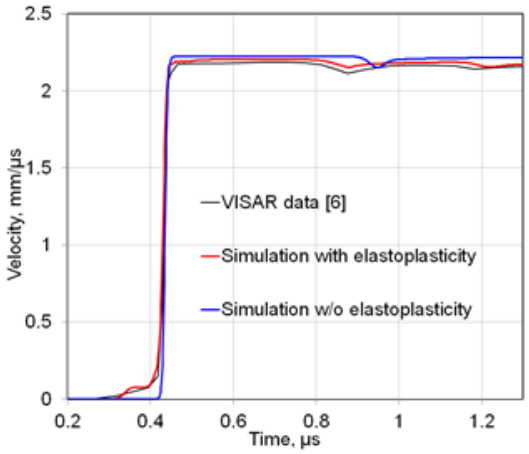

Fig. 4. Free surface velocity of beryllium as a function of time. Target: Be, 3.98 mm; flyer: Ta, 1 mm, velocity 1.418 km/s

Fig. 1, Fig. 3 and Fig. 4 at the top also show simulated curves in the hydrodynamic approximation, which explicitly point at the elastic nature of relief in the experimental curves in [6].

The analysis shows that the simplified model provides a fairly credible assessment of the role of damage and elastoplastic behavior of beryllium under shock loading in a wide range of shock velocities and pressures.

References

1. LASL Shock Hugoniot Data. Edit. By S.P. Marsh. University of California Press. Berkeley. Los Angeles. London. 1980.

2. M. VAN THIEL, J.W. SHANER, E. SALINAS. Compendium of Shock Wave Data. Livermore Lawrence Laboratory Report, UCRL - 50108. V.1, 1977.

3. W. J. EVANS, M. J. LIPP, H. CYNN at al. X-ray diffraction and Raman studies of beryllium: Static and elastic properties at high pressures// Phys. Rev. B 72,094113 (2005).

4. B.A. NADYKTO. In New Models and Numerical Codes for Shock Wave Processes in Condensed Media, edited by I.G. Cameron. Oxford: AWE Hunting BRAE, 1998. P. 205.

5. SESAME: The Los Alamos National Laboratory Equation of State Database. Ed. by S.P. Lyon and J.D. Johnson Los Alamos National Laboratory Document

6. C.D. ADAMS, W.W. ANDERSON, G.T. GRAY III at al. Spall and damage behavior of S200F beryllium. In Shock Compression of Condensed Matter-2009, Eds. M.L. Elert, W. T. Buttler, M.D. Furnish, W.W. Anderson, W.G. Proud. American Institute of Physics, p. 509-512.

7. P.S. FOLLANSBEE, U.F. KOCKS, Acta Metall. 36, pp 81-93 (1988).

8. D.L. PRESTON, D.L. TONKS, D.C. WALLACE. J. Appl. Phys. 93, pp 211-220 (2003).

9. M.B. PRIME, S.R. CHEN, C.D. ADAMS. Advanced plasticity models applied to recent shock data on beryllium. In Shock Compression of Condensed Matter-2011, Eds. M.L. Elert, W. T. Buttler, J.P. Borg, J.L. Jordan, T.J. Vogler. American Institute of Physics, p. 1035-1038.

10. S.M. BAKHRAKH, S.V. VELICHKO, V.F. SPIRIDONOV et al. Voprosy Atomnoi Nauki i Tekhniki, Series "Mathematical Modeling of Physical Processes", 2004, V. 4, pp. 41-50 (in Russian).

11. M.L. WILKINS. Calculation of Elastic-Plastic Flow, in Computational Methods in Hydrodynamics. Moscow, Mir, 1967 (translated into Russian)

A-49

The Structure of Thick-walled Spherical Shell of U-1,5% Mo Alloy After Explosive Loading

Dmitry Belyaev, Eugen Kozlov, Yury Zouev, Igor Svyatov, Alexey Aleksandrov, Ekaterina Levi

Russian Federal Nuclear Center – Zababakhin All-Russia Research Institute of Technical Physics, (RFNC-VNIITF), Snezhinsk, Chelyabinsk region, Russia

Investigation of physical properties of material subjected to high-speed intensive loading is of great interest, as far as besides quick compression of a substance up to high pressure and its adiabatic heating, there are high-speed processes of plasto-elastic deformation, destruction, polymorphous and phase transitions, chemical reactions, electrical polarization, ionization and other physical and chemical phenomena. There is a unique possibility to study fundamental properties of a substance and nonequilibrium processes in extreme conditions. Short-term achievement of high pressure and temperature is obtained most easily and effectively using all-round spherical; explosive loading [1].

This presentation gives the results obtained under metallographic investigation of thick-wall spherical shell out of uranium-molybdenum alloy, which survived after high-level shock-wave loading. Investigation was performed by methods of light microscopy and durometry in meridional shell section.

We revealed four approximately concentrically located zones, which had different structural states, levels of micro hardness, degrees of damage, concentrations, average sizes and volume fractions of nonmetallic inclusions (Fig 1).

The processing and presentation of experimental data containing information about volume distribution of investigated physical values was made using method of color mapping [2, 3].

On the basis of obtained information analysis, some conclusions were made about the details of physical processes that ran during loading, which led to local structural changes and localization of damage and structurally sensitive material parameters related to them: hardness, micro hardness, distribution of nonmetallic inclusions [4].

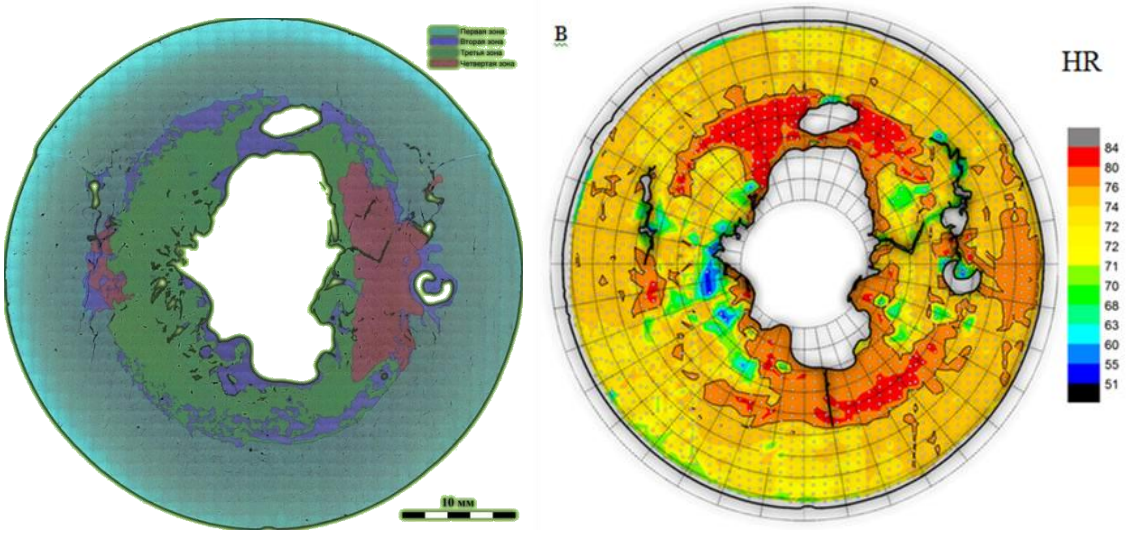

Fig. 1. Meridional shell section with highlighted structural zones (left) and a map of hardness distribution in meridional section (right)

References

1. G.I. KANEL, S.V. RAZORENOV, L.V. UTKIN, V.E. FORTOV, *Shock-Wave Phenomena in Condensed Matter,* p. 408, Yanus, Moscow (1996).

2. E.A. KOZLOV, D.A. BELYAEV, Yu.N. ZOUEV, I.L. SVYATOV, “Spall and Shear Damages of a Shell of U—1.5% Mo Alloy Under Explosive Loading”, XI Russian — US Workshop Fundamental Properties of Plutonium, Snezhinsk, September 12 — 16 (2011).

3. D.A. BELYAEV, Yu.N. ZOUEV, E.A. KOZLOV, I.V. PODGORNOVA, I.L. SVYATOV, “Metallographic Studies of Uranium Shells After Shock-Wave Loading Using Method of Color Mapping”, IX International Ural Workshop “Radiation Damage Physics”, Kyshtym, February 20 — 26 (2011).

4. E.A. KOZLOV et al., “Spall and Shear Destruction in Spherically Converging Shells Out of Iron and Steel. Measurement of Energy and Residual Deformations”, *Deformatsiya i razrusheniye materialov*, **11**, 2 (2008).

A-50

Dynamic Magnetic Response across the Pressure-Induced Structural Phase Transition in CeNi

Alexey Mirmelstein[1], Andrey Podlesnyak[2], Alexander Kolesnikov[2], Georg Ehlers[2], Douglas Abernathy[2], Vladimir Matvienko[1], Gregory Halder[3], Antonio dos Santos[2]

[1]RFNC-VNIITF, Snezhinsk, Chelyabinsk region, Russia, [2]Oak Ridge National Laboratory, Oak Ridge, TN, USA, [3]Argonne National Laboratory, Argonne, IL, USA

Intermediate-valence compound CeNi experiences a pressure-induced first-order structural phase transition with volume jump and as such constitutes an attractive system to study pressure-driven *f*-electron delocalization behaviour in the systems with an unstable *f*-electron shell. By means of x-ray and neutron powder diffraction techniques the structure of high-pressure CeNi phase is determined and the inelastic neutron scattering (INS) technique is employed to study the dynamic magnetic susceptibility of CeNi before and after the structural transition. The INS experiments reveal enhanced Ce 4f–Ni 3d hybridization due to the phase transition while the inelastic 4f magnetic form factor remains unchanged.

A-51

Development of AFM and STM Capabilities for Plutonium

Miles Beaux, Adam Zocco, Miguel Santiago Cordoba, Douglas Vodnik, Stephen Joyce, Michael Ramos, Scott Richmond, Thomas Venhaus, Jeremy Mitchell, Brian Scott, Eve Bauer, Igor Usov

Los Alamos National Laboratory, Los Alamos, NM, USA

The surface behavior of Pu and Pu derivatives has been an ongoing research effort at LANL. Scanning probe microscopy (SPM) techniques such as atomic force microscopy (AFM) and scanning tunneling microscopy (STM) are proven methods for direct 3-dimensional imaging and observation of structure and defects at the meso-, nano-, and atomic scale, and both the occupied and unoccupied electronic states in materials [1]–[3]. However, in spite of the utility of these techniques, as well as calls from theory for their application to Pu materials [4], [5], the development of such SPM capabilities have been exasperated by the difficulties associated with Pu related work. We are pleased to report herein on the development of both AFM and STM capabilities for Pu, and to present preliminary results produced by these capabilities since the introduction of Pu material into these systems in late 2015.

AFM

The AFM utilized is a MultiMode SPM housed in an inert Ar atmosphere (< 1 ppm O_2, < 1 ppm H_2O) glove box. The glove box pressure is maintained between 1.0 and 4.0 mbar below the ambient pressure in the room, which is in turn held at negative pressure relative to the building in order to mitigate the potential for contamination release in the event of a glove box breach. Exhaust lines for the glove box undergo double HEPA filtration prior to tying into building ventilation.

The introduction of Pu samples into the glove box AFM system included a mechanically polished 7 atomic % Ga-stabilized δ-Pu coupon (δ-Pu<7at%Ga>) as well as a PuO_2 film prepared by polymer assisted deposition (PAD). Subsequently, a 2 atomic % Ga-stabilized δ-Pu coupon (δ-Pu<2at%Ga>) was also introduced. Preliminary imaging of these samples collected by tapping mode AFM will be presented, which includes height, amplitude, and phase images. Additionally, images taken utilizing the Peak Force Quantitative Nanomechanical Mapping methodology developed by Bruker will be presented which provides quantitative nano-mechanical surface properties of the samples.

STM

The STM utilized is an Omicron VT STM housed in an ultra-high vacuum (UHV) chamber. Rotary pumps on the UHV system exhaust into the room after undergoing double HEPA filtration. The UHV system is equipped with a sputter gun for cleaning sample surfaces, manipulators for annealing samples, and an Auger spectrometer for determining the cleanliness of samples prior to imaging in the STM. Pu coupons are mounted on Omicron sample plates and inserted into a “vacuum suitcase” (see Figure 1) for transfer from the plutonium facility and/or glove box while maintaining the sample in a controlled environment throughout. The compact design is based on a simple butterfly valve which both holds and isolates the sample.

Preliminary Results

Figure 2 shows AFM images obtained from the surface of the δ-Pu<7at%Ga> coupon. The topography images (amplitude and height) revealed granular surface structure with roughness of approximately 9 nm, grain size of 50 to 150 nm, and grain height of 30 to 60 nm. The

simultaneously obtained phase contrast image reveals sub-μm scale variations in mechanical properties on the surface. Local areas with varying mechanical properties are not always representative of surface topography as indicated by two circled areas. Detailed studies of the nature of these Pu surface irregularities (likely related to chemical composition and crystallographic orientation variations) are underway.

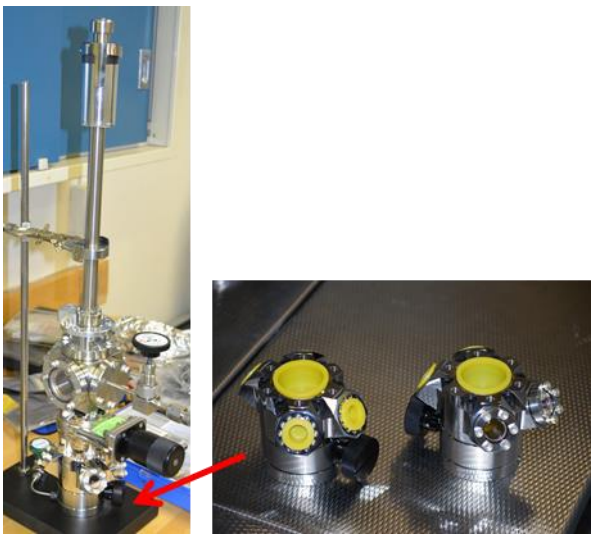

Figure 1. Vacuum suitcase for transfer of samples to the UHV system.

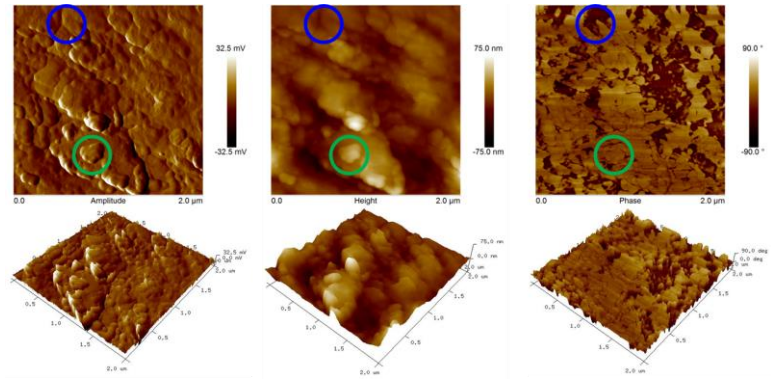

Figure 2. Tapping mode AFM images of 7 atomic % Ga-stabilized δ-Pu.

References

[1] R. Wiesendanger, *Scanning Probe Microscopy and Spectroscopy: Methods and applications*. Cambridge: Cambridge University Press, 1994.

[2] J.-X. Zhu, R. C. Albers, K. Haule, and J. M. Wills, “First-principles study of the Kondo physics of a single Pu impurity in a Th host,” *Phys. Rev. B*, vol. 91, no. 16, Apr. 2015.

[3] K. T. Rim, T. Müller, J. P. Fitts, K. Adib, N. Camillone, R. M. Osgood, E. R. Batista, R. A. Friesner, S. A. Joyce, and G. W. Flynn, “Scanning Tunneling Microscopy and Theoretical Study of Competitive Reactions in the Dissociative Chemisorption of CCl_4 on Iron Oxide Surfaces,” *J. Phys. Chem. B*, vol. 108, no. 43, pp. 16753–16760, Oct. 2004.

[4] J.-X. Zhu, P. H. Tobash, E. D. Bauer, F. Ronning, B. L. Scott, K. Haule, G. Kotliar, R. C. Albers, and J. M. Wills, “Electronic structure and correlation effects in $PuCoIn_5$ as compared to $PuCoGa_5$,” *EPL Europhys. Lett.*, vol. 97, no. 5, p. 57001, Mar. 2012.

[5] T. Das, J.-X. Zhu, and M. J. Graf, “Theory of nodal s±-wave pairing symmetry in the Pu-based 115 superconductor family,” *Sci. Rep.*, vol. 5, p. 8632, Feb. 2015.

A-53

CALPHAD approach a complementary way to solve the plutonium mystery

Benoît Oudot[1], Brice Ravat[1], Aurelien Perron[2], Christine Guéneau[3], Lionel Jolly[1], Patrice Turchi[2], François Delaunay[1]

[1]CEA-VALDUC, Is-sur-Tille, France, [2]LLNL, Livermore, CA, USA, [3]CEA-SACLAY, Gif-sur-Yvette, France

Plutonium metal is a very complex material. Far beyond its radioactive character leading to swelling phenomenon [1] it exhibits six crystal structures with a lot of different physical properties from room temperature to melting and it is very sensitive to corrosion.

The stability range of the ductile δ phase is quite narrow but can be extended to room temperature by alloying Pu with 'δ phase stabilizer' elements such as aluminium, gallium [2]. Nevertheless, thermal treatment below room temperature leads to a partial martensitic transformation of δ-stabilized Pu alloys into the hard and brittle α' phase exhibiting a double C-curve kinetic in a Time-Temperature-Transformation diagram [3]. Upon heating, reverse transformation exhibits a particularly complex behaviour where direct α' → δ phase and indirect α' → β phase transformations are in competition [4-6]. Moreover, even if the plutonium is stabilized with 'δ phase stabilizer' it suffers a degradation process by corrosion during handling, transport and storage.

Thus, this work is based on the power of the coupling between experimental data and phenomenological thermodynamics models based on the CALPHAD (CALculation of PHAse Diagrams) approach and the use of the Thermo-Calc software. Indeed, using thermodynamic simulations on the martensitic reverse transformation highlighted that both reversion modes were possible and that indirect reversion path was more favourable. Moreover, appearance of a new transient pure β phase with solute trapped inside the δ phase has been demonstrated during indirect transformation. [7].

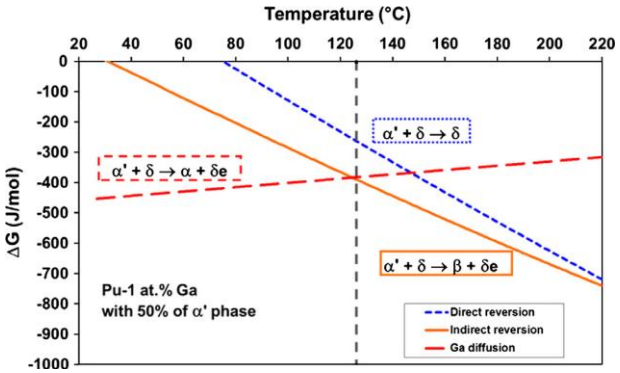

Fig. 1. Thermodynamic driving forces as a function of temperature for direct reversion (blue curve), indirect reversion (orange curve) and only considering a δ phase solute enrichment (red curve) with an initial α' phase fraction set up to 50%. The vertical dashed line represents the indirect reversion temperature determined by simulations.

Once again some CALPHAD calculations performed by adding the oxygen element into the thermodynamic description of the system helps us to determine the corrosion path way and highlighted, like for martensite reversion, a strong dependence of the solute effect. Indeed the calculated ternary diagram at 500K exhibits the coexistence of pure plutonium oxides with plutonium-aluminum compounds requiring a solute diffusion process during the oxidation pathway until the terminal step resulting of the formation of a PuO_2 and Al_2O_3 mixture.

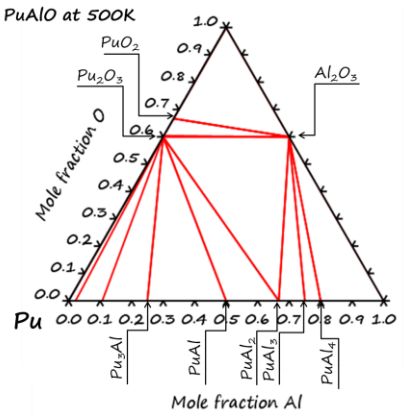

Fig. 2. Isothermal section of the ternary diagram of the PuAlO system at 500K.

Then with two simple examples we underline the powerful approach made by coupling CALPHAD method and experimental data to come through the plutonium complex behaviour and the role played by the solute diffusion process.

References

[1] N. Baclet, B. Oudot, R. Grynspan, L. Jolly, B. Ravat, P.Faure, L.Berlu, G.Jomard *J. Alloys Comp.* **444-445**305-309 (2007).

[2] S.S. Hecker, D.R. Harbur, T.G. Zocco, *Progr. Mater. Sci.* **49**. 429-485(2004).

[2] B. Oudot, K.J.M. Blobaum, M.A. Wall, A.J. Schwartz, *J. Alloys Comp.* **444-445**. 230-235 (2007).

[4] B. Ravat, B. Oudot , A. Perron, F. Lalire, F. Delaunay, *J. Alloys Comp*. **580**. 298-309 (2013).

[7] A. Perron, B. Ravat, B. Oudot, F. Lalire, K. Moutura, F. Delaunay, Acta Mat. 61 7109-7120 (2013).

Acknowledgement

This work was partially done as part of the international agreement on cooperation between DOE-NNSA and CEA-DAM in fundamental science supporting stockpile stewardship.

A-54

Evolution of electronic structures of gamma-Pu, delta-Pu, epsilon-Pu

Li Huang

Institute of Materials, China Academy of Engineering Physics, Sichuan Jiangyou, China

The plutonium metal, which exhibits many exotic and unusual behaviors, is likely the most complex element in the periodic table. Up to now, it is still a big challenge to understand the electronic structures of the six allotropes of plutonium experimentally and theoretically. In the present work, we adopt a modern first-principles approach, namely the combination of density functional theory (DFT) with dynamical mean-field theory (DMFT), to study the electronic structures of the high temperature phases of plutonium, i.e., the gamma-Pu, delta-Pu, and epsilon-Pu systematically. We try to calculate the angle-resolved photo-emission spectra (ARPES) and the orbital-resolved density of states (PDOS), which are shown in Fig. 1 and Fig. 2, respectively. It is clearly seen in these figures, that the band structure of gamma-Pu shows significant band-like and itinerant characters, while the one of epsilon-Pu shows apparent localized and atomic multiple features. More specifically, the bands of gamma-Pu are a bit broader than those of epsilon-Pu, which exhibits sharper atomic multiple peaks in the density of states. In addition, the 5*f* *j*=7/2 state of epsilon-Pu which has a small weight in the Fermi level is probably in the vicinity of Mott-Hubbard metal-insulator transition. Finally, we believe that from the viewpoint of 5*f* electronic correlation strength, epsilon-Pu > delta-Pu > gamma-Pu. To our knowledge, it is the first time to report the theoretical ARPES data for the plutonium metal, so our results will shed new light on the intriguingly electronic properties of plutonium and can be viewed as a critical prediction. The calculations for the low-temperature alpha-Pu and beta-Pu phases are undertaken.

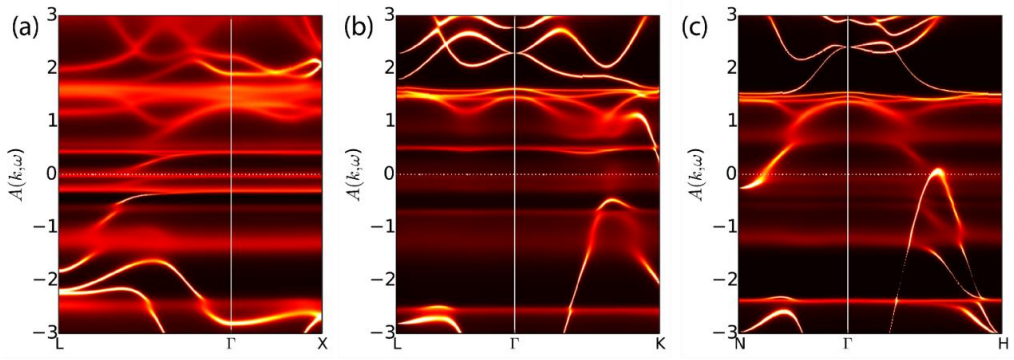

Fig.1 ARPES of (a) gamma-Pu, (b) delta-Pu, and (c) epsilon-Pu, obtained by DFT + DMFT calculations.

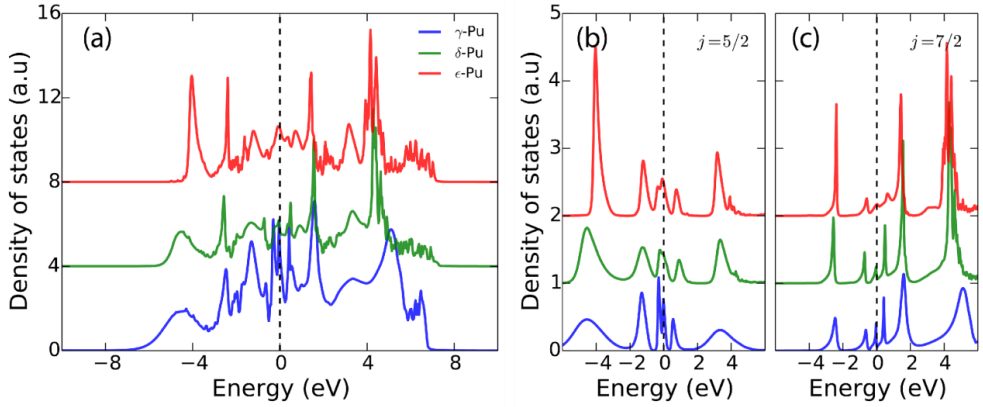

Fig.2 (a) Total, (b) Pu-5*f* *j*=5/2, and (c) Pu-5*f* *j*=7/2 density of states obtained by DFT + DMFT calculations.

A-55

Pu Alloy Oxidation by Water Vapor

Lionel Jolly, Brice Ravat, Benoît Oudot, François Delaunay

CEA - VALDUC, Is-sur-Tille, France

The oxidation of plutonium alloys knows a renewal of interest these last years. New studies call established ideas into question as nature of oxides [1,2]. The goal is to describe first stages of corrosion mechanisms of plutonium metal under oxidant atmosphere at room temperature in real conditions of storage. The knowledge of these first stages is important because they control the corrosion way. Photoelectron spectroscopy (PES) is a powerful technique for the purposes of studying various properties of surfaces, e.g. their composition, oxidation state and chemical and electronic properties.

The plutonium alloy is prepared by electropolishing before introducing to the preparation chamber of the spectrometer in order to remove the most part of oxides.

The X-ray photoelectron spectroscopy (XPS) measurements were performed by an EscaLab 250® by ThermoFisher Scientific out of glove box, using monochromatic Al-Kα X-rays. The initial surface was prepared to get mostly Pu(III) [about 83 at.%] and partially Pu(IV) [about 8 at.%] and Pu(0) [about 9 at.%] [3]. The sample was exposed to several pressures of H_2O (from 2.10^{-7} to 1 mbar) during 5 min at ambient temperature in a preparation chamber of the spectrometer. Spectra are fitted with CasaXPS® by line shapes derived from considered pure phases of prepared surface samples for Pu*4f* and by a Lorentzian shape modified and numerically convoluted with a Gaussian for O1s [4].

XPS analyses of the sample at ambient temperature show that 3 valences of Pu*4f* can coexist in the few 5 nanometers of depth after exposure (cf. Figure 1): Pu(0) [metal], Pu(III) [Pu_2O_3] and Pu(IV) [PuO_2].

The oxidation is quite rapid and seems to saturate even if the metal is still observable (cf. Fig. 1).

The O1s spectra analysis shows the dissociative chemisorption of H_2O at low pressure. Up to 10^{-4} mbar exposure, the adsorbed OH^- species increase with the pressure (cf. Fig. 2). The O^- species, which can be considered as defects in the subsurface, decrease, that is adequate with the Pu(III) oxidation to Pu(IV). After 10^{-4} mbar exposure, H_2O tends to chemisorb to the detriment of the H_2O dissociation. Then, the Pu oxidation saturates and the defects in the subsurface come back.

These results suggest that the H_2O dissociation tends to be complete into 2H + O up to the saturation of the surface, when H_2O molecule tends to chemisorb.

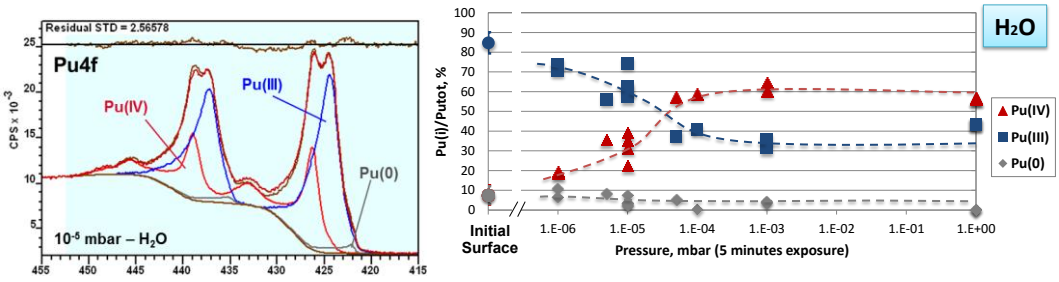

Figure 1: Evolution of the valence Pu4f as a function of the water pressure.

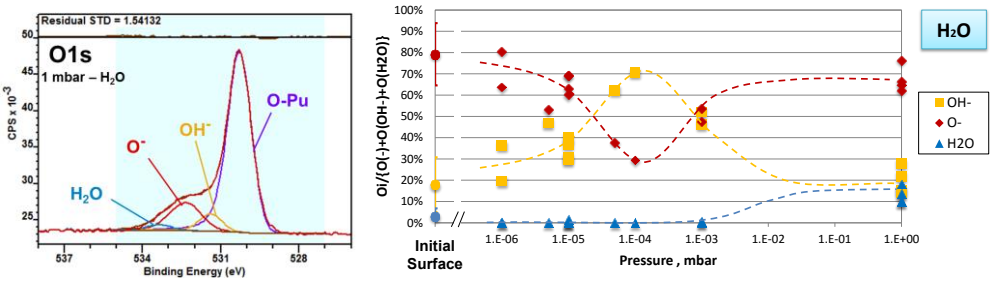

Figure 2: Evolution of the O1s components as a function of the water pressure.

References

[1] H.G. García Flores, P. Roussel, D.P. Moore, D.L. Pugmire (2011) Surf. Sci., 605, 314-320

[2] T. Gouder, A. Seibert, L. Havela, J. Rebizant (2007) Surf. Sci., 601, L77-L80

[3] L. Jolly, P. Berthou, F. Delaunay (2013), Poster P2-18, ECASIA'13, Cagliari, Sardinia, Italy

[4] N. Fairley, CasaXPS®, www.casaxps.com; Casa Software LTD, UK

A-56

Oxidation of Pu-Ga alloyed surfaces and PuO_2 PAD films using Time-of-Flight SIMS

Sarah Hernandez, Thomas Venhaus, David Pugmire, David Moore, Brian Scott

Los Alamos National Laboratory, Los Alamos, NM, USA

Introduction

Delta-plutonium (δ-Pu) is known to oxidize immediately when exposed to air, which can be detrimental to long-term storage [1]. Understanding the nature of the growth and stability of the passive oxide layer on δ-Pu is important to prevent further oxidation or corrosion of the material. Surface science techniques, such as X-ray photoelectron spectroscopy (XPS) and Auger electron spectroscopy (AES), have provided insightful information into understanding the formation and the stability of the oxide [2,3]. However, these surface techniques probe several nanometers deep into the surface and provide limited information on the chemistry at the gas/surface interface.

Time-of-flight secondary ion mass spectroscopy (ToF-SIMS) is a highly surface sensitive technique that probes only the topmost mono-layers of the surface, and provides a comprehensive survey of surface constituents (including hydrogen). However, the relative yields of the secondary ions that constitute the SIMS fragment patterns (e.g., PuO^-, PuO_2^-, PuO_3^-, etc.) are not well understood, and not easily predicted. In this study, we prepared surfaces in vacuum of the most common oxidation state of Pu, 4+ (PuO_2) and 3+ (Pu_2O_3), and measure the resulting fragment patterns in an effort to produce a set of ToF-SIMS "fingerprints" for future gas/surface studies.

Experimental details

ToF-SIMS detects the mass of ejected positive and negative ions from a surface that has been bombarded by a focused, high energy ion beam. To avoid further destruction of the surface, the ion beam may be operated in the low flux static regime (<1nA/cm^2), also known as static ToF-SIMS.

Surface analysis of mechanically polished 2 and 7 at.% gallium (Ga) δ-Pu samples, a 7 at.% electro-polished δ-Pu sample, and a thin epitaxial film of PuO_2, synthesized via the polymer assisted deposition (PAD) process [4], was performed using a Kore ToF-SIMS. This system is equipped with a pulsed 25 keV monoisotopic $^{69}Ga^+$ liquid metal ion gun, a 5 keV Ar^+ sputter gun for depth profiling, and a time-of-flight mass spectrometer capable of a mass resolution of m/Δm = 5000. The system base pressure is approximately 5 x 10^{-10} Torr.

Results

In order to perform a controlled study of the native Pu surface oxidation states and the resultant SIMS fragment patterns, it is necessary to first sputter clean the analysis area of the sample to remove contaminants remaining from the polishing steps. However, sputtering will reduce the oxide due to preferential sputtering of oxygen. XPS analysis has shown that controlled O_2 gas dosing of a sputtered surface can be used to reform the surface to a fully oxidized Pu^{4+} state following the reduction of the oxide from the sputtering [3]. Each mechanically polished Pu-Ga alloyed sample is sputtered to remove the native oxide layers, and dosed with a 20% O_2 and 80% Ar gas mixture at 5 x 10^{-7} Torr to provide an oxygen exposure of 400 L. XPS experiments have revealed that performing this exposure at room temperature will initially create the Pu^{4+} state, but the surface will then auto-reduce quickly to Pu^{3+} [3]. Performing the exposures at low temperatures (< 280 K) will slow the auto-reduction, allowing for SIMS analysis on a stable Pu^{4+} oxide surface.

We observed that there is a unique difference in spectra depending on whether the surface is a Pu^{4+} state or a Pu^{3+} state (Figure 1). After gas dosing, the spectra from the mechanically polished sample are compared with the spectra from the PuO_2 PAD film (Pu^{4+} state as confirmed by XPS) and the electro-polished sample. We also observed the auto-reduction following the exposure at room temperature (Figure 2) and compared this data with published XPS data. The effects of impurities, such as the alloying impurity Ga, will also be discussed.

References

1. J. M. Haschke, T. H. Allen, Los Alamos Science Vol. 1 No. 26, 252- 273 (2000).
2. H. G. Garcia Flores, D. L. Pugmire, IOP Conf. Series: Mater. Sci. and Eng. **9**, 012038 (2010).
3. H. G. Garcia Flores, P. Roussel, D. P. Moore, D. L. Pugmire, Surface Science **605**, 314-320 (2011).
4. T. M. McCleskey, E. Bauer, Q. Jia, A. K. Burrell, B. L. Scott, S. D. Conradson, A. Mueller, L. Roy, X. Wen, G. E. Scuseria, R. L. Martin, Journal of Applied Physics **113**, 013515 (2013).

Acknowledgement

This work is supported by Los Alamos National Laboratory LDRD program.

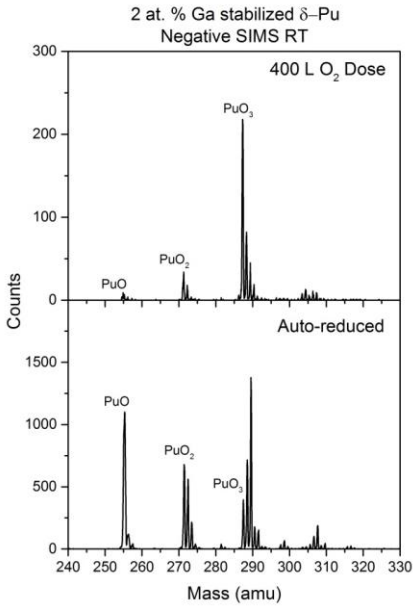

Figure 10: Negative SIMS for mechanically polished 2 at. % Ga sample after 400 L O_2 dosing (top) and after auto-reduction (bottom) at room temperature (RT).

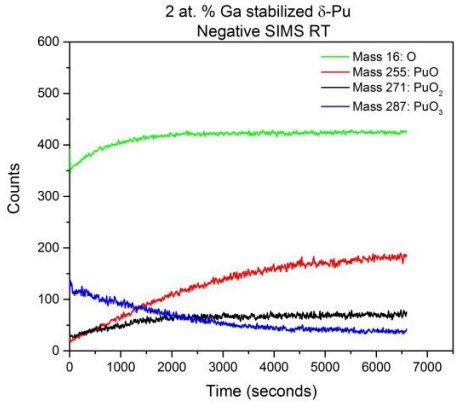

Figure 2: Negative SIMS line spectra profile after 400 L O_2 dosing as a function of time for the 2 at. % Ga sample at room temperature (RT).

A-57

Some results of investigations of particle ejection from a free surface of metals under a shock wave effect

Michael Antipov, Alla Georgievskaya, Vladislav Igonin, Margarita Lebedeva, Konstantin Panov, Valeriy Sadunov, Alexander Utenkov, Igor Yurtov

RFNC-VNIIEF, Sarov, Russia

A process of particle ejection from a free surface of metals under shock wave effects («ejecta») is of great interest. Ejection of particles from a shocked metal surface is sufficiently a complicated process, influenced by the ratio of a lot of factors. The effect of each factor has been the subject of individual investigations. Two-dimensional and three-dimensional numerical methods were developed at VNIIEF to calculate this process. However, these calculations require calibration through using a large number of reliable experimental data.

To study mass of ejecta, spatial distribution of particle density and its change with time the methods of pulse X-ray radiography and piezoelectric pins are generally used.

In the current effort, we presents the new experimental “extended” setup proposed specifically for increasing the accuracy of the X-ray measuring and, concurrently, making it possible to use the method of piezoelectric pins. Some results of investigation of lead ejecta in this setup are presented. The developed algorithm for quantitative measurements of ejecta density by the method of pulse X-ray radiography makes it possible to achieve particle density distribution without using Abel inversion reducing the measuring accuracy.

A-58

Experimental and calculation parameters of benchmark spherical critical assemblies with metal plutonium (^{239}PU (88%)) in α-phase core and beryllium and depleted uranium reflectors

Alexey Kaygorodov, Sergey Vorontsov, Mikhail Kuvshinov, Valentin Khoruzhyi

RFNC-VNIIEF, Sarov, Nizhny Novgorod Region, Russia

The knowledge of nuclear-physics characteristics of «reactor» plutonium [1] is important both for modeling operation of production power reactors, and for ensuring nuclear safety, for example, at treatment of spent nuclear fuel (SNF). Nuclear-physics data are verified by means of carrying out critical mass experiments.

The given paper reports characteristics (mass, sizes, nuclide composition) for critical systems (Keff = 1) with a core made of ^{239}Pu (88%, масс.) in α-phase with a depleted uranium reflector (reflector thickness 2.89 cm and 10.98 cm) and beryllium reflector (reflector thickness 2.10 cm, 8.20 cm and 17.50 cm).

Presented integral (critical mass) experiments with critical assemblies made of ^{239}Pu (88%, mass.) in α-phase have been carried out on FKBN facility [2] in RFNC-VNIIEF. These studies are unique due to exclusive danger work with parts made of such plutonium (both regarding high radioactivity, as well as achievement of unforeseen criticality due to a high density of α-plutonium and, correspondingly, small sizes of critical system).

Studied critical assemblies can be recommended as benchmark ones to be incorporated in the International Reference Book on Nuclear Safety ICSBEP (International Handbook of Evaluated Criticality Safety Benchmark Experiment) [3].

References

1. I.A. Andryushin, Yu.A. Yudin. Propagation risks and problem of reactor plutonium.- Saransk: Krasny Oktyabr, 2007. - 124p.

2. Vorontsov S.V., Kuvshinov M.I. Critical experiments on assemblies with plutonium metal, performed in RFNC- VNIIEF. // VANT. Series «Fizika Yadernykh Reaktorov». -2013. - Issue 3. - P.3-11.

3. International Handbook of Evaluated Criticality Safety Benchmark Experiments. Nuclear Energy Agency, Organization for Economic Cooperation and Development, NEA/NSC/DOC(95).

A-59

Carbonate oxidation of electrorefining salts

Robert Watson, Clare Stawarz

AWE plc, Aldermaston, Reading, UK

Spent electrorefining salts contain about 10wt% Pu (presumed to be $PuCl_3$ and uncoalesced Pu metal) in a NaCl-KCl matrix. A salt distillation process under reduced pressure is proposed to separate the salt matrix from the plutonium species. To prevent any plutonium species being transferred all the plutonium needs to be present as an oxide. An oxidation process using Na_2CO_3 is being investigated. The proposed reactions taking place are :

$$2\ Pu^{3+} + 3\ CO_3^{2-} \rightarrow 2\ PuO_2 + CO + 2\ CO_2$$
$$Pu + 2\ CO_3^{2-} \rightarrow PuO_2 + 2\ CO + 2\ O^{2-}$$

Trials using $CeCl_3$ in NaCl-KCl as a simulant for plutonium showed stirring for 2-3 hr at 710°C gave high yields of oxide (at least 90%). Pieces of cerium metal proved to be more resistant to oxidation under these conditions, but oxide yields of 70 - 80% were achieved either by extending the reaction time or by co-reaction with cerium chloride. A 100% stoichiometric excess of carbonate was required for complete oxidation of the $CeCl_3$. [1]

Trials using $PuCl_3$ in NaCl-KCl, to simulate spent electrorefining salt, showed complete conversion to PuO_2 with stirring for 2 hours at 710°C with 120% excess of Na_2CO_3. The lower potion of the salt contained 98% of the plutonium in 35% of the total salt. XRD of the salt showed the carbonate was completely consumed. [2]

Two trials have been completed using spent electrorefining salts from which alumina crucible fragments retained on a 4mm sieve were removed. A 100% excess of Na_2CO_3 was used, assuming all the plutonium was present as $PuCl_3$. The salt was heated to 735±10°C in a magnesia crucible and stirred at 120rpm with a pitched bladed tantalum stirrer for 2 hours. In both trials the salt separated into a white upper layer and a dark lower layer, Figure 1. In both trials the salt cleaved across the interface between the two phases, in the previously reported studies the salt cleaved along the interface. In one run non-destructive assay showed the plutonium concentration of the white salt phase was 230ppm Pu and the black salt phase about 20% Pu. There was no significant weight loss on the process implying very little carbonate reacted. Examination of the feed and product salts by x-ray diffraction is underway.

Figure 1. Broken product salt.

References

[1] Taylor G and Wilson T 'Evaluation of Molten Salt Carbonate Oxidation for the Treatment of Waste Pyrochemical Salts' Extended Abstract : Pu Futures – The Science 2012, Cambridge, July 2012

[2] Pierce R A, Caldwell T, Paget T and Watson R 'Carbonate oxidation and salt distillation of $PuCl_3$-NaCl-KCl' Abstract at 37th Actinide Separations Conference, Spokane WA, June 2013

© British Crown Owned Copyright 2016/AWE

Published with permission of the Controller of Her Britannic Majesty's Stationery Office.

A-60

Hydrolysis of plutonium under reducing conditions controlled by electrolysis

Hye-Ryun Cho, Young-Sang Youn, E. C. Jung, W. Cha

Korea Atomic Energy Research Institute, Daejeon, Republic of Korea

Introduction

The chemical behaviours of plutonium in aquatic solutions should be understood to ascertain the isolation and immobilization of plutonium in a deep geological system developed for disposing high-level nuclear waste. Under environmental conditions, plutonium can coexist in several oxidation states (Pu(III-VI)) which show drastically different chemical behaviours [1]. It is still difficult to predict dissolved plutonium species and their mobility under underground reducing conditions. Several investigations have been reported on the solubility of plutonium hydroxide in the presence of reducing agents [2-4]. The concentrations of dissolved plutonium species were higher than those estimated with the solubility product of Pu(IV) hydroxide owing to the reduction of Pu(IV). The hydrolysis of Pu(III) and solubility of $Pu(OH)_3$ are important chemical reactions because they may control the initial concentration of dissolved plutonium which forms a mobile or immobile species by interacting with natural matters.

In the present work, the reducing condition is controlled through electrolysis. An electrochemical cell is installed in a glove box purged with Ar gas to prepare plutonium samples under various concentrations and pH levels under electrolytic reducing conditions. The concentrations of hydrogen ions (H^+) in plutonium solutions are reduced using a coulometric pH titration. Chemical speciation for dissolved plutonium is conducted by spectrophotometry adopting a liquid waveguide capillary cell (LWCC), and the solid phase is characterized through x-ray diffraction (XRD).

Experimental

PuO_2 (ORNL, isotopic composition: 99.932% ^{242}Pu) is dissolved, as described in a previous report [5]. The trace amount of Am-241 is removed using an anion-exchange resin (100-200 mesh AG 1-X8, Bio-Rad, USA) in an HCl medium. The background material is converted into $HClO_4$ by repeated evaporation in concentrated $HClO_4$ solutions. An aliquot of a Pu(VI) solution is appropriately diluted using an acidic solution (0.1 M $HClO_4$) and reduced to Pu(III) through electrolysis. The concentration of plutonium is 3.53 mM, which is determined using liquid scintillation counting (LSC, TriCarb 2500 TR/AB, Packard). The initial sample of Pu(III) to investigate the hydrolysis of Pu(III) was prepared through the dilution of a Pu(III) stock solution in 0.1 M $NaClO_4$. The concentration of hydrogen ions is decreased through electrolysis without the addition of an alkaline solution. During the coulometric pH titration, the concentration of plutonium and the oxidation state of Pu(III) are maintained. For example, 20 mL of a Pu(III) sample at a Pu concentration of 0.1 mM, and pH 2 in 0.1 M $NaClO_4$, was prepared in a Teflon reactor. The 10 □A current reduces 0.4 □□mole of H^+ ions to H_2 gas in one hour.

The pH of a sample is measured using a combination glass electrode (Ross type, Orion) calibrated with pH buffers (pH 2.00, 4.01, 7.00 and 10.01, Orion). The absorption spectra of soluble plutonium species are measured using spectrophotometer (Cary5, Varian, Germany) with a sealable quartz cell (Macro117.100F, Hellma) or a LWCC (LWCC-3100, WPI, USA) setup in a glove box [5]. Laser-induced breakdown detection (LIBD) is used for the detection of colloidal nanoparticles. It is a very sensitive method for detecting aqueous particles of a smaller size (< 100 nm) at a low concentration (< ppb) [6].

Results and discussion

Figure 1 shows the absorption spectra of plutonium samples at different pH values measured using a LWCC within a wavelength range of 400 to 700 nm. The absorbance decreases with an increase in pH at a constant concentration of plutonium ([Pu] = 0.08 mM). The characteristic absorption features for the other oxidation states of plutonium (Pu(IV, V and VI)) are not observed in all samples. Therefore, the contribution of dissolved Pu(IV-VI) species can be ignored. The plutonium in the samples may exist in the form of hydrated Pu^{3+} ions, hydrolysis species of Pu(III), colloidal nanoparticles or a precipitate.

Absorption spectra and LIBD signals indicate that two samples at pH 5.07 and 5.51 do not contain colloidal particles whereas trace amounts of colloids are detected using LIBD in samples at pH 5.85 and 6.19. An increase of absorbance for the sample at pH 6.19 in a short wavelength range (400-500 nm) also indicates the formation of plutonium colloids. It means that the samples at pH 5.07 and 5.51 contain only dissolved Pu(III) species with the concentration of approximately 0.08 mM.

Normalized signals for the spectra shown in Figure 1 are consistent with the reference absorption spectrum of hydrated Pu^{3+} ions in 0.1 M $HClO_4$ (data not shown). Therefore, it can be assumed that the decrease of absorbance in a wavelength range of 500 to 700 nm results from the formation of hydrolysis species or a solid phase, which does not absorb light in the region of interest. A quantitative analysis through spectrophotometry indicates that the concentrations of hydrated Pu^{3+} ions are 76.7, 73.8, 44.8 and 31.0 µM for the samples at pH 5.07, 5.51, 5.85 and 6.19, respectively.

The formation constant for the first hydrolysis species of Pu(III) can be determined through spectrophotometry when there is no further hydrolysis species or a solid phase of plutonium in a sample. As shown in Figure 2, the results of a slope analysis (slope = -2 or -3) indicate that Pu^{3+} and $Pu(OH)^{2+}$ ions are dominant in aqueous solutions, which are equilibrated with $Pu(OH)_3$ (s) [7]. The formation constant of $Pu(OH)^{2+}$ species (${}^{*}\beta'_1 = [Pu(OH)^{2+}]\cdot[H^+]/[Pu^{3+}]$) for reaction (1) and the solubility product (${}^{*}K' = [Pu^{3+}]/[H^+]^3$) for reaction (2) are determined at a constant ionic strength of 0.1 M $NaClO_4$, which will be discussed in comparison with the previous results [7].

$$Pu(OH)_3\,(s) + 3H^+ \leftrightarrows Pu^{3+} + 3H_2O \qquad (1)$$

$$Pu^{3+} + nH_2O \leftrightarrows Pu(OH)^{2+} + nH^+ \qquad (2)$$

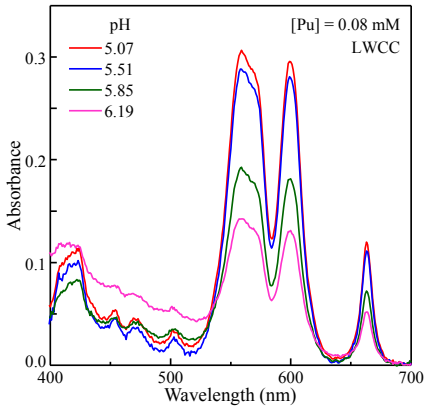

Figure 1. Absorption spectra of plutonium samples are measured using a LWCC. The concentration of plutonium is constant at various pH values.

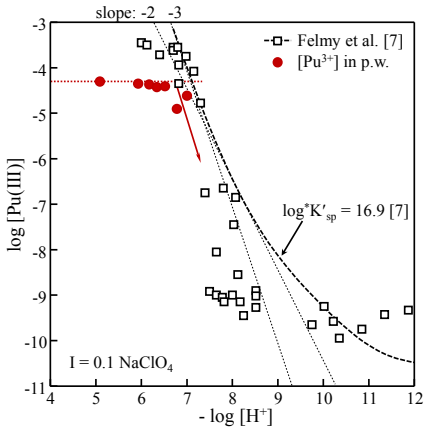

Figure 2. The concentrations of hydrated Pu^{3+} ions quantitatively determined through spectrophotometry are compared with the previously reported data.

Acknowledgement

This work was supported by the nuclear R&D program of the NRF of Korea grant funded by the Korean MSIP.

References

1. G. R. CHOPPIN, “Solution Chemistry of the Actinides”, *Radiochim. Acta*, **32**, 43-53 (1983).

2. H. NILSSON, Y. ALBINSSON and G. SKARNEMARK, “Dissolution of Plutonium(III) Hydroxide at 50 bar H_2”, *Mat. Res. Soc. Symp Proc.*, **807**, 615-620 (2004).

3. K. FUJIWARA et al., “Solubility Product of Plutonium Hydrous Oxide and Its Ionic Strength Dependence”, *Radiochim. Acta*, **90**, 857-861 (2002).

4. D. RAI, et al., “Reductive Dissolution of PuO_2(am): The Effect of Fe(II) and Hydroquinone”, *J. Sol. Chem.*, **31**, 433-453 (2002).

5. H.-R. CHO et al., “Effect of reduction on the stability of Pu(VI) hydrolysis species”, *Radiochim, Acta*, **98**, 555-561 (2010).

6. E. C. JUNG and H.-R. CHO, *Characteristics of the Laser-Induced Breakdown Detection of Colloidal Nanoparticles for Determining Particle Size* in the Delivery of Nanoparticles, ed. A. A. HASHIM, InTech, Ch. 20, 431-452 (2012).

7. A. R. FELMY et al., “The Solubility of Plutonium Hydroxide in Dilute Solution and in High-Ionic-Strength Chloride Brines”, *Radiochim. Acta*, **48**, 29-35 (1989).

A-61

U(VI) adsorption onto alumina, silica, and kaolinite in U(VI)-OH / U(VI)-CO_3 / Ca-U(VI)-CO_3 aqueous systems

Yongheum Jo[1], Jun-Yeop Lee[2], Jong-Il Yun[1]

[1]Department of Nuclear and Quantum Engineering, KAIST, 291 Daehak-ro, Yuseong-gu, Daejeon 34141, Republic of Korea, [2]Institute for Nuclear Waste Disposal, Karlsruhe Institute of Technology, Karlsruhe, Baden-Württemberg, Germany

Uranyl carbonate and ternary calcium uranyl carbonate species, such as $UO_2(CO_3)_3^{4-}$, $CaUO_2(CO_3)_3^{2-}$, and $Ca_2UO_2(CO_3)_3$(aq), have been considered as predominant U(VI) species in neutral and weak-alkaline groundwater. Nonetheless, adsorption mechanism of these uranyl species including carbonate ligands at mineral surfaces has been still unclear. In this work, time-resolved laser fluorescence spectroscopic (TRLFS) characterization of various U(VI) aqueous carbonate species adsorbed onto alumina, silica, and kaolinite in U(VI)-CO_3/Ca-U(VI)-CO_3 systems were conducted to elucidate the adsorption effect of these chemical species.

Uranium(VI) solutions at 88 μmol/L were prepared for the formation of uranyl carbonate and ternary calcium uranyl carbonate species (U(VI)-CO_3/Ca-U(VI)-CO_3 systems). The initial carbonate concentration was adjusted to 0.025 M by adding Na_2CO_3. The pHs were buffered by TRIS and controlled with $HClO_4$ and NaOH in the range of 7.5 to 9.0. $Ca(ClO_4)_2$ was spiked to Ca-U(VI)-CO_3 solutions. The TRLFS analysis of solution showed comparable spectroscopic data with previous studies [1-3], indicating the formation of $UO_2(CO_3)_3^{4-}$, $CaUO_2(CO_3)_3^{2-}$, and $Ca_2UO_2(CO_3)_3$ successively. For the purpose of comparison, U(VI) hydroxide solutions were prepared at pH 5.0, 7.5, and 9.0 in the argon inert atmosphere. Ionic strength of all solutions was kept at 0.1 M with $NaClO_4$.

The batch sorption experiments were performed by mixing the prepared solutions and alumina (Sigma, 544833), silica (Alfa Aesar, L16987), and kaolinite (The Clay Mineral Society, kGa-2) with 5 g/L in solid to liquid ratio. Suspensions were equilibrated for 2 days. After sorption equilibrium, the solid and liquid phases were separated by centrifugation for 30 min at 10,000 g and ultrafiltration with 0.02 μm syringe filter. To measure fluorescence from adsorbed U(VI) species onto mineral, the separated solids were re-suspended by adding background electrolytes. The fluorescence of suspension was obtained by excitation at 266 nm.

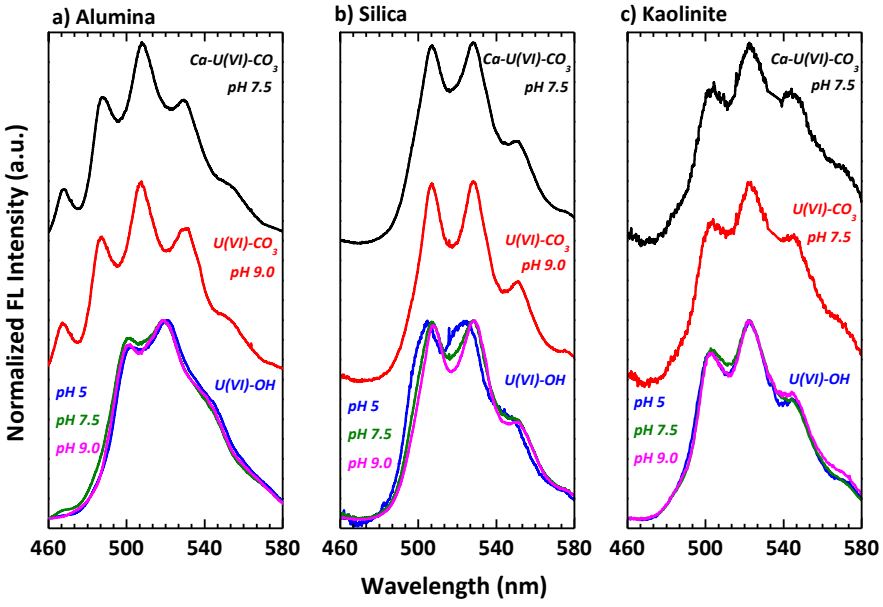

Fig 1. Normalized TRLFS spectra of adsorbed U(VI) onto a) alumina, b) silica, and c) kaolinite

As shown in Fig. 1, spectra of U(VI) adsorbed onto alumina in U(VI)-CO_3/Ca-U(VI)-CO_3 aqueous systems are shifted to lower wavelength with relatively narrower width, as compared those in U(VI)-OH solutions. On the other hand, the spectra of U(VI) adsorbed onto silica and kaolinite were identical regardless of initial aqueous species. The blue-shifted fluorescence spectra with sharp bands are taken into account for the U(VI)-carbonate complexation [4]. Therefore, in analogy to aqueous U(VI) species, these carbonate-like features shown in adsorbed U(VI) species imply the existence of carbonate ligands in U(VI) species adsorbed onto alumina. In contradiction to alumina, for the case of silica and kaolinite, the effect of carbonate U(VI) species was not observed. The presence of carbonate ligands in adsorbed U(VI) was unfavorable, and these ligands surrounding uranyl central ion were detached during adsorption reaction. In ATR-FTIR study [5], the absorption bands of $v_3(CO_3)$ at 1513 cm^{-1} and 1370 cm^{-1} and $v_3(UO_2)$ at 903 cm^{-1} were assigned to bidentate U(VI)-carbonate gibbsite surface species. In the present work, both TRLFS and vibration spectroscopic FTIR results are presented and compared.

References

[1] G. Bernhard et al., “Speciation of uranium in seepage waters of a mine tailing pile studied by time-resolved laser-induced fluorescence spectroscopy (TRLFS)”, *Radiochim. Acta* **74**, 87–91 (1996)

[2] Götz, C. et al., “The Influence of the temperature on the carbonate complexation of uranium(VI): A spectroscopic study”, *J. Radioanal. Nucl. Chem.* **287,** 961–969 (2011)

[3] Lee, J.-Y. and Yun, J.-I., “Formation of ternary $CaUO_2(CO_3)_3^{2-}$ and $Ca_2UO_2(CO_3)_3$(aq) complexes under neutral to weakly alkaline conditions”, *Dalton Trans.* **42**, 9862–9869 (2013)

[4] Wang, Z. et al., ”Cryogenic laser induced fluorescence characterization of U(VI) in Hanford vadose zone pore waters”, *Environ. Sci. Technol*. **38,** 5591-5597 (2004)

[5] Gückel, K. et al., “Binary and ternary surface complexes of U(VI) on the gibbsite/water interface studied by vibrational and EXAFS spectroscopy”, *Chem. Geol.* **326-327**, 27–35 (2012)

A-62

Structural properties of actinides from first principles: important role of Hund's exchange

Bernard Amadon

CEA, Bruyeres le Chatel, France

We utilize a combination of an *ab initio* calculation of effective Coulomb interactions [1] and a full-fledged implementation of DFT+DMFT [2] to study structural properties of pure actinides. We first show that the effective direct Coulomb interaction in actinides is much smaller than usually expected. Secondly, we emphasize the key role of Hund's exchange in combination with the spin-orbit coupling in determining the structural parameters in actinides. Thirdly, using this ab initio description, we reproduce the experimental transition from low volume early actinides to high volume late actinides [3].

References

[1] B. Amadon, T. Applencourt, and F. Bruneval, Screened coulomb interaction calculations: crpa implementation and applications to dynamical screening and self-consistency in uranium dioxide and cerium," Phys. Rev. B 89, 125110 (2014)

[2] B. Amadon, A self-consistent DFT+DMFT scheme in the projector augmented wave method: applications to cerium, Ce2O3 and Pu2O3 with the Hubbard I solver and comparison to DFT+U," Journal of Physics: Condensed Matter 24, 075604 (2012)

[3] Unpublished results, under review (2016)

A-63

Solubility, Hydrolysis and Carbonate Complexation of Plutonium and Neptunium under Repository-Relevant Conditions

Julian Schepperle, David Fellhauer, Xavier Gaona, Marcus Altmaier, Horst Geckeis

Institute for Nuclear Waste Disposal, Karlsruhe Institute of Technology, Karlsruhe, Germany

Plutonium and neptunium are very relevant actinides in the context of nuclear waste disposal because of their high long-term radiotoxic inventory in spent nuclear fuel, the very long half-life of key isotopes ($t_{1/2}$ ^{239}Pu = $2.41 \cdot 10^4$ a; $t_{1/2}$ ^{237}Np = $2.14 \cdot 10^6$ a) and their redox-sensitive character. The internationally favoured option for the final disposal of nuclear waste is storage in deep underground repositories, where reducing conditions are expected to develop after closure due to the anoxic corrosion of steel components. Accurate knowledge of radionuclide solubility and complexation reactions is required to estimate maximum amounts of dissolved radionuclide species potentially mobilized from a repository in the case of water intrusion. Those data represent very relevant source term input parameters for safety assessments. In this framework, the present work provides a comprehensive experimental basis for an accurate thermodynamic description of Pu(IV) and Np(IV) solubility, hydrolysis and complexation with carbonate under reducing conditions. Although several studies exist on this topic (see e.g. Neck et al. [1]), a number of important aspects remain unresolved: a) solubility data for PuO_2(am,hyd) and NpO_2(am,hyd) are missing for $3 < pH < 6$, thus hindering an adequate description of Pu(IV) and Np(IV) behavior in this pH region; b) comprehensive solubility studies with PuO_2(am,hyd) and NpO_2(am,hyd) that cover a wide range of background electrolyte concentrations and pH_m values are so far not available; c) almost all available solubility data for NpO_2(am,hyd) and $pH > 6$ are reported with large uncertainties; d) a very limited data set is available in the literature for the solubility of Pu(IV) and Np(IV) in carbonate containing solutions [2][3].

Undersaturation solubility experiments were performed with PuO_2(am,hyd) and NpO_2(am,hyd) obtained by precipitation from an electrochemically prepared Np(IV) stock solution or by slow "reductive precipitation" of Pu(VI) with hydroquinone, respectively. Independent batch samples were prepared in 0.1 mol $L^{-1} \leq$ [NaCl] $\leq$ 5.0 mol L^{-1} solutions with $2 \leq pH_m \leq 13$ ($pH_m = -\log m_{H+}$). Redox conditions in the investigated systems were fixed by the addition of reducing chemicals. Similar experiments in the presence of 0.1 mol L^{-1} and 0.04 mol L^{-1} Na_2CO_3/$NaHCO_3$ were performed at $8 \leq pH_m \leq 12.5$. Phase separation was performed either by ultrafiltration (10 kD, 2 nm) or ultracentrifugation (90 000 rpm, Beckmann XL-90K ultracentrifuge, Beckmann Type 90 Ti rotor), and an aliquot of the clear supernatant potentially including colloidal species was also collected for selected samples. Measurements of pH_m, redox potential (with pe = 16.9 E_H), and An concentration (liquid scintillation counting (LSC) or sector field inductively coupled plasma mass spectrometry (SF-ICP-MS)) were performed on a regular basis until attaining equilibrium conditions. Experimental results obtained in the absence of carbonate were compared with thermodynamic calculations using the current NEA-TDB selection [4], whereas solubility data gained in carbonate-containing solutions were fitted according with the chemical model previously reported for Th(IV) [5].

The solubility of Pu(IV) and Np(IV) in the acidic pH range systematically decreases with increasing pH_m. Experimentally measured [Pu] are clearly above the concentrations calculated for the equilibrium reaction PuO_2(am,hyd) $\rightleftharpoons$ Pu(IV)(aq). Solvent extraction analysis confirmed that this is due to a major contribution of Pu(III)(aq), which formed in the course of the experiment. In contrast to Pu, the experimentally measured [Np] is in fair agreement with thermodynamic calculations for the equilibrium reaction NpO_2(am,hyd) $\rightleftharpoons$ Np(IV)(aq), and only a very minor impact of ionic strength on the solubility is observed up to 5.0 M NaCl. The

predominance of Np(IV) in the aqueous phase is confirmed by liquid-liquid extraction and capillary electrophoresis (CE) coupled to SF-ICP-MS.

The pe+pH_m values measured under near-neutral to hyperalkaline pH conditions are in the thermodynamic stability field of An(IV) for both Pu and Np. The solubility of PuO_2(am,hyd) and NpO_2(am,hyd) under these conditions is very low, and [An] was quantified by SF-ICP-MS (detection limit ca. $1 \cdot 10^{-12}$ mol L^{-1}). The results reveal a pH and ionic strength independent solubility, with log [Pu(IV)] ≈ –9.2 and log [Np(IV)] ≈ −10.1 corresponding to the equilibrium reaction AnO_2(am,hyd) + 2 H_2O ⇌ $An(OH)_4$(aq).

The presence of carbonate significantly increases the solubility of An(IV) within $8 \leq pH_m \leq 12.5$ (Fig. 1). For the same carbonate concentration, the increase in [NaCl] (and thus in ionic strength) also has a significant impact on the solubility of AnO_2(am,hyd). This observation clearly hints towards the predominance of highly charged An(IV) species in the aqueous phase, as previously reported for Th(IV) under analogous experimental conditions [5]. Preliminary chemical, thermodynamic and activity models are derived for the systems Pu(IV)–OH–CO_3 and Np(IV)–OH–CO_3 based on the newly generated solubility data. These thermodynamic models represent a significant improvement and are highly relevant for calculating reliable An(IV) source term concentrations in the context of safety assessments for nuclear waste repositories.

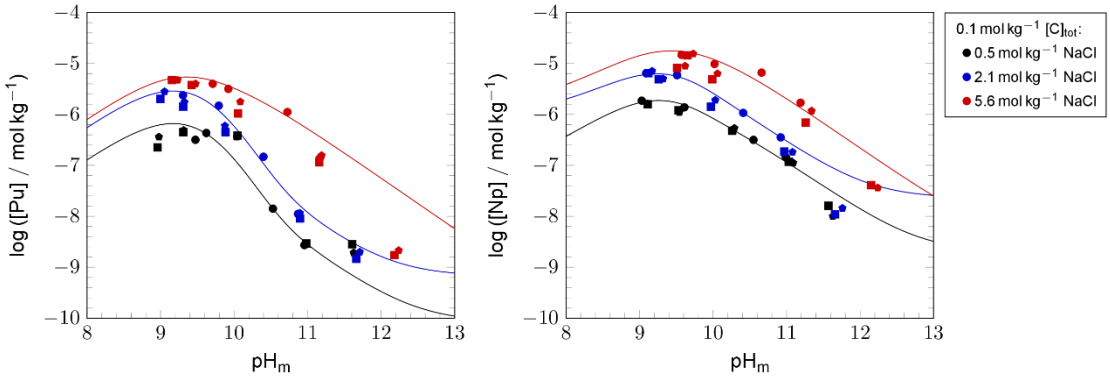

This work was funded by the German Federal Ministry of Education and Research under the research platform ENTRIA.

References

[1] V. Neck, J. I. Kim, *Radiochimica Acta* **2001**, *89*, 1–16.

[2] D. Rai, N. J. Hess, A. R. Felmy, D. A. Moore, M. Yui, P. Vitorge, *Radiochimica Acta* **1999**, *86*, 89–99.

[3] A. Kitamura, Y. Kohara, *Radiochimica Acta* **2004**, *92*, 583–588.

[4] R. Guillaumont, T. Fanghänel, J. Fuger, I. Grenthe, V. Neck, D. A. Palmer, M. H. Rand, *Update on the Chemical Thermodynamics of Neptunium and Plutonium*, Elsevier, Amsterdam, **2003**.

[5] M. Altmaier, V. Neck, M. A. Denecke, R. Yin, T. Fanghänel, *Radiochimica Acta* **2006**, 94, 495–500.

A-64

Thermodynamic stability of the UO_2 surfaces: Interplay between over-stoichiometry and polarity compensation

François Bottin[1], Gérald Jomard[2], Grégory Geneste[1]

[1]CEA, Arpajon, France, [2]CEA, Saint-Paul-lez-Durance, France

The thermodynamic stability of UO_2 surfaces is investigated using *ab initio* calculations in the GGA+*U* framework. Among the seven (100), (110) and (111) terminations studied, we predict that the stoichiometric O-(111) is the most stable one under oxygen-poor or -intermediary environments (see Figure 1).

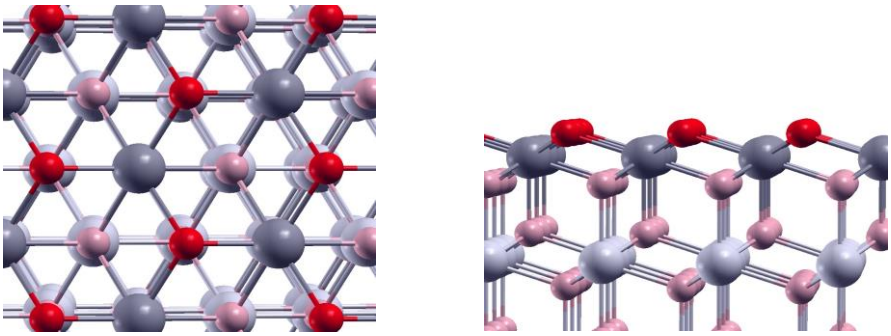

Figure 1: Left (right) panel: Top (side) view of the stoichiometric O-(111) polar termination.

At odds with other fluorite surfaces, the overstoichiometric and polar O_2-(100) and O_2-(111) terminations become the most stable in oxygen-rich environments with strong modifications of the electronic structure within the upper layers. Some U-5*f* surface states are emptied, leading to higher U^{5+} and U^{6+} oxidation states, but leaving the surface insulating. This unexpected polarity compensation mechanism is not observed for other charge transfer compounds [1] (such as PuO_2) and can be related to the *f-f* Mott-Hubbard band gap of the UO_2 material [2]. By considering the most stable stoichiometric and overstoichiometric terminations the Wulff shape of nano-voids in UO_2 crystals can be explained [3].

References

[1] G. Jomard and F. Bottin, Phys. Rev. B **84**, 195469 (2011).

[2] G. Jomard, B. Amadon, F. Bottin and M. Torrent, Phys. Rev. B **78**, 075125 (2008).

[3] F. Bottin, G. Jomard and G. Geneste, Phys. Rev. B **93**, 115438 (2016).

A-65

Analysis of surface chemistry on Pu-Ga alloyed surfaces by Time-of-Flight SIMS

Thomas Venhaus, Sarah Hernandez, Joseph Anderson, David Moore, David Pugmire

Los Alamos National Laboratory, Los Alamos, NM, USA

Introduction

Time-of-flight secondary ion mass spectroscopy (ToF-SIMS) provides a unique analytical technique to probe solid surfaces by producing a comprehensive survey of surface constituents (including hydrogen). ToF-SIMS is highly sensitive with a probe depth of only the topmost mono-layers of the surface. Analysis of the SIMS fragment patterns can also provide information on chemical speciation of adsorbed molecules, especially when exposing surfaces to isotopically labelled gases (e.g. ^{13}CO and $C^{18}O$). This powerful technique, however, has rarely been applied to understanding the reactivity and composition of δ-stabilized plutonium (δ-Pu) surfaces and its oxides.

Plutonium is known to react immediately when exposed to air to form a protective oxide layer [1]. Understanding the nature of the growth and stability of the passive oxide layer on δ-Pu and how the surface layer reacts with atmospheric gases is important to prevent further oxidation or corrosion of the material. Surface science techniques, such as X-ray photoelectron spectroscopy (XPS) and Auger electron spectroscopy (AES) have provided a wealth of information on the surface oxide [2, 3]. SIMS has been demonstrated as a technique capable of distinguishing molecular from dissociative chemisorption on several transition metal surfaces exposed to CO [4]. In this work, we use ToF-SIMS to study the resulting chemistry of the native Pu metal oxide after exposures of a series of common atmospheric gases, which includes H_2, H_2O, N_2, CO, CO_2, and O_2 (for oxygen, see abstract by Hernandez et al.).

Experimental details

ToF-SIMS detects the mass of ejected positive and negative ions from a surface that has been bombarded by a focused, high energy ion beam. To avoid further destruction of the surface, the ion beam may be operated in the low flux static regime (<1nA/cm^2), also known as static ToF-SIMS. Surface analysis of the mechanically polished 7 at.% gallium (Ga) was performed with a Kore ToF-SIMS. This system is equipped with a pulsed 25 keV monoisotopic $^{69}Ga^+$ liquid metal ion gun, a 4 keV Ar^+ sputter gun for depth profiling, and a time-of-flight mass spectrometer capable of a mass resolution of m/Δm = 5000. The system base pressure is approximately 5 x 10^{-10} Torr. Gas dosing was performed *in-situ* at a partial pressure of 1 x 10^{-7} Torr.

Results

The mechanically polished sample was first sputter cleaned briefly with 4 keV argon ions to reduce the surface contamination that remained from the polishing step, while not completely removing the oxide layer. However, the oxide layer was considered to be slightly reduced due to the preferential sputtering of oxygen. Figures 1a (low mass range) and 1b (high mass range) show the resulting positive secondary ion fragment pattern from the Pu surface following a 10 L (1L = 10^{-6} Torr·sec) dose of ^{13}CO at room temperature. If the ^{13}CO had molecularly chemisorbed to the surface, peaks associated with mass 29 would be expected, along with larger clusters containing mass 29 (e.g. $^{239}Pu^{13}CO^+$ at mass 268), as discussed in Ref. 4. Generally, this pattern was not observed in the positive SIMS spectra. Negative SIMS ion fragments, however, revealed peaks associated with ^{13}C ($^{13}C^-$, $^{13}C_2^-$, and $^{13}C_3^-$) in addition to $Pu^{13}C_2^-$, suggesting dissociative adsorption on the surface. In addition to the isotopically

labelled CO, other gases of interest were dosed on the Pu surface similarly, and the results from those exposures are discussed herein.

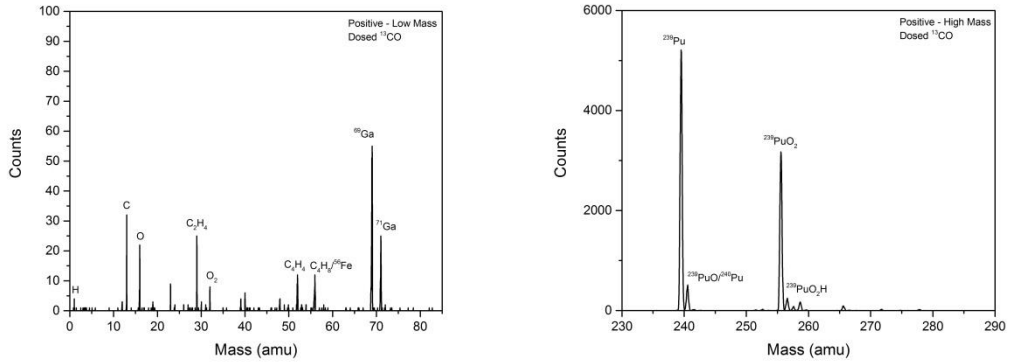

Figure 11: Positive SIMS fragment patterns after ^{13}CO gas exposure for the (a) low masses and (b) high masses on Ga-stabilized δ-Pu surface.

References

5. J. M. Haschke, T. H. Allen, *Surface and Corrosion Chemisty of Plutonium*, Los Alamos Science Vol. 1 No. 26, 252- 273 (2000).
6. H. G. Garcia Flores, D. L. Pugmire, *The growth and evolution of thin oxide films on δ-plutonium surfaces*, IOP Conf. Series: Mater. Sci. and Eng. **9**, 012038 (2010).
7. H. G. Garcia Flores, P. Roussel, D. P. Moore, D. L. Pugmire, *Characterization and stability of thin oxide films on plutonium surfaces,* Surface Science **605**, 314-320 (2011).
8. M. Barber, J. C. Vickerman, J. Wolstenholme, *The application of SIMS to the study of CO adsorption on polycrystalline metal surfaces*, Surface Science **68,** 130-137 ((1977)

A-66

ToF-SIMS Determination of the Partitioning between H and F in Aged Uranium Materials

Scott Donald, Wigbert Siekhaus, Art Nelson

Lawrence Livermore National Laboratory, Livermore, CA, USA

Introduction

Fluorine-containing chemicals play a major role in the standard methodology used to enrich uranium for use in the nuclear industry.[1] While removed during processing uranium to more useable forms, most commonly to UO_2, some amount remains as a minor contaminant and can be detrimental during subsequent processing and use as fuel.[2,3] Specifically, an inherent drawback of many commonly used dry conversion processes is high fluorine in the product.[4] While some work has been done to understand the kinetics of the defluorination process [5,6], no current method is able to remove all of the residual fluorine. With fluorine possessing a higher electronegativity than oxygen, the presence of fluorine in uranium materials may lead to differences in their physical properties and chemical nature; to our knowledge, the exact impact of this fluorine contamination during the aging of uranium samples has not been investigated. This study uses time-of-flight secondary ion mass spectrometry (ToF-SIMS) to provide information on the depth-distribution of fluorine in several aged uranium materials. The partitioning of fluorine and hydrogen in the samples is also discussed.

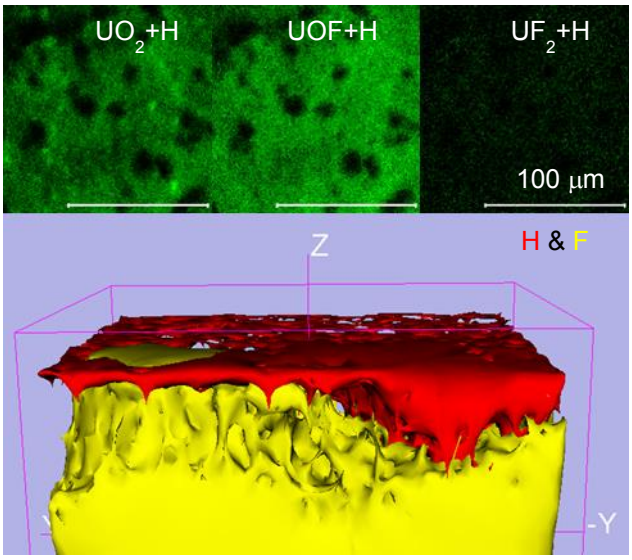

Figure 1. ToF-SIMS positive-ion images, 600 nm lateral resolution, of UO_2+H (top left) UOF+H (top middle) and UF_2+H (top right) for the aged UF_4 single crystal. ToF-SIMS negative-ion depth-profile 3-D image (bottom) of the UF_4 single crystal. Areas of low fluorine ion-counts are not shown for clarity.

Description of the actual work

The samples studied included a uranium tetrafluoride (UF_4) poly-crystal, a uranium poly-crystal polished in water, a thin film of uranium deposited on a silicon wafer, and a polished block of metallic uranium. Aside from the water-polished crystal, all samples had been aged for a period of at least one year at ambient temperature and ~50% relative humidity. ToF-SIMS depth profiles were carried out using a PHI TRIFT III in single-ion source mode. The liquid-metal Ga ion gun was operated at 15 keV with a beam current of 6 x 10^{-8} A, an incidence angle of 45°,

and was used for both sputtering and analysis. Depth-profile raster areas of the ion beam used for sputtering (dc) and imaging (pulsed) were 150 µm x 150 µm and 40 µm x 40 µm, respectively.

Results

In UF_4, the areas comprised of uranium oxide and fluoro-oxide species were found to be associated with a greater concentration of hydrogen than those of uranium tetrafluoride, as displayed in the top of Figure 1. The sputter depth-profile of the UF_4 single crystal is presented in the bottom of Figures 1, with the location of hydrogen and fluorine secondary ions in the depth profile shown as red and yellow, respectively. Increased hydrogen ion count with depth appears to correspond with a decreased concentration of fluorine, an expected result from the reaction of the surface with atmospheric water during aging, but may also indicate a lack of hydrogen solubility in fluorine-rich materials. The mechanism behind the variation in the extent of hydriding (and correlated oxidation) with depth is unknown.

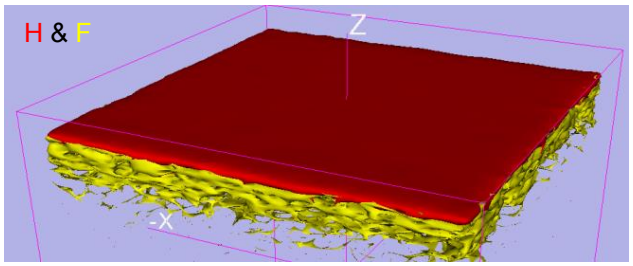

Figure 2. 3-D image of the ToF-SIMS negative ion depth-profile of the U metal poly-crystal polished in water. Image scale is 40 µm x 40 µm x 75 nm.

In both the water-polished uranium sample and sputter-deposited uranium thin film, the areas with hydrogen (red) appear to be limited in depth to the top 7 nm and above a layer of increased fluorine (yellow) concentration, determined to be ~5 nm thick and ~10 nm beneath the surface, as shown in Figures 2 and 3. The traces of hydrogen observed below the fluorine layer are the result of contamination of the reactive surface from the vacuum environment during spectra acquisition.

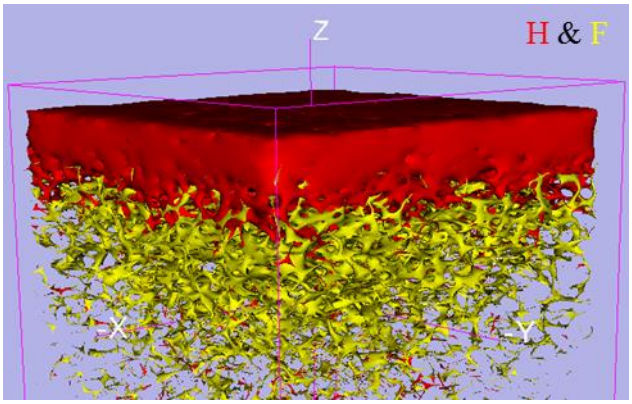

Figure 3. ToF-SIMS 3-D negative ion depth profile image of the aged U thin film on Si. Image scale is 40 µm x 40 µm x 25 nm

In contrast to the water-polished U poly-crystal and U thin film, the distribution of fluorine in the block of U metal does not form an uninterrupted layer below the surface. As displayed in Figure

4, in locations where little to no fluorine (yellow) was found to be present, the concentration of hydrogen (red) appeared in elevated concentrations at increased depth (>30 nm). In contrast to the near-surface-nature of hydrogen seen in the previous samples.

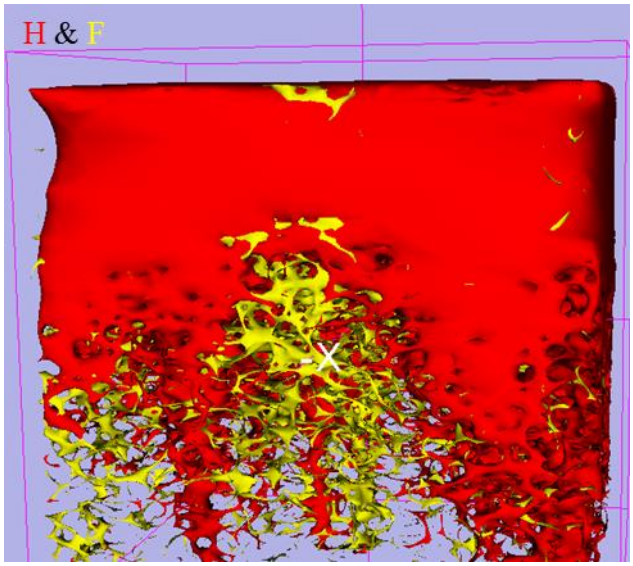

Figure 4. ToF-SIMS 3-D negative-ion depth-profile image of the aged U block. Image scale is 40 μm x 40 μm x 50 nm.

In summary, ToF-SIMS was used to investigate the partitioning of hydrogen and fluorine in aged uranium samples. A majority of samples displayed a hydrogen layer limited to the near-surface region, followed by a uniform layer of elevated fluorine at ~10 nm. In the sample where the subsurface fluorine was non-uniform, hydrogen was seen at elevated concentrations at >30 nm. Based on these results, it appears that hydrogen has limited solubility in areas with elevated concentrations of fluorine, and that the formation of a uniform sub-surface layer of fluorine may influence the aging of uranium materials.

This work was performed under the auspices of the U.S. Department of Energy by Lawrence Livermore National Laboratory under Contract DE-AC52-07NA27344.

References

1. B.H. MCNAMARA, R. SCHEELE, A. KOZELISKY, and M. EDWARDS, “Thermal reactions of uranium metal, UO_2, U_3O_8, UF_4, and UO_2F_2 with NF_3 to produce UF_6,” J. Nucl. Mat. 394, 166 (2009)

2. R.Z. HOU, T. MAHMUD, N. PRODROMIDIS, K.J. ROBERTS, R.A. WILLIAMS, D.T. GODDARD, and T. SEMERAZ, “Synthesis of UO_2F_2 nanoparticles in a tubular aerosol reactor: Reactor design and experimental investigations,” Ind. Eng. Chem. Res., 46, 2020 (2007)

3. L. O. GILPATRICK and L. M. TOTH, “The hydrogen reduction of uranium tetrafluoride in molten fluoride solutions,” J. Inorg. Nucl. Chem., 39, 1817 (1977)

4. C-T. HYANG, “Dry-ADU process for UO_2 production,” J. Nucl. Mat. 199, 61 (1992)

5. Z. X. SONG, X.W. HUANG, Z. F. XIE, Q.R. GE, and R.S. WANG, “Defluorination behavior and mechanism of Uranium Dioxide,” J. Rad. Nuc. Chem. 237, 81 (1998)

6. C. B. YEAMANS, G.W. C. SILVA, G.S. CEREFICE, K.R. CZERWINSKI, T. HARTMANN, A.K. BURRELL, and A.P. SATTELBERGER, “Oxidative ammonolysis of uranium(IV) fluorides to uranium(VI) nitride,” J. Nucl. Mat. 347, 75 (2008)

B-01

Does the Electrochemistry of Plutonium Signal the Unravelling of the Seaborg Concept of the Actinide Series?

Thomas E. Albrecht-Schmitt

Florida State University, Tallahassee, Florida, USA

When Glenn Seaborg introduced the concept of the actinide series as a distinct row of elements much like that of lanthanides, he fundamentally changed the arrangement of the periodic table. The actinide concept is based on a sequential filling of the 5*f* orbitals as one traverses the period. However, the behavior of 5*f* electrons is quite different from that of electrons in 4*f* orbitals. Early in the actinide series the 5*f* electrons are chemically accessible and a multitude of oxidation states are possible. However, starting at americium this behavior disappears and the 5*f* electrons appear to much more localized than found earlier in the series. The situation becomes even more complex starting at californium where electronic bistability occurs, and it appears that the Seaborg concept starts to fail. The departure from conventional understanding becomes even more pronounced in the heaviest actinides. We will use standard reduction potentials in this lecture as indicators of fundamental changes in actinide chemistry. However, reduction potentials are merely manifestations of underlying electronic structure, and we will also seek out the origin of the electronic breaks that occur at plutonium and californium. We will conclude by deciding if it is time to rearrange the periodic table.

B-02

Quantum chemistry and spectroscopic studies of actinide ions with oxygen- and nitrogen- donor ligands in solution

Dominique Guillaumont, Eleonor Acher, Thomas Dumas, Matthieu Audras, Laurence Berthon, Olivia Pecheur

CEA, Bagnols sur Cèze, France

Introduction

Understanding the structure and bonding in actinide ions in solution can provide fundamental information which is essential to predict their behavior and to develop effective solvent extraction separations for waste remediation in advanced nuclear fuel cycles. In complex actinide systems, such information is often lacking because of the difficulty to obtain it solely from experimental data. Quantum chemistry calculations, once associated with experimental data, can be an important tool to obtain structural information and to probe the nature of the metal-ligand bonds.

To achieve the separation of similarly sized ions such as actinide(III) and lanthanide(III), ligands are selected that could enhance covalency in actinide-ligand bonds. Most selective ligands incorporate “soft-donor” sulfur or nitrogen atoms. The detailed knowledge of metal-ligand bonds in these systems is essential to understand and predict ligands selectivity. In the present work we have investigated actinides(III) and lanthanides(III) with a polyaminocarboxylate ligand that form stronger complexes with Am(III) and Pu(III) than with Ln(III). Theoretical calculations were carried out in order to determine to which extent actinides(III) can create more covalent bonds than lanthanides(III) toward this ligand.

To achieve the separation of ions of different ionic radius, “hard-donor” ligands with oxygen atoms are most often used. The knowledge of coordination structures of actinide ions in organic solution with such ligands is the key to understand selectivity. In this work, we have investigated uranium(VI) and plutonium(IV) coordination structures with mono- and bi-functional ligands. It’s only by coupling vibrational and X-ray absorption spectroscopies with quantum chemistry calculations that we were able to elucidate the structures of the actinide complexes in organic solution.

Results

Actinides(III) with O-and N-donor ligands

We studied complexes of trivalent actinides and lanthanides in the presence of a DOTA macrocycle ligand (1,4,7,10-tetraazacyclododecane-tetraacetic acid, Figure 1). DOTA is a polyaminocarboxylate ligand which is a powerful chelating agent with lanthanides(III). Complexes of lanthanides with DOTA have been the subject of many studies over the past years.[1] In contrast, very few studies have been dedicated to actinide complexes.[2] From experimental measurements, we showed that DOTA form slightly stronger complexes with Am(III), and Pu(III) than with Ln(III) and that metal-nitrogen bonds are slightly shorter for actinides than for lanthanides. Quantum chemistry investigations were carried out to establish bonding differences between 4f and 5f elements. Metal-ligand bonds were probed through a topological analysis of the electronic density. The results show that in solution, metal-nitrogen bonds are slightly more covalent for actinides than lanthanides. The role played by solvation effects was analyzed by comparing gas phase and solution calculations. The results indicates that the metal-nitrogen distance shortening from Ln(III) to Am(III) and Pu(III) is only present in solution and disappears in the gas phase.

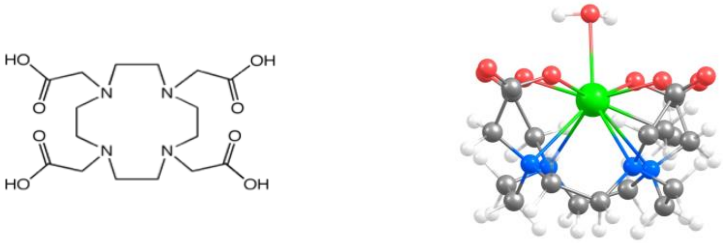

Fig. 1. Left: Structure of DOTA ligand (1,4,7,10-tetraazacyclododecane-tetraacetic acid). Right: Schematic representation of Am(III)-DOTA complex

Uranium(VI) and Plutonium(IV) with O-donor ligands

The coordination structures of uranium(VI) and plutonium(IV) complexes were investigated with O-donor ligands depicted in Figure 2. [3,4] Monofunctional amide ligands and a bifunctional amido-phosphonic acid ligand were investigated. Vibrational IR spectroscopy and EXAFS were employed to probe the molecular environment of uranium(IV) and plutonium(IV) cations. Theoretical chemistry calculations were used to construct and optimize molecular structures corresponding to metal-ion complexes that may form in the organic solution. EXAFS and IR were simulated for the optimized structures. By comparing the simulated spectra with experimental spectra, we were able to deduce the coordination environments of actinide (IV) and (VI) ions.

Fig. 2. Structures of mono- (left) and bi-functional ligands (right).

Fig. 2. Left: Structures of mono- (left) and bi-functional ligands (right).

References

[1] W. P. Cacheris, S. K. Nickle, A. D. Sherry, Inorg. Chem., 26, 958 (1987).

[2] M. Audras, L. berthon, N. Martin, N. Zorz, Ph. Moisy, J. of Radioanal. Nucl. Chem. 303, 1897 (2015).
[3] O. Pecheur, D. Guillaumont, S. Dourdain, L. Berthon, R. Turgis, C. Fillaux, G. Arrachart, F. Testard, Solv. Extr. Ion Exch. http://dx.doi.org/10.1080/07366299.2016.1169146 (2016).
[4] E. Acher, Y. Hacene Cherkakis, T. Dumas, C. Tamain, D. Guillaumont, N. Boubals, G. Javierre, Ch. Hennig, P. Lorenzo, M. C. Charbonnel, Inorg. Chem. http://dx.doi.org/10.1021/acs.inorgchem.6b00592 (2016).

B-03

Thiocyanate complexes of the tri- and tetravalent actinides

Richard Wilson, Tyler Carter

Argonne National Laboratory, Argonne, Illinois, USA

Introduction

It was first hypothesized that the f-electrons play a larger role in directing the chemistry of the actinide elements versus the lanthanide elements in an experiment investigating the elution behaviour of trivalent actinides and lanthanides from an ion-exchange column.[1] The disparate separations behaviour of the actinides relative to the lanthanide elements suggested that differences in the electronic properties of these elements, not their size, was responsible for the unpredicted separations behavior, and could be exploited to selectively separate trivalent lanthanides from actinides. Originally, the presence of thiocyanate (NCS^-) an ambidentate ligand, in trivalent actinide-lanthanide systems was shown to enhance the separation of trivalent actinides over lanthanides and while numerous hypotheses have been posed to including differences in the coordinating atoms (N –vs- S), inner- versus outer-sphere coordination, and increased orbital overlap or covalence.[2-4] Indeed, the origin of the enhanced separation may not even be coordination based, as recent results have demonstrated that enhancements in selectivity in such systems are sometimes dependent on secondary chemical interactions between complexes, extractants, and solvents.[5]

Despite numerous molecules being synthesized as ligands and extractants that demonstrate the separation of trivalent lanthanides from actinides such as soft-donor type molecules as the thiol (S) based- Cyanex extractants, and the N-donor based class of functionalized terpyridine ligands, e.g. BTBP, the chemical differences between the chemical behaviour of the trivalent actinides and lanthanides remains unresolved, particularly as it relates to the chemical interactions between metal and ligand. To this end, we have synthesized a series of actinide and lanthanide thiocyanates to study the interactions between these metals and the thiocyanate anion.

Results

Synthesis of actinide and lanthanide thiocyanate complexes in the presence of a large excess of thiocyanate has demonstrated that a variety of structure types, coordination numbers, and geometries exist depending on the reaction conditions, solvent, and counter cations present. Some examples of the molecular species observed are presented in Figure 1.

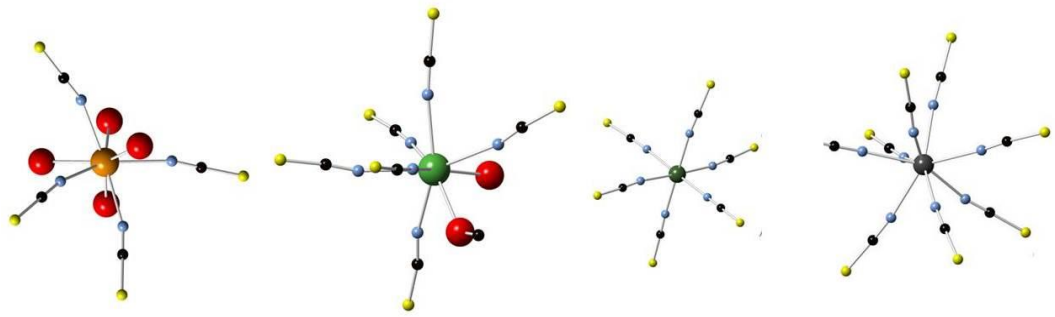

Figure 1: Multiple coordination numbers and polyhedra of lanthanide and actinide thiocyanate complexes, (left to right) $M(NCS)_4(H_2O)_4^-$, $M(NCS)_5(H_2O)_2^{2-}$, $M(NCS)_6^{3-}$, $M(NCS)_7^{4-}$.

Initial studies into the thiocyanate complexes of plutonium, an actinide with stable tri- and tetravalent oxidation states revealed a complex redox behaviour in acidic aqueous media.[6] Initial attempts to isolate a tetravalent plutonium thiocyanate complex resulted in the reduction of the plutonium solution to a characteristically blue Pu(III) solution, consistent with the known redox potentials for both Pu and SCN^-. However, upon concentration deep red crystals, determined by X-ray diffraction to be $[Et_4N]_4Pu(SCN)_8$ were deposited, Figure 2. Significantly, in this complex, and all of the lanthanide and actinide complexes studied, the thiocyanate binds exclusively through the nitrogen, and not the sulfur. Comparison of this structure, with the Th complex synthesized by us, and subsequent spectroscopic characterization demonstrated the unambiguous tetravalent oxidation state of the plutonium ion.

Additional synthesis campaigns with the lanthanides, and Am(III) have revealed an isostructural series of trivalent thiocyanate complexes of the formula, $[Et_4N]_4$ $M(SCN)_7(H_2O)$. These complexes are nearly isostructural with the tetravalent complexes synthesized for Th, U, and Pu, except that the seven thiocyanate ligands and a water molecule are disordered over the eight sites of cubic coordination as shown in Figure 2.

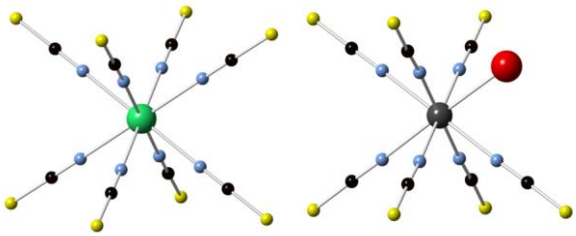

Figure 2. Tetravalent actinide thiocyanate complexes, left, highlighting the cubic eight coordinate system in $M(NCS)_8^{4-}$. Metal in green, nitrogen in blue, carbon in black, and sulphur in yellow. Right, trivalent thiocyanate complexes, $M(NCS)_7(H_2O)^{4-}$.

The single crystal complexes synthesized provide convenient model systems to study the nature of the actinide and lanthanide thiocyanate interaction. We have studied the tetravalent complexes using UV-Vis spectroscopy observing a ligand-to-metal charge transfer band in both the U(IV) and Pu(IV) complexes, but this transition is not present in the trivalent lanthanide or actinide systems. As an alternative to UV-Vis absorption spectroscopy, we have used Raman spectroscopy as a probe of the CN vibrational frequencies of the metal bound thiocyanate groups. In the case of electron donation to or from the thiocyanate molecule, or in the case of a truly covalent interaction, the CN vibrational frequency would be perturbed, an indicator of bond stiffening or weakening. We measured the Raman spectra of all of the complexes synthesized, and those data are presented in Figure 3. These data reveal that the thiocyanate vibrational frequencies are unperturbed by the identity of the metal ion, either 4f or 5f, suggesting that the interaction is principally electrostatic in nature among both the actinide- and lanthanide-thiocyanate complexes.

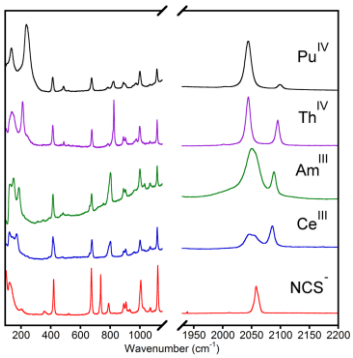

Figure 3: Raman spectra of crystalline lanthanide and actinide thiocyanate complexes highlighting the invariant nature of the CN stretching frequency. Raman spectra of both trivalent and tetravalent metals are shown for comparison.

Summary

This investigation of the actinide and lanthanide thiocyanates, using a combined structural and spectroscopic approach suggests that the principal chemical interaction between the metal and the ligand is electrostatic. Raman spectroscopy of a series of isostructural complexes of the lanthanides and actinides does not reveal a perturbation to the CN vibrational frequency such as might be expected in the case of significant electron donation to the actinide or lanthanide metal center. The sensitivity of the resulting lanthanide and actinide thiocyanate complex to the starting reaction conditions, metal:ligand ratio, solvent polarity, and even counter cation identity, underscores the weak thermodynamic interaction between thiocyanate and the trivalent f-elements.

Acknowledgement

This work was performed at Argonne National Laboratory, operated by UChicagoArgonne LLC for the United States Department of Energy under Contract DE-AC02-06CH11357, and was supported by a DOE Office of Basic Energy Sciences, Chemical Sciences, the Heavy Elements Program.

References

1. Diamond, R. M.; Street, K.; Seaborg, G. T., An Ion-exchange Study of Possible Hybridized 5f Bonding in the Actinides1. *J. Am. Chem. Soc.* **1954,** *76* (6), 1461-1469.

2. Chiarizia, R.; Danesi, P. R.; Scibona, G.; Magon, L., Liquid anion exchange of thiocyanate-nitrate actinide and lanthanide complexes. *J. Inorg. Nucl. Chem.* **1973,** *35* (10), 3595-3604.

3. Moore, F. L., New Approach to Separation of Trivalent Actinide Elements from Lanthanide Elements. Selective Liquid-Liquid Extraction with Tricaprylmethylammonium Thiocyanate. *Anal. Chem.* **1964,** *36* (11), 2158-2162.

4. Choppin, G. R.; Ketels, J., Thiocyanate complexes of some trivalent lanthanide and actinide elements. *J. Inorg. Nucl. Chem.* **1965,** *27* (6), 1335-1339.

5. Ellis, R. J.; Meridiano, Y.; Muller, J.; Berthon, L.; Guilbaud, P.; Zorz, N.; Antonio, M. R.; Demars, T.; Zemb, T., Complexation-Induced Supramolecular Assembly Drives Metal-Ion Extraction. *Chemistry – A European Journal* **2014,** *20* (40), 12796-12807.

6. Carter, T. J.; Wilson, R., The coordination chemistry of homoleptic An(IV) thiocyanates. In *Chem. Eur. Jour.*, Argonne National Laboratory: 2015.

B-04

Quality control tools for the analysis of plutonium in nuclear safeguards, security and safety

Yetunde Aregbe, Rozle Jakopic, Stephan Richter, Goedele Sibbens

EC-JRC-IRMM, GEEL, BELGIUM

Plutonium with its beneficial and fearsome characteristics in the nuclear fuel cycle and in weapons programmes has always been in the focus of research, science, industry and the military. Nowadays, with the long term impact of climate change at the one hand and the increasing energy demand at the other hand, the safe, secure and peaceful use of this extraordinary element is more than ever at the heart of public opinion. According to the Nuclear Energy Agency (NEA), nuclear power is the second-largest source of low-carbon electricity generation worldwide, after hydropower[i]. The framework of nuclear energy in the geopolitical context is diverse and is evolving. The role of nuclear power in some European Union countries is declining whereas some leading actors in other continents are increasingly building on nuclear power [i]. Accountancy and control of nuclear material require analytical measurements that "shall either conform to the latest international standards or be equivalent in quality to such standards" IAEA INFCIRC/153 [ii]. Quality assurance (QA) and quality control (QC) are means to the end of complying with this requirement to provide reliable measurement results and establish confidence in analytical measurement results for the nuclear safeguards and security system. In the European Union Nuclear Safeguards has the rank of European law [iii]. Nuclear reference materials (CRMs) and measurements are tools for enforcement and monitoring of EU legislation, and crucial for conformity assessment with criteria laid down in respective documentary standards supporting the international initiative on a holistic safety, security and safeguards ('3S') concept for nuclear energy [iv]. The JRC being a world-wide renown and accredited provider of metrological quality control tools, such as nuclear certified reference materials (CRMs), nuclear reference measurements, inter-laboratory comparisons (ILCs) and high-quality nuclear targets is fulfilling its obligation under the EURATOM Treaty.

Measurement results have to be traceable to a common reference, namely the respective SI unit, in order to be comparable. To this end, metrological quality control tools are indispensable. They comprise different aspects:

- Method validation and instrument calibration
- Traceability and comparability of measurement results
- Uncertainty of measurement results
- External performance evaluation
- Document/data control and deployment of a quality system

ISO/IEC 17025:2005 on the competence of testing and calibration laboratories has gained due to its wide applicability over the years more and more relevance within the nuclear laboratory community[v]. There are several ISO Guides specifically for the analysis of plutonium with various techniques [vi] and a number of American Society for Testing and Materials (ASTM) consensus standards for the separation, dissolution and analysis of plutonium materials [vii, viii]. Applying one of these reference methods for the analysis of plutonium is not a guarantee to provide a reliable **fit-for-purpose** measurement result. Indispensable to achieve measurement accuracy is the proper application of quality control (QC) and conformity assessment tools.

Nuclear Safeguards

In safeguards this translates that laboratories, particularly the EURATOM on-site laboratories, have to demonstrate that they are meeting the International Target Values (ITVs-2010) for Measurement Uncertainties in Safeguarding Nuclear Materials for Pu analysis [ix, x]. They are uncertainties to be considered in judging the reliability of the measurement results of analytical techniques applied to industrial nuclear and fissile material, which are subject to safeguards verification. Mass spectrometry is one key analytical technique applied by laboratories for plutonium analysis. In Isotope Dilution Mass Spectrometry a known amount of an isotopic certified plutonium reference material (spike CRM) is needed as a calibrant to be gravimetrically blended with the plutonium sample before analysis by mass spectrometric techniques. Large-Sized Dried (LSD) Spikes are used by facility operators and safeguards authorities for accountancy and verification measurements of the uranium and plutonium amount and isotope contents in the reprocessing input solution applying IDMS as shown in Figure 12 and Figure 13 [xi, xii]. This is the highly radioactive solution of dissolved spent fuel, which is stored in input accountancy tanks, and also contains fission products and some activation products [x].

Figure 12 IRMM-1027 Large-Sized Dried spike

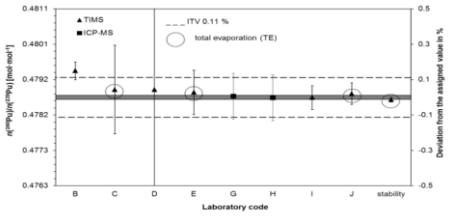

Figure 13 The participant results of the $n(^{240}Pu)/n(^{239}Pu)$ amount ratio in REIMEP-17B with measurement uncertainties (error bars) as reported by the participants (all results and the stability value were reported with expanded uncertainty, k = 2). The grey band represents the assigned value with the expanded uncertainty (k = 2). The dashed line represents the respective ITV-2010 value. The dashed circles indicate the laboratories using total evaporation, a technique strongly recommended for measuring isotope ratios

Nuclear Security

In the 2016 Nuclear Security Summit: Certified Reference Material Fact Sheet it is stated '*To be effective, nuclear forensic analyses must yield accurate and precise results that can withstand scrutiny in a court of law and from the international community. Well-constrained, consistent, and uniform Certified Reference Materials (CRMs) are indispensable for producing high quality analytical results and provide the primary means of demonstrating the accuracy of nuclear forensic measurements'* [xiii]. Americium is a transuranium element, produced by neutron capture in nuclear reactions and from □-decay of ^{241}Pu. To determine the elapsed time since the last chemical purification of plutonium is of relevance in nuclear safeguards and nuclear forensics. IDMS can be applied to measure the $n(^{241}Pu)/n(^{241}Am)$ radio-chronometer, (^{241}Pu, $t_{1/2}$ = 14.325 ± 0.024 a) using a ^{243}Am spike CRM [xiv]. Therefore the JRC and the Commission for the Establishment of Analytical Methods (CEA/CETAMA) that resides within the French Atomic Energy and Alternative Energies Commission are currently jointly preparing a ^{243}Am CRM, see Figure 14.

Figure 14 IRMM-0243 – ^{243}Am certified reference material

Nuclear Safety

Databases of neutron-induced reaction cross sections are maintained by the Nuclear Energy Agency (NEA) of the Organisation for Economic Co-operation and Development (OECD). High quality measurements of neutron cross-sections of the relevant nuclei and materials are being requested in this context of nuclear safety, minimization of high level nuclear waste and safeguards and security. Thin film deposits (called targets) are tailor-made for nuclear physics measurements at the JRC and international accelerator sites. These targets have to be produced by the best available techniques and characterised by state-of-the-art methods [xv]. One indispensable step for the characterisation of plutonium targets is to determine the isotopic mass fractions of the base material by thermal ionisation mass spectrometry (TIMS). By measuring the total alpha activity of the prepared plutonium target with low-geometry alpha-particle counting (LGA) and knowing the respective alpha activity fractions derived from mass spectrometry, the alpha activity for each isotope in the plutonium target can be calculated, and the mass and areal density of the deposited plutonium accurately determined. The quality of the prepared and characterised plutonium targets sets the lower limit of uncertainty that may be achieved in nuclear data measurements. In Figure 15 a ^{242}Pu target prepared by the so-called “molecular plating” on an Al backing for cross-section measurements is shown. This target was prepared for measurements of the ^{242}Pu(*n*,*f*) cross sections [xvi, xvii, xviii].

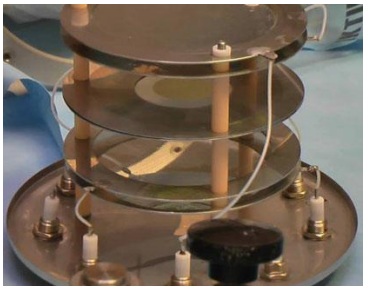

Figure 15 Gridded ionisation chamber with a ^{242}Pu target in the centre as cathode for measurements of ^{242}Pu(n,f) cross sections versus ^{238}U(n,f) at IRMM [xvi]

Summary

Mass spectrometric techniques are applied for accurate measurements of plutonium samples in the fields of nuclear safeguards, nuclear security and nuclear safety[xix]. Laboratories are required to comply with stringent quality requirements for the analysis of plutonium. Metrological tools for mass spectrometric method validation and conformity assessment such as CRMs, the ITVs and the organisation of ILCs are available to the analytical community and are continuously further improved and developed. More recently, reference materials for method validation in age-dating of plutonium materials are also required [xx, xxi]. Neutron data are needed when evaluating the safety and risks related to operation of nuclear power plants, nuclear waste management, or new concepts of nuclear power production. The production of high-quality plutonium targets for experiments to study neutron interaction with matter is a quite special and important field of application. Particularly neutron data on plutonium cross sections are required for Nuclear Resonance Densitometry (NRD), a promising method to accurately quantify the amount of uranium and plutonium in complex materials such as debris of melted nuclear fuel from the damaged Fukushima Daiichi reactor cores [xxii].

B-05

Impurity effects in plutonium alloys

Sue Ennaceur, Paul Roussel

AWE, Aldermaston, Reading, Berkshire., UK

Plutonium is an extremely reactive metal and given the right conditions will form compounds with the majority of the elements in the periodic table. Small concentrations of impurity elements can have dramatic effects in physical properties and the metallurgy of plutonium. For example, the body centred tetragonal □' phase was only discovered once plutonium metal of a suitable purity could be formed coupled with an appropriate technique (1); Small quantities of alloying elements such as aluminium and gallium are sufficient to stabilize the face centred cubic phase at room temperature (2). The impurity elements are typically included at the metal casting stage. These can be included in the original feedstock material or from reaction with environment (gaseous) or from the crucible material. Furthermore, additional impurity atoms are included into the matrix from the radioactive decay process. Knowledge of how these impurity elements/compounds affect the physical properties of plutonium metal and alloys will afford a greater understanding of this material.

Carbon is a ubiquitous impurity in plutonium metals and alloys. The bulk to surface segregation of carbon impurities in plutonium alloys has been reported (3). This process is likely to occur from interstitial dissolved carbon atoms. Plutonium and carbon can form the cubic sub-stoichiometric compound PuC_{1-x} and the sesquicarbide Pu_2C_3. However, the formation of plutonium carbide impurity inclusions in plutonium metal and alloys has not been widely reported. We report the metallographic characterisation of carbide inclusions in plutonium alloys and show the composition is rich in uranium. The affects of these inclusions on material hardness is also presented.

References

1. E. R. Jette, J. Chem. Phys., 23 (1955) 365.

2. S. S. Hecker, D. R. Harbur, T. G. Zocco, Prog. Mater. Sci., 49 (2004) 429.

3. P. Roussel, D. S. Shaw, D. A. Geeson, J. Nucl. Sci. Technol. Supplement 3 (2002) 78.

B-06

Structure of Plutonium(IV) with O-donor ligands from crystallography, extended X-ray absorption fine structure and theoretical calculations

Eleonor Acher, Thomas Dumas, Christelle Tamain, Dominique Guillaumont

CEA MARCOULE, Bagnols sur Cèze, France

Among the various properties that are important for a comprehensive understanding of selective extraction processes, the stoichiometries and coordination structures of actinide ions in the organic solution can provide crucial information regarding extraction mechanisms. In order to study the structure of complexes formed by the extraction of Pu(IV) with N,N-dialkylamides we have combined spectroscopic experiments and theoretical calculations. XRD, EXAFS (extended x-ray absorption fine spectroscopy) and UV-vis spectra together with quantum chemistry calculations have been performed.

N,N-dialkylamides are considered as potential substitutes of the Tributylphosphate (TBP) used in the PUREX process for U(VI)/Pu(IV) extraction and separation from the spent nuclear fuel. One interesting feature of this family of molecules is the strong influence of their alkyl groups on their extracting properties. This dependency is not well rationalized yet and this would be of great interest in order to improve the tuning of the Pu/U extraction and separation by these amides. As a starting point the two amides DEHBA and DEHiBA are studied (shown below). They have been widely investigated and exhibit an interesting extraction behavior for our issue: the extraction of Pu(IV) is strongly decreased from DEHBA to DEHiBA whereas it is not the case for U(VI) for which only a small decrease is observed.

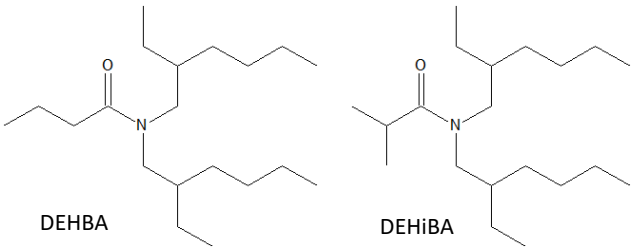

EXAFS analysis of the complex combined with XRD shows that the coordination of Pu(IV) with linear alkyl chain amides is identical in the solution and in the solid state. With branched alkyl chain amides the coordination structure was more difficult to establish unambiguously. DFT calculations were performed on a series of coordination structures. Structural parameters and Debye-Waller factors derived from the DFT calculations were used to compute EXAFS spectra without using fitting parameters. By using this methodology, it was possible to elucidate the structure and show that the branched alkyl chain amide forms partly outer-sphere complexes with protonated ligands bonded to nitrate ions.

B-07

Semiconductivity in Plutonium and Americium Chromates and Molybdates: The Smoking Gun for Energy-Degeneracy- Driven Covalency

Alexandra Arico[1], Alejandro Garza[2], Justin Cross[3], Thomas E. Albrecht-Schmitt[1]

[1]Florida State University, Tallahassee, FL, USA, [2]Rice University, Houston, TX, USA, [3]Los Alamos National Laboratory, Los Alamos, NM, USA

The need to discover unique bonding tendencies in the heavier actinides (Pu-Cf) grows more urgently every day, as this knowledge is necessary for separating these elements in spent nuclear fuel. The PUREX process and its derivatives have satisfied the need to separate uranium from plutonium by exploiting their rich redox chemistries.[1] This tactic is ineffectual for the trivalent actinides beyond uranium, hence, a new approach is imperative. In order to determine bonding tendencies in the heavier actinides, including plutonium, our group employs different ligand systems in synthesis that can potentially access the 5*f*-orbitals. It has been shown in multiple organic extractant studies that the actinides prefer "soft" donor atoms over the lanthanides by an appreciable factor.[2,3] However, there are synthetic challenges involved in preparing such coordination compounds with the actinides, so it would be worthwhile to investigate inorganic ligands that may produce similar preferences. Ligands with high hyperpolarizabilities are attractive in this regard due to their flexible electron cloud; it is important that the bonds of the ligand are strongly polarizable in order to induce a more covalent interaction with the actinide metal. Based on second-harmonic generation measurements as well as second hyperpolarizability calculations, the Group VI transition metal-oxygen bonds have significant bond polarization suitable for our investigation of inorganic actinide compounds.[4] The work presented here is based on a series of *f*-element extended structures synthesized with the chromate moiety (CrO_4^{2-}).

$CsPu_3Mo_6O_{24}(H_2O)$, $CsAm(CrO_4)_2$, and their lanthanide analogues have been prepared. The former actinide compounds are black or dark red semiconductors, whereas the latter are insulators. The trivalent americium compound deviates from the structural and spectroscopic trends observed across the 4*f* chromates; an anticipated result based on the hypothesis that a highly polarizable ligand will influence the bonding with an actinide to be more covalent than with a lanthanide, which predominantly participates electrostatically. The lanthanide chromate series crystallize in three different monoclinic space groups which are related to the ionic radii of the metal centers. Although the ionic radius of 8-coordinate trivalent americium is very similar to that of neodymium (1.108 Å and 1.109 Å, respectively), they do not have the same space group. Instead of crystallizing in the *P*2/*c* space group that $CsNd(CrO_4)_2$ does, the americium compound, $CsAm(CrO_4)_2$, is in the triclinic space group *P*-1. Similar to the Nd analogue, the Am compound adopts a layered topology (Figure 1). The coordination environment of the bi-capped trigonal prism Am center is made up of eight oxygen atoms donated from two chromate tetrahedra. The chromate tetrahedra corner-share with the americium polyhedra to form 2D chains that extend in the *a*-*b* plane, with Cs^+ cations charge-balancing in the interlayer channels.

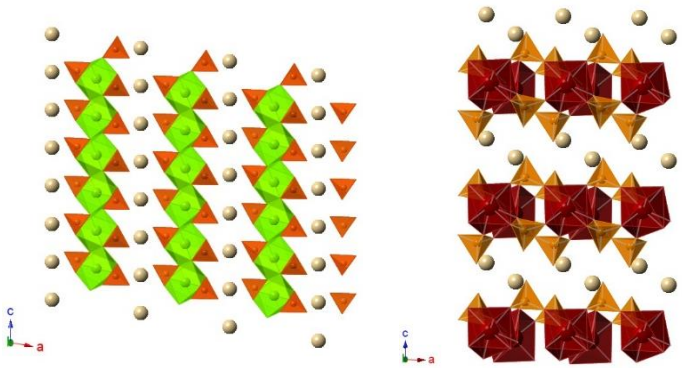

Fig 1. Views along the b-axes of $CsNd(CrO_4)_2$ (left) and $CsAm(CrO_4)_2$ (right)

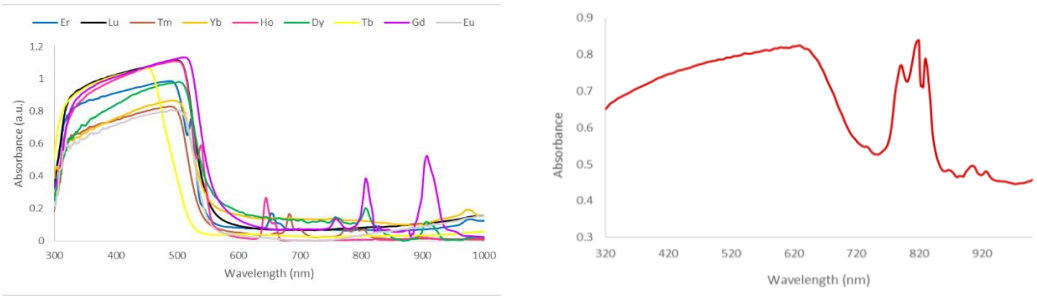

Fig 2. UV-Vis-NIR absorbance of late lanthanide chromates, Eu-Lu (left). UV-Vis-NIR absorbance of $CsAm(CrO_4)_2$ (right).

One of the most striking differences between the 4*f* and 5*f* analogues is the switch from an insulating compound (4*f* elements) to a semiconducting one (Am). This is, of course, accompanied by a dramatic change in color from golds/oranges to a blood red so dark, it appears black to the naked eye. For each of the lanthanide chromates, the absorption spectra have ligand-to-metal charge transfer (LMCT) bands that span the wavelength range of ~300-550 nm, which would explain their gold-orange color (shown in Figure 2). An extrapolation of this data to give the optical energy shows bandgaps in the range of 2.5-2.7 eV for these insulating lanthanide chromates. The americium compound, however, exhibits a very broad LMCT band that extends from 300 nm to ~740 nm. This compound has a band gap of 1.64 eV (Figure 3), evidence of its semiconducting nature. Band structure calculations of this compound give further information on how the 5*f* and 6*d* electrons are participating in bonding with the chromate ligand.

Band-structure calculations show clear degeneracy of the 5*f* orbitals with the 2*p* orbitals of oxygen for plutonium and americium. This degeneracy is absent in the lanthanide analogues.

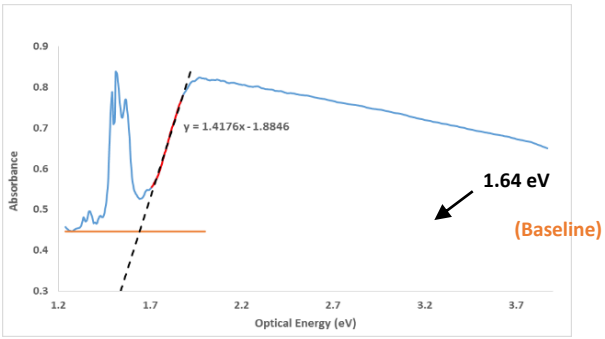

Fig 3. Absorbance vs. Optical Energy of $CsAm(CrO_4)_2$ with a band gap of 1.64 eV.

References:

[1] J.E. Birkett, M.J. Carrott, O.J. Fox, C.J. Jones, C.J. Maher, C.V. Roube, R.J. Taylor, D.A. Woodhead, "Recent developments in the PUREX process for nuclear fuel reprocessing: complexant based stripping for uranium–plutonium separation," *Chimia,* **59**, 898 (2005).

[2] H.H. Dam, D.N. Renhoudt, W. Verboom, "Multicoordinate ligands for actinide/lanthanide separations," *Chem. Soc. Rev.,* **36**, 367 (2007).

[3] M.L. Neidig, D.L. Clark, R.L. Martin, "Covalency in *f*-elements," *Coord. Chem. Rev*., **257**, 394 (2013).

[4] F. Li, X. Hu, R. Sa, L. Niu, "Molecular orbital closed loops analysis of the third-order NLO response of polyanion $[M_8O_{26}]^{4-}$ (M = Cr, Mo, W): a TDDFT study," *Struct. Chem.,* **25**, 539 (2014).

B-08

Evaluation of Covalency in PuF_4 by ^{19}F NMR Spectroscopy

Herman Cho[1], Cigdem Capan[2], Richard Dempsey[2], Sergey Sinkov[1], Bruce McNamara[1]

[1]Pacific Northwest National Laboratory, Richland, Washington, USA, [2]Washington State University, Richland, Washington, USA

We report ^{19}F NMR measurements of magnetic fields at the fluorine sites of PuF_4 aimed at elucidating the electronic structure of the Pu^{4+} centers and the degree of interaction of the valence electrons with F^-. The broadening and shift of the ^{19}F resonance scale linearly with the applied field, indicating that F atoms interact with their two nearest neighbor Pu^{4+} centers primarily through the dipolar fields of the four magnetized valence electrons. Little evidence of a field-independent contact hyperfine coupling is seen. The ^{19}F NMR spectra of PuF_4 are similar in shape and width to spectra of UF_4 obtained by Gabuda et al.[1] despite the former having nominally four valence electrons and the latter two.

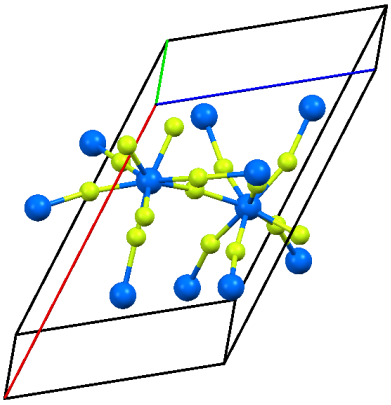

Figure 16: Monoclinic crystal structure of PuF_4 illustrating the coordination of Pu (blue) with eight fluorine atoms (yellow).

We present calculations of the ^{19}F NMR linebroadening and shifts, treating the valence electrons in PuF_4 and UF_4 as being in localized non-interacting atomic orbitals with thermally averaged polarizations. Analyses that assume purely localized $5f^4$ (for PuF_4) and $5f^2$ (for UF_4) electronic configurations for the metal centers systematically underestimate the magnitudes, shifts, and anisotropy of the hyperfine field, suggesting that the magnetic moments are larger than states with only 5f valence electrons. Larger moments may be obtained with mixed valence states such as $5f^46d^1$ for PuF_4, but the best agreement with experimental data is found with admixtures of states such as $5f^4$ and $5f^46d^1$.

The f-level occupancy in isostructural lanthanide[2] and actinide[3] tetrafluorides has previously been investigated by X-ray photoemission and X-ray absorption spectroscopy, and similar findings of mixtures of electronic states have been inferred. These combined results reveal that the Pu electronic configuration is unexpectedly complex, with non-trivial magnetic interactions present even in an insulating compound.

References

1. S. P. Gabuda, L. G. Falaleeva, and Y. V. Gagarinskii, *Physica Status Solidi (b)* **33**, 435 (1969).
2. G. Kaindl, G. K. Wertheim, G. Schmiester, and E. V. Sampathkumaran, Physical Review Letters 58, 606 (1987).
3. A. Y. Teterin, Y. A. Teterin, K. I. Maslakov, A. D. Panov, M. V. Ryzhkov, and L. Vukcevic, Physical Review B 74, 045101 (2006).

B-09

Insight Into Stabilization Mechanisms of the Delta Phase of Plutonium by Deltagen Elements

Boris Dorado, Jordan Bieder, Marc Torrent

CEA, Arpajon, France

The phase transformation of plutonium from the δ to the brittle α-phase can be avoided by alloying pure plutonium with so-called “deltagen” elements, such as gallium, aluminum, americium, etc. While the retaining effect is of course well known, the atomic-scale mechanisms that lead to the δ-phase stabilization have yet to be understood.

In this study, we perform first-principles DFT+*U* calculations in order to investigate the origin of the δ-phase stabilization at low temperature by deltagen elements. In particular, we use the density functional perturbation theory (DFPT) as a tool for calculating the vibrational properties (phonon spectra) of the δ-phase of plutonium containing point defects and alloying elements, which in turn yields information about the material mechanical stability. We show that the phonon spectrum of the δ-phase can display imaginary frequencies, therefore be mechanically unstable at low temperature. When we further condense the associated unstable phonon modes, a distorted fcc structure is found to be more stable than the ideal δ phase. Subsequently, when 3.12 at.% Ga is added in substitution of plutonium, all imaginary frequencies disappear so that the ideal cubic structure is retained. The resulting phonon density of states is then directly assessed against experimental measurements on Ga-stabilized samples. We finally compare the deltagen effect of gallium with that of other elements, such as americium, aluminum, uranium, and iron.

B-10

Density functional theory study on hydriding resistance and surface initial oxidation of plutonium nitride

Bo Sun, Haifeng Liu, Haifeng Song, Hui Zheng

Institute of Applied Physics and Computational Mathematics, Beijing, China

Introduction

Plutonium (Pu) is strategically vital for both energy production and nuclear explosives. However, the surface corrosion of reactive Pu metal might jeopardize its safety and utility when in storage and in use. During the long-term storage, the dioxide PuO_2 overlayer on Pu can be readily reduced to the sesquioxide α-Pu_2O_3 driven by the oxygen-lean conditions [1]. Since α-Pu_2O_3 cannot effectively resist the corrosive gases and is particularly porous to enable the permeation of H_2 molecules, the catastrophic Pu-hydriding reaction will take place soon after the α-Pu_2O_3 overlayer is exposed to hydrogen [2,3]. Relative to the complex Pu oxides, the phase-diagram of Pu-nitride seems to be quite simple with the single-component PuN[4], which is also the promising advanced fuel for future reactors. Thus, it is of high significance to study the environmental adaptability and surface reactions of PuN. However, because of the high radioactivity and toxicity of Pu, the hydriding resistance and the surface initial oxidation behaviors of PuN have not been thoroughly explored by experiments[4], which are calling especially for the atomic-level theoretical studies.

As a continuation of our researches on the surface science and corrosion mechanisms of Pu-metal, recently, we have carried out the first principles calculations and *ab initio* molecular dynamics (AIMD) simulations to explore the electronic structure properties, the stable surface phase, and surface interaction dynamics of PuN. Given the unstable and unreliable roles of Pu-oxide overlayers in preventing the Pu-hydriding, the hydriding resistance and the initial oxidation mechanism of PuN surfaces are the focuses of this talk.

Methodology

Due to the localization-delocalization crossover of Pu-5f electrons, the theoretical description of different Pu compounds remains a considerable challenge[5]. Pu oxides are strongly correlated insulators and can be reasonably described by DFT+*U* and hybrid DFT methods, while calculated to be metallic by pure DFT[6]. PuN is found to be metallic with the same features of 5f states at Fermi-level as the strongly correlated δ-Pu[7]. Both DFT+*U* and hybrid DFT methods are proven to be problematic, whereas pure DFT can give a satisfied description at least with respect to the 5f states nearby Fermi-level[8-10].

In order to investigate the surface reaction dynamics of PuN, the theoretical schemes first need to reasonably describe metallic PuN, and then guarantee the AIMD simulations of the surface interaction with molecules reliable and viable. Based on the overall comparison with the ground-state properties calculated by DFT+*U*, hybrid DFT and DFT+dynamical mean-field theory, we have carefully checked the validity of the spin-polarized DFT (PBE-functional) calculation, using the Vienna *ab initio* simulation program (VASP) [11].

The surface phases of crystal PuN stabilized by both temperatures and nitrogen partial pressures were searched out via *ab initio* thermodynamics method[12]. Then, the AIMD simulations of the interaction dynamics between stable PuN surfaces and molecular H_2 and O_2 were carried out based on the van der Waals density functional (vdW-DF) method[13].

Results and discussion

The spin-polarized PBE calculation can reasonably reproduce the crystal parameters and electronic structures of PuN. Especially, when the spin-orbit coupling effect is considered, the calculated total electronic density of state (DOS) in Figure 1 shows well agreement with the UV-photoelectron spectroscopy (UPS) spectra. The DFT+DMFT method may give further improved description of the quasi-particle peak at Fermi-level, however, it is too time-consuming using this method to do the AIMD simulations. The PDOS results in Figure 1 show that the highest occupied band (HOB) of PuN (with a range of -2 to 0 eV) is mainly the localized Pu-5f, which is similar to that of α-Pu_2O_3. The HOB of PuO_2 is mainly the hybridization of Pu-5f and O-2p states, indicating the stronger affinity of O and Pu than that of N and Pu. As a result, the standard Gibbs energies of formation are -2.84eV and -10.34eV for PuN and PuO_2, respectively[4].

PuN, PuO_2 and α-Pu_2O_3 crystallize in distinct crystal structures and are proven to have different cation-anion bonding properties via the Bader analysis[14], namely, the Pu-O bond is close to ionic while Pu-N is like polar covalent bond. According to the ionic radiuses, we can discuss the crystal compactness parameter (CCP), which is defined as a volume ratio between all the ionic individuals and the crystal matrix. For PuN, PuO_2 and α-Pu_2O_3, the CCPs are calculated respectively to be 0.68, 0.50 and 0.43, among which PuN is compact as δ-Pu (CCP = 0.74) and α-Pu_2O_3 is notably porous. And furthermore, the formation of point defects in PuN is found to be quite difficult.

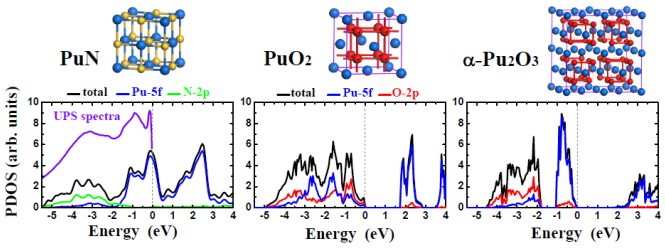

Fig. 1. The crystal structure and calculated projected density of state (PDOS) of PuN, PuO_2 and α-Pu_2O_3. The Fermi level is set to 0 eV. Pu, N and O atoms are denoted by blue, yellow and red spheres, respectively.

Based on the surface energy calculation, the polar stoichiometric PuN(111)-a surface in Figure 2 is found to be most unstable, but it can be stabilized by simply covering one monolayer (1ML) of N atoms on the outmost Pu-layer to be most stable PuN(111)-c surface. That makes an exception to the Tasker's general criteria[15] on the surface stability of an ionic crystal of the NaCl structure such as MgO, indicating that the bonding in PuN is more covalent in nature compared to the typical ionic MgO. When exposed to pure N_2 gas, the PuN(111) and (001) remain to be the stable surface phases under the N-rich and N-lean conditions, respectively.

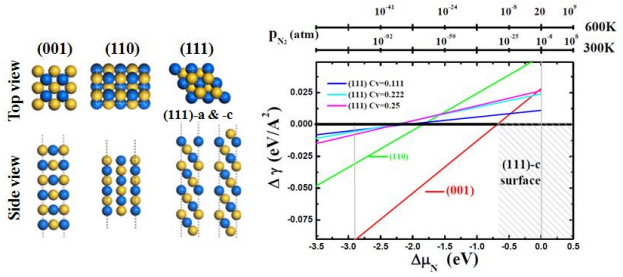

Fig. 2. Left: models of PuN(001), (110) and (111) surface. Right: surface energy difference as a function of N chemical potential, with (111)-c model as the reference.

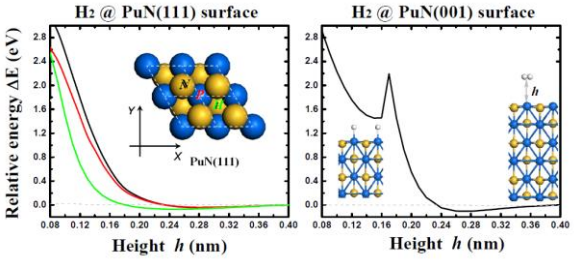

Fig. 3. The energy pathways of H_2 approaching PuN(111) along three channels and PuN(001) surfaces.

Figure 3 presents the interaction properties between H_2 molecule and PuN surfaces. Given the similar UPS spectra of PuN and δ-Pu, it is quite unexpected to find that PuN is really unreactive to molecular and atomic hydrogen, and acts as a diffusion barrier to significantly hinder the permeation of hydrogen. Especially, unlike the exothermic adsorption of atomic H on PuO_2(111) surface, the dissociative adsorption of H_2 on PuN surfaces is proven to be endothermic. One underlying main mechanism is that the trivalent Pu-cation in PuN cannot be further reduced by H atoms, which is also be proven in α-Pu_2O_3. Thus, the compact PuN seems clearly superior in the hydriding resistance to Pu-oxides.

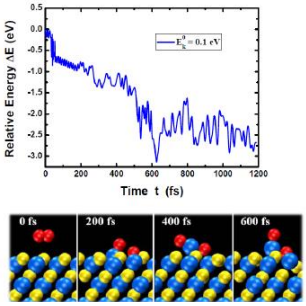

Fig. 4. The NVE-AIMD simulation of the dissociation behavior of O_2 molecule on PuN(111) surface.

However, due to its metallic nature, the clean PuN surface can be readily oxidized. As shown in Figure 4, one O_2 molecule with the initial kinetic energy of 0.1eV will dissociate spontaneously on PuN(111) surface, and interestingly driven by the strong affinity of Pu and O atoms, the heavy Pu cation will segregate out of PuN surface to bond with O. The subsequently dissociated O_2 molecules can uniformly cover PuN surface, which is named the 1ML-O@PuN structure. As a result, 1ML Pu cations will be pulled out of PuN and the residual N anions on subsurface form the N-rich layer, namely, the interlayer of 2ML-N shown in Figure 5.

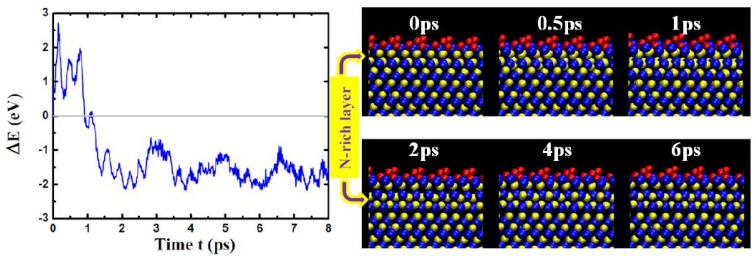

Fig. 5. NVT-AIMD (T=300K) simulation of the adsorption behavior of O_2 on 1ML-O@PuN(111) surface.

The formation process of 1ML-O@PuN is very quick on a timescale (of picoseconds) available to the AIMD simulation. But the further oxidation, for example, the dissociation of O_2 on 1ML-O@PuN(111) surface, will notably slow down since the N-rich layer can help to block the inward

migration of topmost O and the outward segregation of deep Pu. If raising the temperature or the O-adatom coverage on 1ML-O@PuN(111), the N-rich layer will migrate layer-by-layer into the deep layers of PuN as shown in Figure 5. Even when the N-rich layer is buried deeply, the O_2 on 1ML-O@PuN(111) surface still remains at the chemisorption state.

Conclusions and perspective

In summary, our theoretical studies have revealed that the single-component PuN is found to be structurally compact and chemically unreactive to prevent the hydrogen permeation, which makes PuN a potential passivation layer against Pu-hydriding. However, it is also revealed that PuN can be readily oxidized due to the strong affinity of Pu and O atoms. During the initial oxidation, Pu will segregate out of PuN surface to bond with O, forming an ultrathin uniform Pu-oxide film. The residual N atoms will migrate into the deep layers of PuN driven by high temperatures and O-adatom coverages, which can postpone the consequent oxidation of PuN. We expect our current study can inspire experimental interests in exploring the environmental adaptability of PuN and its application in surface passivation of Pu.

References

1. J. M. Haschke, Los Alamos Science **26**, 253 (2000).
2. L. N. Dinh, *et al.*, J. Nucl. Mater. **408**, 171 (2011).
3. G. W. McGillivray, *et al.*, J. Nucl. Mater. **412**, 35 (2011).
4. D. L. Clark, *et al.*, Chaper 7 in The Chemistry of the Actinide and Transactinide Elements, 4th Edition (Volumes 1–6), Springer (2011).
5. K. T. Moore and G. van der Laan, Rev. Mod. Phys. **81**, 235 (2009).
6. X.-D.Wen *et al.*, Chem. Rev. **113**, 1063 (2013).
7. L. Havela, *et al.*, Phys. Rev. B **68**, 085101 (2003).
8. R. Atta-Fynn, *et al.*, Phys. Rev. B **76**, 115101 (2007).
9. L. Petit, *et al.*, Phys. Rev. B **80**, 045124 (2009).
10. X.-D.Wen, *et al.*, J. Phys. Chem. C **117**, 13122 (2013).
11. G. Kresse, *et al.*, Phys. Rev. B **54**, 11169 (1996).
12. K. Reuter, *et al.*, Phys. Rev. B **65**, 035406 (2001).
13. J. Klimeš, *et al.*, Phys. Rev. B **83**, 195131 (2011).
14. R. F. W. Bader, *Atoms in Molecules: A Quantum Theory*. Oxford University Press, New York, (1990).
15. P.W. Tasker, Solid State Phys. **12**, 4977 (1979).

B-11

Understanding the Oxide Layer on Plutonium under Ambient Conditions

Alison Pugmire, David Pugmire, David Moore, Thomas Venhaus

Los Alamos National Laboratory, Los Alamos, NM, USA

The oxidation and corrosion of plutonium continues to be an area of active research, despite over a half of a century of work in this field. Plutonium's high reactivity and chemical complexity has resulted in varied, and often times, perplexing results. For instance, early studies showed that plutonium's oxidation/corrosion process is slow (0.02nm/hr) in dry air for both alpha-phase (α-Pu) and delta-phase plutonium (δ-Pu), but is faster for *α-Pu* (vs. δ-Pu) in humid air (O_2 + H_2O) and faster for *δ-Pu* (vs. α-Pu) in an O_2-free, wet environment (H_2O).[1, 2] In addition to the corrosion rate, questions surrounding the oxide layer composition initially formed in ambient pressures and temperatures have arisen over recent years. Traditionally, the oxide layer has been thought to consist of crystalline plutonium dioxide (PuO_2). Recent studies by our group using x-ray photoelectron spectroscopy (XPS), x-ray absorption fine structure (XAFS), x-ray diffraction (XRD) and spectroscopic ellipsometry (SE), have suggested the initial oxide is amorphous and most likely varies in composition, from PuO_{2-x} (x~1) at the metal-oxide interface to PuO_2 at the very surface (~the top 5 nm).[3-5] Despite the enormous challenges studying plutonium, our understanding of the surface chemistry, metallurgy, oxidation and corrosion, continues to evolve, particularly as more techniques are utilized in studying this complex material.

Plutonium readily oxidizes in atmospheric conditions and quickly forms an oxide layer tens of nanometers thick with a noticeable golden hue. As the metal continues to oxidize over time, it develops a blue-silver color (80-100 nm thick oxide) that turns to a dark blue-purple hue (>100 nm thick oxide) [3, 4, 6]. While the previous XPS and XAFS data provided valuable structural insight, these techniques are only sensitive to either the surface (the top 5 nm using XPS) or the bulk (~ 2.5 μm using XAFS). Previous measurements using SE indicated this technique was ideal because it measures the bulk material while being highly sensitive to subtle changes in the surface.[7] Additionally, SE is an in-situ technique, acquiring valuable, real-time, oxide growth information. Here, we present the results of SE investigations on plutonium metal samples oxidized/corroded in various environments. An ultra-high vacuum chamber (UHV) equipped with a gas manifold and temperature stage was used to control the rate of oxide growth and the environmental conditions (e.g. O_2, H_2O, air, temperature, etc.) An argon ion gun was used to sputter the oxide and study the bare metal. These results will be discussed and compared to previous SE work conducted in laboratory air, as well as information acquired from other techniques (e.g. Auger, XPS, XAFS). This work continues to develop our understanding of the oxide layer by presenting studies from several techniques that probe both the surface and the bulk material.

References

1. J. B. Raynor, J. F. Sackman, "Some Observations on the Oxidation of Unalloyed and d-Stabilized Plutonium Metal," *Plutonium 1965: Proceedings of the 3rd International Congress on Plutonium*, Institute of Metals, (1965).
2. J. M. Haschke, T. H. Allen, L. A. Morales, "Surface and Corrosion Chemistry of Plutonium," *Los Alamos Science,* **26**, 252, (2000).
3. D. L. Pugmire, F. J. Freibert, J. P. Baiardo, "The Optical Properties of the Plutonium/Plutonium Oxide Thin Film System," *Actinide Research Quarterly,* 47, (2013).
4. A. L. Pugmire, D. L. Pugmire, T. J. Venhaus, C. H. Booth, "Structural Insights into the Oxide Formed During the Room Temperature Corrosion of Plutonium," *Pu Futures - The Science ; 2014-09-07 - 2014-09-12 ; Las Vegas, Nevada, United States*, Los Alamos National Laboratory, (2014).
5. D. L. Pugmire, H. G. Garcia Flores, A. L. Pugmire, D. P. Moore, "The Room Temperature Oxidation/Corrosion of delta-Pu: Historical Perspective vs. Modern Understanding,"

Plutonium Futures-The Science 2014 ; 2014-09-07 - 2014-09-12 ; Las Vegas, Nevada, United States, Los Alamos National Laboratory, (2014).
6. D. T. Larson, D. L. Cash, "Plutonium Oxide Thickness - Color Correlation," The Dow Chemical Company(1968).
7. D. L. Pugmire, H. G. G. Flores, "The Optical Properties of the Pu/Pu Oxide Thin Film System," *Plutonium Futures – The Science 2012*, University of Cambridge, UK, (2012).

B-12

Alpha Radiolysis of Nitric Acid Solutions with Plutonium

Laurent Venault[1], Guillaume Garaix[1], Amaury Costagliola[2], Philippe Moisy[1], Guillaume Blain[2], Johan Vandenborre[2], Massoud Fattahi-Vanani[2], Nicolas Vigier[3]

[1]CEA Marcoule, Bagnols sur Ceze, France, [2]Subatech EMN, Nantes, France, [3]AREVA NC, Paris La Défense, France

The industrial nuclear fuel reprocessing, especially the separation of uranium from plutonium, is based on some adjustment of the oxidation states of actinide ions in solution. The efficiency of the process requires controlling perfectly these changes in oxidation states. However, some radiolytic phenomena are going to induce the formation of oxidizing or reducing species towards actinide ions as a result of the radioactive decay of these elements. Then, radiolysis can impact the redox behavior of plutonium in solution and affect the separation of this latter from uranium. As actinides are mainly α emitters, it is necessary to well characterize the α-radiolytic phenomena in order to well understand and predict the redox behavior of plutonium in reprocessing.

The aim of this study is to better describe the redox behavior of plutonium in aqueous nitric acid solution due to alpha radiolysis, partly owing to its own radiative decay. In a first step, radiolytic formation of H_2O_2 and HNO_2, the major products in solution from nitric acid radiolytic decomposition [1, 2], have been quantified. In the second step, it appeared that the sole effects of α-radiolysis on the nitric acid media can't account for the redox behavior of plutonium but that specific chemical reactivity of plutonium should be considered too.

The accumulation of nitrous acid HNO_2 in nitric acid solutions of plutonium (+IV) is shown on figure 1 as a function of the deposited dose in solution for different concentration of nitric acid. It appears that in a first step when the dose is lower than about 1000 $J.L^{-1}$, the formation and accumulation of nitrous acid is very high but they slow down in a second step for higher doses. Moreover it can be demonstrated that the fast accumulation of nitrous acid is correlated to the formation of transient plutonium(+III) in solution as it can be seen from figure 2.

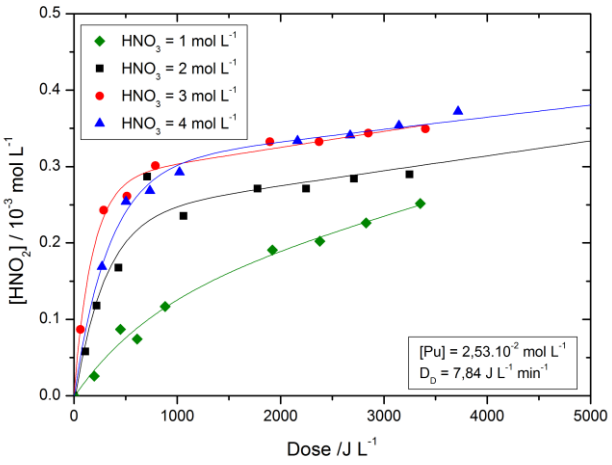

Fig. 1. Variation of HNO_2 concentration in solution under the effect of plutonium induced radiolysis in nitric acid solutions as a function of the deposited dose.

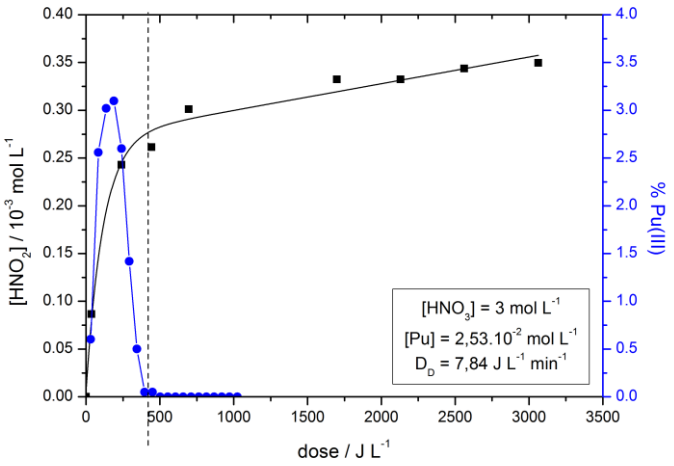

Fig. 2. Variation of HNO_2 concentration and Pu(III) ratio under the effect of plutonium induced radiolysis in à 3 M nitric acid solution as a function of the deposited dose.

However, it appears that the HNO_2 radiolytic yield in nitric acid solutions containing plutonium are lower than the ones obtained through the irradiations of nitric acid solutions using some helium ions beams [3]. On the opposite, these results are consistent with the HNO_2 radiolytic yields determined in experiment using ^{244}Cm or ^{210}Po in nitric acid solutions [4, 5].

These results seem to indicate that the oxidation-reduction reactions of plutonium ions are involved in the radiolytic formation and consumption mechanism of nitrous acid. In nitric acid solutions without plutonium the reaction between HNO_2 and H_2O_2 can account for the total or partial consumption of these species. In the presence of ^{244}Cm or ^{210}Po, neither H_2O_2 nor HNO_2 are involved in some oxidation or reduction reactions with these solutes. But, Pu(IV) can be reduced to Pu(III) by reaction with H_2O_2 whereas Pu(III) can be oxidized by reaction with HNO_2 leading to the formation of nitric oxide NO which can react with nitric acid to give back some HNO_2. Moreover, NO_3° radical is commonly quoted as a transient species to account for the radiolysis of nitric acid [6]. This radical can be considered as a potential oxidizing reactant towards Pu(IV) to produce Pu(V) which can disproportionate in Pu(IV) and Pu(VI). Then, Pu(VI) can be reduced by reacting with H_2O_2. Finally, it appears essential to take into account all the oxidation-reduction reactions of plutonium ions in nitric acid solution to well estimate the radiolytic yield of nitrous acid and compare it to the experimental data.

References

[1] M. V. Vladimiraova and al., *High Energ. Chem.*, **3** (1969) 477-478

[2] P. K. Bhattachary and al., *Int. J. Radiat. Phys. Chem.*, **5** (1973) 91-99

[3] G. Garaix and al., *Rad. Phys. Chem.*, **106** (2015) 394-403

[4] M. V. Vladimirova and al., *High Enrg. Chem.*, **6** (1972) 54-57

[5] N. N. Andreichuk and al., *Sov. Radiochem.*, **26** (1984) 740-745

[6] Y. Katsumura and al., *J. Phys. Chem.*, **95** (1991) 4435-4439

Keywords: alpha radiolysis, nitric acid, plutonium, hydrogen peroxide, nitrous acid

B-13

Reductive Dissolution of PuO_2 and CeO_2 in the Presence of Ti Particles and Ultrasound Irradiation

Matthieu Virot[1], Xavier Beaudoux[1,2], Tony Chave[1], Gilles Leturcq[2], Gauthier Jouan[3], Laurent Venault[2], Philippe Moisy[2], Sergey I. Nikitenko[0]

[1]Institut de Chimie Separative de Marcoule (ICSM), Bagnols sur Ceze, France, [2]CEA Marcoule - CEA/DEN/MAR/DRCP, Bagnols sur Ceze, France, [3]CEA Marcoule - CEA/DEN/MAR/DTEC/SECA/LCC, Bagnols sur Ceze, France

Plutonium dioxide is a dense and hard material. It is particularly inert towards most chemical substances and is very refractive to dissolution especially when fired at high temperature. Acidic non complexing media cannot dissolve this material in agreement with the high positive free energy related to this process ($\Delta rG° = 32\text{-}41$ kJ.mol^{-1}) [1,2]. The most famous media for dissolution of PuO_2 requires the use of catalytic amount of fluoride ions F^- in boiling and concentrated nitric acid [3]. This complexing dissolution route however suffers from some drawbacks related to the relatively low rate of dissolution, the equipment corrosion, and the effluent management. Due to the existence of four relatively stable oxidation states of Pu in acidic media, redox dissolution of PuO_2 can be considered. Oxidative dissolution of PuO_2 can be enabled with oxidants having redox potentials higher than ~1.2 V/SHE for PuO_2^{2+}/PuO_2 couple, or 1.4-1.6 V/SHE for PuO_2^{2+}/PuO_2 couple [1-3]. Strong oxidant cations such as Ce(IV), Ag(II), or Am(V,VI) allow to successfully dissolve PuO_2 with the possibility of regenerating the oxidant ions with ozone or electrochemistry. Although very fast dissolutions are observed at almost room temperature for such processes, the overconsumption of oxidant ions in the presence of organic materials or fission products in the dissolver can be problematic. The reductive dissolution route can be performed with redox couples having potentials below ~0.5 V/SHE which may solve the corrosion problems and propose milder reaction conditions [1-3]. However, reported studies remain scarce and do not allow satisfactory dissolution kinetics and yields, in addition to the use of non-compatible reagents or solvents for nuclear industry.

In parallel, sonochemistry (i.e., chemical reaction driven by ultrasound) can be an efficient tool to accelerate processes and initiate in situ redox reactions. Recent studies demonstrated that the sonication of aqueous nitric solutions allows the control and stabilization of the oxidation state of actinide ions [4,5]. The effect observed in sonochemistry are not related to direct interactions of ultrasound waves with molecules but derive from acoustic cavitation, which is the nucleation, growth, and rapid implosive collapse of gas- and vapor-filled micro-bubbles. At collapse, extreme conditions reached inside the bubbles lead to the formation of excited and radical species that recombine and react in solution. In addition, physical phenomena accompanying these effects are able to activate extended solid surfaces through the erosion or fracture of grains, the increase of reactive surface area, and depassivation of surfaces. For instance, the oxidative dissolution of uranium carbide and metallic plutonium was found to be improved under ultrasound irradiation [4,6]. Furthermore, studies devoted to the dissolution of CeO_2 and PuO_2 in H_2O_2 or HCOOH systems showed significant improvements under ultrasound irradiation [7]; however, reported kinetics were too low to consider any direct application.

In this context, the sonochemical and reductive dissolution of PuO_2 was investigated under relatively mild conditions. Due to its redox properties and crystallographic similarities, ceria was first investigated as an inactive surrogate for PuO_2. After preliminary studies, “hot” experiments were carried out in Atalante facility (Marcoule) in a dedicated glove box where an ultrasonic reactor is implemented. Several oxides were prepared by thermal conversion of oxalate precursors and were rigorously characterized before experiments (SEM, XRD, BET, etc.). Dissolutions were followed by SEM and by UV-Vis spectrophotometry for PuO_2 and ICP-AES for CeO_2. The quantitative dissolution of both oxides is observed at 33-35°C under ultrasound irradiation (20 kHz, Ar, 0.5-0.7 W.mL^{-1}) in 0.5-1.0 M HNO_3 / 0.1 M $[N_2H_5][NO_3]$ / 1-3 M HCOOH in the presence of Ti particles inserted in the reactor as a generating source of reducing agents.

Ultrasound allows the activation of Ti through the depassivation of its surface usually strongly non-reactive in nitric solutions. During sonication, dissolution rates and yields can be highly improved in the presence of dilute fluoride aliquots through the injection of NH_4F or HF which allow the chemical depassivation of Ti surface. The rapid and complete dissolution of PuO_2 can be achieved under these conditions and is accompanied by Pu(III) accumulation in solution (Figure 1). Reductive dissolution in such dilute and mild conditions is a promising alternative towards the dissolution of this refractory oxide and the related reduced equipment corrosion and effluent generation.

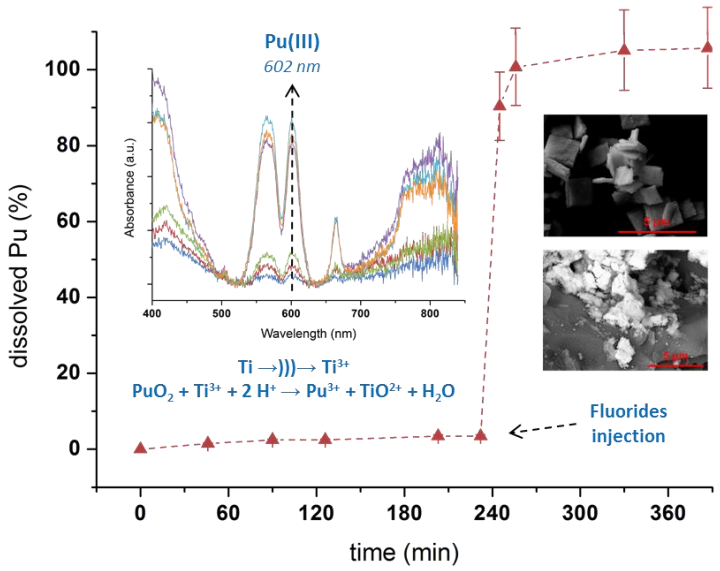

Figure 1: Dissolution kinetic of PuO_2 (14 $m^2.g^{-1}$, 150 mg) observed under ultrasound (20 kHz, Ar, 0.45 $W.mL^{-1}$) at 35°C in 0.5 M HNO_3 / 0.1 M $[N_2H_5][NO_3]$ / 2 M HCOOH (50 mL) in the presence of Ti particles (140 mg, 325 mesh). Fluorides (50 mM) were injected at 230 min. Insets highlight the accumulation of Pu(III) in solution in such system with UV-Vis spectroscopy, the proposed dissolution mechanism, and SEM pictures of PuO_2 (5 $m^2.g^{-1}$) before and after dissolution (bright colors: Pu, and dark colors: Ti) in similar conditions.

References

[1] C. Madic, P. Berger and X. Machuron-Mandard, in *Transuranium Elements, a Half Century*, eds. L. Morss and J. Fuger, ACS, Washington, DC, 1992, ch. 44, pp. 457-468.

[2] J. L. Ryan and L. A. Bray, in *Actinides Separations*, Eds. J. D. Navratil and W. W. Schulz, ACS Symposium Series, Washington, DC, 1980, ch. 34, 499-514.

[3] G. P. Nikitina, Y. E. Ivanov, A. A. Listopadov and L. B. Shpunt, Radiochemistry, 1997, 39, 109-122.

[4] S. I. Nikitenko, L. Venault, R. Pflieger, T. Chave, I. Bisel and P. Moisy, Ultrason. Sonochem., 2010, 17, 1033-1040.

[5] M. Virot, L. Venault, P. Moisy and S. I. Nikitenko, Dalton Trans., 2015, 44, 2567-2574.

[6] M. Virot, S. Szenknect, T. Chave, N. Dacheux, P. Moisy and S. I. Nikitenko, J. Nucl. Mater., 2013, 441, 421-430.

[7] F. Juillet, J. M. Adnet and M. Gasgnier, J. Radioanal. Nucl. Ch., 1997, 224, 137-143.

B-14

Shedding a new light on the superconductivity of $PuCoGa_5$: A heat capacity study on single crystals below 1 K

Jean-Christophe Griveau, Eric Colineau, Rachel Eloirdi, Pedro Amador Celdran, Roberto Caciuffo

ITU, Karlsruhe, Germany

Plutonium based superconductor $PuCoGa_5$[1] still remains a fascinating system. It presents a record superconducting transition temperature T_c ~ 18.5 K, one order of magnitude above all *5f* based systems reported ever and an estimated critical field Hc_2~ 80 T, similar to features of High Tc oxides Superconductors. One key aspect for the studies of $PuCoGa_5$ is the self-decay effect taking place in the material due to the presence of ^{239}Pu atoms. This is generating defects and disorder in the material that could be at the origin of artifacts misleading conclusions on the ground state of the system. Moreover, a self-heating is preventing reliable deep analysis at low temperatures where fundamentals properties can unambiguously be determined. Several studies[2] based on ageing pointed out the importance of pure single crystals with low self-heating reducing defects creation to clearly progress on the understanding of the ground state properties of the compound. But despite intensive works performed since its discovery very important questions remains unanswered such as the coupling mechanism at the origin of the superconductivity and the symmetry of the superconducting order parameter. Here we report a low temperate study on the basic properties of $PuCoGa_5$ single crystals of isotope ^{239}Pu and ^{242}Pu in the normal and in the superconducting state. Magnetization and heat capacity have been examined down to 1.8 and 0.6 K respectively giving access to new features related especially to the superconducting features and suggesting new scenarios for the ground state and the origin of the coupling mechanism.

References

1 J.L. Sarrao et al., Nature, **420** (2002) 297.

2 F. Jutier et al. EPL, **78** (2007) 57008.

B-15

Plutonium and americium solvent extraction processes: recent development in europe

Andreas Geist

Karlsruhe Institute of Technology (KIT), Karlsruhe, Germany

Background

The separation of transuranium elements (TRU = neptunium, plutonium, americium and curium) from used nuclear fuel serves several purposes: On one hand, TRU can be re-used as fuel, minimising the consumption of fresh uranium.[xxiii] This is primarily the case for plutonium recycling, offering the additional advantage of slowing down the increase in plutonium stockpile. On the other hand, TRU recycling has potential benefit related to final waste disposal. Most notably, a high level waste repository could be significantly more compact due to the long term heat load being reduced if TRU are not emplaced into the repository.[xxiii,xxiv] The recycling of TRU requires their prior separation from the used nuclear fuel, i.e. from fission products. For this purpose solvent extraction processes are developed in many countries. The focus is on plutonium and americium since plutonium can easily be re-used in MOx fuel and since plutonium and americium are the main contributors to the long term heat load.

TRU separations in Europe

The PUREX process is commercially operated in France and in the UK to separate uranium and plutonium. Americium cannot be separated in the PUREX process. Hence, multi-cycle approaches are developed to separate and purify the TRU (see Figure 1).

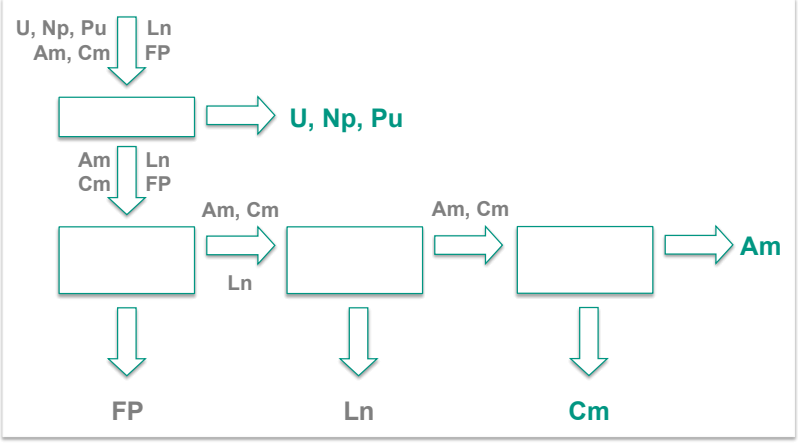

Figure 1. TRU separation using a sequence of solvent extraction processes: 1. PUREX to separate U, Np, Pu; 2. separation of Am, Cm and fission lanthanides from other fission products (DIAMEX process); 3. separation of Am and Cm from fission lanthanides (SANEX process); 4. separation of Am from Cm. Ln = fission lanthanides; FP = other fission products. Horizontal arrows, solutes extracted; vertical arrows, solutes rejected.

The PUREX process is used to separate uranium and plutonium and, by slight process modifications, also neptunium.[xxv] Next, americium and curium, together with the chemically similar fission lanthanides (all being present as trivalent cations), are separated from the PUREX raffinate by so-called DIAMEX processes.[xxvi,xxvii] Americium and curium are then separated from the lanthanides by SANEX processes.[xxviii,xxix] Separating trivalent americium and curium ions from lanthanide ions is only viable by applying soft (i.e. nitrogen or sulphur) donor ligands which have a stronger affinity for actinide ions.[xxx] Recently, processes that merge DIAMEX and SANEX into one process have successfully been demonstrated.[xxxi,xxxii,xxxiii]

Curium does not contribute to long term heat load; however, it complicates fuel fabrication because of its high neutron dose rate and short term heat load. For this reason, downstream processes have been developed to separate Cm(III) from Am(III), such as the SESAME process

developed at the French Alternative Energies and Atomic Energy Commission (CEA)[xxxiv] or the LUCA process developed at Jülich Research Centre.[xxxv]

Processes for separating only americium

To simplify this multi-cycle procedure, processes are being developed which extract only Am(III) from PUREX raffinate, routing Cm(III) together with the fission products to the high level waste (see Figure 2). This results in a significant simplification, requiring less solvent extraction cycles.

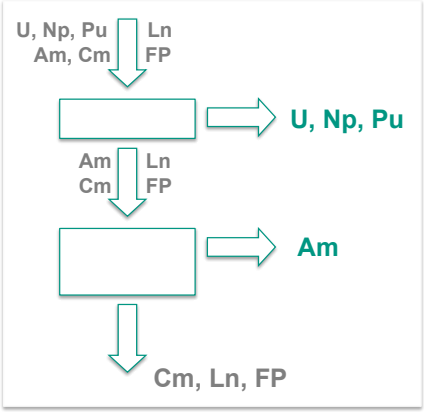

Figure 2. Simplified TRU separation scheme taking advantage of directly separating only Am from the PUREX raffinate solution: 1. PUREX to separate U, Np, Pu; 2. Am-only extraction .

Extracting agents useful under the high-acidity conditions encountered when processing PUREX raffinate have a rather low separation factor for Am(III) over Cm(III) (typically ≈ 1.6), requiring a large number of stages to achieve sufficient separation. Combining such an extracting agent with an aqueous phase complexing agent having reverse selectivity yields separation factors of 2.5–3. This significantly reduces the number of stages required. Adding ligands capable of selectively stripping actinide ions from the organic phase, processes are developed for separating only americium from PUREX raffinate. Examples are the French EXAm[xxxvi,xxxvii] process and the EURO-EXAm and AmSel[xxxviii] processes developed in the European SACESS project.

Processes for TRU co-separation

Grouped Actinides Extraction (GANEX) processes are developed for the homogeneous recycling of TRU, addressing proliferation concerns: GANEX processes do not generate a pure plutonium product since the TRU are not separated from each others throughout the process.

The CEA developed and successfully hot-tested such a process.[xxxix] Using extracting and complexing agents developed in European research programmes on actinide separations, two further versions of GANEX processes were developed: the CHALMEX process[xl] and the EURO-GANEX process.[xli,xlii] The latter was successfully hot-tested.[xliii]

One of the challenge in designing such processes is developing solvent formulations that are capable of extracting Pu(IV) in sufficiently high concentrations, together with other TRU of various oxidations states.[xliv]

Conclusions and outlook

Recycling TRU as nuclear fuel requires highly selective and efficient separations processes. Solvent extraction is the method of choice. In the framework of European research programmes funded by EURATOM and national programmes, a suite of solvent extraction processes has been developed and tested. The most promising ones are further studied and developed, both from a fundamental point of view and to improve their technology readiness level (TRL).

B-16

From the stars through the ocean abyss: the long travel of super-nova Pu-244 into VERA's particle detector

Peter Steier[1], Anton Wallner[1,2], Thomas Faestermann[3], Jenny Feige[1,8], Chana Feldstein[4], Klaus Knie[3,5], Gunther Korschinek[3], Walter Kutschera[1], Avishai Ofan[4], Michael Paul[4], Francesca Quinto[1,6], Georg Rugel[3,7]

[1]University of Vienna, Vienna, Austria, [2]Australian National University, Canberra, Australia, [3]Technische Universität München, Garching, Germany, [4]Hebrew University, Jerusalem, Israel, [5]GSI Helmholtz-Zentrum fu ¨r Schwerionenforschung, Darmstadt, Germany, [6]Institute for Nuclear Waste Disposal, Eggenstein-Leopoldshafen, Germany, [7]Helmholtz-Zentrum Dresden-Rossendorf, Rossendorf, Germany, [8]Technische Universität Berlin, Berlin, Germany

The astrophysical question

All but the lightest elements in the cosmos were produced by nucleosynthesis in stars. Half of the nuclides heavier than iron - including all actinides - are generated in explosive environments. Their production requires a very short and intense burst of neutrons, known as rapid neutron capture or r-process nucleosynthesis. However, the relevant astrophysical sites, and the history of the r-process during the Galactic chemical evolution remain a mystery.

The most frequently occurring candidates for r-process nucleosynthesis are core-collapse (type II) supernovae, with a rate of about 1 to 2 per 100 years in the Galaxy. However, recent models suffer difficulties on whether very heavy events can really be produced in these explosions. Other less frequent scenarios, e.g. neutron-star mergers are discussed as alternatives. During every event, the interstellar medium is enriched with fresh nucleosynthetic products. Depending on the rate of these events, also radionuclides with sufficiently long half-live will accumulate in the interstellar medium. With a half-live of 81 My, ^{244}Pu can place strong constraints on recent r-process frequency and production yield.

It is known that ^{244}Pu was present in the early solar system with an abundance of 0.8% relative to ^{238}U. Therefore, new heavy r-process nuclei had been injected by an event no more than a few half-lives before the gravitational collapse of the protosolar nebula. Nowadays, this primordial ^{244}Pu has decayed to undetectable levels on earth. However, if r-process nucleosynthesis is frequent, ^{244}Pu should be present at a steady-state abundance in interstellar matter. ^{244}Pu from recent nucleosynthesis can reach the Earth in two ways: a relatively close supernova may inject it to our planet directly, or the shock front of the explosion may sweep up ^{244}Pu accumulated in interstellar dust and transport it to Earth

We have carried out a search for live interstellar ^{244}Pu in deep-sea reservoirs[1], which are expected to accumulate interstellar dust particles over long time periods. The abundances found were by about two orders of magnitude lower than expected from continuous production in the Galaxy. Our findings indicate that ^{244}Pu has not accumulated to a steady state in the interstellar matter, and thus supernovae did not contribute significantly to actinide nucleosynthesis for the past few hundred million years. Actinide nucleosynthesis, as mapped through live ^{244}Pu, seems to be very rare.

The search for ^{244}Pu

Accelerator Mass Spectrometry (AMS) utilizes a particle accelerator adopted from nuclear physics as a big mass spectrometer. The higher particle energy improves the ion optical properties, allows the complete destruction of interfering molecular isobars, and reduces the probability of scattering and tailing processes responsible for background in conventional mass spectrometers. Detectors for particles in the MeV energy range have no dark-count rate, and allow additional identification. The AMS facility VERA at the University of Vienna was optimized and extended over the years for the detection of actinides. ^{244}Pu can be detected practically without instrumental background and high sensitivity.

Two kinds of deep-sea archives were investigated: with a growth rate of a few millimetres per million years, hydrogenous crusts will strongly concentrate elements and particles. The higher accumulation rate of deep-sea sediments (mm/ky) results in a better time resolution but requires much larger sample volumes. We used a deep-sea manganese crust (237 KD from cruise VA13/2, collected in 1976) with a growth rate between 2.5 mm per My and 3.57 mm per My; it originates from the equatorial Pacific at a depth of 4,830 m and covers the last 25 My. Our second sample, also from the Pacific Ocean, is a piston-core deep-sea sediment (7P), extracted during the TRIPOD expedition as part of the Deep-Sea Drilling Project (DSDP) at 3,763 m water depth and covers a time period of about 0.5–2.1 My before present.

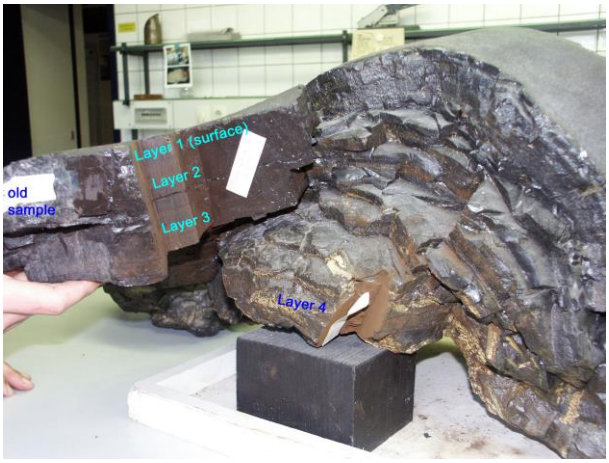

Crust sample 237 KD. This FeMn crust (with a total thickness of 25cm) was sampled in 1976 from the Pacific Ocean at 4,830m water depth

The crust sample was split in four layers, the top 1 mm, was used for measuring the anthropogenic Pu contamination originating from atmospheric atomic-bomb tests from ca 1950 to 1963. The 12 individual pieces processed with masses between 30 and 360 g were dissolved, and ^{236}Pu was added as a spike to trace the chemical yield. The plutonium was extracted by Ca co-precipitation and several and anion exchange, co-precipitated with 2 mg Fe, and converted to oxide by combustion, suitable for the Cs-sputter ion source used for AMS. As a low yield of ^{236}Pu was observed for some samples, their stored solutions were reprocessed and Pu was separated by TRU resin. The sediment samples were processed by alkali fusion and liquid-liquid extractions, ^{242}Pu was used as a tracer in this case.

The AMS measurement procedure was a sequence of alternating counting periods of ^{236}Pu, ^{239}Pu, ^{244}Pu and again ^{236}Pu (^{242}Pu instead of ^{236}Pu for the sediment samples). All samples were repeatedly measured until they were completely exhausted, and lasted 5 to 20 hours. After the AMS measurement of the deep-sea samples, reference samples containing a well-known isotope ratio of ^{244}Pu/^{242}Pu were measured. The measured ratios reproduced the nominal values within 4%. The overall yields for the 12 crust samples were between 0.06×10^{-4} and 1.54×10^{-4}.

A clear anthropogenic ^{239}Pu and ^{244}Pu signal, originating from atmospheric atomic-bomb tests from ca. 1950 to 1963, was observed in the top layer of the deep-sea manganese crust (16 events of ^{244}Pu detected). However, only two atoms of ^{244}Pu were detected in the deeper layers of the crust sample, and one in the sediment. This is two orders of magnitude less than expected. One additional crust sample, the lowest layer of the crust material, was of hydrothermal origin where no extraterrestrial ^{244}Pu could accumulate. This sample was chemically prepared and measured in the same way as the other crust samples and served as a process blank for potential chemistry and machine background.

References

1. A. Wallner, T. Faestermann, J. Feige, C. Feldstein, K. Knie, G. Korschinek, W. Kutschera, A. Ofan, M. Paul, F. Quinto, G. Rugel, P. Steier. Abundance of live Pu-244 in deep-sea reservoirs on Earth points to rarity of actinide nucleosynthesis. Nature Communications 6:5956 (2015)

B-17

Real-time, fast neutron assay of plutonium and related materials

Malcolm J. Joyce

Lancaster University, Lancaster, UK

Introduction

The mainstay of neutron assay for fissile materials has long been the proportional counter utilizing thermal neutron capture reactions in either ^{10}B (as a constituent of boron trifluoride gas) or ^{3}He (helium). Such detectors are very stable in use, well understood and relatively immune to the influence of omnipresent γ-ray contamination. However, leakage of boron trifluoride is potentially hazardous due to the liberation of hydrogen fluoride and ^{3}He is supply-constrained. Perhaps most importantly, the efficiency of detection in either case is often optimized by thermalizing the neutron field prior to detection. In doing this a significant proportion of the temporal information associated with the neutron field is lost which complicates the ease with which properties such as neutron energy & multiplicity are extracted, and also the finesse with which uncorrelated, accidental events are rejected.

Organic scintillation detectors provide a different approach to neutron assay in which the interaction of an incident fast neutron is manifest as a pulse of light. This is usually converted to an electrical signal by a photo cathode and amplified either by a photomultiplier tube (PMT) or silicon photomultiplier (SiPM). In contrast to thermal neutron detectors based on ^{10}B and ^{3}He referred to above, organic scintillators are sensitive to fast neutrons (typically above an energy threshold of 500 keV) and the light is evolved with sufficient speed to enable a much greater proportion of the temporal characteristics to be retained through to the voltage pulse corresponding to each event.

However, organic scintillators have several disadvantages associated with them. Firstly, early variants of the scintillation media were toxic and highly flammable. This restricted their adoption in industrial environments. Over the last ten years low-hazard, low-flashpoint alternatives have become available whilst recently a solid alternative was synthesized for applications where liquids were not suitable. Secondly, the scintillant also responds to photon radiations with γ rays being the principal source of contamination in neutron environments. It has been known for over 50 years [1] that a subtle distinction in pulse shape offers the potential to separate neutrons from γ rays due to the difference in linear energy transfer of neutrons over photons and the associated long decay of the former. The pulses from organic scintillators are necessarily fast (with durations of the order of ~ 50 ns) and this places significant performance requirements on the data acquisition electronics. Since 2010 ultra-fast, integrated real-time data acquisition systems have been available to provide for the power, pulse-shape discrimination and pulse synchronization requirements of organic scintillation detector systems. In this paper a summary of the achievements to date with organic scintillation detector systems for the assay of nuclear materials containing ^{240}Pu, ^{235}U and ^{244}Cm will be described.

Instrumentation and experimental set-up

The instrument that constitutes the basis for this research is the mixed-field analyser (MFA) [2]. The MFA is a single-unit device that provides the high-voltage supply required for the PMTs on organic scintillation detectors with pulse-shape discrimination (PSD) processing from raw input pulse through to the output of a corresponding transistor-transistor logic (TTL) pulse for every neutron and γ ray that is detected. The MFA requires 330 ns to process each event but maintains the synchronization with every event in turn to within a limiting jitter of $\pm$ 6 ns thus retaining the fast-neutron temporal information for each event; this enables coincident data to be extracted from mixed radiation fields in real-time without the requirement for pre-detection thermalisation. A dedicated graphical user interface is used to configure the MFA which includes the specification of the PSD threshold, the trigger threshold and the calibration of the pulse-height spectra. This is configured over an integrated Ethernet connection. Once set up,

the MFA operates entirely independently of any user involvement and is available in a modular form factor to control groups of four scintillation detectors at a time.

Interval time distribution measurements

Fundamental to both passive and active neutron coincidence counting is the duration over which neutrons are emitted from fission, irrespective in a qualitative sense of the specific isotope in question. A schematic of the timescale of fission and neutron detection assuming thermalisation is required (i.e. for ^{3}He or ^{10}B) is shown in Fig. 1 below for a $\log_{10}$ scale and linear scale in a) and b), respectively. At the point in the evolution of a fission event beyond which fission is inevitable (when the fission fragment nucleon distributions are formed and the associated Coulomb repulsion overwhelms cohesion often referred to as the point of scission), ~10% of the prompt neutron emission is suspected to occur (dependent on specific isotope in question). The fission fragments accelerate away from each other extremely rapidly and heat up as they acquire sphericity emitting the remaining 90% of the prompt neutron emission. It is estimated that the period over which prompt neutron emission occurs is between 10^{-18} and 10^{-13} after scission. If the number of neutrons is counted following the stimulus of a first, trigger neutron event across a range of bins in time, then a peaked distribution of neutron counts versus time is obtained referred to as the interval time distribution (ITD). In terms of detection of the prompt neutrons it is necessary for them to firstly traverse the distance between the source of emission and the detector(s) which introduces a relatively significant source of delay given the timescales involved and also causes the arrival times of the emitted neutrons at the detector system to become dispersed due to the distribution in energies associated with the fission spectrum; this can be a benefit in terms of spectroscopy but places a further limit in the context of fast timing that is manifest as a broadening of the ITD. It is difficult to conceive of an experimental set-up in which the source-detector distance can be reduced much beyond a limiting traverse delay of ~5 ns given the need for a finite detector thickness in which the neutron interaction occurs and unavoidable intermediate boundaries such as the detector housing and sample container. It is this variance in source-detector distance and the depth of the detector volume that yields a limiting range in timing in the nanosecond region post-scission despite the neutron emission being over a factor of 10^{4} earlier than this. A range of neutron energy from 0.5 MeV (a reasonable estimate for the low-energy cut-off in organic scintillators) through to 5 MeV (~5% probability level of a typical Watt spectrum) over a distance or detector depth of 10 cm yields a range in elapsed time between the scission and time of detection of 10 ns through to ~3 ns, respectively.

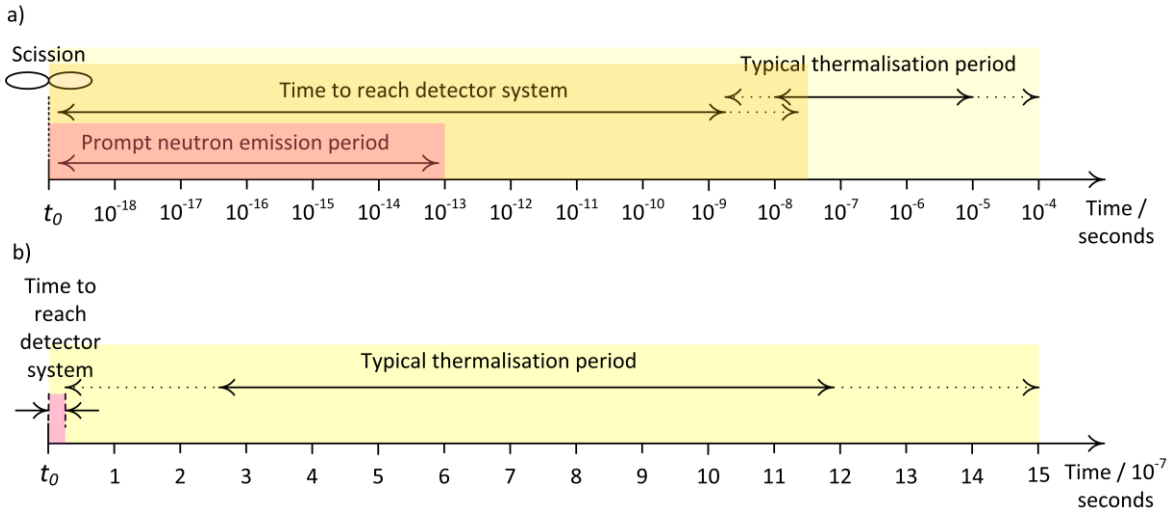

Figure 1: Schematic timelines for neutron emission and detection a) $\log_{10}$ and b) linear timescales.

Where themalisation is necessary in order to exploit the high neutron capture cross-sections in either ^{3}He or ^{10}B, the most popular approach is to use a hydrogenous moderator to slow the neutrons to thermal energies. Most often high-density polyethylene is used, with reasonable estimates for the time necessary for slowing down and capture on either ^{10}B or ^{3}He being of the

order of 10 μs. This requirement adds a very significant factor in time of ~10^3 that is manifest perhaps most significantly in requiring that coincidence gates are of the order of microseconds in length are needed. This overlaps with the time taken for neutrons to scatter in the environment or to be evolved from uncorrelated processes such as (α, n) reactions. Consequently the proportion of uncorrelated, non-fission 'accidental' events that are confused with 'reals' is much larger for the case of thermal neutron coincidence detector systems because of the need to allow for slowing down time. This is demonstrated most clearly in terms of the ITDs or Rossi-α distributions reproduced in Fig. 2 for thermal neutron detection systems (left) [3] and for fast neutron, organic scintillator systems (right) [4]. The slow rate of die-away for thermalized systems relative to fast results in very significant accidentals rate that persists long after the reals from fission have subsided; the equivalent in the fast domain is of the order of ~15 ns in width (corresponding to the spectral width of the fission burst with zero accidentals as time $\rightarrow \infty$.

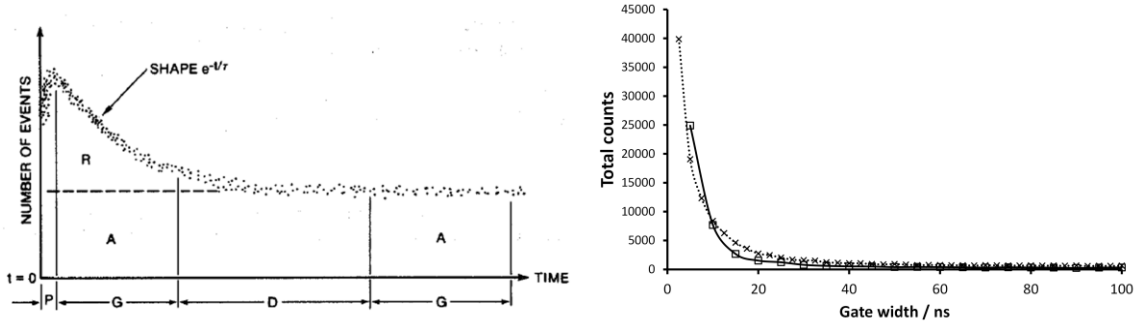

Figure 2: Total coincident neutron counts for detectors requiring thermalisation (left) [3] versus time and for the organic liquid scintillant EJ-309 (right) dotted line: experimental measurements with ^{252}Cf, solid line: MCPN5 simulations [4].

Plutonium studies

Plutonium is often assessed via neutron coincidence methods on a passive basis via the neutron emission from spontaneous fission in the even-numbered isotopes, predominantly ^{240}Pu. ^{240}Pu typically constitutes 6-7% wt. plutonium depending on the origin of the material yielding ~1000 neutrons s^{-1} g^{-1} with average number of neutrons per fission $\bar{\nu}$ of 2.2 which presents an attractive possibility for fast neutron coincidence counting. In Fig. 3a plot of doubles fast neutron events per 100 s acquisition versus plutonium mass is given which has been corrected for accidentals, acquired with four EJ-309 organic scintillation detectors [5].

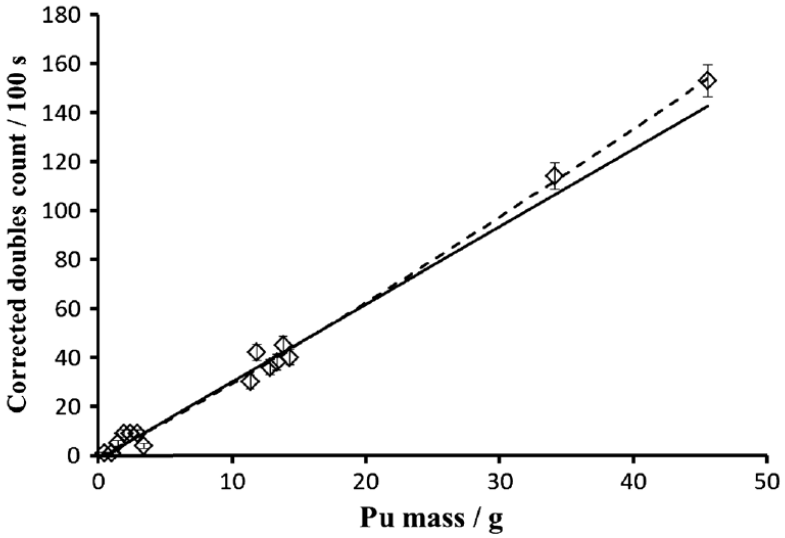

Figure 3: Coincident fast neutron doubles per 100s acquisition period versus plutonium dioxide mass corrected for accidentals with linear (solid) and non-linear (dashed) weighted least-square fits, taken with four EJ-309 detectors [5].

Uranium studies

In comparison with plutonium, uranium presents somewhat different challenges in terms of non-intrusive assay due to relatively weak γ-ray spectroscopy signatures and only a weak spontaneous fission decay pathway associated with ^{238}U. The latter is difficult to exploit for either fissile mass assessment or enrichment analysis due to the overburden of ^{238}U ubiquitous in low-enriched uranium-based nuclear fuels & feedstock materials and the corresponding insensitivity to changes in its abundance due to changes in ^{235}U enrichment. Consequently active neutron assay (alternatively termed interrogative assay) is often used in which a source of neutrons is used to induce neutron emission via stimulated fission in the ^{235}U content. Usually a low-energy neutron source such as americium-lithium (AmLi), a moderated source or indeed a combination of both is used to stimulate neutron emission. The principle hence forward is similar to the passive assay of plutonium described above with the additional complication that in addition to the removal of the omnipresent background contribution, it is also necessary to account for the neutron contribution from the source and also for the contribution from spontaneous fission in ^{238}U. The former usually has to be measured in the absence of the sample (i.e. the uranium under assessment) whilst the latter has to be measured in the absence of the source. Where the assessment of large samples is required (such as fuel assemblies etc.) they can constitute dense neutron scatterers in their own right and thus the perturbation they introduce to the stimulating neutron field has to be accounted for. Data for this assessment are shown in Figure 4 for singles (left) and doubles (right) acquired with a AmLi source and four EJ-309 detectors over a series of 1-hour acquisition periods [6].

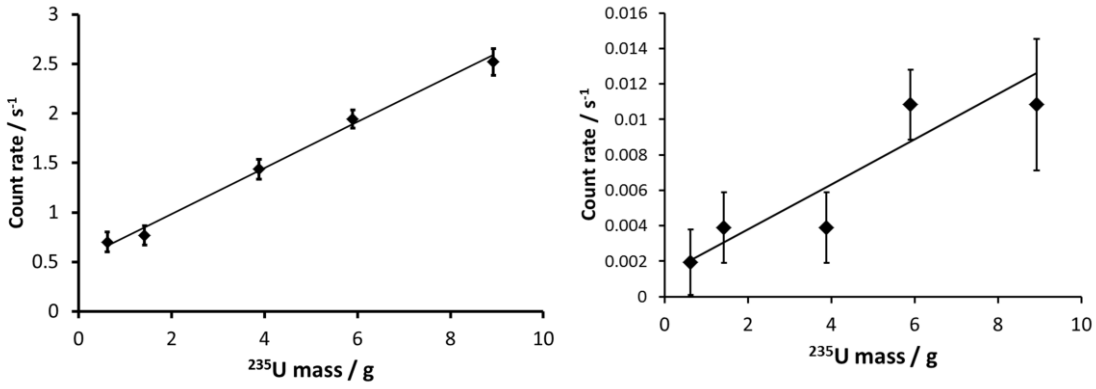

Figure 4; Fast neutron counts for fission induced in low-enriched U_3O_8 samples of 200 g with AmLi for singles (left) and doubles (right) using 4 EJ-309 detectors and 1-hour count duration [6].

Curium studies

Curium is a rather different case to most uranium and plutonium isotopes because of the very significant neutron emission rate from ^{244}Cm and to a lesser extent that from ^{242}Cm, in particular [7]. The aim of curium assessment is usually to differentiate neutron emission from its spontaneous fission from that of plutonium derived from ^{240}Pu; however this is difficult especially in wastes and irradiated fuels where curium arises in levels of abundance as a minor actinide that can swamp the ^{240}Pu component in many systems. An interesting differentiating feature however is the fission-borne fast neutron multiplicity as has been measured with four EJ-309 detectors for ^{244}Cm and ^{252}Cf in Fig. 5. A clear, real-time difference in multiplicity is observed for these isotopes through to triples in both case with only a 20-minute acquisition period with sources of 105 s^{-1} (^{252}Cf) and 16000 (^{244}Cm).

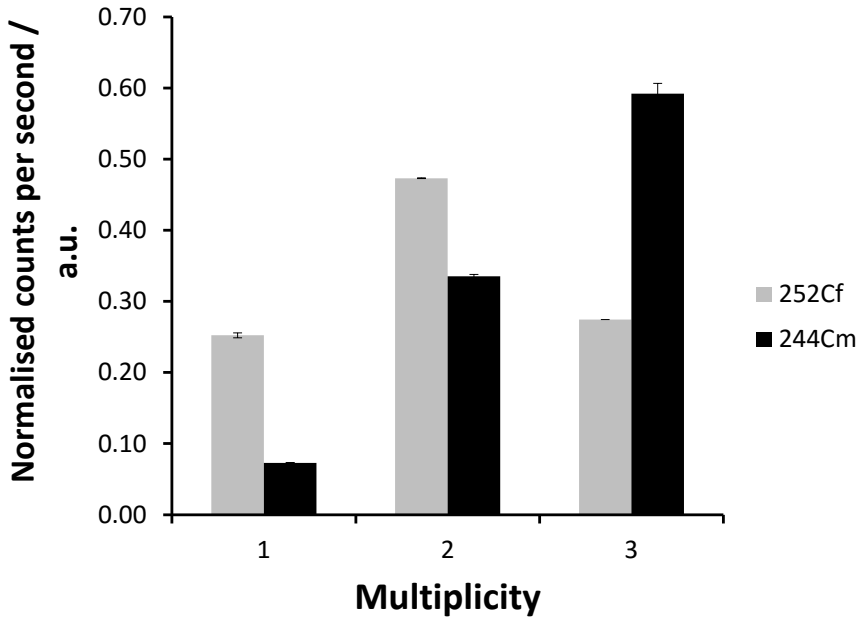

Figure 5: Normalised fast neutron counts versus multiplicity for passive assay of ^{252}Cf and ^{244}Cm, four detectors, typical acquisition time 20 minutes.

Summary

In this abstract three examples of measurements that have been performed with organic liquid scintillation detectors have been described on plutonium and related materials. These and related measurements will be elaborated upon in the paper given at the conference.

References:

[1] 'A scintillation counter with neutron and gamma-ray discriminators', F. D. Brooks, Nucl. Inst. Meth. 4 (3) pp. 151-163 (1959).

[2] 'The Design, Build and Test of a Digital Analyzer for Mixed Radiation Fields', M. J. Joyce, M. D. Aspinall, F. D. Cave, K. Georgopoulos and Z. Jarrah, IEEE Trans. Nuc. Sci **57** (5) pt. 2 2625-2630 (2010).

[3] N. Ensslin, Principles of neutron coincidence counting, chapter 16, 'Passive non-destructive assay manual', pp. 457-492, http://www.lanl.gov/orgs/n/n1/panda/00326411.pdf

[4] 'Fast neutron multiplicity counting with zero accidentals', R. Sarwar, Plutonium Futures 2016 (this meeting).

[5] 'Real-time, fast neutron coincidence assay of plutonium with a 4-channel multiplexed analyser and organic scintillators', IEEE Trans. Nuc. Sci. 61 (3) pp. 1340-1348 (2014).

[6] 'Active fast neutron singles assay of 235U enrichment in small samples of triuranium octoxide', In review, Progress in Nuclear Energy, (2016).

[7] 'Field examples of waste assay solutions for curium-contaminated wastes', P. Chard, S. Croft, I. Hutchinson, T. W. Turner, A. Ross and B. Greenhalgh, 12th ASME International Conference on Environmental Remediation and Radioactive Waste Management, ICEM2009-16259, pp. 95-105.

B-18

Nanoparticle Plutonium Formation, Growth, and Morphology with Advanced *in-situ* Liquid Cell Electron Microscopy

Edgar Buck

Pacific Northwest National Laboratory, Richland, WA, USA

In this presentation, the history of Pu contamination at the Hanford site will be reviewed, including the various disposal locations, the quantities of Pu and co-contaminants disposed, and recent research efforts designed to unravel the chemical form of Pu in the environmental samples. Microanalytical information will also be presented for the sediments at the Z-9 site. The information will include the chemical characterization of the sediments at two bore holes drilled at the Z-9 sites. Although the majority of the plutonium is present as oxide, using both electron microscopy (EM) and x-ray absorption spectroscopy evidence was found for the formation of nano-sized mixed Pu and iron phosphate hydroxides that are structurally related to rhabdophane-group minerals. The Pu-phosphate formation may depend on the local microenvironment in the sediments, availability of phosphate, and hence the distribution of these minerals may control long-term migration of Pu in the soil. The presentation will also focus the role of *in-situ* EM can play in understanding nanoparticle formation and its subsequent interaction with substrates.

The analysis and identification of Pu-bearing particles and phases in soils and sediments presents several challenges in the areas of low-level detection, as well as in the collection of representative samples. Within the 200 area at the Hanford site in eastern Washington State, the 216 Z-Plant area, also termed the Plutonium Finishing Plant, conducted Pu recovery operations that resulted in organic and aqueous wastes being disposed at several 'cribs' or ground trenches. These organic wastes consisted of carbon tetrachloride mixed with lard oil, tributyl phosphate, and dibutyl butyl phosphonate. One of the main disposal areas was known as the 216-Z9 trench which was one of three major disposal facilities, received a total of about 1.3×10^7 L of liquid waste. The Z9 trench was defined as the "worst case" representative of several disposal sites impacted by discharges from the Z-plant complex.

Iron (II) minerals, when in isolation, will control the fate of Pu; however, in a sediment with clay, calcite, and other soil minerals present as we observed in the Z9 sediments, other phases and elements may have a significant impact on the Pu chemistry. Nevertheless, the complexity found in the natural environments may lead to the formation of phases that may not be predicted in laboratory set-ups. Understanding the chemistry of Pu in complex media requires tools that can probe micro-environments. We have been exploring the use of *in-situ* EM to investigate the precipitation of Pu. All designs of cells for *in-situ* electron microscopy incorporate a membrane that prevents evaporation of the liquid sample in the microscope vacuum. In Figure 1, and example of an *in-situ* EM observation of Pu oxalate growth in solution is shown. We will describe other observations of Pu behaviour, morphology, and compositional changes studied with these new EM methods.

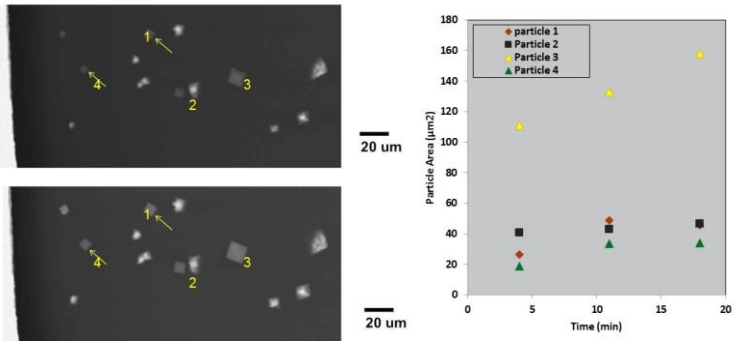

Figure 1. Formation and growth of Pu(IV) oxalate in solution observed in the electron microscope

B-19

Chemical Speciation of uranium oxide and plutonium oxide materials for forensic science

Marianne Wilkerson, Miles Beaux, Sarah Hernandez, Stephen Joyce, Andrew Nelson, Alison Pugmire, David Pugmire, Amy Ross, Brian Scott, Igor Usov, Gregory Wagner, Angelique Wall, Laura Wolfsberg

Los Alamos National Laboratory, Los Alamos, NM, USA

We are investigating morphology and chemical speciation of actinide oxide materials for development of signatures that could be indicative of provenance and history of unknown samples. Previous studies reveal that morphology and chemical signatures of uranium oxide compounds important to conversion processes may be measured by scanning electron microscopy and powder X-ray diffraction analysis [1,2]. Measurements of uranium oxide materials stored under conditions of high relative humidity suggest that these signatures may change. Nuclear processes conducted to concentrate or purify plutonium also are chemical in nature, providing opportunities for chemical or elemental impurities from the process to be incorporated into the plutonium product. Plutonium oxides readily form on plutonium metal as a dispersible “rust” of yellow-olive material. A number of mechanisms to understand corrosion on plutonium surfaces have been proposed [3], but our understanding of the complexity of plutonium oxide systems, their morphologies, and chemical behavior precludes our ability to develop forensics signatures based on these properties. To better understand potential morphology and chemical signatures that could be useful for nuclear forensic science, we are conducting studies to characterize a high-purity PuO_2 thin film for comparison with a range of plutonium oxide powders produced from oxidation of plutonium metal.

Here, we will discuss our investigations of morphology and chemical signatures from both uranium oxide and plutonium oxide materials. Specifically, we will present results from a study to characterize both high-purity and legacy uranium trioxide powders that were stored under controlled conditions of temperature and relative humidity. Chemical speciation was characterized by powder X-ray diffraction analysis and synchrotron-based X-ray absorption spectroscopy, and addition of water to the lattice was modelled using density functional theory. For our plutonium oxide studies, we initiated work with epitaxial PuO_2 thin films prepared using polymer assisted deposition, a water-based process, to determine potential changes in lattice structure of plutonium oxides [4]. These films were characterized by powder X-ray diffraction analysis and X-ray absorption spectroscopy, as well as other surface sensitive techniques [5]. We compare these results with measurements of the chemical speciation and morphology from highly oxidized plutonium metal.

References:

[1] A. L. Tamasi, Kevin S. Boland, K. Czerwinski, J. K. Ellis, S. A. Kozimor, R. L. Martin, A. L. Pugmire, D. Reilly, B. L. Scott, A. D. Sutton, G. L. Wagner, J. R. Walensky, and M. P. Wilkerson, "Oxidation and hydration of U3O8 materials following controlled exposure to temperature and humidity,” Anal. Chem. vol. 87, no. 8, pp. 4210-4217, 2015.

[2] A. L. Tamasi, L. J. Cash, W. T. Mullen, A. R. Ross, C. E. Ruggiero, B. L. Scott, G. L. Wagner, J. R. Walensky, S. A. Zerkle, and M. P. Wilkerson, “Comparison of morphologies of a uranyl peroxide precursor and calcination products,” J. Radioanal. Nucl. Chem., DOI 10.1007/s10967-016-4692-x.

[3] H. G. García-Flores, P. Roussel, D. P. Moore, and D. L. Pugmire, “Characterization and stability of thin oxide films on plutonium surfaces,” Surf. Sci, vol. 605, no. 3-4, pp. 314-320, 2011.

[4] B. L. Scott, J. J. Joyce, T. D. Durakiewicz, R. L. Martin, T. M. McCleskey, E. Bauer, H. Luo, and Q. Jia, “High quality epitaxial thin films of actinide oxides, carbides, and nitrides: advancing understanding of electronic structure of f-element materials,” Coord. Chem. Rev. vol. 266-267, pp. 137-154, 2014.

[5] M. F. Beaux, S. A. Joyce, D. P. Moore, D. L. Pugmire, I. O.Usov, T. J. Venhaus, Private Communication.

B-20

Redox speciation of actinides using capillary electrophoresis coupled to ICP-MS

Christian Willberger, Samer Amayri, Verena Häußler, Raphael Scholze, Tobias Reich

Johannes Gutenberg University Mainz, Mainz, Germany

Redox-sensitive, radiotoxic and long-lived ^{239}Pu ($t_{1/2}$ = 2.411 × 10^4 a), besides other actinides such as ^{237}Np ($t_{1/2}$ = 2.14 × 10^6 a) or ^{238}U ($t_{1/2}$ = 4.468 × 10^9 a), is part of the high-level radioactive waste in spent nuclear fuels. The nuclear waste will be stored in a deep geological repository with argillaceous rocks, crystalline rocks or salt as potential host rocks.[1] Under natural conditions, those actinides exhibit a wide distribution of possible oxidation states with different speciations in aquifers. In the case of Pu, for example, not only the oxidation states Pu(III) up to Pu(VI) can be attained in aqueous solution but moreover there are versatile possibilities of different complexation partners and coordination numbers. The design of the repository has to ensure that the radioactive waste is isolated from the environment for periods of up to one million years. Therefore, for the safety assessment of a future geological repository it is very important to gain a deep understanding of the geochemical behavior of the actinides. For this reason it is essential to have a reliable and efficient analytical method for determining the exact speciation of actinides at environmentally-relevant concentrations as in the case of a possible leakage from the repository.

For analyzing the oxidation states and the different speciations of the actinides in different media, the separation capability of capillary electrophoresis (CE) was coupled with the high sensitivity of ICP-MS. With this setup we achieved separation and quantification of different actinide oxidation states within less than 20 minutes and limits of detections of approximately 1 × 10^{-9} M[2-3] which is expected for actinides in the far field of a repository.

The electrophoretic mobilities (μ_e) of the actinides Th and U – Am (c = 5 · 10^{-7} M) in different oxidation states in 1 M HCl, 1 M $HClO_4$ and Opalinus clay pore water[4] (only for Pu(V)) have been determined with CE-ICP-MS with 1 M acetic acid as background electrolyte. The μ_e of the Pu oxidation states +III to +VI have been measured. The values seem to be independent from the respective acid and are in good agreement

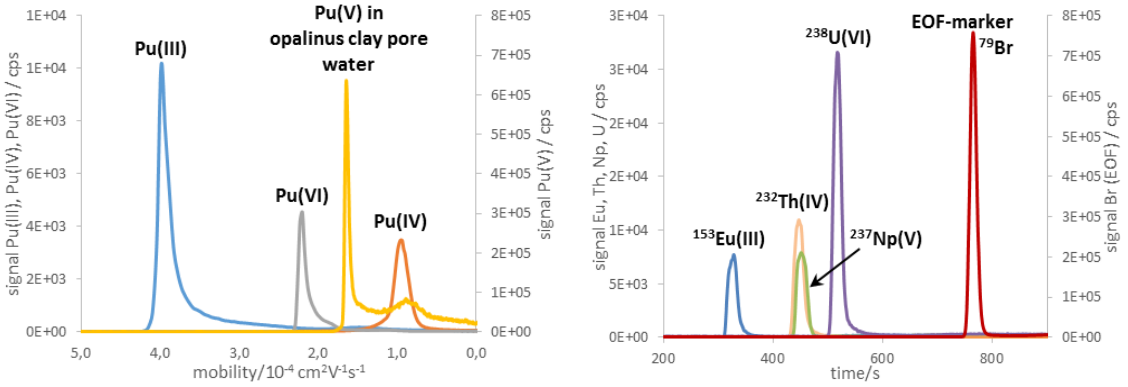

Figure 1: Electropherograms of the Pu oxidation states (left) and the redox-stable analogues (right)

with both the available literature data[5-6] and with redox stable analogues (Eu(III), Th(IV), Np(V), U(VI)) that have also been investigated. Fig. 1 shows the electropherograms of the different Pu species and of the related redox-stable elements.

The trend in the μ_e for the actinides U – Pu turned out to be Ac(III) > Ac(VI) > Ac(V) > Ac(IV). The μ_e of Am(III) (μ_e(Am(III)) = 3.86·10^{-4} cm^{2}V^{-1}s^{-1}), U(IV) (μ_e(U(IV)) = 0.34·10^{-4} cm^{2}V^{-1}s^{-1}) and

U(VI) (μ_e(U(VI)) = 1.51·10^{-4} cm^{2}V^{-1}s^{-1}) have been measured for the first time under these experimental conditions.

Furthermore, a systematical approach for calculating values for the μ_e of actinides in instable oxidation states that were not feasible for CE-ICP-MS experiments is introduced. This schema is confirmed by measurements of already estimated values which have been measured afterwards. The estimated value for U(IV), for example, is μ_e(U(IV)) = 0.28·10^{-4} cm^{2}V^{-1}s^{-1}. This is in very good agreement with the experimental data given above.

The results of this systematic determination of the values for μ_e were applied to investigate the speciation and kinetics of Np(V) reduction by hydroxyl ammonium hydrochloride as a function of temperature.[7] The corresponding kinetic parameters will be presented.

Acknowledgement

This work was financially supported by the Federal Ministry for Economic Affairs and Energy under contract No.02E10981.

References

[1] Hoth, P.; Wirth, H.; Reinhold, K.; Bräuer, V.; Krull, P.; Feldrappe, H. *Endlagerung radioaktiver Abfälle in Deutschland*, BGR Bundesanstalt für Geowissenschaften und Rohstoffe: Hannover/Berlin, Deutschland, **2007**.

[2] Stöbener, N.; Amayri, S.; Gehl, A.; Kaplan, U.; Malecha, K.; Reich, T. *Anal. Bioanal. Chem.* **2012**, 404, 2143–2150.

[3] Kuczewski, B.; Marquard, C. M.; Seibert, A.; Geckeis, H.; Kratz, J. V.; Trautmann, N. *Anal. Chem.* **2003**, 75, 6769–6774.

[4] Van Loon, L. R.; Soler, J. M.; Bradbury, M. H. *J.Contam. Hydrol.* **2003**, 61, 73–83.

[5] Bürger, S.; Banik, N. L.; Buda, R. A.; Kratz, J. V.; Kuczewski, B.; Trautmann, N. *Radiochim. Acta* **2007**, 95, 433–438.

[6] Graser, C.-H.; Banik, N. L.; Bender, K. A.; Lagos, M.; Marquard, C. M.; Marsac, R.; Montoya, V.; Geckeis, H. *Anal. Chem.***2015**, 87, 9786–9794.

[7] Willberger, C.; Amayri, S.; Reich, T.: Redox speciation of neptunium using capillary electrophoresis coupled to ICP-MS. In S. Neumeier, P. Kegler & D. Bosbach (ed.), *8th European Summer School on Separation Chemistry and Conditioning as well as Supramolecular, Intermolecular, Interaggregate Interactions* (p. 59) **2014**, Jülich: Zentralbibiliothek, Verlag, ISSN: 0944-2952.

B-21

ThermAc - a collaborative project investigating aquatic chemistry and thermodynamics of actinides at elevated temperature conditions

Marcus Altmaier[1], Felix Brandt[5], Vinzenz Brendler[2], Ion Chiorescu[6], Elisenda Colas[7], Hilde Curtius[5], Francesco Endrizzi[1], Carola Franzen[2], Xavier Gaona[1], Mireia Grive[7], Seven Hagemann[4], Carsten Koke[3], Dmitrii A. Kulik[8], Sven Krüger[6], Jun-Yeop Lee[1], Martin Maiwald[3], Tres Thoenen[8], Petra J. Panak[3], Andrej Skerencak-Frech[3], Robin Steudtner[2]

[1]Karlsruhe Institute of Technology, Institute for Nuclear Waste Disposal (KIT-INE), Karlsruhe, Germany, [2]Helmholtz-Zentrum Dresden-Rossendorf, Institute of Resource Ecology, Dresden, Germany, [3]University of Heidelberg, Institute for Physical Chemistry, Heidelberg, Germany, [4]Gesellschaft für Reaktor und Anlagensicherheit (GRS), Braunschweig, Germany, [5]Jülich Research Center, Institute of Energy and Climate Research (IEK-6), Jülich, Germany, [6]Technische Universität München, Theoretical Chemistry, München, Germany, [7]Amphos21 Consulting, Barcelona, Spain, [8]Paul Scherrer Institute, Laboratory for Waste Management (PSI-LES), Villigen, Switzerland

The ThermAc project is extending the chemical understanding and available thermodynamic database for actinides, long-lived fission products and relevant matrix elements in aquatic systems at elevated temperatures. To this end, a systematic use of estimation methods, new experimental investigations and quantum-chemistry based information is used. ThermAc has started in March 2015 and is projected for three years, running until 28.02.2018. The project is funded by the German Federal Ministry for Education and Research (BMBF) and is coordinated by KIT-INE.

The ThermAc project is developed with the aim of improving the scientific basis for assessing nuclear waste disposal scenarios at elevated temperature conditions. Adequate scientific tools must be available to assess the related chemical effects and their impact upon safety. A clear focus of ThermAc is on long-lived actinides in oxidation states III, V and VI, with selected fission products and important redox controlling matrix elements like Fe also receiving attention. Tetravalent actinides and detailed investigations of redox processes are excluded from the current ThermAc work programme. ThermAc mainly addresses the temperature range from ~5°C up to ~90°C, focusing on systems at low or intermediate ionic strength. Chemical analogs for the actinide elements will be used, especially in order to gain information on solid phase transformation processes. Ion-interactions are treated with the Specific Ion Interaction Theory (SIT), in agreement with the approach favored by the NEA-TDB project. In addition to batch titrations and solubility investigations to obtain thermodynamic parameters, also various spectroscopic tools are used to identify species, their stoichiometry and structure. Quantum chemical calculations are used to support the interpretation of experimental findings, and establish a fundamental understanding of chemical effects on a molecular level.

Within the scope of ThermAc, a significant impact can be realized within a strong collaborative and integrated concept with the following strategic components:

(1) Systematic use of estimation methods for thermodynamic data and model parameters.

(2) Comprehensive experimental validation of the estimations.

(3) Fundamental studies for improved process understanding of actinide chemistry at elevated T.

(4) Comprehensive critical evaluation of the work performed within (1-3).

A key result from the comparison of predictions based upon estimation methods with new experimental data derived within ThermAc will be the assessment of the use of estimations methods to set up a workable thermodynamic database for elevated temperatures with high applicability to nuclear waste disposal issues. In this context it will be clarified, to which extent

systems will remain critical with regard to available thermodynamic data, and which relevant processes at elevated temperatures are still not sufficiently understood.

Acknowledgement: *This project has received funding from the German Federal Ministry for Education and Research (BMBF). KIT-INE is working under the contract 02NUK039A.*

B-22

Traces of Pu isotopes originated from burnt-up fuel in Fukushima exclusion zone

Renata Kierepko[1,2], Atsuyuki Sorimachi[3,4], Shinji Tokonami[4], Sarat Sahoo[1]

[1]Fukushima Research Headquarter, National Institute for Quantum and Radiological Science and Technology, Chiba, Japan, [2]Institute of Nuclear Physics, Polish Academy of Sciences, Krakow, Poland, [3]Department of Radiation Physics and Chemistry, Fukushima Medical University, Fukushima, Japan, [4]Institute of Radiation Emergency Medicine, Hirosaki University, Hirosaki, Japan

The accident in Fukushima Dai-ichi Nuclear Power Plant (FDNPP) released high activity of fission and neutron activation products in the environment. Total amount of released Pu is still unknown. Estimations so far indicates that dispersion from FDNPP is about 0.01 – 0.1 % of total Pu isotopes released from Chernobyl NPP accident. This implies activity of distributed Pu (for FDNPP) at the level GBq. It is assumed that more amounts might be deposited close to NPP in early April 2011. However, due to sequence of hydrogen explosion (Unit 3 contained MOX fuel rods) that caused emission of radioactive elements to the atmosphere and depending on meteorological conditions, a highly radioactive plume was moved on the north - western direction of FDNPP. As a consequence of coprecipitation on 15 March 2011, a large area was affected by wet deposition. The highly contaminated area, within 30 km radius of FDNPP was defined as an exclusion zone. This work focused on Pu isotopes as traces of non-volatile elements of burnt-up fuel which were dispersed and could be deposited on that area. Previous papers reported no significant increase of $^{239+240}$Pu activity and rather rarely provided information on ^{238}Pu activity concentration in samples from exclusion zone. In the present studies, hot spots (places with high dose rate above 2 μSv h^{-1}) in Namie district were selected. Samples of upper layer soil and plants were collected as well as mud from small “artificial collectors” of water like e.g. small dips below downspout of rain gutter, trench that was a part of road drainage system and dips in the road, etc. The activity level of caesium isotopes (^{134}Cs, ^{137}Cs) in collected samples reached value 5 MBq kg^{-1} (signature of high and relatively fresh contamination) while $^{239+240}$Pu and ^{238}Pu reached 0.3 Bq kg^{-1} and 0.5 Bq kg^{-1}, respectively. These values were significantly higher than average activity concentration of Pu in Japanese soil estimated as a 0.15 Bq kg^{-1}. The activity ratio, ^{238}Pu and $^{239+240}$Pu used as a sources marker, was determined as a 0.5 for Chernobyl accident. Our study reveals higher level of Pu activity ratio in some samples in exclusion zone. That indicates very well the nuclear burnt-up fuel non-volatile elements impact on sampling area. More results in details and their interpretation will be presented at the conference.

B-23

On the Raman Spectrum of Plutonium dioxide: vibrational and crystal electric field modes

Mohamed Naji[1], Nicola Magnani[1], Laura Bonales[2], Sara Mastromarino[1,3], Jean-Yves Colle[1], Joaquin Cobos[2], Dario Manara[1]

[1]European Commission, Joint Research Centre, Institute for Transuranium Elements (ITU), Karlsruhe, Germany, [2]Centro de Investigaciones Energéticas, Medioambientales y Tecnológicas (CIEMAT), Madrid, Spain, [3]Università degli di Roma La Sapienza, Rome, Italy

Raman spectrum of plutonium dioxide can have important applications in nuclear waste management, nuclear forensic and safeguard activities. The spectrum of plutonium dioxide (PuO_2) has been studied in a few research laboratories in the last couple of decades. It consists of only one triply degenerate T_{2g} (LO1, q = 0) Raman active vibrational mode, and one T_{1u} (LO2) forbidden mode. The latter is activated by Frenkel-type oxygen defects, as suggested in recent literature for an analogous mode predicted and observed in UO_2. However, the Raman spectrum of plutonium dioxide was reported up to higher Raman shift energies (beyond 1500 cm^{-1}) only recently. A few crucial features of the high-energy part of the PuO_2 Raman spectrum remain to-date unclarified, which has not permitted a satisfactory definition of a precise Raman fingerprint for PuO_2. Among those features, the most remarkable are two strong peaks consistently observed by Sarsfield et al. (Sarsfield, Taylor et al. 2012) at 2120 ± 10 cm^{-1} and 2620 ± 10 cm^{-1}. Despite some attempts, the nature of these two lines could not be clearly defined. Sarsfield et al. analysed in depth various possible attributions for them, both in terms of higher-order phonon combinations and surface impurity modes, but could not find any satisfactory assignment. Nevertheless, these authors suggested their assignment to excitations with electronic origin.

In this research, the Raman spectrum of plutonium dioxide has been studied both experimentally and theoretically. Particular attention has been devoted to the identification of the high energy modes, the attribution of which has so far been controversial. The experimental part of this study was carried out with the help of an original encapsulation technique which permits, for the investigation of this material, the use of different excitation laser sources (1.9 – 2.54 eV), and the employment of the triple subtractive spectrometer configuration. The first feature is important for the identification of resonant and electronic Raman bands; the second is necessary for the study of the anti-Stokes (AS) spectrum. In particular, the analysis of the AS spectrum in parallel to the Stokes one allowed us to reasonably estimate a temperature dependence of the observed Raman modes, especially the above-mentioned high-energy bands. Moreover, theoretical CF calculations performed in the present research soundly support the attribution of these high-energy lines to PuO_2 CF transitions. Such a conclusion, together with the already sound theoretical and experimental description of the vibrational part of the Raman spectrum, allows us to propose a consistent Raman fingerprint for plutonium dioxide.

B-24

Resonant Laser-SNMS on actinides for spatially resolved ultra-trace analysis

Clemens Walther[1], Hauke Bosco[1], Michael Franzmann[1,2], Linda Hamann[1], Mohammad Tanha[1], Klaus Wendt[2]

[1]Leibniz Universität Hannover, Institute for Radioecology and Radiation Protection, Hannover, Germany, [2]Johannes Gutenberg-Universität Mainz, Institute of Physics, Mainz, Germany

The transport mechanisms and geochemical behavior of actinides in natural systems is of major importance to evaluate their distribution in geological formations at contaminated areas and storage sites. The composition analysis and spatial imaging of hot particles, sorption on mineral surfaces and migration of trace concentrations of radionuclides requires an excellent suppression of organic background and isobaric contamination in combination with high spatial resolution while maintaining the natural structure of the sample.

The new resonant Laser-SNMS system at the IRS Hannover was developed to cover those specifications by combining the high element selectivity of resonance ionization with the non-destructive analysis of a static TOF-SIMS with spatial resolution down to 70 nm. This system was planned based on a test installation at the nuclear chemistry department of the University Mainz [1]. After the setup of a Ti:Sa laser system and the adaption of an IONTOF TOF.SIMS 5 for laser post-ionization we achieved a platform for a broad range of radioecological measurements.

The laser-ionization of a neutral particle cloud above the sample required a simulation of the expanding particles and a simulation based optimization of the TOF analyzer due to different ionization behavior. The results of this optimization were verified by a gain of laser ion signal and improved measurement conditions during several tests. The sensitivity was increased by almost one order of magnitude to about 1E-4 as demonstrated by measuring uranium in a 200 nl droplet of a 1 ppb uranium standard solution and by measuring well defined uranium spheres. The sensitivity will be further improved by a two stage extraction process. First mass spectra of synthetical uranium and plutonium samples demonstrated the expected suppression of interfering elements and molecules, which was confirmed with environmental samples. In MOX fuel Pu-238 and U-238 were successfully discriminated. Furthermore, with the ability to retrace the origin of the resonant laser ions, it was possible to create isotope selective images of environmental sample material. For preselection of sample material, the technique of alpha track analysis is applied and further refined for application on environmental bulk samples with a system capable to ablate few atomic layers and to detect on a single ions level.

We present first resonant Laser SNMS Measurements on Pu and U samples. Natural minerals from Afghanistan close to Kabul containing enhanced levels of natural radioactivity were characterized. First results on particles from the Chernobyl exclusion zone and from the evacuated zone close to the Fukushima Daichii nuclear power plant are presented.

References

[1] N. Erdmann, J.-V. Kratz, N. Trautmann, G. Passler, Analytical and Bioanalytical Chemistry, 2009, Volume 395, Number 6, Page 1911

B-25

On the Highest Oxidation State of Plutonium in Compounds

Jun Li

Theoretical Chemistry Center, Department of Chemistry, Tsinghua University, Beijing, China

The oxidation state is a central concept in chemistry [1,2]. The highest known oxidation state is +8, as exemplified in tetra-oxides MO_4 (M = Ru, Os, Hs, Xe) of group-VIII metal and less-inert noble gas. Despite claims of octavalent states of Pu and Cm in MO_4 compounds, whether or not such high oxidation state is stable for actinides is still unclear. We have investigated the electronic structures of PuO_4 PuO_nF_{8-2n}, PuS_4 and analogous complexes by using *ab initio* wavefunction theory and density functional theory [3-5]. It has been shown that the exotic low-spin high-oxidation state of Pu(VIII) is highly unstable against intramolecular electron transfer. The more common plutonyl$^+$ unit seems to be preferred with Pu(V) oxidation state, even in tetraoxygen species. We can conclude that the highest oxidation states An(VIII) of the actinides become more and more unlikely from uranium onward in the 5f actinoid series.

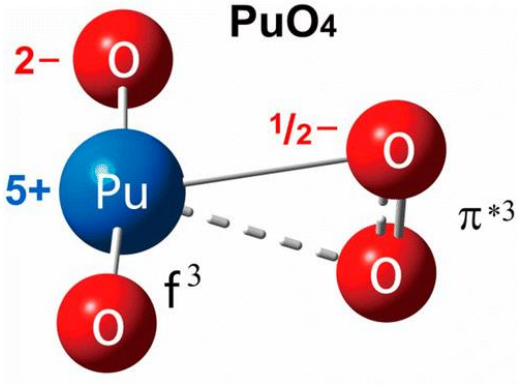

References

[1] P. Karen, P. McArdle, J. Takats, “Towards a Comprehensive Definition of Oxidation State (IUPAC Technical Report)”, *Pure Appl. Chem*. **2014**, *86*, 1017-1081.

[2] H. Xiao, H.-S. Hu, W. H. E. Schwarz, J. Li, "Theoretical Investigations of Geometry, Electronic Structure and Stability of UO_6: Octahedral Uranium Hexoxide and Its Isomers", *J. Phys. Chem. A* **2010**, *114*, 8837−8844.

[3] W. Huang, W.-H. Xu, J. Su, W. H. E. Schwarz, J. Li, "Oxidation States, Geometries, and Electronic Structures of Plutonium Tetroxide PuO_4 Isomers: Is Octavalent Pu Viable?", *Inorg. Chem*. **2013**, *52*, 14237-14245.

[4] W. Huang, P. Pyykko, J. Li, " Is octavalent Pu(VIII) possible? Mapping the series PuO_nF_{8-2n} (n=0-4)", *Inorg. Chem*. **2015**, *54*, 8825-8831.

[5] W. Huang, W.-H. Xu, W.H.E. Schwarz, J. Li, "On the Highest Oxidation States of Metal Elements in MO_4 Molecules (M = Fe, Ru, Os, Hs, Sm, and Pu)", *Inorg. Chem*. **2016**, *55*, 4616-4625.

B-26

Structural properties of plutonium systems revealed by high resolution XANES and RIXS techniques

Tonya Vitova

Karlsruhe Institute of Technology (KIT), Insitute for Nuclear Waste Disposal (INE), Karlsruhe, Germany

Advanced spectroscopy methods, which provide precise speciation, redox state, and electronic structure information, are needed to benchmark and drive improvement of geochemical/thermodynamic modeling and quantum chemical computational methods. Reliable speciation analyses and accurate determination of oxidation states of actinide elements (An) are essential in geochemical modelling codes, which coupled to thermodynamic databases are used to predict An reactivity under varying conditions.[1-3] One scenario under consideration in safety assessment studies of nuclear waste repositories is water intrusion and interaction with the waste matrix. The fate of any released An is predominantly governed by its redox state. Specifically for Pu it has been shown that up to four Pu oxidation states may coexist under environmentally relevant conditions, each having different potential migration pathways in the environment. It is also known that Pu(IV) has a high tendency towards hydrolysis, polymerization and subsequent colloid formation under environmental conditions, depending on the aqueous solution redox potential. These colloids are believed to be in equilibrium with ionic solution species and in this case are part of the thermodynamic system of Pu aqueous chemistry. However, their formation is still not well understood and their role for Pu redox chemistry remains controversial.

Fundamental understanding of the electronic structure of An is important to reveal why specific N-donor ligands used to separate An from lanthanide elements (Ln), such as n-Pr-BTP (2,6-bis(5,6-dipropyl-1,2,4-triazin-3-yl)pyridine), have high bonding affinity to trivalent An cations compared to their chemical homolog Ln(III).[4] Quantum chemical calculations are used to help predict An electronic structure and hybridization with N-donor orbitals to understand selectivity, as well as An properties: however, such calculations remain computationally challenging.[5-7] Using advanced spectroscopic methods to secure knowledge of An redox speciation and electronic structure can improve predicting An environmental behavior and provide benchmark data for improvement of quantum chemical codes.

High energy resolution XANES (HR-XANES) spectroscopy technique, also named high energy resolution fluorescence detected XANES (HERFD-XANES) or partial fluorescence yield XANES (PFY-XANES), has been extensively developed and applied over the last decade (see, for example [8]). Its application for speciation, redox state, and electronic structure investigations of An elements is recently gaining momentum. HR-XANES at the An $M_{4,5}$ and L_3 edges provide much more narrow spectral features compared to the conventional XANES, due to reduced contribution of core-hole lifetime broadening effects.[9-11] The HR-XANES therefore contains additional information, as it is rich in resolved resonant spectral features for specific An oxidation states.[10,12,13] The An $M_{4,5}$ edge HR-XANES probes directly the An valence unoccupied 5*f* states (3*d*→5*f*) and thus yields insight to the role these frontier orbitals play in hybridization with ligands and bond formation.[14]

The utility of HR-XANES spectroscopy technique in studies of An elements was the motivator for installing and commissioning a multi-analyzer Johann type X-ray emission (XES) spectrometer (MAC-spectrometer) at the INE-Beamline for actinide research at the ANKA synchrotron radiation facility, Karlsruhe, Germany.[11,15] The MAC-spectrometer is ultimately destined to be the central instrument at the radioactive end station of the newly constructed beamline for catalysis and actinide research (CAT-ACT-Beamline). Our set-up is optimized for An $M_{4,5}$ edge HR-XANES and XES/Resonant inelastic X-ray scattering (RIXS) experiments; absorption of 3-4 keV photons by air is minimized by a He environment enclosing sample, crystals, and detector, thereby enhancing efficiency. This instrument, combined with access to

the controlled laboratory at the Institute for Nuclear Waste Disposal (INE) in close proximity, is globally unique, enabling An $M_{4,5}$ edge HR-XANES and XES/RIXS investigations of solid and liquid phase radioactive materials, including under extreme conditions. Using the MAC-spectrometer at a dedicated beamline will facilitate discovery in studies of the transuranium elements, as presently HR-XANES and RIXS publications are mainly limited to uranium containing materials.[9,10,12-14,16]

The characterization capabilities of the Pu $M_{4,5}$ and L_3 edge HR-XANES technique will be highlighted by recent results obtained for both model and complex Pu materials studied at the INE-Beamline.

A number of examples for determination of Pu redox states in liquids and solid systems will be discussed. Comparison of U/Np/Pu M_4/M_5 HR-XANES spectra of UO_2^{2+}, NpO_2^{2+}, PuO_2^{2+} as well as Pu M_5/L_3 HR-XANES of various Pu oxidation states (Pu(III)-Pu(VI)) in aqueous solution will be presented. The changes of the Pu 5*f* and 6*d* unoccupied valence states and the energy shifts of the absorption edges of the spectra as a function of the additional electronic density on Pu upon reduction of Pu from P(VI) to Pu(III) will be revealed. It will be shown that the An *3d4f* RIXS spectra can be applied to detect the level of localization of 5*f* states across the An series. It will be demonstrated that the Pu L_3 edge HR-XANES is a suitable technique for detection of small changes in the Pu-O bond distances for plutonyl species. This is of particular interest for samples with Pu content below the limit of detection of EXAFS. The high sensitivity of the Pu $M_{4,5}$ edge HR-XANES technique compared to the Pu L_3 edge XANES/HR-XANES for detection of An oxidation states present in small amounts in mixtures will be highlighted. Results from characterization of Pu oxidation states in a highly active glass sample from the "Verglasungseinrichtung Karlsruhe" (VEK),[17] which contains vitrified high level liquid nuclear fuel reprocessing waste, and a glass simulate containing variable Pu loadings prepared in reducing and oxidizing conditions will be presented. The importance of the results will be discussed in terms of the strategy of using simplified simulates to understand more complex industrial glass samples and the knowledge targeted to predict the long term behavior of vitrified nuclear waste stored in a long term nuclear waste repository.

Acknowledgement

We acknowledge the Helmholtz Association of German Research Centers and the Karlsruhe Institute of Technology for the Helmholtz Young Investigators Group grant (VH-NG-734). The results are obtained in collaboration with Markus Altmaier, Sebastian Bahl, Paul Bagus, Kathy Dardenne, Melissa A. Denecke, David Fellhauer, Javier Gaona, Horst Geckeis, Ernesto Gonzalez-Robles, Bernhard Kienzler, Sylvain Peuget, Volker Metz, Ivan Pidchenko, Tim Prüßmann, Jörg Rothe, Joseph Somers.

References

1. Denecke, M. A. Coordin Chem Rev 2006, 250(7-8), 730-754.

2. Geckeis, H.; Lutzenkirchen, J.; Polly, R.; Rabung, T.; Schmidt, M. Chem Rev 2013, 113(2), 1016-1062.

3. Altmaier, M.; Gaona, X.; Fanghanel, T. Chem Rev 2013, 113(2), 901-943.

4. Panak, P. J.; Geist, A. Chem Rev 2013, 113(2), 1199-1236.

5. Moore, K. T.; van der Laan, G. Rev Mod Phys 2009, 81(1), 235-298.

6. Wen, X. D.; Martin, R. L.; Henderson, T. M.; Scuseria, G. E. Chem Rev 2013, 113(2), 1063-1096.

7. Neidig, M. L.; Clark, D. L.; Martin, R. L. Coordin Chem Rev 2013, 257(2), 394-406.

8. Bergmann, U.; Glatzel, P. Photosynth Res 2009, 102(2-3), 255-266.

9. Rueff, J. P.; Raymond, S.; Yaresko, A.; Braithwaite, D.; Leininger, P.; Vanko, G.; Huxley, A.; Rebizant, J.; Sato, N. Phys Rev B 2007, 76(8).

10. Vitova, T.; Kvashnina, K. O.; Nocton, G.; Sukharina, G.; Denecke, M. A.; Butorin, S. M.; Mazzanti, M.; Caciuffo, R.; Soldatov, A.; Behrends, T.; Geckeis, H. Phys Rev B 2010, 82(23).

11. Rothe, J.; Butorin, S.; Dardenne, K.; Denecke, M. A.; Kienzler, B.; Loble, M.; Metz, V.; Seibert, A.; Steppert, M.; Vitova, T.; Walther, C.; Geckeis, H. Rev Sci Instrum 2012, 83(4).

12. Vitova, T.; Denecke, M. A.; Göttlicher, J.; Jorissen, K.; Kas, J. J.; Kvashnina, K.; Prüßmann, T.; Rehr, J. J.; Rothe, J. Journal of Physics: Conference Series 2013, 430(1).

13. Kvashnina, K. O.; Butorin, S. M.; Martin, P.; Glatzel, P. Phys Rev Lett 2013, 111(25).

14. Vitova, T.; Green, J. C.; Denning, R. G.; Loble, M.; Kvashnina, K.; Kas, J. J.; Jorissen, K.; Rehr, J. J.; Malcherek, T.; Denecke, M. A. Inorg Chem 2015, 54(1), 174-182.

15. Walshe, A.; Prussmann, T.; Vitova, T.; Baker, R. J. Dalton T 2014, 43(11), 4400-4407.

16. Booth, C. H.; Medling, S. A.; Jiang, Y.; Bauer, E. D.; Tobash, P. H.; Mitchell, J. N.; Veirs, D. K.; Wall, M. A.; Allen, P. G.; Kas, J. J.; Sokaras, D.; Nordlund, D.; Weng, T. C. J Electron Spectrosc 2014, 194, 57-65.

17. Dardenne, K.; González-Robles, E.; Rothe, J.; Müller, N.; Christill, G.; Lemmer, D.; Praetorius, R.; Kienzler, B.; Metz, V.; Roth, G.; Geckeis, H. Journal of Nuclear Materials 2015, 460(0), 209-215.

B-27

Crystal dynamics of neptunium dioxide

Luigi Paolasini[1], Pablo Maldonado[2], Peter M. Oppeneer[2], Tom R. Forrest[3], Nicola Magnani[4], Alexei Bosak[1], Gerard H. Lander[4], Roberto Caciuffo[4]

[1]ESRF – The European Synchrotron, 71 avenue des Martyrs CS 40220, 38043 Grenoble cedex 9, France, [2]Department of Physics and Astronomy, Uppsala University, Box 516, S-75120 Uppsala, Sweden, [3]Diamond Light Source,, Harwell Science and Innovation Campus, Didcot Oxfordshire OX11 0DE, UK, [4]European Commission, JRC-ITU, Postfach 2340, D-76125 Karlsruhe, Germany

The energy-wavevector dispersion relation for normal modes of vibration propagating along high-symmetry lines in NpO_2 at room temperature has been determined by measuring the coherent one-phonon scattering of X-rays from a ~1.2 mg single-crystal specimen. The results are compared against ab initio phonon dispersion simulations computed within the first-principle density functional theory in the generalized gradient approximation plus Hubbard U correlation (GGA+U) approach, taking into account third-order anharmonicity effects in the quasi-harmonic approximation. Good agreement with the experiment is obtained for calculations with an on-site Coulomb parameter U = 4 eV and Hund's exchange J = 0.6 eV in line with previous electronic structure calculations. Thermal expansion, heat capacity, thermal conductivity, phonon linewidth, and thermal phonon softening are calculated and compared with available experimental data.

The inelastic X-ray scattering (IXS) experiment was carried out on a high-quality single crystal of NpO_2 using the ID28 beamline at ESRF with an incident energy E=17.794 keV, provided by a flat Si (999) perfect crystal back-scattering monochromators followed by a horizontally focusing multilayer. As severe sample photo-absorption is present, data have been collected in reflection geometry. A beam spot size of 30x80 μm^2 on the sample surface was obtained by using a multilayer focusing configuration. The sample of dimension of $0.4\times0.3\times0.3$ mm^3 was oriented with the specular direction along the (100) crystal axis and the (011) axis in the scattering plane. To avoid contamination of the environment, the crystal was encapsulated between two single crystal diamond slabs of $0.5\times5\times5$ mm^3 at the JRC Institute of Transuranium Elements in Karlsruhe. Examples of typical IXS constant-Q energy scans collected at room temperature are shown in Fig. 1. We have investigated different Brillouin zones in order to optimize the inelastic structure factor for the different optic branches. Optic phonons arise mainly from oxygen vibration modes and are very weak.

The good agreement of the experimental results with the ab initio calculated phonon dispersions indicates that the GGA+U approximation provides a good description of the phononic system, and allows for the study of its thermodynamic properties. The calculated heat capacity, bulk modulus, and thermal conductivity are in good agreement with the measured quantities. The failure in the description of the thermal expansion at high temperatures stresses the limitation of the quasi-harmonic approximation to study actinide oxides beyond ~ 1000 K. We show that optical phonons contribute significantly to the heat transport due mainly to their large velocities and short lifetimes. Compared with UO_2, the main differences in the phonon density of states are a softening of the optical modes and an increase of the peak centered around 55 meV, whereas the acoustic modes in NpO_2 are shifted to higher frequencies. The calculated value at 0 K of the bulk modulus in NpO_2 is in agreement with the experimental value and slightly smaller than the one determined by high-pressure X-ray diffraction for UO_2. NpO_2 has a smaller thermal conductivity than UO_2, at least in the temperature range 600 to 1000 K for which experimental values are available This is accounted for by our simulation, which overestimates the experimental value for NpO_2 by $\sim$20% at 600 K and underestimate it by ~1% at 1000 K [1].

The second part of the experiment was performed at low temperature (10 K) searching for phonon anomalies in the acoustic region below 15 meV. Indeed, according to previous work [2] in NpO_2 the magnetic dipole s are quenched in the ordered phase, and the primary order parameter is the rank-5 (triakontadipole) magnetic multipole. This exotic magnetic order is

accompanied by an order of electric quadrupoles that are arranged in a type-I, 3-k longitudinal structure. The ground-state quartet of the Np ions is split in the ordered phase, with a singlet-doublet-singlet sequence. The singlet-doublet and singlet-singlet single-ion transitions give rise to dispersive multipolar excitation branches centred around 6 and 13 meV. Similarly to what observed by inelastic neutron scattering in UO_2 [3], it is expected that a strong interaction between magnetic and vibrational modes occurs through the mediation of electric quadrupole fluctuations. This will affect the phonon acoustic modes centered around 13 meV and at 6 meV.

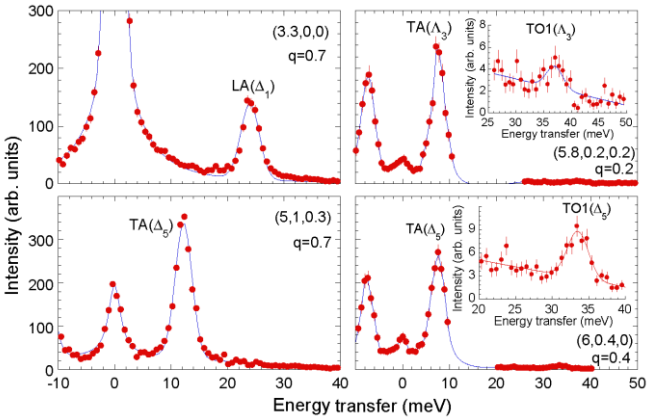

Figure 1. Examples of constant-Q inelastic X-ray scattering energy scans collected at room temperature for NpO_2 around different Brillouin zone centres. The intensity data are in arbitrary units but have been scaled for the same factor. To be noticed is the difference in intensity between acoustic and optic phonon modes.

We have measured the LA (6-ζ, 0, 0), TA (6, ζ, 0) and TA (5, -1, ζ) phonon branches at 10 K. Whereas the LA phonon intensities decreases smoothly from the zone centre to the zone boundary, as expected from the first-principle phonon calculations (that provide an excellent match to the measured dispersion curves), the two measured TA branches present an anomaly at the reduced wavevector ζ = 0.8, reflected in a drastic loss of intensity of the corresponding phonon group, as shown in Fig. 2 for the TA (6, q, 0) branch. This wavevector corresponds to about 13 meV, exactly where the theoretical prediction assumes the existence of dispersive mean-field magnetic modes. This issue will be the subject of further investigations on ID28 in order to check whether the intensity anomaly is an experimental artefact or if it really related to the order of the magnetic triakontadipoles.

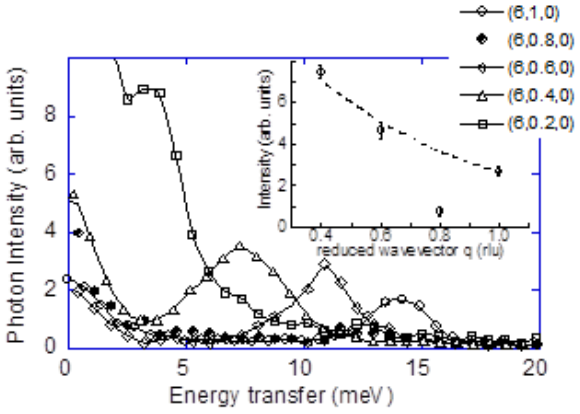

Figure 2. Intensity evolution of the transverse acoustic (6, ζ, 0) branch showing a drastic decrease of the intensity of the phonon group at ζ = 0.8 rlu (black dots). Notice also that the (610) is a Brillouin zone boundary. The inset shows the q dependence of the phonon group integrated intensity.

References

[1] P. Maldonado *et al.*, *Phys. Rev. B.* **93**, 144301 (2016)

[2] P. Santini *et al., Phys. Rev. Lett.* **97**, 207203 (2006)

[3] R. Caciuffo *et al., Phys. Rev. B.* **84**, 104409 (2011)

B-28

Study of the 5f electronic states in uranium-plutonium mixed oxides using high resolution XANES

Philippe Martin[1], Michal Strach[1], Damien Prieur[2], René Bès[3], Renaud C. Belin[4], Dario Manara[2], Christophe Valot[1], Tonya Vitova[5], Tim Prussmann[5], Kathy Dardenne[5], Jörg Rothe[5]

[1]CEA, DEN, DTEC, Centre d'études nucléaires de Marcoule, Bagnols-sur-Cèze F-30207, France, [2]European Commission, Joint Research Centre, Institute for Transuranium Elements, , P.O.Box 2340, D-76125 Karlsruhe, Germany, [3]Antimatter and Nuclear engineering, Department of applied Physics, Aalto University, Finland, [4]CEA, DEN, DEC, Centre d'études nucléaires de Cadarache, Saint Paul lez Durance, F-13115, France, [5]Karlsruhe Institute of Technology (KIT), Institute for Nuclear Waste Disposal, P.O. Box 3640, D-76021 Karlsruhe, Germany

Uranium−plutonium mixed oxide fuels $U_{1-y}Pu_yO_{2-x}$ are currently studied within the frame of the fourth generation (GEN-IV) of nuclear reactors and more specifically for sodium-cooled fast neutron reactors (SFRs). GEN-IV's main purpose is to manage more efficiently the energetic resources by recycling valuable actinides such as U and Pu from spent nuclear fuels. Because of their specific neutronic spectrum, SFRs will also be able to burn long-lived minor actinides (MAs) such as Am, Np, and Cm recovered from used fuel. This could lead to a drastic decrease in both radiotoxicity and heat load of ultimate wastes favoring the ecological footprint of their final disposal [1]. In such complex mixed oxide systems, both the homogeneity of the cation distribution into the fluorite UO_2 structure and the oxygen stoichiometry significantly affects most of the fuel properties (thermal conductivity, melting temperature, diffusion phenomena, etc.) [2–5]. Furthermore, the americium valence state in $U_{0.54}Pu_{0.45}Am_{0.01}O_{2-x}$ mixed oxides is directly affected by the cation distribution homogeneity [6].

These properties depend mainly on the complexity of U and Pu electronic structures, in particular the unfilled actinide 5f and 6d valence shells. A theoretical modeling and predictions of the electronic structure behavior remains challenging in such system and need to be supported by experimental observations.

An element-selective probe to study the electronic structure of actinides is provided by X-ray spectroscopy at core thresholds. Up to now, X-ray Absorption Near Edge Spectroscopy (XANES) at the L_{III} edge has been the most commonly reported method to determine the oxidation states of U, Pu, Np and Am in mixed oxides [7–10]. However, despite their relative low energy range (3-4 keV) which is now mainly offset by the high photon flux available, experiments at the $M_{4,5}$-edge are increasingly reported because such edges allow direct probing of the 5f orbitals. Nevertheless, the accuracy is strongly limited by the core-hole broadening of the $2p_{3/2}$ (> 8 eV) and $3d_{3/2,5/2}$ (> 3 eV) initial states at the L_{III} and $M_{IV,V}$-edges, respectively. These values prevent to observe the expected small electronic structure modifications induced by the plutonium incorporation within the UO_2 lattice [11] using standard XANES collected on $(U,Pu)O_{2.00}$ samples.

To overcome the latter difficulty, an emission spectrometer can be used to collect High Energy Fluorescence Detected XANES (HERFD-XANES) allowing the collection of spectra with a virtually reduced core-hole [12,13]. A reduction from 3-4 eV to less than 1 eV at the actinide's $M_{IV,V}$-edges can be so obtained [14]. Such experimental set-up is now available at the INE beamline [15,16] located at the synchrotron source ANKA (Karlsruhe, Germany) and application of HERFD-XANES on highly radioactive materials such as $(U,Pu)O_2$ is now possible.

To our knowledge, we report here the first HERFD-XANES measurements at uranium M_{IV} and plutonium M_V edges collected on $(U,Pu)O_2$ samples. The samples were prepared by a co-grinding process that involves direct co-milling of UO_2 and PuO_2 powders described in Ref. [17]. The humidity was adjusted to prepare stoichiometric materials, so as to obtain monophasic $(U_{1-y}Pu_y)O_{2.00}$ solid solution [18] with y ranging from 0.25 to 0.62.

In Figure 1, the HERFD-XANES spectra collected at Pu M_{IV} edge on $(U,Pu)O_{2.00}$ are compared to $Pu(+IV)O_2$ and $Pu(+III)PO_4$ [19] reference compounds. As expected, the presence of a

Pu(+III) fraction can be discarded as the spectra collected on $U_{0.54}Pu_{0.46}O_{2.00}$ and $U_{0.38}Pu_{0.62}O_{2.00}$ samples are aligned to the PuO_2 spectra. Nevertheless, a broadening of the main peak located at ~3775.5(2) eV compared to PuO_2 can be observed for the two MOX samples. The latter would be due to the modification of the plutonium empty 5f states induced by the formation of the $(U,Pu)O_{2.00}$ solid solution.

In figure 2, the HERFD-XANES spectra collected on UO_2 and MOX samples at U M_{IV} edge are shown. No broadening of the main peak located at ~3725.5(2) eV is observed. But, a clear shift to higher energy as a function of the Pu content of the main peak is observed. A partial oxidation of U^{4+} cation to U^{5+} and/or U^{6+} can be excluded because as illustrated by HERFD-XANES results obtained on UO_2, U_4O_9 and U_3O_8 [14] this would had led to the presence of a supplementary peak instead of an energy shift. Similarly to plutonium edge, these HERFD-XANES could be due to the modification of the uranium 5f states induced by the substitution of uranium by plutonium in the $(U,Pu)O_2$ solid solution.

The energy resolution achieved by using an emission spectrometer at $M_{IV,V}$ edges of the actinide allows to observe experimentally the modification of the electronic structure of both uranium and plutonium 5f valence states induced by the introduction of plutonium within the UO_2 lattice in $(U,Pu)O_{2.00}$ compounds. These results will be compared to theoretical calculations.

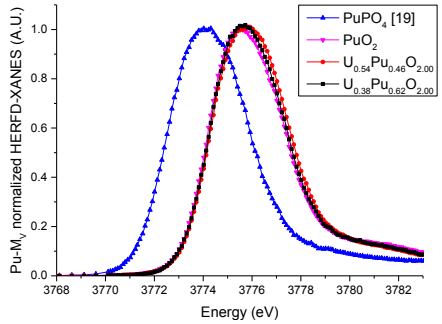

Figure 1: Plutonium-M_V HERFD-XANES

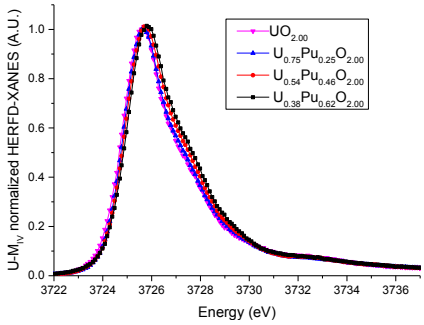

Figure 2: Uranium-M_{IV} HERFD-XANES

References

[1] S. Pillon, 3.05 - Actinide-Bearing Fuels and Transmutation Targets, in: R.J.M. Konings (Ed.), Compr. Nucl. Mater., Elsevier, Oxford, 2012: pp. 109–141.

[2] F. De Bruycker et al., J. Nucl. Mater. 419 (2011) 186–193.

[3] M. Beauvy, J. Nucl. Mater. 188 (1992) 232–238.

[4] Y. Philipponneau, J. Nucl. Mater. 188 (1992) 194–197.

[5] C. Duriez et al., J. Nucl. Mater. 277 (2000) 143–158.

[6] R. Vauchy et al., J. Nucl. Mater. 456 (2015) 115–119.

[7] J.-F. Vigier et al., Inorg. Chem. 54 (2015) 5358–5365.

[8] D. Prieur et al.,J. Nucl. Mater. 434 (2013) 7–16.

[9] M. Chollet et al., J. Alloys Compd. 662 (2016) 448–454.

[10] R. Vauchy et al., Inorg. Chem. 55 (2016) 2123–2132.

[11] K.O. Kvashnina et al., Anal. Chem. 87 (2015) 8772–8780.

[12] J.-P. Rueff et al., J. Electron Spectrosc. Relat. Phenom. 188 (2013) 10–16.

[13] P. Glatzel et al., Catal. Today. 145 (2009) 294–299.

[14] K.O. Kvashnina, S.M. Butorin, P. Martin, P. Glatzel, Phys. Rev. Lett. 111 (2013) 253002.

[15] T. Vitova et al., J. Phys. Conf. Ser. 430 (2013) 012117.

[16] J. Rothe et al., Rev. Sci. Intrum. (2012) 043105.
[17] T. Truphémus et al., J. Nucl. Mater. 432 (2013) 378–387.
[18] R.C. Belin et al., J. Nucl. Mater. 465 (2015) 407–417.
[19] K. Popa et al., J. Solid State Chem. 230 (2015) 169–174.

C-01

Pu-238 and the Pu sustainment work at Los Alamos

David L. Clark

Los Alamos National Laboratory, Los Alamos, NM, USA

The first isotope of plutonium to be discovered was ^{238}Pu, produced in 1940 by bombarding uranium with deuterons. Its short half-life (87.7 yr) was conducive to tracer studies that allowed its separation and identification. Today, ^{238}Pu is readily obtained by neutron bombardment of ^{237}Np, and separated by ion exchange techniques.

^{238}Pu has found important application in radioisotope power systems – nuclear power systems that derive their energy from the heat produced by spontaneous decay, as distinguished from nuclear fission. Most radioisotope power systems use ^{238}Pu as an isotope heat source. We describe here an overview of the production, purification, component fabrication, actual applications, and disposal of this very important isotope.

By far, the most prevalent application has been for space and interplanetary exploration. For this application, heat source fuel is enriched to 83.5% in ^{238}Pu isotope, and oxygen atoms in $^{238}PuO_2$ are enriched in ^{16}O to reduce the neutron emission rate to as low as 6000 n/s/g. The ^{238}Pu isotope provides 99.9% of the thermal power in heat source fuel. Radioisotope Thermoelectric Generators (RTGs) have been used in the United States to provide electrical power for spacecraft since 1961 in Space Nuclear Auxiliary Power (SNAP) units to power satellites and remote instrument packages on the moon. Early SNAP units were powered with plutonium metal. Voyager missions employed Multihundred Watt Radioisotope Thermoelectric Generators (MHW-RTGs) that consisted of 24 100-W heat sources of $^{238}PuO_2$. The current systems employ General Purpose Heat Sources (GPHS) of hot pressed 150g pellets of $^{238}PuO_2$.

C-02

^{241}Am Production for Use in Radioisotope Power Systems

Catherine Campbell[1], Cheryl Carrigan[1], Michael Carrott[1], Chris Maher[1], Bliss McLuckie[1], Chris Mason[1], Colin Gregson[1], Tamara Griffiths[1], Josh Holt[1], Mark Sarsfield[1], Robin Taylor[1], Tim Tinsley[1], Keith Stephenson[2]

[1]National Nuclear Laboratory, Sellafield, UK, 2European Space Agency, Noordwijk, The Netherlands

The Voyager 1 space probe has left our solar system and will continue to send valuable scientific data back to earth until at least 2020. Despite being 20 billion km away the probe still has enough power to transmit signals from interstellar space because of the plutonium-238 (^{238}Pu) battery it carries.

^{238}Pu is used as a power source for space probes, orbiters and rovers and is proven as an effective source of power where the use of solar generated power is impractical. Historically, Europe has relied on collaborations with the USA and Russia to access these nuclear power sources, however, during 2009 the European Space Agency (ESA) funded a project to examine the cost and practicality of European produced Radioisotope Power Systems (RPS). The study concluded that a small number of radioisotopes could be of practical use in RPSs either as Radioisotope Heating Units (RHUs); for use in Radioisotope Thermoelectric Generators (RTGs) or in a Stirling Radioisotope Generator (SRG). On further review two leading candidates, ^{241}Am and ^{238}Pu, were selected for a more detailed study. Whilst ^{238}Pu was recognized as the isotope of choice for use in RPSs, the costs of establishing a European based production facility for ^{238}Pu was deemed prohibitively expensive. The radioisotope ^{241}Am was identified as a potential alternative to ^{238}Pu because of its availability within the nuclear fuel cycle, despite its lower power density of ~ 0.11 W_{th}/g, (around ¼ that of ^{238}Pu materials).

During the reprocessing of spent nuclear fuel, plutonium is separated as a chemically pure plutonium dioxide (PuO_2) product and placed into storage, containing around 3-11% w/w of the ^{241}Pu isotope. During storage the ^{241}Pu isotope beta decays to ^{241}Am with a half-life of 14.4 years.

$$^{241}_{94}Pu \xrightarrow{\beta \ 14.4y} {}^{241}_{95}Am$$

Reprocessing of spent nuclear fuel has resulted in the creation of hundreds of kg of ^{241}Am that is constantly growing into the civil plutonium stockpile in the UK. Over the past few years a process for separating ^{241}Am from PuO_2 was defined and a concept production plant designed, based on a mass balance flowsheet. Experimental underpinning of the flowsheet was required to provide a proof-of-concept and then developed to technology readiness level (TRL) 5 by operating at full scale americium (4.8g/L) and plutonium (96 g/L) concentrations. This development work culminated in a process that efficiently separates ^{241}Am from PuO_2 powder providing an americium product of high purity (> 99%) and at high recovery (> 99.9%), while generating a plutonium product that is less radioactive and easier to fabricate into new mixed oxide (MOx) fuel.

A series of trials where the americium nitrate product is converted to americium oxalate and then decomposed to produce americium oxide were also performed to establish optimal powder properties. This americium oxide material is then used to produce ceramic pellets and comments will be made on the challenges associated with high temperature sintering of this material.

C-03

Studies Related to the Fabrication of $^{238}PuO_2$ Ceramic Fuel Pellets and the Surrogate CeO_2

Daniel Kramer

University of Dayton, Dayton, Ohio, USA

Since the development of radioisotope thermoelectric generators (RTGs) at Mound Laboratories (Miamisburg, Ohio) over fifty years ago, several different fuel forms have been employed for the application of the radioisotope ^{238}Pu. Since plutonium-238 in its elemental state has several disadvantages, the fuel currently employed for deep space missions by the U.S is an oxide – $^{238}PuO_2$. $^{238}PuO_2$ in the form of ceramic pellets have supplied all of the thermal energy for radioisotope powered spacecraft launched in the U.S. over the last ~20 years. These spacecraft/missions include Cassini/Saturn (NASA/ESA - 17 nations - launched 1997 and now in its 2nd extended mission), New Horizons/Pluto (launched 2006 - Pluto flyby July 2015), and the Mars rover Curiosity (launched 2011 - landed Aug 2012) which utilizes the latest U.S. RTG called an MMRTG (Multi-Mission Radioisotope Thermoelectric Generator).

The current MMRTG contains 32 $^{238}PuO_2$ ceramic fuel pellets which provide all of the thermal energy that is converted into electrical power for the rover Curiosity. The process steps used in the fabrication of $^{238}PuO_2$ fuel pellets utilize a number of classical ceramic fabrication techniques including ball milling, sieving, compaction, hot pressing, and sintering. The various ceramic processing parameters are carefully controlled (i.e. t-T-P) which results in $^{238}PuO_2$ fuel pellets which have the required physical and mechanical properties that meet/exceeds all of the required safety and operational parameters. Since $^{238}PuO_2$ is highly radioactive, great care needs to be taken in the performance of all of the ceramic processing operations to ensure personnel safety.

The application of a non-radioactive surrogate material, for performing various ceramic developmental processing endeavors in support of space nuclear power efforts, would result in reduced personnel exposure, and a significant reduction in associated costs. Over the last several years there have been a number of ceramic based processing studies performed utilizing CeO_2 as a surrogate material for PuO_2. CeO_2 is also being investigated since it has many expected physical and chemical properties similar to PuO_2 in terms of crystal structure, general oxidation behavior, etc. As with any surrogate material there are limitations on how well the selected material truly mirrors the actual material of interest. Besides the large radiological differences between CeO_2 (which is non-radioactive) and a $^{238}PuO_2$ fuel pellet (which is highly radioactive and which produces ~0.41W_{th}/gram), several other differences have recently been observed during ceramic pellet processing experiments which may limit the application of CeO_2 as a ceramic processing surrogate for $^{238}PuO_2$. A discussion of some aspects of $^{238}PuO_2$ pellet processing/modeling and the application of CeO_2 as a $^{238}PuO_2$ surrogate will be presented.

C-04

Redox Stability and Separation Chemistry of Actinyl Cations Coordinated by Schiff Base Ligands

Christiain Bustillos[1,2], Roy Copping[2,3], Andrew Gaunt[2], Cory Hawkins[1,4], Iain May[2], Mikael Nilsson[1], Sean Reilly[2], Brian Scott[2]

[1]Department of Chemical Engineering and Materials Science, University of California, Irvine, CA, USA, [2]Science, Technology and Engineering, Los Alamos National Laboratory, Los Alamos, NM, USA, [3]Medical Radioisotope Program – Isotope Development Group, Oak Ridge National Laboratory, Oak Ridge, TN, USA, [4]Chemistry Department, Tennessee Tech University, Cookeville, TN, USA

Introduction

The actinyl cations of uranium, neptunium and plutonium dominate the +V and +VI oxidation state chemistry of these actinide elements. Typically these linear dioxo moieties ($\{AnO_2\}^{+}$/$\{AnO_2\}^{2+}$) are sterically demanding and only allow coordination around the equatorial plane of the metal center. Conveniently, Schiff base ligands are typically tetra- or penta-dentate and can readily coordinate around the equatorial plane of uranyl(VI), with structural and spectroscopic characterization of a suite of complexes reported. Furthermore, it has been shown that such ligands can stabilize uranyl(V), a moiety that can readily disproportionate to uranyl(VI) and uranium(IV) in most solutions. A few examples of the application of Schiff base ligands for uranyl(VI) extraction, and of neptunyl(V) and neptunyl(VI) coordination, indicate a broader applicability of Schiff base coordination.[1] It is in this context that we now report a summary of U(VI), Np(VI), Np(V), Pu(VI) and Pu(V) chemistry in the presence of selected Schiff base ligands, both organic soluble and aqueous soluble (Fig. 1). Our particular focus was on developing separation processes where the presence of the Schiff base altered conventional actinyl solvent extraction chemistry, and on our attempts to control actinyl(VI/V) redox chemistry.

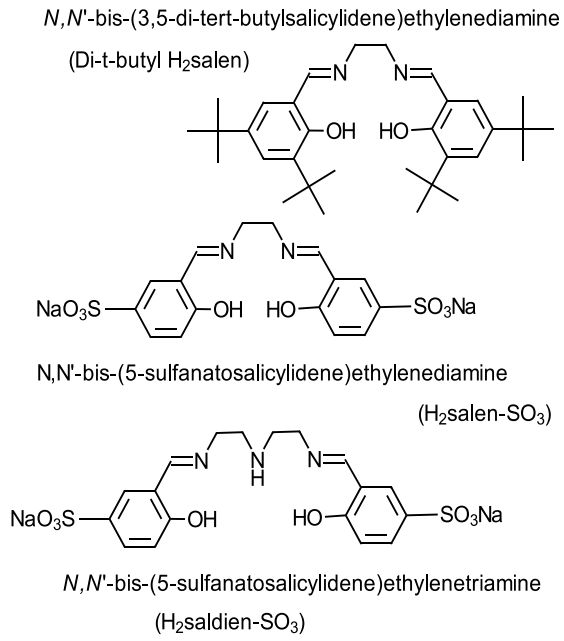

Fig. 1. Schiff base ligands used in these actinyl complexation and solvent extraction studies.

Experimental

All three ligands were synthesized following conventional organic synthesis techniques, with many of the details associated with the solvent extraction experiments and the uranium spectroscopic and structural measurements previously reported.[2] Synthetic, spectroscopic and structural neptunium and plutonium chemistries were performed using techniques refined for previous Np and Pu coordination chemistry projects.[3]

Results and Discussion

The di-t-butyl H_2salen ligand shown in Fig. 1 will readily deprotonate and coordinate to actinyl(VI) cations in organic solvent, with isostructural complexes structurally characterized for $\{UO_2\}^{2+}$, $\{NpO_2\}^{2+}$ and $\{PuO_2\}^{2+}$. A structural representation of the Pu(VI) complex is shown in Fig. 2, with classical tetradentate coordination observed around the equatorial plane of the $\{PuO_2\}^{2+}$ moiety through coordination by the two imine nitrogens and two deprotonated phenolic oxygens. A 5th equatorial site is occupied by an acetonitrile molecule.

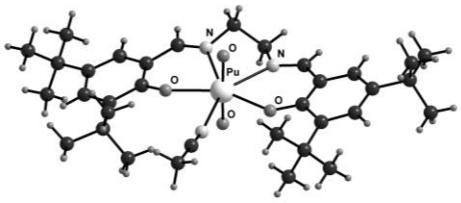

Fig 2. Structural representation of PuO_2(di-t-butyl-salen)(CH_3CN).
Only the Pu, N & O atoms have been labelled, for clarity.

Competitive solvent extraction experiments were performed with U(VI) and a lanthanide cation, Dy(III), using di-t-butyl H_2salen as the extractant in the organic phase (1-octanol/toluene) and ethylenediaminetetraacetic acid (EDTA) in the aqueous phase. The contrasting steric demands of the two cations assisted in the selective extraction of the actinyl cation in this system, with the lanthanide cation remaining in the aqueous phase post-contact.

Sulfonato functionalization allows for aqueous phase solubility of Schiff base ligands (Fig. 1), with both 4- and 5- coordinate ligand systems studied. While the coordination chemistry with actinyl cations remains unchanged, as evidenced through structural characterization of uranyl(VI) complexes, there are changes in redox stability *vs.* organic soluble species. Both H_2salen-SO_3 and H_2saldien-SO_3 will reduce Np(VI) to Np(V), and coordinate the $\{NpO_2\}^{+}$ moiety. In contrast, Pu(VI) can be stabilized by H_2salen-SO_3 but we were unable to stabilize Pu(V).

Switching from an organic soluble Schiff base ligand to aqueous soluble Schiff base ligands allows for the design of a different set of solvent extraction experiments. With the Schiff base ligand now in the aqueous phase, and HDEHP (bis(2-ethylhexyl)phosphoric acid) in the toluene organic phase a significant change in f-element extraction chemistry could be observed. For H_2salen-SO_3 partial ligand hydrolysis and ligand mediated reduction of Np(VI) to Np(V) add complications to data analysis. Despite these complications the trend is clear, selective H_2salen-SO_3 'hold-back' of the two actinyl cations greatly enhances the separation of U & Np from trivalent Eu and Cm (Fig. 3).[2] This is a reversal of extraction behavior for both uranyl(VI) and neptunyl(V) in this conventional solvent extraction system.

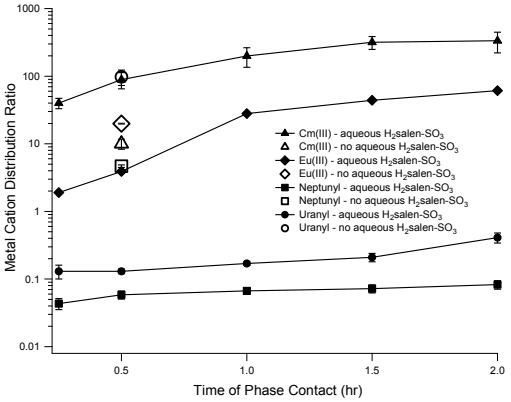

Fig. 3. Distribution ratios at various phase contact times for uranyl(VI) (depleted uranium), neptunyl(V/VI) (^{237}Np), Eu(III) ($^{152/154}$ radiotracer) and Cm(III) (^{244}Cm). The aqueous phase contained H_2salen-SO_3 in mildly acidic solution and the organic phase contained HDEHP in toluene.

Acknowledgements

This work was supported by the University of California under the UCOP Grant ID# 12-LF-237294, a grant that was awarded jointly to UC Irvine and Los Alamos National Laboratory. In addition, C.G. Bustillos acknowledges the support of the Los Alamos National Laboratory Seaborg Institute for Summer Research Fellowships. Los Alamos National Security, LLC, operates Los Alamos National Laboratory for the National Nuclear Security Administration of the Department of Energy under contract DE-AC52-06NA25396.

References

[1] See, for examples, (a) Hardwick, H.C.; Royal, D.S.; Helliwell, M.; Pope, S.J.A.; Ashton, L.; Goodacre, R.

and Sharrad, C.A. *Dalton Trans.* 2011, **40**, 5939-5992. (b) Chguryan, D.G.; Dzyubenko, V.I.; Grigor'ev, M.S.; Yanovskii, A.I. and Struchkov, Yu.T. *Radiokhimiya*, 1988, **30**, 41-46. (c) Sahu, S.K. and Chakravortty, V. *J. Radioanal. Nucl. Ch*. 1998, **227**, 163-165. (d) Takao, K. and Ikeda, Y. *Inorg. Chem.* 2007, **46**, 1550-1562. (e) Copping, R.; Mougel, V.; Den Auwer, C; Berthon, C.; Moisy, P.; Mazzanti, M. *Dalton Trans.* 2012, **41**, 10900-10902.

[2] (a) Hawkins, C.A.; Bustillos, C.G.; Copping, R.; Scott, B.L.; May, I. and Nilsson, M. *Chem. Commun*. 2014, **50**, 8670-8673. (b) Hawkins, C.A.; Bustillos, C.G.; Copping, R.; May, I. and Nilsson, M. Actinide and Fission Product Partitioning and Transmutation, Thirteenth Exchange Meeting, Seoul, Republic of Korea 23-26 September 2014, NEA/NSC/R(2015)2, 315-323. (c) Hawkins, C.A.; Bustillos, C.G.; May, I.; Copping, R.; Nilsson, M. submitted for review, *Dalton Trans*.

[3] Berg, J.M.; Gaunt, A.J.; May, I.; Pugmire, A.L.; Reilly, S.D.; Scott, B.L.; Wilkerson, M.P. *Inorg. Chem.* 2015, **54**, 4192-4199.

C-05

Actinide Polyrotaxanes: From Hydrothermal Synthesis to Structural Regulation

Wei-Qun Shi

Laboratory of Nuclear Energy Chemistry, Institute of High Energy Physics, Chinese Academy of Sciences, Beijing, China

Metal-organic materials with dynamic components, such as mechanically-interlocked rotaxane molecules (MIMs), integrate the attractive feature of flexibility into rigid frameworks as well as broad functionalities. Among plenty of rotaxane-based coordination polymers, transition metal ions and lanthanide ions have been intensively studied due to their rich coordination patterns and availabilities. However, polyrotaxanes containing actinide cations, such as uranyl or thorium cations, have been never reported. Hence, we are currently pursuing the preparation of actinide polyrotaxanes from uranyl cation and pseudorotaxanes ligands containing cucurbituril. This effort has finally succeeded to produce a series of uranyl polyrotaxanes with a rich library of structures from one dimension to three dimensions. Moreover, we found that the diversity of topologic structures is in close relationship with the direction role of different uranyl secondary building units.

C-06

PuF_4 Lattice Effects Due to Aging

Amanda Casella, Calvin Delegard, Kaylyn McCoy, Bruce McNamara, William Karl Pitts, Sergey Sinkov

Pacific Northwest National Laboratory, Richland, WA, USA

In 1971 approximately 150 grams of PuF_4 were set aside for use as a neutron source to detect the aqueous-organic interface in solvent extraction operations. This material was doubly-encapsulated, preserving the PuF_4 sample in a hermetic environment for approximately 40 years when it was repackaged to retrieve the original material. Degradation effects in the PuF_4, initially observed by a muting of the expected tan-pink color were confirmed by loss of detail in the diffuse reflectance spectrum and lack of crystalline structure, aside from that of trace PuO_2, on x-ray diffraction. Optical and scanning electron microscopy with energy dispersive spectroscopy were also performed on the sample to characterize morphology and sample composition.

This presentation will summarize the characterization results of the 45 year old PuF_4 sample and describe findings from thermal annealing which appear to restore some of the crystalline structure as verified by x-ray diffraction and restoration of the expected sample color.

C-07

The Kinetic Evolution of Self-Irradiation Damage in Face-Centered Cubic Pu-Ga Alloys

Franz Freibert

Los Alamos National Laboratory, Los Alamos, NM, USA

There is little doubt that the alpha decay process of Pu results in significant impact when hosted in a solid. In face-centered cubic (FCC) Pu-Ga metal alloys the impact of self-irradiation includes changes at the atomic scale to include accumulation of daughter products (i.e., U, He, Np and Am) and changes at the bulk scale to include thermo-physical and mechanical properties changes. However, there is little to no understanding for how the mechanistics of the decay cascade, which occurs on the nanosecond temporal scale over micrometer spatial scale, evolves as lattice disruption and damage via kinetic and energetic processes.

In other FCC metals (i.e. steels, Al alloys, etc.), displacements introduced into the lattice via a decay cascade produces Frenkel pairs and other point defects. As Frenkel pairs diffuse and extended defects form, absorption at existing sinks or in the matrix typically lead to damage accumulation and void swelling. However, in Pu-Ga alloys there has been observed little in the way of damage accumulation and no void swelling. Previously, the behavior of Pu aging related volume swelling to saturation has been well-described by a first order differential relationship of Pu-decay damage production balanced against thermal annealing in the form $\Delta V/V_o = A[1-exp(-Bt)]$.[1] In that model, A is a function of the decay rate, defect volume and the alloy composition; and B is an Arrhenius function describing the activation energy for the lattice recovery process scaled by an atomic hopping frequency. Here point defects responsible for the volume increase result directly from the damage cascade without evolution to extended defect structures.

Although effectively utilized, this model has been replaced by a more universal expression provides greater insight into Pu aging and defect evolves under a broader set of kinetic and energetic processes over range of time and temperature. The Johnson-Mehl-Avrami (JMA) equation applied in the form $X(t,T) = A[1-exp(-Ct^n)]$ is a more useful expression which applies to generalized Time-Temperature-Transformation (TTT) diagrammatic descriptions of kinetic processes and phase transformation. [2] Here C and n are a geometric growth function and Avrami exponent, respectively; which better account for accounts for the kinetic evolution of extended defect structures that in this formalism can be viewed in this formalism as a second phase. Damage ingrowth data when fitted to the JMA form reveals the energetics and time dependency of formation increase with increasing Ga composition, likely associated with the contraction of the lattice with increasing composition. Furthermore, a Ga compositional dependent crossover behavior to a time independent process is revealed. At sufficiently high temperatures, annealing occurs likely via extended defect dissociation and bulk recombination of Frenkel pairs at traps, sinks or in the matrix all leading to damage annihilation and finally to lattice recovery. Once again, when this phenomenon is analyzed by way of the JMA quantification of the TTT diagram description, energetics and time dependency of these recovery processes are revealed.

Included in this presentation will be a brief description of the JMA model in light of the TTT diagram. Furthermore, parameters obtained from volume expansion data fitted to the JMA model will be discussed as a means to explore kinetic evolution of Pu self-irradiation lattice modifications and to explain various aspects of damage accumulation and recovery in FCC Pu-Ga metal alloys.

References:

1) Freibert, F. J., J. N. Mitchell, D. S. Schwartz, A. Migliori, “Radiogenic-Thermally Coupled Lifetimes in Defects of Aged δ-phase Pu-Ga Alloys;” ANS Conference: Plutonium Future 2014 - Proceedings of a Topical Conference on Plutonium and Actinides; September 7-12, 2014; Las Vegas, NV.

2) Martin, J. W., R. D. Doherty, and B. Cantor. (1997). Stability of Microstructure in Metallic Systems, Cambridge University Press, pg. 183.

C-08

Oxidation study of Pu stabilized in δ-phase

Brice Ravat, Lionel Jolly, Benoît Oudot, François Delaunay

CEA - VALDUC, Is-sur-Tille, France

Introduction

To improve our knowledge of plutonium oxidation related to safe and long term storage, the reactivity of a highly metastable δ-Pu alloy was studied under controlled atmosphere composed of dry or wet oxygen atmosphere at different temperatures. The originality of this work lies in an *In situ* X-ray diffraction (XRD) analysis performed during the oxidation process enabling the phase identification as well as the characterization of the oxides growth kinetics.

Experimental details

In situ X-ray diffraction (XRD) analyses were performed under dry and wet atmospheres of O_2 during different isothermal holds using a temperature chamber (TTK 450 Anton Paar®) installed in a θ/θ diffractometer (BRUKER AXS D8 Advance®) placed inside a glove box. The oxide surfaces were also examined by scanning electron microscopy at the end of exposure.

Description of the original model of Rietveld analysis develop for oxides thickness assessment

In order to be able to analyze the microstructure of the Pu oxides, the recorded diffraction diagrams were analyzed using a novel method based on a modified Rietveld refinement. Indeed, whereas classical Rietveld refinement is adapted to phase mixture analysis, this approach enables to assess the thickness of the staked layers considering the absorption mass coefficients of the different observed phases. More precisely, the thickness determination of each layer is based on the analysis of the discrepancy of the theoretical (structure factor) and observed peak diffraction intensities in the recorded X-ray diagram resulting from the variation of beam absorption with the incidence angle. This formalism was developed and integrated into the TOPAS5 software enabling a full profile refinement.

Phase analysis after exposure under O_2 atmosphere

Before oxidation kinetics studying, analysis of the nature of Pu oxides occurring during oxidation process was first performed. As an illustration, a typical X-ray diagram recorded during an isothermal hold at 150°C (valid for dry and wet O_2 atmospheres exposure) is given in Fig. 1. Phase analysis has confirmed the presence of PuO_2 and Pu_2O_3 occurrence during oxidation process. The polymorphic character of Pu_2O_3 was also evidenced since the analysis of XRD diagrams has revealed the cubic and hexagonal (co-called α and β phases) crystallographic structures of the sesquioxide. But on the other hand, the observation of the occurrence of the body-centered monoclinic structure of Pu corresponding to the stable phase of pure Pu at 150°C was absolutely unexpected. Indeed the destabilization of the δ-phase resulting from oxidation was never reported in the literature. It may be connected to the emergence of an area depleted on δ-stabilizer element at the alloy-oxides interface involving the activation of solute diffusion occurring during the oxidation process.

Oxidation kinetics analysis under dry oxygen atmosphere

In-Situ X–ray diffraction analyses coupled to the innovative method of Rietveld refinement enabled to characterize the oxidation kinetics by following individually the growth of each phases occurring during the oxidation process. As example, Fig.2 shows the oxides layers thicknesses against time for the isothermal hold of 150°C for 120 hours under a dry atmosphere of 100 mbar of O_2. The obtained results confirm that the total oxide thickness curves exhibit a paralinear behaviour (related to oxygen diffusion activation into the material) at the beginning of oxidation progress as mostly observed in early works thanks to microbalance monitoring the reaction. The individual behaviour analysis of each phase allows us to highlight that this paralinear evolution is mainly connected to the growth of the α-Pu_2O_3 layer since β-Pu_2O_3 contribution remains relatively slight and the PuO_2 layer is very thin at the beginning of oxidation. We can also deduce that the Pu β-phase occurrence seems to be linked to the Pu_2O_3 emergence. Then after 60 hours of exposure the total oxide thickness increase results essentially from the increase in the PuO_2 layer since the thickness of other phases seem to saturate.

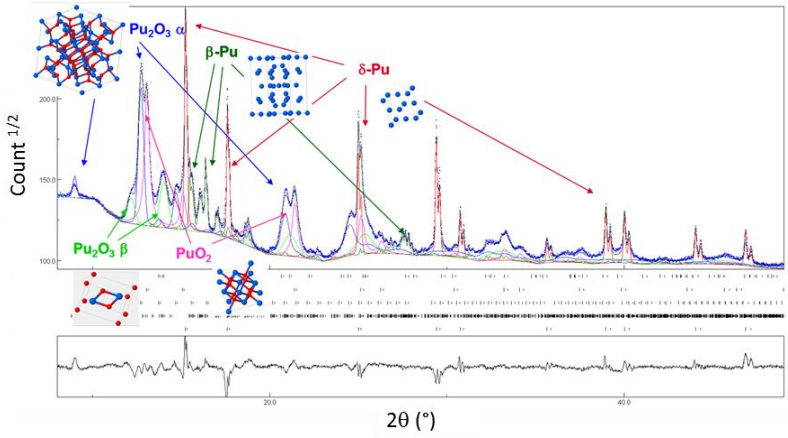

Fig. 1: Analysis of X-ray diffraction diagram revealing the presence of PuO_2, α and β Pu_2O_3 , as well as Pu β-phase after an isothermal hold of 150°C for 120 hours under a dry atmosphere of 100 mbar of O_2.

Influence of wet atmosphere and temperature on the oxidation kinetics

Under same O_2 pressure and temperature conditions, wet atmosphere causes a breakaway in the oxidation kinetics as shown in Fig 3 involving water molecules in the acceleration of the oxidation rate. This acceleration of oxidation process is exclusively linked to the PuO_2 layer growth. Further SEM analyses have revealed the presence of surface spalling. Lattice parameter analysis of α-Pu_2O_3 layer also has showed an increase in a compressive stress which consequently could be at the origin of the surface cracking and subsequently promoting the acceleration of the oxidation rate. Finally, the temperature appears to be an accelerating factor of the oxidation rate as well.

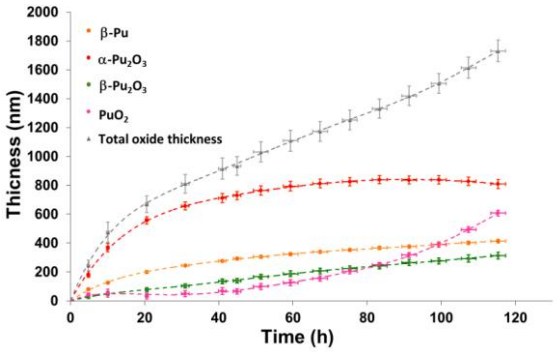

Fig. 2: Thickness of PuO_2, α and β Pu_2O_3 , as well as Pu β-phase deduced from X-Ray diffraction analysis during the isothermal hold of 150°C for 120 hours under a dry atmosphere of 100 mbar of O_2.

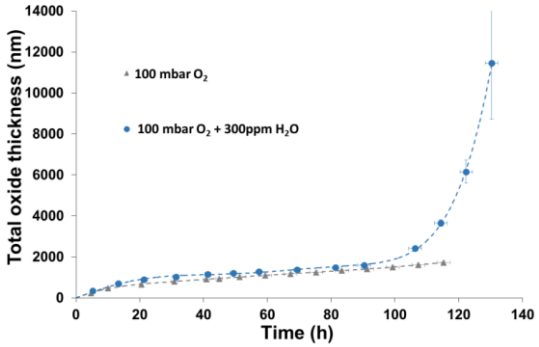

Fig. 3: Total oxide thickness deduced from X-Ray diffraction analysis during the isothermal hold of 150°C for 120 hours under a dry and wet atmosphere.

C-09

Water interactions with actinide oxide surfaces

Bengt Tegner[1], Andrew Kerridge[2], Nikolas Kaltsoyannis[1]

[1]The University of Manchester, Manchester, UK, [2]Lancaster University, Lancaster, UK

The interactions between water and the actinide oxides UO_2 and PuO_2 are important when considering the long-term storage of spent nuclear fuel. However, experimental studies in this area are severely limited by plutonium's intense radioactivity, and hence we have recently begun to investigate these interactions computationally. In this contribution we will report the results of first principles calculations of the electronic and geometric structures of AnO_2 bulk and AnO_2 surfaces (An = U, Np, Pu), as well as the interaction of water with the latter. Strongly-correlated effects are taken into account using a Hubbard corrected potential, which enables us to perform efficacious plane-wave density functional calculations of extended systems. In particular, we will compare results of water adsorption on AnO_2 (111), (110), and (100) with the corresponding results on CeO_2, focusing on the energetics and structural properties of molecular versus dissociative adsorption, for both partially and fully covered surfaces.

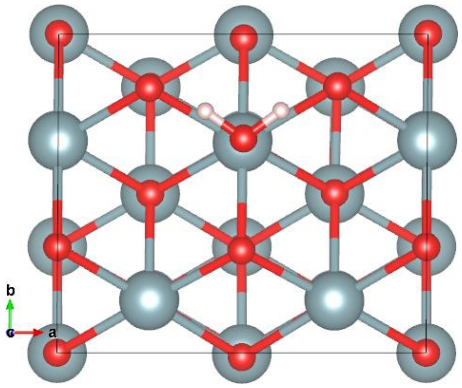

Figure 17 Single water molecule adsorbed on the UO_2 (111) surface. Uranium atoms are grey, oxygen atoms are red and hydrogen atoms are pink.

C-10

How does Pu(IV) interact with hyperphosphorylated protein osteopontin ?

Gaëlle Creff[1], Hervé Michel[1], Jérôme Roques[3], Claude Vidaud[2], Christophe Den Auwer[1]

[1]ICN-Université de Nice Sophia Antipolis, Nice, France, [2]CEA Marcoule, Bagnol-sur-Cèze, France, [3]IPN-Université Paris Orsay, Orsay, France

In case of release of actinides in the environment, contamination of the living organisms can occur and induce radiological and chemical toxicities. Whatever the way of integration, the radioelement is absorbed, and then either directly excreted, or transported by blood, linking with different biological ligands toward target organs [1]. Once absorbed by the organs, the radioactive heavy element might take the place of essential elements by chemical or steric analogy (calcium and iron for example), leading to serious alterations of the organ function. Excretion rates and the nature of the target organs depend on the radioelement itself and its speciation. While at the macroscopic scale many studies have described the impact of such elements on animals, quantified the excretion and the retention rates and identified the main target organs, information concerning the mechanisms of transport, accumulation and storage at the molecular level still remain very scarce [2]. This deficiency in terms of data comes from the difficulty to combine the actinide chemistry (strong tendency to hydrolysis) with the physiological conditions. But the need for mechanistic data at the molecular level is essential to go towards a deeper understanding of toxicological processes related to actinides and to propose new solutions for cure.

Regarding the possible target organs and based on several different studies, the bone matrix appears as a privileged target for most of the actinides[i]. The objective of our research work is to elucidate the mechanisms of interaction of actinides with the bone matrix at the molecular scale. The bone is a complex system composed of a cellular matrix and an extra cellular matrix (ECM), presenting a mineral and an organic phase. The organic part of ECM is composed of various proteins, including osteopontin (OPN). This hyper-phosphorylated and non-structured macromolecule, which has recently been identified, is particularly important in the process of osteogenesis [3] and might play a crucial role in the *in vivo* accumulation of actinides in the regions of bone growth, capable of inducing bone cancer [4]. Moreover it is well known that actinides present a very strong chemical affinity for phosphate groups, whether from organic or mineral origin. We have studied the interaction of the OPN protein in solution with the actinides at oxidation state (IV) because they present the highest affinity for bone matrix (it retains 70% of Th(IV), 50% of Pu(IV) and 30–50% of Np(IV) while only 10 to 15% of U(VI)), more precisely with Pu(IV) and Th(IV), the latter being a less radioactive surrogate with simpler RedOx chemistry (therefore more easily manipulable than all the other actinides (IV)).

For that purpose, we have implemented a combination of experimental and theoretical techniques among which X-ray Absorption Spectroscopy (XAS) combined with density functional theory calculations (DFT) and attenuated total reflection Fourier transform infrared (ATR-FTIR) in order to determine the local organization around the An(IV) cation.

Firstly, we studied the interaction of Th(IV) with OPN. The results evidenced an important interaction of the cation with the phosphoryl groups which is qualitatively in agreement with the macroscopic observation concerning the retention rate of thorium by the bone matrix [5]. Preliminary ATR-FTIR spectroscopic analysis performed on a reduce mimetic peptidic sequence of the protein showed a complexation by both carboxylates, through a bidentate coordination, and phosphates functions. DFT calculations were also performed for the Th(IV)-peptide complex and in agreement with IR spectroscopic data. The Th(IV) coordination sphere is composed of one bidentate carboxyl group and two monodentate phosphoryl groups with characteristic distances of 3.06 Å between the thorium atom and the carbon and 3.88 Å between the thorium atom and the phosphorus. Four water molecules complete the coordination sphere of the cation in order to bring the thorium coordination number to 8.

Surprisingly, the Pu(IV) coordination sphere appears rather different than for Th(IV) (figure 1). In particular, we noticed a difference for the contributions above 3Å which are attributed to

phosphorus atoms. This observation seems to indicate a smaller interaction of Pu(IV) than Th(IV) for the peptide and OPN phosphate functions. A detailed discussion on the two coordination modes will be proposed. Impact of the experimental conditions (as pH) on the structure will also be presented.

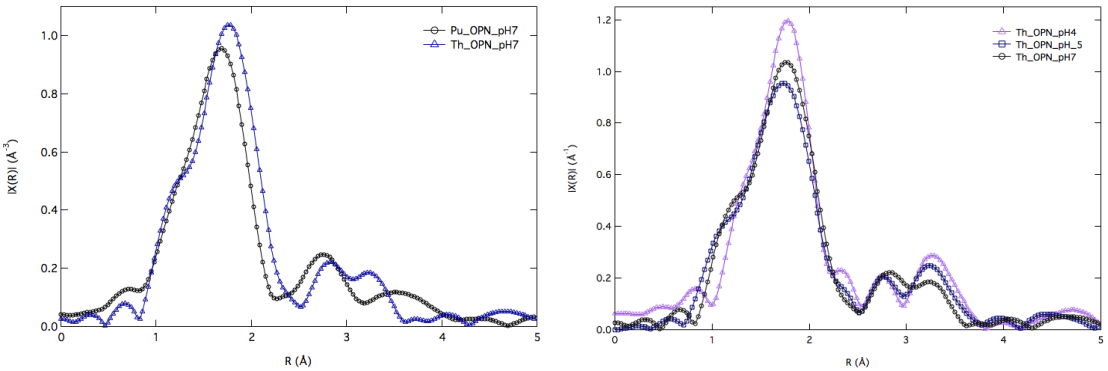

Figure 1a : FT of EXAFS signal for Pu(IV)-OPN and Th(IV)-OPN complexes in solution at pH 7; 1b FT of EXAFS signal for Th(IV)-OPN complexes in solution at different pH values.

In order to complement this structural data, a study at the actinide trace scale with OPN at pseudo physiological conditions has been performed. We used size dependent micro filtration combined with alpha spectrometry and ICP-HRMS to determine the plutonium and thorium behaviors respectively towards OPN uptake. This approach complements the structural data with pseudo physiological conditions that can mimic possible Pu(IV) contamination. Partition data obtained with α spectrometry for ^{238}Pu(IV) at trace scale (100 Bq/L or 0.16 ppt) in aqueous solution at physiological pH are summarized in table 1. Data for the ^{238}Pu(IV)-OPN, ^{238}Pu(IV)-BSA and ^{238}Pu(IV)-blank samples are compared. This demonstrates, although qualitatively, the affinity of Pu(IV) for OPN and not for BSA. The results will be discussed in comparison with the data obtained for Th(IV) using ICP-HRMS.

	protein free Pu (filtrate)		protein-Pu complex (filter)		Total	
Sample description	%^{238}Pu	error (%)	%^{238}Pu	error (%)	%^{238}Pu	error (%)
control Pu:NTA = ε:1	80.0	4.6	4.0	2.4	84.0	5.2
Pu:NTA:BSA = ε:1:0.2	83.7	4.3	2.9	1.4	86.6	4.5
Pu:NTA:BSA = ε:1:10	75.3	3.6	12.1	3.4	87.4	5.0
Pu:NTA:OPN$_f$ = ε:1:10	9.9	0.6	76.6	5.4	86.5	5.5

Table 1 Partition percentage of ^{238}Pu(IV) calculated from ^{238}Pu(IV) activity in each sample: filtrate or filter (deduced from alpha spectrometry peaks integration) and ^{238}Pu(IV) activity initially added in the protein solution. The stoichiometry is given in mole fractions with respect to 1 NTA molecule; ε represents ^{238}Pu(IV) at the trace scale starting with 100 Bq/L (or 6.62 10^{-13} mole/L).

Table 1 Partition percentage of ^{238}Pu(IV) calculated from ^{238}Pu(IV) activity in each sample: filtrate or filter (deduced from alpha spectrometry peaks integration) and ^{238}Pu(IV) activity initially added in the protein solution. The stoichiometry is given in mole fractions with respect to 1 NTA molecule; ε represents ^{238}Pu(IV) at the trace scale starting with 100 Bq/L (or 6.62 10^{-13} mole/L).

In conclusion, the present work is an elucidation of the interaction mechanisms of Pu(IV) with human OPN protein. It highlights the role of phosphorylated domains in the complexation mechanisms. It also underlines the structural differences between Pu(IV) and Th(IV) although the latest is considered as a chemical surrogate of Pu(IV).

References:

[1] A. F. Eidson, *Health Physics*, 1994, **67**, 1-14.

[2] P. W. Durbin, *Actinides in animals and man, in The chemistry of the actinide and transactinide elements*, 4th edition, L. R. Morss, N. M. Edelstein, J. Fuger, J. J. Katz, Ed. Springer, 2011, Vol. 5, p. 3339

[3] J. Sodek, B. Ganss and M. D. McKee, *Critical Reviews in Oral Biology & Medicine*, 2000, **11**, 279-303.

[4] C. Vidaud, D. Bourgeois, D. Meyer, *Chem. Res. Toxicol.*, 2012, **25**, 1161.

[5] G. Creff, S. Safi, J. Roques, H. Michel, A. Jeanson, P-L Solari, C. Basset, E. Simoni, C. Vidaud, C. Den Auwer*, Inorg. Chem.*, **2016**, 55, 29–36.

C-11

Self-assembly of plutonium sulfate dimers from a chloride matrix

Amy Hixon, Ginger Sigmon

University of Notre Dame, Notre Dame, IN, USA

Introduction

Plutonium sits near the middle of the actinide series and marks the transition from early to late actinide elements. Thorium, uranium, and neptunium, which lie to the left of plutonium, have delocalized electrons and are similar to transition metals in their chemistry whereas the elements heavier than plutonium have localized electrons and behave similarly to the lanthanide elements. The electrons associated with plutonium appear to be neither fully localized nor delocalized, challenging our understanding of the nature of chemical bonding in heavy element compounds and complexes. In addition, there is a general lack of information on solid state plutonium complexes and the relationship between solid- and aqueous-phase coordination chemistry, which hinders the development of accurate chemical models.

We report the synthesis and single crystal structures of two Pu(IV) sulfate complexes synthesized in the presence of potassium sulfate salts in dilute hydrochloric acid. A comparison of these structures with similar thorium, uranium, and neptunium sulfate structures will shed light on trends across the early actinide series and serve as a basis for future studies with late actinide elements.

Methods

$K_{12}[Pu_2Cl_6(SO_4)_4]_2$ **(1)**: 100 µL of a 50 mM Pu(IV) stock solution was added to 75 µL of 0.1 M K_2SO_4 in a glass vial. The vial was covered with parafilm and small holes cut in the parafilm to allow for slow evaporation. Within one week, large orange crystals formed. Crystals were selected for single crystal X-ray diffraction, as described below.

$K_8Pu_2(SO_4)_8 \cdot 5H_2O$ **(2)**: 100 µL of a 50 mM Pu(IV) stock solution was added to 200 µL of 0.5 M K_2SO_4 in a glass vial. The vial was covered with parafilm and small holes cut in the parafilm to allow for slow evaporation. Within one week, large orange crystals formed. Crystals were selected for single crystal X-ray diffraction, as described below.

Single Crystal X-ray Diffraction: Single crystals of **1** and **2** were picked by hand and mounted on a Bruker Quazar single crystal X-ray diffractometer for structure determination.

Results

The compound $K_{12}[Pu_2Cl_6(SO_4)_4]_2$ **(1)** crystallizes in the monoclinic space group $P2_1/n$ with unit cell a = 7.295(4) Å, b = 13.933(8) Å, c = 12.862(8) Å, and β = 99.62(1)°. The structure consists of an eight-coordinate Pu(IV) center bonded to three sulfate tetrahedra (two edge sharing and one vertex sharing) and three chlorine atoms (see Figure 1a). Two of the sulfate tetrahedra form a bridge to a second Pu(IV) center to form a dimer. Potassium atoms found between the dimers provide charge balance. A brief search of the literature and of the Inorganic Chemistry Structural Database (ICSD) suggests that this is the first dimer to contain both sulfate and chlorine.

Increasing the potassium sulfate concentration yields the compound $K_8Pu_2(SO_4)_8 \cdot 5H_2O$ **(2)**, which crystallizes in the monoclinic space group $P2_1/c$ with unit cell a = 12.363(2) Å, b =

11.125(2) Å, c = 13.467(2) Å, and β = 111.71(2)°. In contrast to compound **1**, compound **2** exhibits nine-fold coordination of the Pu(IV) center; the bridging sulfate groups in both dimers are similar. Although the single crystal structure of **2** was previously reported by Wilson (2011), we report here a new synthetic route to its formation from solution. Whereas Wilson (2011) synthesized compound **2** from a Pu(IV)-sulfate stock solution and potassium sulfate, we report synthesis of an identical compound from a Pu(IV)-chloride stock solution and potassium sulfate.

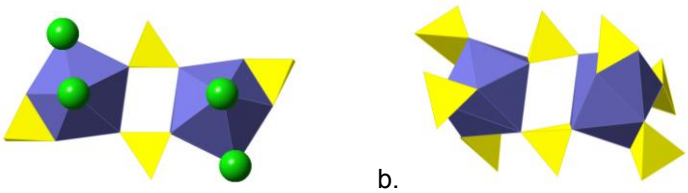

Fig. 1: a) shows the $K_{12}[Pu_2Cl_6(SO_4)_4]_2$ dimer, b) shows the $K_8Pu_2(SO_4)_8 \cdot 5H_2O$ dimer. Plutonium, chloride, and sulfate are depicted in blue, green, and yellow, respectively.

Sulfate dimers have also been reported for thorium and uranium. Schnaars and Wilson (2012) crystallized a U(IV) dimer structure identical to compound **2** with various alkali metal cations. A slightly varied dimer is found for thorium. In $Na_{10}[Th_2(SO_4)_9(H_2O)_2]3H_2O$ two thorium centers are bridged by only one sulfate tetrahedron in a vertex-sharing configuration (Albrecht et al., 2011). Although no crystallographic studies have been performed on Np(IV) sulfates, aqueous-phase investigations show that Np(IV) will bond with sulfate in both edge- and vertex-sharing modes (Hennig et al., 2008). This suggests that changes in coordination environment occur across the early actinides and highlights the need for further research in this area.

Summary

Here we report the single crystal structures and synthesis of two Pu(IV) sulfate dimers synthesized in the presence of potassium sulfate in hydrochloric acid. Current synthetic efforts are focused on producing other alkali metal plutonium sulfate materials and on identifying the chloride:sulfate ratio that represents the transition from a mixed plutonium dimer (i.e., one containing both sulfate and chloride) to a sulfate-only dimer.

Acknowledgements

This work is supported by the Office of Basic Energy Sciences of the U.S. Department of Energy as a part of the Materials Science of Actinides Energy Frontier Research Center (DE-SC0001089).

References

Albrecht, A.J.; Sigmon, G.E.; Moore-Shay, L.; Wei, R.; Dawes, C.; Szymanowski, J.; Burns, P.C. The crystal chemistry of four thorium sulfates. *J Solid State Chem* **2011**, *184*, 1591-1597.

Hennig, C.; Ikeda-Ohno, A.; Tsushima, S.; Sheinost, A.C. The sulfate coordination of Np(IV), Np(V), and np(VI) in aqueous solution. *Inorg Chem* **2009**, *12*, 5350-5360.

Schnaars, D.D.; Wilson, R.E. Uranium(IV) sulfates: Investigating structural periodicity in the tetravalent actinides. *Inorg Chem* **2012**, *51*, 9481-9490.

Wilson, R.E. Structural periodicity in plutonium(IV) sulfates. *Inorg Chem* **2011**, *50*, 5663-5670.

C-12

Coordination polymers of tetravalent neptunium with aromatic polycarboxylate ligands

Nicolas Martin[1], Juliane März[2], Natacha Henry[1], Christophe Volkringer[1,3], Atsushi Ikeda-Ohno[2], Christoph Hennig[2], Thierry Loiseau[1]

[1]Université de Lille, Lille, France, [2]Helmhotz Zentrum Dresden Rossendorf, Dresden, Germany, [3]Institut Universitaire de France, Paris, France

Coordination polymers are organic-inorganic complexes built up from the association of metallic centers with O- or N-donor ligands. In the particular case of actinides, previous literatures mainly have reported the synthesis of solid networks bearing U(VI) or Th(IV). Trans-uranium elements have been much less studied due to their high radiotoxicity and limited amount of the material source. Among the possible oxidation states of actinides (An), the tetravalent state has been investigated most actively and large polynuclear oxo-clusters have been isolated for U[1,2] or Pu[3]. In contrast, there is very few data concerning Np(IV) compounds. In 2012, Takao *et al.*[4] reported the presence of a hexanuclear cluster of Np(IV) in an aqueous solution, which is the only polyoxo cluster reported for Np(IV) thus far. The knowledge of the formation of such polynuclear An(IV) species could be of significant importance for the fate of An in contaminated soils containing O-donor ligands, such as humic acids or organic pollutants (e.g. phthalates).

In the present work, we studied the crystallization of Np(IV) with various aromatic polycarboxylate ligands in different solvents and analyzed their crystal structures. In water, an infinite chain of $Np_2O_2(H_2O)_2(1,2\text{-bdc})_2$ were isolated in the presence of phthalate. This compound crystallizes as aggregates of orange plates, whereas the analogue compound with uranium is obtained as green crystals. With mellitic acid the oxidation of Np(IV) to Np(V) was observed and led to large green plates. Single-crystal XRD analysis revealed layers of $\{NpO_7H_2O_{0\text{-}2}\}$ units linked to each other *via* trans-dioxo neptunyl bonds. Similar coordination environments have been observed in the other neptunium(V) compounds[5].

The use of other solvents allowed the crystallization of large polynuclear discrete Np(IV) clusters. For example, using DMF, the hexanuclear unit of $[Np_6O_4(OH)_4]$ has been obtained with different dicarboxylic ligands and is the basic building unit to form an open-framework structure (Figure 1, left). The corresponding structures revealed for the first time the isolation of the hexanuclear cluster An_6O_8 with Np(IV). These clusters are linked by the ligand creating tetrahedral and octahedral voids in the structure.

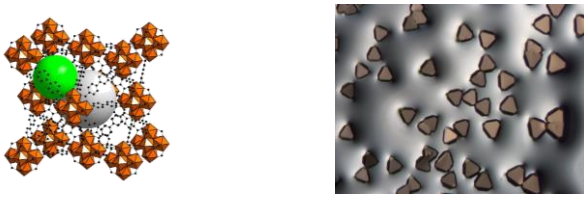

Figure 1 : View of the structure (left) and optical microscope picture (right) of $[Np_6O_4(OH)_4L_6(H_2O)_6]$

References

1 C. Falaise, C. Volkringer, J. F. Vigier, A. Beaurain, P. Roussel, P. Rabu, T. Loiseau, *J. Am. Chem. Soc.* 2013, **135**, 15678.

2 B. Biswas, V. Mougel, J. Pécaut, M. Mazzanti, *Angew. Chemie - Int. Ed.*, 2011 **50**, 5745.

3 L. Soderholm, P. M. Almond, S. Skanthakumar, R. E. Wilson, P. C. Burns, *Angew. Chemie - Int. Ed.* 2008, **47**, 298.

4 K. Takao, S. Takao, A. C. Scheinost, G. Bernhard, C. Hennig, *Inorg. Chem.* 2012, **51**, 1336.

5 I. A. Charushnikova, N. N. Krot, Z. A. Starikova, *Radiochemistry* 2001, **43**, 492.

C-13

Plutonium Oxide Processing Platform for Nuclear Forensics Applications

David Meier, Joel Tingey, Gregg Lumetta

Pacific Northwest National Laboratory, Richland, WA, USA

The National Technical Nuclear Forensics Center (NTNFC) within the Domestic Nuclear Detection Office (DNDO) of the Department of Homeland Security (DHS) has funded a domestic national laboratory to establish both laboratory scale (up to 200 g Pu per batch) and bench-scale (up to 10 g Pu per batch) capabilities to produce plutonium oxide (PuO_2) for use in identifying and validating nuclear forensics signatures associated with the chemical processing of plutonium oxide. The laboratory scale system is being developed in three glove boxes within a Category-II nuclear facility in the United States. This capability will be a flexible processing system used quarterly on various flow sheets associated with the plutonium nitrate precipitation methods including Pu(III) and Pu(IV) oxalate. The bench-scale system has been established in a series of gloveboxes within the same facility on the PNNL campus and its functionality was demonstrated with plutonium procured from a national laboratory in February 2016 The following unit operations are included in both systems: 1) dissolution of as-received PuO_2, 2) purification of the Pu nitrate solution by anion exchange, 3) concentration of the purified Pu nitrate solution by evaporation, 4 precipitation, and 5) thermal conversion of precipitated plutonium species to PuO_2. This paper and presentation will describe the development efforts for establishing the laboratory scale and the bench scale efforts as well as the preliminary characterization of the product materials using various analyses.

C-14

Production of Plutonium-238 for Deep Space Missions

Robert Wham

Oak Ridge National Laboratory, Oak Ridge, TN, USA

The Department of Energy (DOE) is responsible for maintaining the national capability to support the design, development, production, deployment and safety of Radioisotope Power Systems (RPSs) for National Aeronautics and Space Administration (NASA) and national security missions. DOE and its predecessor agencies have been producing radioisotope power systems for over fifty years. Radioisotope power systems uniquely enable missions that require a long-term, unattended source of electrical power and/or heat in harsh and remote environments. These systems are reliable, maintenance–free, and capable of producing heat and electricity for decades. ^{238}Pu serves as the heat source for all RPS launched by the United States.

Radioisotope Power Systems have enjoyed highly successful use in the United States, having been used on 27 space missions to date. NASA, in partnership with DOE, has deployed RPSs on breathtaking missions to the Moon, Mars, and the outer planets. Four active RPS-powered missions continue to provide information at Mars, Saturn, Pluto, and beyond the boundary of our Solar System.

The ^{238}Pu production process consists of the fabrication of neptunium-237 (^{237}Np) targets, irradiation of the targets in a nuclear reactor, and recovery of ^{238}Pu from the irradiated targets through chemical extraction. In the past, ^{238}Pu was produced at DOE's Savannah River Site (SRS) in South Carolina on an incremental basis during large–scale production of weapons–grade Pu, using reactors that have since been shut down. The last ^{238}Pu production in these reactors occurred in 1988. After DOE stopped producing ^{238}Pu, DOE's remaining inventory, supplemented by purchases from Russia, has been used to continue to supply power systems. NASA and DOE have begun a multi-year project to re-establish the capability to make ^{238}Pu using existing DOE facilities. This talk describes that project and the status of the effort.

Production of ^{238}Pu requires irradiation of ^{237}Np in a nuclear reactor with a high neutron flux to enable reasonable production rates. DOE has selected two research reactors with sufficient flux — the Advanced Test Reactor (ATR) at Idaho National Laboratory (INL) and the High Flux Isotope Reactor (HFIR) at Oak Ridge National Laboratory (ORNL) for this purpose.

Figure 1 outlines the production of ^{238}Pu which involves the following five steps:

1. NpO_2 in storage at INL must be put into shipping containers and shipped to ORNL for use in producing ^{238}Pu.
2. NpO_2 that has been in storage requires purification to remove its decay daughter, ^{233}Pa, which emits a low-energy gamma ray that contributes to worker dose during subsequent target fabrication activities. Purification and recycling of neptunium require conversion to an oxide form for target fabrication.
3. Targets are fabricated by blending NpO_2 with aluminum powder and pressing the mixture into a pellet. Multiple pellets are then clad in an aluminum tube and sealed by welding.
4. Targets are irradiated in either ATR or HFIR. Irradiation times vary from one to six cycles, depending on the specific location in the reactor core and the buildup of undesirable isotopes such as ^{236}Pu.
5. Irradiated targets go through a series of chemical processing steps to recover and purify both neptunium and plutonium. Plutonium is shipped to the Los Alamos National Laboratory (LANL), and neptunium is recycled back to target fabrication.

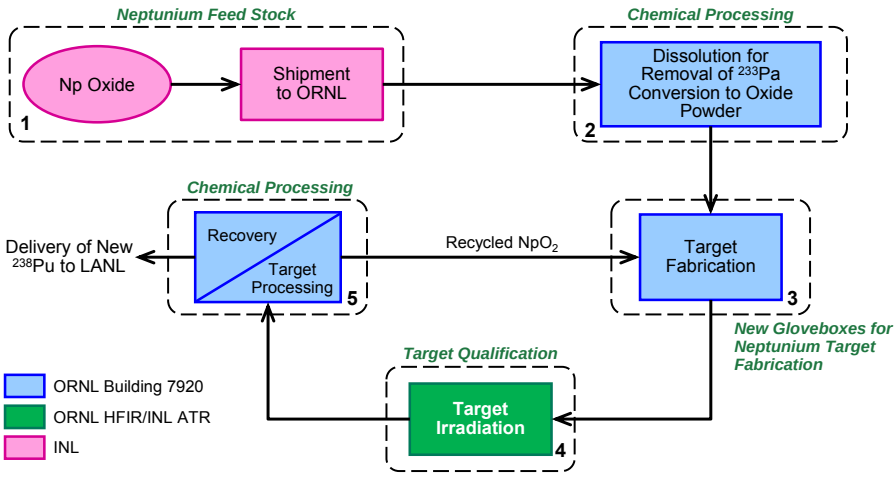

Figure 1. ^{238}Pu production flow diagram.

While ^{238}Pu was produced at the SRS site, there are modifications to the processes necessary in order to use existing DOE infrastructure. The two major areas requiring development are:

(1) A new small, dense target for irradiation of NpO_2 must be developed. The SRS targets were very large and not very dense (only 6 vol% NpO_2 in the aluminum matrix). Current DOE research reactors have a much smaller volume and must be loaded to a density of ~ 20 vol% NpO_2. The problem is that a small portion of the ^{237}Np fissions releasing significant amounts of fission heat. The targets must be designed to operate at temperatures lower than the melting point of aluminum (~650°C).

(2) Research staff at both Savannah River National Laboratory and INL identified process improvements to reduce costs and wastes using solvent extraction to recover Np/Pu instead of the anion exchange process used originally at SRS. This process modification requires additional development and testing.

Furthermore, the process chemistry is affected by the ^{238}Pu concentration as well as the presence of fission products. The high radiation fields cause the chemicals used in the processing to degrade. The efficiency of separation and recovery is impacted significantly by these changes in process chemistry. This talk will describe current status of development underway to test and scale up the various process steps required to produce ^{238}Pu.

C-15

Selective Separation of Electrochemically Generated Am(VI)

Christopher Dares[1,2], Thomas J Meyer[1], Bruce Mincher[3]

[1]The University of North Carolina at Chapel Hill, Chapel Hill, NC, USA, [2]Florida International University, Miami, FL, USA, [3]Idaho National Laboratory, Idaho Falls, ID, USA

Key to successful implementation of nuclear energy to supply future energy needs are viable waste reprocessing and remediation schemes. Irradiated nuclear fuel includes a small fraction of transuranic elements including plutonium, neptunium, and minor actinides such as americium which constitute the major component of long-term radiotoxicity and heat generation. It is imperative therefore to develop closed nuclear fuel recycling schemes which not only improve uranium efficiency, but, also minimize the volume of high level waste generated. In these schemes, Am must be separated from the lanthanides prior to transmutation as their high neutron cross-section would otherwise disrupt the fission efficiency of the recycled fuel.

Arguably, one of the most difficult steps is the partitioning of americium which has a similar ionic radius to the other minor actinides, and lanthanides present, and has a common +3 oxidation state. In acidic solutions, its coordination chemistry is therefore similar leaving few options for selective separation. Traditionally, separation has been achieved through solvent extraction techniques utilizing ligands which preferentially bind Am(III) by making us of the slightly more diffuse 5f-orbitals of Am compared to the 4f-orbitals of the lanthanides.

Recently, work has been performed to exploit the oxidative chemistry available in acidic solutions by using chemical oxidants to generate Am(VI). Am(VI) exists as the dioxo cation $[Am^{VI}O_2]^{2+}$, and features a greatly altered charge density, and ligand preferences providing a new platform for selective separation. Multiple challenges exist in oxidizing Am(III) to its higher oxidation states, particularly the high potential for the intermediate Am(IV/III) couple at E^o = 2.6 V vs. SCE in 1 M acid. This severely limits the availability of chemical oxidants, many of which introduce complications further on in the waste stream. To circumvent these additional complications, and further simplify waste processing, we approached the partitioning of Am in the waste stream by electrochemical oxidation of Am(III) to Am(VI).

Our electrodes are comprised of a thin layer of conductive metal oxide nanoparticles (tin-doped indium oxide, nITO) which were subsequently derivatized with a covalently bound terpyridine ligand known to have an affinity for Am(III). With these electrodes, we have demonstrated the oxidation of Am(III) to Am(VI) at potentials as low as 1.8 V vs. SCE in non-complexing media. The Am(VI) generated is not infinitely stable, and reduced back to Am(III) over time. However, it is sufficiently stable that it can be separated by liquid-liquid extraction using diamylamylphosphonate, a complexant known to selectively extract Am(VI). We will discuss these results, and the factors affecting extraction efficiency.

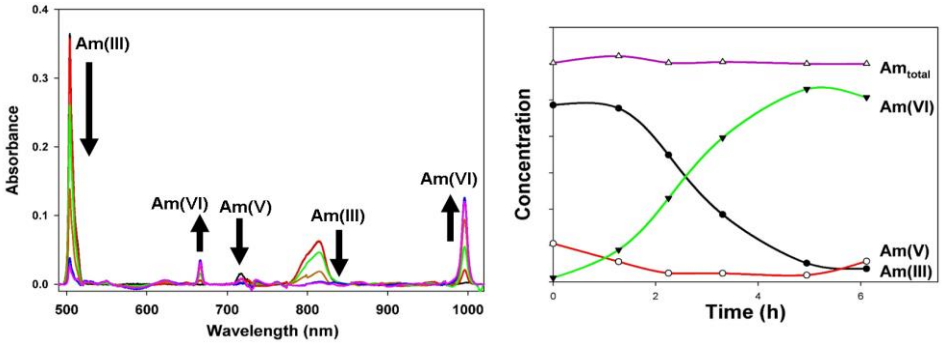

C-16

Reprocessing and beyond - the management of spent oxide and Magnox fuel in the UK held by the NDA

Danny Fox

Nuclear Decommissioning Authority, Moor Row, Cumbria, UK

Introduction

In the UK, the Nuclear Decommissioning Authority (NDA) is responsible for the management of spent nuclear fuel arising from commercial gas-cooled power reactors, i.e. the Magnox and Advanced Gas Cooled Reactors (AGRs), as well as that from experimental and prototype reactors produced in the early days of nuclear power development.

The largest quantity of spent fuel, at least several thousands of tonnes, which the NDA manages arises from the UK's AGR fleet operated by EDF Energy. Of the remainder, Magnox fuel stocks currently represent about two thousand tonnes and other fuels some hundreds of tonnes, ranging from intact commercial Light Water Reactor (LWR) fuel to various 'exotic fuels', some in quantities as small as a few kilogrammes. The exotic fuels are in various chemical and physical forms and, sometimes, conditions of damage and degradation. Examples of fuels classified as 'exotic' include legacy experimental/prototype thermal and fast reactor fuels as well as research reactor fuels, and residues from post irradiation examination programmes.

[The NDA is not responsible for the management of fuel from Sizewell B or a potential 'New Build' programme.]

The NDA Strategies for spent fuel management

Historically, bulk Magnox and AGR fuels have been reprocessed at Sellafield in the Magnox and THORP plants respectively.

Right from the start Magnox fuel has been reprocessed, in part, because of its susceptibility to corrosion and the NDA strategy remains to reprocess all Magnox fuel, as set out in the Magnox Operating Programme (MOP). Over 53,000 tonnes of Magnox fuel has been reprocessed since the early 1960s and based on typical plant performance, Magnox fuel reprocessing is expected to finish around 2020. However, for a number of reasons it may not be practicable to reprocess all of the spent Magnox fuel in the MOP inventory and when Magnox reprocessing operations cease there are likely to be relatively small amounts of fuels left over to manage.

The THORP plant was built to reprocess UK origin AGR fuel and overseas origin LWR fuel under commercial contracts. THORP is expected to complete its reprocessing contracts in 2018 by which time over 9,000 tonnes of domestic and overseas oxide fuel will have been reprocessed. Thereafter all unreprocessed AGR fuel, including future arisings, amounting in total to some several thousands of tonnes, will be committed to interim storage pending a future decision on whether to declare them as waste for disposal in a Geological Disposal Facility (GDF). This approach has been assessed by the NDA to be presently the most viable and cost-effective option. In delivering this strategy sufficient space to receive and manage all the AGR fuel from EDF Energy's fleet of power stations will have been created by reprocessing fuel in existing fuel storage ponds, which avoids having to build additional storage capacity for AGR fuel. If reprocessing was extended it would mean gradually replacing many of the Sellafield plants which support THORP's operations at great expense. This would divert key resources from NDA's primary focus of decommissioning and clean-up.

The Dounreay site stores quantities of ‘exotic fuels’ which were not reprocessed prior to closure of the site’s reprocessing plant and, in addition to the stocks of commercial reactor fuels, Sellafield holds some ‘exotic fuels’. The NDA has taken a series of decisions to transfer all of the exotic fuels at Dounreay to Sellafield for management. This strategy of consolidation provides better value to the UK taxpayer as it enables the accelerated clean-up and decommissioning of the Dounreay sites making it more cost-effective in the long term. In most cases the exotic fuels will be managed alongside bulk fuels which share common characteristics. For example, we are reprocessing fuel from the Dounreay Fast Reactor (DFR) alongside spent Magnox fuel. This maximises the opportunity to use existing facilities and provides best value for money. In other cases, such as the mixed oxide fuels from the Dounreay Prototype Fast Reactor (PFR), we have decided to store this fuel alongside AGR fuel in THORP facilities.

For planning purposes we are assuming that following a period of interim storage for several decades the NDA’s spent fuels will be disposed of in a GDF. Our subsidiary, Radioactive Waste Management Limited (RWM), is responsible for implementing geological disposal of spent fuels that are subsequently declared as waste. Accordingly, RWM is responsible for carrying out R&D on the disposability of fuels and the performance of the disposal system.

Research and Development activities in support of managing spent fuels at the end of reprocessing

The NDA, either directly or through its Site Licence Companies (SLCs), supports Research and Development activities on a range of technologies to underpin its spent fuel management strategies. NDA’s over-arching strategy is that, where possible, R&D is undertaken by the SLCs and their suppliers. However, NDA carries out research directly in relation to its primary function of decommissioning and clean-up of UK legacy sites and, as part of this, NDA also maintains a directly funded R&D programme to inform strategy, deliver innovation, and maintain and develop skills in spent fuel management.

Spent Magnox Fuel

As noted earlier, when Magnox reprocessing operations cease there could be some fuel left over as it may simply become impractical to reprocess the ‘tail-off’ of arisings. Projections of this inventory range from a few tonnes to a few hundred tonnes of fuel depending on a number of factors.

In addition to the MOP inventory, the decommissioning programmes for legacy ponds and silos at Sellafield include the management of significant stocks of Magnox fuel derived material in a variety of forms from fuel rods and debris to cladding residue and sludge.

Figure 1. Typical Magnox Type Fuel Rods

The NDA is working with Sellafield Ltd on options so that any remaining Magnox fuel, following the completion of reprocessing, can be safely and cost-effectively managed through interim storage prior to disposal. Dependent on the nature of the residual material options include;

- Drying and storage in weld sealed containers
- Storage in vented and shielded containers.
- Encapsulation in cement wasteforms.
- Extended storage in containers in chemically dosed ponds.

Work on the technology of drying Magnox fuel is well advanced and there is high confidence that this option is deployable if it was required. The storage of Magnox fuel in vented shielded containers is being developed as part of a programme to manage materials held within legacy ponds at Sellafield. Depending on the nature and amount of material left over at the end of reprocessing unreprocessed material could be suitable for containerised storage or for encapsulation in one of the waste plants operating at or scheduled to be built at Sellafield.

Synergies will be sought in the development and deployment of technology options within the decommissioning and spent fuel management strategies to ensure that alternative options to reprocessing enable any unreprocessed Magnox fuel to be safely and cost-effectively managed. Overall this work will inform how the MOP is optimised to balance the types and amounts of fuel, if any, remaining for interim storage at the end of reprocessing.

RWM is carrying out R&D on the disposability of fuels including understanding fuel conditioning/packaging options and their impacts on the performance of the disposal system.

In addition, work with RWM and ongoing coordination of the decommissioning and spent fuel management strategies will address the future requirements to enable any disposal of spent Magnox fuel material designated as waste. This work will seek to;

- Build on development of interim storage options such as drying and cemented wasteforms as options to enable Magnox fuel disposal.
- Establish, with RWM, the impact of alternative Magnox fuel disposal options on the alternative concepts for a GDF.
- Seek alternative technologies, if appropriate, to optimise safe, cost-effective disposal, which may include alternative fuel treatment, encapsulation, and packaging routes.

The options chosen for ongoing development will be influenced by the quantities of Magnox fuel material for disposal, synergies with other metal fuel residue under NDA management, and broader experience of managing metal fuels through to disposal.

Spent Oxide Fuel

For oxide fuels we have considerable operational experience and technical knowledge for the management of AGR fuel in pond storage. AGR fuel is dismantled and stored as pins in open cans. The fuel has been stored successfully for over 25 years in ponds on the Sellafield site. In readiness for the completion of THORP reprocessing, Sellafield Ltd continues to develop its approach for the interim wet storage of AGR spent fuel to the point of packaging for disposal.

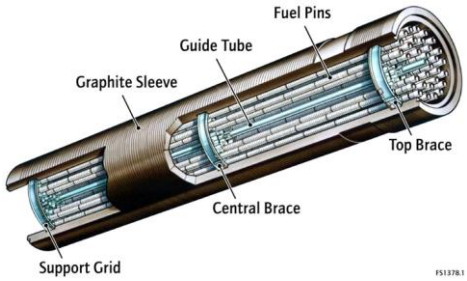

Figure 2.Undismantled AGR fuel element showing pins

R&D is being funded by NDA and Sellafield Ltd covering a number of areas in support of the interim storage of oxide fuels for at least several decades, particularly for stainless steel clad AGR fuel which is unique to the UK, in order to;

- Develop and maintain the fundamental science, knowledge base and skills to further underpin extended fuel storage,
- Extend the known wet storage duration of AGR fuel through storage trials and ongoing post storage examination of long-stored fuel from operational ponds.
- Improve monitoring of spent fuel in storage and the condition of storage facilities.
- Support contingency options in the event of unanticipated fuel failures, which includes;
    - Support of improved detection and mitigation options to manage any fugitive radioactive release from wet stored fuel.
    - Researching fuel drying options to support fuel packaging, disposal, and, in the case of AGR fuel, to examine the potential of drying and dry storage for future adoption in preference to prolonged wet interim storage if this became technically or economically preferable.

The NDA's responsibility includes management of some oxide fuels which have been cut up for fuel examination, resulting in pin sections and fuel debris; some of this material is not suitable for reprocessing in Thorp. The SLCs are currently engaged in preparations to secure the interim storage of this material, where necessary by adoption of suitable measures for the containment of the radioactive material.

RWM is also carrying out R&D on the disposability of oxide fuels and the performance of the disposal system. Ongoing coordination with RWM on the spent fuel management strategy will address the future requirements to enable any disposal of spent oxide fuel. Current work includes disposal system requirements, understanding the impacts of oxide fuel behaviour during interim storage, fuel conditioning/packaging options and the effects of water carryover, and the interaction of ground water with AGR fuel.

Fuel drying development, noted earlier, will include consideration of drying fuel segments and fuel debris, as well as drying fuel with perforated cladding. Other options including treatment, immobilisation technologies and package development will also be explored where appropriate to support ongoing storage and disposal of oxide fuel materials.

Summary

In the UK, the NDA manages a diverse range of spent fuels arising from commercial gas-cooled power stations and also experimental and prototype reactors which are now shutdown. Commercial reprocessing operations in the UK are scheduled to finish this decade and any remaining fuels will be committed to interim storage, pending a future decision about disposal to a geological disposal facility. This paper discusses how, through its Site Licence Companies and subsidiaries, the NDA supports its spent fuel management strategies by funding research

and development activities. These R&D activities cover a range of technologies and approaches for the interim storage of spent fuel to the point of and including disposal. The development of these technologies will ensure the safe and cost-effective management of spent fuels over many decades.

C-17

Gas-Phase Reactions of Water with Actinide Dioxide Cations, PaO_2^+ to CfO_2^+: The "Enigmatic" Behavior of Plutonium

John K. Gibson[1], Monica Vasiliu[2], Phuong Diem Dau[1], Richard Wilson[3], Kirk Peterson[4], David Dixon[2]

[1]Lawrence Berkeley National Laboratory, Berkeley, California, USA, [2]University of Alabama, Tuscaloosa, Alabama, USA, [3]Argonne National Laboratory, Argonne, Illinois, USA, [4]Washington State University, Pullman, Washington, USA

Introduction

Among the most fundamentally important reactions of metal oxides are with water. Bimolecular metal ion-molecule reactions in the gas phase can reveal essential chemistry that illuminates, and possibly predicts, condensed phase behaviour.[1] Such relatively simple reactions, performed in the absence of perturbations from surrounding solvent molecules or lattice atoms, are relatively amenable to accurate theoretical treatment, which enhances understanding of experimental observations and provides an evaluation of the validity of computational methodologies. The gas-phase encounter of a metal dioxide cation with water results in physisorption hydration, reaction 1, or chemisorption hydrolysis, reaction 2.

$$MO_2^+ + H_2O \rightarrow MO_2(H_2O)^+ \qquad (1)$$

$$MO_2^+ + H_2O \rightarrow MO(OH)_2^+ \qquad (2)$$

Exothermic barrier-less reaction 1 occurs for all MO_2^+. Reaction 2 can be observed if reaction 3 is exothermic and has a sufficiently low barrier for proton-transfer.

$$MO_2(H_2O)^+ \rightarrow MO(OH)_2^+ \qquad (3)$$

Reaction 3 reveals hydrolysis at a molecular level, can be accurately computationally modelled, and elucidates metal-oxygen bonding. The hydroxide product of reaction 3 is also the intermediate for oxo-exchange reaction 4 with isotopically labelled $H_2{}^{18}O$.

$$MO_2^+ + H_2{}^{18}O \rightarrow MO^{18}O^+ + H_2O \qquad (4)$$

Elementary gas-phase bimolecular reactions such as reactions 1-4 provide a fundamental basis to understand chemistry of metal oxide ions in aqueous solutions, including hydrolysis and oxo-exchange.[2-5]

Methods

Ion-molecule reactions studied by quadrupole ion trap mass spectrometry (QIT-MS) establish whether association of metal dioxide cations with water result in hydrates (reaction 1) or hydroxides (reaction 2). Ligand-exchange distinguishes between these isomers. Using ligands L, such as acetone, that exhibit higher gas basicities than H_2O, occurrence of exothermic reaction 5 reveals a hydrate structure; non-occurrence indicates the alternative hydroxide isomer, $MO(OH)_2^+$.

$$MO_2(H_2O)^+ + L \rightarrow MO_2(L)^+ + H_2O \qquad (5)$$

Reaction 4 is also studied in the QIT-MS to determine if spontaneous oxo-exchange occurs. Potential energy surfaces (PESs) for isomerization reaction 3 and oxo-exchange reaction 4 are calculated at the coupled cluster CCSD(T) level extrapolated to the complete basis set limit with additional corrections including scalar relativity and spin-orbit. The experimental observations are compared with predictions from calculated PESs. The gas-phase results are evaluated to

illuminate hydrolysis and oxo-exchange of metal oxide cations in aqueous solution, as well as fundamental aspect of bonding in MO_2^+ ions.

Results and Discussion

The energies and structures resulting from gas-phase addition of water to metal oxide cations, MO_2^+, have been assessed by experiment and theory for several metals. An example of experimental results is shown in Figure 1, where it is apparent that oxo-exchange reaction 4 occurs more rapidly for M = Pa versus M = U.[2] The computed PESs for these exchange processes are shown in Figure 2. Because the computed TS1 barrier for M = U is only 1.3 kcal/mol below the reactant energies, whereas TS1 is at -7.0 kcal/mol for M = Pa, faster exchange for PaO_2^+ is accurately predicted.[4] An experimental observation in both solution and

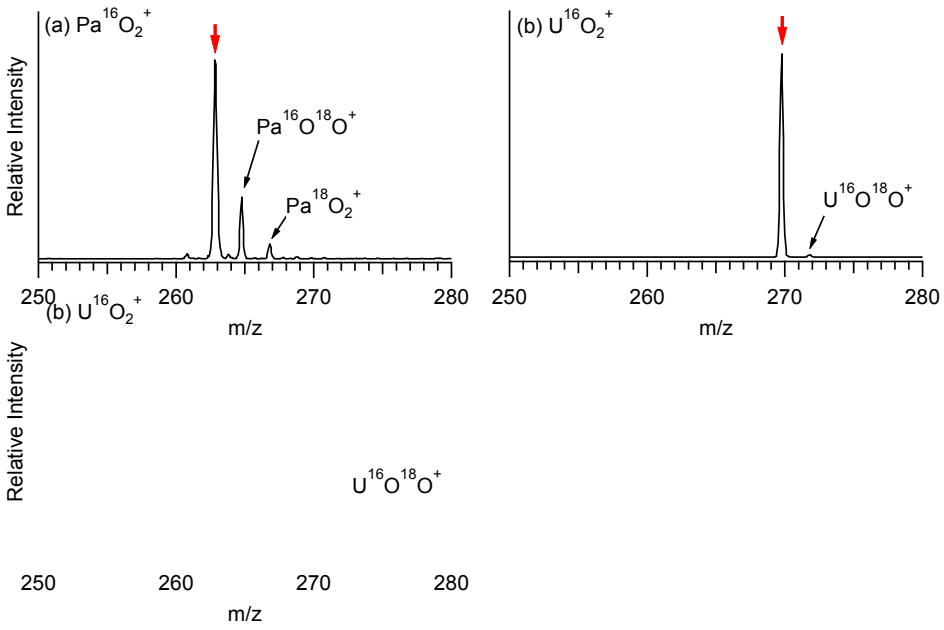

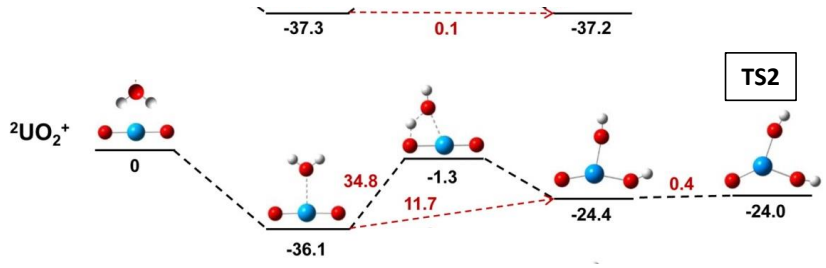

Figure 2. Computed potential energy surfaces for addition of water to UO_2^+ and PaO_2^+. Indicated energies relative to the separated reactants are in kcal/mol.[4] "An" denotes an actinide.

Referring to Figure 2, a key aspect of the association of H_2O to a MO_2^+ ion is whether the physisorption hydrate, $MO_2(H_2O)^+$, or chemisorption hydroxide, $MO(OH)_2^+$, is lower in energy; that is, whether isomerization reaction 3 is endothermic or exothermic. Ligand-exchange experiments, reaction 5, have revealed that the lower-energy isomer is $MO_2(H_2O)^+$ for M = Pr, U, Np, Pu and Am, but $MO(OH)_2^+$ for M = Nb and Ta; for M = Pa, a mixture of $PaO_2(H_2O)^+$ and $PaO(OH)_2^+$ is produced, suggesting that the two isomers are close in energy. These results are in accord with calculated PESs, including that for M = Pa in Figure 2, which correctly predicts that the physisorption and chemisorption isomers are essentially degenerate in energy, to within 0.1 kcal/mol. The computed PESs also accurately predict that oxo-exchange reaction 4 should occur for M = Pa and U (TS1 < 0), but not for M = Pr, Np, Pu, and Am (TS1 > 0). The gas-phase molecular results elucidate the previously "enigmatic" observation that solution oxo-exchange occurs more rapidly for UO_2^+ than PuO_2^+, despite that the uranium-oxygen bonds are distinctively strong.

An intriguing aspect of isomerization reaction 3 is that it provides a measure of the energy necessary to disrupt the covalent bonding in the linear actinyl ions, AnO_2^+ (An = actinide), by converting a covalent An=O bond to two ionic An-OH bonds. The greater the covalent character of an An=O bond, the greater will be the diminishment in bonding upon disruption of this bond to yield ionic An-OH bonds. Thus, reaction 3 should be energetically less favourable as the covalent character of the An=O bond in the reactant increases, regardless of the intrinsic strength of the An=O bond. The reasoning behind this interpretation is that any covalent contribution to An-O bonding is lost, or substantially diminished, upon converting the An=O bond to two An-OH bonds. Preliminary computed energies for reaction 3, which are consistent with experimental observations, indicate for the actinide elements An = Pa-Cm a maximum endothermicity at Pu or Am (tentative computed energies are similar for Pu and Am). This result can be interpreted as indicating an increase in An=O covalency from Pa to Pu/Am, followed by a decrease in covalency for Cm and beyond. This is in accord with a recent bonding analysis that indicated an increase in covalency from PaO_2^+ to PuO_2^+ (heavier AnO_2^+ were not considered).[5] The conclusion that covalency in the AnO_2^+ molecular ions increases across the actinide series is in accord with similar considerations for solid AnO_2.[6] Because the 5f orbitals contract across the actinide series, this seemingly anomalous increase in covalency has been attributed to a better match between the energies of the actinide 5f and oxygen 2p valence orbitals in the region of Pu, an effect referred to as energy-degeneracy driven covalency. The present results demonstrate this same trend for molecular actinyl ions, and indicate a maximum covalency for PuO_2^+ or AmO_2^+. A consequence is that AmO_2^+ does not exhibit oxo-exchange despite that the Am-O bond dissociation energies are even lower than for PuO_2^+.

The experiment and theory results demonstrate similar hydrolysis characteristics for the three group 5 metal oxide ions, NbO_2^+, TaO_2^+ and PaO_2^+. This is in analogy with aqueous solution chemistry where none of the three oxides is resistant to hydrolysis. An interesting experimental and theory observation is that the group 5 lanthanide oxide ion, PrO_2^+, exhibits neither hydrolysis nor oxo-exchange.

The studies were extended to addition of a second water molecule to the primary products. If the initial water addition results in a hydrate, then the secondary product is a bis-hydrate, $MO_2(H_2O)_2^+$. If the primary product is a hydroxide, then the secondary product can be a hydroxide hydrate, $MO(OH)_2(H_2O)^+$, or a tetrahydroxide, $M(OH)_4^+$. The experimental results suggest $NbO(OH)_2(H_2O)^+$, $Ta(OH)_4^+$ and $Pa(OH)_4^+$ as the most stable isomers. Although the preliminary PESs predict $M(OH)_4^+$ as the more stable and kinetically accessible isomer for all three metals, the calculations correctly predict that $NbO(OH)_2(H_2O)^+$ is relatively close in energy to $Nb(OH)_4^+$. These molecular results reveal the underlying basis for the facile aqueous solution hydrolysis of Nb(V), Ta(V) and Pa(V).

Summary

Combined experiment/theory studies of gas-phase bimolecular metal oxide cation-water reactions elucidate solution hydrolysis and provide fundamental insights into metal-oxygen bonding. The intrinsically stable nature of the actinyl(V) hydrates, $AnO_2(H_2O)^+$, was

demonstrated in the gas phase by experiment and theory for An = U, Np, Pu, Am, as well as for the lanthanide Pr. The contrasting susceptibility of MO_2^+ to hydrolyze to $MO(OH)_2^+$ for M = Pa, Nb and Ta was also demonstrated. Experiment and theory are also in accord that oxo-exchange with water should occur for PaO_2^+ and UO_2^+, the two AnO_2^+ ions with the highest bond dissociation energies, but not for NpO_2^+, PuO_2^+ or AmO_2^+. A key overall interpretation of the results is that the An=O bonds in the AnO_2^+ ions are least covalent for Pa and most covalent for Pu or Am. Although computations have been extended to CmO_2^+, BkO_2^+ and CfO_2^+, performing experiments for these unstable ions is challenging.

Acknowledgements

This work was supported by the U.S. Department of Energy, Office of Basic Energy Sciences, Heavy Element Chemistry, at LBNL under Contract No. DE-AC02-05CH11231 (P.D.D. and J.K.G), through a subcontract from Argonne National Laboratory (D.A.D.), and through Grant No. DE- FG02-12ER16329 (K.A.P.). R.E.W. was supported by the U.S. Department of Energy Basic Energy Sciences, Early Career Research Award Program, under Contract DE-AC02-06CH11357. D.A.D. thanks the Robert Ramsay Fund at the University of Alabama.

References

(1) Rutkowski, P. X.; Michelini, M. C.; Gibson, J. K.: Proton Transfer in Th(IV) Hydrate Clusters: A Link to Hydrolysis of Th(OH)(2)(2+) to Th(OH)(3)(+) in Aqueous Solution. *Journal of Physical Chemistry A* **2013**, *117*, 451-459.

(2) Dau, P. D.; Wilson, R. E.; Gibson, J. K.: Elucidating Protactinium Hydrolysis: The Relative Stabilities of $PaO_2(H_2O)(+)$ and PaO(OH)(2)(+). *Inorganic Chemistry* **2015**, *54*, 7474-7480.

(3) Rios, D.; Michelini, M. C.; Lucena, A. F.; Marçalo, J.; Gibson, J. K.: On the Origins of Faster Oxo Exchange for Uranyl(V) versus Plutonyl(V). *Journal of the American Chemical Society* **2012**, *134*, 15488-15496.

(4) Vasiliu, M.; Peterson, K. A.; Gibson, J. K.; Dixon, D. A.: Reliable Potential Energy Surfaces for the Reactions of H_2O with ThO_2, PaO_2^+, UO_2^{2+}, and UO_2^+. *Journal of Physical Chemistry A* **2015**, *119*, 11422-11431.

(5) Kaltsoyannis, N.: Covalency Hinders $AnO_2(H_2O)^+$ à $An(OH)_2^+$ Isomerization (An = Pa-Pu). *Dalton Transactions* **2016**, *45*, 3158-3162.

(6) Prodan, I. D.; Scuseria, G. E.; Martin, R. L.: Covalency in the Actinide Dioxides: Systematic Study of the Electronic Properties Using Screened Hybrid Density Functional Theory. *Physical Review B* **2007**, *76*.

C-18

Thermal expansion study of the heavy-fermion superconductor $^{242}PuCoGa_5$

Rachel Eloirdi[1], Nicola Magnani[1], Carlotta Giacobbe[2], Pedro Amador Celdran[1], Jean-Christophe Griveau[1], Eric Colineau[1], Gerard H. Lander[1], Roberto Caciuffo[1]

[1]European Commission, Joint Research Centre (JRC), Institute for Transuranium Elements (ITU), Karlsruhe, Germany, [2]European Synchrotron Radiation Facility, Grenoble, France

$PuCoGa_5$ has the highest T_c (18.5 K) of any heavy-fermion superconductors. Fourteen years after its discovery our understanding of this material remains at best confused. The presence of valence fluctuations has been recently suggested by resonant ultrasound spectroscopy [1]. To address this point, we have performed high-resolution x-ray diffraction measurements on an encapsulated powder sample [2] of $^{242}PuCoGa_5$. The sample has been prepared as single crystal by the self-flux method using a charge of 242-plutonium metal obtained by an amalgamation process [3].

The x-ray diffraction patterns measured from 300 K to 5 K show that the tetragonal symmetry is preserved down to 5 K. The c/a ratio decreases with increasing temperature to become almost constant above ~150 K. The volume thermal expansion coefficient α_V has a jump at T_c, a factor ~20 larger than the change predicted by the Ehrenfest relation. As a consequence, the volume expansion deviates from the curve expected for the conventional anharmonic behaviour described by a simple Grüneisen-Einstein model. The observed differences are about ten times larger than the statistical error bars.

References

[1] B. J. Ramshaw et al., PNAS **112**, 3285 (2015).

[2] A. H. Hill, T. Klimczuk, R. Springell and H. C. Walker, *J. Appl. Cryst.* **46**, 567-569 (2013).

[3] Y. Shiokawa, K. Hasegawa, K. Konashi, M. Takahashi, K. Suzuki, J. Alloys Comp. **255**, 98 (1996).

C-19

Electrode reduction of actinyl ions followed by deposition in weak acid solution

Yoshihiro Kitatsuji, Kazuki Ouchi, Haruyoshi Otobe

Japan Atomic Energy Agency, Tokai, Ibaraki 319-1195, Japan

Introduction

Formation of insoluble particle of actinide (An) in the aqueous solution has much effect on migration of them in environmental. The actinide ions which have large electric charge tend to form complex with ligand such as hydroxide, organic compound, etc. and to aggregate making colloids. Many thermodynamic studies concerning complex formation of actinide with ligand and solubility of them have been actively carried out. The reaction mechanism of formation of particles such as colloids is quite complicated. Especially, redox of An(IV) / An(V) accompanied formation or braking the An-O bond of actinyl ion, so that it is not sufficient only to consider the hydrolysis of electrolysis products. The authors have recently studied the formation of colloidal particle of actinide by focusing the mutual relation between redox reactions and aggregation of the ions.

Methods

Gold electrodes were employed as the working electrode to avoid generation of H_2. Voltammetry was performed by using an Au microelectrode (25 □m in diameter) in order to facilitate the discrimination of deposition onto the electrode surface. A platinum wire and a silver-silver chloride electrode (SSE) with 1 M LiCl were employed as the counter and the reference electrodes, respectively. Stripping voltammogram was recorded by scanning the potential at a constant rate after preelectrolysis applying a constant potential for a period of time. Electrochemical Quartz Crystal Microbalance (EQCM) was measured by using the 8 MHz AT-cut quartz crystal (13.7 mm in diameter) with Au electrodes (5.1 mm in diameter).

Stock solution of actinide was in 0.1 M $HClO_4$. The acidity of the solution was adjusted in pH range between 2.0 and 4.0 by adding NaOH. The concentration of the supporting electrolyte of the sample solution for electrochemical measurements is fixed to be 1 M $NaClO_4$.

Results and discussion

Autocatalytic reduction of Uranium(V)

Uranium(VI) ion is reduced to U(V) when U is electrolyzed at the potential of -0.35 V vs SSE. And the U(V) disproportionate to produce U(IV) in acidic solution of pH < ca. 2. On the other hand, immediately disproportionation of U(V) was not observed in the solution of pH higher than 2.

Therefore U(V) exist stably for several minutes. However, disproportionation of U(V) progress after formation of U(IV) aggregate in the solution [1]. Electrolytic reduction was also affected by existence of U(IV). On the controlled potential electrolysis, the steady current due to reduction of U(VI) to U(V) was recorded at the beginning of electrolysis. Then the current turns to increase several minute later. The surplus current suggests further reduction to U(IV) occurred. The EQCM study showed the deposition of reduction product of U(VI) onto the electrode surface coincident with the observation of surplus current. These results suggest that the reduction of U(V) was catalyzed by its reduction product, that is U(IV), deposited on the electrode.

Electrodeposition of Np(IV)

Reduction of Np(V) is electrochemically irreversible reaction, and its overpotential is so large that the reduction current of it in the acidic solution is not observed within the potential window. However, Np(V) is reduced to Np(IV) by electron transfer reaction with Np(III)/Np(IV) mediator [2]. When acidity of the solution was lower than pH 3.0, reduction current of Np(V) was appeared at ca. -0.75 V vs SSE in the cyclic voltammogram. The reduction current showed the characteristic of electrodeposition. Oxidation current of deposited species is also appeared at +0.5 V when reduction of Np(V) was observed. Unlike uranium, the electrodeposition occurred quickly with electrode reduction of Np(V). Then the reduction of Np(V) was inhibited by formation of deposit layer on the electrode. The reduction of Np(V) and deposition occurred at more positive potential in the solution of higher pH. Stripping currents due to oxidation of Np(IV) were uniform up to 30 sec of preelectrolysis time in the solution of pH 3.0. For longer preelectrolysis time, oxidation current peak shifts more positively, it indicates the stabilization of deposited Np species.

Acknowledgement

This work was supported by JSPS KAKENHI Grant Number 15H04247, 26249148.

References

[1] Yoshihiro Kitatsuji, Haruyoshi Otobe, Takaumi Kimura, Sorin Kihara, Electrochim. Acta, 141(2014)6-12.

[2] Yoshihiro Kitatsuji, Takaumi Kimura, Sorin Kihara, J. Electroanal. Chem. 641(2010)83-89.

C-20

Numerical Simulation on Breeding and Burning Process of Plutonium in Fusion Fission Hybrid Reactor for Energy (FFHR-E)

Xueming Shi, Xianjue Peng

Institute of Applied Physics and Computational Mathematics, Beijing, China

A neutronics calculation of a Fusion Fission Hybrid Reactor for Energy (FFHR-E), which can breed and burn plutonium in the blanket without separation of transuranium from the spent fuel, is presented.

The Fusion core parameters are similar to the International Thermonuclear Experimental Reactor (ITER). The D shaped plasma torus is stretched to a semi-cylinder for simplification. The inner border lines, around which the blanket is constructed, remains the same as in ITER except that the diverter part has been simplified. Along the poloidal direction, the blanket is cut into 17 fission fuel modules and 3 divertor modules. Along the blanket radial direction, the blanket is divided into the first wall, the fission fuel zone, the tritium breeding zone and the shield zone, the total depth of the blanket is around 1 meter. An alloy of natural uranium and Zirconium (U-10Zr) is adopted in the fission blanket, which is cooled by light water. Li4SiO4 is selected as the the tritium breeder.

In order to model the three dimensional neutron transport and burnup process in the hybrid, a linkage code MCORGS is used. MCORGS is coupled to MCNP and ORIGEN-S and have already been validated through several typical benchmarks. It is assumed that the thermal power in the blanket is maintained to 3000MWth in the neutronic burnup calculation, the fusion power is then adjusted accordingly, since the average blanket energy multiplication (M) is increasing in a long period. M and Tritium Breeding Ratio(TBR) can be maintained at 10 and 1.15 respectively, over tens of years continuous irradiation without any reprocessing of fission fuel. However, since it is impossible for the fuel clad to withstand the neutron irradiation over such a long period, simplified reprocessing without separation of transuranium from uranium is adopted. It is assumed that the spent fuel is reprocessed every five years in this paper, since the maximum displacement per atom (dpa) for the fuel clad is about 9 dpa/year.

Two kind of reprocessing scenarios are compared

(i) Only part of the fission products is removed. This may be done by simplified pyro-reprocessing. Heat up the spent fuel to a high reprocessing temperature by decay heat, fission product elements whose boiling points are below the temperature will evaporate.

(ii) All the fission products are removed. This may be done by simplified aqueous-reprocessing or adavanced pyro-reprocessing.

Three reprocessing temperature, i.e. 1700K, 2100K and 2500K are compared. Under 1700K, the following elements of fission products will be removed, i.e Kr, Xe, Br, I, As, Cs, Se, Rb, Cd, Te, Yb, Sr. Under 2100K, another three elements Sb, Eu, Sm will be removed, among them, Eu and Sm are strong neutron absorber. Under 2500K, another 5 elements Tm, Ag, In, Ga will be removed. It is shown that both TBR and M under 2100K are much better than those of 1700K. However, if the temperature is raised from 2100K to 2500K, there are little improvement in both TBR and M. It is highly suggested that the reprocessing temperature of 2100K is adopted.

In the following research, scenario 1 is used every 5 years, scenario 2 is introduced every 60 years, which is a typical lifetime of one fission reactor. In the first 60 years, the average TBR and M are 1.15 and 12. From the second to tenth 60 years, the average TBR and M are above 1.3 and 16. It shows the possibility of breeding and burning plutonium by this simplified but proliferation resistant reprocessing.

C-21

Thermodynamic Properties of Pu as a Function of Ga Content

Daniel Schwartz, Jeremy Mitchell, Franz Freibert

Los Alamos National Laboratory, Los Alamos, New Mexico, USA

The thermal properties of plutonium are strongly influenced by alloying with gallium. Clear evidence of this can be seen in the dramatically expanded delta-Pu phase stability field at Ga concentration (C_{Ga}) > 0.75 at.% Ga. We have been investigating the fundamental elevated temperature thermal behavior of Pu as a function of Ga content. Previous work shows that Pu-2 at.% Ga has heat capacity ~15% higher than the Dulong-Petit high temperature limit, while Pu-7 at.% Ga displays normal behavior. Pu-3 at.% Ga is currently being measured to narrow down the critical C_{Ga} where normal harmonic behavior begins, and these results will be reported.

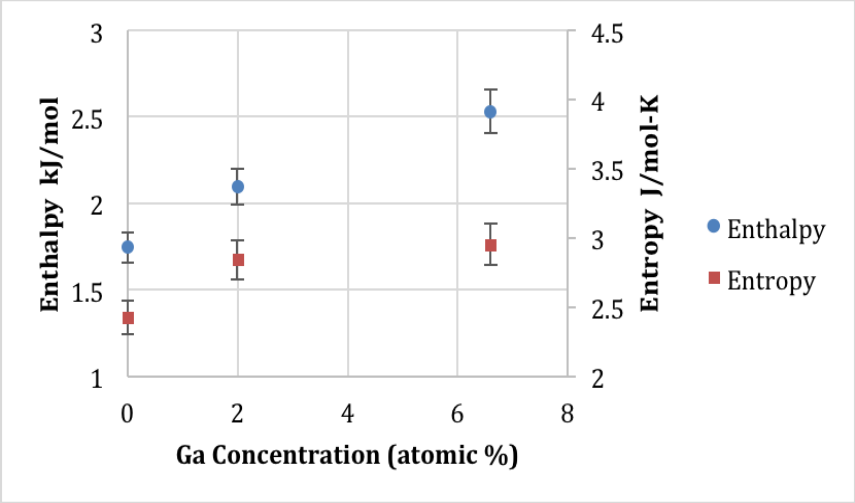

Figure 1. The enthalpy and entropy of Pu delta-epsilon transition as a function of Ga content.

The enthalpy and entropy of the delta-epsilon transformation is also being explored as a function of Ga content (figure 1). These thermodynamic functions are strongly influenced by C_{Ga}, although there is some indication that changes in entropy begin to slow at high C_{Ga}. Ga additions move the delta-epsilon phase boundary to significantly higher temperatures ($T_{delta\text{-}epsilon}$ for Pu-7 at.% Ga is >130K higher than for unalloyed Pu). These results will be discussed in detail.

Finally, we will discuss a series of thermal measurements on Pu alloyed with *sub*-delta stability levels of Ga, in the 100 to 600 ppm Ga range. These alloys show significantly altered enthalpies for all the phase transformations, and the changes are not systematic.

C-22

A Temperature Investigation of δ-phase ^{239}Pu-Ga Alloys

Alice I. Smith[1], Adrian S. Losko[1,2], Sven C. Vogel[1], Scott Richmond[1], Michael Ramos[1]

[1]Los Alamos National Laboratory, Los Alamos, NM, USA, [2]University of California Berkeley, Berkeley, CA, USA

The phase diagram of Pu-Ga alloys has been a subject of interest and controversy for decades, and only recently an agreement has been reached in the matter of the two phase diagrams, the metastability of the δ phase, and the "equilibrium" phase diagram vs. the "working" phase diagram [1-2]. Phase stability and phase transformations in binary plutonium alloys affect mechanical properties, microstructure, corrosion behaviour, and structural integrity, and are critical for a variety of applications, from metallurgy to nuclear energy and weapons research. A clear and detailed understanding of phase stability and phase transformations is necessary in order to predict the behaviour and response of materials to unexpected stimuli. Despite the many years of theoretical and experimental research, the mechanism behind the phase stability, in connection to phase transformations, is not completely understood.

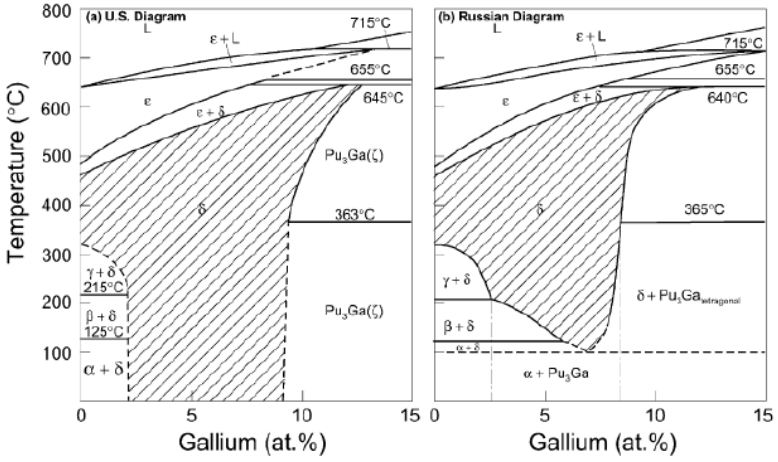

Fig. 1. The US (a) and Russian (b) Pu-Ga phase diagrams.

We present an experimental study of the transformation behavior of δ-phase ^{239}Pu-Ga alloys upon thermal cycling. Two high-purity, polycrystalline ^{239}Pu samples, stabilized with 2.0 and 7.0 at.% Ga in the δ-phase, were vacuum degassed, and homogenized by annealing for 100 hours at 450°C (525°C for the ^{239}Pu-7at.%Ga sample) in a Sieverts apparatus [3]. Each sample was sealed in a cylindrical vanadium double-wall container, with helium exchange gas.

Neutron diffraction data were collected at ambient pressure and over a wide range of temperatures (28-675K), on the high-pressure preferred orientation (HIPPO) neutron time-of-flight powder diffractometer [4], located at the Manuel Lujan Jr. Neutron Scattering Center, Los Alamos Neutron Science Center (LANSCE) [5]. Structural refinements were carried out by Rietveld method [6] implemented in the GSAS software package [7].

In addition, energy-resolved neutron tomography characterization was performed at room temperature and ambient pressure on the FP5 beamline, also located at LANSCE [8]. Measurements were collected on both samples, before and after each thermal cycle (heating/cooling). The tomographic reconstruction, with energy ranges corresponding to ^{239}Pu neutron absorption resonances, allows us to quantify the ^{239}Pu density, enabling sample reconstruction, along with identification of physical features, such as sample dimensions, physical defects (cracks, holes, foreign inclusions, etc.), and variations in the distribution of the

alloying element. Analysis of the transmission spectra allows for mapping of isotope concentrations.

The collected data will contribute to a better understanding of the phase stability and phase transformations in ^{239}Pu-Ga alloys, in connection to the evolution of the average structure and microstructure, at different temperatures and alloying element compositions.

Acknowledgments

This research was supported by the US Department of Energy through the NNSA for the FY2015 and FY2016 Lujan Center Nuclear and Materials Research User Program. Los Alamos National Laboratory is operated by Los Alamos National Security LLC under Contract DE-AC52-06NA25396.

References

1 Hecker S.S., Timofeeva L.F., *Los Alamos Science* 2000; 26:244.
2 Hecker et al., *Progress in Materials Science* **49** (2004) 429-485.
3 S. Richmond et al., IOP Conf. Ser: Mater. Sci. Eng. **9**, 012036 (2010).
4 H.-R. Wenk, L. Lutteroti, S. C. Vogel, Nucl. Instr. Methods Phys. Res. A **515**, 575 (2003)

5 Lisowski & Schoenberg, Nuclear Instr. and Methods in Phys. Res. A 562 (2006) 910–914

6 H. M. Rietveld, Journal of Applied Crystallography, 1969, **2**, 65.

7 A. Larson and R. V. Dreele, “General Structure Analysis System (GSAS)”, Tech. Rep. (Los Alamos National Laboratory Report LAUR 86-748, 2004).

8 A. S. Tremsin et al., Neutron News **24**:4, 28-32 (2013)

C-23

Experimental studies to support storage of PuO_2 in the UK

Colin Gregson[1], Robin Orr[1], Howard Sims[2], Robin Taylor[1], Kevin Webb[1], David Woodhead[1], Paul Cook[3], Jeff Hobbs[3], Helen Steele[3]

[1]National Nuclear Laboratory, Sellafield, Cumbria, UK, [2]National Nuclear Laboratory, Culham Science Park, Abingdon, Oxfordshire, UK, [3]Sellafield Ltd, Sellafield, Cumbria, UK

Reprocessing operations at the Sellafield Site in Cumbria, United Kingdom, have resulted in the production of a large amount of plutonium dioxide (PuO_2) and plutonium containing materials. These materials must be safely and securely stored until its re-use or final disposal. Even if reused, storage will be required for several decades.

Since the mid-1970s, PuO_2 in the UK has been stored in sealed, welded packages. This provides safe containment of the PuO_2 during storage and prevents contamination of the powder, so that future re-use options are not foreclosed. The principal mechanism by which a package might fail under normal storage conditions is from gas pressurization. Historically, the safe storage of PuO_2 has been assured by empirical criteria, controlling conditions during production and packaging of the PuO_2, and inspection of stored packages. Therefore pressurization has rarely occurred, and where it has done so it has been associated with plant mal-operations. However, to underpin ongoing storage of these materials for future decades Sellafield Ltd and the UK National Nuclear Laboratory are undertaking experimental studies to improve the understanding of the mechanisms and controlling factors affecting package pressurization.

Pressurization of packages might be expected to occur by number of processes:

- Gas pressurization from self-heating,
- Helium in-growth from alpha decay,
- Desorption of adsorbed gases, particularly water,
- Radiolysis of water adsorbed on PuO_2,
- Gas generation from degradation of polythene included in some packages.

Gas pressurization from self-heating of the initial fill gas of the package is unavoidable but relatively modest. Current experimental studies have, therefore, focused on water adsorption/desorption and the radiolysis of water in the package. Future experiments are planned to investigate the buildup and release of helium in PuO_2 powder, generated by alpha decay. Previous studies on helium accumulation/release in PuO_2 and uranium oxides has generally focused on fuel pellets that have much larger grain sizes and mobility has often been analysed at temperatures above powder storage conditions and therefore those studies may not be directly applicable [2].

Water adsorption on PuO_2

Understanding the variation in water sorption with temperature is important to quantify the contributions to pressurization from desorption of water upon self-heating during storage. In addition, the amount of adsorbed water on the powder surface also influences the initial hydrogen gas generation rate from radiolysis [1]. PuO_2 is strongly hygroscopic and quickly adsorbs moisture during handling. A number of studies have investigated the state of water on PuO_2 surfaces. Stakebake [3] proposed that water is present as strongly bound chemisorbed

(dissociated) water, a quasi-chemisorbed (strongly hydrogen bonded) layer, and finally weakly bound physisorbed water. In a more recent review, Haschke [4] compiled the available literature data and presented a similar model, but concluded that five distinct sorption states could be identified. Finally, Paffett has investigated the physisorption of water on a low surface area PuO_2 powder and concluded it to be well well-described by the Brunauer–Emmett–Teller (BET) model over a wide range of relative humidity [5]. However, uncertainty remains in reconciling the reported observations, in quantifying strongly bound and physisorbed water as a function of temperature and vapour pressure, and also understanding the influence of particle morphology and specific surface area.

Stored PuO_2 in the UK is derived mainly from reprocessing, either from spent uranium metal fuels from UK Magnox reactors (referred to as "Magnox" PuO_2) or from reprocessing of spent oxide fuels in the Thorp reprocessing plant ("Thorp" PuO_2). In both reprocessing plants the PuO_2 is produced via plutonium oxalate precipitation and decomposition. Operating conditions in these plants has varied over the years, resulting in a range of powder properties, particularly specific surface area. Experiments have therefore measured water adsorption on seven different sources of PuO_2 powders, with specific surface area between 2.3 $m^2.g^{-1}$ and 37 $m^2.g^{-1}$. Samples were either used as-received from the production plant, prepared by re-calcining Magnox PuO_2 at a temperature above the original calcination temperature to lower the specific surface area (SSA), or by calcination of plutonium oxalate to give high SSA PuO_2.

The variation in water adsorbed with vapour pressure and temperature was determined by measuring the pressure of a sealed Inconel vessel, containing a known quantity of water and PuO_2, as a function of temperature. The overall approach is similar to the method developed by Paffett *et al.* [5].

Fig. 1. Vessel (front) and furnace (back, insulation removed) for water sorption studies.

The water adsorption, expressed as statistical monolayers coverage, increases with relative humidity. It is notable that results for different PuO_2:water mass ratios give similar sorption curves with relative humidity, which implies that the enthalpy of sorption for physisorption is very similar to the enthalpy of liquefaction. Furthermore, our experiments show similar results for all PuO_2 powders investigated, covering a wide range of calcination temperatures and associated specific surface areas. However, these results show some differences from the observations reported by Paffett *et al.* [5] for physisorption of water on PuO_2. Paffett *et al.* reported adsorption curves that fitted the BET model over a wide range of relative humidity whereas the PuO_2 samples investigated in the present study show lower sorption levels than the BET model at high relative humidity. Despite progress understanding the physisorption of water on PuO_2, uncertainty remains about the quantity and properties of strongly bound water on the oxide surface. The results from these and ongoing studies will be used to refine models of the water sorption on PuO_2 powders in storage.

Radiolysis of water adsorbed on PuO_2

Radiolysis of water adsorbed on PuO_2 generates hydrogen and under some conditions oxygen [6], raising the question of whether pressurisation from gas generation or flammable atmosphere could occur during long-term storage. Experiments in this study have so far focussed on measurements of the radiolytic yields of hydrogen gas from a wide range of PuO_2 and $(U,Pu)O_2$ powders exposed to atmospheres of fixed RH in either air or nitrogen. Our experimental results, combined with the available literature data [6], show for PuO_2 a trend of increasing $G(H_2)$ with the number of monolayers of water adsorbed onto the oxide surface. Only with a high number of monolayers of water on the surface of PuO_2 does the hydrogen yield approach that of bulk water. This is in contrast to studies of other metal oxides such as UO_2 and CeO_2 using γ irradiation or helium ion irradiation [7] that are reported to show the opposite trend and cannot, therefore, be used as analogues of PuO_2/water interactions. Despite this overall trend, differences are observed in the hydrogen yields from the various sources of PuO_2 studied and from changing the gas phase atmosphere between nitrogen and air. These differences highlight the potential complexity of the system and the importance of gas phase reactions under experimental conditions.

Even low $G(H_2)$ values would imply a pressurisation of stored PuO_2 packages over long timescales yet that is not observed in practice. Clearly, “back-reactions” must limit the build-up of hydrogen in sealed packages. These may involve surface (catalysed) recombination reactions and/or radiolytic processes that need to be characterised to fully understand the reaction chemistry occurring in PuO_2 storage packages and will be the focus of future work.

References

1. H.E. Sims *et al.*, “Hydrogen yields from water on the surface of plutonium dioxide,” *J. Nucl. Mat.*, **437** (2013) 359.

2. (a) C. RONCHI and J. P. HIEMAUT, “Helium diffusion in uranium and plutonium oxides”, *J. Nucl Mat.*, **325** (2004) 1 (b) Z. TALIP *et al.*, “Thermal diffusion of helium in 238Pu-doped UO_2”, *J. Nucl. Mat.*, **445** (2014) 117.

3. J.L. STAKEBAKE and L.M. STEWARD, “Water vapor adsorption on plutonium dioxide,” *J. Colloid Interface Sci.*, **42** (1973) 328.

4. J. M. HASCHKE and T.E. RICKETTS, “Adsorption of water on plutonium dioxide,” *J. Alloys Compd.*, **252** (1997) 148.

5. M.T. PAFFETT *et al.*, “A critical examination of the thermodynamics of water on actinide oxide surfaces,” *J. Nucl. Mat.*, **322** (2003) 45.

6. (a) D. K. VEIRS et al., “Water radiolysis on plutonium dioxide: Initial results identifying a threshold relative humidity for oxygen gas generation”, Los Alamos report LA-UR-12-26423 (2012) (b) J. M. DUFFEY and R. R. LIVINGSTON, “Gas generation testing of plutonium dioxide”, WSRC-MS-2002-00705 (2002) (c) M. V. VLADIMIROVA and I. A. KULIKOV, “Formation of H_2 and O_2 in Radiolysis of Water Sorbed on PuO_2”. *Radiochemistry* **44** (2002) 86.

7 J. A. LAVERNE and L. TANDON, “H_2 production in the radiolysis of water on UO_2 and other oxides”, *J. Phys. Chem. B*, **107** (2003) 13623.

C-24

Irradiation testing of fuels for plutonium and minor actinide transmutation

P. Ralph Hania

NRG, Petten, The Netherlands

Studies towards transmutation of plutonium and (some of) the minor actinides in fast spectrum reactors have been conducted for a few decades, mainly in Europe, the US and Japan. Main drivers have been the growing stockpiles of separated plutonium in several countries in the 20th century and a decision in some countries to pursue lifetime and volume reduction of spent fuel waste. In Europe several institutes have worked together to perform irradiation tests to assess the in-core behavior of candidate fuels and/or matrices carrying the long-living actinide waste, including mixed oxides, nitrides and ceramic-ceramic and ceramic-metallic composites.

The aim of this contribution is to provide a limited overview of experimental assessment of candidate transmutation fuels. The reasons behind and results of some of these fuel tests will be presented, with a focus on the HFR Petten but citing other work as well.

C-25

How alpha decays of actinides will affect the nuclear glass structure: evidence of competitive effects between damage generation from recoil nuclei and recovery processes from alpha particles

Sylvain Peuget[1], Anamul Haq Mir[1], Thibault Charpentier[2], Laura Martel[3], Joseph Somers[3], Thierry Wiss[3], Jean-Marc Delaye[1], Marcel Toulemonde[4], Serge Bouffard[4], Christophe Jégou[1]

[1]CEA, DEN, DTCD, SECM, Laboratoire d'Étude des Matériaux et Procédés Actif, Bagnols sur Cèze, France, [2]NIMBE, CEA, CNRS, Université Paris-Saclay, CEA Saclay, Gif sur Yvette, France, [3]European Commission, Joint Research Centre (JRC), Institute for Transuranium Elements (ITU), Karlsruhe, Germany, [4]CIMAP-GANIL (CEA-CNRS-ENSICAEN-Univ. Caen), Caen, France

Borosilicate glasses, besides their numerous applications, have been recognized as valuable materials for the conditioning of nuclear wastes. Among the long term behavior issues, the structural evolution of the glass under irradiation (beta and alpha decays) [1] is of primary importance, along with its chemical durability in a deep-geological repository [2,3]. Alpha decay from minor actinides is the main source of atomic displacements in the glassy network under repository conditions. Therefore so as to guarantee the long-term behavior of containment glasses in the nuclear waste repository, studies have been conducted since 1970 in Europe, in the USA and in Japan, on the effects of irradiation in nuclear glasses[1]. Since 2001 an important research program was started in France on the consequences of alpha decays on the properties of the French borosilicate glass, called SON68 glass, which was recently reviewed in [4]. The radiation damage induced by alpha decay was investigated by examining glass specimens, doped with a short-lived actinide ^{244}Cm, irradiated by light and heavy ions, irradiated in research reactor by using the nuclear reaction $^{10}B(n,\alpha)^{7}Li$ and by performing Molecular Dynamic (MD) simulation of displacements cascades.

These studies have shown that some macroscopic properties vary appreciably with the accumulation of alpha decay, but then stabilize after integrating doses of the order of 4×10^{18} $\alpha \cdot g^{-1}$. The glass density decreases by about 0.6%, its Young's modulus by about 15% and its hardness by about 30%, while its fracture toughness increases by around 50%. These variations with alpha decay dose follow a direct impact model[4], $f_a = 1-\exp(-v_i D_\alpha)$, where f_a is the damage volume fraction, v_i is the damage volume per event (g) and D_α is the alpha decay dose per g. Such an evolution indicates that only a single alpha decay event is enough to induce a full transformation of the material to the saturated damaged state.

Heavy ion irradiation in the MeV energy regime, simulating damage induced by the recoil nuclei (RN) of alpha decays, correctly reproduced the macroscopic property variation versus alpha decay dose observed on ^{244}Cm doped glass (figure 1), with a saturation phenomenon occurring after an energy deposition by nuclear collision of around $5x10^{20}$ keV.cm^{-3} (30MGy). Moreover MD simulation of the accumulation of displacements cascades generated by heavy ion also showed a glass swelling following a similar exponential variation with dose (figure 1). This good agreement between alpha decay and heavy ion irradiations studies suggests that the nuclear collisions induced by the recoil nuclei is responsible of the variation of macroscopic properties evolution observed under alpha decay irradiation. Nevertheless the density variation observed under heavy ions external irradiation is greater than under alpha decay irradiation showing that heavy ion irradiation do not fully reproduce the phenomena occurring during an alpha decay event.

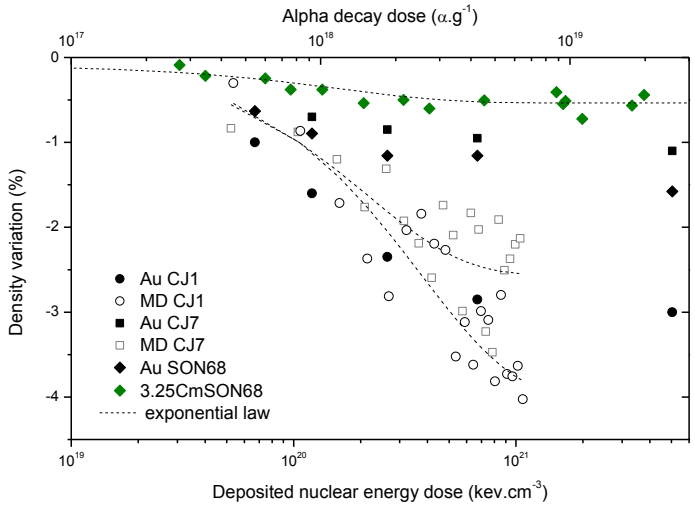

Figure 1. Density variations of 3.25wt% $^{244}CmO_2$ doped SON68 glass, of borosilicate glass (CJ1, CJ7, SON68) irradiated by gold ions (1-7 MeV), and of borosilicate glass (CJ1, CJ7) irradiated with MD simulation by accumulation of 600 eV cascades, [4]

In parallel to the macroscopic studies, SEM and TEM characterizations have been performed on ^{244}Cm doped glass and showed that alpha decay radiation damage do not induce a modification of the glass microstructure up to the nanometer scale (figure 2). The glass is still homogeneous, with no phase separation, crystallisation or bubbles formation up to an alpha decay dose corresponding to several thousand years of disposal of nuclear glass canister. Heavy ion and $^{10}B(n,\alpha)^{7}Li$ irradiations have confirmed the stability of SON68 glass microstructure under extreme irradiation conditions.

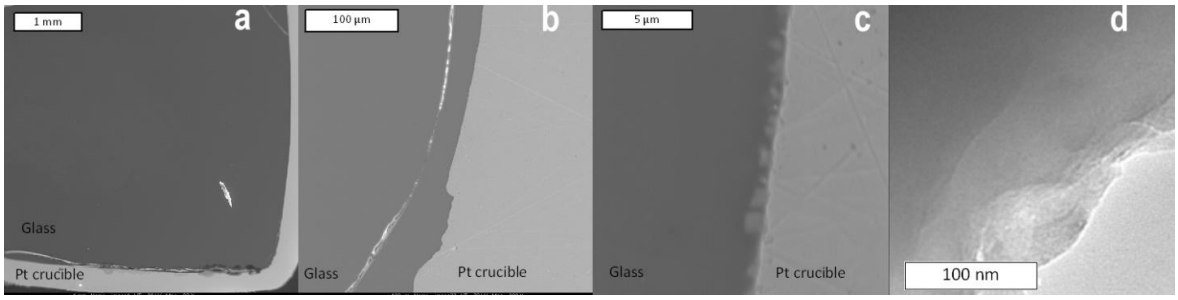

Figure 2. a to c**,** SEM pictures of a SON68glass doped with 3.25wt% of $^{244}CmO_2$ after an alpha decay dose of 1.5 x $10^{19}\alpha$/g. d, TEM picture of a SON68glass doped with 1.2wt% of $^{244}CmO_2$ after an alpha decay dose of 8 x $10^{18}\alpha$/g

So as to understand the origin of the changes in macroscopic properties under alpha decay irradiation, the short and medium range order of the irradiated glass was probed with various spectroscopic techniques, mainly NMR, Raman and XANES.

Some changes in the local order around the main cations have been identified. Heavy ion irradiation showed a change in boron (figure 3) and aluminum coordination numbers and an increase in the glass depolymerization [4-6]. These observations have been correlated with other structural transformations observed by Raman spectroscopy and Molecular Dynamic simulation (MD) studies [4,7]. In addition to the modifications of the local order around the cations, molecular dynamics and external irradiation studies [4,8] also revealed an evolution of the medium-range order, involving both changes in the bond angles between network formers and broadening of the ring-size distributions indicating increasing disorder with irradiation. A recent calorimetric study showed an increase of the fictive temperature of the damaged glass [9], suggesting that the driver of these structural evolution could be associated to a local melting process followed by a high quenching rate step, due to the RN displacement cascade [10]. Therefore a model of

irradiation induced vitrification involving ballistic disordering and fast quenching events has been proposed to explain the glass restructuration under alpha decay irradiation [9] that suggests that the nuclear damage generated by RN controls the glass transformation [4].

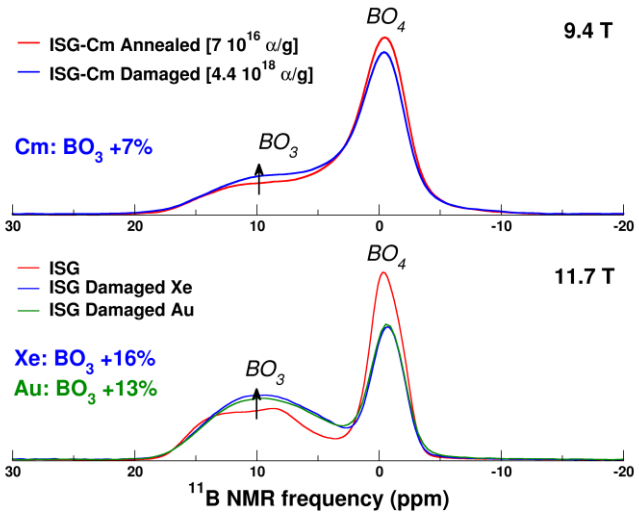

Figure 3 : Upper Panel: Comparison between the ^{11}B MAS NMR spectra (9.4T) of a damaged and annealed ^{244}Cm doped ISG glasses[11]. Lower Panel: Comparison between the ISG and ISG-damaged with Xe (92MeV) and Au (1-7MeV) irradiation [4,6] acquired at higher magnetic field (11.7T) Spectra are normalized to the same area.

Nevertheless, the amplitude of either macroscopic property and structural parameter changes observed under alpha decay irradiation are much lower than those generated by heavy ion irradiation that simulate the effect of the RN (Figure 1 and 3) [11]. Moreover recent results using sequential and simultaneous ion irradiations [12,13] have shown that the electronic energy loss of the alpha particle (AP) induces partial repair of the damage generated by heavy ions. Therefore the final damaged glassy state of actinides doped glasses is certainly controlled by both type of events and associated competitive mechanisms, damage generation from RN and self-healing from AP. This competitive mechanism can be understood in the framework of the unified thermal spike phenomenology [14]. Under this phenomenology, the energy loss of the ions causes local heating around the ion path and in certain cases can induce local melting and ion track formation (the local temperature depends on the energy loss of the ions). This mechanism has been used to describe the ion track formation during 92MeV Xe ion irradiation (high electronic stopping power) [6] and 1 to 7 MeV Au ion irradiation (high nuclear stopping power) [14]. This thermal spike description is in full agreement with the modifications of the local order observed in borosilicate glass under such irradiation conditions [4,6] mainly a decrease of boron coordination number and an increase of non-bridging oxygen concentration (NBO). Indeed in borosilicate glasses, it is well known that the increase of the temperature induces a shift of the reaction $BO_4 \leftrightarrow BO_3$ + NBO to the right [15] and so favors trigonal boron and NBO. In the irradiation with alpha decay, however, RN and AP simultaneously irradiate the material. The RN induce very high pseudo-temperature inside the displacement cascades [10] (which can be qualified as ballistic melting in the framework of unified thermal spike phenomenology), higher than the glass melting temperature, which results in a similar glass transformation as for heavy ion external irradiation. On the contrary, 99% of AP energy is lost in electronic collisions with a very low electronic stopping power of around 0.5 keV/nm, which is insufficient, according to the thermal spike calculation [12], to reach the glass melting temperature and then generate the same damage level as heavy ions. Nevertheless, temperatures of around 600 K can be reached [12] which are high enough to induce a partial repair of the irradiated glassy structure, as has been shown by numerous calorimetric experiments performed on actinides doped glasses [1,9,16]. So the partial repair of the glassy structure can occur via defect recombination activated by the AP thermal spike, which does not need to exceed the glass transition temperature but rather activate the defect recombination. Therefore the lower damage level observed in the ^{244}Cm doped glass can be explained by the competitive effect between damage generation by the RN and partial damage repair due to AP.

To conclude, alpha decay accumulation in nuclear glass induces a slight modification of the glassy state involving both decay product of alpha disintegration, RN and AP. We propose that the final structure is therefore the result of the “supervitrification” due to the ballistic melting in RN tracks and the subsequent AP partial damage repair due to a thermal self-healing mechanism.

References

1 Weber, W. J. *et al.* Radiation effects in glasses used for immobilization of high-level waste and plutonium disposition. *Journal of Material Society* **12**, 1946-1978 (1997).

2 Vienna, J. D., Ryan, J. V., Gin, S. & Inagaki, Y. Current Understanding and Remaining Challenges in Modeling Long-Term Degradation of Borosilicate Nuclear Waste Glasses. *International Journal of Applied Glass Science* **4**, 283-294, doi:10.1111/ijag.12050 (2013).

3 Cailleteau, C. *et al.* Insight into silicate-glass corrosion mechanisms. *Nature Materials* **7**, 978-983, doi:10.1038/nmat2301 (2008).

4 Peuget, S., Delaye, J. M. & Jégou, C. Specific outcomes of the research on the radiation stability of the French nuclear glass towards alpha decay accumulation. *Journal of Nuclear Materials* **444**, 76-91, doi:http://dx.doi.org/10.1016/j.jnucmat.2013.09.039 (2014).

5 Peuget, S. *et al.* Comparison of radiation and quenching rate effects on the structure of a sodium borosilicate glass. *Journal of Non-Crystalline Solids* **378**, 201-212 (2013).

6 Mendoza, C. *et al.* Oxide glass structure evolution under swift heavy ion irradiation. *Nuclear Instruments and Methods in Physics Research Section B: Beam Interactions with Materials and Atoms* **325**, 54-65, doi:http://dx.doi.org/10.1016/j.nimb.2014.02.002 (2014).

7 Delaye, J. M., Peuget, S., Calas, G. & Galoisy, L. Comparative effects of thermal quenching and ballistic collisions in SiO2–B2O3–Na2O glass. *Nuclear Instruments & Methods in Physics Research Section B-Beam Interactions with Materials and Atoms* **326**, 256-259, doi:http://dx.doi.org/10.1016/j.nimb.2013.10.061 (2014).

8 Delaye, J. M., Peuget, S., Bureau, G. & Calas, G. Molecular dynamics simulation of radiation damage in glasses. *Journal of Non-Crystalline Solids* **357**, 2763-2768, doi:10.1016/j.jnoncrysol.2011.02.026 (2011).

9 Maugeri, E. A. *et al.* Calorimetric Study of Glass Structure Modification Induced by a Decay. *Journal of the American Ceramic Society* **95**, 2869-2875, doi:10.1111/j.1551-2916.2012.05304.x (2012).

10 Peuget, S. *et al.* Irradiation stability of R7T7-type borosilicate glass. *Journal of Nuclear Materials* **354**, 1-13, doi:10.1016/j.nucmat.2006.01.021 (2006).

11 Charpentier, T. *et al.* Self-healing capacity of nuclear glass observed by NMR spectroscopy. *Scientific Reports* **6**, doi:10.1038/srep25499 (2016).

12 Mir, A. H. *et al.* Defect recovery and damage reduction in borosilicate glasses under double ion beam irradiation. *EPL (Europhysics Letters)* **112**, 36002 (2015).

13 Mir, A. H. *et al.* Mono and sequential ion irradiation induced damage formation and damage recovery in oxide glasses: Stopping power dependence of the mechanical properties. *Journal of Nuclear Materials* **469**, 244-250, doi:10.1016/j.jnucmat.2015.12.004 (2016).

14 Toulemonde, M. *et al.* Synergy of nuclear and electronic energy losses in ion-irradiation processes: The case of vitreous silicon dioxide. *Phys. Rev. B: Condens. Matter Mater. Phys.* **83**, 9, doi:054106 10.1103/PhysRevB.83.054106 (2011).

15 Wu, J. & Stebbins, J. F. Quench rate and temperature effects on boron coordination in aluminoborosilicate melts. *Journal of Non-Crystalline Solids* **356**, 2097-2108, doi:10.1016/j.jnoncrysol.2010.08.015 (2010).

16 Primak, W. & Roberts, F. P. Stored energy in a radioactive waste borosilicate glass: Its frequency factor and kinetics and its source. *Nuclear Science and Engineering* **86**, 191-205 (1984).

C-26

Recent progress in actinide phosphates chemistry

Karin Popa[1], Gilles Wallez[2], Damien Bregiroux[2], Philippe E. Raison[1], Laura Martel[1], Yulia Arinicheva[3], Stefan Neumeier[3], Joseph Somers[1], Rudy Konings[1]

[1]European Commission, Joint Research Centre, Institute for Transuranium Elements, Karlsruhe, Germany, [2]Sorbonne Universités, UPMC Univ Paris, Paris, France, [3]Forschungszentrum Jülich, IEK-6, Juelich, Germany

Ceramic nuclear waste forms are potential alternative materials for the storage and final disposal of very long-lived radioisotopes. Different classes of phosphates (*e.g.* monazites, diphosphates, britholites, thorium phosphate-diphosphate, NZP-like phosphates) are considered, since they may incorporate significant amounts of actinides in different oxidation states. Some of them, of natural occurrence, have demonstrated long-term chemical and mechanical stability [1], indicating their potential for actinide disposal, should a policy of partitioning and conditioning be followed for the back end of the fuel cycle. Such compounds are also under consideration for space applications (zero or negative thermal expansion, space batteries, etc.). We present here recent findings on the preparation and the characterisation of pure phases of actinides-containing phosphates and their relevance for the conditioning of the nuclear waste.

1. Monazites

Natural monazite minerals (Ce-, La-, and Nd-monazites) and their synthetic analogues $M^{III}PO_4$ (M^{III} = Bi, La, Ce, Pr, Nd, Sm, Eu, Gd, Tb, Dy, Pu, Am, and Cm) all crystallise in the monoclinic space group $P2_1/n$ (14) [2]. We have prepared $PuPO_4$ through different synthesis routes [3-6]. As plutonium can exist in both +III and +IV oxidation states in $PuPO_4$ and PuP_2O_7, respectively, investigation of Pu-monazite is of particular interest. High resolution XANES measurements confirm the +III valence state of plutonium, in agreement with valence bond derivation. The presence of the americium (as a β^- decay product of plutonium) in the +III oxidation state was determined based on XANES spectroscopy. [4].

Thermal behaviour, lattice parameter evolution and decomposition of $PuPO_4$ have been reported earlier by our group and it was found that $PuPO_4$ decomposes to the corresponding oxides under a nitrogen atmosphere above 1100 °C [5]. The heat capacity and the magnetic properties of $PuPO_4$ have also been measured [6].

Pure-phase $La_{1-x}Pu_xPO_4$ solid solutions with monazite structure were obtained for the compositions with x= 0.01, 0.05, 0.10, 0.15. The lattice parameters follow linear trend with composition confirming solid solution formation. XRD-patterns of the compounds with x=0.25 and 0.50 revealed the formation of two phases: $(La,Pu)PO_4$ with a monazite structure and Pu-oxide, and is likely a consequence of the disparate thermal stability limits of the end members. The molar fraction of Pu in the monazite phase was estimated using the Rietveld refinement of the XRD data in order to determine the solubility of Pu in $LaPO_4$ within the monazite structure. The structural incorporation of Pu(III) on the La(III) sites into the monazite structure is currently studied trough ^{31}P MAS-NMR, EXAFS and XANES measurements. The ^{31}P spectra of two actinide-based monazites are presented in **Fig 1**. They are characterized by one main peak representative of a P atom surrounded by four oxygen and four cations (Pu or La) called $(PO_4)(Pu)_4$ or $(PO_4)(La)_4$ units. The small extra peaks (red arrows) which are the NMR signature of a good solid solution, which in this material indicates the presence of very low amount of Am (from ^{241}Pu decay) to give $(PO_4)(La)_3(Pu)_1$ or $(PO_4)(Pu)_3(Am)_1$ units.

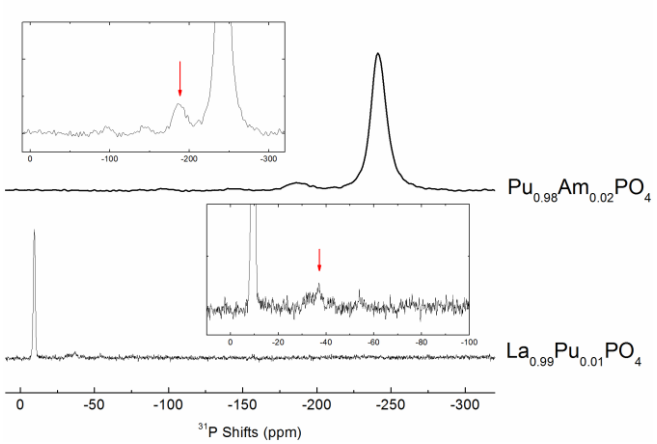

Fig. 1 ^{31}P MAS NMR spectra of two monazite solid solution acquired at 55 kHz and their corresponding zoom in the insets.

2. Cheralites

The mineral cheralite is an analogue of monazite $CePO_4$, in which cerium is replaced randomly by two different cations with similar ionic radii. The archetype, $CaTh(PO_4)_2$, originally named brabantite, was described by Rose [7]. Based on steric considerations, Podor *et al.* [8] established the criteria of the stability of $M^{II}M^{IV}(PO_4)_2$ compounds in the cheralite form. Several Th-cheralites of Ca, Cd, Sr, Pb, and Ba form under hydrothermal conditions [9,10]. Ca-free derivates often result in non-cheralite forms.

Moreover, $CaNp(PO_4)_2$ and $CaU(PO_4)_2$ crystallize in the monoclinic $P2_1/n$ space group [11,12]. However, no Pu(IV) or Ce(IV) cheralites exists, due to the redox behavior of these elements at high temperature [13]. Complete monazite-cheralite solid solutions were obtained and well characterized several times by different authors: $CePO_4$-$CaTh(PO_4)_2$, $LaPO_4$-$CaTh(PO_4)_2$ and $LnPO_4$-$CaTh(PO_4)_2$-$CaU(PO_4)_2$(with *Ln* = La, Nd, Gd) [14-16]. Thermal stability studies indicated that heat treatment caused gradual decomposition of $CaTh(PO_4)_2$ into the corresponding oxides above 1250 ^{o}C [5,17]. Thus, conventional sintering of this material cannot be applied. We have achieved rapid densification, of such powders, without decomposition, using the spark plasma sintering (SPS) method. Fully densified pellets of pure cheralite were produced and used for further thermal diffusivity and hardness measurements.

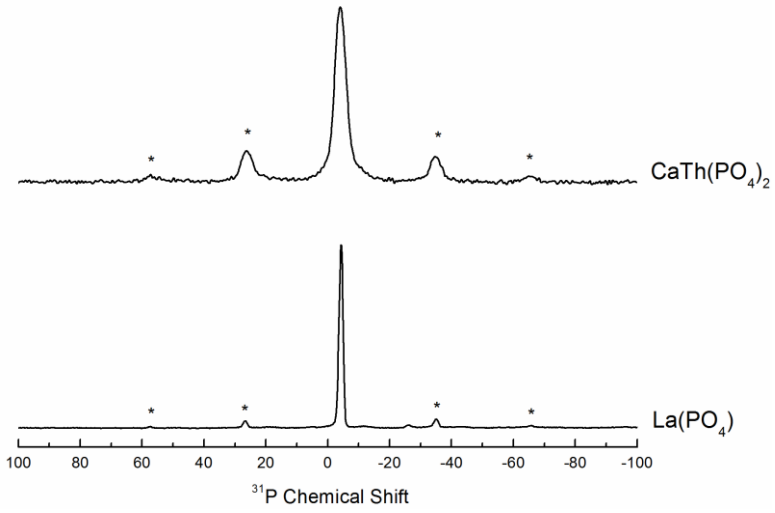

Fig. 2 ^{31}P MAS NMR spectra of $CaTh(PO_4)_2$ and $LaPO_4$ acquired at 5 kHz. The stars stand for the spinning sidebands.

Within this study, the ^{31}P MAS NMR was used to complete the structural characterisation of the synthetic cheralite (**Fig. 2**). Both $LaPO_4$ and $CaTh(PO_4)_2$ present a single ^{31}P NMR peak in agreement with their crystallographic structure.

3. Yavapaiites

Yavapaiite mineral crystallizes in the C2/m monoclinic space group and consists of layers running parallel to the (a,b) plane built up of corner-connected *M'*O_6 octahedra and PO_4 tetrahedra [18]. Several structural classes of phosphates stem from yavapaiite at room temperature:

(a) "low-yavapaiite" for small cations *M* and *M'* (Ca to Sr and Ge to Zr, respectively), crystallize in the C2/c space group [19]. This form, together with the yavapaiite itself, cannot incorporate actinides into their structures.

(b) "super-yavapaiite" is made of cations big enough (*i.e.* barium actinide phosphates) to form polyhedra of higher coordination [20]. The super yavapaiite structure crystallizes in the C2/c space group. The structure is made of (100) layers of BaO_{14} polyhedra alternating with dense slabs of *M*'O_8 square-based antiprisms and PO_4 tetrahedra. The uncommon BaO_{14} units are distorted elongated hexagonal bipyramids. The high level of coordination of the two cations is consistent with their large size.

4. Relationship between the cheralite and yavapaiite structures

The existence of two very different structures, cheralite and yavapaiite, stems from the difference of ionic size of the *M* and *M'* cations [21]. The high ratio between the ionic radii of the divalent and tetravalent cations in yavapaiite forms results in the ordering of these cations into well differentiated polyhedra, typically a large one for M^{II} and a small one for M^{IV}. The link between these two structural families could be observed in the case of $SrNp(PO_4)_2$, which crystallizes in the orthorhombic space group Cmca [22]. Though this structure exhibits alternate layers of SrO_{10} and NpO_8 polyhedra, like in yavapaiite, it is the most strongly linked to the cheralite form.

5. Relevance in the nuclear waste management

As a potential candidate for the specific immobilization of long-life radionuclides, the chemical durability of cheralite compounds were extensively studied, confirming their chemical durability [23]. The degradation of the chemical durability induced by the presence of tetravalent uranium is explained by its tendency to oxidize at the solid-liquid interface during the dissolution process.

Because of the anisotropy of the crystal structure, yavapaiite and derived compounds show a strongly anisotropic thermal expansion. We have analyzed the expansion mechanism of room temperature and high temperature forms of $BaZr(PO_4)_2$. In the yavapaiite form, the thermal expansion results in the unfolding of the $[Zr(PO_4)_2]_n^{2-}$ layers, involving various phenomena such as bridging oxygen rocking motion in the Zr-O-P linkage. The resulting cell parameters thermal expansion are 34.0, -4.1 and 7.3 10^{-6} K^{-1} for a, b and c, respectively. In the high temperature form, the unfolded $[Zr(PO_4)_2]_n^{2-}$ layers cannot expand further, so that the crystal structure only expands along the c-axis. In contrast, lanthanide monophosphates with the cheralite structure, show almost isotropic thermal expansion [24].

References

[1] D. Bregiroux, R. Belin, P. Valenza, F. Audubert, D. Bernache-Assollant, *J. Nucl. Mater.* **366** (2007) 52-57

[2] N. Clavier, R. Podor, N. Dacheux, *J. Eur. Ceram. Soc.* **31** (2011) 941-976

[3] C. Thiriet, R.J.M. Konings, F. Wastin, *J. Nucl. Mater.* **344** (2005) 56-60

[4] K. Popa, P.E. Raison, L. Martel, P.M. Martin, D. Prieur, P.L. Solari, D. Bouëxière, R.J.M. Konings, J. Somers, *J. Solid State Chem.* **230** (2015) 169-174

[5] R. Jardin, C.C. Pavel, P.E. Raison, D. Bouëxière, H. Santa-Cruz, R.J.M. Konings, K. Popa, *J. Nucl. Mater.* **378** (2008) 167-171

[6] O. Beneš, K. Popa, V. Reuscher, A. Zappia, D. Staicu, R.J.M. Konings, *J. Nucl. Mater.* **418** (2011) 182-185

[7] D. Rose, *Neues. Jahrb. Mineral. Monatsh.* **6** (1980) 247-257

[8] R. Podor, M. Cuney, C.N. Trung, *Am. Mineral.* **80** (1995) 1261-1268

[9] J.M. Montel, J.-L. Devidal, D. Avignant, *Chem. Geol.* **191** (2002) 89-104

[10] K. Popa, T. Shvareva, L. Mazeina, E. Colineau, F. Wastin, R.J.M. Konings, A. Navrotsky, *Am. Miner.* 93 (2008) 1356-1362

[11] Y. Dusausoy, N.E Ghermani, R. Podor, M. Cuney, *Eur. J. Mineral.* **8** (1996) 667-673

References

[12] P.E. Raison, R. Jardin, D. Bouëxière, R.J.M. Konings, T. Geisler, C.C. Pavel, J. Rebizant, K. Popa, *Phys. Chem. Minerals* **35** (2008) 603-609

[13] K. Popa, D. Bregiroux, R.J.M. Konings, T. Gouder, A.F. Popa, T. Geisler, P.E. Raison, *J. Solid State Chem.* **180** (2007) 2346-2355

[14] Y. Hikichi, K. Hukuo, J. Shiokawa, *Nippon Kagaku Kaishi* **12** (1978) 1635-1640

[15] R. Podor, M. Cuney, *Am. Mineral.* **82** (1997) 765-771

[16] R.J.M. Konings, M. Walter, K. Popa, *J. Chem. Thermodynamics* **40** (2008) 1305-1308

[17] P.E. Raison, S. Heathman, G. Wallez, C.E. Zvoriste, D. Bykov, G. Ménard, E. Suard, K. Popa, N. Dacheux, R.J.M. Konings, R. Caciuffo, *Phys. Chem. Miner.* **39** (2012) 685-692

[18] E.J. Graeber, A. Rosenzweig, *Am. Miner.* **56** (1971) 1917-1933

[19] K. Popa, G. Wallez, D. Bregiroux, P. Loiseau, *J. Solid State Chem.* **184** (2011) 2629-2634

[20] D. Bregiroux, K. Popa, R. Jardin, P.E. Raison, G. Wallez, M. Quarton, M. Brunelli, C. Ferrero, R. Caciuffo, *J. Solid State Chem.* **182** (2009) 1115-1120

[21] D. Bregiroux, K. Popa, G. Wallez, *J. Solid State Chem.* **230** (2015) 26-33

[22] G. Wallez, D. Bregiroux, K. Popa, P.E. Raison, C. Apostolidis, P. Lindqvist-Reis, R.J.M. Konings, A.F. Popa, *Eur. J. Inorg. Chem.* (2011) 110-115

[23] O. Terra, N. Dacheux, F. Audubert, R. Podor, *J. Nucl. Mater.* **352** (2006) 224-232

[24] L. Perrière, D. Bregiroux, B. Naitali, F. Audubert, E. Champion, D.S. Smith, D. Bernache-Assollant, *J. Eur. Ceram. Soc.* **27** (2007) 3207-3213

C-27

Chemical Bond Nature in $Cs_2AnO_2Cl_4$

Yury Teterin[1,3], Anton Teterin[1], Kirill Ivanov[1], Mikhail Ryzhkov[2], Konstantin Maslakov[3], Stepan Kalmykov[3], Vladimir Petrov[3], Dmitry Suglobov[3]

[1]NRC "Kurchatov Institute", Moscow, Russia, [2]Ural Department of RAS, Institute of Solid State Chemistry, Ekaterinburg, Russia, [3]Radiochemistry Division, Chemistry Department, Lomonosov Moscow State University, Moscow, Russia, [4]V.G. Khlopin Radium Institute, St.-Petersburg, Russia

Chemical bond features in $Cs_2AnO_2Cl_4$ (An=U,Np,Pu) due to the participation of electrons of the filled An 6p and O 2s (Cl 3s) atomic shells were studied. Quantitative analysis was done of the valence electrons x-ray photoelectron spectra structure in the binding energy (BE) range of 0 eV to ~35 eV for dicaesium tetrachlorodioxoactinate ($Cs_2AnO_2Cl_4$) single crystal. This compound contains the neptunyl group NpO_2^{2+}. The BEs and structure of the core electronic shells (~35 eV – 1250 eV), as well as the relativistic discrete variation (RDV) calculation results for the $AnO_2Cl_4^{2-}$ (D_{4h}) cluster reflecting Np close environment in $Cs_2NpO_2Cl_4$ were taken into account. The experimental data show that the many-body effects due to the presence of cesium and chlorine contribute to the outer (0 – ~15 eV BE) valence molecular orbitals (OVMO) spectral structure much less than to the inner (~15 – ~35 eV BE) (IVMO) one. The filled An 5f electronic states were theoretically calculated and experimentally confirmed to present in the valence band of $Cs_2AnO_2Cl_4$. It corroborates the suggestion on the direct participation of the An 5f electrons in the chemical bond. The An 6p atomic orbitals (AO) participate in formation of both the inner (IVMO) and the outer OVMO valence molecular orbitals (bands). The filled An 6p and the O 2s, Cl 3s electronic shells were found to take the maximum part in the IVMO formation. The MO composition and the sequence order in the binding energy range 0 eV – ~35 eV in $Cs_2AnO_2Cl_4$ were established. The experimental and theoretical data allowed a quantitative MO scheme for $Cs_2AnO_2Cl_4$ in the BE range0 – ~35 eV, which is fundamental for both understanding the chemical bond nature in $Cs_2AnO_2Cl_4$ and the interpretation of other x-ray spectra of $Cs_2AnO_2Cl_4$. The contributions to the chemical binding for the $UO_2Cl_4^{2-}$ ($NpO_2Cl_4^{2-}$) clusters were evaluated to be: the OVMO contribution – 76% (49%), the IVMO contribution – 24% (51%).

C-28

Integrated surface science lab station for spent corrosion studies

Thomas Gouder, Rachel Eloirdi, Frank Huber, Roberto Caciuffo

European Commission, Joint Research Centre, Institute for Transuranium Elements, Karlsruhe, Germany

Surface reactions play an important role in the storage of spent nuclear fuel. In particular, knowledge of the reaction mechanisms is important for prediction of the fuel behaviour under special conditions and under long term storage. One promising route for establishing the reaction mechanisms in the complex fuel is to replace it by simplified model systems. These allow addressing part-aspects of the overall process in so called single effect studies. In our approach, the fuel matrix is represented by sputter deposited thin films of actinide oxides (ThO_2, UO_2, PuO_2, mixed oxides, etc.) into which fission products, minor actinides, cladding or waste container materials are incorporated by co-deposition. The surface reactivity of these systems is studied in a two-step process. 1. Single surface-gas interactions are investigated by studying the gas adsorption under UHV. While being different from real world corrosion conditions, the reaction parameters can be closely controlled (gas dosage, mixing, temperature…). 2. Real world reactions are probed under atmospheric conditions, e.g. by performing electrochemistry studies.

We will first present the surface science lab station (Fig. 1) at ITU, which is dedicated to these studies. Basic idea was to integrate sample preparation, analysis and surface reactions in one single, well controlled environment to ensure unaltered, representative surfaces (avoiding e.g. contact with lab atmosphere). The machine is available to external users and its flexible design enables it fulfilling a great number of different tasks.

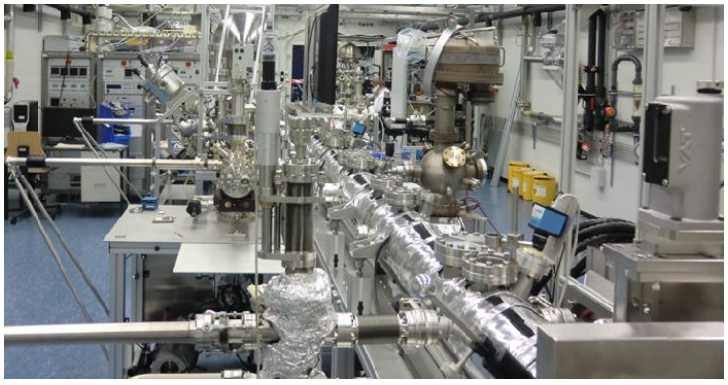

It allows carrying out sample preparation, and reactivity studies under UHV and ambient pressure. In future the system will be working with transuranium elements. Special emphasis is given to the combination of spectroscopy techniques (XPS, UPS, BIS, TPD, HREELS, Kelvin probe) probing the average surface, and mapping techniques probing local reactivity aspects (AFM running under ambient pressure, combined with electrochemistry) will be presented. Another important aspect is the gap between ultra-high vacuum conditions, imposed by most surface spectroscopies, and the ambient reaction conditions (aqueous environment) of spent fuel during storage. To assess it, diagnostic techniques running under both conditions are being implemented (e.g. Kelvin probe measuring the surface potential under UHV and ambient pressure). The system is equipped with three preparation chambers, allowing producing thin films (sputter deposition and evaporation) and carrying out surface reactions (adsorption of molecular and atomic oxygen, hydrogen etc.).

The system has a modular setup, where the various techniques are mounted in individual chambers, which can be connected to the station on demand. Separation into independent devices ensures robust operation of such complex facility.

In a second part of the talk we will report on an ongoing study of $UCeO_x$ films, used as surrogates for U-Pu MOX. Films have been prepared from the elemental targets (U, Ce) by

sputter deposition in presence of oxygen. Oxygen content was adjusted by the oxygen pressure and postdeposition exposure to atomic oxygen. Goal was to study the surface reactivity of off-stoichiometric films towards a series of reactants intervening in nuclear waste corrosion reactions (H_2O, O_2, H_2, H_{atomic}). Information on surface stoichiometry and morphology was obtained by XPS, UPS an AFM.

C-29

Effect of Doping Level on Dissolution Behavior of Rare-Earth Doped UO_2

Jeongmook Lee[1], Jandee Kim[1], Young-Sang Youn[1], Jong-Goo Kim[1], Sang-Eun Bae[1,2], Yeong-Keong Ha[1], Jong-Yun Kim[1,2]

[1]Korea Atomic Energy Research Institute, Daejeon, Republic of Korea, [2]University of Science and Technology, Daejeon, Republic of Korea

The concept for the disposal of high level nuclear waste like spent nuclear fuel is based on multiple barriers including the fuel waste form, containers, and a deep geologic environment [1]. To design reliable and safe geological repositories for long-term storage it is important to understand the change of characteristics of spent nuclear fuel with time, and the storage environment affected by spent nuclear fuel [2]. In the spent nuclear fuel after irradiation in a nuclear power plant, there are nearly ~95% of UO_2 and large number of fission products such as rare-earth (RE) elements [2,3]. These products would lead to many changes on physical and chemical properties of the fuel like thermal conductivity, phase stability and the relevant fuel performance [4,5]. The key changes influence the chemical reactivity of the fuel are the RE doping and non-stoichiometry of the UO_2 matrix when the fuel waste will expose to groundwater at container failure [1]. In this work gadolinium and thorium were chosen as a representative trivalent and tetravalent element of RE, respectively. Gadolinium or thorium doped uranium dioxide pellets with several doping level up to 10 mol% were manufactured from mixture of Gd_2O_3 or ThO_2 and UO_2 powder, respectively. By regulating oxygen potential, RE doped UO_2 and $UO_{2\pm x}$ pellets were also produced. X-ray diffraction (XRD), scanning electron microscopy (SEM), and Raman spectroscopy were used to confirm the physical properties of RE (Gadolinium or thorium) doped uranium dioxides. The substitution of gadolinium and thorium atoms into the UO_2 fluorite lattice was found by the change of lattice parameters evaluated from XRD spectra. Especially, The stoichiometric difference of Gd doped UO_2 was confirmed using the relation between lattice parameter and doping level. The microstructures of RE doped uranium dioxide surface were observed by SEM, and they showed that there was markedly difference with doping level and stoichiometric difference on surface of UO_2 matrix. Raman spectra showed surface structure of each pellet of Gd doped UO_2 affected by gadolinium doping level. For electrochemical behavior and dissolution properties in carbonate solutions, a standard three-electrode system was employed with RE doped uranium dioxide used as the working electrode. Electrochemical results showed the influence of RE doping level and stoichiometric difference of the UO_2 matrix on kinetics of oxidation and dissolution of uranium dioxide.

References

[1] Shoesmith, D.W., (2000) J.Nucl. Mater. 282, 1-31.

[2] Ewing, R.C. (2015) Nat. Mater. 14, 252–257.

[3] Konings, R.J.M., Wiss, T. and Beneš, O. (2015) Nat. Mater. 14, 247–252.

[4] Amaya, M., Hirai, M., Kubo, T. and Korei, Y. (1996) J. Nucl. Mater. 231, 29-33.

[5] Cobos, J., Papaioannou, D., Spino, J. and Coquerelle, M. (1998) J. Alloy. Comp. 271-273, 610-615.

C-30

A new strategy for stabilizing uncommon oxidation states learned from an extraordinarily complex mixed-valent uranium phosphonate framework

Chengliang Xiao[1], Lanhua Chen[1], Juan Diwu[1], Thomas E. Albrecht-Schmitt[2], Shuao Wang[1]

[1]Soochow University, Suzhou, Jiangsu, China, [2]Florida State University, Tallahassee, Florida, USA

Compounds containing U(V) are difficult to produce, primarily because of its inherent instability toward either being disproportionated to U(IV) and U(VI) or oxidized to U(VI), despite the fact that U(V) is known to exist widely in the natural environment as the intermediate species during the reduction of U(VI) to U(IV). Here, we demonstrated that $U^{V}O^{2+}$ ions can be located at $U^{VI}O_2^{2+}$ lattice sites during mild reduction and crystallization under hydrothermal conditions, yielding an extraordinarily complicated and rare mixed-valent uranium phosphonate compound that simultaneously contains U(IV), U(V), and U(VI). The presence of uranium with three oxidation states was confirmed by various characterization techniques including X-ray crystallography, X-ray photoelectron, electron paramagnetic resonance, Fourier transform infrared, UV-vis-NIR absorption and diffuse reflectance spectroscopies, magnetism measurements, and synchrotron radiation X-ray absorption spectroscopy. This work is highly informative for further understanding of the reduction process of U(VI) and the existence of highly mobile pentavalent actinides in the environment while the synthetic strategy presented could be substantially utilized for making a new family of pentavalent actinide compounds followed with better illustration of their structure-property relationships. More importantly, we believe the strategy of simultaneous reduction and crystallization can be fancily utilized for stabilizing the uncommon oxidation states of other elements in general.

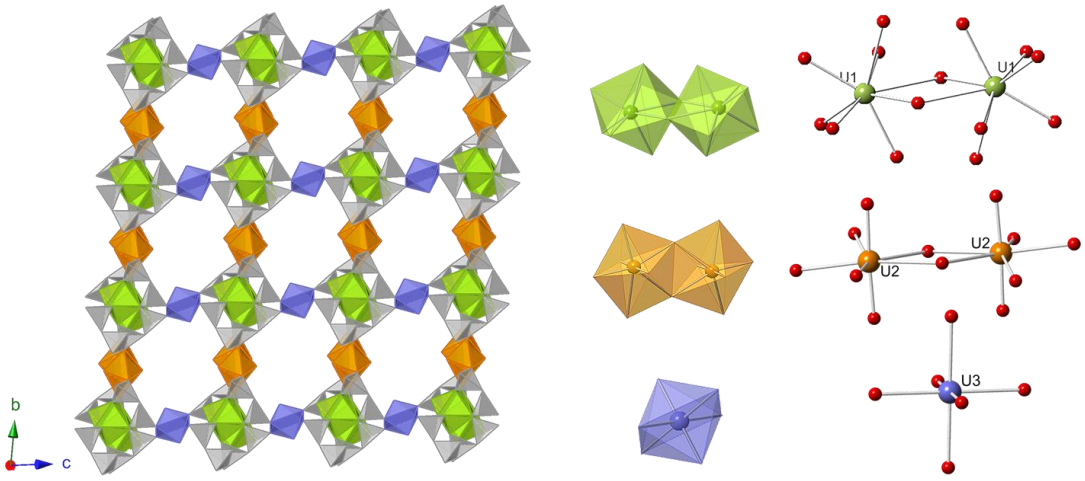

Figure 1. Polyhedral view of compound $[N(C_2H_5)_4]_{1.5}(H_3O)_{1.5}(U^{VI}O_2)_2(U^{V}O_2)U^{IV}{}_2[CH_2(PO_3)_2]_4$ along the *a* axis (green polyhedron: U(1); orange polyhedron: U(2); navy-blue polyhedron: U(3);

C-31

Uranium-Hydride Initiation Times before and after outgassing in Vacuum at 300C to determine the Influence of Hydrogen Content in Uranium on Hydride Initiation Time.

Wigbert J. Siekhaus

Lawrence Livermore National Laboratory, Livermore, CA

The hydride initiation time of cold rolled uranium exposed to air for 25 minutes after polishing in air with water as lubricant, and subsequently to 0.1 bar hydrogen at 35C (after 16 hr outgassing in vacuum at 75 C), has been reported to occur be 1000 to 3000 s [1]. Hydride initiation on hydrogen-free uranium requires that hydrogen penetrate through the uranium-oxide layer (either by diffusion or through a crack) to the metal, react with it and increase its local hydrogen concentration above the hydrogen solubility limit so that UH_3 can form. [2-3]. However, uranium is typically (as e.g. in reference [1]) super-saturated in hydrogen, and hence every hydrogen atom arriving at the metal/oxide interface will begin UH_3 formation immediately. Removing hydrogen from uranium by outgassing it in vacuum would, in contrast, require some time to bring the local hydrogen concentration above the solubility limit, and hence should increase the hydride initiation time. Uranium is also supersaturated in carbon, resulting in approximately fifty 2-6 μm-size carbide inclusions/mm^2. Pre-existing UH_3 accumulates at the interface between carbide and metal [4,5], and during polishing and subsequent exposure to air forms an oxide that incorporates hydrogen, and is hence is most likely more permeable to hydrogen at 0.1 bar than the UO_2 formed on uranium metal. Alternately, said hydrogen-containing oxide may be more likely to form stress- cracks due differences in thermal expansion coefficients between uranium metal and said oxide, or uranium carbide and uranium metal. Preferential hydriding attack at carbide-inclusion has been observed at low temperature and low hydrogen pressure experiments [6], as well as at high hydrogen pressures [7]. Removing hydrogen through vacuum outgassing eliminates said hydrogen containing oxide, and hence may increase the hydride initiation time. The diffusion coefficient of hydrogen in uranium is sufficiently high [8] and the decomposition temperature of UH_3 sufficiently low [9] so that hydrogen can be removed from uranium by vacuum-outgassing at moderate temperatures that do not affect its crystal structure. We present an experimental study of hydride initiation times in which we exposed to hydrogen uranium disks (~ 2mm thick, cold rolled material), prepared following the procedure used in reference [1], either 'as is' or outgassed in ultra-high vacuum (UHV) at 300 C. We find that while 'as is' samples initiate as in reference [1], an outgassed sample initiated hydriding substantially later, as shown in figure 1.

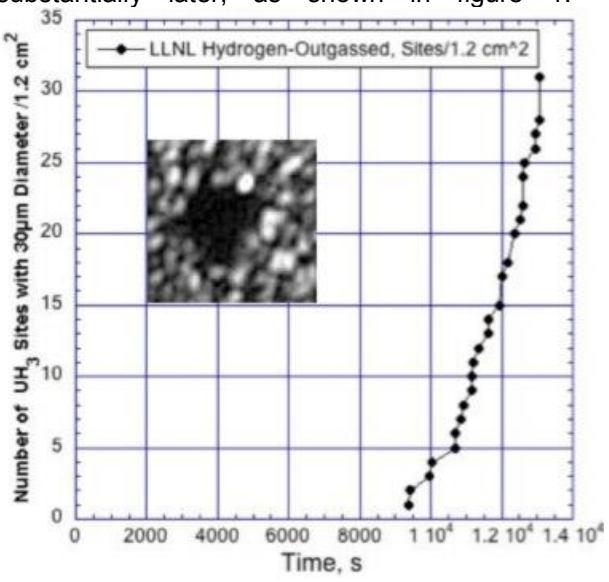

Figure 1. The number UH_3 sites of 30μm diameter on the surface of vacuum-outgassed uranium exposed at 30 C to 0.1 bar H_2 as a function of exposure time. The image in the graph is a UH_3 pit of ~30 μm diameter.

The first hydride pit appears at ~9500 s, which is, according to reference [1], later by a factor three or more than what is typically observed.

The data shown in figure 1 imply that vacuum-outgassed uranium exposed to hydrogen begins hydride pit formation substantially later than is 'typical' for uranium super-saturated in hydrogen [1]. However, other factors may be at play, and convincing proof that hydrogen-content

influences hydride pitting awaits results from the same sample hydrided before and after removal of hydrogen. That work is in progress, and will be shown at the conference.

Acknowledgments

Lawrence Livermore National Laboratory under Contract DE-AC52-07NA27344 performed this work under the auspices of the U.S. Department of Energy.

References

9 J.R. Petherbridge, J. P. Knowles, S. G. Bazley, Solid State Ionics, 292 (2016) 110-115.
10 J. Glascott, Philosophical Magazine, 94 (2014) 3, 221-241
11 J. Glascott, Philosophical Magazine, 94 (2014) 13, 1393-1413
12 L.W. Owen, R.A. Scudamore, Corrosion Science, 6 (1966) 461-468.
13 W.J. Siekhaus, P.K. Weber, I.D. Hutcheon, J.E.P. Matzel, W. McLean, J Alloy Compd., 645 (2015) 225-229.
14 R. Schulze et al., Los Alamos National Laboratory, private communication.
15 N.J Harker, T.B. Scott, C.P. Jones, J.R. Petherbridge, J. Glascott. Solid State Ionics 241, (2013) 46-52.
16 G.L. Powell, in: J.S. Morrell (Ed.) Uranium Processing and Properties, Springer, New York, 2013, pp. 173-188.
17 G.L. Powell, in: J.S. Morrell (Ed.) Uranium Processing and Properties, Springer, New York, 2013, pp. 189-206.

C-32

Lipophilic pyridine-2,6-bis(1H-1,2,3-triazol-4-yl) structure as selective chelating unit for direct actinides extraction from purex raffinate

Annalisa Ossola[1], Eros Mossini[1], Elena Macerata[1], Marco Giola[1], Mario Mariani[1], Arturo Arduini[2], Alessandro Casnati[2]

[1]Politecnico di Milano, Milano, Italy, [2]University of Parma, Parma, Italy

The management and safe disposal of high level radioactive waste generated during the operational time in the nuclear power plants is one of the greatest issue of the nuclear industry. The actinide isotopes are the main responsible for the radiotoxicity of the waste; their long half-lives pose questions about the storage of a vitrified mass for a long time and also concerning the necessity of a long term surveillance of the repositories [1]. The removal of the long lived isotopes from the spent nuclear fuel or their transmutation into stable or short-lived elements could allow to overcome these problems. In order to guarantee an efficient actinide transmutation, all the radionuclides characterized by an high neutron capture cross section must be separated from the rest, otherwise they would prevent fission reactions [2]. These goals can be achieved by means of hydrometallurgical processes, thanks to specific molecules able to co-extract or separate minor actinides (MA) and lanthanides (Ln) from the PUREX feed containing also other fission and corrosion products [3].

It is well-know from literature that the possibility to separate MA from Ln lies in the slightly softer nature of actinides ions in respect to the lanthanides ones. This is probably due to the greater spatial extension of the 5f orbital that give them the possibility to create bond with soft donor atoms (such as N, S and P). The ligand behavior towards MA and Ln depends on several factors, among them the complexing site structure plays a crucial role [4].

In the present research work, different innovative lipophilic molecules were synthetized with the purpose of being selective for MA. They are characterized by the same ligand core, that is pyridine-2,6-bis(1H-1,2,3-triazol-4-yl), and were studied with the aim to verify their behavior towards MA and Ln families. Since solubility was the main hindrance of these ligands, many attempts were made in order to find the best experimental conditions in which their selectivity could be reliably assessed. Several liquid-liquid extraction tests were performed with a synthetic aqueous feed spiked with representative radionuclides and the ligand extraction efficiency and selectivity were evaluated. In some cases, the ligands behavior was investigated as a function of the nitric acid concentration in the aqueous feed or the ligand concentration in the organic solvent, in order to evaluate the impact of these fundamental parameters on the extracting properties.

The selectivity of the ligand core for MA was demonstrated, once the experimental conditions in which good ligands solubility and efficiencies were found. These promising results justify further investigation on the ligands, in order to better investigate the selectivity and assess the stability towards hydrolysis and radiolysis, the loading capacity and the complexation mechanism, such as by UV-Vis and ESI-MS analyses.

References

[1] Mahajan, G.R.; Prabhu, D.R.; Manchanda, V.K.; Badhake, L.P. (1998) Waste Manage. 18, 125-133

[2] Fermvik, A.; Grüner, B.; Kvíčalová, M.; Ekberg, C. (2011), Radiochim. Acta 99, 113-119

[3] IAEA, Assessment of Partitioning Processes for Transmutation of Actinides (2010), IAEA-TECDOC-1648

[4] Madic, C; Lecomte, M.; Boussier, H.; Dozol, J-F. (2004). Advanced chemical separations of minor actinides from high active nuclear wastes. Euradwaste '04, (p. 955). France

C-33

Incorporation of soluble radionuclides into high oxidation state actinide solid matrix

Yaxing Wang[1], Xuemiao Yin[1], Juan Diwu[1], Thomas E. Albrecht-schmitt[2], Shuao Wang[1]

[1]Soochow University, suzhou, China, [2]Florida State University, talahassee, USA

Deep geological disposal is a preferred option for management of nuclear waste in many countries, especially for the vast amounts of used nuclear fuel and other high level radioactive waste. However, release of high toxicity and long half-live radionuclides during long term storage is a primary concern. Uranyl crystal compounds formed during corrosion and oxidative alteration of used nuclear fuel can act as a host to incorporate transuranium elements by charge-balance substitution, which may decrease the mobility of these radionuclides. In our recent study, compatible crystal lattice is proposed to sequestrate soluble radionuclides, especially for minor actinides and fission products which hold relatively long half-live. One case is that two new uranyl vanadates were synthesized and structurally characterized, trivalent lanthanide cations were further inserted into their layers and frameworks through substitution of interlayer ions. Another case is that unusual case of aliovalent substitutional disorder of SeO_3^{2-} /IO_3^- trigonal pyramids was observed in the structure of $Th(IO_3)_2(SeO_3)$. Furthermore, crystal lattice models, $Eu(IO_3)_3$, was chosen to investigate the mechanism of simultaneous sequestration of radionuclides ^{129}I and ^{79}Se.

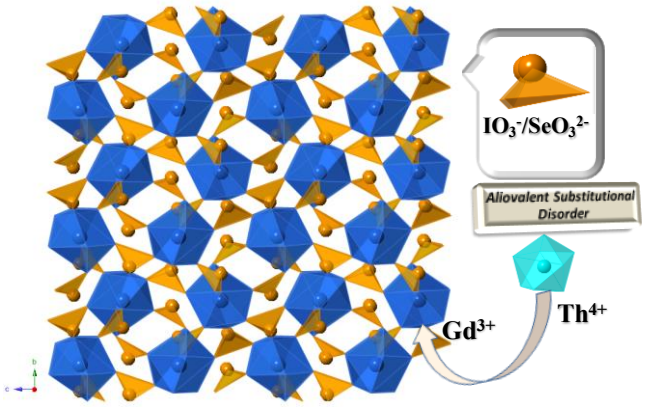

References

Wang, Y.; Yin, X.; Zhao, Y.; Gao, Y.; Chen, L.; Liu, Z.; Sheng, D.; Diwu, J.; Chai, Z.; Albrecht-Schmitt, T. E.; Wang, S.*, Insertion of Trivalent Lanthanides into Uranyl Vanadate Layers and Frameworks. ***Inorg. Chem.*** **2015**; *54*, 8449–8455

Wang, Y.; Wang Y,; Yin, X.; Chen, L.; Liu, Z.; Sheng, D.; Diwu, J.; Chai, Z.; Albrecht-Schmitt, T. E.; Wang, S.*, Crystal Structure of $Th(IO_3)_2(SeO_3)$ Containing Aliovalent Substitutional Disorder of SeO_3^{2-}/IO_3^- Trigonal Pyramids: New Insights into Fate of Radionuclides ^{79}Se and ^{129}I in the Environment, ***unpublished***

C-34

Recent investigations of solid state chemistry of actinides at Soochow university

Shuao Wang

Soochow University, Suzhou, China

During the past one year, progresses have been made on the solid state chemistry of actinides for several different projects. These include: (1) the first uranyl polycatenated framework that can effectively remove cesium from aqueous solutions; (2) several thorium based metal organic frmawork compounds with ultra-large channels and porosity as well as new thorium coordination features; (3) an "in-situ ion-exchange" strategy to create new hereobimetallic 4f-5f complexes in the vanadate system; (4) several extremely complicated uranyl phosphonates with unusual low-temperature phase transition features and combinations of uranyl coordination environments.

C-35

Vibrational properties of uranium and plutonium

Johann Bouchet, François Bottin, Boris Dorado

Commissariat a l'Energie Atomique, Bruyeres le Chatel, France

Density functional theory (DFT) has been an extraordinary successful tool to understand the ground state properties of the actinides and to show the fundamental role played by the 5f electrons. The inclusion of temperature effects in the calculations is even more challenging but crucial for studying the rich phase diagram exhibited by these elements.

Usually, thermal vibrations of atoms can be taken into account via the so-called quasiharmonic approximation (QHA). In this framework, the phonon dispersion relations are calculated at 0 K using density functional perturbation theory (DFPT) and the temperature is included only via the thermal dilatation, i.e., by computing the phonon spectrum at different volumes. This method has been applied with success to Th. However with only one f electron and a fcc structure, Th does not show all the complexity found in the heavier actinides. In particular, this method cannot be used on structures stabilized at high temperature by anharmonic effects and therefore dynamically unstable at 0 K such as the bcc structure adopted by the whole actinide series before the melting point.

Here we show the results of a new method based on ab-initio molecular dynamics simulations to obtain the phonon spectrum of a material at high temperature and capture the anharmonic effects [1]. Whereas all previous attempts based on the QHA failed to reproduce the behavior of the phonon modes of uranium as a function of temperature, this method can capture the effects responsible for the CDW phase transition in α-U [2]. We also show the phonon spectrum of the γ bcc structure at high temperature. Using the phonon density of states we calculate the free energies of the α and the γ structure to obtain the transition line in pressure and temperature.

We also present new results for the phonon spectra of the α, δ and ε phases of plutonium and we discuss the different mechanisms governing the stability and the phase transition of these structures.

References:

[1] O. Hellman, I. A. Abrikosov, and S. I. Simak, Phys. Rev. B **84**, 180301 (2011).

[2] J. Bouchet and F. Bottin, Phys. Rev. B **92**, 174108 (2015)

C-36

A state-of-the-art report within NEA-TDB to assess modeling and experimental approaches in aqueous high ionic-strength solutions

Marcus Altmaier[1], Davide Costa[2], Andrew Felmy[3], Helge Moog[4], Roberto Pabalan[5], Marilena Ragoussi[2], Don T. Reed[6], Wolfgang Runde[7], Punam Thakur[8], Wolfgang Voigt[9]

[1]Karlsruhe Institute of Technology, Institute for Nuclear Waste Disposal (KIT-INE), Karlsruhe, Germany, [2]OECD Nuclear Energy Agency, Boulogne-Billancourt, France, [3]Washington State University, Pullman WA, USA, [4]Gesellschaft für Anlagen- und Reaktorsicherheit, Braunschweig, Germany, [5]U.S. Nuclear Waste Technical Review Board, Arlington VA, USA, [6]Los Alamos National Laboratory, Carlsbad NM, USA, [7]Los Alamos National Laboratory, Los Alamos NM, USA, [8]Carlsbad Environmental Monitoring & Research Center, Carlsbad NM, USA, [9]Technical University of Freiberg, Freiberg, Germany

Within the scope of the OECD Nuclear Energy Agency (NEA) Thermochemical Database (TDB) Project, the preparation of a State of the Art Report (SOAR) to assess the modeling and experimental approaches used to describe high ionic-strength solutions is a current activity. This state of the art report builds on past NEA-TDB documents [1] and focuses on ionic strengths $I \geq 3$ M where the Pitzer formulation [2,3], rather that the SIT approach, is recommended and usually applied. The focus of this SOAR update is on the nuclear waste disposal aspects that apply to repository concepts in bedded and domed rock salt formations, although there is also relevance to other geologic disposal concepts where transient high ionic-strength aqueous conditions can exist. This SOAR assessment activity is the first step in the development of a comprehensive high quality and self-consistent Pitzer data set that can describe the aqueous actinide and brine chemistry for all predicted repository conditions to address low-probability brine-inundation scenarios that are a necessary part of the safety case for a nuclear waste repository in salt [4].

The aqueous solution properties treated within the Pitzer approach that pertains to a nuclear waste repository in salt is divided into different categories: (i) “Oceanic” for the main components of high ionic-strength brine including interactions of main components with carbonate, (ii) “Radionuclide/actinide” for the key radionuclides (and their analogs) and their interactions with main inorganic and organic ligands that need to be addressed to support the safety case, and (iii) “Others” including selected non-radioactive elements of high relevance like iron or lead. The vast majority of the available literature deals with the brine chemistry associated with “oceanic” systems (~1000 species-specific) and this remains a very active area of research for a number of reasons outside of the nuclear repository application. For the radionuclide/actinide data set, there are new data reported for all the key oxidation states of the actinides but there are significantly less literature publications (~65) on this key topic. There is especially a significant lack of temperature-variable data for the radionuclide/actinide data set as well as ternary species and a number of gaps exist in current database applications. A critical assessment of these key data gaps will be provided.

References:

[1] Allard et al. 1997. “Modelling in Aquatic Chemistry.” OECD Publications, 724 pp., ISBN 92-64-15569-4.

[2] Pitzer, K.S. 1973. “Thermodynamics of Electrolytes. I. Theoretical Basis and General Equations.” *Journal of Physical Chemistry, 77*, (2), 268–277.

[3] Pitzer, K.S. 1991. “Ion Interaction Approach: Theory and Data Correlation.” Chapter 3 of *Activity Coefficients in Electrolyte Solutions*. 2nd Edition. Pitzer, 152709 K.S., ed. Boca Raton, Florida: CRC Press.

[4] Reed, D.T. and M. Altmaier (eds.), “Proceedings of the Third International Workshop on Actinide and Brine Chemistry in a Salt-Based Repository (ABC-Salt III),” Los Alamos National Laboratory Report LA-UR-15-21114, Los Alamos, NM, USA (2015).

C-37

The OECD/NEA update book on the chemical thermodynamics of U, Np, Pu, Am and Tc

Ingmar Grenthe[1], Xavier Gaona[2], Andrey Plyasunov[3], Linfeng Rao[4], Wolfgang Runde[5], Andrew Felmy[6], Bernd Grambow[7], Rudy Konings[8], Anna L. Smith[9], Emily Moore[8], Kastriot Spahiu[10], Davide Costa[11], Marilena Ragoussi[11]

[1]Royal Institute of Technology, Stockholm, Sweden, [2]Karlsruhe Institute of Technology, Institute for Nuclear Waste Disposal, Karlsruhe, Germany, [3]Institute of Experimental Mineralogy, Russian Academy of Sciences, Moscow, Russia, [4]Lawrence Berkeley National Laboratory, Berkeley, USA, [5]Los Alamos National Laboratory, Los Alamos, USA, [6]Washington State University, Pullman, USA, [7]SUBATECH, Nantes, France, [8]European Commission, JRC, Institute for Transuranium Elements, Karlsruhe, Germany, [9]Delft University of Technology, Delft, The Netherlands, [10]SKB, Stockholm, Sweden, [11]OECD Nuclear Energy Agency (NEA), Paris, France

Within the scope of the OECD Nuclear Energy Agency (NEA) Thermochemical Database (TDB) Project, a comprehensive critical review of thermodynamic data available for inorganic compounds and aqueous complexes of U, Np, Pu, Am and Tc with focus on the relevance to waste management safety is in preparation. The review work covers all new studies available since the release of the previous NEA–TDB update volume [1]. A unique feature of this update is the inclusion of a survey of thermodynamic data obtained by quantum chemical methods that works well for reactions in gas-phase, but not for reactions in solution. This part of the review is not "critical" and only intended to demonstrate the development in a rapidly expanding field. Thermodynamic data obtained using these methods are not selected, but listed for information. The release of the new update volume is foreseen for the second half of 2017. The most relevant modifications and improvements with respect to [1–5] will be summarized in this contribution.

Uranium

Most of the newly published thermodynamic data on the hydrolysis of U(VI) and U(IV) are consistent with the previous selection in [1] and [2]. The main improvement in the data selection for these species is related with the availability of enthalpy data and SIT ion interaction coefficients for both monomeric and polyatomic species. Several publications dealing with U(VI) peroxide aqueous species have been critically reviewed, and the reported species included in the thermodynamic selection. The formation of ternary species Ca/Mg–U(VI)–CO_3 is relevant in the context of nuclear waste disposal because of the predominant role that these species can play in certain repository concepts. This review concluded that the experimental data give sufficient evidence of their existence, and stability constants for the formation of $M_xUO_2(CO_3)_3^{2x-4}$ are selected for M = Mg, Ca, Sr, Ba and x = 1 and 2. The new update volume deals also with the critical review of a number of U(III), U(IV), U(V) and U(VI) (binary, ternary and quaternary) solids and mineral phases, including alkali and alkaline-earth uranates, halides, phosphates, arsenates, silicates, carbonates and borates. Coffinite was found to be a special case in view of inconsistencies in the newly reported data on thermodynamic properties and solubility. A need for additional solubility or enthalpy calorimetric data is emphasized

Neptunium

Several new references on the hydrolysis of Np(VI), Np(V) and Np(IV) are available in the literature. Only the Np(VI) system has been updated with the selection of anionic hydrolysis species forming in alkaline pH conditions. New insights on the Np(IV)–OH–CO_3 system were reported since the release of [1], although thermodynamic data available for this system are only recommended for scoping calculations. Solubility data for NpO_2CO_3(s) are considered to update the Np(VI)–carbonate system, which holds now a closer consistency with the analogous U(VI) system. New studies on the interaction of silicate with Np(VI), Np(V) and Np(IV) were

conducted in the last decade. These studies clearly hint towards the formation of stable Np–silicate aqueous species, but reported thermodynamic data are only recommended for scoping calculations until more comprehensive studies are available. Thermodynamic data selected in [1] and [3] for the Np(V)–phosphate and Np(V)–sulfate systems are updated in the present review according with new spectroscopic, calorimetric and chromatographic studies.

Plutonium

New experimental studies available for Pu(VI) and Pu(IV) have been used to update the thermodynamic data for the corresponding hydrolysis schemes. The new update volume provides a critical review of thermodynamic data available for pure solid phases ($PuO_2(OH)_2{\cdot}H_2O$(cr), PuO_2(cr), PuO_2(am,hyd), Pu_2O_3(cr), $PuO_{1.61}$(cr), $Pu(OH)_3$(s)), but also for the mixed PuO_{2+x}(s,hyd) phase, for which a large number of studies were published since the release of [1]. Thermodynamic data selected in [1] and [3] for Pu(III)–phosphate aqueous species and solid compounds are updated according with new solubility experiments reported in the literature. Selected values are now in reasonable agreement with Am(III). New data available for Pu(VI) and Pu(IV) carbonate systems are consistent with the selection in [1] and [3]. As for Np, new thermodynamic data reported for Pu(VI)– and Pu(IV)–silicate systems are only recommended for scoping calculations.

Americium

The analogy between Am(III) and Cm(III) aqueous system is further exploited in this update volume for the selection of thermodynamic data of Am(III). The same hydrolysis scheme and thermodynamic data as in [1] and [4] are retained, except for the new selection of the ternary aqueous species Ca–An(III)–OH forming in alkaline solutions with [Ca] ≥ 0.5 M. The Am(III)–fluoride system is updated with new enthalpy data, which was determined in Cm(III)–TRLFS (time resolved laser fluorescence spectroscopy) studies at elevated temperatures. Based on new experimental evidences available for the sulfate system, the initial selection in [4] is favored by the present review in contrast to the updated selection in [1]. The study of the system An(III)–phosphate is complicated by the very low solubility of the $AnPO_4$(s) phase. Besides the selection of $AmH_2PO_4^{2+}$ in [1], new Cm(III)–TRLFS results obtained under alkaline pH conditions provide sound evidence for the selection of the species $AnHPO_4^{+}$. In spite of the new experimental studies available on the Cm(III)–carbonate system, the previous selection in [1] is retained by this review. Experimental data available for the An(III)–silicate system are somewhat discrepant, but the most reliable studies support the previous selection in [1].

Technetium

A number of relevant experimental studies on the solution chemistry Tc thermodynamics were published since the release of the previous update volume [1]. The main changes with respect to [1] and [5] affect the hydrolysis scheme of Tc(IV) and the solubility-controlling oxide $TcO_2{\cdot}xH_2O$(s), which are updated in this review according to the new data available. In addition, an activity model for Tc(IV) hydrolysis species in chloride media is also available. New publications reporting Tc(IV)–chloride species forming under very acidic conditions have been critically reviewed, and the reported species included in the current thermodynamic selection. There are still many solid-phase data missing, that make it difficult to obtain accurate thermodynamic values, specifically for the metal and oxide phases that are often times based on Re-analogues.

Appendix and guidelines

The update book on the chemical thermodynamics of U, Np, Pu, Am and Tc will also include relevant updates and modifications of appendix and guidelines: (i) a methodology for ionic strength corrections of enthalpy data will be provided; (ii) as originally done in [2], an Appendix D will be included summarizing estimation methods for entropy and heat capacities of solid phases, which will be extended to Np and Pu; (iii) guidelines for the estimation of errors will be updated; (iv) a new series of tables with thermodynamic data recommended only for scoping calculations will be included in Appendix E.

References:

[1] R. Guillaumont, T. Fanghänel, J. Fuger, I. Grenthe, V. Neck, D. A. Palmer, M. H. Rand. Vol. 5. Update on the Chemical Thermodynamics of Uranium, Neptunium, Plutonium, Americium and Technetium, OECD Nuclear Energy Agency Data Bank, Amsterdam, The Netherlands, (2003).

[2] I. Grenthe, J. Fuger, R. J. M. Konings, R. J. Lemire, A. B. Muller, C. Nguyen-Trung, H. Wanner. Vol. 1. Chemical Thermodynamics of Uranium, OECD Nuclear Energy Agency Data Bank, Amsterdam, The Netherlands, (1992).

[3] R. J. Lemire, J. Fuger, H. Nitsche, P. Potter, M. H. Rand, J. Rydberg, K. Spahiu, J. C. Sullivan, W. J. Ullman, P. Vitorge, H. Wanner. Vol. 4. Chemical Thermodynamics of Neptunium and Plutonium, OECD Nuclear Energy Agency Data Bank, Amsterdam, The Netherlands, (2001).

[4] R. J. Silva, G. Bidoglio, M. H. Rand, P. B. Robouch, H. Wanner, I. Puigdomenech. Vol. 2. Chemical Thermodynamics of Americium, OECD Nuclear Energy Agency Data Bank, Amsterdam, The Netherlands, (1995).

[5] J. A. Rard, M. H. Rand, G. Anderegg, H. Wanner. Vol. 3. Chemical Thermodynamics of Technetium, OECD Nuclear Energy Agency Data Bank, Amsterdam, The Netherlands, (1999).

C-38

Solubility, hydrolysis and chloride complexation of Np(V) in alkaline, dilute to concentrated NaCl, $MgCl_2$ and $CaCl_2$ solutions

David Fellhauer, Xavier Gaona, Kathy Dardenne, Marcus Altmaier

Karlsruhe Institute of Technology, Institute for Nuclear Waste Disposal, Karlsruhe, Germany

A thorough understanding of the principal geochemical processes of actinide elements in aqueous solutions is highly relevant for the long-term safety assessment of nuclear waste repositories. Solubility phenomena strongly control the radionuclide source term, i.e. the maximum amount of dissolved radionuclide species potentially mobilized from the near-field of a repository in the case of water intrusion. Due to its long half-life and abundance in spent nuclear fuel, ^{237}Np is an element of high relevance in this context. In aqueous solutions, the pentavalent oxidation state of Np is thermodynamically stable over a wide range of E_h and pH conditions. The solubility and hydrolysis behavior of Np(V) has been subject of several studies that were mainly performed in NaCl or $NaClO_4$ solutions as background electrolyte. According to a widely accepted chemical model [1], the solubility of Np(V) in dilute to concentrated NaCl-NaOH solutions is controlled by equilibrium reactions between the binary hydroxide solid phase $NpO_2OH(am)$ and the aqueous species $NpO_2(OH)_n^{1-n}$ with n = 0 to 2.

In the last few years, we have performed new solubility experiments with Np(V) in alkaline, dilute to concentrated NaCl [2], $MgCl_2$, and $CaCl_2$ [3] solutions which reveal that the current chemical model for Np(V) needs to be extended. The formation of so far not considered ternary M-Np(V)-OH(s) solid phases with M = Na, Ca (e.g. $Ca_{0.5}NpO_2(OH)_2(s,hyd)$) readily takes place under these conditions. Our comprehensive experimental data show that the latter have significantly lower solubilities compared to binary $NpO_2OH(am)$. From the systematic dependence of the solubility of these well-defined solid compounds on pHm and ionic strength, important information about the Np(V) hydrolysis model and especially the corresponding thermodynamic constants are derived, which help to solve some contradictory discussions on this issue [4]. Furthermore, clear indications for the formation of ternary hydrolysis complexes, $Ca_xNpO_2(OH)_y^{2x+1-y}$, in Ca containing solutions are obtained. From the comprehensive solubility data up to pH_m = 10, where hydrolysis of Np(V) is negligible, and additional Vis/NIR and Np-L3 EXAFS spectroscopic investigations of aqueous Np(V) solutions in $MgCl_2$ and $CaCl_2$ solutions, a detailed description of the innersphere chloro complexation of Np(V) is achieved.

In the presentation, the new experimental results and the corresponding thermodynamic equilibrium data (solubility products, complex formation constants, ion interaction parameters derived within both the SIT and Pitzer approaches) are summarized.

References:

[1] Guillaumont, R., Fanghänel, Th., Fuger, J., Grenthe, I., Neck, V., Palmer, D.A., Rand, M.H. (OECD, NEA-TDB), Chemical thermodynamics vol. 5, update on the chemical thermodynamics of uranium, neptunium, plutonium, americium and technetium, Elsevier, North-Holland, Amsterdam (2003).

[2] Petrov, V.; Gaona, X.; Fellhauer, D.; Dardenne, K.; Kalmykov, S. N.; Altmaier, M., Abstract No. A1-3, 13th International Conference on Chemistry and Migration Behaviour of Actinides and Fission Products in the Geosphere, Migration ’11, Beijing, China, 18-23 September, 2011.

[3] Fellhauer, D.; Rothe, J.; Altmaier, M.; Neck, V.; Runke, J.; Wiss, T.; Fanghänel, Th., Radiochim. Acta (2016) (DOI 10.1515/ract-2015-2489).

[4] Neck, V., Geochim. Cosmochim. Acta 70, 4551-4555 (2006).

C-40

Examination of actinide (Pu(IV,V,VI), Np(V), and U(VI)) sorption on rutile (TiO_2)

Andreas Schnurr, Brian Powell

Environmental Engineering and Earth Sciences, Clemson University, Clemson, SC, USA

Introduction

Nuclear weapons production and testing in the last decades created a legacy of Pu contamination in several forms and locations e.g. Hanford Reservation (11800 Ci ^{239}Pu; 1, 2) and Nevada Test Site (240000 Ci $^{238\text{-}240}$Pu; 3). The final disposal in deep geological formations is considered to be the safest way to keep high level radioactive waste from the biosphere. For the safety assessment of nuclear waste concepts, the potential intrusion of groundwater and therefore contact with waste forms have to be taken into account.

Actinides, especially Pu with a variety of simultaneously existent redox states at environmental most important pH conditions in the aqueous phase, exhibit very complex solid-water interface reactions with mineral surfaces. To predict concepts for safety assessment, therefore, it is necessary to achieve a better understanding of sorption processes and sorption mechanism. Such studies are particularly relevant for plutonium due to observations of enhanced subsurface transport at several sites around the world (4 – 7). Characterization of the processes responsible for enhanced migration are necessary for the development of reliable waste performance models.

Motivation

Former studies from Mangold and Powell (8) with uranium sorption to hematite showed a trend in dependency of ionic strength and elevated temperature. Batch-sorption studies (25 to 80°C in 0.01 and 1.0 M NaCl), potentiometric titrations (25 to 50°C in 0.01, 0.1, 0.4, and 1.0 M NaCl), and calorimetric titrations (0.01, 0.1, 0.4, and 1.0 M NaCl) were conducted. As expected uranium sorption to hematite was found to increase with increasing temperature due to the endothermic driven process and slightly decrease with increasing ionic strength. Potentiometric titrations show a drop in the pH_{PZC} of hematite from pH ~ 9.3 (25°C) to pH ~ 7.3 (50°C), that the increased sorption due to a less positively charged surface is reasonable for increased temperature. Isothermal calorimetric acid/base titrations conducted at four different ionic strengths reveal a positive increase in reaction heat with increasing ionic strength. The author's suggestion is that surface protonation and/or chloride outer-sphere surface complexation reactions are endothermic (at 25°C). However, a self-consistent thermodynamic model of these data has not yet been assembled which can describe/predict these processes. Due to the complexity of iron oxide minerals, we performed the experiments in this study with an idealized surface. The TiO_2 mineral (rutile) is a well-known metal oxide used in several previous studies (e.g. 9) and is stable against dissolution for a wide pH range of interest.

Overall, we are expecting similar tendencies/results with this mineral surface as seen in previous solid-water interface reaction studies of actinides onto iron oxides (e.g. hematite and goethite) or onto clay minerals (e.g. montmorillonite), but the detailed characterization of surface specific reactivity of rutile should allow development of a thermodynamic working model capable of describing changes in actinide sorption as a function of ionic strength and temperature. This will be a results driven modeling effort using the idealized rutile surface. It should then be possible to transfer the model construct from rutile to systems with similar metal oxide surfaces e.g. hematite.

Experimental

The investigations in this study include batch-sorption studies of actinides (Pu, Np, and U at trace level concentrations < 10^{-6} M) onto rutile (constant solid to liquid ratio; 1 g/L) in NaCl solutions (0.01, 0.1, 0.4, and 1.0 M) at three different temperatures (20 to 65°C), acid-base potentiometric titrations of rutile in the same background electrolyte solutions with increased mineral surface concentration (16 g/L). Finally, two types of isothermal calorimetric titrations (acid-base and actinide sorption) will complete a broad thermodynamic set of experimental data to derive a thermodynamic working model. The chemical speciation of actinide surface complexes will be monitored using x-ray absorption spectroscopy (XANES/ESAFS) and Fourier Transform Infrared Spectroscopy (FT-IR) and the batch sorption and titration data will be modeled using reactions which are self-consistent with species identified using these spectroscopic techniques.

References

[1] K. J. Cantrell, “Transuranic Contamination in Sediment and Groundwater at the U.S. DOE Hanford Site,” PNNL-18640, Pacific Northwest National Laboratory: Richland, WA (2009).

[2] A. R. Felmy et al., “Plutonium contamination issues in Hanford soils and sediments: Discharges from the Z-Plant (PEP) complex,” *Phys. Chem. Earth*, **35**, 292 (2010).

[3] D. K. Smith et al., “An inventory of long-lived radionuclides residual from underground nuclear testing and the Nevada test site,” *J. Environ. Radioactiv.*, **67**, 35 (2003).

[4] T. E. Payne et al., “Trench ‘Bathtubbing’ and Surface Plutonium Contamination at a Legacy Radioactive Waste Site,” *Environ. Sci. Technol.*, **47**, 13284 (2013).

[5] A. B. Kersting et al., “Migration of plutonium in ground water at the Nevada Test Site,” *Nature*, **397**, 56 (1999).

[6] A. P. Novikov et al., “Colloid transport of plutonium in the far-field of the Mayak Production Association, Russia,” *Science*, **314**, 638 (2006).

[7] P. H. Santschi et al., “Organic Nature of Colloidal Actinides Transported in Surface Water Environments,” *Environ. Sci. Technol.*, **36**, 3711 (2002).

[8] J. Mangold and B. A. Powell “unpublished data”.

[9] L. G. J. Fokkink et al., “Temperature Dependence of the electrical Double Layer on Oxides: Rutile and Hematite,” *J. Colloid. Interf. Sci.*, **127**, 116 (1988).

C-41

Evolution of the morphology of $(U_{0,45}Pu_{0,55})O_2$ powder during dissolution in nitric acid

Gilles Leturcq, Alexis Neuschwander, Yannis Ziouane, Bénédicte Arab-Chapelet

CEA, Marcoule, France

Dissolution of mixed $(U,Pu)O_2$ oxides with more than 35% of Pu is complex. According to the study of Warin et al. [1], from this amount, the undissolved percent in nitric acid increases drastically with the Pu content of the oxide. Authors allocated this result to the rearrangement of the crystal structure of the mixed oxide: below 35%, $(U,Pu)O_2$ have a face centered cubic crystal structure while beyond this amount it adopts a centered cubic structure. This lack of solubility has also been observed by Vollath et al. [2]. They noted a significant decline of the dissolution kinetic when the content of Pu exceeds 35%.

Then, a better understanding of the phenomena involved in the dissolution of Pu-riched $(U,Pu)O_2$ is of interest. Particularly, this work deals with the modification of the surface morphology of the oxide during dissolution in nitric acid. In literature, little information is available about the impact of the morphology on the dissolution of compounds containing high amounts of PuO_2. The interest of this study is to expose if there is a significant change of the morphology (form, grain size, density and porosity) of the powder but also if there is a modification of the crystal lattice during the dissolution of a $U_{0.45}Pu_{0.55}O_2$ powder obtained by sol-gel process. Such study is done using SEM and BET measurements at different dissolution progress steps. X-ray diffraction enable the study of the evolution of the microstrain rates of the oxide during the dissolution.

On Ce/Nd and Th/Nd mixed oxide powders with a respective amount of 0.7/0.3, Horlait [3] proved that the specific surface area grows with dissolved fraction. In the case of Th/Nd mixed oxide, this rise was continuous during all the duration of the dissolution experiment while a nonlinear increase was observed on Ce/Nd oxide for which, the increase is sharp at the beginning and slow down with the progress of dissolution. For both oxides, Horlait concluded that the specific surface area evolves during the dissolution until it reaches the limit value would be obtained by grains after crushing to isolate the crystallites. However, once isolated, the dissolution of theses crystallites should continue. Two mechanisms are then imaginable, whether a dissolution by a preferential path into the solid or a uniform dissolution of the crystallite. The second case seems more realistic physically and would induce a slowly diminution of the specific surface area until the complete dissolution of the solid. By simplifying the grain at a spherical model, the decrease of the surface area would follow a law belonging to a core shrinking model.

Such study has never been realized on uranium, plutonium mixed oxides and it has to be noticed that the initial morphology of the powder of our $(U,Pu)O_2$ powder is different from those used on Horlait's study.

References:

[1] D.Warin, Mansard, *Contribution à l'étude de la solubilité nitrique des combustibles MOX*, Internal communication CEA, 1989.

[2] D.Vollath, H.Wedemeyer, *On the dissolution of $(U,Pu)O_2$ solid solutions with different Pu contents in boiling nitric acid*, Nuclear technology 71, 1985.

[3] D.Horlait, *Structural characterization of mixed oxides $MIV_{1-x}LnIII_xO_{2-x/2}$ (M = Ce, Th) prepared by oxalic route. Multiparametric study of the dissolution and microstructural evolution,* doctoral thesis, university of Montpellier II, 2011.

C-42

Overview: National Research Laboratory in Nuclear Forensic from México

Héctor Hernández-Mendoza, Elizabeth Teresita Romero-Guzmán

Instituto Nacional de Investigaciones Nucleares, Estado de México, Mexico

According to recommendations of the International Atomic Energy Agency (IAEA), Mexico is taking steps to combat illicit trafficking of nuclear material. The creation of a National Research Laboratory in Nuclear Forensic (LANAFONU its acronym in Spanish; Laboratorio Nacional de Investigaciones en Forense Nuclear) has been assigned to Instituto Nacional de Investigaciones Nucleares (ININ) at 2014. The aims of this laboratory is to combat illicit trafficking of nuclear material, optimize the scientific processes and techniques used to analyze nuclear material (orphan radioactive sources), measure the effect of ionizing radiation of possible exposure –acute or chronic- as consequence of manipulation, management, transport, and final storage. Today, LANAFONU facility had been focused in optimization of protocols for emergency and routine to measure alpha in environmental and biological samples using Inductively Coupled Plasma with Sector Field Mass Spectrometry (ICP-SFMS). The activities principal at LANAFONU are: i) Optimization of methods to measure of Pu isotopes by AS (Alpha Spectrometry), ICP-SFMS and AMS (Accelerator Mass Spectrometry), ii) develop of radiochemical methods for routine situations and nuclear emergencies, iii) participation in scientific technical committee on nuclear forensics, iv) participation in international inter-comparison exercises to optimize and validate methods v) and v) consolidation of LANAFONU at the IAEA. Finally, the laboratory has the challenge to establish collaborations in nuclear forensic investigations with other countries and to acquire international standard parameters to perform this type of analysis.

C-43

Diffusion Characteristics of Surrogate Nuclear Material Alloys

John Auxier II[1,2], Christopher Eley[1,2], Joshua Gurka[1,2], Duncan Brocklehurst[1,2], Howard Hall[1,2]

[1]Radiochemistry Center of Excellence, Knoxville, TN, USA, [2]Institute for Nuclear Security, University of Tennessee, Knoxville, TN, USA

The proliferation of special nuclear material (e.g. ^{235}U, ^{233}U, and ^{239}Pu), or SNM, is of concern to the national and international community. Upon interdiction of the materials, it is important to be able to characterize the samples in order to determine their age, origin, and possible processing history. It is the focus of this work to demonstrate the development of new techniques that can be used for metal chronometry and origin identification. The first effort will demonstrate the ability to use scanning electron microscopy (SEM) coupled with electron dispersive spectroscopy (EDS) to determine surface morphology and impurity diffusion within the metallic samples. This movement of impurities can be related to a time signature that allows for the determination to chronometric signatures of the materials. Secondly, SNM undergo predominantly alpha particle decay, which will create defect regions inside the material. The defect sites will increase as the samples ages from its last processing time, and will change the electrical conductivity of the measurements. Therefore, sensitive conductivity measurements have been performed on pure metals and alloys. The change in conductivity observed will allow for the identification of the age of the materials. These techniques can be combined with traditional techniques, such as mass spectrometry, to allow for the development of forensic signatures that can be related to the age and processing history of the material.

C-44

Benchmark spherical critical assemblies with a core made of plutonium metal ^{239}Pu (98 %) in δ - phase and compound reflectors

Alexey Kaygorodov, Sergey Vorontsov, Mikhail Kuvshinov, Valentin Khoruzhyi

Rfnc-Vniief, Sarov, Nizhny Novgorod Region, Russia

The knowledge of nuclear-physics characteristics of plutonium is important both for modeling operation of production power reactors, and for ensuring nuclear safety, for example, at treatment of spent nuclear fuel (SNF). Nuclear-physics data are verified by means of carrying out critical mass experiments.

Objects of presented studies are six spherical critical assemblies with a core made of plutonium metal ^{239}Pu(98 %) in δ-phase [1] and compound reflectors, containing alternating layers made of ((CH_2)n+Fe), (C+Fe) and (Pb+Fe). Critical parameters (K_{eff} =1) (geometry form, sizes and masses) for each assembly have been determined in the experiments on FKBN facility in RFNC-VNIIEF. The paper presents results of critical experiment analysis, performed by M.I. Kuvshinov, A.A. Malinkin and V.P. Egorov in RFNC-VNIIEF on the facility FKBN in the year of 1963 [2,3].

Experimental values $K_{eff.}$ are compared to calculation ones, obtained using various nuclear data libraries (BAS, ENDF/B7.1, JEF-3, JENDL-4, CENDL-3) [4]. Agreement between calculation and experiment depends on the type of assembly. Library JEF-3 are more preferable for three types of assemblies.

Presented critical assemblies can be recommended as benchmark ones to be incorporated into the International Reference Book on Nuclear Safety ICSBEP (International Handbook of Evaluated Criticality Safety Benchmark Experiment) [1].

References

[1] International Handbook of Evaluated Criticality Safety Benchmark Experiments. Nuclear Energy Agency, Organization for Economic Cooperation and Development, NEA/NSC/DOC(95). Volume I. PU-MET-FAST. Valuators (VNIIEF) M.V. Gorbatenko, V.P. Gorelov, V.P. Yegorov, V.G. Zagrafov, V.I. Ilyin, M.I. Kuvshinov, V.I. Yuferev

[2] Vorontsov S.V., Kuvshinov M.I. Critical experiments on assemblies with plutonium metal, performed in RFNC - VNIIEF. // VANT. Series «Fizika Yadernykh Reaktorov». -2013. - Issue 3. - P.3-11. XIII International workshop «Plutonium Fundamental Properties». Workshop materials. Edited by V.A. Nadykto. FSUE «RFNC - VNIIEF», Sarov. September 9-13, 2013. P106-109. [2].

[3] Kuvshinov M.I., Vorontsov S.V., Gorelov V.P. et al. Benchmark critical experiments on the facility FKBN-2M. VANT. Series «Fizika Yadernykh Reaktorov». -2000. - Issue 2/3. P.142-154.

[4] Kuvshinov M.I., Vorontsov S.V., Khoruzhii V.Kh. Experimental and calculation parameters of benchmark spherical critical assemblies with a core made of plutonium metal (^{239}PU (98%)) in δ – phase and compound reflector, containing layers made of polyethylene and steel. VANT. Series «Fizika Yadernykh Reaktorov». - 2015- Issue 4. P.12-24.

C-45

Characterization of Ce, U, and Pu Metal Produced by Calcium Reduction

Kaylyn McCoy[1,2], William Karl Pitts[1], Amanda Casella[1], Calvin Delegard[1]

[1]Pacific Northwest National Laboratory, Richland, WA, USA, [2]University of Utah, Salt Lake City, UT, USA

Metal buttons of cerium, uranium, and plutonium were produced from their respective tetrafluorides using the classic (Ames Process) calcium reduction method. Batches were performed on the 1- and 10-gram scale with CeF_4. The 1-gram batches had difficulties in coalescence while the 10-gram batches produced quality metal buttons with greater than 75% yield. This method (10-gram scale) was then performed using UF_4 and PuF_4, to produce metal buttons for analysis.

This presentation will discuss the experimental process used for the conversion along with basic physical characteristics of the metals. Additionally, detailed characterization will be presented such as purity of the materials as examined by scanning electron microscopy with energy dispersive X-ray spectroscopy, phase properties measured by X-ray diffraction, and grain structures analysed by optical microscopy.

C-46

The Multi-Isotope Process Monitor: Deployment at the H-Canyon Nuclear Separation Facility

David Meier[1], Lindsay Sexton[2], Jamie Coble[3]

[1]Pacific Northwest National Laboratory, Richland, WA, USA, [2]Savannah River National Laboratory, Aiken, SC, USA, [3]University of Tennessee-Knoxville, Knoxville, TN, USA

The Multi-Isotope Process (MIP) Monitor is an approach to online process monitoring for Material Control & Accounting (MC&A) and facility process controls needed for efficient operations. The MIP Monitor measures gamma-emitting radionuclides present in feed, product, and waste streams of a nuclear reprocessing or separation facility. These radionuclides are measured by gamma spectrometry and compared to spectral patterns representing “normal” process conditions using multivariate analysis. By targeting specific gamma-emitting radionuclides, the MIP Monitor approach is compatible with the use of small, portable, medium resolution gamma detectors that may be easily deployed throughout an existing facility.

The distribution radionuclides in a reprocessing or separation stream is related to several operational variables, including nitric acid concentration, organic phase (TBP) concentration\ and used nuclear fuel characteristics. In an effort to achieve consistent industrial processes with reproducible conditions, the distribution of each radionuclide carried within the organic and aqueous phases should be relatively constant for a given type of used fuel. Also, the distribution of radionuclides in both product, organic and waste streams at each stage in the facility should be relatively reproducible.

Researchers at national laboratories and Universities are working to deploy the MIP Monitor at the H-Canyon Nuclear Separations Facility located on the Savannah River Site. The goal of the deployment project is to continuously gather and process the spectral data in the hot and warm sampling aisles at the H-Canyon facility during actual used nuclear fuel separation campaigns. The information gathered could be used to improve safety, material security, efficiency, material and process controls, and overall plant performance to aid both the regulator and the plant operator. In addition, demonstrating the operation of the MIP Monitor in a full-scale facility will help to advance the technological readiness and realize the benefits associated with the technique. This technology is intended to support the Department of Energy’s (DOE) Nuclear Energy’s Fuel Cycle Research and Development (FCR&D) and Materials Protection, Accounting and Control Technology (MPACT) program. This paper will present an overview of the MIP Monitor deployment project, detail our experimental deployment plan at H-Canyon, and present preliminary plutonium data from current deployment efforts.

C-47

Investigation of the Electronic Structure of Transuranic Elements Utilizing a Redox Active Ligand.

Shane S. Galley[1], Scott A. Pattenaude[2], Suzanne C. Bart[2], Thomas E. Albrecht-Schmitt[1]

[1]Florida State University, Tallahassee, Fl, USA, [2]Purdue University, West Lafayette, IN, USA

Introduction

The majority of actinide coordination complexes have been investigated in aqueous media with ligands that do not react with dioxygen or hydrolyze. Non-aqueous chemistry of transuranium elements is underexplored owing to the enhanced challenges of finding soluble starting materials, solvents that do not rapidly degrade from radiolytic reactions, and isotopic scarcity. Of course, overcoming the hurdles of air-sensitive, nonaqueous, transuranium chemistry opens up avenues that have never been explored, and allows us to more deeply understand structure, reactivity, and physical properties in heavy elements.

Here, we focus on utilizing the redox active ligand 2,4,6,8-tetrakis(*tert*-butyl)-9-hydroxyphenoxanone (DOPO) to complex with the mid-to-heavy actinides under non-aqueous conditions. DOPO has been well established in transition metal chemistry for stabilizing various oxidation states of the metal while mediating multi-electron processes[1-4] Recently, DOPO has been used in uranium chemistry for multi-electron oxidative addition and reductive elimination.[4] We are interested in using the DOPO ligand to synthesize tris-chelate complexes in order to study the electronic structures of trans-uranic elements and to measure the effects of a redox-active ligand on the heavier actinides.

Description Of The Actual Work

Synthesis of $An(DOPO)_3$ complexes has been accomplished using nonaqueous conditions. $AnBr_3$ (An: Pu, Am, and Cf) were dissolved in pyridine. The DOPO ligand was slowly introduced to the reaction flask in a 3:1 ratio of ligand to metal. Upon standing, large block-shaped crystals formed. Crystallographic data revealed that the tris-chelating complexes of $Pu(DOPO)_3$, $Am(DOPO)_3$, and $Cf(DOPO)_3$ do not form a isomorphous series.

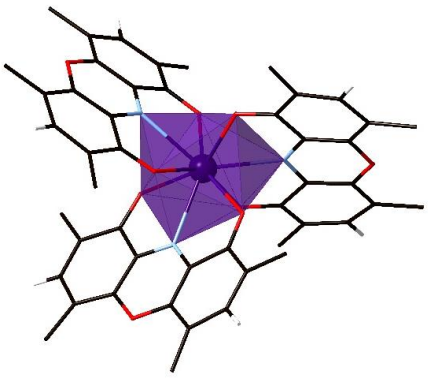

Figure 1. *A view of An(DOPO)3 (An: Pu, Am, Cf) complex showing the nine-coordinate tricapped trigonal prismatic coordination environment of the An(III) cation created by three, tri-dentate, dioxophenoxazine ligands. The tert(butyl) groups have been omitted for clarity.*

Results

The molecular structure of $An(DOPO)_3$' (An: Pu, Am, Cf) contains actinide ions surrounding by three DOPO molecules leading to a nine-coordinate tri-capped trigonal prism geometry shown in **Figure 1**. The structural data suggests that $Pu(DOPO)_3$ is in the tetravalent state, whereas the Am and Cf are most likely in the trivalent state. The UV-Vis spectrum of $Pu(DOPO)_3$ is dominated by intraligand charge-transfer bands, therefore the Pu^{IV} *f-f* transistions are obstructed and the oxidation of Pu cannot be determined from the spectrum. In **Figure 2**, the bond lengths of the three DOPO ligands coordinating to the Pu center are listed. Two of the DOPO molecules have very similar bond lengths which correspond to the monoanionic DOPO ligand. The bond lengths of the third DOPO molecule deviate from those of the first two DOPO molecules. This is evidence that the third DOPO ligand is in the dianionic form, which supports the suggestion that plutonium is in the tetravalent state. In comparison to $Am(DOPO)_3$, and $Cf(DOPO)_3$, the DOPO ligands in those complexes exhibit uniform bonding throughout each structure. This suggests that each ligand is monoanionic, which stabilizes the trivalent state of Am and Cf.

Magnetic studies have been performed on $Am(DOPO)_3$. The magnetic susceptibility data show that the $Am(DOPO)_3$ is non-magnetic, which is typical for the $5f^6$ ground state. This confirms that the ligands are monoanionic and do not possess the radical character that has been found in other systems.[2] However, further magnetic studies will be performed on $Pu(DOPO)_3$ to investigate the magnetic properties and to probe to the radical that was generated from the dianionic DOPO ligand to stabilize the Pu(IV) center.

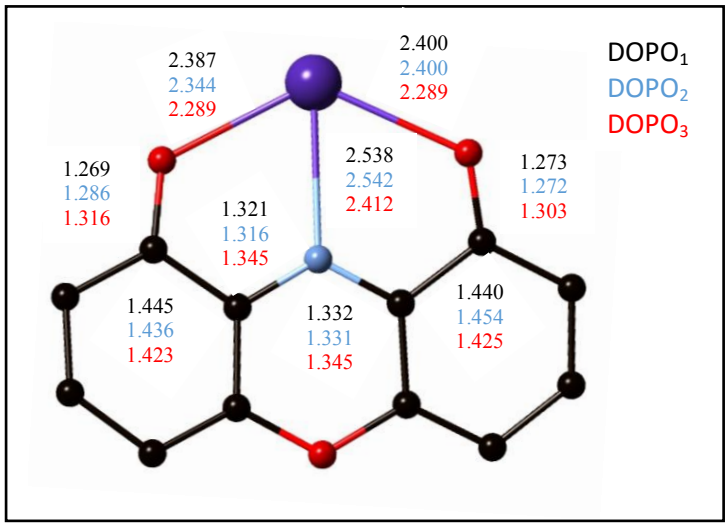

Figure 2: *Bond distances (Å) of $Pu(DOPO)_3$.*

References

[1] E. P. Ivakhnenko, A. G. Starikov, V. I . Minkin, K. A. Lyssenko, M. Y. Antipin, V. I. Simakov, M. S. Korobov, G. S. Borodkin, P. A. Knyazev," Synthesis, Molecular and Electronic Structures of Six-Coordinate Transition Metal (Mn, Fe, Co, Ni, Cu, and Zn) Complexes With Redox-Active 9-hydroxyphenoxazin-1-one Ligands." *Inorganic Chemistry* **2011,** *50*, 7022-7032

[2] L. G. Ranis, K. Werellapatha, N. J. Pietrini, B. A. Bunker, S. N. Brown, "Metal and Ligand Effects on Bonding in Group 6 Complexes of Redox-Active Amidodiphenoxides," *Inorganic Chemistry*, **2014**, *53*, 10203-10216.

[3] E. M. Matson, S. R. Opperwall, P. E. Fanwick, S. C. Bart, “Oxidative Addition of Halogens to Uranium(IV) Bis(amidophenolate) Complexes,” *Inorganic Chemistry*, **2013**, *52*, 7295-7304.

[4] S. A. Pattenaude, C. S. Kuehner, W. L. Dorfner, E. J. Schelter, P. E. Fanwick, S. C. Bart, “Spectroscopic and Structural Elucidation of Uranium Dioxophenoxazine Complexes.” *Inorganic Chemistry* **2015,** *54,* 6520-6527.

C-48

Fast neutron multiplicity counting with zero accidentals

Rashed Sarwar[1], Malcolm J Joyce[1], Colin H Zimmerman[2]

[1]Engineering Department, Lancaster University, Lancaster, Lancashire, UK, [2]Central Laboratory, National Nuclear Laboratory, Sellafield, Cumbria, UK

The development and initial Rossi-α, Feynman Y and neutron coincidence distribution results of a Field-Programmable Gate Array (FPGA) based system for the real-time multiplicity analysis with organic liquid scintillation detectors will be described. Passive neutron multiplicity counting is a well-documented method used widely in the analysis of special nuclear material with the objective of quantifying the plutonium content of a given sample by deploying time-correlated thermal neutron detection techniques [1]. The application of this method can be seen primarily in the discipline of nuclear safeguards associated with the implementation of arms control treaties and the prevention of the illicit use of civilian nuclear materials from bulk material storage facilities etc. Historically, the primary choice of detectors for this purpose have been helium-3 detectors due to the large cross-section of ^{3}He for thermal neutrons. Despite very high efficiency, detecting thermal neutrons requires the thermalization of the neutrons emitted from fission which on average have a kinetic energy of 2 MeV. As a consequence, the use of these detectors requires large coincidence windows (in the order of tens of microseconds) [2] as can be observed in Figure 1. This leads to significant number of accidental counts and large uncertainties preventing the determination of high order multiplicities. Moreover, the incident energy of the neutron is lost due to thermalization and, further, there is a growing shortage in the supply of He-3 itself [3].

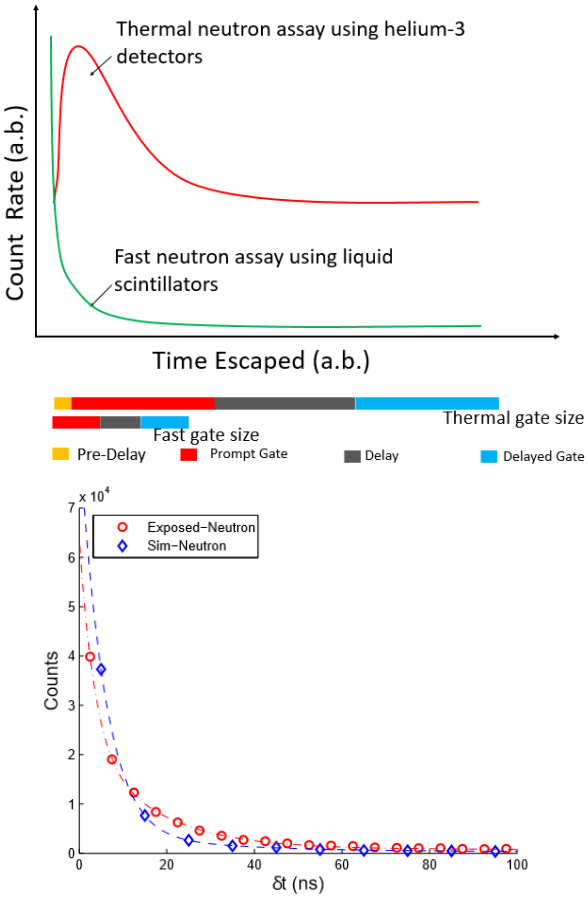

Figure 1: (left) Theoretical Rossi-α distribution for both thermal and fast neutron detectors [1, 4]. (right) Rossi-α distribution of californium-252 source and its corresponding MCNP6 simulated validation showing good agreement

A solution to this is the use of liquid scintillation detectors for fast neutron multiplicity analysis or coincidence counting. Despite having lower detection efficiency compared to ^{3}He detectors, liquid scintillation detectors are blessed with very small detection die-away [4]. Moreover, the neutrons do not have to be thermalized as the scintillators, which are hydrogen based compounds, have relatively high cross-sections for elastic scattering, the primary mode of neutron detection in these detectors. This allows small coincidence windows (in the order of tens of nanoseconds) thereby registering only minimal accidental counts, as depicted in Figure 1 (left) via the Rossi-α [1] distribution. A reconstructed fast neutron multiplicity distribution will be demonstrated in this paper using a prototype system developed using a field-programmable gate array coupled with four mixed-field analysers [5]. The system is capable of determining the Rossi-α (see Figure 2 (right)), Feynman-Y [6] and the neutron coincidence distribution in real-time as well as providing time-of-flight analysis. Results from experiments using both correlated and uncorrelated sources will be presented along with the corresponding MCNP6 simulation results for validation purposes. As illustration, the Rossi-α distribution using a correlated source is presented in Figure 2 which shows good agreement between the experiment and the simulation. Additionally, preliminary analysis of joint neutron-gamma multiplicities will be discussed as well as the unfolding of neutron spectra from the Rossi-α distributions.

References

[1] N. Ensslin, Principles of neutron coincidence counting, chapter 16, ‘Passive non-destructive assay manual’, pp. 457-492, http://www.lanl.gov/orgs/n/n1/panda/00326411.pdf

[2] D. L. Chichester, S. A. Pozzi, J. L. Dolan, A. C. K. M. T. Kinlaw, M. Flaska, A. Enqvist, J. T. Johnson, and S. M. Watson, 'MPACT Fast Neutron Multiplicity System Design Concepts (2012)', https://inldigitallibrary.inl.gov/sti/5547277.pdf.

[3] A.J. Keller, 'An Increasingly Rare Isotope', Physics 241, Stanford University, 2011.

[4] M. J. Joyce, J. Adamczyk, M. D. Aspinall, F. D. Cave, and R. Plenteda, 'Real-time, fast neutron detection for stimulated safeguards assay', Proceeding of the 37th ESARDA symposium on Safeguards and Nuclear Non-Proliferation (2015).

[5] 'M. J. Joyce, K. A. A. Gamage, M. D. Aspinall, F. D. Cave, and A. Lavietes, 'Real-Time Fast Neutron Coincidence Assay of Plutonium With a 4-Channel Multiplexed Analyzer and Organic Scintillators', IEEE Transactions on Nuclear Science, vol. 61, no. 3, pp. 1340-1348, June 2014.

[6] R.P. Feynman, F. De Hoffmann, and R. Serber, 'Dispersion of the neutron emission in U-235 fission', Journal of Nuclear Energy (1954), Volume 3, Issue 1, 1956, Pages 64-IN10

C-49

Synthesis and Vapor Pressure Determination of Volatile Quadrivalent Neptunium Complexes

Aaron Johnson, Jacon Davies, Kevin Carney

Idaho National Laboratory, Idaho Falls, Idaho, USA

Ionization in a thermal ionization mass spectrometer (TIMS) instrument occurs during thermal desorption of a chemically purified material off of a source filament. During this process, a portion of the desorbed material is ionized through thermal action. Thus, the total amount of material ionized (which directly correlates to the sensitivity of the spectrometer), is largely governed by two properties: the elements ionization energy, and its volatility. For example, plutonium has a low vapor pressure but also a low ionization potential, hence it exhibits moderate sensitivity in a TIMS analysis. However, neptunium exhibits both higher vapor pressure and ionization potential than plutonium, resulting in poor TIMS sensitivity. This is a major disadvantage when the primary isotope of interest is of significantly low abundance; commonly only 0.1-0.2% of the sample can be ionized which complexes analyses. To increase the sensitivity of the mass spectrometer, a more efficient method of introducing these compounds into the mass spectrometer is desirable. Currently Idaho National Laboratory is developing a new ionization method involving direct capillary introduction of gaseous neptunium compounds directly into a spark source chamber. Initial estimates of this source configuration predict an ionization efficiency of approximately 1-10%, representing an order of magnitude increase. A major complexity to this approach is that it requires the chemical modification of neptunium to increase its volatility. β-Diketone chelates of metals are well known for their high volatility. In this work, chelates of quadrivalent neptunium and 6,6,7,7,8,8,8-heptafluoro-2,2,-dimethyl-3,5-octanedione (FOD), 1,1,1,2,2-pentafluoro-6,6-dimethylheptane-3,5-dione (PDHD), and 1,1,1-Trifluoro-5,5-dimethyl-2,4-hexanedione (TDHD), and 2,2,6,6-tetramethyl-3,5-heptanedione (TMHD) were synthesized and characterized by FTIR, NMR, and in some cases single crystal XRD. The compounds were then tested for their stability and sublimation temperature by thermogravimetric analysis. Ultimately, the goal of this work is to determine the vapor pressures, as well as thermodynamics of sublimation for these compounds. To do this, a modified Knudsen effusion cell coupled to a quartz crystal microbalance was employed. This method allows for the precise determination of compounds of very low vapor pressures. Once vapor pressures have been determined at varying temperatures, the Clausius-Clapeyron equation can then be applied to determine $\Delta H_{sublimation}$ and $\Delta S_{sublimation}$. Overall, the methods and results of this study will be applied to similar compounds of U, Pu, and Th.

C-50

Simulant corium materials for investigations in the frame of severe accident studies

Alice Seibert[1], David Bottomley[1], Dario Manara[1], Sara Mastromarino[2], Luca Soldi[3], Emtethal Kassim[1], Damien Prieur[1], Philippe E. Raison[1], Thierry Wiss[1], Didier Pellotiero[1], Joseph Somers[1], Vincenzo V. Rondinella[1]

[1]Europäische Kommission, Joint Research Centre, Institut für Transurane, Karlsruhe, Germany, [2]Delft University of Technology Faculty of Applied Sciences, Nuclear Energy and Radiation Applications, Delft, The Netherlands, [3]Politecnico di Milano, Energy Department, Milan, Italy

Introduction

In a severe accident scenario with melting of fuel and cladding mixed UO_2-ZrO_2 phases called "corium" are formed. For LWR typical core inventories range from U/Zr molar ratios of 40/60 to 60/40 and this is the zone of interest in the UO_2-ZrO_2 phase diagram for UO_2-fuelled reactors. However for MOX-fuelled reactors the fuel composition range extends from 7-9 wt% PuO_2 in UO_2 to about 20 wt% PuO_2 in UO_2 in fast reactors. Therefore this requires knowledge of the PuO_2-UO_2-ZrO_2 diagram. Samples have been made that simulate the compositions of coria expected from MOX or fast reactor fuel inventories and also beyond to higher PuO_2 contents in order to understand the form of this phase diagram.

Real corium, due to interactions with structural materials contains elements such as Fe, In, Ag, B and others from in-vessel structures and structural materials, as well as fission products. The behaviour of such complex ceramics at high temperature, the influence of the oxygen potential (steam) and fission products under these extreme conditions is essential for modelling of severe accident scenarios and a priori determination of the fuel's safe performance limits. Beside the accident research on real large scale samples (investigation of TMI samples as well as Chernobyl lavas and investigations such as the Phebus project [1]), smaller scale severe accident testing facilities permit a detailed understanding of the mechanisms and elucidation of the important material properties (melting and cooling behavior, thermal conductivity, etc.) that determine reactor core degradation in a severe accident. Material properties like hardness and chemical durability are also an important factor when it comes to decommissioning of severely damaged reactors e.g. at Fukushima.

Results

Samples simulating corium materials formed under severe nuclear reactor accidents were synthesized using various methods and used for thermodynamic investigations, e.g. melting point under inert and oxidative conditions, as well as thermal conductivity measurements and mechanical testing.

As the melting behaviour of uranium dioxide is atmosphere-dependent, a difference is expected also for the mixed U,Zr-oxide materials. First results were obtained on the pure U,Zr-system [2]; additionally, the influence of the plutonium content was considered recently ([3] and this study).

Self-crucible laser flash pyrometry [4] of a series of samples with varying U,Zr,Pu-content has been performed under different atmospheres: reducing (Ar-6%H_2), inert (Ar) and oxidizing (air). Results from these melting point investigations are now combined with X-Ray absorption spectroscopy and XRD to provide a correlation with the obtained solidification temperatures and in particular the uranium valence.

The laser flash results showed a variation due to a) composition and b) atmosphere (redox condition). For U,Zr-materials and U,Pu,Zr-materials with high uranium content the solidification temperature generally decreases when melted and re-melted under air atmosphere, but

remains nearly constant in inert or reducing atmosphere. Repeated laser shots under air show a rapid drop in primary transition point (and also other transition points), indicating that at ~3000 K there is a very rapid interaction between liquids and their atmospheres. These findings imply that uranium is the main agent taking up oxygen. XANES investigation on a series of U,Zr-oxide materials and an 8 wt% Pu content composition showed clear evidence of a UL III line typical of higher oxides of U therewith corroborating the interpretation. XRD has demonstrated the presence of cubic and tetragonal phases attributable to U, Pu and Zr-dominated phases and the possible presence of U_4O_9 reflections in some samples.

Conventional EDX analysis was only able to confirm qualitatively the main elements and certain element-rich phases. Area analysis deviated from expected compositions when uranium and plutonium in concentration > 10 at% were present. This is thought to be due to the fluorescence effects of uranium and plutonium (particularly of U from Pu-decay). Only analysis using a shielded SEM has enabled quantification for some samples.

Conclusions

Differing results under neutral, reducing and air atmospheres for the UO_2-, PuO_2- and ZrO_2-mixtures can be interpreted by the major influence of UO_2 oxidising beyond stoichiometry in air atmosphere, resulting in lower solid/liquid transition temperatures, whereas the highest melting point is observed for stoichiometric dioxide compositions. Accordingly the UO_2 poor, PuO_2, ZrO_2–rich compositions show relatively constant melting points, unaffected by the change of atmosphere.

References

[1] P. D. W. Bottomley et al. Ann Nucl Ener, 2014, 65, 345.

[2] A. Seibert, D. Manara et al. to be published

[3] A. Quaini et al. J Nucl Mater, 2015, 467, 660

[4] D. Manara et al. Rev Sci Instr, 79, 2008, 113901

C-51

New insight in the Am-O phase diagram by coupling experimental HT-XRD and Calphad thermodynamic modelling.

Enrica Epifano[1], Romain Vauchy[1], Renaud C. Belin[3], Florent Lebreton[1], Alexis Joly[1], Christine Guéneau[2], Philippe Martin[1]

[1]DEN/DTEC/SECA/LCC CEA, Cadarache Saint-Paul-Lez-Durance, France, [2]DEN/DPC/SCCME/LM2T CEA, Saclay Gif-sur-Yvette, France, [3]DEN/DEC/SESC/LLCC, Cadarache Saint-Paul-Lez-Durance, France

Minor actinides (MA) like Am, Np and Cm significantly contribute to the long-term radiotoxicity of the spent nuclear fuel. One of the options envisaged for reducing the nuclear waste inventory is the transmutation of these elements in fast neutron reactors. The possibility of using advanced fuels, mainly UO_2 doped with MA, has led to the necessity of investigating the structural and thermodynamic properties of such compounds. In this frame, the attention is mainly focused on U-Am mixed oxides [1,2].

The assessment of the thermodynamic behaviour of the U-Am-O ternary system is not possible without a thorough knowledge of the associated binary systems. Unfortunately, experimental data on the Am-O are rare due to the difficulty of handling such radiotoxic samples. Nevertheless, various representations of the Am-O phase diagram have been proposed [3-6].

Recently, a Calphad thermodynamic modelling of the Am-O system has been proposed by Gotcu *et al.*, [7] and integrated in the TAF-ID database [8]. In this representation (cf. Figure 18) for an O/Am ratio ranging between 1.5 and 2.0, three phases are reported: a dioxide (AmO_{2-x}) with a large hypo-stoichiometric single-phase domain, a hexagonal sesquioxide (A-Am_2O_3) and an intermediate cubic phase ($AmO_{1.62}$). Moreover, for the americium dioxide, a miscibility gap is reported for 1150K <T <1300K and 1.7<O/Am< 1.95.

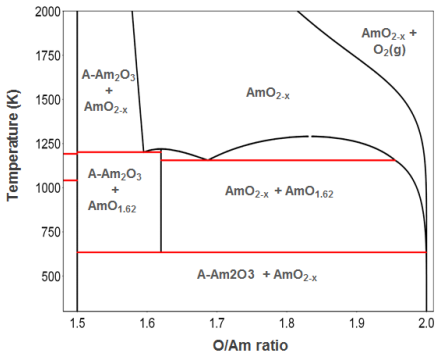

Figure 18. Am-O phase diagram computed with the Calphad model of Gotcu *et al*. [7]

Recently, we compared our results obtained by *in situ* High-Temperature X-ray Diffraction (HT-XRD) to thermodynamic computations performed with the Gotcu model [9]. More precisely, the behaviour of AmO_{2-x} under air up to 1900 K and the phase boundary between AmO_{2-x} and AmO_{2-x} + A-Am_2O_3 were investigated. A general consistency was found and allowed us to establish for the first time the relation between the AmO_{2-x} lattice parameter, the O/Am ratio and temperature.

In this work, we have continued the investigation of the Am-O phase diagram by HT-XRD, focusing the attention on the region with O/Am ranging between 1.6 and 2.0 and intermediate temperatures between 700 and 1400 K. Our data show that the intermediate $AmO_{1.62}$ phase has an existence domain, similarly to the body centred cubic (BCC) $PuO_{1.61\pm x}$ phase observed in the

Pu-O system. Furthermore, until this moment, our HT-XRD data have not pointed out the existence of a miscibility gap.

Based on these results an improved thermodynamic model of the Am-O system will be presented in this work. The introduced modifications rely on our HT-XRD data and other recent studies published in literature [10]. As shown in Figure 19-(a), in our model we have added a low-temperature BCC sesquioxide phase ($AmO_{1.52}$) and an existence domain for the $AmO_{1.62}$ phase. In this improved phase diagram, the similarity with the Pu-O system (Figure 19-(b)) is more evident than in the previous one. Anyway, some differences still remain, especially concerning the temperature limits of stability of the dioxides.

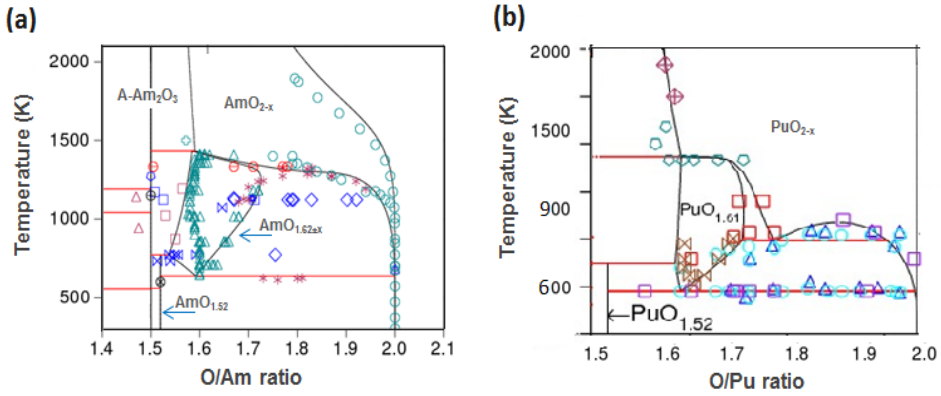

Figure 19. (a) Preliminary result of the Am-O Calphad assessment (this work). (b) Pu-O phase diagram computed with the Calphad model according to Gueneau *et al.* [11]

Considering that the experimental evidences reported in literature are not unequivocal [3], further HT-XRD measurements are scheduled before the conference with the aim to conclude on the presence or not of a miscibility gap in the Am-O system.

References

1. D. Horlait, F. Lebreton, T. Delahaye, N. Herlet, P. Dehaudt, *Procedia Chem.*, vol.7, pp. 485–492, 2012.

2. D. Prieur, A. Jankowiak, T. Delahaye, N. Herlet, P. Dehaudt, P. Blanchart, *J. Nucl. Mater.*, vol. 414, pp. 503–507, 2011.

3. C. Sari and E. Zamorani, *J. Nucl. Mater.*, vol. 37, no. 3, pp. 324–330, 1970.

4. H. Okamoto, *J. Phase Equilibria*, vol. 12, no. 6, pp. 696–697, 1991.

5. C. Thiriet and R. J. M. Konings,*J. Nucl. Mater.*, vol. 320, no. 3, pp. 292–298, 2003.

6. H. Okamoto, *J. Phase Equilibria Diffus.*, vol. 32, no. 6, pp. 572–573, 2011.

7. P. Gotcu-Freis, J.-Y. Colle, C. Guéneau, N. Dupin, B. Sundman, R. J. M. Konings, *J. Nucl. Mater.*, vol. 414, no. 3, pp. 408–421, 2011.

8. www.oecd-nea/science/taf-id.com.

9. E. Epifano, R. C. Belin, C. Gueneau, J-C. Richaud, R. Vauchy, M. Strach, P. M. Martin, Sci. Basis Nucl. Wste Manag. XXXIX, Montpellier, France (2015)

10. F. Lebreton, R. C. Belin, T. Delahaye, P. Blanchart, *J. Solid State Chem.*, vol. 196, pp. 217–224, 2012.

11. C. Gueneau, C. Chatillon, B. Sundman, *J. Nucl. Mater.*, vol. 378, pp. 257-272 (2008).

C-52

Structure and stability of EDTMP and DOTMP complex with Th(IV) for nuclear medicine

Tomoo Yamamura[1], Masaru Furuya[1], Suguru Ohta[1], Koshin Washiyama[2]

[1]Institute for Materials Research, Tohoku University, Sendai, Miyagi, Japan, [2]School of Health Sciences, Faculty of Medicine, Kanazawa University, Kanazawa, Ishikawa, Japan

Radionuclide therapy is one of the fields of nuclear medicine and it uses tumor specific antibody, and/or peptide that labeled with radionuclide which emitted charged-particle such as α particle, β - particle, and Auger electron for treatment of tumors. β - particle emitters, such as ^{89}Sr, ^{90}Y, and ^{131}I have been used for clinical field in Japan, and ^{32}P, ^{153}Sm, ^{186}Re have also been used in the United States and Europe. Alpha-particles are radiations of high liner energy transfers (LETs). Therefore, the cytotoxicity that induced by α -particles are far more potent than low LET β - particles. Due to the short range of α -particles in tissue, α -emitting radionuclides are suited for targeting micrometastases and single tumor cells. Therefore, several α -emitters such as ^{211}At, ^{213}Bi), ^{223}Ra), and ^{225}Ac) have used for clinical trial of leukemia, melanoma, bone metastases, and so on. Especially, ^{227}Th, ^{223}Ra, and ^{225}Ac are the parent of decay chain nuclides. These nuclides act as in vivo generator and emit more potent radiation to tumor than single α -, β -particle emission.

In this study, the stability constants and crystallographic structure of the thorium complexes with DOTMP and EDTMP ligands (Fig. 1) which are often used for labeling alpha emitters to antibodies and peptides.

The stability constants and crystallographic structure of the thorium complexes with DOTMP and EDTMP ligands which are often used for labeling alpha emitters to antibodies and peptides. The bonding between thorium metal and nitrogen is found to be the longest, i.e. the weakest, found ever. A tendency of relatively small stability constants log K_{ML} with EDTMP and DOTMP ligands with Th(IV) ion are similar to those with alkaline earth ions such as Ca(II), and differs very much from those with d-transition metal ions. The tendency is consistent with the weak support by nitrogen donors.

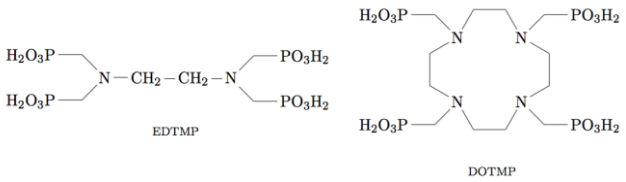

Fig. 1 Chemical structures of EDTMP and DOTMP

C-53

Assessment of PuO_2^{2+} solubility in high borate media

Mark Silver

Florida State University, Tallahassee, Florida, USA

Geological nuclear waste repositories offer expansive, dry environments to contain radioactive materials safely for large, albeit estimated, periods of time. Currently, the Waste Isolation Pilot Plant (WIPP) is the only geological repository accepting transuranic (TRU) waste in the United States. WIPP stores each container of radioactive waste in the confines of rock salt, which is set to surround and entomb the waste for tens of thousands of years until enough material decays to longer-lived species. Scientific models are currently addressing the potential premature breach of one of these containers, thereby leaking TRU material into the rock salt surrounding. The rock salt environment at WIPP contains a very high borate concentration, [B] = 166 ppm, the third highest complexing anion in the salt after chloride and sulfate.

Scientific models fail to address with accuracy the solubility of higher-valent actinides in the presence of the WIPP rock salt, especially the divalent plutonium dioxide cation, PuO_2^{2+}. Work in this area has exposed the presence of two PuO_2-borate species, an inaccuracy in the models which adds to necessity of these measurements, and it is one of the main focuses of this research to quantify and characterize these two species.

With the intent of safely determining this chemistry, ^{242}Pu was chosen due to its significantly longer half-life (3.45×10^5 yrs.) and traceable optical features in absorption spectroscopy (λ = 830 nm, ε_{830nm} = 550 M^{-1} cm^{-1}). Solution-state UV-vis-NIR absorption spectroscopy was used to analyze samples of PuO_2 in borate solutions at various concentrations and pH = 7 – 9.26. The immediate observation is the presence of these two species, assigned to complexes involving monoborate and tetraborate in solution. These species shift the assigned 830 nm absorption feature of PuO_2^{2+} to 816 nm and 848 nm. The former shift will be the second reported species to cause a hypsochromic peak shift of this PuO_2^{2+} absorption feature. Characterization of these borate species in solution will most effectively be performed by ^{11}B-NMR spectroscopy. While no heavy elements will be presence in this technique, this provides an accurate picture of borate speciation which can be compared to aforementioned observations. EXAFS analysis has also been conducted on a series of PuO_2-borate solutions with the intent of gathering additional evidence to compare and determine the identity of these two complexes. Additionally, high-ionic strength measurements involving 0.01 – 5 M NaCl / $MgCl_2$ provide more evidence in the way of improving scientific models in relation to the Pitzer model.

Finally, preparation of crystalline phases of PuO_2-borate materials at ambient temperatures and pressures have been targeted with the intent of identifying putative $M_aPuO_2[B_bO_c(OH)_d]A_e$ ($M = Na^+, Mg^{2+}$; $A = Cl^-$) species which may exist in solution. $PuO_2[B_8O_{11}(OH)_4]$ is the only single-crystal structure in the literature which contains hexavalent plutonium, and is part of an isotypic series containing the actinyl units UO_2^{2+}, NpO_2^{2+}, and PuO_2^{2+}. It is expected that PuO_2^{2+} will behave similar to UO_2^{2+} and coordinate in a variety of structure-types when different cations and anions are available in the matrix of crystallization. Crystallization as a single-phase will determine how effective these solids are at providing complex information of PuO_2-borate in solution.

C-54

Elastic Modulii of Various Innovative Fuel Materials

Tarik A. Saleh, Joshua White, Ursula Carvajal Nunez, Laura A. Tucker, Ryan Leon

Los Alamos National Laboratory, Los Alamos, NM, USA

Resonant Ultrasound Spectroscopy (RUS) is a powerful means of measuring the elastic modulus of materials very accurately. As such it is a useful tool for characterizing novel materials, measuring the changes in properties due to damage (radiation or otherwise), and as an initial measure of quality in small scale fabrication, specifically to this presentation, in pellets of novel fuel types. This talk will cover RUS measurements on various fuel materials, including uranium oxide, uranium/plutonium mixed oxide fuels, and, particularly, uranium silicides. Many similar pellets of U_3Si_2, U_3Si_5 and USi were measured and compared to literature values, and moduli measurements from nanoindentation. Experimental equipment, environment, and challenges while measuring moduli on these actinide bearing materials will be highlighted. This work is part of the US Department of Energy -Fuel Cycle Research and Development - Advanced Fuel Campaign, focusing on the properties of various high density fuels in order to generate candidates for next generation reactors and accident tolerant fuels.

C-55

Aging Effects Interacting with Microstructure

Saryu Fensin, Steve Valone

Los Alamos National Lab, Los Alamos, NM, USA

Aging effects, especially as related to helium (He) have been explored over the years in gallium (Ga) -stabilized fcc-phase plutonium (δ-Pu). Mechanical response of Pu that underwent accelerated aging, under uniaxial stress conditions, at quasi-static strain rates, has shown that although the yield stress for δ-Pu increases with age it causes a substantial decrease in the material's ductility. The reason behind this change in properties has been attributed to many effects including the presence of point defects and He bubbles that are generated due to self-irradiation in Pu as it ages. However, all the origins contributing to this phenomenon have not been identified. In this work, we explore Ga segregation, as a function of age, as another mechanism that could affect these properties.

Specifically, we use Monte Carlo simulations using the MEAM Pu potential, to investigate Ga segregation as a function of free surface orientation, grain boundary type and Ga concentration. Preliminary results indicate that Ga segregates *away* from free surfaces irrespective of orientation and Ga concentration. These results also show that Ga preferentially segregates to boundaries based on GB structure. For example, it was observed that Ga segregated away from all Σ5 symmetric tilt boundaries but preferentially segregated to over-coordinated regions within Σ11 asymmetric tilt boundaries. We will discuss these results and some addition molecular-dynamics simulations to understand the reasons behind these observations.

C-56

Electrical transport in uranium compounds URhX_5 (X = Ga, In)

Yoshinori Haga[1], Yuji Matsumoto[2], Naoyuki Tateiwa[1], Etsuji Yamamoto[1], Jiri Pospisil[1], Zachary Fisk[3]

[1]Japan Atomic Energy Agency, Tokai, Japan, [2]Nagoya Institute of Technology, Nagoya, Japan, [3]University of California, Irvine, Irvine, USA

Rare earth and actinides compounds crystalizing in the tetragonal $HoCoGa_5$-type structure (115 compounds) have attracted attention for the last decade because of novel phenomena arising from strong electron correlations. Among them uranium analogues UTX_5 (T: can be formed by replacing cobalt site with a series of transition metals. A change of *d*-electron count systematically alters their ground states from paramagnetic metal (T = Fe, Ru, Os), semimetal with low carrier concentration (T = Co, Rh, Ir) and antiferromagnetic metal (T = Ni, Pd, Pt). Experimental and theoretical Fermi surface investigations strongly suggested rigid band picture in these compounds and successfully explained the electronic states.

On the other hand, we recently reported a new member of UTX_5 : $URhIn_5$, only a uranium 115 compound with indium as a constituent element [1,2]. In comparison to the isoelectronic analogue $URhGa_5$, $URhIn_5$ has significantly larger unit cell volume. As a result the ground state of $URhIn_5$ becomes antiferromagnetic, in contrast to nonmagnetic in $URhGa_5$, indicating that the rigid band picture is no more valid. In the present paper, we report electronic state investigation in $URhIn_5$ by means of electrical transport measurements as well as de Haas-van Alphen effect [3]. The experimental data strongly suggest a formation of a gap on the Fermi surface in the antiferromagnetic state leaving a small conduction carrier concentration. Anomalous temperature dependence of the effective carrier number at low temperature was suggested from a simple two-band analysis.

References

[1] Y. Matsumoto *et al*., Phys. Rev. B **88**, 045120 (2013).

[2] H. Sakai *et al*., Phys. Rev. B **88**, 045123 (2013).

[3] Y. Matsumoto *et al*., JPS Conf. Proc. **3**, 011097 (2014)

C-57

Experimentally Validated Casting Simulations of Unalloyed Plutonium

Meghan Gibbs, Deniece Korzekwa

Los Alamos National Laboratory, Los Alamos, NM, USA

Computational simulations of the casting process can be used as part of a combined experimental/computational approach in order to produce quality castings. Such simulations provide the opportunity for optimization of process parameters and experimental setup which lead to a higher quality product. The other aspect of using an experimental/computational approach is the ability to refine and improve simulations based on experimental results. Casting of unalloyed plutonium is challenging due to large volumetric phase transformations incurred during cooling, particularly the 9% volume decrease of β->α transformation at 117 °C. Previously, nominally pure plutonium pucks and rods were manufactured via slow controlled cooling through the critical phase fields, using two geometries, pucks and rods [1].

This work explores utilizing the experimental data from the production of the puck and rod parts to validate simulations performed using the LANL developed computer code TRUCHAS. Simulations will be compared to experimental data. In addition, validated simulations will be rerun to incorporate code improvements and compared to the initial simulations. TRUCHAS is a casting simulation code that covers the entire casting process from mold and metal heating with electromagnetic or radiative heating, pouring and fill, through non-isothermal solidification. Recent developments in the code provide improved electromagnetic heating, view-factor based radiation heat transfer, and a rudimentary microstructure model.

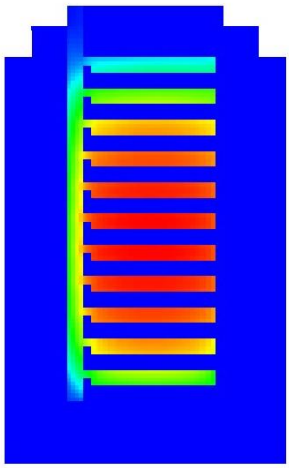

Figure 1: A cross section of the 10 uniform puck mold showing solidification start time. Withing the pucks, the red (darker) indicates the longest time and blue (lighter) the shortest time.

References

1. D.R. Korzekwa, F.J Freibert, P.J. Crawford, J.W. Gibbs, D.A. Korzekwa, R.M. Aikin, Jr., “Fabrication of Unalloyed Plutonium,” Plutonium Futures – The Science 2010, p. 415. Keystone, CO, September 19-23, 2010.

C-58

Magnetic susceptibility and fluctuations of the electron density in the δ-plutonium

Arkadij Volkov, Aleksandr Povzner

Ural Federal University, Ekaterinburg, Russia

In the case of δ-plutonium, according to the LDA+U+SO-results [1], large fluctuations of the magnetic moments should have place in the basic state of 5f-electrons. On the other hand, the analysis of experimental data on the electronic and magnetic properties leads to the conclusion about the fluctuations of from the basic configuration of 3+ to 4+ and 2+ states of plutonium ions, which lead to the observed Kondo-like behavior of the magnetic subsystem [2] and not described by ab initio calculations.

In this paper, the self-consistent procedure that combines the results of LDA+U+SO electronic structure calculations (in the method of FP-LAPW) and model description of the thermal fluctuations of the spin and charge density of d- and f-electrons, shows that large fluctuations of the spin moments lead to fluctuations in the occupation numbers of orbitals.

The Hamiltonian of LDA-model - $H_0 = \sum_{\mathbf{k},l,\sigma} \varepsilon^{(\mathrm{LDA})}_{\mathbf{k},l,m} a^{+}_{\mathbf{k},l,m,\sigma} a_{\mathbf{k},l,m,\sigma}$ was supplemented by the terms of the spin-spin and charge interactions to account for Hubbard correlations

$$H_U^{(l)} = U^{(l)} \sum_{\mathbf{v},m} \delta n_{\mathbf{v},l,m,\uparrow} \delta n_{\mathbf{v},l,m,\downarrow} + \widetilde{U}^{(l)} \sum_{\mathbf{v},m\neq m'} \delta n_{\mathbf{v},l,m,\uparrow} \delta n_{\mathbf{v},l,m',\downarrow} + \left(\widetilde{U}^{(l)} - J^{(l)}\right) \sum_{\mathbf{v},m\neq m',\sigma} \delta n_{\mathbf{v},l,m,\sigma} \delta n_{\mathbf{v},l,m',\sigma} \Big/ 2 \quad (1)$$

Here $\varepsilon^{(\mathrm{LDA})}_{\mathbf{k},l,m}$ is energy of the electron with quasimomentum **k,** orbital – *l* and magnetic – *m* quantum numbers, which is calculated in the LDA+U+SO-approximation without spin imbalance; $U^{(l)}$ is the Coulomb interaction energy of the electrons of the same orbital (*l*,*m*)=(*l*,*m*′); $\widetilde{U}^{(l)} = U^{(l)}_{m\neq m'} - 2J^{(l)}$; $U^{(l)}_{m\neq m'}$ is the Coulomb interaction energy of the electrons of different orbitals - (*l*.*m*)≠(*l*,*m*′); $J^{(l)}$ is the Hund exchange interaction energy of the electrons of different orbitals ((*l*.*m*)≠(*l*,*m*′)); $\delta n_{\mathbf{v},l,m,\sigma} = n_{\mathbf{v},l,m,\sigma} - \left\langle n_{\mathbf{v},l,m,\sigma} \right\rangle_0$ is the operator of deviations from the values of the occupation numbers $\left\langle n_{\mathbf{v},l,m,\sigma} \right\rangle_0$ found in the LDA+U+SO-approximation; $n_{\mathbf{v},l,m,\sigma} = a^{+}_{\mathbf{v},l,m,\sigma} a_{\mathbf{v},l,m,\sigma}$; $a^{+}_{\mathbf{v},l,m,\sigma}\left(a_{\mathbf{v},l,m,\sigma}\right)$ and $a^{+}_{\mathbf{k},l,m,\sigma}\left(a_{\mathbf{k},l,m,\sigma}\right)$ are the creation (annihilation) of an electron in the state (*l*, *m*) with spin σ at the site ν and their Fourier transforms, respectively.

For the self-consistent calculation of the statistic sum corresponding to the Hamiltonian (1), we introduced the stochastic inhomogeneous exchange and charge fields that fluctuating in space and time. Estimates of the most probable configurations of stochastic fields were carried out in the approximation of a saddle point for the free-energy functional. In the method of generating functional the Green's function of the electrons was found. It was found that the electronic LDA-spectrum split into spectrums of the spin-symmetric (α=+1) and spin-antisymmetric (α=+1) states. These energy spectrums have the form

$$\varepsilon^{(\mathrm{LDA})}_{\mathbf{k},l,m} \rightarrow \varepsilon^{(\mathrm{LDA})}_{\mathbf{k},l,m} - \alpha U^{(l)} \left\langle M^2_{(l,m)} \right\rangle^{1/2} + U^{(l)} \Delta n^{(l,m)}(T) \Big/ 2 \quad (2)$$

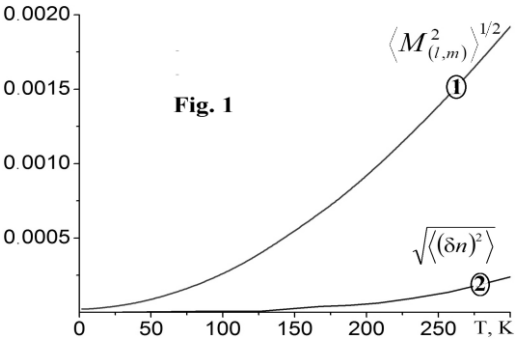

Fig. 1

where $\Delta n^{(l,m)} = N_0^{-1}\sum_{\nu,\sigma}\left\langle \delta n_{\nu,l,m,\sigma}\right\rangle$ is a change in the filling of the (*l*,*m*)-orbital, $\left\langle M^2_{(l,m)}\right\rangle^{1/2}$ is the amplitude of the spin-density fluctuations of electrons in the (*l*,*m*)-state at site.

The temperature increase in the the amplitude of the spin-density fluctuations (Fig. 1, curve 1) leads to the filling of the spin-symmetric states at the expense of other states LDA-bands (with $l \neq l'$) and at the expense of the spin-antisymmetric states of the same the LDA-band. This leads to a temperature increase of the charge fluctuations (Fig. 1, curve 2), as well as the occurrence of temperature-induced local magnetic moments at $T>T^*$. The last thing accompanied by filling spin-symmetric states of f-electrons, analogously to as it is in the Kondo effect.

The spin magnetic susceptibility (see Fig.2) is described by the expression

$$\chi = \sum_{l=f,d}\chi^{(l)} + \chi^{(sp)} + J\chi^{(f)}\chi^{(d)}$$

and due to the renormalization of the electron spectrum (2) the susceptibility of f-electrons ($\chi^{(f)}$) satisfies the Curie-Weiss law for $T>T^*$. The susceptibility of d-electrons ($\chi^{(d)}$) does not have these temperature dependence features. It varies weakly with increasing *T* as well as the susceptibility of the system s- and p-electrons ($\chi^{(sp)}$).

Renormalizations (2) electronic energies of different orbitals by spin fluctuations are significant in the formation of the orbital susceptibility, since there are additional transitions between states with different values of $\alpha = \pm 1$. Estimates show that the orbital contribution a little over 70% of the total magnetic susceptibility.

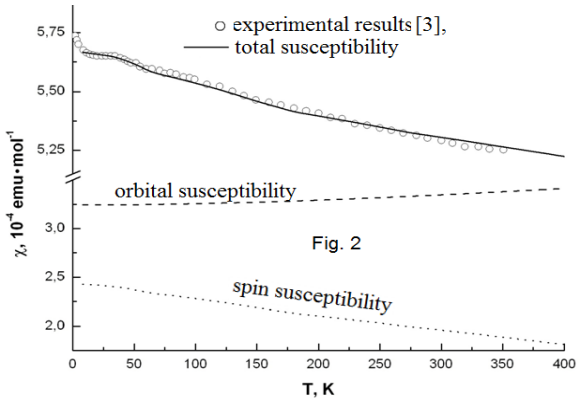

Fig. 2

The total spin and orbital magnetic susceptibility compared with experimental data on $Pu_{0.957}Ga_{0.043}$ [3] in Fig.2.

The calculations were used the values of the parameters of the intra-atomic electron interaction: $U^{(f)}$=2.67 eV, $U^{(d)}$=1.8 eV (in the ab initio calculations [1], wherein the effect of the exchange enhance is not considered - $U^{(f)}$=2.50 eV), and of the Hund exchange interaction J_H=0.5 eV. The average distance between multiplet energies Δ_l=2 eV, which corresponds to half the distance between the centers of the $f^{5/2}$ and the $f^{7/2}$ multiplets bands energy, and the value of the spin-orbit interaction - 0.35 eV, as in [1]. In addition, when calculating the density of states (Fig. 3) and susceptibility (Fig. 2) used parameters of fd-exchange interaction - $J = 0.1U^{(f)}$ and the imaginary part of the Pauli susceptibility of non-interacting electrons $B^{(f)}$=1 and $B^{(d)} = B^{(f)}U^{(d)}g_0^{(d)}(\varepsilon_F)/\left(U^{(f)}g_0^{(f)}(\varepsilon_F)\right)$.

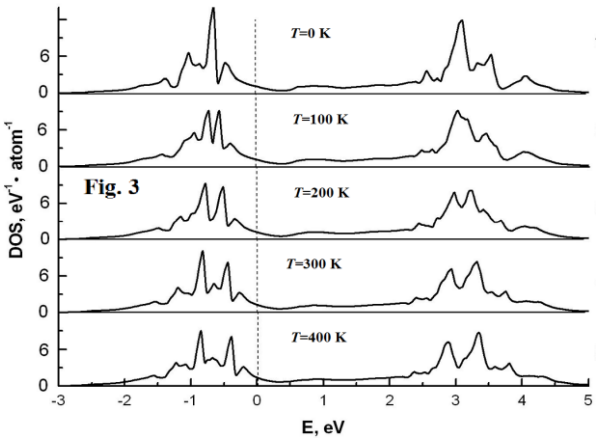

Fig. 3

The density of electron f-states, according to our calculations, is much greater than the density of d-states. The change density of electron states with temperature leads to the fact that the average occupation numbers of sites by f,d-electrons decreases with increasing temperature and increases filling of sp-bands. In particular value Δn_f = - 0.2 electrons/site and Δn_d = - 0.013 electrons/site for *T*=400 K. Obtained by us temperature changes valence are accompanied by charge fluctuations, the maximum mean square value of fluctuations the number of f-electrons at a site is $\sqrt{\sum_{\nu}\left(\delta n_{\nu}^{(f)}\right)^2 / N_0}$ ~0.01 electron/site, and d-electrons to an order of magnitude less. These

estimates suggest that that the effect of valence fluctuations (fluctuations of the occupation numbers) is weak compared to the arising Kondo lattice. At that estimation a concentration of the radiation impurity by the scheme [3] is different from previously presented by tens of percent.

References

1. A. O. Shorikov, A. V. Lukoyanov, M. A. Korotin, et.al., Phys. Rev. B, 72 (2005), 024458

2. E. S. Clementyev, A. V. Mirmelstein, JETP, 109 (2009) p. 128

3. S. K. McCall, M. J. Fluss, B. W. Chung, et.al., PNAS 103 (2006) p. 17179

C-59

Modeling and validation of the Pu 239 surface alpha spectrum using MCNPX coupled with CINDER'90

Laura A. Tucker, Scott Richmond, Tarik A. Saleh

Los Alamos National Laboratory, Los Alamos, NM, USA

Alpha decay in plutonium is well understood, however, the energy and number of alpha particles that escape the surface is less well known. How this field changes with sample size and age and isotopic composition is critical to understanding radiation damage in materials surrounding the plutonium. MCNPX (Monte Carlo N-particle eXtended), a radiation transport code coupled with CINDER'90, an isotopic transmutation code that calculates nuclide inventories, is used to model the alpha spectrum of a Pu239 sample, and the subsequent field at the surface. MCNPX allows us to calculate the reaction rates and track the isotopes as cross section data to create a temporally resolved nuclide inventory solution. This solution is used as an input for CINDER'90 which gives us the alpha spectrum and the nuclide inventory in a spatial homogeneous region. The model will be validated against an experiment consisting of a Pu239 sample suspended in a spherical stainless steel vessel. The vessel will be hermetically sealed and connected to an electrometer and a pressure transducer. The vessel then will be filled with different gases at different pressures. The alpha spectrum will be calculated from the pressure versus current relationship.

C-60

Effects of Aqueous Phase Complexants on Lanthanide and Actinide Oxalate Solubilities

Hannah Colledge, Cheryl Carrigan, Robin Taylor, Mark Sarsfield

National Nuclear Laboratory, Cumbria, UK

With the development of advanced reprocessing flowsheets for future actinide recycling, complexing ligands are increasingly being used in separation processes due to their affinity to selectively bind to lanthanides and/or actinides and carry them into the desired phase. As a result, the safety and chemical effects of these ligands (e.g. Diethylene-triamine-pentaacetic acid (DTPA)) or their degradation products (e.g. acetic acid), which could be carried over from the partitioning process into the downstream conversion process, need to be considered.

Our investigations have focused on determining the effects of acidity and temperature on the downstream oxalate precipitation process, in the presence of these complexing agents, initially focusing on DTPA and acetic acid. Experimental measurements of residual metal ion solubilities in the oxalate mother liquor (OML) were made to determine the effects, if any, of aqueous phase ligands on actinide complexation. Initial experiments were carried out using neodymium (III) as a non-active simulant for americium (III) prior to commencing a second series of active experiments with thorium (IV), which can be considered as a simulant for plutonium (IV).

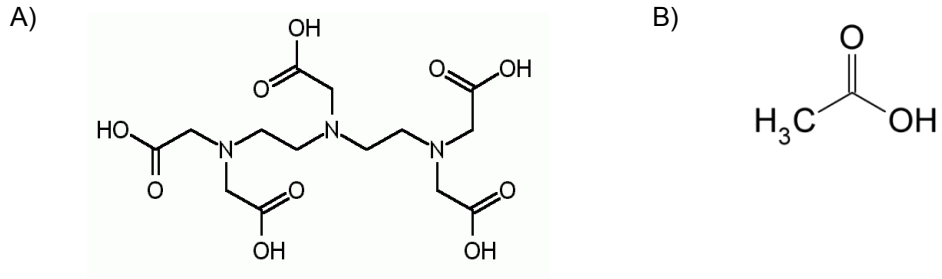

Figure 1: Chemical Structure of A) DTPA and B) Acetic Acid

A reaction carousel was used to carry out up to 12 oxalate precipitation experiments simultaneously. For each experiment, neodymium nitrate was added into a reaction tube with nitric acid, DTPA (if required), acetic acid (if required), ultra-pure water and oxalic acid. At specific time intervals, an aliquot of the working solution from each reaction tube was filtered via a centrifugal ultra-filter (10 kDa MWCO) and analysed by ICP OES (Inductively Coupled Plasma – Optical Emission Spectroscopy). The experimental conditions focused on varying the acidity between 0.3 M and 1 M HNO_3 and the temperature between ambient and 60 °C. DTPA concentration varied from 0.025 M to 0.07 M and the concentration of acetic acid was maintained at 0.05 M.

The ICP-OES results indicated that as the temperature and acidity of the working solution increased the solubility of neodymium in the oxalate mother liquor also increased. Consequently, ambient temperature and a lower acidity (0.3 M HNO_3) were the appropriate conditions for neodymium (III) oxalate formation, giving the lowest solubility values.

With regards to aqueous phase ligands, the presence of acetic acid appeared to have a minimal effect on oxalate precipitation with the concentration of neodymium in the OML remaining

similar to the oxalate-only (“blank”) samples throughout the various experimental runs. However, the addition of DTPA to the oxalate precipitation reaction frequently reduced the solubility of neodymium in solution in comparison to the blank experiments. A series of experiments with varying concentrations of DTPA showed that as the concentration of DTPA introduced to the reaction mixture increased, the concentration of neodymium in the OML consequently decreased.

From the initial investigations it was clear that DTPA had an effect on metal ion solubilities during oxalate precipitation and as a result some analyses of the neodymium oxalate precipitate were completed. Analysis techniques used included Raman spectroscopy, elemental analysis and thermo-gravimetric analysis. The elemental analysis indicated that the oxalate solid with DTPA contained $C_2H_4NO_2$ in addition to the neodymium oxalate precipitate expected, which would correspond to an amino acetate group. This was further supported by the presence of a C-N stretch in the Raman spectrum. An alternative interpretation of the elemental analysis results investigated the effects of charge balance and the number of coordination sites in order to give an estimated molecular formula for the DTPA oxalate precipitate; $Nd_5(DTPA)(C_2O_4H_2)_5(H_2O)_{20}.22H_2O$. These combined results suggest that a fragment of the DTPA structure may have become incorporated into the structure of the neodymium oxalate precipitate and further investigations are ongoing.

Similar solubility experiments are being undertaken with thorium (IV) and plutonium (IV) nitrates in place of neodymium (III) nitrate to extend the studies to tetravalent actinide ions. In addition to investigating the effects of acidity and temperature on the downstream oxalate precipitation process, varying oxalate concentrations will be applied to obtain a range of solubility measurements in order to compare with existing literature data. It is envisaged that the solubility data obtained will feed into solubility models, which can ultimately be used to compare actinide oxalate solubilities with and without the carryover of complexing ligands from upstream separation processes.

C-61

Characterization of *f*-element oxide stoichiometry and phases through Raman Spectroscopy

Jared Stritzinger, George Goff, Dave Wayne

Los Alamos National Laboratory, Los Alamos, NM, USA, LA-UR-16-23355

Introduction

The fluorite structure is well represented in the lanthanide and actinide series by the MO_2 oxides of Ce, Pr, Tb, Th, U, Np, Pu, Am, Cm and Cf. These oxides are often thought of as stoichiometric; however, $MO_{2\pm x}$ often is a better reflection the true non-stoichiometric nature of these oxides.

The fluorite structure consists of the general formula MO_2 or MX_2, which places the metal cation in a cubic coordination environment and O or X anion in a tetrahedral coordination environment. The arrangement of atoms imparts unusual structural stability that accommodates additional anions or the loss of anions. This stability is linked to metal cations that can access multiple oxidation states, allowing for the structure to easily offset the accompanying change in charge with the addition or loss of anions. This characteristic keeps the over-all structure of the metal lattice consistent, while coordination environments shift based on the anions present.

Raman spectroscopy is sensitive to shifts in the coordination environments as symmetry is broken and new vibrational modes are allowed. The stoichiometric fluorite structure type shows O_h^5 symmetry with one Raman active mode arising from the T_{2g}. Examination of sub-stoichiometric praseodymium oxides and a variety of uranium oxides show the effect of oxygen stoichiometry on the fluorite structure and the resulting Raman spectroscopy. This allows for multiple phases to be distinguished with Raman Spectroscopy in samples where bulk characterization such as powder x-ray diffraction shows one phase.

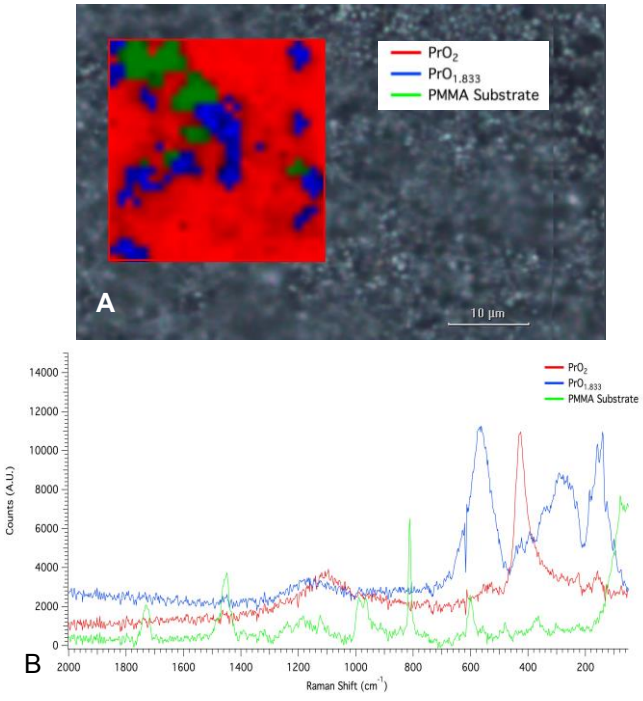

Figure 1: A) Raman map of surface indicating different PrO_x phases B) Raman spectra of various

Experimental and Results

Samples of praseodymium and uranium oxides were prepared through firings at various temperatures and leeching in acid environments. Powder samples were mounted on a poly(methyl-methacrylate) substrates for powder x-ray diffraction and micro-Raman spectroscopy.

A sample of PrO_2 prepared by leaching Pr_6O_{11} ($PrO_{1.833}$) in 0.1 M HCl for 2 hours. Powder X-ray diffraction showed a single phase with unit cell edge of 5.4Å, which is consistent with the PrO_2 reported edge of 5.393Å. When a 625 μm^2 area of the sample surface, Figure 1A, was mapped with Raman spectroscopy, the sample surface showed two phases, both the fluorite and $PrO_{1.833}$. While the bulk of the sample was converted to the PrO_2 fluorite structure, about 20% of the sample remained $PrO_{1.833}$ and is not

observed in the powder X-ray diffraction, Figure 2.

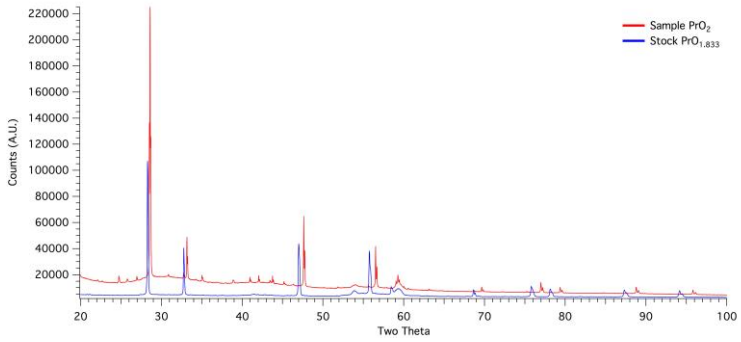

Figure 2: Powder X-ray diffraction of PrO_2 and $PrO_{1.833}$

The robustness of the Fluorite structure is reflected in powder x-ray diffraction measurements that show only a small change in the unit cell edge as the amount of $MO_{2\pm x}$ is varied and the symmetry of the metal lattice remains the same. The results of the powder x-ray diffraction of PrO_2 demonstrate this as the metal cations of $PrO_{1.833}$ occupy roughly the same lattice positions as PrO_2, with the same peaks only slight shifted. The major structural difference is the loss of one oxygen from the cubic coordination environment in approximately one third of the metal sites and is not reflected, as oxygen sites in $PrO_{1.833}$ are disordered over the structure and are poor x-ray scatterers compared to praseodymium atoms, the anion substructure can be difficult to resolve.

Raman spectroscopy provides a method to determine differing local phases and stoichiometry at the surface of a sample by probing the local coordination environment. This is important for providing insight to oxides where bulk analysis through powder x-ray diffraction relies on the over-all lattice and may indicate one phase where multiple non-stoichometric phases are present.

C-62

Physical Properties and Nuclear Magnetic Resonance of Antiferromagnetic $PuPt_3$

Eric D. Bauer[1], Andrew M. Mounce[1], Adam P. Dioguardi[1], Paul H. Tobash[1], Jeremy Mitchell[1], Thomas E. Albrecht-Schmitt[2], Joe D. Thompson[1]

[1]Los Alamos National Laboratory, Los Alamos, NM, USA, [2]Florida State University, Tallahassee, FL, USA

The PuX_3 (X=Rh, Pd, Pt) compounds crystallize in the cubic Cu_3Au structure and order antiferromagnetically at low temperature. The Neel temperature of $PuRh_3$ is T_N=6 K, whereas T_N=24 K in $PuPd_3$. The reported Neel temperature of $PuPt_3$ varies between T_N=40-60 K, suggesting sensitivity to growth and/or annealing conditions. The magnetic susceptibility follows a (modified) Curie-Weiss law at high temperature with an effective moment ranging between 1.0-1.3 μ_B, indicating localized Pu 5f electrons in these materials. Neutron diffraction measurements reveal that the ordered moment of $PuPd_3$ is 0.8 μ_B. Herein, we report the physical properties of $PuPt_3$ obtained by measurements of magnetic susceptibility, electrical resistivity, specific heat, and ^{195}Pt nuclear magnetic resonance. Two antiferromagnetic transitions are observed at T_{N1}=64 K and T_{N2}=57 K in $PuPt_3$, along with a ferromagnetic-like transition at T_c~20 K. These phase transitions are also observed in specific heat measurements. A spin-density-wave anomaly is found in electrical resistivity measurements at T_{N1}=65 K in $PuPt_3$, similar to the behavior of Cr or URu_2Si_2, with small anomalies at T_{N2} and T_c. The 195Pt Knight shift measurements follow the Curie-Weiss behavior of the bulk magnetic susceptibility in the paramagnetic state and exhibit more complicated behavior below T_{N1}. Spin-lattice-relaxation $1/T_1$ measurements reveal an increase of $1/T_1$ between 100 K and 65 K, indicating the presence of antiferromagnetic spin fluctuations. The physical properties of $PuPt_3$ and the behavior of the Pu 5f electrons will be discussed.

C-64

Complexation Behavior and Solubility of the Ternary Systems Ca/Mg-UO_2-CO_3 under Weakly Alkaline Conditions

Jun-Yeop Lee[1], Marika Vespa[1], Ezgi Yalcintas[1], Xavier Gaona[1], Kathy Dardenne[1], Jörg Rothe[1], Thomas Rabung[1], Marcus Altmaier[1], Jong-Il Yun[2]

[1]KIT-INE, Karlsruhe, BW, Germany, [2]KAIST, Daejeon, Daejeon, Republic of Korea

Formation behavior and structural characteristics of ternary Ca/Mg-UO_2-CO_3 aqueous complexes are investigated by means of time-resolved laser fluorescence spectroscopy (TRLFS) and extended X-ray absorption fine structure (EXAFS). In view of their potential relevance in controlling the solubility of U(VI) in carbonate-containing solutions, the solubility of ternary Ca/Mg-UO_2-CO_3 solid phases is studied under weakly alkaline pH conditions and varying [Ca(II)]/[Mg(II)], C_{tot} and temperature. The emphasis of the present work is to derive comprehensive chemical and thermodynamic models for the investigated ternary systems (including both aqueous species and solid compounds), and further to determine their spectroscopic and structural properties.

In the study of ternary Ca/Mg-UO_2-CO_3 aqueous species, the U(VI) stock solution was prepared by dissolution of $UO_2(NO_3)_2{\cdot}6H_2O$ and diluted to a total U(VI) concentrations of 1 mM and 0.1 mM. The pH of the solution was adjusted in the range of 7.4 to 9.0 with TRIS/MES buffer solutions. Total inorganic carbon concentration was initially set to 50 mM with Na_2CO_3/$NaHCO_3$, and total Ca(II) and Mg(II) ion concentrations were controlled with the addition of $Ca(ClO_4)_2$ and $MgCl_2{\cdot}6H_2O$, respectively. Ionic strength was adjusted at 0.1 M H/$NaClO_4$ for Ca(II) system and 0.15 M NaCl–$NaHCO_3$–Na_2CO_3 for Mg(II) system.

Fig. 1a and 1b show U(VI) fluorescence spectra obtained under increasing [Ca(II)] and [Mg(II)], respectively. The characteristic fluorescence peak positions previously reported [1] in combination with the increase in fluorescence intensity with increasing earth-alkaline metal ion concentration support the formation of ternary Ca/Mg-UO_2-CO_3 aqueous complexes. The coupling of slope analysis and evolution of fluorescence lifetime reveals the formation of two different ternary U(VI) carbonate species for Ca(II) and Mg(II), $CaUO_2(CO_3)_3^{2-}$ /$Ca_2UO_2(CO_3)_3$(aq) and $MgUO_2(CO_3)_3^{2-}$/$Mg_2UO_2(CO_3)_3$(aq), respectively. The stability constants extrapolated to infinite dilution according to specific ion interaction theory compare well with data reported in the literature for $CaUO_2(CO_3)_3^{2-}$, $Ca_2UO_2(CO_3)_3$(aq) and $MgUO_2(CO_3)_3^{2-}$, whereas this is the first time that the stability constant for $Mg_2UO_2(CO_3)_3$(aq) has been determined. EXAFS results support the formation of ternary Ca/Mg-UO_2-CO_3 aqueous species, showing similar molecular structure to the Liebigite ($Ca_2UO_2(CO_3)_3{\cdot}10H_2O$) except for the shorter U-Mg distance compared to U-Ca distance which is related with differences in ionic radii of both earth-alkaline metal ions.

Solid phases $Ca_2UO_2(CO_3)_3{\cdot}xH_2O$(cr) and $Mg_2UO_2(CO_3)_3{\cdot}yH_2O$(cr) were synthesized as described in the literature [2] and characterized by XRD, SEM-EDS, DTA and quantitative chemical analysis. Preliminary results on the solubility of these solid phases under weakly alkaline conditions, $25 \leq T\ (°C) \leq 80$, and varying [Ca]/[Mg] and C_{tot} will be presented in this contribution. The results obtained in this work contribute to an accurate description of the chemical speciation and solubility of U(VI) in natural environments along with geochemical boundary conditions relevant in the safety assessment of deep-geologic repository.

The spectroscopic part of this work was supported by the Nuclear Safety Research Program (1305032-0315-CG100) through the Korea Foundation of Nuclear Safety (KOFONS), granted financial resource from the Nuclear Safety and Security Commission (NSSC), Republic of Korea.

The solubility part of this work received funding from the German Federal Ministry for Education and Research (BMBF) under the contract number 02NUK039A.

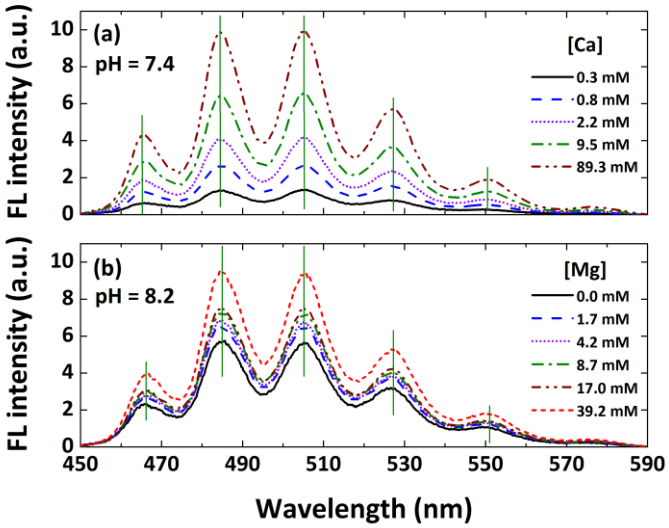

Fig 1. Fluorescence spectra of (a) Ca-UO_2-CO_3 and (b) Mg-UO_2-CO_3 species obtained as a function of earth-alkaline metal ion concentration

References

[1] G. Geipel, S. Amayri and G. Bernhard, *Spectrochim. Acta, Part A*, 2008, **71**, 53-58.

[2] N. G. Chernorukov, A. V. Knyazev, E. V. Vlasova and N. Y. Kuznetsova, *Radiochemistry (Moscow, Russ. Fed.)*, 2009, **51**, 244-249.

C-65

Physical nature of light actinides longevity in the dynamic failure phenomenon

Alexandr Uchaev, Nadezda Selchenkova, Valeriy Punin, Elena Kosheleva

Russian Federal Nuclear Center – VNIIEF, Sarov, Russia

It is known that a number of actinides are nuclear energy materials that can be used in pulsed research facilities, where they are subject to high-intense action [1, 2].

As a rule, relaxation of strongly non-equilibrium states is accompanied by destructive processes [3, 4]. In papers [3, 5] it is shown, that from a self-similarity property of damageability accumulation there results a bond between the amplitude of critical pressure $P(t)$ and the material longevity *t*, defined as

$$P(t)^{\gamma} t = const,$$

where $\gamma \approx 3{,}8$. This very condition specifies the ability for simulating the dynamic failure process under laboratory conditions when scaling the real time process [3].

The longevity is composed of the waiting time of failure centers occurrence $t_{wt.}$ and the time of clustering of failure centers cascade $t_{c.}$, when connectivity in the failure centers system, and a percolation cluster arise. In papers [2, 4] it was shown that $t_{wt.} >> t_c$. Due to this correlation, $t_{wt.}$ time determination evaluates the time boundary of maintaining the functional properties of metals under extreme conditions.

In case of mechanical systems the role of generalized susceptibility χ is played by compressibility *K,* related to a density variable – the density of failure centers $N(t) = \int J(t)dt$ [4, 6]. The centers formation rate *J(t)* of a number of studied metals, as the research results show, presented in paper [4], have similar values.

It was applied R/S analysis [7] for determination Hearst index of failure centers distribution in the failure surface of metallic Pu [8], subject to shock-wave effect and the failure surfaces of copper and steel samples, affected by a thermal shock. Hearst index H_{Pu} = 0,7, H_{Cu} = 0,66, H_{Fe} = 0,65 possess similar values, what justifies to the similarity of failure processes in the mentioned samples. It is demonstrated, that physical nature of light actinides longevity, placed in the extreme conditions (thermal shock action) in the range of non-equilibrium states $t \sim 10^{-6} – 10^{-10}$ s is determined by the time of formation of critical concentration of failure centers cascade (changing the body connectivity) which are a percolation cluster.

The unique mechanism of the dynamic failure process (the loss of the body connectivity through clustering of failure centers cascade), the unique order parameter (final density *N(t)* of failure centers) and similar space dimension, where the process is going on, specify the physical nature of metals longevity, involving fissile materials.

References

1. Physical encyclopaedia / Chief Editor A.M. Prokhorov. M.: The Great Russian Encyclopaedia. V. 3. 1992. P. 327.

2. Physical encyclopaedia / Chief Editor A.M. Prokhorov. M.: The Great Russian Encyclopaedia. V. 5. 1998. P. 148.

3. R.I.Ilkaev, V.T.Punin, A.Ya.Uchaev, S.A.Novikov, E.V.Kosheleva, L.A.Platonova, N.I.Selchenkova, N.A.Yukina. Time regularities of the process of metals dynamic failure, conditioned by hierarchy properties of dissipative structures – failure centers cascade. // Academy for Sciences Reports, 2003, vol. 393, № 3. - P. 326-331.

4. R.I.Ilkaev, V.T.Punin, A.Ya.Uchaev, N.I.Selchenkova, L.A.Platonova, E.V.Kosheleva, A.S.Konkin. Physical nature of metals longevity in the dynamic failure phenomenon //Nuclear Physics and Engineering. 2010, vol. 1, № 2, p.99-103.

5. R.I.Ilkaev, A.Ya.Uchaev, S. A. Novikov, N.I. Zavada, L.A.Platonova, N.I.Selchenkova. Universal properties of metals in the dynamic failure phenomenon. // Academy for Sciences Reports, 2002, vol. 384, № 3, P. 328-333.

6. Uchaev A.Ya., Punin V.T., Selchenkova N.I., Kosheleva E.V. On synergetic and athermic processes in the dynamic destructive phenomena. Zababakhin scientific lectures: Collection of report abstracts of XI International Conference, 16-20 April 2012. – RFNC – VNIITF, Snezhinsk. - P.198-199.

7. Feder J. Fractals: Translated from English _M.: Mir. 1991. - 254 p.

8. Golubev V.K., Sobolev Yu.S., Trunin I.R. On determination of conditions of failure of plutonium and its alloy with gallium under shock loading // Problems of Strength. 1998. №5. P. 100-105.

C-66

Effect of geometry and time-amplitude characteristics of external high-intensity action on metals longevity employed in the nuclear power engineering

Alexandr Uchaev, Valeriy Punin, Nadezda Selchenkova, Elena Kosheleva

Russian Federal Nuclear Center – VNIIEF, Sarov, Russia

The paper presents study results of metals dispersion under shock-wave loading (ShWL) affected by pulses of relativistic electron beams. Cu, Al samples with applied disturbances in the form of pyramidion with different apex angles are loaded.

Study results of metals dispersion process reported in the paper, have shown that at ShWL there originates dissipative structures' spectrum, which is similar to the spectrum of dissipative structures in the dynamic failure phenomenon. At specific time-amplitude characteristics of external action the dispersion process occurs from the pyramidion vertices (shock wave (ShW) energy is cumulated by the medium itself at specified geometry) [1].

The paper shows that the process of dispersion and dynamic failure with ShW length shorter than geometric dimensions of applied disturbances may occur not from the disturbance foundations, but from their vertices. The dispersion process is preceded by processes of hydrodynamic metal flows. This fact should be taken into account when developing high-intensity impulse technology.

References

Kosheleva E.V., Punin V.T., Selchenkova N.I., Uchaev A.Ya.// Common regularities of hierarchy relaxation processes in metals under the action of penetrating radiation pulses. 2015. Sarov: RFNC-VNIIEF. – 211 p.

C-67

Measurement of the diffusivity and permeability of hydrogen in plutonium

Scott Richmond

Los Alamos National Laboratory, Los Alamos, NM, USA

The diffusivity of hydrogen and deuterium in δ-Pu and ε-Pu has been measured and the data are included here. The measurements were made at very dilute solution, H/Pu <0.001, to minimize vacancy-H self-trapping [1]. To make the measurement a fixed volume of hydrogen was opened to a 17.5 mm diameter Pu-2at.%-Ga metal sample 1.25 mm thick which had been cut in half (half-moon shaped). The sample was held at constant temperature in a Sieverts type apparatus and pressures and concentrations of hydrogen were kept well within the Pu-H solution region to avoid any precipitation of hydride. The equilibration time was monitored and the diffusivity (D) determined after 5 time-constants (τ) assuming $\tau = l^2/(\mathrm{Pi}^2 \square D)$, where l is the thickness, using the method described by Glicksman [2]. The measurements are shown in Figure 1.

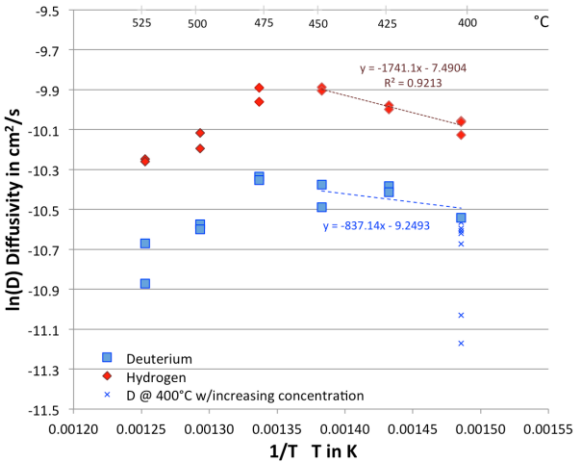

Figure 1. Diffusivity of hydrogen and deuterium in δ-Pu and ε-Pu metal, 2 at. % Ga.

The data in Figure 1 give an activation energy for diffusion of ~0.1 eV for hydrogen in the range 400–450 °C, which is consistent with the density functional theory calculations of Taylor et al [3]. A series of diffusivity measurements taken at 400 °C while allowing the concentration to increase from <0.0001 D/Pu up to D/Pu 0.001 resulted in a continuous decrease in diffusivity. The decreasing diffusivity at increasing concentration and at any temperature above 475 °C is attributed to vacancy-H self-trapping.

Virtually all transport of hydrogen in metals occurs as a diffusing solution of interstitial atoms. The permeability is the product of the amount of hydrogen in solution in a metal and how fast that hydrogen can diffuse in that metal. The rate of hydriding under ideal conditions is controlled by the permeability, P, where $P=D*K_S$ and D is the diffusivity and K_S is the Sieverts constant. K_S, however, varies wildly in Pu [4]. Wipf [5] has shown that the heat of solution, ΔH_S, dominates the value of the permeability and this is very true for Pu with ΔH_S varying from -0.4eV in Pu-7at.%-Ga alloy to -0.8eV in unalloyed Pu. For comparison of Pu to other materials figure 2 shows plots of hydrogen permeabilities from S. A. Steward's "Review of Hydrogen Isotope Permeability Through Materials"[6] together with data for steel [7] and plutonium. The Pu-H permeabilities were determined during hydrogen adsorption and desorption with Pu coupons with well-characterized geometries and chemistries in a Sieverts type apparatus. Notably, the permeability of δ-Pu exceeds that of palladium below 500 °C.

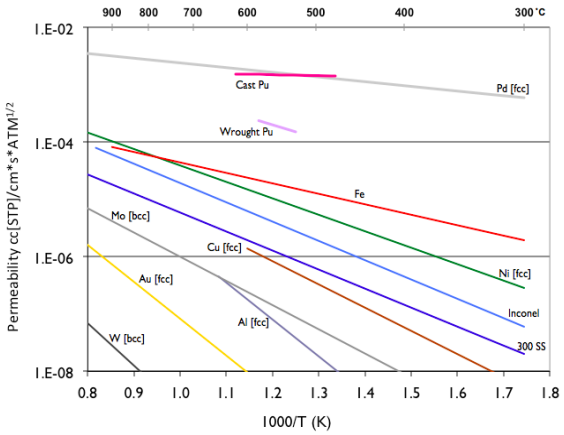

Figure 2. Hydrogen permeabilities in various metals (Steward[6], LeClaire[7], Richmond- this work).

A review of hydriding rate data by Mulford and Swift [8] also found that hydrogen permeation of δ-Pu metal varies with the square root of the hydrogen pressure but generally does not vary with temperature, consistent with figure 2. The general invariance in *P* with temperature is due to K_S and *D* changing in opposite directions but with nearly equal magnitude with temperature, depending on the processing and composition of the alloy. The large difference in permeability between wrought and cast plutonium is due to impurity trapping, which significantly reduces diffusivity (H trapping is well described by Wert [9]).

Conclusion

Plutonium is highly permeable to hydrogen with a correspondingly high diffusivity. Both the diffusivity and permeability are strongly affected by gallium content and vacancy-H self-trapping in addition to impurity trapping.

References

1. Daniel S. Schwartz, Scott Richmond, Alice I. Smith, Alison Costello and Christopher D. Taylor (2012). *Hydrogen-Vacancy Effects in Pu-2 at. % Ga Alloys*. MRS Proceedings, 1444, mrss12-1444-y01-04 doi:10.1557/opl.2012.1125.

2. M. E. Glicksman, *Diffusion in solids : field theory, solid-state principles, and applications*; Wiley : New York, 2000; pp107-133

3. Taylor C. D.; Hernandez S. C.; Francis, M. F.; Schwartz D. S.; Ray A. K. J. Phys.: Condens. Matter 2013, 25, 265001.

4. Richmond, S.; Bridgewater, J. S.; Ward, J. W.; Allen, T. H. IOP Conf. Ser.: Mater. Sci. Eng. 2010, 9, 012036.

5. Wipf, H. Phys. Scr. 2001, T94, 43–51.

6. Steward, S. A., *Review of Hydrogen Isotope Permeability through Materials*; Report UCRL-53441; Lawrence Livermore National Laboratory: Livermore, CA, 1983.

7. Le Claire, A. D. Diffusion and Defect Data 1983, 33, 1–66.

8. Mulford, R. N.; Swift, D. C. AIP Conf. Proc. 2003, 673, 179–181.

9. Wert, C. A. Trapping of Hydrogen in Metals. In *Hydrogen in Metals II: Application-Oriented Properties*; Alefeld, G., Völkl, J., Eds.; Springer Berlin Heidelberg: Berlin, Heidelberg, 1978; pp 305–330.

D-01

Synthetic Transuranic Chemistry: Bridging the Knowledge Gap to Uranium

Andrew Gaunt

Los Alamos National Laboratory, Los Alamos, New Mexico, USA

Elucidation of trends in metal-ligand orbital interactions and 5f/6d contributions to covalent bonds can only be achieved if attempts are made to extend recent advances in uranium (and to a smaller extent, thorium) chemistry to transuranic elements. Great progress has been realized through a whole slew of new uranium molecules exhibiting a range of different metal-ligand multiple bond motifs. Examples span terminal chalcogenides, nitrides, and imido species to name a few. As the actinide series is traversed from left to right, the energies of the 5f orbitals drop while those of the 6d remain relatively constant, and oxidation state also influences metal-based orbital energies and their energy match with different ligand donor types. Conducting transuranic chemistry under inert atmospheric conditions in organic solvents allows access to a range of model complexes that can provide a detailed level of bonding and electronic structure detail that is not possible under the more extensively studied aqueous/aerobic conditions where ionic bonding interactions dominate. Beyond actinyl dioxo cations, it is unknown whether transuranic ions exhibit sufficient 5f/6d orbital energy matching and spatial overlap with alternative ligand donor groups that have the potential to engage in multiple-bonding. Following presentation of practical considerations, motivational context, and how the field has evolved during the current century, investigations into the pursuit of neptunium and plutonium metal-ligand multiple bonds with oxo, sulfido, nitrido, and imido groups will be presented, including development of essential new synthetic access routes along with successful isolation and characterization of the first non-dioxo transuranic metal-ligand multiple bond.

Modern era research in the small field of air- and moisture-sensitive non-aqueous transuranic synthetic chemistry is grounded in the development of low valent precursors such as $PuI_3(THF)_4$, $PuI_3(py)_4$, $Pu[N(SiMe_3)_2]_3$, $NpI_3(THF)_4$ reported by Sattelberger, Clark and coworkers , along with $[Pu(MeCN)_9][PF_6]_3$ reported by Neu and coworkers.[1,2] This foundation was expanded by Gaunt, Neu and coworkers, who provided structural verification of previously reported precursors, established $PuBr_3(THF)_4$ as a new starting material, demonstrated that the synthetic procedures various precursors could be scaled-down, and provided structural verification of several of the Pu(III) molecules.[3] These precursors were utilized to facilitate a systematic bonding comparison across an isostructural series of La(III), Ce(III), U(III), and Pu(III) complexes with S, Se, and Te donor ligands.[4] The results revealed that the actinide bonds to the soft chalcogen atoms exhibited an enhanced degree of covalency compared to the corresponding lanthanide bonds, a result of greater 5f versus 4f participation in the metal-ligand orbital overlap (in collaboration with Kaltsoyannis, UCL/University of Manchester, UK). Similar conclusions were drawn from subsequent studies of complexes of the same metal ions with dithio- and diseleno-phosphinates, ligands which from a structural perspective closely mimic proposed actinide-selective separation agents.[5,6]

The next phase of the research was to target transuranic metal-ligand multiple bonds. In related uranium chemistry, several of the synthetic routes begin from an initial An(IV) precursor, no examples of which were available for Np(IV) to Pu(IV) for anhydrous organic-solvent mediated chemistry. We prepared new organic soluble salts of the $[PuCl_6]^{2-}$ and $[Pu(NO_3)_6]^{2-}$ anions, analyzed them by single-crystal X-ray diffraction and vis/NIR spectroscopic techniques, and have utilized them in complexation reactions with air- and moisture-stable ligands.[7] However, a neutral, organic solvent soluble molecule is preferable for air- and moisture-sensitive chemistry. In this regard, the neutral An(IV)-chloride-DME solvento adducts, $AnCl_4(DME)_2$ (Fig. 1), were developed and characterized (DME = 1,2-dimethoxyethane) for both neptunium and plutonium.[8]

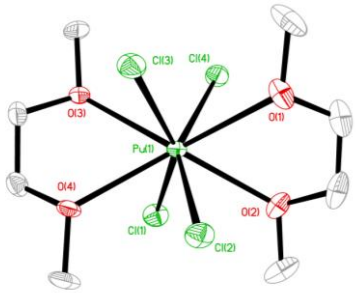

Fig. 1. Thermal ellipsoid representation (at the 50% probability level) of the solid-state crystal structure of $PuCl_4(DME)_2$.

The DME-chloride adducts opened up new avenues of exploration in the pursuit of a deeper understanding of bonding, reactivity, redox properties, and covalency trends across the 5f series. Three main thrusts will be discussed. Firstly, in collaboration with Liddle (University of Manchester, UK), we have demonstrated that the sterically bulky triamidoamine $TREN^{TIPS}$ scaffold ($TREN^{TIPS}$ = $\{N(CH_2CH_2NSiPr^i_3)\}^{3-}$) can be installed onto Np(IV) and Pu(IV), along with characterization of the resultant complexes.[9] For both Np and Pu, the An(IV) molecules can be reduced over a potassium mirror, resulting in generation of the corresponding An(III) species, which offer a vacant coordination site on which to attempt to install An-ligand bonds with multiple-bonding character (Fig. 2). Our initial reactivity studies with oxygen atom transfer reagent will be discussed.

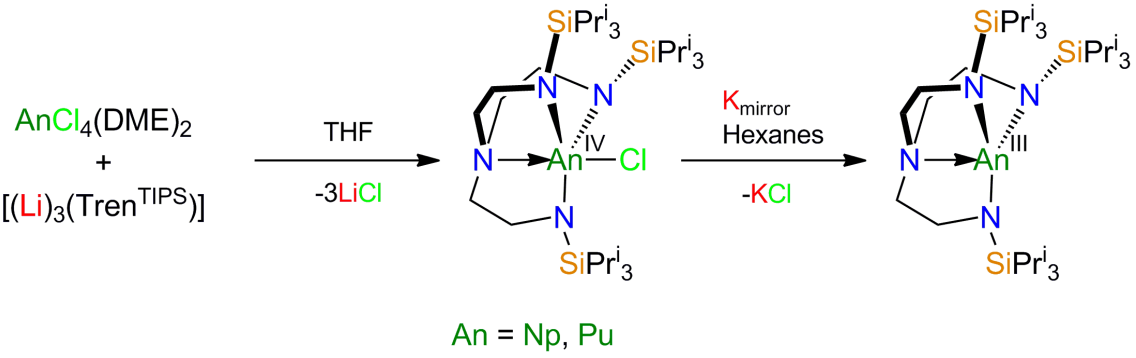

Fig 2. Synthetic route for installation of the $TREN^{TIPS}$ framework onto Np(IV) and Pu(IV) metal ions.

The second thrust is a collaboration with Hayton (University of California, Santa Barbara) in the pursuit of functionalities containing An=E (E = S, Se, Te) multiple bonds. Progress will be presented on the synthetic strategy of converting the $AnCl_4(DME)_2$ adducts to tris(amide) monochloride molecules that will serve as isolable intermediates, followed by installation of trityl chalcogenolate anions that are expected to undergo reductive cleavage resulting in formation of An=E bonds.

The third thrust is a collaboration with Boncella (Los Alamos National Laboratory) to extend his discovery of bis(imido) analogs of the uranyl ion to transuranic elements. Numerous synthetic routes are being explored to a various imido containing species for neptunium and plutonium. Most notably, the first transuranic non-dioxo motif containing metal-ligand multiple-bonding character has been successfully isolated, in the form of a linear Np(V) bis(imido) species containing functionalized bypyridine co-ligands and one chloride anion (Fig. 3).[10] The short Np-

N bond distances are comparable to the U(V) analog and electronic structure calculations have been performed by Batista (Los Alamos National Laboratory). Further reactivity studies and investigations of electronic properties are ongoing.

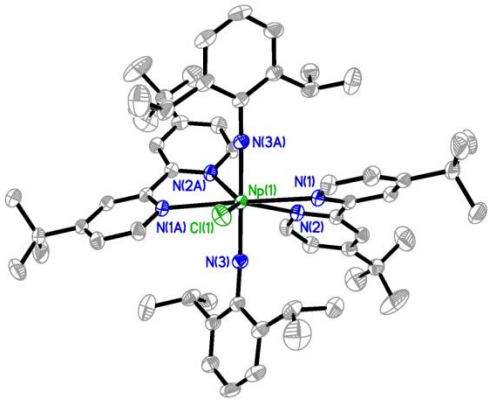

Fig. 3. Thermal ellipsoid representation (at the 50% probability level) of the solid-state crystal structure of the bis(imido) containing Np(V) molecule with substituted bipyridines as co-ligands.

Finally, the future outlook for the field will be discussed, including limitations, obstacles still to be overcome, and highly desirable target molecules that may become within reach in the near future.

References

1.Avens, et al., *Inorg. Chem.* **1994**, *33*, 2248.
2. Enriquez, et al., *Chem. Commun.* **2003**, 1892.
3. (a) Gaunt,et al., *Inorg. Chem.* **2008**, *47*, 8412. (b) Gaunt, et al., *Inorg. Chem.* **2008**, *47*, 26.
4. Gaunt, et al., *Inorg. Chem.* **2008**, *47*, 29.
5. Macor, et al., *Dalton Trans.* **2015**, *44*, 18923.
6. Jones, et al., *Chem. Sci.* **2013**, *4*, 1189.
7. Reilly, et al., *Inorg. Chem.* **2012**, *51*, 9165.
8. Reilly, et al., *Dalton Trans.* **2014**, *43*, 1498.
9. Brown, et al., *Chem. Commun.* **2016**, *52*, 5428.
10. Brown, et al., *J. A, Chem. Soc.* **2015**, *137*, 9583.

D-02

Role of atomic multiplets in intermediate valence PuB_6

Alexander B. Shick[1], Ladislav Havela[2], Alexander I. Lichtenstein[3], Mikhail I. Katsnelson[4]

[1]Institute of Physics ASCR, Prague, Czech Republic, [2]Charles University, Prague, Czech Republic, [3]University of Hamburg, Hamburg, Germany, [4]Radboud University, Nijmegen, The Netherlands

The electronic structure of PuB_6, an actinide analog of SmB_6, was investigated making use of a combination of the density functional theory in a local density approximation (LDA), and the exact diagonalization (ED) of an effective discrete Anderson impurity model [1]. Intermediate valence ground state with the f-shell occupation n_{4f} =5.5 for the Pu atom in PuB_6 is calculated. This ground state is a non-magnetic singlet with all angular momenta of the 5f-bath cluster equal to zero. The 5f-shell magnetic moment is completely compensated by the moment carried by the electrons in the conduction band.

Already in DFT, PuB_6 is an insulator with a small amount of holes near the X-point, and the indirect band gap of < 60 meV (see Fig. 1). This band gap becomes direct in DFT+ED calculations supporting the idea of "topological Kondo insulator" in PuB_6.

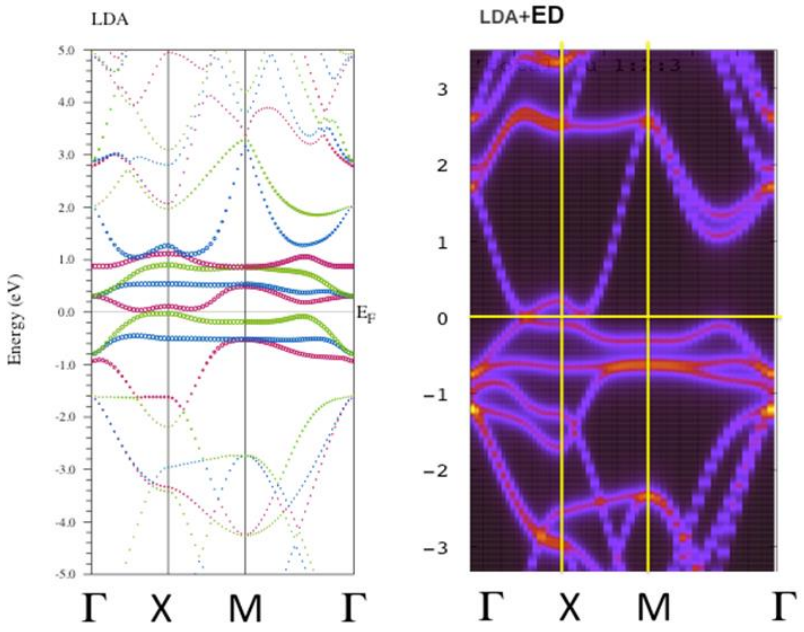

Fig. 1. PuB_6 LDA and LDA+ED band structure.

The f-orbital density of states (fDOS) obtained from LDA+ED for the Pu atom PuB_6 is shown in Fig. 2 in comparison with the fDOS for $PuCoGa_5$.The many-body resonances near the Fermi energy are produced by f^6-to-f^5 multiplet transitions are in a way analogues to the *Racah* peaks, specific

transitions between *Racah* multiplets [2] of f^n-to-$f^{n-1,n+1}$. Three peak structure: f^6-to-f^5 multiplet transitions are better resolved than f^5-to-f^4 transitions. This suggests partial delocalization of f^5 multiplet, and illustrates the “dual” nature of the f states in Pu compounds.

The non-magnetic character of PuB_6 , as well as δ-Pu and $PuCoGa_5$ is associated with the valence fluctuations due to Coulomb interaction between f- and d-states. When there is a mixing of magnetic [f^5] and non-magnetic [f^6] multiplets the resulting state is non-magnetic. Our calculations show that hybridization between f-shell and other non-f electrons plays a role and leads to formation of the multi-orbital Kondo-like singlet ground state.

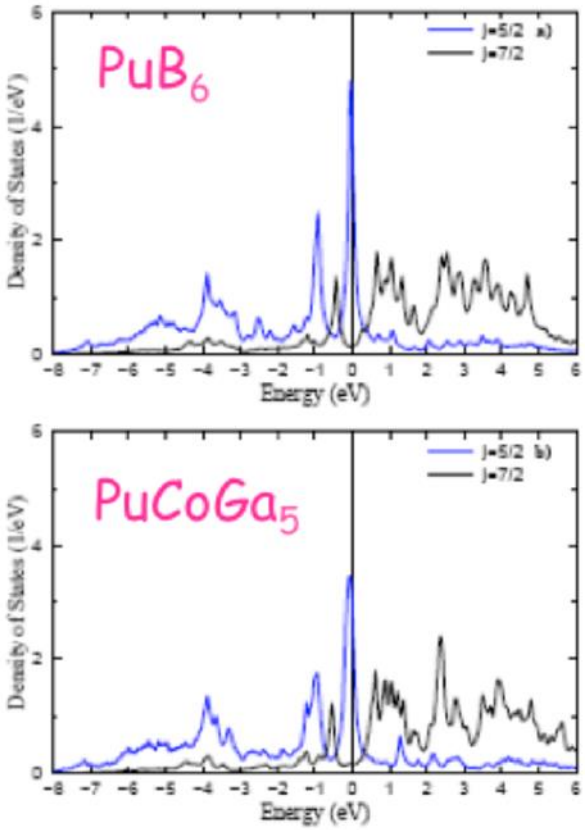

Fig. 2. f-electron density of states (j = 5/2, 7/2 projected) for the Pu atom in PuB_6 and $PuCoGa_5$.

References

[1] A. B. Shick, L. Havela, A. I. Lichtenstein, M. I. Katsnelson, Scientific Reports 5, 15429 (2015).

[2] G. Racah, Phys. Rev. 76, 1352 (1949).

D-03

Resonant inelastic X-ray scattering of actinide materials

Kristina Kvashnina[1,2]

[1]*The European Synchrotron, Grenoble, France,* [2]*Helmholtz-Zentrum Dresden-Rossendorf, Dresden, Germany*

This contribution will provide an overview of applications of advanced X-ray spectroscopic techniques that take advantage of the resonant inelastic X-ray scattering (RIXS) processes in the hard and tender X-ray range [1]–[7]. Figure 1 shows a schematic drawing of the X-ray emission spectrometer with a spherically bent crystal analyser installed at the Rossendorf beamline (ROBL) at the European Synchrotron Radiation Facility in Grenoble [8]. The spectrometer is constructed for studying the nuclear materials and environmental applications by high energy resolution fluorescence detection (HERFD) X-ray absorption spectroscopy (XAS), X-ray emission spectroscopy (XES) and RIXS techniques at the An L_3 and $M_{4,5}$ edges.

We will show here few examples of the electronic structure studies of complex materials, nanosystems and intermetallic compounds by means of HERFD and RIXS and discuss the phenomena related to the crystal field splitting, oxidation state and number of the 5f electrons. In connection with presented results, the capabilities and limitations of the experimental techniques and theoretical methods will be discussed.

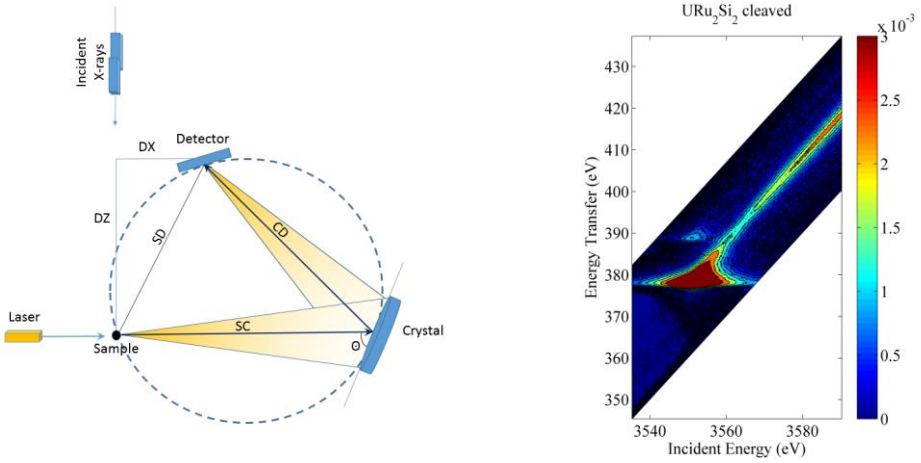

Figure 1. left: A schematic drawing of the Johann-type X-ray emission spectrometer; right: core to core RIXS data of the URu_2Si_2 sample recorded at the U M_5 edge.

References

[1] K. O. Kvashnina, S. M. Butorin, P. Martin, and P. Glatzel, “Chemical State of Complex Uranium Oxides,” *Phys. Rev. Lett.*, vol. 111, no. 25, p. 253002, Dec. 2013.

[2] T. Vitova, M. A. Denecke, J. Göttlicher, K. Jorissen, J. J. Kas, K. Kvashnina, T. Prüßmann, J. J. Rehr, and J. Rothe, “Actinide and lanthanide speciation with high-energy resolution X-ray techniques,” *J. Phys. Conf. Ser.*, vol. 430, p. 012117, Apr. 2013.

[3] K. O. Kvashnina, Y. O. Kvashnin, and S. M. Butorin, “Role of resonant inelastic X-ray scattering in high-resolution core-level spectroscopy of actinide materials,” *J. Electron Spectros. Relat. Phenomena*, vol. 194, pp. 27–36, Jun. 2014.

[4] K. O. Kvashnina and F. M. F. de Groot, “Invisible structures in the X-ray absorption spectra of actinides,” *J. Electron Spectros. Relat. Phenomena*, vol. 194, pp. 88–93, Jun. 2014.

[5] K. O. Kvashnina, Y. O. Kvashnin, J. R. Vegelius, A. Bosak, P. M. Martin, and S. M. Butorin, “Sensitivity to Actinide Doping of Uranium Compounds by Resonant Inelastic X-ray Scattering at Uranium L 3 Edge,” *Anal. Chem.*, vol. 87, no. 17, pp. 8772–8780, Sep. 2015.

[6] T. Vitova, J. C. Green, R. G. Denning, M. Löble, K. Kvashnina, J. J. Kas, K. Jorissen, J. J. Rehr, T. Malcherek, and M. A. Denecke, “Polarization Dependent High Energy Resolution X-ray Absorption Study of Dicesium Uranyl Tetrachloride.,” *Inorg. Chem.*, vol. 54, no. 1, pp. 174–82, Jan. 2015.

[7] A. L. Smith, P. E. Raison, L. Martel, D. Prieur, T. Charpentier, G. Wallez, E. Suard, A. C. Scheinost, C. Hennig, P. Martin, K. O. Kvashnina, A. K. Cheetham, and R. J. M. Konings, “A New Look at the Structural Properties of Trisodium Uranate Na 3 UO 4,” *Inorg. Chem.*, vol. 54, no. 7, pp. 3552–3561, Apr. 2015.

[8] K. O. Kvashnina and A. C. Scheinost, “A Johann-type X-ray emission spectrometer at the Rossendorf beamline,” *J. Synchrotron Radiat.*, vol. 23, no. 3, May 2016.

D-04

Synthesis, reactions, and structures of gas-phase actinide oxide nitrate complexes: Relative stabilities and An oxidation states in $AnO_3(NO_3)_2^-$ (An = U, Np, Pu)

Rémi Maurice[1], Eric Renault[2], Phuong Diem Dau[3], Yu Gong[3], Philip X. Rutkowski[3], John K. Gibson[3]

[1]SUBATECH, UMR CNRS 6457, IN2P3/EMN Nantes/Université de Nantes, Nantes, France, [2]CEISAM, UMR CNRS 6230, Université de Nantes, Nantes, France, [3]Chemical Sciences Division, Lawrence Berkeley National Laboratory, Berkeley, California, USA

Gas-phase actinide oxide nitrate complexes can be obtained in various ways. While such complexes can be "directly" produced by electrospray ionization (ESI) of actinide nitrate solutions, more "exotic" complexes can be generated by collision-induced dissociation (CID). In this work, we study the formation of $AnO_x(NO_3)_y^-$ (An = U, Np, Pu) complexes by ESI and CID. While complexes with standard oxidation states for actinides can be obtained by ESI (up to +VI), $AnO_3(NO_3)_2^-$ complexes result from CID. Since these latter species could in principle exhibit to a +VII oxidation state if An = Pu or Np, it is crucial to properly assign the oxidation states. Due to the employed experimental mass spectrometry approach, limited insights can be obtained from experiment concerning molecular geometries and electronic structures. It is thus crucial to perform quantum mechanical calculations, in particular to determine the electronic structures of the formed complexes and assign the actinide oxidation states.

We have used density functional theory with the hybrid PBE0 exchange-correlation functional to determine the molecular geometries of the $AnO_x(NO_3)_y^-$ complexes of interest and evaluate their electronic structures in terms of oxidation states. Scalar relativistic effects are implicitly taken into account by means of energy-consistent pseudopotentials. To assign oxidation states, we compute the geometries, atomic charges and spin densities, and we compare those obtained for the $AnO_3(NO_3)_2^-$ (An = U, Np, Pu) complexes to those for $AnO_x(NO_3)_y^-$ cases for which there is little doubt concerning the An oxidation states. In particular, we have shown that Pu has a +VI oxidation state in the $PuO_3(NO_3)_2^-$ complex [1]; CID results in a Pu-$O^{\cdot}$ multiradical bonding and is not a way to reach oxidation states higher than Pu(VI). Indeed, the ground state of $PuO_3(NO_3)_2^-$ exhibits a radical oxygen atom that is antiferromagnetically coupled to the spin-triplet plutonyl unit. The structures in the An=U and Np cases will also be discussed, and the corresponding oxidation states attributed in a similar fashion.

Reaction energies will be also determined to assess the relative stabilities of these $AnO_3(NO_3)_2^-$ complexes. Two types of experimentally studied reactions will be considered:

(1) $AnO_3(NO_3)_2^- + NO_2 \rightarrow An^{VI}O_2(NO_3)_3^-$

(2) $AnO_3(NO_3)_2^- + HNO_2 \rightarrow An^{VI}O_2(OH)(NO_3)_2^- + NO_2$

While for An=U and An=Pu, similar reaction energies are obtained, the An=Np case appears to be an outlier within the series, with $NpO_3(NO_3)_2^-$ being relatively more stable than $UO_3(NO_3)_2^-$ and $PuO_3(NO_3)_2^-$, in agreement with experimental reactivity observations. This trend will be put in perspective with the computations concerning the oxidation states of the $AnO_3(NO_3)_2^-$ complexes. This work constitutes a nice example of joint theory/experiment study, in which oxidation states are convincingly assigned by correspondence between information obtained from experiments and quantum mechanical calculations.

Reference:

[1] R. Maurice, E. Renault, Y. Gong, P. X. Rutkowski, J. K. Gibson, “Synthesis and structures of plutonyl nitrate complexes : Is plutonium heptavalent in $PuO_3(NO_3)_2$?”, Inorg. Chem., 2015, 54, 5367−2373.

D-05

Redox chemistry of Pu, Np and U under alkaline to hyperalkaline pH conditions

Xavier Gaona

Karlsruhe Institute of Technology, Institute for Nuclear Waste Disposal, Karlsruhe, Germany

Actinide aqueous chemistry is a relevant, multifold and scientifically challenging research field of inorganic chemistry. In the context of nuclear waste disposal, actinides represent the main contributors to the radiotoxic inventory in a repository in the long term. Because of their specific electronic configuration, several oxidation states of actinides (+III to +VII) can exist in aqueous solution. This imposes a differential chemical behaviour as a function of the boundary redox conditions, which is of special concern for the safety case of repositories for nuclear waste disposal. In this framework, it is essential to continuously reduce experimental and systematic uncertainties, fill existing gaps in thermodynamic databases and improve knowledge and available data for more complex and relevant (geo)chemical systems.

This presentation focuses on plutonium, neptunium and uranium as relevant examples of the experimental and conceptual approaches employed at KIT–INE for investigating actinide aquatic chemistry and thermodynamics. Based upon experimental studies characterizing actinide redox transformation processes, separate series of solubility experiments with actinide solid phases are performed in dilute to concentrated saline systems. Solubility experiments are combined with advanced techniques available at KIT–INE for the characterization of solid and aqueous phases: EXAFS, (synchrotron-based) in-situ XRD, TRLFS, TEM, among others. Comparison with other actinides are systematically considered in the interpretation of the experimental results, analysing consistency along the actinide series and taking advantage of the well-known chemical analogies between actinides of the same redox state.

Selected examples will be presented and discussed in this contribution:

- Redox chemistry of Pu(III/IV) under alkaline to hyperalkaline pH conditions: on the role of Pu(III) in cementitious systems

- Complexation of iso-saccharinic acid with Pu(III/IV) under alkaline to hyperalkaline pH conditions

- Redox chemistry of U(IV/VI) under alkaline to hyperalkaline pH conditions: on the formation of anionic U(IV) hydrolysis species

- Np(VI) solubility in alkaline NaCl media: analogies with U(VI) and Pu(VI)

- Formation of Np(VII) under hyperalkaline oxidizing conditions

All studies included in this presentation aim at deriving comprehensive thermodynamic models of the investigated systems, which can be implemented in thermodynamic databases for geochemical model calculations.

D-06

Towards explaining anomalous properties of unalloyed and alloyed Pu appearing after the long-term storage at the liquid He temperature

Boris Nadykto

Russian Federal Nuclear Center VNIIEF, Sarov, Russia

Anomalous properties of unalloyed and alloyed Pu appear after the long-term storage of their specimens. In [1-3], densities of Pu were measured over the storage period of 3000-4000 h and then extrapolated to the saturated densities. Dilatometry data [1-3] show that long-term storage of unalloyed α-Pu specimens at the temperature of liquid helium (T=4 K) lead to ~ 10% reduction in α-Pu density ρ_α, from 20.3 g cm^{-3} to 18.4 g cm^{-3} that is significantly lower than ρ_α at the room temperature. Under the same conditions, the density of δ-Pu alloyed with 6 at.% Al ρ_δ increases by ~ 16%, from 15.8 g/cm^3 to 18.4 g/cm^3, the density, which is identical to that of unalloyed α-Pu ρ_α . This long-standing puzzle is qualitatively explained by a hypothetic amorphizaton [1-3]; however, physical nature and mechanism/mechanisms of the "amorphizaton" is still poorly understood. Here we show that ρ_α decreases due to the formation of nano-sized voids due to α--decay, while the evolution of ρ_δ is a two-stage process: δ-α' phase transition and plastic deformation of δ-phase followed by the expansion of α' in the same manner as that of α-phase.

Cooling of unalloyed α-Pu to cryogenic temperatures is known to lead to reduced bond lengths in the α -Pu lattice and increased density [4]. However, the density of α-Pu after the long-term storage at the temperature of liquid He is unexpectedly lower than that at the room temperature. This anomaly may be explained by the formation of voids due damages to the crystalline structure induced by α-decay products. Such an explanation is quite logical, because microscopic damages to the crystalline structure due to α-decay are often found in nature, in minerals, where radiohalos or pleochroic halos are formed around U inclusions. However, in this case, rates, at which specimen density changes over time, should depend on the intensity of α-decay. No experimental data on densities of specimens of unalloyed ^{242}Pu and ^{238}Pu or alloyed ^{239}Pu and ^{238}Pu with different fraction of ^{238}Pu stored at T=4K are currently available. However, experiments at the room temperature [5] show that the density of specimens of ^{238}Pu is much lower than that of ^{239}Pu, while the intensity of α-decay of ^{238}Pu is much higher than that of ^{239}Pu.

In [6-7], X-ray diffraction (XRD) studies of thin films of ^{238}Pu and ^{239}Pu, which were produced by vapor deposition and were initially free of radiogenic He, were carried out. The hydrostatic density of these 1-10 μm films was not measured. Instead, specimens were studied by XRD at the room temperature for 340 days. The measured lattice parameters of ^{238}Pu, whose density is generally much lower than that of ^{239}Pu, was, however, found to be very close to those of ^{239}Pu. The maximum change in atomic volume for ^{238}Pu was less than 1% over the storage period and tended to decrease as the storage time is growing. The experimental data are likely to indicate that lower compared to ^{239}Pu density of ^{238}Pu is related to the larger void volume formed in ^{238}Pu due to the higher intensity of α-decay.

Based on the theoretical work [9], in which a macroscopic model of shock impact produced by the recoil atom on the crystalline structure of the surrounding material was developed, we show that swelling of unalloyed α-phase Pu can be explained by the formation of nano-sized voids due to damages to the crystalline structure by the recoil atom. A significantly larger change in Pu density at the liquid He temperature compared to the room temperature were shown to be caused by the difference in mobility of atoms and relaxation of voids being formed due to the large difference in Pu properties (viscosity, shear strength) at room temperature and T=4 K. Since radiation-induced amorphization is a kinetic process involving both the formation and annealing of radiation-induced voids, the formation of a void volume at lower temperatures, where annealing is very small, if not negligible, requires much smaller expose than at the room temperature. These considerations lead us to conclude that the main reason of the anomalous behaviour of α-Pu density exhibited during long-term storage at T=4 K is amorphization via the

formation of significant amount of void volumes, which are induced by damages to the crystalline structure by recoil atoms.

Amorphization itself leads to a marked drop in solid density and, hence, cannot explain the observed ~ 16% growth of the density of alloyed δ-Pu. However, the formation of specimens of identical density under prolonged irradiation of unalloyed α-Pu and alloyed δ-Pu can be explained by a gradual δ→α′ phase transformation driven by α-decay followed by swelling of α′-Pu being formed due to the aforementioned δ→α′ transformation. In [8], alloyed δ-phase Pu is shown to transform into the α′-phase under static pressure. The development of a short-time pressure pulse produced by the recoil atom and the possibility of δ→α′ transformation has been discussed in [9]. The XRD analysis carried out in [1] is consistent with [8]. Experiments [1] revealed no signs of α-phase in the δ-phase Pu alloy after a 900 h storage at T=4K, which is expectable due to the short storage time. Not detecting α′-Pu in the specimens are most likely due to small fraction of the α′-phase formed after 900 h [1] and smear of X-ray reflections caused by strong deformations at nano-scale. Based on the data [1], Pu density decreases due to the δ→α′ transformation by ~1% that corresponds to the presence of 6% of α′-Pu. Another possible reason for not detecting α′-phase in the XRD studies [1] is that T=4 K electronic phase transitions may not be accompanied by structural phase transitions due to the low mobility of lattice atoms. Due to the electronic phase transition, for example, under compression, the size of Pu atoms and bond lengths in the lattice alter, while the lattice type remains unchanged. This means that the number of isomorphic phases at low temperatures may be much larger than that at the room or elevated temperatures. These considerations lead us to conclude that the evolution of alloyed δ-phase Pu is to be a two-stage process. The first stage includes the formation of the α′-phase and plastic deformation of the δ-phase. During the second stage, the α′-phase swells in the same manner the unalloyed α-phase. Such a scenario is consistent with the measurements [1] showing that unlike unalloyed α-phase, the compression of δ-Pu cannot be described by a single exponent. According to [1], the rate, at which the density of δ-Pu is growing over the first 500 hours is 1.4 times higher than the rate , at which ρ_δ is growing over the following 3500 h till the end of the experiment.

It is also important to note that further experimental studies of disperse inclusions [11] in Pu and its alloys such as voids, pores or bubbles are needed in order to make a definitive conclusion about the nature of anomalous behaviour of Pu properties during long-term storage at low temperatures. It is important to note that changes in the lattice properties alone are not representative of the actual bulk density variations because the presence of nano-sized and larger disperse inclusions, which may not impact the lattice properties, can cause large changes in the bulk density. The present study also lead us to conclude that it would be very important to study phase transformations in solids, not necessarily actinides, at extremely low temperatures in further detail and to investigate the impact of atomic mobility on structural and electronic phase transformations.

References

1. J.A.C. Marples, A. Hough, M.J. Mortimer at al., Plutonium 1970 and other Actinides Conference, Santa Fe, edited by W.N. Miner, AIME, New York, 623 (1970)
2. J.A.C. Marples, R.O.A. Hall. J. Nucl. Mater. 39, 212-216 (1972).
3. S.S. Hecker, J.C. Martz. In Ageing Studies and Lifetime Extension of Materials. Edited by. L.G. Mallinson. 23 (2000)
4. A.C. Lawson, J.C. Lashley, P.S. Riseborough. J. Alloys Compd. 444-445, 274 (2007).
5. A.G. Seleznev, N.S. Kosulin, V.D. Shushakov Radiochemistry. 43(2), 101-106.(1995)
6. S.I. Gorbunov, A.G. Seleznev. Radiochemistry. 43(2), 101-106. (2001)
7. S.I. Gorbunov, A.G. Seleznev. International Workshop on Fundamental Properties of Plutonium. VNIIEF, Sarov, Russia, 24 – 27 June 2002, 17-19, (2002)
8. S.S. Hecker, D.R. Harbur, T.G. Zocco. Prog. Mater. Sci. 49 (1-3), 429-485 (2004).
9. B.A. Nadykto, O.B. Nadykto. In *Ageing Studies and Lifetime Extension of Materials* L.G. Mallinson, ed. , 415 (2000)
10. W.J. Weber, RC. Ewing, C.R.A. Catlow, T. Diaz de la Rubia at al. J. Mater. Res. 13, 1434 (1998).
11. A. Schwartz, M.Wall, T. Zocco, W. Wolfer. Phil. Mag. 85, 479 (2005).
12. J.R. Jeffries, M.A. Wall, K.T. Moore, A.J. Schwartz. J. Nucl. Mat. 410, 84 (2011).

D-07

Probing He bubbles in naturally aged and annealed □-Pu alloys using small-angle x-ray scattering

Jason R. Jeffries[1], Tony van Buuren[1], Trevor Willey[1], Mark A. Wall[1], Dave Ruddle[1], Jan Ilavsky[2], Patrick Allen[1]

[1]Lawrence Livermore National Laboratory, Livermore, CA, USA, [2]Argonne National Laboratory, Argonne, IL, USA

The self-irradiation of Pu alloys generates He that is trapped within the metal matrix in the form of He bubbles. The distribution of these He bubbles in δ-phase Pu-Ga alloys exhibits a peak near a radius of 0.7 nm, and this size is remarkably stable as function of material age. When annealed, the He bubbles in δ -Pu alloys grow, coarsening the distribution. However, the magnitude of this coarsening is uncertain, as different experimental methods reveal bubbles that differ by at least one order of magnitude.

Small-angle x-ray scattering (SAXS) is a powerful, synchrotron-based technique that can probe a wide range of bubble sizes, while providing a bulk measurement as opposed to the small sample volumes probed by transmission electron microscopy (TEM). As such, we have turned to SAXS experiments on plutonium to enhance our understanding of He bubbles in aged material. Owing to the change in electron density between the Pu matrix and the He bubble, transmitted x-rays are scattered strongly, and the extent of this scattering can be modeled to extract a distribution of scatterers spanning sizes from sub-nm up to μm. The results on naturally aged specimens of Ga-stabilized δ-Pu are in very good agreement with TEM measurements, and results of annealed specimens (425 °C/24 hours) indeed reveal bubble coarsening, in qualitative agreement with TEM results. Because they are bulk measurements with substantially reduced uncertainty in the bubble density (number of bubbles per unit volume), SAXS measurements can be used to quantitatively analyze the amount of He residing in bubbles. Our results show that, while the bubble distribution indeed coarsens with annealing, there is also a loss of He amounting to about 85%.

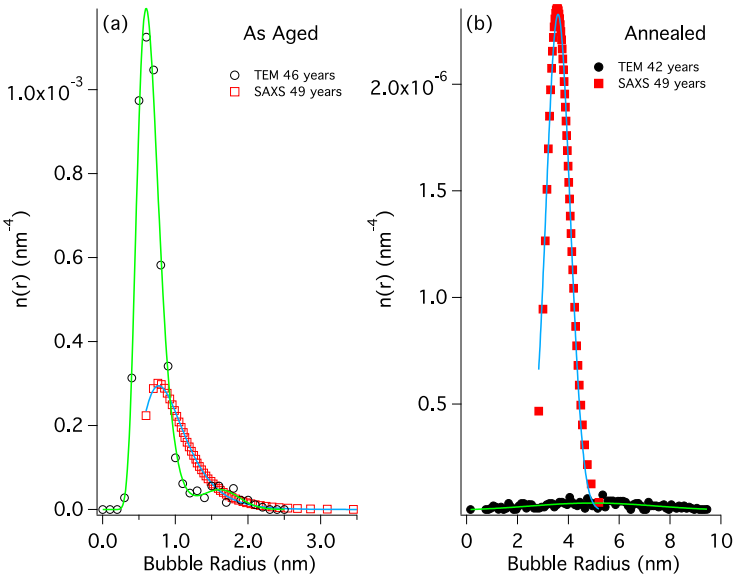

Figure 20: A comparison of bubble distributions for naturally aged and annealed samples of δ-Pu extracted fro SAXS and TEM experiments.

This work was performed under the auspices of the U.S. Department of Energy by Lawrence Livermore National Laboratory under Contract DE-AC52-07NA27344.

D-08

Oxidation state of plutonium: recent studies in inorganic compounds

Denis Bykov[2], Anna L. Smith[2], Karin Popa[1], Damien Prieur[1], Philippe Martin[3], Rudy Konings[1], Philippe E. Raison[1]

[1]European Commission- JRC-ITU, Karlsruhe, Germany, [2]Delft University of Technology, Delft, The Netherlands, [3]Commissariat à l'Energie Atomique. CEA-DEC, Saint Paul Lez Durance, France

The electronic configuration of plutonium is $(Rn)5f^6 6d^0 7s^2$, similar to its analogue element in the lanthanide family, samarium $(Rn)4f^6 5d^0 6s^2$. But unlike the latter, plutonium exhibits numerous oxidations states, in solution but also in the solid-state. Optical solution absorption spectra have been reported for Pu(III), Pu(IV), Pu(V), Pu(VI) and Pu(VII). Pu solutions have characteristic colours, blue, tan, green, violet, depending of the valence of plutonium, its concentration in solution and the anions the plutonium is associated with. Though in the solid-state the most common valences are III and IV, plutonium can form various ternary/quaternary complex compounds where Pu has the valences V, VI and more rarely VII. Many of those compounds have already been reported in the literature and studied extensively [1][2]. We have recently investigated and revisited a certain number of compounds that can form at different stages of the nuclear fuel cycle, in which the oxidation states of plutonium vary from (III) to (VII). The trivalent oxidation state was found in $PuPO_4$ [3] and $Pu_2Zr_2O_7$. In $PuPO_4$, the trivalent oxidation state of plutonium was established to be extremely stable up to high temperature [4] whilst in the zirconate pyrochlore, plutonium(III) can readily turn into Pu(IV) under oxidizing conditions [5], like the sesquioxyde Pu_2O_3 turns into PuO_2. Pu(IV) was observed in the pyrophosphate compound PuP_2O_7 [6]. Higher oxidation states have been observed in the ternary system Na-Pu-O, which has recently been revisited [7][8] in the framework of the safety assessment of Sodium-cooled Fast Reactors (SFRs). In case of a breach in a cladding element, sodium would enter the pin and react with the oxide fuel $(U,Pu)O_2$ to form new phases with lower thermal conductivity and density than the fuel, leading to fuel swelling and creation of hot spots. In the Na-Pu-O system, depending of the (Na+An)/O ratio, oxygen potential and temperature, the following compounds can form: Na_2PuO_3, Na_3PuO_4, Na_4PuO_5, Na_5PuO_5, Na_5PuO_6. In those ternary compounds, plutonium is the central atom of an oxoplutonate anion where the oxidation state varies from (IV) to (VII).

All compounds have been characterized by X-Ray diffraction and their crystallographic structures refined by Rietveld analysis or determined ab-initio when the structure was unknown (i.e. Na_5PuO_6 and Na_3PuO_4) [7][9]. The valence state of plutonium in the different compounds has been assessed by the Bond-valence method based on the interatomic distances determined from the crystallographic structural refinements. For some selected materials the oxidation state of plutonium has been determined experimentally by X-ray Absorption Near Edge Structure spectroscopy (XANES) at the synchrotron radiation sources ESRF and SOLEIL [3][10].

A summary on the crystallographic data for the various compounds is given in table 1.

	Compound	symmetry	Space group	a(Å)	b(Å)	c(Å)	β°	Z	Volume Å^3	Ref
Pu(III)	$PuPO_4$	Monoclinic	$P2_1/n$	6.759	6.980	6.447	103.63	2	295.59	[3]
	$Pu_2Zr_2O_7$	Cubic	Fd-3m	10.692				8	1222.3	[5]
Pu(IV)	PuP_2O_7	Triclinic	P1	*~8.6*	*~8.6*	*~8.6*	*~89.9*	4	*~640*	[6]
	Na_2PuO_3	Monoclinic	C2/c	5.965	10.313	11.772	109.97	4	680.56	[10]
Pu(V)	Na_3PuO_4	Orthorhombic	Fmmm	13.302	9.634	6.651		8	852.3	[9]
	Na_5PuO_5	Monoclinic.	C2/m	10.953	4.616	6.565	71.31	2	314.30	[7]
Pu(VI)	Na_4PuO_5	Tetragonal	I4/m	7.519		4.619		2	261.14	[7]
Pu(VII)	Na_5PuO_6	Monoclinic	C2/m	5.816	9.980	5.747	110.76	2	311.87	[7]

Table1: Crystallographic data of ternary plutonium compounds studied in the present work

Our presentation will provide an insight into the different crystallographic structures and discuss the oxidation states and cationic radii of plutonium in those materials.

References

[1] "Die Reaktion der Oxide der Transurane mit Alkalioxiden-I Ternäre Oxide der Sechswertigen Transurane mit Lithium und Natrium" - C. Keller, L. Koch, K.H. Walter, J. Inorg. Nucl. Chem. 27 (1965) 1205–1223.

[2] "Die Reaktion der Oxide der Transurane mit Alkalioxiden-II Ternäre Oxide der Sechswertigen Transurane mit Lithium und Natrium" - C. Keller, J. Inorg. Nucl. Chem. 27 (1965) 1225–1232.

[3] "Structural investigations of PuIII phosphate by X-ray diffraction, MAS-NMR and XANES spectroscopy" - K. Popa, P.E. Raison, L. Martel, P.M. Martin, D. Prieur, P.L. Solari, D. Bouexiere, R.J.M. Konings, J. Somers - Journal of Solid State Chemistry 230 (2015) 169–174

[4] "The high-temperature behaviour of $PuPO_4$ monazite and some other related compounds"

R. Jardin, C.C. Pavel, P-E. Raison, D. Bouëxière, H. Santa-Cruz, R. J.M. Konings, K. Popa

J. Nucl. Mat.378 (2008) 167–171

[5] “Fundamental and technological aspects of actinides oxide Pyrochlores: relevance for immobilization matrices” - P.E. Raison, R.G. Haire, T. Sato, T. Ogawa

Mat. Res. Soc. proc., “Scientific Basis for Nuclear Waste Management”, 556(1999) 3-10

[6] "Triclinic-cubic phase transition and negative expansion in the actinide IV (Th, U, Np, Pu) diphosphates" - G. Wallez, P.E. Raison, N. Dacheux, N. Clavier, D. Bykov, L. Delevoye, K. Popa, D. Bregiroux, A.N. Fitch, R.J.M. Konings - Inorg. Chem., 51(7) (2012) 4314-4322.

[7] "Synthesis and crystal structure investigations of ternary oxides" in the Na–Pu–O system"

D.M. Bykov P.E. Raison, R.J.M. Konings, C. Apostolidis, M. Orlova

Journal of Nuclear Materials 457 (2015) 54–62

[8] Anna L. Smith - PhD - "Structural and thermodynamic properties of sodium actinide ternary oxides" University of Cambridge. Churchill College. July 2015 -

[9] "Structural investigation of Na_3NpO_4 and Na_3PuO_4 using X-ray diffraction and ^{237}Np Mössbauer spectroscopy" - A.L. Smith, A. Hen, P.E. Raison, E. Colineau, J.C.Griveau, N. Magnani, J.P.Sanchez, R. J.M.Konings, R. Caciuffo, A.K. Cheetham - Dalton Transactions 44 (42), (2015) pp. 18370-18377

[10] "Structural properties and charge distribution of the sodium uranium, neptunium and plutonium ternary oxides: a combined X-ray diffraction and XANES study" - A. L. Smith, P. Martin, D.Prieur, A. Scheinost, P.E.Raison, A.K. Cheetham, R.J.M.Konings - Inorganic Chemistry 2016, 55 (4), pp 1569–1579

D-09

Synthesis, Structure, and Characterization of a Pair of Berkelium Iodates: Developments in assessing bonding character in actinides beyond Plutonium

Mark Silver

Florida State University, Tallahassee, Florida, USA

Recent experiments involving late actinides (those beyond curium) have revealed to what extent covalency exists in the bonding of those compounds containing these actinides. Bulk-scale quantities of ^{249}Bk were handled for the first time ever with the intent of collecting sufficient solid-state evidence to characterize the structural, optical, and magnetic properties of the 5*f* ^{8}-center, in addition to describing the bonding within certain coordination environment.

f-Block iodate materials have been prepared using all available and stable isotopes (including ^{249}Cf), so a meaningful comparison between the structures and bonding of the lanthanide and actinides, as well as focusing on the changes between the actinide series, and berkelium can be made. With such uncanny resemblance in redox chemistry compared to cerium, the possibility of producing an intermediate-valent berkelium material isotypic with that of $Ce_2(IO_3)_6(OH_x)$ (x = 0.44) was pursued.

The proposed synthetic route used $Bk(OH)_4$, converted from $BkCl_3$ first, in combination with a 9 M-excess of iodic acid were heated at 180 °C for three days. The products of the reaction were the tri- and tetravalent iodates materials, $Bk(IO_3)_3$ (>99 %) and $Bk(IO_3)_4$ (<1 %), respectively. $Bk(IO_3)_3$ was found to adopt the $Cf(IO_3)_3$ structure-type, with a nine-coordinate tricapped trigonal coordination environment, while the tetravalent iodate crystallized in the $Zr(IO_3)_4$ structure-type with a square antiprismatic geometry surrounding the metal-center.

A comprehensive series of techniques were used to ascertain as much information from these short-lived products. UV-vis-NIR absorption and fluorescence (λ_{Ex} = 420 nm) measurements were collected at a range of temperatures approaching liquid nitrogen. Emission spectra confirm the presence of trivalent berkelium within the $Bk(IO_3)_4$ single-crystal analyzed, supporting the intermediate-valent nature of this material. Magnetic susceptibility measurements of the trivalent material revealed a significantly reduced magnetic moment for the 5*f* ^{8}-system (7.8 μ_B compared the calculated 9.72 μ_B for Bk^{III}). Quantum mechanical calculations were performed in order to describe the orbital participation in bonding between iodate groups and berkelium of both coordination environments and oxidation states. Currently, other quantum mechanical methods are being employed to discern the electronic and magnetic structures of both materials are being conducted. It is expected that the results from these analyses offer even greater observation into these two iodate systems than what has been gathered experimentally.

D-10

First-principles studies of plutonium oxides and their surface interactions with gaseous molecules

Ping Zhang

Institute of Applied Physics and Computational Mathematics, Beijing, China

Plutonium is very easy to react with oxygen in the environment to form surface oxides, such as PuO_2 and Pu_2O_3, due to its strong chemical activities. It is a crucial research goal in the plutonium community to fully understand the characteristics of these surface plutonium oxides by studying the competitive diversity in 5*f* orbitals, such as delocalization/localization, spin-orbit coupling, directionality and anisotropy in chemical bonding. We have carried out systemic first-principles calculations to study the plutonium oxides and their surface interaction with gaseous molecules. Our research progress, which can be summarized as follows: (1) The electronic structure, mechanical, and thermodynamic properties of the plutonium oxides have been studied by DFT+*U* theory. By comparing with the ground-state electronic structures of a series of actinide oxides, it is found that the covalent Pu-O, U-O, and Np-O bonds are all stronger than that of Th-O one, i.e., the ionicity in the Th-O bond is strongest in these difference actinide oxides. (2) The dielectric function and optical properties of PuO_2 and α-Pu_2O_3 have been calculated and compared with each other by using the linear-response theory in the framework of DFT+*U*. The results provide a useful optical criterion to distinguish different plutonium oxides. (3) We have obtained the DFT+*U* phonon dispersions of PuO_2 and α-Pu_2O_3. Prominently, our predicted phonon dispersion of PuO_2 was subsequently confirmed by inelastic X-ray scattering measurement from Lawrence Livermore National Laboratory and the Argonne National Laboratory. (4) We have studied the thermodynamic equilibrium and oxidation–reduction transformation between PuO_2 and α-Pu_2O_3. The obtained spontaneous reduction conditions of $PuO_2 \rightarrow \alpha$-Pu_2O_3 are in good agreement with the experiments. (5) The point defects and helium diffusion behavior in PuO_2 have been investigated from first principles. It is revealed that the most stable dissolved sites in PuO_2 are linked to the concentration of oxygen vacancies. Helium atoms tend to occupy the octahedral interstitial sites and oxygen vacancies in intrinsic and oxygen-vacancy pre-existing PuO_2 systems, respectively. (6) Our first-principles molecular dynamic simulations based on DFT+*U*+vdW approach show that it is difficult for H_2 to get close to the PuO_2 surface directly. However, H_2 can penetrate into the α-Pu_2O_3 layer and then reach the plutonium layer while still keeping its molecular state. This theoretical result supports the experimental observation that α-Pu_2O_3 can accelerate the hydrogenation of plutonium with respect to PuO_2. (7) PuO_2(111) has been found to be the most stable surface, while for PuO_2(001), there is a prominent surface reconstruction. (8) The interactions between H_2O molecules and plutonium oxide surfaces have been largely clarified by our most recent first-principles studies. (9) The temperature-dependent diffusion coefficients of oxygen defects in plutonium oxides have been theoretically predicted.

D-11

Radiolysis of H_2-O_2 mixtures at the interface with ceramic oxides

Luke Jones[1], Howard Sims[2], Robin Orr[3], Simon Pimblott[1]

[1]University of Manchester, Moor Row, Cumbria, UK, [2]National Nuclear Laboratory, Abingdon, Oxfordshire, UK, [3]National Nuclear Laboratory, Seascale, Cumbria, UK

The UK has a significant quantity of civil separated plutonium in interim storage at the Sellafield site, which is stored as the oxide powder in welded steel canisters. During long term storage, there are several mechanisms that could lead to potential pressurization of the canisters. These are:

- He accumulation from α decay
- Decomposition of polymeric packing materials
- Steam generation from self-heating
- H_2 formation from chemical reaction of PuO_2 and H_2O, producing a postulated PuO_{2+x} phase
- Radiolysis of adsorbed water

Several of these mechanisms involve the interaction of PuO_2 with H_2O and are poorly understood. The radiolysis of adsorbed moisture, which, under certain circumstances, could lead to detonable atmospheres of H_2 and O_2 being generated inside the canisters is of concern. A significant body of work has been undertaken to investigate the production of H_2 from adsorbed moisture on PuO_2, however, little attention / focus has been given to the recombination of the resulting H_2 and O_2, which could lead to a steady state inside the canisters (Reaction 1).

$2H_2 + O_2 \leftrightarrow 2H_2O$ (Reaction 1)

This project aims to investigate the radiolysis of H_2 and O_2 gas mixtures to determine whether recombination occurs at ambient temperatures. CeO_2 and ZrO_2 have been used extensively as inactive surrogates of PuO_2 and these powders will be used to investigate the presence of an oxide powder, and to what extent this has on the gas phase chemistry. Several ratios of H_2-O_2 will be investigated ranging from H_2 excess to O_2 excess atmospheres to gain a better understanding of mechanisms occurring inside the storage canisters.

^{60}Co γ-rays and accelerated H^+ and He^{2+} ions are utilized as external radiation sources to simulate the decay modes present inside the storage containers.

Gas Chromatography is used to investigate the depletion rate of H_2 and O_2 from the headspace.

D-12

Preparation and Characterization of Intrinsic Plutonium Colloids by Sonolysis of PuO_2 in water

Elodie Dalodière[1], Matthieu Virot[1], Vincent Morosini[1], Tony Chave[1], Thomas Dumas[2], Christoph Hennig[3], Thierry Wiss[4], Oliver Dieste Blanco[4], Tolek Tyliszcak[5], David Shuh[5], Laurent Venault[2], Philippe Moisy[2], Sergey I. Nikitenko[1]

[1]Institut de chimie separative de Marcoule, bagnols sur ceze, France, [2]CEA, nuclear energy division, bagnols sur ceze, France, [3]Helmholtz zentrum dresden-rossendorf, Dresden, Germany, [4]European commission JRC ITU, Karlsruhe, Germany, [5]Advanced light source LBNL, Berkeley, USA

Colloidal species of Pu(IV) were shown to play a central role in the speciation of plutonium in various aqueous wastes and in biosphere. However, these particles are still poorly studied and no predictive model about their formation, behavior and separation is available. This work is focused on the preparation and characterization of stable salt-free Pu(IV) colloids using ultrasonic treatment of PuO_2 in pure water. Sonochemistry (i.e., chemistry under ultrasound) is known to enable the formation of nanoparticles with controlled properties without any side chemicals. Sonochemistry does not arise from a direct interaction of ultrasonic waves with molecules but rather from the acoustic cavitation phenomenon, which is a set of consequent events: the nucleation, growth, and rapid implosive collapse of gas- and vapor-filled microbubbles reaching an acoustic resonance size. At collapse, high local pressures and temperatures (more than thousand Celsius degrees and several hundred atmospheres) lead to in situ generation of radical and excited species. It has long been known that water sonolysis under argon leads to the homolytic splitting of water molecules producing $OH^{\bullet}$ and $H^{\bullet}$ radicals which can recombine into H_2 inside the cavitation bubbles and H_2O_2 at the bubble liquid interface. Additional mechanical effects of ultrasound in heterogeneous solid/liquid systems (acceleration of mass transfer, surface erosion, grain-size reduction, etc.) originate from numerous secondary effects of acoustic cavitation, such as acoustic streaming, micro-jetting, splashing, shock waves and shearing forces.

Salt-free Pu colloids were prepared by applying 20 kHz power ultrasound to PuO_2 suspensions in pure water under Ar or Ar/(10%)CO atmospheres. These sonochemical colloids were found to be very stable (> 6 months) and were then compared to hydrolytic Pu(IV) colloids obtained by the dilution in pure water under vigorous stirring of a concentrated Pu(IV) solution previously stabilized in 2 M HNO_3. The yield of sonochemical Pu colloid (alpha spectroscopy) was found to increase with PuO_2 specific surface area and by using reducing carrier gas mixture (Figure 1. a.). Kinetic data evidenced that both chemical and mechanical effects driven by acoustic cavitation strongly contribute to the mechanism of Pu colloid formation. At first, the fragmentation of initial PuO_2 particles accelerates the overall process providing larger surface of contact between cavitation bubbles and solids. Furthermore, hydrogen formed during sonochemical water splitting enables reduction of Pu(IV) to more soluble Pu(III) at the bubble/solution interface, which then reoxidizes yielding Pu(IV) colloids (Figure 1.b. and c.). Comparative studies using HR-TEM, Pu LIII-edge XAS, and STXM/NEXAFS (O K-edge) techniques revealed that both colloids (sonochemical and hydrolytic) are composed of quasi-spherical nano-crystalline particles of PuO_2 (*fcc*, $Fm\bar{3}m$ space group confirmed) measuring about 7 nm and 3 nm (Figure 1.d.), respectively. XANES spectra confirmed that Pu is in (+IV) oxidation state for all of the studied samples. The EXAFS spectra of colloidal PuO_2 nanoparticles were fitted using a triple oxygen shell model for the first coordination sphere of Pu(IV). Confrontation of HR-TEM and EXAFS studies highlighted the correlation between the number of Pu-O and Pu-Pu interactions and the particle size expressed as atomic surface-to-volume ratio. The STXM/NEXAFS studies indicated that the oxygen state of hydrolytic Pu colloid is influenced by hydrolyzed Pu(IV) species in much more extent than PuO_2 nanoparticles composing sonochemical colloid. More generally, hydrolytic and sonochemical Pu colloids can be described as core-shell nanoparticles made of quasi-stoichiometric PuO_2 cores with hydrolyzed Pu(IV) moieties at the surface shell.

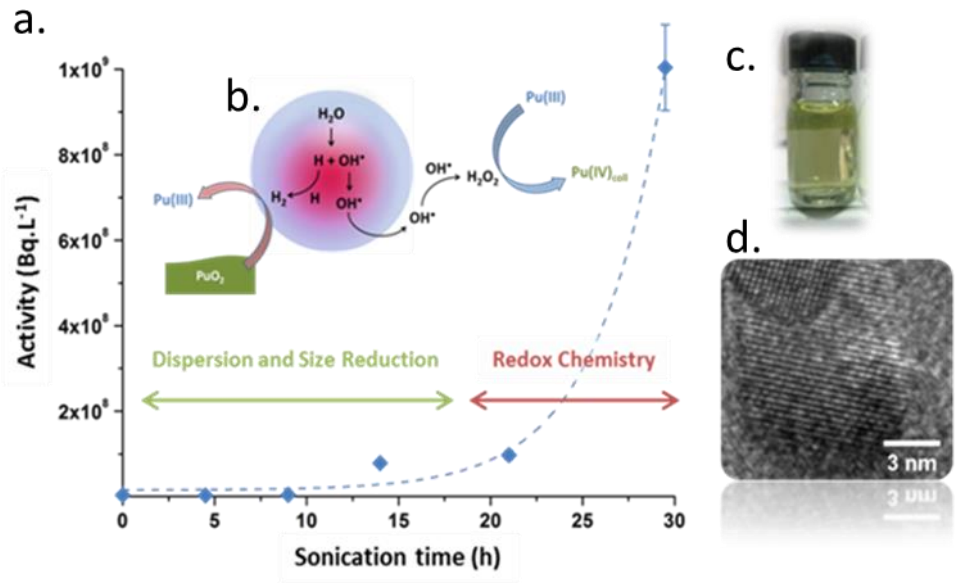

Figure 21 : **a.** Kinetic curve of Pu colloid formation during sonolysis of PuO2 in water at 20 kHz (Pac = 0.34 $W.mL^{-1}$) in the presence of 10%CO/Ar gas mixture at 20°C obtained by alpha spectroscopy measurement. **b.** Reactional scheme of the formation of Pu colloid formed by sonochemistry.
c. Picture of Pu colloids obtained under sonication. **d.** HR-TEM image of sonochemical Pu colloid.

D-13

Spectroscopic and mass spectral characterization of uranium fluoroanions formed from an ionic liquid

Christoper Zarzana[1], Gary Groenewold[1], Michael Benson[1], Kristyn Johnson-Roscioli[1], Jonathan Martens[2], Jos Oomens[2], Rika Hagiwara[3], Tetsuya Tsuda[4]

[1]Idaho National Laboratory, Idaho Falls, Idaho, USA, [2]Radboud University, Institute for Molecules and Materials, FELIX Laboratory, Nijmegen, The Netherlands, [3]Kyoto University, Kyoto, Japan, [4]Osaka University, Suita, Suita, Japan

Faster, easier, and greener approaches for manipulation of actinide elements is a topic of ongoing interest, driven by the need to more efficiently recover uranium from geologic media, and from waste liquids and slurries. Ionic liquids have terrific potential in these processes, since they have exceptionally low vapor pressures, can be recovered, and can display remarkable dissolution properties. Research at the INL has pursued identification of ionic liquids for fast low temperature conversion of actinide elements directly into their fluorides, at room temperature. In particular, the fluorohydrogenate class of ionic liquids has shown remarkable potential. These materials have nitrogen-based cations (such as imidazolium derivatives), and a unique anion consisting of fluoride complexed with two and three molecules of HF. Surprisingly, these ionic liquids display a remarkable propensity for dissolving a wide variety of inorganic compounds.

Initial studies by Hagiwara and coworkers showed that the N-ethyl-N'-methylimidazolium (EMIm+) chloride would take up between two and three HF molecules when exposed to anhydrous HF, forming the fluorohydrogenate anions (FHF) and emitting HCl in the process. The resulting ionic liquid was a non-viscous, low vapor pressure substance that nevertheless maintained the aggressive attributes of HF. For example, exposure of glass surfaces to the EMImFHF resulted in a solution, that when analyzed using electrospray ionization mass spectrometry, contained an abundant ion at m/z 123 that corresponded to $[SiF_5]^-$, and lower abundance ions corresponding to $[CaF_3]^-$, and $[AlF_4]^-$. This indicated that the IL was attacking the normally impervious glass surfaces. Subsequent experiments showed that this approach was compatible with many elements, including zirconium and uranium oxides. Treatment of UO_2 with a 9:1 molar excess of EMImFHF completely dissolved the oxide, producing a deep blue solution after three days.

The blue U-IL solution was diluted with acetonitrile to micromolar concentrations and analyzed using The negative ion ESI-MS of the UO_2-EMImFHF solution revealed an abundant ion at m/z 352 that corresponded to $[UF_6]^-$ that is unbound to the EMIm cations that surround it in the condensed phase. This implies that the fluorohydrogenate ionic liquid oxidized the tetravalent UO_2 upon dissolution, removing the oxo ligands in the process, and taking the uranium only to the 5+ oxidation state instead of the usually encountered 6+ state. Infrared multiphoton dissociation (IRMPD) spectroscopy in collaboration with the FELIX laboratory (Free Electron Laser for Infrared eXperiments, Nijmegen, The Netherlands), of this ion resulted in photoelimination of a fluorine radical at about 510 cm^{-1}, very nearly the same frequency predicted by DFT (502 cm^{-1}) for $[UF_6]^-$. The cation mode produced an abundant ion at m/z 574 that corresponded to the $[(EMIm)_2UF_6]^+$. This complex exhibited a band corresponding to U-F stretching modes in the region around 528 cm^{-1}, slightly blue shifted from the uncomplexed $[UF_6]^-$ anion. Careful examination of the portions of the IRMPD spectrum corresponding to the imidazolium ring hydrogen atoms showed both in-plane, and out-of-plane vibrational modes, and that the latter were strongly shifted upon complexation, which indicates that these H atoms, particularly the methyne-H atom, were responsible for coordinating with the fluorine atoms on the UF_6^- complex.

Complexes containing the uranyl ion are also observed in the UO_2-EMImFHF solutions. An abundant complex can be observed at m/z 679 in the positive mode that corresponds to the formula $[(EMIm)_3UO_2F_4]^+$. Collisional activation of this complex eliminates neutral EMImF, so it was hypothesized that the complex structure was two EMIm cations surrounding $UO_2F_3^-$, with

an additional pendant EMImF. However, subsequent IRMPD measurements suggest that this uranyl species is the octahedral $UO_2F_4^{2-}$ anion. IRMPD measurements of this complex reveal two intense bands at around 872 cm^{-1} and 405 cm^{-1} corresponding to uranyl and U-F stretches respectively. The peak at 405 cm^{-1} corresponded to an octahedral U-F stretching mode that was in excellent agreement with the frequency predicted by DFT calculations. The peak at 872 cm^{-1} corresponds to the intense uranyl asymmetric stretch, again in good agreement with the DFT calculations. Collision-induced dissociation of the $[(EMIm)_3UO_2F_4]^+$ complex resulted in serial elimination of first HF and then the [EMIm-H] radical, to furnish the complex $[(EMIm)_2UO_2F_3]^+$. An intense uranyl stretching band was measured at 906 cm^{-1}, which was ~30 cm^{-1} blue shifted compared to the $[(EMIm)_3UO_2F_4]^+$ complex; this is precisely what is expected as a result of reduced donation of electron density to the uranyl metal center by the complex containing only three fluoride ligands, compared to the complex containing four. Consistently, the U-F stretching modes in $[(EMIm)_2UO_2F_3]^+$ were also shifted to the blue, to about 444 cm^{-1}, about 40 cm^{-1} higher than that for $[(EMIm)_3UO_2F_4]^+$; fewer fluoride ligands tightens the overall complex, with the bonding of each fluoride being markedly stronger. The shift was also consistent with the DFT predictions.

The remarkable dissolution properties of the EMImFHF ionic liquid suggested that other fluorohydrogenates may also be effective. Accordingly, fluorohydrogenate ILs containing N-methyl pyridinium, N-methyl,N-butylpiperidinium, and N-butyl-N'-methylimidazolium (BMIm) were also synthesized and evaluated for their ability to dissolve UO_2. Of these ionic liquids, only the BMImFHF generated a blue solution indicative of the formation of UF_6^-, however its rate of dissolution was significantly slower compared to EMImFHF.

The results of the dissolution studies open up a wide range of possibilities for production of metal fluorides directly from oxides and salts, at room temperature, and without the safety problems associated with handling anhydrous HF or other fluorinating agents. Companion studies have shown that in addition to uranium, the fluorohydrogenates will also fluorinate Fe, Nb, Zr, Ti, and several other transition metals. It may be possible to fluorinate other actinide elements, a development that would be of interest for physical inorganic, and organometallic studies if nothing else. Further, it may be possible to achieve recovery of dilute concentrations of uranium from oxidic gangue material, which may hold potential for resource recovery and analytical sample collection.

D-14

Electronic Structure of PuTe and Related Materials from Photoemission

John Joyce[1], Kevin Graham[1], Tomasz Durakiewicz[1], Gerard H. Lander[2], Miles Beaux[1], Paul H. Tobash[1], Eric D. Bauer[1], Jeremy Mitchell[1], Scott Richmond[1]

[1]Los Alamos National Laboratory, Los Alamos, NM, USA, [2]European Commission, Joint Research Centre, Institute for Transuranium Elements, Karlsruhe, Germany

The complexity of Pu electronic structure is manifest in the details of the 5*f* electron character. There is often both a localized/itinerant boundary and a multivalent component to the Pu 5*f* electronic structure. Using photoelectron spectroscopy (PES) in a variety of forms we detail the experimental electronic structure for PuTe and relate these finding to delta-phase Pu metal (δ-Pu). While many Pu materials have a 5*f* configuration or occupancy around 5, PuTe along with the other mono chalcogenides have a significantly larger 5*f* electron count.[1,2] In fact, PuTe with a 5*f* occupancy of around 5.5 has more $5f^6$ character than any other measured Pu compound. By contrast, the 5*f* occupancy of δ-Pu is around 5.2 electrons.[3] There are characteristic electronic structure features for localized and itinerant 5*f* electrons as observed in photoemission as well as distinct features of the $5f^6$ electronic configuration.[3,4] As one end point in the electronic structure of Pu materials, PuTe has been popular in electronic structure calculations which include dynamical mean field theory (DMFT) calculations and the prediction of a topological insulator (TI) state.[5,6]

The valence band PES data for PuTe and δ-Pu is shown in figure 1 with δ-Pu in red and PuTe data in blue. The top frame of the figure shows the first two eV of the valence band which includes a characteristic three peak structure (TPS) in PuTe that is well described by atomic multiplet theory as arising from a $5f^6$ initial state of the Pu.[7] The spectral intensity between two and five eV in the PuTe valence band data is attributed to a $5f^5$ electronic configuration. The δ-Pu data shows two regions, one at the Fermi level that includes $5f^5$ itinerant character and a sharp peak very near the Fermi energy as well as a more localized $5f^5$ component centered around -1 eV. Superimposed on the $5f^5$ character for δ-Pu is a small component of the $5f^6$ character represented by the TPS.

In the lower frame of figure 1 we show the full valence band region for PuTe and δ-Pu. The PuTe spectrum has been scaled so that there is no part of the PuTe that is greater in intensity than the δ-Pu. In this way we can subtract the PuTe spectrum from the δ-Pu spectrum. Using this methodology we estimate the $5f^6$ component in the δ-Pu spectrum to be no more than 20% of the valence band spectral intensity. Also in figure 1, it is observed that the first peak in PuTe is distinctly different in binding energy than the quasiparticle peak in δ-Pu. Moreover, the TPS which agrees very well with the atomic multiplet calculations is a strong indication of localized 5*f* character in this part of the valence electronic structure.

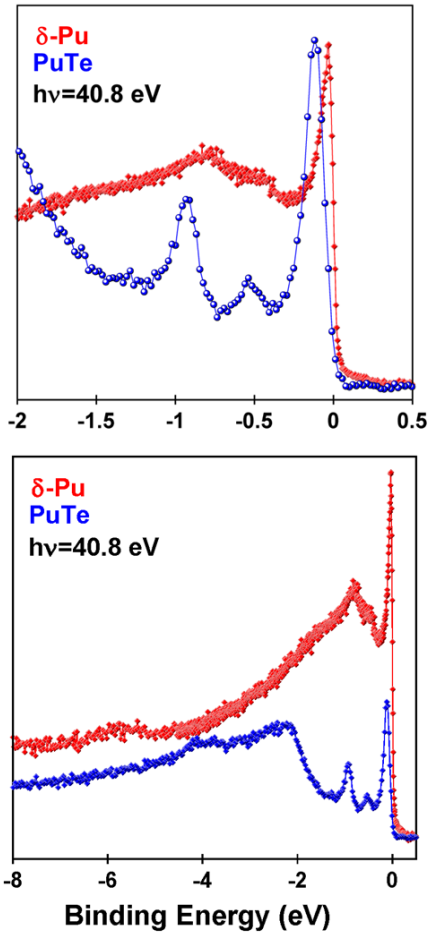

Fig. 1: PES valence band data for PuTe and δ-Pu.

Following the calculations and prediction for a TI state in PuTe,[6] we conducted angle-resolved photoemission (ARPES) on single crystal PuTe samples. In figure 2 we show typical ARPES data for PuTe. The lower axis is binding energy and the vertical axis is collection angle which translates into crystal momentum. There is no angle-dependence to the data whatsoever. This is true for a range of energies and collection angles with the ARPES data always being invariant in angle.

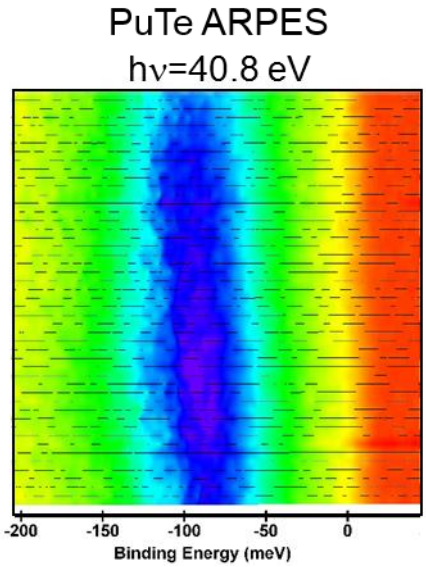

Fig. 2: ARPES data for PuTe. Red is low intensity and purple is high intensity. The peak is dispersionless.

While we did not observe a TI state in PuTe, we contend that this may well be the result of the mixed valence of PuTe ($5f^5$ and $5f^6$ configurations) where the calculation was for a pure $5f^6$ configuration.[6] The prediction of a TI state in AmN may hold more promise as the 5*f* configuration in AmN should be closer to integer valent. The data in figure 2 covers the range of the first peak in the TPS energy region.

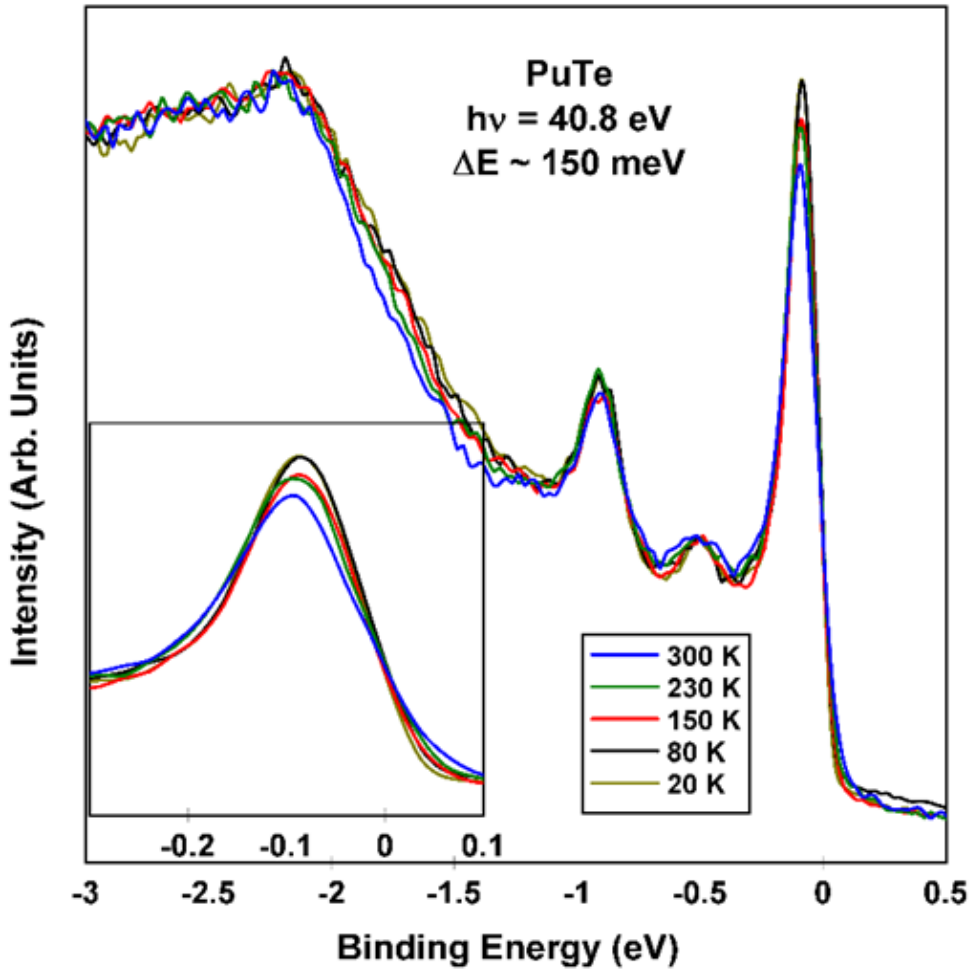

Fig. 3: Temperature dependent PES data for PuTe.

In figure 3 we show temperature dependent PES data for PuTe. The data cover a temperature range from 20 to 300 K. This temperature interval includes the 80 to 300 K range covered by a DMFT calculation in 2010.[5] The experimental temperature dependence shows far less variation than the temperature dependence predicted by the 2010 DMFT calculations. It is noted that the temperature dependence of the second and third peaks in the TPS region is less than that observed in the first peak. In the inset for figure 3 we show details of the temperature dependence for the first peak of the TPS. This temperature dependence is very similar to the dependence predicted for a peak less than 100 meV wide and 75 meV or less below the Fermi energy. In short, most of the temperature dependence is a result of Fermi-Dirac statistics. The strong temperature dependence predicted in the 2010 DMFT calculation for a 5*f* occupancy of

5.2 can be moderated by selecting a larger 5*f* occupancy value closer to 5.5 while still using DMFT.

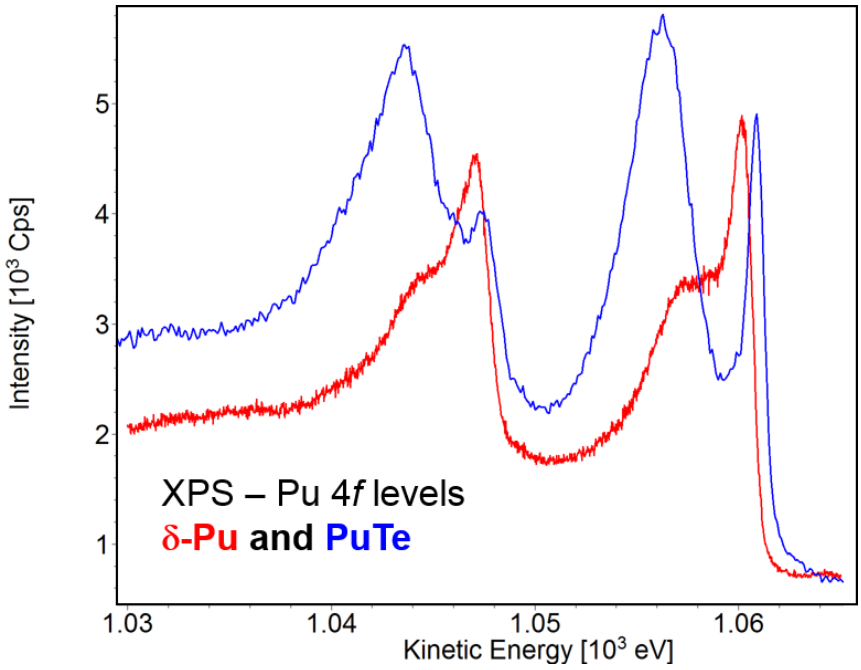

Fig 4: XPS Pu 4*f* core-level data for PuTe (blue) and d-Pu (red).

In figure 4 we show XPS data revealing two separate components for each of the spin-orbit split Pu 4*f* core-level components. While the shifts in the 4*f* core-level data do not exactly track the details of the multivalent and localized/itinerant character of the valence band data, there is clear indication of the existence of multiple electronic configurations and PuTe at the far extreme of the Pu spectrum.

Recent high resolution, angle-resolved and temperature dependent PES data on PuTe and δ-Pu reveal an electronic structure with multiple valence states ($5f^5$ and $5f^6$ at least) for both Pu materials as well as 5*f* electrons in localized and itinerant states for δ-Pu metal.

PES and ARPES research is supported by the US DOE, office of Basic Energy Sciences, division of Materials Science and Engineering. XPS research is supported by the US Department of Homeland Security, Domestic Nuclear Detection Office, under HSHQDC-15-X-B0004 and HSHQDC-12-X-00062.

References:

[1] T. Gouder et al., Phys. Rev. Lett. **84**, 3378 (2000).

[2] T. Durakiewicz, et al., Phys. Rev. B. **70**, 205103 (2004).

[3] J.-X. Zhu, et al., Phys. Rev. B, **76**, 245118 (2007).

[4] J.M. Wills, et al., J. Electr. Spectr. Rel. Phenom. **135** 163-166 (2004).

[5] C.-H. Yee, et al., Phys. Rev. B **81**, 35105 (2010).

[6] X. Zhang et al., Science **335**, 1464 (2012).

[7] F. Gerken, et al., J. Phys. F: Met. Phys. **13**, 1571 (1983).

D-15

Exploring actinide recognition, sensitization, and cellular uptake by bio-inspired platforms

Rebecca Abergel

Lawrence Berkeley National Laboratory, Berkeley, CA, USA

From the danger posed by potential contamination of individuals with radioactive fission products after a nuclear event to the therapeutic use of short-lived alpha-emitting isotopes for cancer treatment, the solution chemistry of actinides has become increasingly relevant to a number of applied problems. Understanding the fundamental bonding interactions of selective *f*-element ligands presents a rich set of scientific challenges and is critical to the characterization of transuranic actinide coordination chemistry in environmentally and biologically relevant species and to the development of highly efficient separation reagents or new therapeutic agents. Our approach to these challenges uses a combination of biochemical and spectroscopic studies on both in vitro and in vivo systems to characterize the selective binding of actinide ions by natural and biomimetic hard oxygen-donor ligands and the subsequent macromolecular recognition of the resulting actinide complexes displayed by protein-based metal transport systems.

The photophysics and solution thermodynamic behavior of trivalent and tetravalent actinide complexes formed with selected siderophores and synthetic analogs such as multidentate hydroxypyridinonate and catecholate ligands were probed. In addition to the recently described intramolecular sensitization of Am(III) and Cm(III) luminescence using these chromophore-bearing ligands, we report the unprecedented solution stabilization of Bk(IV), when complexed with hydroxypyridinone moieties from the octadentate ligand 3,4,3-LI(1,2-HOPO), and the first comprehensive characterization of sensitized Bk(IV) luminescence through the so-called antenna effect. Moreover, while most investigated ligands were shown to sensitize the luminescence of one or several lanthanide ions as well as that of Cm(III) through multi-photon excitation processes, subsequent specific binding of the metal complexes to secondary entities such as proteins that participate in endogenous metal homeostasis mechanisms resulted in significant enhancement of the intramolecular energy transfer processes. Particular metal-uptake pathways may therefore be used to create “double-antennas” for the sensitization of actinide luminescence, which in turn may lead to gains in sensitivity and enhanced detection of these ions in complex environmental samples.

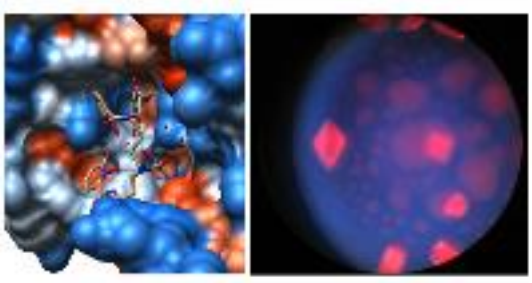

Figure 1. Crystal structure (left) and bright luminescence (right) of the ternary protein complex of Scn:[Cm(3,4,3-LI(1,2-HOPO))]$^{-}$.

Among those probed, one outstanding metal complex transporter is the mammalian siderophore-binding protein siderocalin (Scn), which appears as a potential player in the

physiological transport of actinides. Controlled in vitro assays demonstrated that intracellular plutonium uptake could occur through sidero- calin-mediated endocytosis, providing a previously unidentified target for preventing actinide incorporation and subsequent cellular damage. Crystallographic studies also revealed remarkable aspects of the protein's interactions with chelated metals, including Th(IV), Pu(IV), Am(III), Cm(III), Bk(IV), and Cf(III), establishing series of isostructural systems that can be used to derive trends along the 5*f*-element sequence.

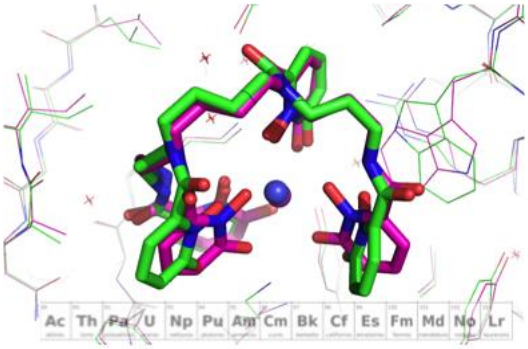

Figure 2. Superimposed crystal structures of the ternary protein complexes Scn:[M^{III}(3,4,3-LI(1,2-HOPO))]$^{-}$, where M is Am, Cm, or Cf, displaying subtle metal-binding differences.

These results will be discussed with a perspective on how such studies have important implications for the use of spectroscopic methods to exploit the fundamental knowledge of the role of *f*-electrons in actinide bonding for the development of new transport, separation, luminescence, and therapeutic applications.

D-16

Examination of aging processes occurring during plutonium sorption to solid phases

Brian Powell

Clemson University, Anderson, SC, USA

Understanding the subsurface migration of plutonium is vital for the development of robust and reliable performance assessment models of actinide bearing waste disposal facilities. Sorption of plutonium (and other actinides) to mineral surfaces represents the primary means by which migration of plutonium is slowed in the subsurface. Over the past several decades, our understanding of sorption mechanisms and the species involved has greatly increased. This is primarily due to the incorporation of advanced analytical techniques such as x-ray absorption spectroscopy, x-ray photoelectron spectroscopy, nanoSIMS, and electron microscopy. However, in most cases quantification of the extent of sorption is done using batch adsorption experiments where researchers monitor the forward sorption reaction and less frequently examine desorption. Without analysis of the desorption processes, “aging” phenomena will not be observed. In this presentation, “aging” will be used as a broad term intended to capture any process by which the chemical or physical nature of the sorbed species is altered such that desorption behaviour is hysteretic, irreversible, or unexpectedly slow. While slow or irreversible desorption of plutonium and other actinides has been observed by a number of research teams, we have only a limited understanding of the underlying processes causing the observed behaviour[1-3]. This presentation will discuss three aging processes using previous and ongoing studies.

Redox mediated aging processes

Numerous studies over the past 30 years have examined surface mediated oxidation and reduction reactions which profoundly alter the sorption behaviour of plutonium[1, 2, 4-19]. Reduction of weakly sorbing Pu(V) to insoluble and strongly sorbing Pu(IV) can change the extent of plutonium sorption by orders of magnitude. Field and laboratory studies of plutonium sorption to natural soils and pure minerals have demonstrated the importance of both sorption and reduction of Pu(V) as well as desorption of plutonium which is frequently found as Pu(V) in the aqueous phase. However, it remains unknown if Pu(IV) is desorbing then oxidizing to Pu(V) in the aqueous phase or if Pu(V) is formed on the surface then desorbs. Furthermore, the exact mechanisms of surface mediated Pu(V) reduction to Pu(IV) remain unknown. A series of batch desorption experiments using Pu contaminated soils from the United States Department of Energy Savannah River Site have demonstrated that desorption of Pu is several orders of magnitude slower than sorption and appears to be coupled to oxidation of Pu(IV). These observations are consistent with recent flow cell experiments examining plutonium sorption to goethite and montmorillonite clays[20, 21] as well as previous field studies[22, 23]. In the context of these data, the underlying mechanisms potentially responsible for surface mediated plutonium redox reactions will be discussed, with an emphasis on the role of water as a potential reductant. A series of laboratory studies using pure phase minerals have attempted to examine role of radiolysis, disproportionation, precipitation/co-precipitation, and electron shuttling in Pu(V) reduction to Pu(IV). While the results are promising, they remain inconclusive and we are left with the unproven working hypothesis that surface mediated reduction of Pu(V) is coupled to the oxidation of water which is only possible due to an increased reduction potential of sorbed Pu(IV) complexes relative to aqueous Pu(IV) species.

Formation of surface precipitates

Relatively recent studies have demonstrated that plutonium readily forms nanocolloids or surface precipitates when plutonium concentrations are sufficiently high[24-28]. However, the crystallinity and morphology of the observed precipitates vary based on the mineral surface, the aqueous chemistry (i.e. changes in pH, ionic strength, and the presence of complexing ligands), and the concentration of plutonium. Formation of surface precipitates could represent a hysteretic and potentially irreversible reaction and the thermodynamic favorability of the disordered PuO_2 type phases which are commonly observed could also help to facilitate reduction of Pu(V) to Pu(IV). A review of these recent studies will be provided with an emphasis on the factors which appear to control precipitate crystallinity and morphology.

Non-redox based aging processes

Due to the inherent sensitivity of plutonium to undergo oxidation/reduction reactions, the redox driven processes discussed above are an inherent complicating factor when examining plutonium sorption to mineral surfaces. Therefore, examining systems with redox stable actinides or aqueous conditions which maintain a single plutonium oxidation state are useful to understand non-redox based aging processes. These processes may include transition from one physical site to another with stronger sorption affinity or a change in the speciation or strength of interaction of the sorbed actinide with the mineral surface. Recent studies of plutonium sorption to goethite in the presence desferrioxamine B have demonstrated that a non-redox based aging process increases the strength of Pu interactions with goethite over a 6 month period[29]. As the pH decreases, the extent of change in the “aging” process increases with time[29]. Thus, the sorbed plutonium appears to become less labile over time. Similar behaviour was modelled by Tinnacher et al.[3], when using a consecutive, two site sorption model was used to describe the slow but reversible sorption kinetics of Np(V) sorption to goethite. To aid in the discussion of these data, current batch sorption, isothermal titration nanocalorimetery, potentiometry, and x-ray absorption spectroscopy experiments examining Eu(III), Np(V), Pu(IV), and Pu(V) sorption to pure minerals will be discussed to gain an understanding of the underlying energetic driving forces of the sorption reactions (i.e. sorption enthalpy and entropy). These data indicate that sorption of actinides is controlled by formation of inner sphere complexes and displacement of hydrating waters.

References

1. Lu, N.; Cotter, C. R.; Kitten, H. D.; Bentley, J.; Triay, I. R., Reversibility of sorption of plutonium-239 onto hematite and goethite colloids. *Radiochimica Acta* **1998,** *83*, (4), 167-173.

2. Lu, N.; Reimus, P. W.; Parker, G. R.; Conca, J. L.; Triay, I. R., Sorption kinetics and impact of temperature, ionic strength and colloid concentration on the adsorption of plutonium-239 by inorganic colloids. *Radiochimica Acta* **2003,** *91*, 713-720.

3. Tinnacher, R. M.; Zavarin, M.; Powell, B. A.; Kersting, A. B., Kinetics of neptunium(V) sorption and desorption on goethite: An experimental and modeling study. *Geochim. Cosmochim. Acta* **2011,** *75*, (21), 6584-6599.

4. Duff, M. C. In *Speciation and transformations of sorbed Pu on geologic materials: wet chemical and spectroscopic observations*, Plutonium in the Environment, 2001; Kudo, A., Ed. Elsevier Science Ltd. : 2001; pp 139-157.

5. Duff, M. C.; Hunter, D. B.; Triay, I. R.; Bertsch, P. M.; Kitten, J.; Vaniman, D. T., Comparison of two micro-analytical methods for detecting the spatial distribution of sorbed Pu on geologic materials. *Journal of Contaminant Hydrology* **2001,** *47*, (2-4), 211-218.

6. Hixon, A. E.; Arai, Y.; Powell, B. A., Examination of the effect of alpha radiolysis on plutonium(V) sorption to quartz using multiple plutonium isotopes. *Journal of Colloid and Interface Science* **2013,** *403*, 105-112.

7. Hixon, A. E.; Powell, B. A., Observed Changes in the Mechanism and Rates of Pu(V) Reduction on Hematite As a Function of Total Plutonium Concentration. *Environmental Science & Technology* **2014,** *48*, (16), 9255-9262.

8. Hu, Y. J.; Schwaiger, L. K.; Booth, C. H.; Kukkadapu, R. K.; Cristiano, E.; Kaplan, D.; Nitsche, H., Molecular interactions of plutonium(VI) with synthetic manganese-substituted goethite. *Radiochimica Acta* **2010,** *98*, (9-11), 655-663.

9. Kirsch, R.; Fellhauer, D.; Altmaier, M.; Neck, V.; Rossberg, A.; Fanghanel, T.; Charlet, L.; Scheinost, A. C., Oxidation State and Local Structure of Plutonium Reacted with Magnetite, Mackinawite, and Chukanovite. *Environmental Science & Technology* **2011,** *45*, (17), 7267-7274.

10. Morgenstern, A.; Choppin, G. R., Kinetics of the oxidation of Pu(IV) by manganese dioxide. *Radiochimica Acta* **2002,** *90*, (2), 69-74.

11. Olsson, M.; Jakobsson, A. M.; Albinsson, Y., Sorption of Pu(VI) onto TiO2. *Journal of Colloid and Interface Science* **2003,** *266*, (2), 269-275.

12. Powell, B. A.; Fjeld, R. A.; Kaplan, D. I.; Coates, J. T.; Serkiz, S. M., Pu(V)O2+ adsorption and reduction by synthetic hematite and goethite. *Environmental Science & Technology* **2005,** *39*, (7), 2107-2114.

13. Powell, B. A.; Fjeld, R. A.; Kaplan, D. I.; Coates, J. T.; Serkiz, S. M., Pu(V)O-2(+) adsorption and reduction by synthetic magnetite (Fe3O4). *Environmental Science & Technology* **2004,** *38*, (22), 6016-6024.

14. Sanchez, A. L.; Murray, J. W.; Sibley, T. H., The Adsorption of Plutonium-Iv and Plutonium-V on Goethite. *Geochim. Cosmochim. Acta* **1985,** *49*, (11), 2297-2307.

15. Shaughnessy, D. A.; Nitsche, H.; Booth, C. H.; Shuh, D. K.; Waychunas, G. A.; Wilson, R. E.; Gill, H.; Cantrell, K. J.; Serne, R. J., Molecular interfacial reactions between Pu(VI) and manganese oxide minerals manganite and hausmannite. *Environmental Science & Technology* **2003,** *37*, (15), 3367-3374.

16. Romanchuk, A. Y.; Kalmykov, S. N.; Aliev, R. A., Plutonium sorption onto hematite colloids at femto- and nanomolar concentrations. *Radiochimica Acta* **2011,** *99*, (3), 137-144.

17. Romanchuk, A. Y.; Kalmykov, S. N.; Novikov, A. P.; Zakharova, E. V., Regularities of the Sorption Behavior of Actinide Ions on Mineral Colloid Particles. *Russian Journal of General Chemistry* **2011,** *81*, (9), 2029-2038.

18. Zavarin, M.; Powell, B. A.; Bourbin, M.; Zhao, P. H.; Kersting, A. B., Np(V) and Pu(V) Ion Exchange and Surface-Mediated Reduction Mechanisms on Montmorillonite. *Environmental Science & Technology* **2012,** *46*, (5), 2692-2698.

19. Zavarin, M.; Zhao, P. H.; Dai, Z. R.; Kersting, A. B., Plutonium sorption and precipitation in the presence of goethite at 25 and 80 degrees C. *Radiochimica Acta* **2014,** *102*, (11), 983-997.

20. Begg, J. D.; Zavarin, M.; Kersting, A. B., Plutonium Desorption from Mineral Surfaces at Environmental Concentrations of Hydrogen Peroxide. *Environmental Science & Technology* **2014,** *48*, (11), 6201-6210.

21. Begg, J. D.; Zavarin, M.; Zhao, P. H.; Tumey, S. J.; Powell, B.; Kersting, A. B., Pu(V) and Pu(IV) Sorption to Montmorillonite. *Environmental Science & Technology* **2013,** *47*, (10), 5146-5153.

22. Demirkanli, D. I.; Molz, F. J.; Kaplan, D. I.; Fjeld, R. A.; Serkiz, S. M., Modeling long-term plutonium transport in the Savannah River Site vadose zone. *Vadose Zone Journal* **2007,** *6*, (2), 344-353.

23. Kaplan, D. I.; Powell, B. A.; Demirkanli, D. I.; Fjeld, R. A.; Molz, F. J.; Serkiz, S. M.; Coates, J. T., Influence of oxidation states on plutonium mobility during long-term transport through an unsaturated subsurface environment. *Environmental Science & Technology* **2004,** *38*, (19), 5053-5058.

24. Romanchuk, A. Y.; Kalmykov, S. N.; Egorov, A. V.; Zubavichus, Y. V.; Shiryaev, A. A.; Batuk, O. N.; Conradson, S. D.; Pankratov, D. A.; Presnyakov, I. A., Formation of crystalline $PuO_{2+x}{\cdot}nH_2O$ nanoparticles upon sorption of Pu(V,VI) onto hematite. *Geochim. Cosmochim. Acta* **2013,** *121*, 29-40.

25. Powell, B. A.; Dai, Z.; Zavarin, M.; Zhao, P.; Kersting, A. B., Stabilization of Plutonium Nano-Colloids by Epitaxial Distortion on Mineral Surfaces. *Environmental Science & Technology* **2011,** *45*, (7), 2698-2703.

26. Batuk, O. N.; Conradson, S. D.; Aleksandrova, O. N.; Boukhalfa, H.; Burakov, B. E.; Clark, D. L.; Czerwinski, K. R.; Felmy, A. R.; Lezama-Pacheco, J. S.; Kalmykov, S. N.; Moore, D. A.; Myasoedov, B. F.; Reed, D. T.; Reilly, D. D.; Roback, R. C.; Vlasova, I. E.; Webb, S. M.; Wilkerson, M. P., Multiscale Speciation of U and Pu at Chernobyl, Hanford, Los Alamos, McGuire AFB, Mayak, and Rocky Flats. *Environmental Science & Technology* **2015,** *49*, (11), 6474-6484.

27. Soderholm, L.; Almond, P. M.; Skanthakumar, S.; Wilson, R. E.; Burns, P. C., The structure of the plutonium oxide nanocluster [Pu38O56Cl54(H2O)(8)](14-). *Angewandte Chemie-International Edition* **2008,** *47*, (2), 298-302.

28. Schmidt, M.; Lee, S. S.; Wilson, R. E.; Knope, K. E.; Bellucci, F.; Eng, P. J.; Stubbs, J. E.; Soderholm, L.; Fenter, P., Surface-Mediated Formation of Pu(IV) Nanoparticles at the Muscovite-Electrolyte Interface. *Environmental Science & Technology* **2013**, doi: 10.1021/es4037258.

29. Wong, J. C.; Zavarin, M.; Begg, J. D.; Kersting, A. B.; Powell, B. A., Effect of equilibration time on Pu desorption from goethite. *Radiochimica Acta* **2015,** *103*, (10), 695-705.

D-17

Characterization of actinide oxides by Raman spectroscopy: from model systems to real spent fuel

Christophe Jégou[1], Sylvain Peuget[1], Sandrine Miro[1], Zeynep Talip[1], Lionel Desgranges[2], Ritesh Mohun[2], Guillaume Guimbretière[3], Aurelien Canizares[3], Patrick Simon[3]

[1]CEA DEN DTCD, 30207 Bagnols sur Ceze Cedex, France, [2]CEA DEN DEC, 13108 Saint Paul Lez Durance Cedex, France, [3]CNRS UPR3079 CEMHTI, 45071 Orleans Cedex, France

Over the last few years, many applications have been found for Raman spectroscopy in the characterization of nuclear materials, particularly for actinide-based oxides, irradiated in a nuclear reactor or not [1-3]. Raman spectroscopy enables remotely-performed measurements, which limits the risks of contamination and of irradiation for workers. It enables structural information to be recorded quickly and requires no destructive sample preparation prior to the measurement.

The characterization of highly radioactive materials like UOX-type (UO_2 base) and MOX ($(U,Pu)O_2$ base) irradiated fuels by Raman spectroscopy is therefore possible today [4,5], but the interpretation of the data acquired needs understanding based on prior theoretical and experimental studies on simpler systems. Irradiated fuel remains an extremely complex material, basically consisting of an actinide oxide which is the source of fission reactions in a reactor. It is known that these fission reactions lead to a modification in the fuel chemistry through the generation of fission products and of minor actinides, irradiation damage within the fluorite structure, a local evolution of its microstructure depending on the local burnup, and so on…

The objective of this presentation is firstly to summarize the methodology implemented to help in interpreting Raman spectra for irradiated fuels. This methodology associates several experimental approaches, ranging from:

- the Raman spectroscopy characterization of model actinide oxides like UO_2, PuO_2, ThO_2, $(U,Pu)O_2$, [7-12]
- the taking into account of irradiated fuel chemistry based on simple or complex systems (UO_2 doped with trivalent elements, Simfuel…), [13-15]
- the study of the effects of irradiation on these model oxides through external irradiation experiments (alpha, electrons…) or the characterization of alpha emitter materials having undergone damage, [16-19]
- the taking into account of the material's stœchiometry and of its reactivity to oxidation depending on the medium and the temperature, [9, 20-21]
- through to the acquisition of Raman data on the irradiated fuel itself.

Considerable progress has been made over recent years in interpreting the Raman spectra for actinide oxides without defects and close to the stœchiometry. This progress has enabled a better understanding of the origin of the lines observed (purely electronic process, phonons and resonant processes…) and their evolution depending on the nature of the actinide present in the fluorine structure (position of the T2g line and intensity of the resonance lines depending on the gap width) [22-25]. For the oxides showing defects of chemical origin or related to the irradiation, the presence of a triplet has been observed between 500 and 700 cm^{-1} and has been the subject of several investigations recently. For example Figure 1 shows the Raman spectrum of irradiated UO_2 when analyzed with the 633nm laser. It can be seen that along with the T2g, there are the presence of three additional peaks in the range of 500-700 cm^{-1} denoted as U1 (~ 527 cm^{-1}), U2 (~ 572 cm^{-1}) & U3 (~ 630 cm^{-1}). The obtained results for PuO_2 (alpha emitter material) are consistent with those previously observed after irradiating UO_2.

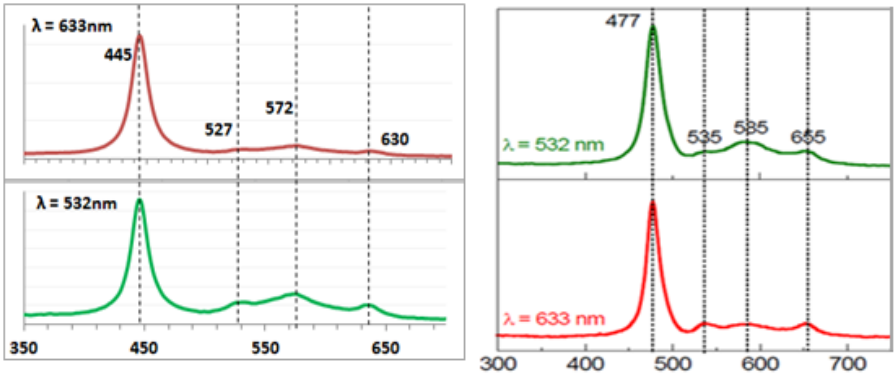

Figure 1: Raman spectra of (a) UO_2 (b) PuO_2 when characterized using the 633nm red laser & 532nm green laser [19].

The activation of these modes occurs through various stresses, like chemical doping, irradiation or oxidation in air, which will be discussed. The appearance of this triplet of defects has finally been observed for irradiated fuels (Figure 2), which is consistent with the studies on simple systems but without it being possible to fully discriminate all the effects at this stage.

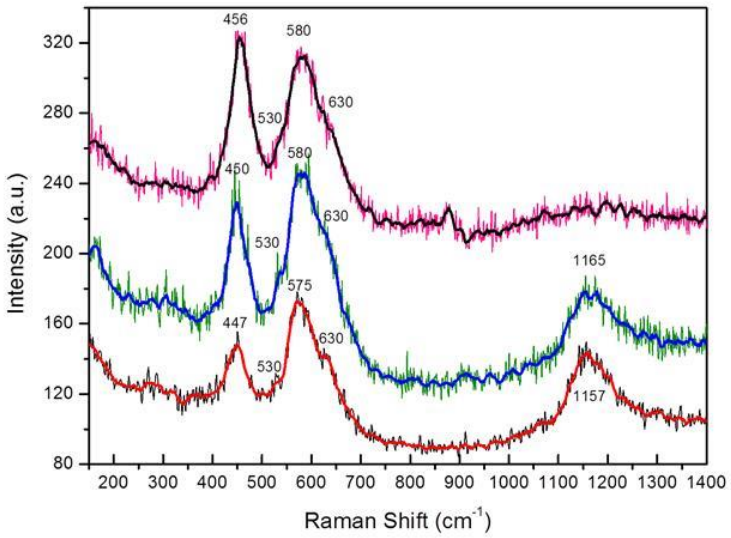

Figure 2: Raman spectra of UOX60 spent fuel sample in central zone (black - raw data; red - smoothed data) and in Rim zone (green - raw data; blue - smoothed data) and of plutonium enriched aggregates (pink – raw data; black – smoothed data) (MOX47 spent fuel). The laser power on the sample during the Raman acquisition is around 1.2mW [5].

Secondly, the focus will be on the use of Raman spectroscopy to follow the structural evolutions caused by the alteration of fuel (irradiated in a nuclear reactor or not) under water radiolysis. In the case of highly heterogeneous Mimas MOX fuels (Figure 3), the spatial resolution of this technique enables the local oxidation of the $(U,Pu)O_2$ matrix depending on the plutonium content to be followed [9, 26], and an identification of the nature of the precipitated phases is possible. The evolution of the defect formation kinetics under water and under alpha irradiation will also be examined through studies enabling in-situ monitoring of the behavior of a UO_2/water interface under alpha irradiation.

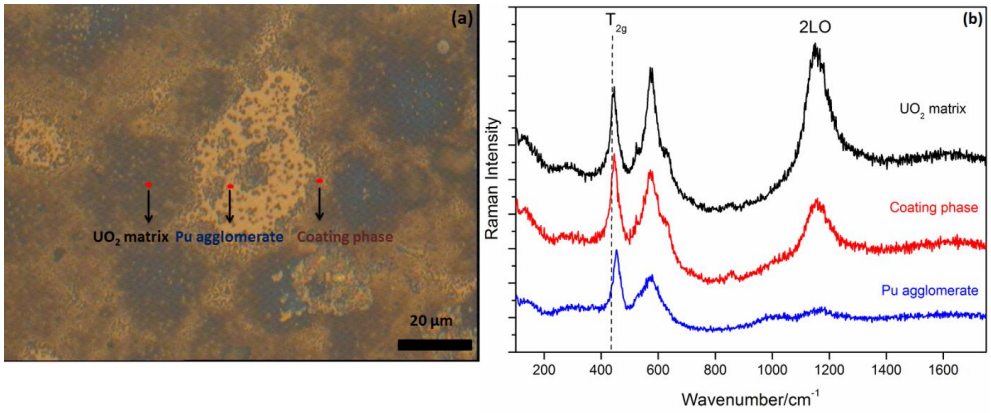

Figure 3: Image (a) and Raman spectra (b) of UO_2 matrix, coating phase and Pu agglomerate of MIMAS MOX disk.

References :

[1] R. Caraballo et al., In: Pro. HotLab Conference, Session PIE1, Idaho Falls USA (2013).
[2] G. Guimbretière et al., IEEE Trans. Nucl. Sci. (2014), 61, 2045.
[3] M. Naji et al., J. Raman Spectrosc. 46 (2015) 750.
[4] C. Jégou etal., J. Nucl. Mater. 399 (2010) 68.
[5] C. Jégou etal., J. Nucl. Mater. 458 (2015) 343.
[6] G.C. Allen et al., J. Nucl. Mater. 144 (1987) 17.
[7] R.G. Begun, G. M., Haire, *J. Less-Common Met.* (1990), 162, 129.
[8] D. Manara, B. Renker, J. Nucl. Mater. 321 (2003) 233.
[9] C. Jégou etal., J. Nucl. Mater. 405 (2010) 235.
[10] M.J. Sarsfiel et al., J. Nucl. Mater. 427 (2012) 333.
[11] F. Pointurier, O. Marie, J. Raman Spectrosc. 44 (2013) 1753.
[12] R. Böhler et al., J. Nucl. Mater. 448 (2014) 330.
[13] L. Desgranges et al., Inorg Chem. 51 (2012) 9147.
[14] Z. Talip et al., J. Am. Cer. S. 98 (2015) 2278.
[15] H. He et al., Can. J. Chem. 85 (2007) 702.
[16] P.R. Graves, Appl. Spectrosc. 44 (1990) 1665.
[17] G. Guimbretière et al., Appl. Phys. Lett. 100 (2012) 251914.
[18] G. Guimbretière et al., Appl. Phys. Lett. 103 (2013) 041904.
[19] R. Mohun et al., NIMB. 374 (2016) 67.
[20] H. He, D. Shoesmith, Phys. Chem. Chem. Phys. 12 (2010) 8108.
[21] L. Desgranges et al., J. Raman Spectrosc. 43 (2012) 455.
[22] T. Livneh, E. Sterer, *Phys. Rev. B* 73 (2006) 085118-1.
[23] J. Lv et al., J. Raman Spectrosc. 47 (2016) 345.
[24] B. Dorado, P. Garcia, Phys. Rev. B. 87 (2013) 1395139.
[25] L. Desgranges et al., JOM. 66 (2014) 2546.
[26] M. Odorowski et al., J. Nucl. Mater. 468 (2016) 17.

D-18

Identification of Processes Controlling Pu Transport Behavior Under Field Conditions

Annie Kersting

LLNL, Livermore, CA, USA

Introduction of Pu into the environment results from both nuclear energy production, and the legacy of nuclear weapons. Faster progress is needed towards cleaning up contaminated sites as well as developing a permanent nuclear waste storage facility that can safely isolate long-lived actinides and fission products from the biosphere. Significant uncertainty still remains on how long-lived radionuclides will behave in the environment. Plutonium (Pu) is of particular interest because of its high toxicity and long half-life ($t_{1/2}$ ^{239}Pu 2.4 x10^4 yrs). Pu is redox sensitive which in turn controls its stability and solubility in the environment. The behavior of Pu will be controlled by its interactions with mineral surfaces. Understanding the sorption and desorption reactions rates of Pu is key to predicting colloid facilitated transport rates in the environment.

In this talk, I will present result from investigations of both sorption and desorption rates of Pu(IV) and Pu(V) from different common environmental minerals, clay and Fe-oxide. We investigated Pu behavior over a large range of concentrations (10^{-15} – 10^{-5} M) found in the environment at circumneutral pH. For Pu concentrations below solubility, the sorption isotherms for both montmorillonite and goethite were linear, although the rates of sorption were significantly different. On the goethite surface Pu(V) was rapidly reduced to Pu(IV) with equivalent Pu(IV) and Pu(V) K_d values obtained after 1-week. In contrast, Pu(V) was reduced much more slowly to Pu(IV) on the montmorillonite surface, taking longer than 3 weeks but less than 6 months. Desorption rates for montmorillonite were slow but not irreversible and were on the time scale of years to tens of years. Desorption rates of goethite are currently underway.

An additional aim of this work is to bridge our laboratory-derived, mechanistic understanding of Pu sorption/desorption behavior with mechanisms that may be encountered in the field. Can the process of sorption/desorption to clays and Fe-oxides explain the transport observed at the Nevada Nuclear Security Site (formerly Nevada Test Site), NV, U.S.A.? We will compare our experimentally derived rates to observations of Pu transport at the Nevada Test Site, NV U.S.A. under conditions similar to those explored experimentally.

D-19

Study of combustion synthesis of solid solutions (U1-yAn/Lny)O2±x under air atmosphere

Guillaume Peter-Soldani[1], Eléonore Welcomme[1], Xavier Deschanels[2], Francis Abraham[3], Stéphane Grandjean[4]

[1]CEA, DEN, DRCP/SERA/LCAR, F-20207 Bagnols-sur-Cèze Cedex, France, [2]CEA, DEN, DRCP/ICSM/LNER, F-20207 Bagnols-sur-Cèze Cedex, France, [3]Université Lille Nord de France- UCCS/UMR CNRS 8181 ENSCL-USTL, F-59652 Villeneuve d'Ascq Cedex, France, [4]CEA, DEN, DRCP, F-20207 Bagnols-sur-Cèze Cedex, France

Within the framework of the research carried out on the treatment and recycling of nuclear spent fuel for the 4th generation systems, various conversion routes of actinide(s) into solid oxide are of interest. Among them, thermal denitration based on a single thermal treatment consists in concentrating solution and decomposing the nitrate salt formed to actinide oxide. Conventionally, the direct thermal denitration of plutonium and uranium nitrate solutions leads to powder characteristics not compatible with direct shaping of nuclear fuel pellets. Moreover, this method does not permit to obtain the desired UO_2+PuO_2 or $(U,Pu)O_2$ mixed oxides in a single thermal step, but a phase mixture (e.g. UO_3 and PuO_2 or U_3O_8 and PuO_2) requiring thus an additional reduction step. In this study, an alternative route has been explored: the solution combustion synthesis (SCS) also called self-propagating high-temperature synthesis (SHS) involving a fuel (metal nitrate) and an oxidizer (glycine) to form $(U,Pu)O_2$ oxide. This method has been already applied to U based mixed oxide syntheses (U,Th and U,Ce), additional step being required in many cases to reduce U_3O_8 into UO_{2+x}. To simplify the synthesis pathway, synthesis parameters were thoroughly explored in this work, and namely the fuel/oxidizer ratio. As a result, an improved combustion method tested on (U,Th; U,Ce; U,Nd) surrogate systems led us to the desired monophasic $(U_{1-y}Ln_y)O_{2\pm x}$ ($0\leq y\leq 1$) solid solutions in a single step. Then, this method was successfully applied to the targeted (U,Pu) system. Some characteristics of the mixed oxide powder have also been linked to synthesis conditions.

D-20

Synthesis and dissolution of mixed oxides $(U_{1-x}Pu_x)O_2$ with different morphologies

Yannis Ziouane, Gilles Leturcq, Bénédicte Arab-Chapelet, Sophie Lalleman

CEA, Marcoule, France

Introduction

The dissolution of spent nuclear fuel in nitric acid is one of the main steps of nuclear fuel recycling in France. For this purpose, it is necessary to understand and quantify the impact of fuel characteristics on $(U_{1-x}Pu_x)O_2$ dissolution kinetics. In this study, a focus on the impact of the oxide morphology on dissolution kinetics was done. Three different morphologies were synthesized thanks to sol gel process (big heap of about 200µm consisting of sintered grains) on the one hand and oxalic precipitation (one platelet morphology and one hexagonal morphology) on the other hand. Significant differences in dissolution kinetics were observed. Therefore, the morphology of the powders was found to be a key parameter that has to be considered in $(U,Pu)O_2$ dissolution kinetic studies.

Synthesis and Characterizations

As the aim of this study is to elucidate the effect of the morphology of the powder on its dissolution, different synthesis routes had to be used to make different AnO2 (with An = U, Pu or (U,Pu)) samples exhibiting different morphologies. In all cases, concentration, purity and oxidation of monometallic solutions were determined by UV-visible spectroscopy.

The oxalic conversion is usually reported to synthetize actinide oxides [1]. This process is based on an oxalic precipitation (mixing oxalic acid and an actinide nitrate solution) followed by a calcination step under controlled atmosphere. In this study, two different oxalates were precipitated resulting in different morphologies: one characteristic of platelet morphology [2] and the other one of the hexagonal stick morphology [3]. Articles referring to the sol-gel method deal with the synthesis of microspheres [4,5]. In this work, to synthesize powders, protocol was modified as follows. A metallic nitrate solution (U/Pu final ratio fixed in this solution) was mixed with urea ($CO(NH_2)_2$) and HMTA (hexamethylenetetramine) at low temperature (~5°C). Once urea and HMTA were dissolved into the cold actinide solution, the solution was stirred and heated at 80°C. HMTA was decomposed at high temperature causing an increase in pH and the hydrolysis of uranium. In a few minutes, solution jellified. Heat treatments were performed for all precursors up to 850°C with a rate of $40°.min^{-1}$ Compounds were maintained to this temperature for 90 min then cooled down to room temperature.

Several characterizations were performed on the synthetized oxides powders. XRD analyses of the powders validates compounds are single phase AnO_2 (with An = U, Pu or (U,Pu)) but also permitted to determine some structural parameters: the lattice parameters, the crystallite sizes and the microstrain rates. In all cases, actinide oxides were synthetized and lattice parameters close to a perfect $AnO_{2.00}$ were obtained. The specific surface areas which are dependent on the morphology of the compound were calculated by the Brunauer–Emmett–Teller (BET) 5 points method. SEM micrographs (figure 1) are used to authenticate the presence of a good and homogeneous morphology for each material. The crystallite sizes defined by XRD analyses were confirmed and agglomerate sizes were determined.

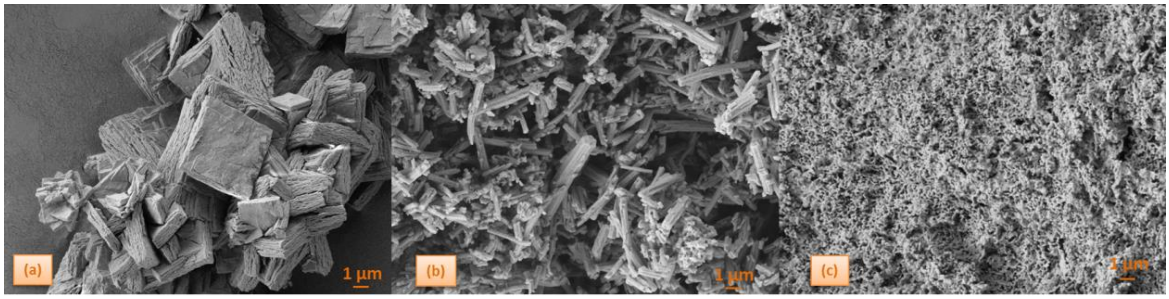

Figure 1: SEM micrographs of UO_2 and PuO_2 powders in secondary electron mode: a 5000x magnification for two PuO_2 obtained by oxalic precipitation from two different precursors (a and b) and for an UO_2 acquired by sol-gel route (c).

Dissolution

The dissolution of UO_2 (figure 2) appears different depending on the compounds in the same experimental conditions (i.e. $[HNO_3]$ = 1,5M at 50°C). These dissolution kinetics results has been published in ATALANTE 2016 proceeding and points out the complexity of the relationship between the morphology (porosity, grain size, microstrain rates, form and size of agglomerate) of oxides powders and the dissolution kinetics. Previous characterizations were essential to understand which parameters have an effect on the determination of dissolution kinetics. The porosity, the grain sizes and the crystal defects (microstrain rates) impact the dissolution kinetics. The morphology seems to be a key parameter to determine the dissolution kinetics. Similar studies conducted on the PuO_2 and on a $U_{0,75}Pu_{0,25}O_2$ will be presented at the conference and it will be proposed a relation between the effect of the plutonium content and the different structural parameter on the dissolution kinetics.

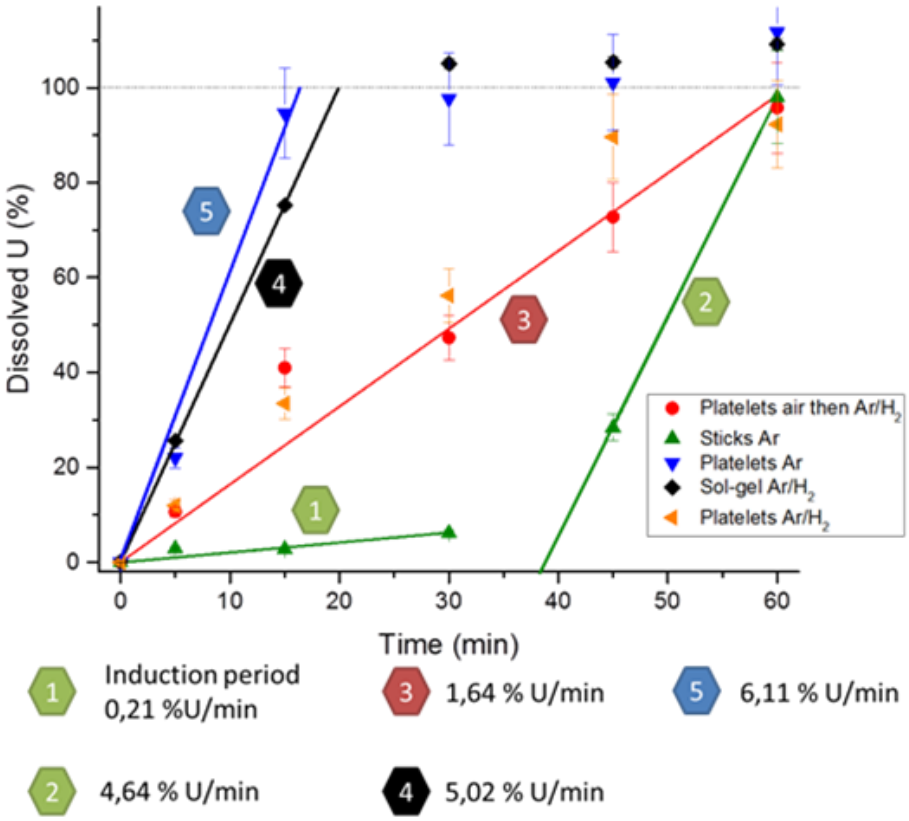

Figure 2: Same experimental conditions and different morphologies conducing to different dissolution kinetics.

Conclusion

In conclusion, this results points out that the morphology is a key parameter that have to be considered in studies dealing with $(U,Pu)O_2$ dissolution kinetics. Some results correlating the material characterizations to the dissolution kinetics will be presented in details at the conference.

References

[1] Hingant N, Clavier N, Dacheux N, Hubert S, Barré N, Podor R, Aranda L (2011) Preparation of morphology controlled Th1−xUxO2 sintered pellets from low-temperature precursors. Powder Technology 208: 454-460.

[2] Abraham F, Arab-Chapelet B, Rivenet M, Tamain C, Grandjean S (2014) Actinide oxalates, solid state structures and applications. Coordination Chemistry Reviews. Volumes 266-267: 28-68.

[3] Grandjean S, Arab-Chapelet B, Robisson A.C, Abraham F, Martin Ph, Dancausse J-Ph, Herlet N, Léorier C (2009) Structure of mixed U(IV)–An(III) precursors synthesized by co-conversion methods (where An = Pu, Am or Cm). Journal of Nuclear Materials 385: 204-207.

[4] Vaidya V.N (2008) Sol-gel process for ceramic nuclear fuels. Journal of Sol-Gel Science and Technology: 369-381.

[5] Jeong K-C, Kim Y-K, Oh S-C, Cho M-S, Lee Y-W, Chang J-W (2005) UO3 intermediate particle preparation using the Sol-gel process. Transactions of the Korean Nuclear Society autumn meeting Busan, Korea, October 27-28.

D-21

Differential sorption behavior of U(VI) and Pu(VI) dependent on their redox chemistry

Stefan Hellebrandt[1], Karah E. Knope[2,5], Sang Soo Lee[2], Aaron J. Lussier[3], Joanne E. Stubbs[4], Peter J. Eng[4], Lynda Soderholm[2], Paul Fenter[2], Moritz Schmidt[1]

[1]Helmholtz-Zentrum Dresden-Rossendorf, Dresden, Saxony, Germany, [2]Argonne National Laboratory, Lemont, IL, USA, [3]University of Notre Dame, Notre Dame, IN, USA, [4]University of Chicago, Chicago, IL, USA, [5]Georgetown University, Washington, DC, USA

In a recent paper (Schmidt et al. 2013) our group suggested the surface-catalyzed formation of Pu(IV)-oxo-nanoparticles due to an enhanced concentration of Pu(III) at the surface of muscovite mica in equilibrium with a small amount of Pu(IV). The study took three possible pathways for the reaction into account: (1) Pu(III) adsorbs on the muscovite surface, where the oxidation to Pu(IV) takes place. (2) The oxidation of Pu(III) to Pu(IV) happens in solution, whereupon Pu(IV) adsorbs on the surface. In both cases (1) and (2) the increased Pu(IV) concentration leads to oligomerization and afterwards the formation of Pu(IV)-oxo-nanoparticles. Another pathway (3) is the formation of Pu(IV)-oxo-nanoparticles in solution which subsequently adsorb at the mica surface. This pathway was considered less likely, due to a clear enhancement of the reaction in the presence of the interface, which cannot be explained by this process. Motivation of the current study was to test the viability of these mechanisms, but also to investigate the interfacial reactivity of Pu's various oxidation states.

The mobility of radionuclides in the environment and thus their hazard potential will be controlled by their reactivity at the water/mineral interface. Thus, it is necessary to understand how Pu behave in contact with mineral surfaces on a molecular level, to make reliable long-term predictions about the safety of a nuclear waste repository. In order to understand these processes analytical methods shall ideally be both surface specific and sensitive. X-ray reflectivity techniques, particularly resonant anomalous X-ray reflectivity (RAXR) and crystal truncation rod (CTR) measurements have proven to be a successful combination to investigate geochemical interfacial regimes (Fenter 2002). Plutonium is one of the most important radionuclides in term of nuclear waste disposal due to its long half-life period and high radiotoxicity. That's why it has been subject of different studies over the last decades. While these studies could show an enhancement of the mobility of plutonium in the presence of colloidal matter (Kersting et al., 1999 and Novikov et al., 2006), the formation of Pu(IV)-nanoparticles is still content of ongoing research (e.g. Kersting 2013, Walther & Deneke 2013).

In the current study a comparison of the interaction of UO_2^{2+} and PuO_2^{2+} ([Pu] = 0.1 mmol L^{-1}, [U] = 1 mM mmol L^{-1}, I(NaCl) = 0.1 mol L^{-1}, pH 3.2 ± 0.2) with muscovite mica and the effect of the actinides' different redox properties were investigated using a combination of surface X-ray diffraction, alpha spectrometry and grazing-incidence X-ray adsorption near-edge structure (GI-XANES) spectroscopy. RAXR data of a Pu(VI) solution in contact with muscovite show a broad Pu distribution, which cannot be explained by simple ionic adsorption of PuO_2^{2+}, indicating the formation of Pu(IV)-oxo-nanoparticles. Alpha spectrometry confirms these findings; the occupancy was determined to be ~ 8.3 Pu/A_{UC} (where A_{UC} = 46.72 $Å^2$ is the unit cell area). This means the mechanism of the redox partner independent formation of Pu(IV)-nanoparticles previously observed for Pu(III) can be confirmed for Pu(VI) as well.

UO_2^{2+} shows clearly different performance. No RAXR signal was observable, indicating no adsorption of UO_2^{2+}. The persistence of the hexavalent oxidation state of U was confirmed by GI-XANES spectroscopy. Furthermore, Alpha spectrometry and GI-XANES spectroscopy showed very weak signals or no signal at all, in agreement with the RAXR findings. Assuming that the sorption behavior of UO_2^{2+} and PuO_2^{2+} is equivalent excluding their redox chemistry, no Pu(VI) should be present at the surface. Therefore, the previously proposed mechanism (1) cannot contribute significantly to the observed formation of Pu(IV)-oxo-nanoparticles from Pu(VI) solution. To distinguish mechanisms (2) and (3) UV/Vis spectroscopy was performed similar to our previous study. No Pu(IV) was detectable, even if measured over a longer periode

of time than available for the X-ray reflectivity experiment. Hence mechanism (3) also appears to be implausible. Apparently, the observed formation of Pu(IV)-nanoparticles follows mechanism (2). Because of the redox properties of Pu, an equilibrium of Pu(IV), Pu(V) and Pu(VI) will be present in solution. Thus available Pu(IV) will adsorb on the muscovite (001) basal plane. The tetravalent oxidation state of interfacial Pu was confirmed by GI-XANES spectroscopy. Since a threshold is reached polymerization occurs as a consequence of hydrolysis, through an olation (Knope et al., 2015) or oxolation (Knope & Soderholm, 2013) mechanism.

References

Fenter, P. (2002): *Rev. Mineral. Geochem.*, **49**, 149-221.

Kersting, A. B.; Efurd, D. W.; Finnegan, D. L.; Rokop, D. J.; Smith, D. K.; Thompson, J. L. (1999): *Nature*, ***397***, 56-59.

Novikov, A. P.; Kalmykov, S. N.; Utsunomiya, S.; Ewing, R. C.; Horreard, F.; Merkulov, A.; Clark, S. B.; Tkachev, V. V.; Myasoedov, B. F. (2006): *Science*, ***314***, 638-641.

Kersting, A. B. (2013): *Inorganic Chemistry*, **52**, 3533-3546.

Walther, C., & Denecke, M. A. (2013): *Chem. Rev.*, **113**, 995-1015.

Schmidt, M., Lee, S. S., Wilson, R. E., Knope, K. E., Bellucci, F., Eng, P. J., Stubbs, J. E., Soderholm, L., Fenter, P. (2013): *Environ. Sci. Technol.*, **47**, 14178-14184.

Knope, K. E.; Skanthakumar, S.; Soderholm, L. (2015): *Inorganic Chemistry, **54***, 10192-10196.

Knope, K. E.; Soderholm, L. (2013): *Chemical Reviews, **113***, 944-994.

D-22

Synthesis and structural characterization of a new water soluble actinide(IV) hexanuclear cluster $[An_6(OH)_4O_4]^{12+}$ (with An = U, Np, Pu).

Christelle Tamain[1], Thomas Dumas[1], Dominique Guillaumont[1], Christoph Hennig[2], Philippe Guilbaud[1]

[1]CEA, Nuclear Energy Division, Marcoule, RadioChemistry & Processes Department, F-30207 Bagnols sur Cèze, France, [2]Helmholtz-Zentrum Dresden-Rossendorf, Institute of Resource Ecology, Bautzner Landstr. 400, D-01314 Dresden, Germany

Among the different processes (precipitation, sorption, colloid formation…) affecting the actinide migration in the environment, complexation is particularly important as it increases the amount of actinide in solution, the actinide release and the migration rates.[1] It is often assumed that actinide(IV) chemistry in the environment is influenced by its speciation and particularly its hydrolysis. However, soluble oligomer species resulting from hydrolysis-complexation competition are largely absent from thermodynamic descriptions of aqueous speciation.

Actinide(IV) clusters were intermitently studied during the last fifty years before seeing a renewed interest in the last decade.[2] Several studies on tetravalent actinides described oxo-hydroxo hexanuclear species, $[An_6(OH)_4O_4]^{12+}$, stabilized by small organic ligands such as carboxylic acid[3,4,5] or small amino acid.[6,7,8] These structures were mainly described with Th(IV) and U(IV) whereas only once was reported for Pu(IV) and none for Np(IV).

Herein we report the structure of new actinide(IV) hexanuclear core species $[An_6(OH)_4O_4]^{12+}$ (An = U, Np, Pu). The cluster is stabilized with a polyamino carboxylic acid, DOTA (1,4,7,10-tetraazacyclododecane-1,4,7,10-tetraacetic acid), which is an hydrophilic ligand considered in separation processes and in actinide interaction with human body.

The structure determined by single crystal XRD is made of a hexanuclear core built from six plutonium(IV) connected through four oxo (μ_3O^{2-}) and four hydroxo (μ_3OH^-) alternate bridges (Figure 1). This cluster is decorated and stabilized by four DOTA molecules coordinating the four equatorial Pu(IV) cations. Each ligand is linked to one plutonium metallic center by one oxygen atoms of two of its carboxylic acid functions. The third arm acts as a bridging carboxylate group with one oxygen atoms connected to one equatorial adjacent plutonium cation. The last carboxylic branch of the molecule stays uncoordinated to any metallic center. All the water molecules and unbonded oxygen atoms of each carboxylic acid of each DOTA ligand are connected through hydrogen bonds leading to a stable configuration.

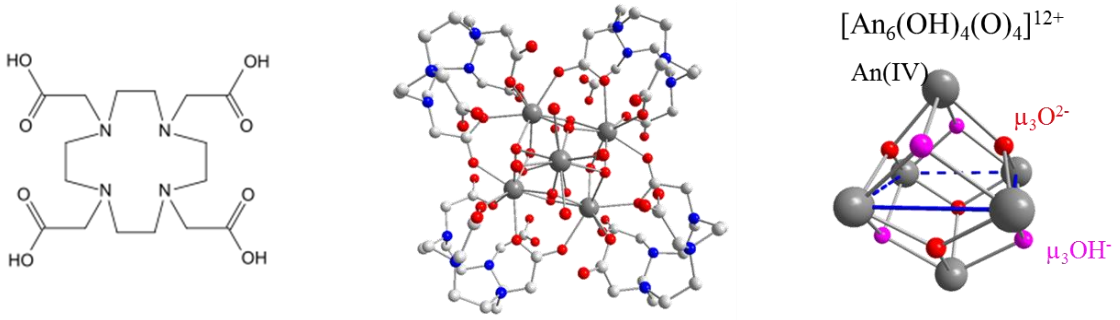

Figure 1: DOTA ligand (left), plutonium cluster structure (middle) and plutonium hexanuclear core without DOTA ligands (right).

X-ray absorption near-edge structure (XANES) and Extended X-ray Absorption Fine Structure (EXAFS) were employed to characterize the actinide speciation in the solution after dissolution of the crystals in aqueous solution. The best fit spectra based on hexanuclear complexe crystal structure are in excellent agreement with the experimental one. All actinide(IV) shells are well reproduced by the model. Moreover, the UV-visible absorption spectrum of the actinde(IV) solution recorded presents the same signature and overall shape as the crystal UV-vis reflectance ones. These structural characterizations demonstrate the existence of these An(IV) clusters as water soluble complexes. Even though, from U(IV) to Np(IV), the existence of soluble hexanuclear core species has already been demonstrated, it is the first time that Pu(IV) hexanuclear core are identified in aqueous solution. Moreover, these analyses reveal that UV-visible spectroscopy can be used as a probe to identify the soluble An(IV) cluster.

Beyond a complete structural resolution of the solid state cluster (single-crystal XRD) and of the complex in solution (X-ray absorption), some physical-chemical characteristics were investigated. Based on UV-visible spectroscopy, the pH stability range in aqueous solution was determined for each An(IV). The absence of modification in the spectrum shape indicates a large pH range stability: 0.6<pH<4.0, 0.6<pH<5.3 and 0.6<pH<5.3 for plutonium(IV), neptunium(IV) and uranium(IV) respectively. These ranges are widder than the one determined for An-formate (Th, U, Np)[4,8] or Th-glycine[6] systems. The competition between complexation and hydrolysis seems to be in favour of complexation with DOTA even in moderate acidic media. The solubility of the complex in aqueous solution was evaluated, after saturation of an aqueous solution (pH = 2.5), to settle between 14 and 20 $g.L^{-1}$. These values are very high compared to the solubility considered up to now in environmental models. These results confer a particular interest to these actinide DOTA-hexanuclear core species.

References

1. R. J. Silva and H. Nitsche, *Radiochimica Acta*, 1995, **70/71**, 377.

2. J. Qui, P.C. Burns, *Chemical Reviews*, 2013, **113**, 1097.

3. M. Vasiliu, K.E. Knope, L. Soderholm, D.A. Dixon, *J. Phys. Chem. A*, 2012, **116**, 6917.

4. K. Takao, S. Takao, A. Scheinost, G. Bernhard, C. Hennig, *Inorg. Chem.*, 2012, **51**, 1336.

5. G. Nocton, J. Pécaut, Y. Filinchuk, M. Mazzanti, *Chem. Commun.*, 2010, **46**, 2757.

6. C. Henning, S. Takao, K. Takao, S. Weiss, W. Kraus, F. Emmerling, A. Scheinost, *Dalton Trans.*, 2012, **41**, 12818.

7. K.E. Knope, R.E. Wilson, M. Vasiliu, D.A. Dixon, L. Soderholm, *Inorg.Chem.*, 2011, **50**, 9696.

8. S. Takao, K. Takao, W. Kraus, F. Emmerling, A. C. Scheinost, G. Bernhard, C. Hennig, *Eur. J. Inorg. Chem.*, 2009, 4771.

[i] http://www.iea.org/publications/freepublications/publication/WEO2015SpecialReportonEnergyandClimateChange.pdf

[ii] http://www.iaea.org/Publications/Documents/Conventions/index.html

[iii] http://europa.eu/legislation_summaries/institutional_affairs/treaties/treaties_euratom_en.htm

[iv] JRC thematic report Science for Standards: a driver for innovation; chapter 4 Nuclear safety and security, EUR 25942 EN

[v] ISO/IEC 17025:2005 General requirements for the competence of testing and calibration laboratories, International Organization for Standardization, Geneva

[vi] http://www.iso.org/iso/home/search.htm?qt=Nuclear+fuel+technology+plutonium&sort=rel&type=simple&published=on

[vii] http://www.astm.org/search/fullsite-search.html?query=plutonium&resStart=10&resLength=10&toplevel=products-and-services&sublevel=standards-and-publications&

[viii] http://webstore.ansi.org/FindStandards.aspx?SearchString=plutonium&SearchOption=1&PageNum=0&SearchTermsArray=plutonium%7cnull%7cnull

[ix] International Target Values 2010 for Measurement Uncertainties in Safeguarding Nuclear Materials, IAEA-STR-368, Vienna, November 2010

[x] K. Casteleyn ,et al. On-site Laboratories of Euratom: Ten Years of Excellent Results and Time to Renew; *proceedings INMM 2011*

[xi] Surugaya N1, Hiyama T, Verbruggen A, Wellum R; *Anal Sci*. 2008 Feb;24(2):247-52.

[xii] R. Jakopič, J. Bauwens, R. Bujak, C. Hennessy, F. Kehoe, U. Jacobsson, S. Richter and Y. Aregbe; Preparation and certification of the IRMM-1027 series of large-size dried spikes for the measurement of plutonium and uranium content in dissolved irradiated nuclear fuel by isotope dilution mass spectrometry – in preparation

[xiii] http://static1.squarespace.com/static/568be36505f8e2af8023adf7/t/56fd8d821d07c0659bf96d7b/1459457410885/Nuclear+Forensics+CRM.pdf

[xiv] Wellum R, Verbruggen A, Kessel R (2009) A new evaluation of the half-life of ^{241}Pu. *J Anal At Spectrom* 24:801–807

[xv] Sibbens G, Eykens R, Moens A, Peeters M, Luyckx K, Sapundjiev, D, Aregbe Y (2010) Target preparation and characterisation at IRMM. Proceedings of the Scientific Workshop on Neutron Measurements, Theory and Applications, Nuclear Data for Sustainable Nuclear Energy, 28-30 April 2009, Geel Belgium; JRC Scientific and Technical reports EUR23883EN-2010: 159–164

[xvi] G Sibbens, A. Moens, R. Eykens, D. Vanleeuw, F. Kehoe, H. Kühn, R. Wynants, J. Heyse, A. Plompen, R. Jakopič, S. Richter, Y. Aregbe. *Journal of Radioanalytical and Nuclear Chemistry* February 2014, Volume 299, Issue 2, pp 1093-1098

[xvii] Accurate Nuclear Data for Nuclear Energy Sustainability. http://www.andes-nd.eu/. Accessed 24 July 2012

[xviii] P. Salvador-Castiñeira, T. Bryś, R. Eykens, F.-J. Hambsch, A. Moens, S. Oberstedt, G. Sibbens, D. Vanleeuw, and M. Vidali, *Physical Review* C 88, 064611 (2013)

[xix] Sergei Boulyga, Stefanie Konegger-Kappel, Stephan Richter and Laure Sangély, J. Anal. At. Spectrom., 2015, 30, 1469

[xx] Wallenius M, Mayer K (2000) Age determination of plutonium material in nuclear forensics by thermal ionisation mass spectrometry. *Fresenius J Anal Chem* 366(3):234–238

[xxi] M. Sturm, S. Richter, Y. Aregbe, R. Wellum, S. Mialle, K. Mayer, T. Prohaska *Journal of Radioanalytical and Nuclear Chemistry* October 2014, Volume 302, Issue 1, pp 399-411

[xxii] P. Schillebeeckx, B. Becker, H. Harada, S. Kopecky Neutron Resonance Spectroscopy for the Characterisation of Materials and Objects, Report EUR 26848 EN

[xxiii] Poinssot, C.; Bourg, S.; Ouvrier, N.; Combernoux, N.; Rostaing, C.; Vargas-Gonzalez, M.; Bruno, J., *Energy* **2014,** *69*, 199–211.

[xxiv] *Potential Benefits and Impacts of Advanced Nuclear Fuel Cycles with Actinide Partitioning and Transmutation*; NEA No. 6894, OECD, Nuclear Energy Agency (NEA), Paris: 2011.

[xxv] Dinh, B.; Moisy, P.; Baron, P.; Calor, J.-N.; Espinoux, D.; Lorrain, B.; Benchikouhne-Ranchoux, M. In *Proc. Internat. Solvent Extr. Conf. (ISEC 2008)*, Moyer, B. A., Ed. Tucson, AZ, USA, 15–19 September, 2008.

[xxvi] Serrano-Purroy, D.; Baron, P.; Christiansen, B.; Malmbeck, R.; Sorel, C.; Glatz, J. P., *Radiochim. Acta* **2005,** *93,* 351–355.

[xxvii] Magnusson, D.; Christiansen, B.; Glatz, J. P.; Malmbeck, R.; Modolo, G.; Serrano-Purroy, D.; Sorel, C., *Solvent Extr. Ion Exch.* **2009,** *27,* 26–35.

[xxviii] Modolo, G.; Wilden, A.; Geist, A.; Magnusson, D.; Malmbeck, R., *Radiochim. Acta* **2012,** *100,* 715–725.

[xxix] Modolo, G.; Geist, A.; Miguirditchian, M., Minor actinide separations in the reprocessing of spent nuclear fuels: recent advances in Europe. In *Reprocessing and Recycling of Spent Nuclear Fuel*, Taylor, R., Ed. Woodhead Publishing: 2015.

[xxx] Panak, P. J.; Geist, A., *Chem. Rev.* **2013,** *113,* 1199–1236.

[xxxi] Warin, D.; Poinssot, C.; Bourg, S. In *Proc. Internat. Conf. GLOBAL 2011,* Makuhari, Japan, 11–16 December 2011, paper 478580.

[xxxii] Wilden, A.; Modolo, G.; Schreinemachers, C.; Sadowski, F.; Lange, S.; Sypula, M.; Magnusson, D.; Geist, A.; Lewis, F. W.; Harwood, L. M.; Hudson, M. J., *Solvent Extr. Ion Exch.* **2013,** *31,* 519–537.

[xxxiii] Wilden, A.; Modolo, G.; Kaufholz, P.; Sadowski, F.; Lange, S.; Sypula, M.; Magnusson, D.; Müllich, U.; Geist, A.; Bosbach, D., *Solvent Extr. Ion Exch.* **2015,** *33,* 91–108.

[xxxiv] Donnet, L., Adnet, J. M., Faure, N., Bros, P., Brossard, Ph., Josso, F. In *Proc. 5th Information Exchange Meeting on Actinide and Fission Product Partitioning and Transmutation,* Mol, Belgium 1998, OECD-NEA, Paris, France (1999), pp. 161–168.

[xxxv] Modolo, G.; Kluxen, P.; Geist, A., *Radiochim. Acta* **2010,** *98,* 193–201.

[xxxvi] Bollesteros, M.-J.; Calor, J.-N.; Costenoble, S.; Montuir, M.; Pacary, V.; Sorel, C.; Burdet, F.; Espinoux, D.; Hérès, X.; Eysseric, C., *Proc. Chem.* **2012,** *7*, 178–183.

[xxxvii] Chapron, S.; Marie, C.; Arrachart, G.; Miguirditchian, M.; Pellet-Rostaing, S., *Solvent Extr. Ion Exch.* **2015,** *33,* 236–248.

[xxxviii] Wagner, C.; Müllich, U.; Geist, A.; Panak, P. J., *Solvent Extr. Ion Exch.* **2016,** *34,* 103–113.

[xxxix] Miguirditchian, M.; Roussel, H.; Chareyre, L.; Baron, P.; Espinoux, D.; Calor, J.-N.; Viallesoubranne, C.; Lorrain, B.; Masson, M. In *Proc. Internat. Conf. GLOBAL 2009*, Paris, France, 6–11 September, 2009.

[xl] Halleröd, J.; Ekberg, C.; Löfström-Engdahl, E.; Aneheim, E., *Nukleonika* **2015,** *60* (4), 829–835.

[xli] Carrott, M.; Geist, A.; Hérès, X.; Lange, S.; Malmbeck, R.; Miguirditchian, M.; Modolo, G.; Wilden, A.; Taylor, R., *Hydrometallurgy* **2015,** *152*, 139–148.

[xlii] Carrott, M.; Bell, K.; Brown, J.; Geist, A.; Gregson, C.; Hérès, X.; Maher, C.; Malmbeck, R.; Mason, C.; Modolo, G.; Müllich, U.; Sarsfield, M.; Wilden, A.; Taylor, R., *Solvent Extr. Ion Exch.* **2014,** *32,* 447–467.

[xliii] Malmbeck, R.; Carrott, M. J.; Geist, A.; Hérès, X.; Magnusson, D.; Miguirditchian, M.; Modolo, G.; Sorel, C.; Taylor, R. J.; Wilden, A., In *Proc. Internat. Solvent Extr. Conf. (ISEC 2014)*, Würzburg, Germany, 7–11 September, 2014; pp 39–44.

[xliv] Brown, J.; McLachlan, F.; Sarsfield, M.; Taylor, R.; Modolo, G.; Wilden, A., *Solvent Extr. Ion Exch.* **2012,** *30,* 127–141.

LATE SUBMISSIONS

A-42

Plutonium Chemistry in the WIPP: Update and Path Forward

Donald Reed[1], Russ Patterson[2]

[1]Los Alamos National Laboratory, Carlsbad, NM, USA, [2]DOE-CBFO, Carlsbad, NM, USA

The Waste Isolation Pilot Plant (WIPP) continues on its path to recovery to resume operations in 2017 since the operational problems that occurred in early 2014. This will be done in a series of steps that will likely invoke design changes in the WIPP underground, revised acceptance criteria for TRU waste shipped to the WIPP site, and a strengthened safety case. An update of these activities and the expected path forward will be provided.

What remains constant throughout all these potential changes is that the core safety case for long-term containment of TRU waste has remained intact. The underground fire and very small subsequent Am/Pu release have been shown to be operational in nature and, in many respects, the resilience and performance of the salt Formation has been re-affirmed by these problems. In this context there has been essentially no change in the core safety case that supports the long-term performance of the WIPP TRU repository.

Plutonium, especially in the longer term, continues to be the actinide of most concern with respect to release in the WIPP concept. The oxidation state distribution and solubility/speciation of plutonium, in this context, only becomes important in the low-probability of brine inundation due to human intrusion scenarios. In this context, a long-term study to evaluate the impacts of reduced iron on the likely oxidation state distribution and correspondingly low solubilities of plutonium under repository-relevant conditions has been completed. Additionally redox-invariant analogs for Pu(III) and Pu(IV) have also been completed. These results continue to support overall performance assessment calculations although there continues to be some challenges in the speciation and modeling of plutonium in this system.

The role and importance of iron chemistry in the redox reactions of multivalent metals, including actinides, has been well established and reported previously [1,2]. There are also important links between the subsurface microbiology and this iron chemistry and this chemistry is a key pathway by which microbial processes influence metal speciation. Current WIPP PA assumptions are for a 50/50 distribution of Pu(III/IV) under the conditions where the low probability of dissolved brine release could occur. With low-activity Pu isotopes (e.g., Pu-242), the Pu(III) is the predominant oxidation state in the long term. For higher activity isotopes (e.g. $\geq$ Pu-239 in activity) significant Pu(IV) is also noted and appears to be predominant. In all cases investigated, the measured dissolved concentration/ solubility of plutonium remains low (see Figure). Overall, these results continue to confirm current WIPP PA assumptions. A key result of these long-term studies is that the reactivity of reduced iron is critical to the long-term performance of the repository and, once self-sealing occurs, will remove oxygen, produce hydrogen, and further react to reduce higher-valent metals and actinides to establish strongly reducing conditions.

The results of these long-term plutonium studies to determine the likely redox distribution and overall solubility will be updated and presented.

References:

(1) D. T. Reed, J. F. Lucchini, S. B. Aase and A. J. Kropf. Radiochim. Acta., 94 (2006) 591-597.

(2) D. T. Reed, M. K. Richmann, J-F. Lucchini and M. Borkowski, “Reduction of Higher-Valent Plutonium by Iron Under Waste Isolation Pilot Plant (WIPP)-Relevant Conditions; Data Summary and Recommendations.” Los Alamos report LA-UR-10-01254. Los Alamos National Laboratory, Los Alamos NM, USA.

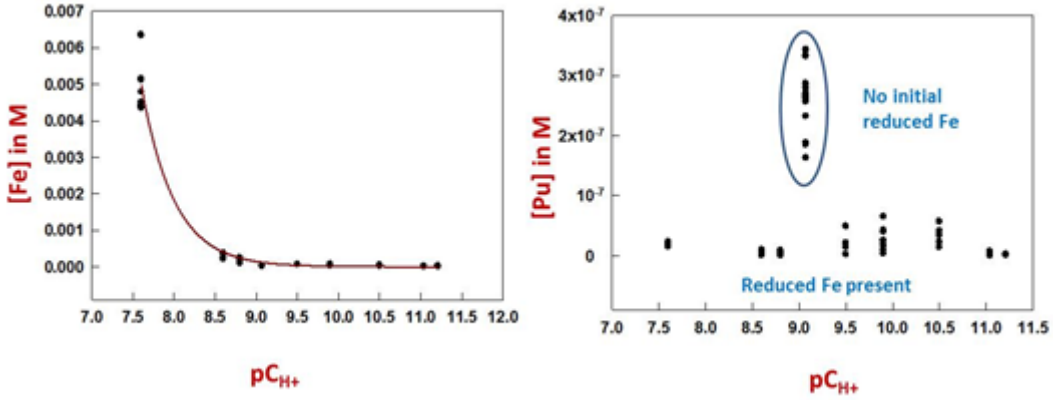

Figure. Concentration of Fe and Pu in WIPP brine for long-term (~8 year experiments) as a function of pC_{H+}. These results show the importance of reduce Fe as well as the low (~10^{-8} M) plutonium concentrations observed.

This publication is a Conference and Workshop report by the Joint Research Centre (JRC), the European Commission's in-house science and knowledge service. It aims to provide evidence-based scientific support to the European policy-making process. The scientific output expressed does not imply a policy position of the European Commission. Neither the European Commission nor any person acting on behalf of the Commission is responsible for the use which might be made of this publication.

Legal Notice
Neither the European Commission nor any person acting on behalf of the Commission is responsible for the use which might be made of this publication.

European Commission

Contact information
European Commission, Joint Research Centre (JRC), Directorate for Nuclear Safety and Security (DNSS),
Nuclear Safety Department, Advanced Nuclear Knowledge (Unit G.i.5)
D-76125 Karlsruhe, P. O. Box 2340, Germany
E-mail: JRC-KRU-INFO@ec.europa.eu
Tel.: (+49-7247)951-382
Fax: (+49-7247)951-590

JRC Science Hub
https://ec.europa.eu/jrc

Catalogue Number LC-NA-28059-EN-N (online)
EUR 28059 EN
ISBN 978-92-79-58851-8 (pdf)
ISSN 1831-9424 (online)
doi:10.2789/069707 (online)
JRC Pubsy 102724

Publications Office of the European Union, Luxembourg

© European Atomic Energy Community, 2016

This publication was compiled and edited by Roberto Caciuffo.

How to obtain EU publications

Our publications are available from EU Bookshop (http://bookshop.europa.eu),
where you can place an order with the sales agent of your choice.

The Publications Office has a worldwide network of sales agents.
You can obtain their contact details by sending a fax to (352) 29 29-42758.

Europe Direct is a service to help you find answers to your questions about the European Union
Free phone number (*): 00 800 6 7 8 9 10 11
(*) Certain mobile telephone operators do not allow access to 00 800 numbers or these calls may be billed.

A great deal of additional information on the European Union is available on the Internet.
It can be accessed through the Europa server http://europa.eu

LC-NA-28059-EN-N

JRC Mission

As the science and knowledge service of the European Commission, the Joint Research Centre's mission is to support EU policies with independent evidence throughout the whole policy cycle.

EU Science Hub
ec.europa.eu/jrc

@EU_ScienceHub
EU Science Hub - Joint Research Centre
Joint Research Centre
EU Science Hub

doi:10.2789/069707 (online)

Publications Office